Symposium Proceedings: Nuclear Data Problems for Thermal Reactor Applications

EPRI

EPRI NP-1098
Project 975-1
BNL-NCS-25047
ENDF-270
Symposium Proceedings
June 1979

Keywords:
Nuclear Data
Cross Sections
Data Uncertainties
Thermal Reactors
Benchmark Experiments
Criticals
Fissile Elements
Actinides
Fission Product Data
Decay Heat
$^{252}Cf\ \overline{\nu}$

Prepared by
Electric Power Research Institute
Palo Alto, California

ELECTRIC POWER RESEARCH INSTITUTE

Symposium Proceedings:
Nuclear Data Problems for Thermal Reactor Applications

NP-1098
Research Project 975-1
BNL-NCS-25047
ENDF-270

Symposium Proceedings, June 1979

BROOKHAVEN NATIONAL LABORATORY
Upton, New York

May 22–24, 1978

Prepared by

P. F. Rose and S. Pearlstein
National Nuclear Data Center
Brookhaven National Laboratory
Upton, New York 11973

and

Odelli Ozer
Project Manager
Nuclear Power Division
Electric Power Research Institute

Prepared for

Electric Power Research Institute
3412 Hillview Avenue
Palo Alto, California 94304

ORDERING INFORMATION

Requests for copies of this report should be directed to Research Reports Center (RRC), Box 50490, Palo Alto, CA 94303, (415) 961-9043. There is no charge for reports requested by EPRI member utilities and affiliates, contributing nonmembers, U.S. utility associations, U.S. government agencies (federal, state, and local), media, and foreign organizations with which EPRI has an information exchange agreement. On request, RRC will send a catalog of EPRI reports.

NOTICE

Prepared by
Electric Power Research Institute
Palo Alto, California

ABSTRACT

The proceedings of a symposium on the status of nuclear data for thermal reactor applications are presented. The following areas were specifically addressed in the symposium:

1. Status of the microscopic nuclear data of importance to thermal reactors
2. Status of clean critical benchmark experiments used for testing the validity of nuclear data and computational methods
3. Status of fission product and heavy actinide data and related integral experiments
4. Problems associated with using nuclear data files in calculations and industry experience with the dependence of reactor design methods on nuclear data uncertainties

Problem areas and recommendations for further development are discussed.

PREFACE

BACKGROUND

During the past four years, the Electric Power Research Institute (EPRI) has supported an extensive nuclear data development effort. This effort, which had for its overall objective the development of a national "industry standard" nuclear data base, has focused on improving the performance of the reference nuclear data library, ENDF/B, in applications of interest to the U.S. utility industry. Research was undertaken to test the adequacy of the fourth version of the ENDF/B file (ENDF/B-IV) in thermal reactor benchmark calculations, to determine the sensitivity of light water reactor calculations to nuclear data, and to attempt to correct a number of major data-related discrepancies.

The Symposium on Nuclear Data Problems for Thermal Reactor Applications was convened to review the status of nuclear data problems in light of results obtained from these EPRI-sponsored activities and to determine priorities for the continuing development of ENDF/B-V. The symposium was organized by the National Nuclear Data Center (NNDC) at Brookhaven National Laboratory, as part of EPRI Research Project 975-1. NNDC has played a key role in coordinating the nationwide development of ENDF/B.

The symposium primarily addressed the needs of the thermal reactor community and focused on (1) microscopic cross sections of importance to reactor design, (2) clean critical benchmarks and analysis of clean critical experiments, (3) dependence of power reactor benchmarks on nuclear data, and (4) interaction of methods and data in industrial experience.

Round table discussions, in which papers were reviewed in depth, were organized for each session. The sessions were followed by a formal preparation of summaries that evaluated the present status of the subject under discussion, indicated future directions for development, and made specific recommendations to funding agencies. The final summaries are reproduced in Section 1 of this document.

ACKNOWLEDGMENTS

The editors gratefully acknowledge the effort of the session chairmen in directing the round table discussions and in preparing a summary of the sessions. The fine cooperation received from the symposium participants and the efforts of Ms. Z. Laskowsky in preparing this summary in conformance with EPRI editorial requirements are also gratefully acknowledged.

CONTENTS

Section 1

SUMMARY

Section 1

SUMMARY

REVIEW OF MICROSCOPIC CROSS SECTIONS OF IMPORTANCE TO REACTOR DESIGN--
Session Chairman: B. R. Leonard, Jr.

Average Number of Neutrons Produced per Fission

An important paper of this session was the review by J. R. Smith of the value of $\bar{\nu}$ for ^{252}Cf and ratio measurements for the thermally fissile nuclides.

Smith's paper, "Status of ^{252}Cf $\bar{\nu}$ and Its Impact on Thermal Parameters," presents the results of an extensive reanalysis of the measurements of $\bar{\nu}$ using the manganese bath technique. Several of the values represent a significant modification of the originally reported results. In addition, the value of $\bar{\nu}$ obtained using the boron pile technique has been significantly modified by a reanalysis of the experiment by Ullo (1).

Spencer's recent and ongoing measurements at Oak Ridge National Laboratory (ORNL) on the $\bar{\nu}$ value for ^{252}Cf have resulted in a value larger and somewhat discrepant with the mean of other extensively evaluated experiments (2). Spencer's experiments, however, have undergone extensive external and internal analysis. When Spencer's measurements are factored into the reevaluated results of nine other experiments, Smith arrives at a current weighted mean value of $\bar{\nu}_t(^{252}Cf) = 3.766$ n/fission. Since it is apparent that there are systematic errors in the reported values, the precision of the mean, ± 0.007, is not a realistic error assignment. A more realistic error assignment has not yet been made but would probably be of the order of ± 0.02 n/fission.

Smith notes that the values for the ratio of $\bar{\nu}$ (^{235}U) to ^{252}Cf obtained by Boldeman (3) are discrepant with the ratio deduced by Gwin (4) from his measurements. Gwin has experimental evidence that this difference is due to physical effects caused by finite thickness of the foil used for the measurements for the thermally fissile nuclei.

Primary Fissile and Fertile Materials

The following comments are based primarily on the paper presented by L. W. Weston, "Review of Cross Section Data Important to the Uranium Plutonium Fuel Cycle in Thermal Reactors," and the Session III round table discussion.

^{233}U. The whole energy region below 0.1 eV should be definitively remeasured and reevaluated, taking into particular account the consistency of partial and total cross sections and the behavior near the 0.1 eV anomaly. Measurements should include at least σ_T, σ_f, σ_c, and $\bar{\nu}(E)$.

^{235}U. The low-energy fission cross-section data reported in slow-chopper and linear accelerator (LINAC) experiments from the Belgian laboratories at MOL and GEEL probably have systematic errors in the interpretation of the energy scale. In principle, these data can be corrected, and the corrected data should be incorporated in the simultaneous least squares (LSQ) of the partial cross sections in the thermal region. Identical problems exist for the fission data for ^{233}U, ^{239}Pu, and ^{241}Pu.

In the resolved resonance region, there is a need for an improved evaluation utilizing existing knowledge of resonance spin states and multilevel fission theory.

^{238}U. Four new measurements have been reported for the resonance parameters of the three lowest-energy neutron resonances. The results of these measurements are reasonably consistent and differ significantly from previously accepted values.

The shape of the capture cross section in the thermal neutron region should be reevaluated using the new resonance parameters. The measured absorption cross sections near zero neutron energy will constrain the thermal cross section to values near those presently accepted, $\approx$2.7 b. The self-indication results reported from Rensselaer Polytechnic Institute (RPI) should be analyzed for the higher energy resonances, in particular the p-wave levels, to aid in the evaluation of the higher energy strength functions.

Integral benchmark comparisons indicate that the capture contribution in the unresolved resonance region is too large. A reexamination of the components of the strength function might improve this situation.

^{239}Pu. The thermal cross-section data need reevaluation considering the possible problem in the energy scale of the MOL and GEEL fission cross-section data. The effect of the energy variation of $\bar{\nu}$ in the thermal region on the interpretation of all the thermal data should be evaluated.

^{240}Pu. The resonance parameters of the 1 eV resonance need to be determined more accurately. This resonance self-shields significantly at low concentrations, and the self-shielding changes dramatically with changes in isotopic density. The present status is that there are two discrepant groups of parameters that cannot, apparently, be reconciled. Benchmark calculations of critical experiments at Battelle, Pacific Northwest Laboratories (BNWL spheres) indicate a possible problem in the ^{240}Pu cross section.

There are new direct capture measurements in the thermal energy region below the 1 eV resonance reported by Weston and Todd (5). The ^{240}Pu thermal capture also shows up in the ^{239}Pu capture data of Gwin et al. The thermal capture is known from irradiation experiments. The capture cross section of the 1 eV resonance in its wings, however, is poorly known. New capture and transmission measurements through the 1 eV resonance could contribute significantly to improved knowledge of this cross section.

^{241}Pu. New capture and fission cross-section data in the thermal energy range have been reported by Weston and Todd (6). The shape of the capture cross section differs significantly from that previously deduced from total and fission cross-section data (e.g., ENDF/B-IV). The new capture data are in the direction of improving agreement with the $\eta(E)$ reported by Smith in his presentation. A simultaneous LSQ evaluation in the thermal region is needed, including the possibility of an energy-dependent $\bar{\nu}$.

The data in the resonance region indicate that the average value of Γ_γ is larger than previously deduced.

^{232}Th. Two new measurements of thermal capture cross sections were reported informally in Session III. These values (2200 m/s) were:

7.37 ± 0.11 b	Chrien et al., Brookhaven National Laboratory (BNL)
7.33 ± 0.17 b	Poenitz, Argonne National Laboratory (ANL)

These results confirm the previously used values of about 7.4 b. The accuracy obtained with the activation technique has been significantly improved by new determinations of the yield of the 411 keV ^{233}Pa gamma ray decay as:

38.6 ± 0.5/100	Gehrke, Helmer, and Reich, Idaho National Engineering Laboratory (INEL)
38.6 ± 1.5/100	Poenitz (ANL)

New values of the parameters of the first four positive energy resonances have been obtained by Chrien. The reported values were:

E_o (eV)	Γ_n (meV)	Γ_γ (meV)
21.78	2.1 ± 0.1	24 ± 1.5
23.43	3.7 ± 0.2	26 ± 1.5
56.49	4.0 ± 0.3	25 ± 2
69.07	41.2 ± 3	22.6 ± 2

The new parameters are consistent within assigned errors with those evaluated by Derrien (7).

It was pointed out that the preliminary version V ^{232}Th file failed to include a contribution in the resolved energy range of the missed p-wave resonances. Addition of this background file will increase the shielded resonance capture integral significantly.

Recent RPI measurements of total cross sections from ∿0.01 to 20 eV should serve as a strong constraint in determining the shape of the capture cross section near thermal. Capture measurements planned at RPI should also serve to determine this low-energy shape.

Heavy Actinides

General conclusions were also presented relating to the actinides. Some of these comments are based on "Nuclear Data for Actinide Production and Depletion Calculations," a paper given by R. W. Benjamin of the Savannah River Laboratory (SRL) in Session IV.

With the advent of the ENDF/B-V actinide file, evaluated nuclear data for the transactinium isotopes are suitable for current studies and calculations of thermal reactor transmutation effects. There are a few experimental measurements for these isotopes beyond those currently planned or in progress that would appear to be valuable for future user needs. There is a lack, however, of recognized, well-documented production-depletion studies that can be used to test the data. Recommendations are made in three areas: microscopic experimental measurements, evaluations, and benchmarks.

Experimental Measurements. A number of experimental measurements would be worthwhile, but all of them would have to be classed as second or third priority. These are listed below in order of importance.

- ^{242m}Am - integral capture to 10%
- ^{241}Am - differential capture branching ratio
- ^{242}Cm - integral capture to 20%
- ^{237}Np - better definition of (γ,n) and $(n,2n)$
- ^{251}Cf - differential fission
- ^{250}Cf - low-energy total or capture
- ^{246}Cm - differential total or capture below 20 eV
- ^{247}Cm - differential fission below 30 eV
- ^{233}Pa - differential capture to 5% below 2 eV. There are some additional incompletely analyzed total cross-section data from measurements on the materials testing reactor (MTR) fast chopper. Analysis of these data would provide resonance parameters at higher energies than the available analysis by Simpson allows (8).

Measurements in progress are listed in Table 1 of Benjamin's paper.

Evaluations. Several reevaluations to incorporate recent experimental data into ENDF/B-V are in progress. These are also listed in Table 1 of W. B. Wilson and T. R. England's paper, "Status of Fission Product Data for Absorption Calculations." The only additional isotope for which a reevaluation could be made profitably is ^{242}Cm. The objective would be to incorporate the low-lying resonance data from the USSR into the version V evaluation (which contains a picket fence resonance region).

Benchmarks. There are at present no recognized, well-documented depletion benchmarks for the actinides. Such experiments should be defined, then carried out and analyzed in a form useful for data testing.

Fission Products

In the area of fission product yield, the paper by W. H. Walker, "Cross Sections and Yields Important for Fission Product Absorption in Thermal Reactors," demonstrated a consistent set of fission product yield data for the important long-term nuclides. The major uncertainty noted was for the Xe yield from ^{241}Pu fission.

Round Table Discussion

At the round table discussion for this session an informal paper was given by N. E. Holden and J. R. Stehn of Brookhaven National Laboratory (BNL) on thermal parameters of the fissile nuclides.

With recent reanalyses of various measurements of $\bar{\nu}$ and alpha experiments, Holden and Stehn used the LSF program (9) to determine the effect of the reanalyzed results on the thermal parameters of the fissile nuclei. As a benchmark for the determination of the changes to the various parameters, the LSF calculation "Q4" is listed. This was a quasi-final ENDF/B-IV evaluation. With the exception of ^{233}U, the Q4 corresponds to approximately the recommended ENDF/B-IV values.

Among the various changes to the input, a lower ^{239}Pu half-life value and a slightly higher but more exact ^{233}U half-life value were included. The results of Okazaki's analysis of his 1964 Chalk River alpha irradiation experiment (10) and the results of the Mathematical Applications Group, Inc. (MAGI), on the 1968 Durham and Lounsbury alpha irradiation experiments were used (11, 12).

The $\bar{\nu}$ values for ^{252}Cf correspond to Smith's evaluation of the manganese bath experiments, Boldeman's evaluation of the liquid scintillator experiments, and Ullo's evaluation of the Colvin-Sowerby boron pile (13) and the Spencer liquid scintillator experiments. The only $\bar{\nu}$ ratios to ^{252}Cf that were used correspond to Gwin's measurement and Boldeman's measurement corrected for foil-thickness effects.

The results in Tables 1-1 through 1-4 include Q4, all changes listed above, and a calculation with all ^{252}Cf $\bar{\nu}$ values and all $\bar{\nu}$ ratios involving ^{252}Cf eliminated from the input.

Table 1-1

RESULTS FOR ^{233}U

Quantity	Calculations		
	Q4	All Changes	No ^{252}Cf $\bar{\nu}$
σ_{TOTAL}	591.85	589.01 ± 3.79	589.16
σ_{Scat}	11.98	12.23 ± 0.68	12.22
σ_{abs}	579.87	576.78 ± 3.10	576.95
σ_{fiss}	533.67	530.38 ± 22.9	530.56
σ_{capt}	46.20	46.40 ± 2.36	46.38
η(2200 m/s)	2.284	2.295 ± 0.006	2.294
α(2200 m/s)	0.0866	0.0875 ± 0.0018	0.0874
$\bar{\nu}_T$	2.482	2.496 ± 0.023	2.495
^{252}Cf $\bar{\nu}_T$	3.7566	3.769 ± 0.032	-
$T_{1/2}$	$1.572(10)^5$ y	$1.591(10)^5$ y ± $0.001(10)^5$	$1.591(10)^5$ y

Table 1-2

RESULTS FOR ^{235}U

Quantity	Calculations		
	Q4	All Changes	No ^{252}Cf $\bar{\nu}$
σ_{TOTAL}	698.47	697.60 ± 1.93	697.65
σ_{Scat}	15.56	16.14 ± 1.21	16.11
σ_{abs}	682.92	681.46 ± 11.6	681.54
σ_{fiss}	585.70	582.61 ± 4.90	582.92
σ_{capt}	97.22	98.85 ± 1.13	98.63
η(2200 m/s)	2.074	2.083 ± 0.018	2.082
α(2200 m/s)	0.1660	0.1697 ± 0.002	0.1692
$\bar{\nu}_T$	2.419	2.436 ± 0.004	2.434
^{252}Cf $\bar{\nu}_T$	3.7566	3.769 ± 0.032	-

Table 1-3

RESULTS FOR ^{239}Pu

Quantity	Calculations		
	Q4	All Changes	No ^{252}Cf $\bar{\nu}$
σ_{TOTAL}	1019.78	1025.77 ± 3.44	1024.68
σ_{Scat}	8.03	7.85 ± 1.00	7.88
σ_{abs}	1011.75	1017.93 ± 3.39	1016.80
σ_{fiss}	742.05	748.08 ± 46.	748.46
σ_{capt}	269.71	269.84 ± 2.95	268.34
η(2200 m/s)	2.107	2.121 ± 0.013	2.117
α(2200 m/s)	0.3635	0.3607 ± 0.0083	0.3585
$\bar{\nu}_T$	2.873	2.886 ± 0.007	2.876
^{252}Cf $\bar{\nu}_T$	3.7566	3.769 ± 0.032	-
$T_{1/2}$	24,374y	24,122 ± 31y	24,122y

Table 1-4

RESULTS FOR ^{241}Pu

Quantity	Calculations		
	Q4	All Changes	No ^{252}Cf $\bar{\nu}$
σ_{TOTAL}	1383.96	1386.50 ± 7.16	1388.07
σ_{Scat}	11.05	11.02 ± 1.39	11.01
σ_{abs}	1372.91	1375.47 ± 6.72	1377.06
σ_{fiss}	1008.71	1006.61 ± 22.	1006.76
σ_{capt}	364.20	368.87 ± 5.04	370.31
η(2200 m/s)	2.156	2.166 ± 0.007	2.166
α(2200 m/s)	0.3611	0.3664 ± 0.0052	0.3678
$\bar{\nu}_T$	2.934	2.960 ± 0.010	2.963
^{252}Cf $\bar{\nu}_T$	3.7566	3.769 ± 0.032	

REVIEW OF CLEAN CRITICAL BENCHMARKS AND ANALYSIS OF CLEAN CRITICAL EXPERIMENTS--
Session Chairman: J. Hardy, Jr.

Summary

Plutonium and Mixed-Oxide Experiments. Only the eigenvalue measurements and the BNWL homogeneous nitrate solution criticals can be considered an adequate set for testing data and computational methods. These experiments cover a range of H/^{239}Pu and ^{240}Pu content. They are both bare and fully reflected with water, and corrections due to fill tubes and other experimental perturbations are minimal. Their chief deficiency appears to be the uncertainty in atomic densities due to limitations of the analytical techniques employed.

The homogeneous PuO_2-polystyrene assemblies may be of somewhat less value as benchmarks because of the perturbing effects of the plastic coatings on the compacts and possible particle-size effects.

Among the heterogeneous lattice experiments, the Pu-Al fuel rod measurements that were repeated without Lucite sleeves and the mixed-oxide rod lattices are the most useful. Some were critical experiments and others were done by critical approach techniques; the critical experiments should probably be given more weight.

Experimental integral parameter results in the BNWL mixed-oxide lattices are difficult to interpret. In addition, a significant problem exists with respect to the thermal disadvantage factors, which presently have a calculation-experiment ratio (C/E) on the order of 1.1 to 1.2.

Homogeneous ^{235}U Criticals. With ENDF/B-IV, ^{235}U aqueous homogeneous criticals show calculated k_{eff} values ranging systematically from 0.994 for large thermal systems to 1.01 at 45% leakage. This trend is thought to be due mostly to an underprediction of leakage resulting from a too-soft fission spectrum. The ^{235}U capture and fission resonance integrals are also important. For ENDF/B-IV, the fission resonance integral is 9 b above the best integral value of 275 ± 5 b (above 0.5 eV), and the capture integral is low. This results in an epithermal alpha at least 5% below integral measurements.

Recent differential fission spectrum measurements for ^{235}U indicate that the Maxwellian model is inadequate and a more complex representation is required. Furthermore, the ENDF/B-IV mean energy ($\overline{E}_p$ = 1.985 MeV) is too low. An equilibrium spectrum based on a Watt shape with $\overline{E}_p$ = 2.027 MeV (which fits the differential data reasonably well), plus a 10-b reduction of the ENDF/B-IV ^{235}U fission resonance integral, can remove the k_{eff} trend observed for homogeneous criticals. This would also significantly improve the epithermal alpha of ^{235}U. A more complex spectrum representation, the Steen standard model with $\overline{E}_p$ = 2.073 MeV, also fits the differential data and can eliminate the k_{eff} leakage trend, but this requires a ^{235}U epithermal alpha no greater than ENDF/B-IV. In either case, an increase of ∿0.5% in $\overline{\nu}$ is also required to eliminate the k_{eff} bias.

ENDF/B-IV gives a fission age in H_2O of 25.5 cm^2, significantly below the measured value of 26.4 ± 0.3 cm^2. The equilibrium spectrum based on the Watt shape, with $\overline{E}_p$ = 2.027 MeV, provides only slightly better agreement. The Steen standard model, with $\overline{E}_p$ = 2.073 MeV, leads to very good agreement. It also produces good agreement with integral measurements of fission spectrum averaged cross sections: $\overline{\sigma}_f(^{238}U)$ and $\overline{\sigma}_f(^{238}U)/\overline{\sigma}_f(^{235}U)$.

^{238}U-^{235}U-H_2O Experiments. The slightly enriched uranium, H_2O-moderated TRX-1 and -2 critical lattices have been analyzed by eight laboratories using ENDF/B-IV data. These experiments show adequate consistency. The analyses give a reasonably coherent picture of nuclear data performance and of consistency among the different methods of calculation. The strong correlation of calculated k_{eff} and ρ^{28} (the ratio of epithermal to thermal ^{238}U capture) suggests that ^{238}U resonance capture is the principal difference among the calculative methods. Differences are particularly apparent between the new RAHABR (SRL* results) (14), RCP01/MUFT7 (Bettis Atomic Power Laboratory [BAPL] results), and RECAP/HAMMER and REPC/HAMMER (BNL results).

Although other integral parameters are in adequate agreement with experiment, the best calculative methods give ρ^{28} about 3-5% high, and correspondingly low k_{eff} (∿0.985 in TRX-1 and 0.990 in TRX-2). A 0.5% increase of ^{235}U $\overline{\nu}$ would significantly improve k_{eff} for both TRX-1 and TRX-2.

Although new resonance parameters for the low-energy resonances of ^{238}U reduce ρ^{28} by 2.5%, this has been partially compensated for in preliminary ENDF/B-V by a significantly increased s-wave strength function so that the net reduction of ρ^{28} from version IV is only about 1%.

The BAPL full-core Monte Carlo analyses of TRX-1 and TRX-2 give excellent agreement with corresponding cell Monte Carlo plus-B_1 leakage corrections for integral parameters. However, the BNL RECAP analyses show a difference between the RECAP/HAMMER and full-core RECAP results for ρ^{28} but not for δ^{25}. It is thought that this is mostly due to statistics (flux shape convergence) in the full-core RECAP.

^{238}U-^{235}U-D_2O Experiments. Material B^2 and integral parameters are currently being measured in a coaxial uranium-fuel-D_2O-moderated critical lattice at the Savannah River Laboratory. Reaction rate parameters agree with earlier measurements, but the measured B^2 in the critical facility is 0.52 m^{-2} lower than in the exponential. The experimental results do not at present satisfy the internal consistency criterion, although all known systematic errors have been accounted for and well-known experimental techniques are used.

Consistency analysis of the MIT-1, -2, and -3 Cross Section Evaluation Working Group (CSEWG) benchmark lattices shows that the experimental results are inconsistent. Material bucklings from these subcritical experiments are significantly higher than predicted by consistency analysis or calculation. This material buckling discrepancy is a problem common to all D_2O subcritical experiments, and all of the "benchmark quality" D_2O lattice experiments that have appeared in the literature have been subcritical experiments.

Three new D_2O subcritical experiments have been proposed as CSEWG thermal benchmarks. These experiments are later experiments in the MIT Heavy Water Lattice Project than MIT-1, -2, and -3, and appear to have a greater consistency between the measured activation parameters. The material buckling discrepancy observed for MIT-1, -2, and -3 is also observed for these lattices.

Th-^{233}U Experiments. There is substantial evidence from the calculated eigenvalues of homogeneous criticals and thorium-uranium lattices to support hardening of the fission neutron spectrum for ^{233}U. The new harder ^{233}U fission spectrum proposed by Steen significantly reduces the leakage bias observed in calculations of k_{eff}. All results obtained with the Steen spectrum (and ENDF/B-IV cross sections) appear

to scatter about a horizontal line (versus leakage fraction) that depicts an overall underprediction of k_{eff} by 0.3-0.4%. Such a residual bias can easily be accommodated by raising the value of $\bar{\nu}$, which would affect all assemblies equally.

There is reasonable consistency among the integral thorium capture measurements, given their experimental errors. With ENDF/B-IV, experiment-calculation ratios (E/C) range from 10% high to 3% low, with experimental uncertainties ranging from ± 2% to ± 5%. It is difficult to judge the adequacy of predictions of thorium resonance capture without a firm value for thermal σ_a since the measured ThO_2 rod resonance integral (RI) is proportional to σ_a (from normalization) and calculated ρ^{02} is inversely proportional to σ_a. Assuming that the value σ_a = 7.4 b is adequate, the comparisons suggest that ENDF/B-IV predictions of thorium resonance capture are ∿3% low.

The light water breeder reactor (LWBR) thorium gives slightly better overall agreement with experiment because of a 3% increased resonance capture and a 1% reduced σ_a. For the Leonard thorium, the reduced resonance capture and 3% higher σ_a result in E/C nominally + 10%. ENDF/B-V includes the Leonard resonance evaluation except for the parameters of the lowest resonances, taken from Derrien (15), but the ENDF/B-IV σ_a has been maintained. Therefore we would infer the prospects for ENDF/B-V as follows:

- Reducing σ_a to 7.4 b would shift the predictions obtained from the Leonard evaluation by 3%.
- Furthermore, Leonard has stated that additional capture should be added to account for missed p-wave resonances (16). This would improve the comparison with experiment by several percent.
- Recent measurements of the low-energy shape of the thorium capture cross section could conceivably add another 0.3-0.5 b to the RI (unshielded), which would bring the overall prediction of capture measurements into very good agreement with experiment.

Recommendations

1. It would be extremely desirable to have a good set of carefully determined reaction rate ratios in mixed-oxide lattices. These should include ρ^{28}, δ^{28}, δ^{25}, and δ^{49}, as well as capture and fission ratios between the uranium and plutonium isotopes, and thermal disadvantage factors.

2. It is highly desirable to have additional analyses of the BNWL homogeneous plutonium experiments and the mixed-oxide experiments with ENDF/B-IV and -V data.

3. In order to resolve the 2-4% methods differences observed in ^{238}U resonance capture, it is important that new calculations of high accuracy be performed to establish a consensus. The comparison should be made for the TRX-1 infinite lattice cell with ENDF/B-IV. VIM and other Monte Carlo programs should be employed for this. In addition, the methods comparison of ENDF-230 should be extended to include recent calculations. The most important results of these comparisons should be made readily accessible to interested persons.

4. It is recommended that the preliminary ENDF/B-V ^{238}U be examined to see whether the differential data can accommodate a 0.2-0.3 b reduction in shielded capture integral.

5. For D_2O-moderated uranium lattices, new measurements in critical experiments are needed for cross-section testing purposes. Any such experiments should utilize simple single-rod assemblies at or near natural ^{235}U enrichment and should measure a complete set of activation and reactivity parameters. The results of these experiments should satisfy the consistency analysis before acceptance as a cross-section testing benchmark.

6. ^{235}U $\bar{\nu}$ should be increased $\sim$0.5% (over ENDF/B-IV) on the basis of k_{eff} results for homogeneous criticals and TRX lattices.

7. The ENDF/B-IV ^{235}U fission spectrum should be hardened. The Watt shape with $\bar{E}_p$ = 2.03 MeV proposed for ENDF/B-V will partially correct k_{eff} errors for high-leakage criticals. The remainder can be corrected by an increased epithermal alpha for ^{235}U. The capture and fission resonance integrals of ^{235}U should be reviewed in light of integral data and improvements incorporated into ENDF/B as soon as possible (perhaps as a mod to version V).

8. The ^{235}U fission spectrum requires further investigation in order to reconcile differential and integral experiments.

9. The thorium thermal-capture cross section should be determined to < 1%, and additional measurements are desirable. Recent experiments tend to support the value of 7.4 b.

10. The shape of the thorium capture cross section should be well-measured up to 20 eV, and current efforts in this area should be encouraged. This range contributes a significant amount of unshielded epithermal capture in lattices.

11. New ^{233}U-ThO_2 critical benchmark-quality lattices should be measured using H_2O (D_2O) as moderator. This should include a complete set of integral parameters for comparison with predictions of individual reaction rates. The number of reliable thorium integral capture measurements is quite limited.

12. ^{233}U $\bar{\nu}$ should be raised by 0.3-0.4% to bring the calculated ^{233}U-Th k_{eff} into agreement with experiment after a harder ^{233}U spectrum (perhaps the Steen standard spectrum) is adopted.

13. Additional fission spectrum measurements are desirable, particularly for ^{233}U.

Some Criteria for Integral Benchmark Experiments to Test Nuclear Data for Thermal Reactors

Some major criteria for a good thermal reactor benchmark experiment were formulated by the Thermal Data Testing Subcommittee of the CSEWG. Although most of these criteria are obvious, because of the exigencies of real life they have hardly ever been fulfilled. It is also true that many experiments on which much effort was expended are not useful as benchmarks because of significant failings in one or more of these areas.

Experiments can be arranged in a rough hierarchy, from the most specific differential measurement to the most complex application test, as follows:

1. Differential experiments (of varying resolution)
2. Simple integral experiments of a fairly specific nature--e.g., dilute RIs, age, etc.
3. Homogeneous criticals
4. Simple lattice experiments (criticals and exponentials)
5. Complex mock-ups used to test overall design models

Homogeneous criticals test thermal criticality parameters, resonance integrals, moderation and leakage properties, and fission spectra for specific combinations of moderator and fissile material.

Lattice experiments should extend this to useful combinations of materials in heterogeneous configurations that can be interpreted with a minimum of ambiguity. Geometries should be simple and as easy to model in calculations as possible. Perturbations due to control rods, shields, experimental devices, reentrant holes, etc., should be as small as possible and preferably should not exist at all.

Typically, a series of a few uniform rod lattices with different spacing is most desirable. Where possible, these lattices should be large enough to establish a usable, asymptotic, simply buckled region (small cores intended to study leakage are an exception). Such simple geometry permits relatively unambiguous analysis and ease of interpretation and makes the experiment useful to as many analysts as possible.

Although criticality is useful, integral parameter measurements provide much more specific tests of important data types. Parameters such as ρ^{28}, δ^{25}, δ^{28}, and conversion ratio (CR*) should be measured. Radial and axial activation shapes should be measured with different detectors (fast, thermal, or intermediate).

Various combinations of moderator, fissile, and fertile materials are useful in distinguishing the effects of individual materials. The following series is an example.

^{235}U-^{232}Th-H_2O

^{235}U-^{232}Th-D_2O

^{233}U-^{232}Th-D_2O

^{235}U-^{238}U-H_2O

^{235}U-^{238}U-D_2O

Critical experiments are preferred to exponentials. Exponential experiments have frequently been difficult to interpret.

Current calculative methods (e.g., Monte Carlo) can readily handle all sorts of geometry and composition variations. For this reason, a few carefully done experiments, carefully chosen to span the range of lattices of interest, are more useful than many poorly done ones. The experiments should not try to do too much. Good measurements of a few parameters are probably better than an approach that tries to cover everything in sight.

It is not clear, for example, that much more can be learned about nuclear data by doing experiments with both metal and oxide fuel. The choice of using detector foils versus grinding or dissolving fuel pellets should depend on practical considerations of availability and experimental technique.

Measurements at elevated temperatures can be useful, primarily to test Doppler effect in resonance capture.

Experiments should be documented in complete detail in at least one single lab report. Experimenters should be available for questions, and they should keep original lab notes and records. It is desirable that an experiment be analyzed as it is being done so that inconsistencies can be discovered and investigated.

Materials, geometries, standards, and other relevant parameters should be well characterized.

Experiments should be adequately funded and staffed, and they should not be performed under deadline pressures.

Measurements should be repeated enough times to establish reproducibility. A careful error analysis should be part of the experiment. Systematic experimental effects (e.g., foil perturbations, cadmium box effects, room return) should be minimized by a judicious choice of methods, and unavoidable effects should be studied by experiment and calculation.

Alternative methods should be used, when possible, to provide cross checks.

DEPENDENCE OF POWER REACTOR BENCHMARKS ON NUCLEAR DATA--Session Chairman: D. Diamond

Because the topics covered in this session were not necessarily related to one another, each paper is discussed separately.

Integral Decay-Heat Measurements and Comparisons to ENDF/B-IV and -V

T. R. England presented results from Los Alamos Scientific Laboratory (LASL) and Hanford Engineering Development Laboratory (HEDL) on recent comparisons of integral decay measurements with summation calculations. The experiments measured the decay power following pulsed and long-term thermal neutron irradiation of ^{233}U, ^{235}U, and ^{239}Pu. The summation calculations used ENDF/B-IV decay data and yields from versions IV and V. The comparisons were very good for ^{235}U and almost as good for ^{233}U. For ^{239}Pu the percent difference between calculation and the LASL experiment as a function of cooling time averaged $\sim$ 9% and ranged as high as 14%.

Generalized LSQ methods were applied to the ^{235}U and ^{239}Pu decay-heat measurements and calculations to arrive at the ANS-5 standard on decay heat. (A series of exponentials is fit to the data.) Results for ^{235}U imply uncertainties of less than 2% (1σ) for the "infinite" exposure case for all cooling times greater than 10 seconds. The uncertainties for ^{239}Pu are on the order of 4%. This standard is particularly important for use in analyzing the loss-of-coolant accident (LOCA) in light water reactors (LWRs).

Comparisons of experimental β and γ spectra with summation calculations using ENDF/B-IV were also included. The effect of noble gas lost during cooling and corrections for absorption during irradiation were also discussed.

Great experimental and analytic progress has resulted from the efforts of recent years. However, efforts should not cease until the field is in a state that will

be satisfactory for some time. There is an urgent need to understand in detail the extent to which recent experiments are discrepant among themselves and with summation calculations. The most striking contrast presented at this conference concerned the apparent agreement of the LASL 20,000-s irradiation data with summation calculations for ^{235}U and the disagreement for ^{239}Pu. Discrepancies between LASL and ORNL measurements for ^{239}Pu of $\sim$8% need to be resolved.

Considerable effort has gone into reducing the uncertainty in the ^{235}U decay-heat curve. This is of great economic importance to LWR vendors in analyzing the LOCA and of great technical importance in mitigating the effects of the LOCA. It is recommended that reactor engineers be made aware of these advances. There is also a need for benchmarks for long-term ($>10^5$ s) heating and spectrum measurements.

Only one measurement has been obtained for ^{233}U for cooling times under 100 s. Experimental decay-heat curves for this nuclide need to be established. There are longer-term data available in a French measurement.

There are no benchmark measurements for ^{238}U, although several percent of all fissions occur in this nuclide in current designs. This situation should be rectified.

Detailed NaI(Tl) spectra now exist for ^{235}U, ^{239}Pu, and ^{241}Pu that can aid the study of decay data files in searches for likely improvements. Ge(Li) spectra on an absolute basis should be acquired for short irradiations and a variety of cooling times to allow detailed benchmarking of the fission product yield and decay data files.

While the literature now shows detailed estimates of the (small) uncertainties to be expected in present summation-method decay-heat estimates, it would be desirable to ascertain what the spread in decay-heat estimates would be using various worldwide evaluations of the relevant quantities. Such a study could provide another way to sense the uncertainty in the summation estimates of decay heat. There are data available in England, France, and perhaps Japan that might be suitable for use in these comparative studies.

The delayed neutron yields and spectra can be calculated from the fission product files. The quality of such calculations should be examined for use in improving evaluated delayed neutron yields, spectra, and temporal dependencies.

Status of Fission Product Data for Absorption Calculations

W. B. Wilson reviewed progress in fission product nuclear data for absorption buildup calculations in thermal reactors. Detailed sensitivity studies were presented. These calculations were done with the EPRI-CINDER code and showed the effect on fission-product absorption of thermal and epithermal cross sections, yields, decay constants, and branching ratios. The procedure was to identify 64 major absorbers that contributed more than 0.1% of thermal, epithermal, or total absorption. The sensitivity to 291 parameters that affect the absorption by these nuclides was then calculated, and rankings were made of the most important parameters.

Effective absorption cross sections as a function of irradiation time calculated with ENDF/B-IV were compared with those derived for irradiation samples produced in the MTR. These showed good agreement for thermal cross sections. The agreement was poor for resonance integrals, with the calculations lying below the measurements. The combined data for thermal absorption calculations were in good agreement with the measurements.

Several recommendations can be made on the basis of this work. The sensitivities need to be combined with uncertainties in the basic data in order to understand the overall uncertainty in fission product absorption calculations. The discrepancy between calculation and measurement-inferred resonance integral needs to be resolved. New benchmark measurements are needed in order to resolve this matter, especially since it is considered impractical to reanalyze the original BAPL experiments. Another unexplored approach would be to use the measured number densities available from, for example, W. Maeck's cumulative yield measurements (17). The densities depend on cross sections and it would be possible to use the measured densities with ENDF/B-IV cross sections and compare with summation calculations.

Data Processing for Power Reactor Fuel Cycle Codes

The importance of physics models in processing codes was demonstrated by R. E. MacFarlane of LASL. Cross-section processing for the reactor fuel-cycle codes EPRI-CELL and EPRI-CPM was discussed with emphasis on the self-shielding methods. Tables of resonance cross sections versus background cross sections are generated using a detailed pointwise solution of the slowing-down equations in an infinite homogeneous medium. Equivalence relations were given to account for non-1/E flux, intermediate resonance effects, and heterogeneity. An example using CPM for a pin cell showed a 2.2% decrease in ^{238}U resonance absorption due to the CPM values of

the λ parameters. Another example showed that a 30% effect on the diffusion coefficient arises from self-shielding of elastic scattering. Comparisons of ENDF/B-IV and the original E-CELL library for a pressurized water reactor (PWR) isotopics problem are good if ^{238}U absorption is reduced by about 15%. The NJOY processing code used for producing CELL and CPM libraries was described briefly.

The Relationship Between Basic Nuclear Data and LWR Fuel Cycle Parameters

D. Harris described work being done at RPI to analyze the sensitivity of water reactor fuel cycle parameters and costs to uncertainties in nuclear data. A sequence of batch depletion, core analysis, and fuel cost codes (referred to as Path B) determines the changes in fuel cycle parameters and costs for changes in few-group microscopic cross sections, in fission yields, and in decay data. For cases that are found to be significant from Path B analysis, the sensitivities of few-group data to basic nuclear data are determined by detailed calculations (referred to as Path A).

Analyses of pressurized and boiling water reactors with recycle and throwaway options show substantial sensitivities of fuel cycle parameters and costs to $\overline{\nu}$, κ, and thermal and resonance cross sections of fissile nuclides. There is less sensitivity to cross sections for fission products and fertile nuclides. Discussion of this paper focused on combining the computed sensitivities with nuclear data uncertainties.

It is recommended that the computed RPI sensitivities be combined with nuclear data uncertainties to yield uncertainties in end-of-cycle reactivities and end-of-exposure inventories. For this purpose, nuclear data uncertainty information would be useful for resonance parameters and for thermal cross sections and shapes. The sensitivity and uncertainty information should be used to indicate the advisability of additional measurements in ranges (such as thermal energies) that are found to be important.

INTERACTION OF METHODS AND DATA IN INDUSTRIAL EXPERIENCE--Session Chairman: B. Zolotar

There is a need for a conceptual separation between pure cross-section benchmarks and design testing. Both aspects are necessary in the overall cross-section effort. The range of available benchmarks and the benchmark process should be extended to include more emphasis on power reactor applicability. Such an extension can at the same time allow for a greater diversity in the experimental groups responsible for

the benchmarks. Obtaining calculations from a wider variety of contributors is also important. Particular attention should be paid to selecting benchmarks that include:

- Temperature effects
- Oxide lattices representative of BWR and PWR enrichment, spectra, and composition
- Isotopics

In the analysis of criticals, particular care should be taken in calculating leakage effects. Potential problems in leakage calculations can be caused by both cross-section and methods deficiencies.

Although there is some conflicting evidence, there does appear to be a problem in calculating the temperature dependence of reactivity. It is not clear if the problem lies with methods or data. Detailed Monte Carlo calculations would be extremely useful in looking at the temperature discrepancies.

Sophisticated methods are coming into more routine use for reactor design and operations support. Along with these methods ENDF/B-based libraries are now being used for thermal reactor design calculations. The use of ENDF/B-IV with a minimum of well-defined changes has shown good success in calculating LWR cases. However, the remaining discrepancies still need to be resolved. In particular, this and other sessions have pointed to discrepancies in:

- ^{238}U resonance capture
- Pu cross sections
- ^{235}U fission spectrum
- Thermal $\bar{\nu}$ values

The use of ENDF/B data in such design analysis will require that special care be taken in the ENDF/B effort to ensure that thermal reactor needs are considered. ENDF/B revisions should be released within a time frame that allows for such considerations. Once these data are being used for routine production analysis, data modifications should not be made without very strong justification.

Although discrepancies observed in the course of power reactor analysis can be indicative of data problems, it is premature to use such analyses directly in the ENDF/B data testing process. All users of ENDF/B are encouraged to provide results to the CSEWG data testing subcommittee.

NOTES AND REFERENCES

1. J. J. Ullo, Report WAPD-TM-1287, August 1977.
2. R. R. Spencer, 1977: Personal communication to B. R. Leonard, Jr.
3. J. W. Boldeman. In Neutron Standards and Applications. NBS Special Publication 493, 1977, p. 182.
4. R. G. Gwin et al. Measurements of the Average Number of Prompt Neutrons per Fission of ^{239}Pu and ^{235}U. Report ORNL/TM-6246, 1978.
5. L. W. Weston and J. H. Todd. Nucl. Sci. Eng., Vol. 63, 1977, p. 143.
6. L. W. Weston and J. H. Todd. Nucl. Sci. Eng., Vol. 65, 1978, p. 460.
7. H. Derrien. "Evaluation of ^{232}Th Resonance Parameters." In Resonance Parameters of Fertile Nuclei and ^{239}Pu, ed. P. Ribon Saclay. NEANDC(E) 163 U, May 1974.
8. O. D. Simpson et al. Nucl. Sci. Eng., Vol. 55, 1974, p. 273.
9. D. McPherson and J. H. Johnson. LSF: An Interpreter for a Class of Least Square Fitting Problems. AECL-3415, May 1972.
10. A. Okazaki and E. K. Sokolowski. In Proc. Conf. on Nuclear Data for Reactors, Helsinki, Vol. 1, 1970, p. 703.
11. MAGI--A Monte Carlo Analysis of a Chalk River Experiment on Cross Sections of Fissile Nuclides. Palo Alto, Calif.: Electric Power Research Institute, December 1975. NP-163.
12. M. Lounsbury, R. W. Durham, and G. C. Hanna. In Proc. Conf. on Nuclear Data for Reactors, Helsinki, 1970.
13. D. W. Colvin and M. G. Sowerby. In Proc. Symp. on Physics and Chemistry of Fission, Salzburg, Vol. 2, 1965, p. 25.
14. Two sets of results from Savannah River Laboratory are differentiated by referring to one set as SRL and to the other as SRL*.
15. H. Derrien. "Evaluation of ^{232}Th Resonance Parameters." In Resonance Parameters of Fertile Nuclei and ^{239}Pu, edited by P. Ribon Saclay. NEANDC(E) 163 U, May 1974.
16. B. R. Leonard: Personal communication to J. Hardy, Jr.
17. W. J. Maeck. "Fission Yields: Measurement Techniques and Data Status." In Neutron Standards and Applications, NBS Special Publication 493, October 1977, p. 146.

Section 2

REVIEW OF CROSS SECTION DATA IMPORTANT TO THE URANIUM-PLUTONIUM FUEL CYCLE IN THERMAL REACTORS

Review of Cross Section Data Important to the Uranium-Plutonium Fuel Cycle in Thermal Reactors*

L. W. Weston
Oak Ridge National Laboratory, Oak Ridge, TN 37830

INTRODUCTION

Since there are hundreds of cross sections involved in the design of a thermal reactor, this paper will be limited to the imporportant fissile and fertile nuclide cross sections with emphasis on the problems and discrepancies in these cross sections. Before considering such problems it should be noted that the overall data base and the evaluations of this data base have improved markedly in recent years - even with a dramatic reduction in experimental measurements. The fact that discrepancies still exist should not overshadow the fact that experimenters and evaluators have made progress in providing an increasingly reliable differential cross section data base for reactors.

IMPORTANT CROSS SECTIONS

When a uranium fueled reactor is first loaded, the important cross sections are obviously those of ^{235}U, ^{238}U, water, and the structural materials. For economic reasons a reactor core must achieve high burn-up and as a result a number of other nuclides are formed by transmutation following neutron absorption. The cross sections of these nuclides become important according to their abundance and nuclear parameters. Table 1 shows the actinide nuclide concentrations[1] in spent fuel 150 days after reactor discharge (34 GWD/T) from a light water reactor (LWR). The table corresponds to an equilibrium fuel cycle with loading of 3.3% enriched uranium. This table indicates clearly that not only the uranium isotopes are important but also the plutonium isotopes, and to some extent ^{237}Np, and $^{241,243}Am$.

Advances in sensitivity and uncertainty analysis are beginning to yield detailed, quantitative information on the sensitivity of reactor parameters to cross sections and their uncertainties.[2-5] Such analysis not only indicates which nuclides present important problems but also at what neutron energy regions. With this information available, experimenters may concentrate more on the areas of critical importance.

*Research sponsored by the Reactor Research and Technology Division, U. S. Department of Energy under contract W-7405-eng-26 with the Union Carbide Corporation.

Table 1

Actinide Nuclide Concentrations in Spent Fuel*

Nuclide	Concentration (grams/T HM)
U-234	119
U-235	7560
U-236	4580
U-238	942000
Np-237	500
Pu-238	180
Pu-239	5270
Pu-240	2200
Pu-241	1050
Pu-242	380
Am-241	47
Am-242m	1
Am-243	105

*Taken from ref 1.

URANIUM - 235

A major discrepancy[6,7] exists for ^{235}U between irradiation experiments and other combinations of measurements from which the ratio of capture to fission (alpha) can be derived. This discrepancy exists for both ^{233}U and ^{235}U and is illustrated for the case of ^{235}U in Table 2 which was taken from ref 7. There is about a 9% discrepancy in alpha as derived from the differential cross section measurements, η and $\bar{\nu}$ measurements, and critical experiments as compared to that derived from irradiation experiments. Considerable effort has so far failed to uncover the source of the discrepancy. This discrepancy cannot be removed except by new experiments or by reevaluation and correction of the existing experiments.

There are remaining disturbing differences[8,9] in the experimental measurements of the absolute value of $\bar{\nu}$ as well as the value of $\bar{\nu}$ derived from η and alpha measurement [$\bar{\nu} = \eta(1+\alpha)$]. These data continue to receive intensive attention and new measurements of $\bar{\nu}$ are being carried out.[10,11] There continue to be discrepancies in the measurements, however, evaluations yield acceptable uncertainties because of the quantity of input data.

A major step forward in the evaluation of the cross sections over the neutron energy region important to thermal reactors has been carried out by Leonard, Kottwitz, and Thompson.[12] Their evaluation of ^{235}U involved the use of a nonlinear least squares fitting technique for determining the energy dependence of the

cross sections. These studies have indicated several important problems which include: (1) the data of Gwin et al.[13] is somewhat inconsistent when interpreted as the capture and fission cross sections as compared to being interpreted as the absorption cross section and ratio of capture to fission, (2) the fission cross section data of Deruytter and Wagemans[14] appear to have a discontinuity at 0.21 eV, and (3) the capture cross section data of de Saussure et al.[15] above 0.4 eV should be normalized upward by as much as 14%. These data have dominated ENDF/B resonance evaluation and are now clearly in doubt.

There is a need[7] for more accurate knowledge of the cross sections below 2200 m/sec. There is an appreciable fraction of neutrons in a LWR with velocities less than 2200 m/sec and the shapes of the cross sections are poorly known.

Table 2

2200 m/sec Alpha Values for ^{235}U Input Data.*

Method	σ_C/σ_F
$\frac{\sigma_T - \sigma_S}{\sigma_F}$	0.158 ± 0.005
$\bar{\nu}/\eta$	0.155 ± 0.006
Critical Exps.	0.153 ± 0.005
Mean	0.155 ± 0.003
Irradiation Exps.	0.169 ± 0.003

*Taken from Ref 7.

URANIUM - 238

Neutron absorption in the resonances of ^{238}U is of great importance in a LWR. Resonance absorption accounts for about half of the capture in ^{238}U.[2] Because of the large amount of ^{238}U in a fuel pin of a reactor, these resonances are highly self-shielded from neutron absorption. The calculation of resonance absorption in ^{238}U in a uranium fueled reactor is very complex.

There has been a long standing discrepancy between resonance capture calculated from the experimental differential cross sections as compared to integral experiments. Integral experiments yield lower resonance capture, especially in high self-shielded systems. This discrepancy is apparently in the process of being

partially resolved because of several factors. Recent experimental measurements[16-19] of the resonance parameters have brought about the reduction of the capture widths of the first three s-wave levels by about 15% and increased the neutron widths of the levels at 20.0 and 36.8 eV, by about 10% for the ENDF/B-V evaluation.[20] This apparently has removed about one third of the discrepancy.[21] It has been pointed out clearly by Olsen et al.[16] and by Harris et al.[21] that a multilevel representation of the cross section must be used in the interpretation of experimental measurements and may be important in highly self-shielded reactor systems. This is illustrated in Fig. 1 which compares experimental data of the transmission of neutrons through a thick sample of ^{238}U with a single level and multilevel representation of the cross section. The difference is due to resonance-resonance interference in the scattering channels and due to resonances outside the resolved resonance region.

The other fact that has been brought up concerning the resonance absorption discrepancy in ^{238}U is simply that computer codes for calculating reactor performance must use an adequate description of the cross section or significant errors may be introduced.

Since possible solutions to the problem of the discrepancy in ^{238}U resonance absorption have been brought forth, the discrepancy cannot be considered as serious as previously. Further evaluation and testing of recent results and calculation methods are needed.

A more accurate determination of the cross sections for ^{238}U up to 1-eV neutron energy would be very desirable.[20] Even though the 2200 m/sec cross section is well known, the shapes of the cross section vs neutron energy are difficult to describe in terms of the known positive energy resonances and reasonable assumptions concerning bound levels. The assumption of the capture cross section being inversely proportional to neutron velocity in the thermal region of neutron energies could be incorrect.

Recent fuel cycle cost sensitivity studies for a PWR and BWR by Becker et al.[5] indicate that the cost sensitivity to nuclear data uncertainties for ^{238}U and other fertile nuclides are not as large as one might think. This is because the creation of more or less fissile nuclide tends to compensate for uncertainties in fertile nuclide absorption. One must be careful with this conclusion since results can be different[22] according to whether criticality is reset with control rods or with ^{235}U enrichment as was used in the above study.

PLUTONIUM

The concentration of the plutonium isotopes in a thermal reactor after extended operation is not negligible as can be seen in Table 1. If plutonium is recycled in thermal reactors, the figures in Table 1 for spent fuel would not change appreciably[1] except for increased build-up of ^{242}Pu, ^{243}Am, and ^{244}Cm. The

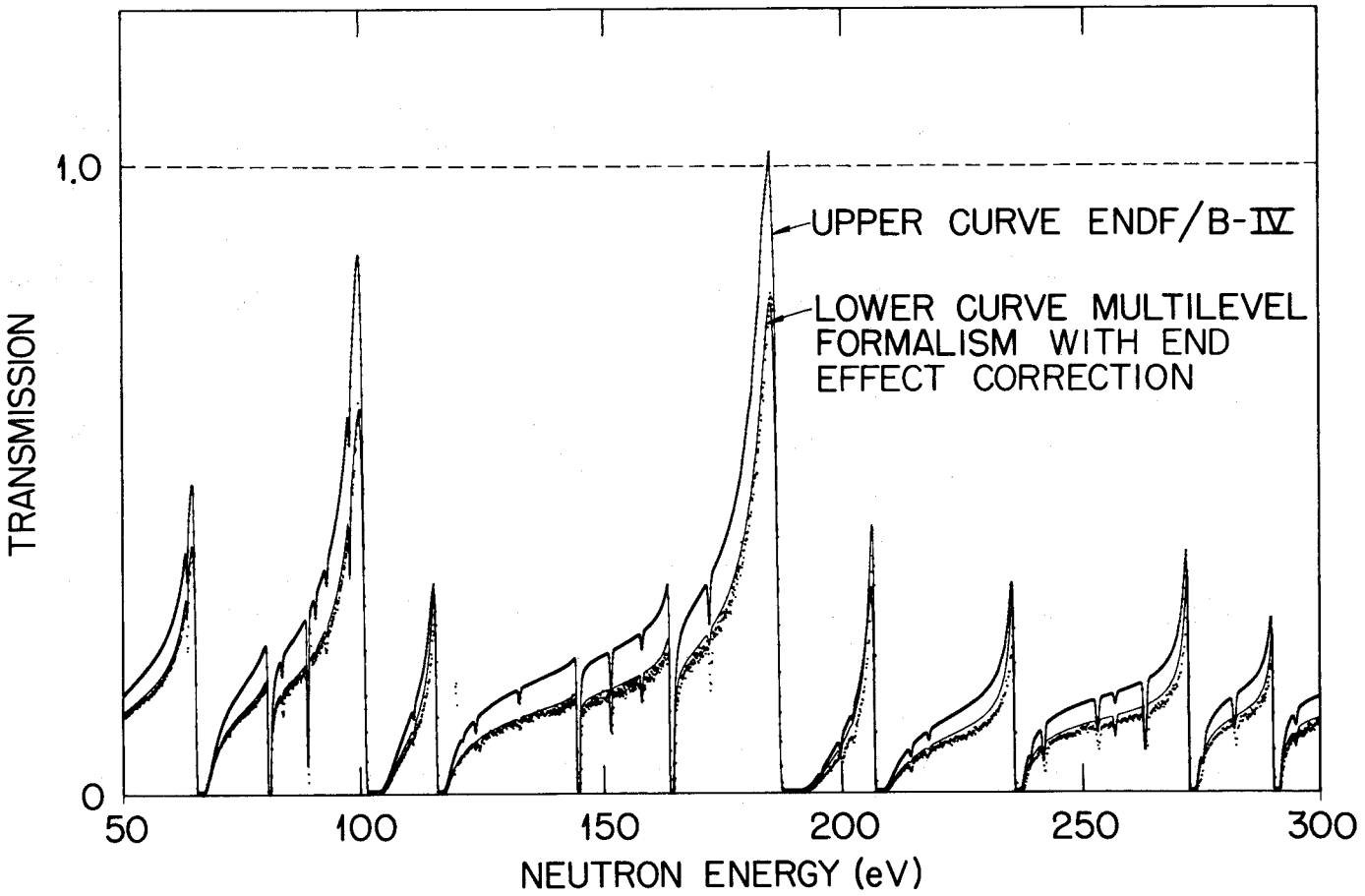

Fig. 1. Measured transmission through 1425 mils of ^{238}U. The upper curve is the corresponding resolution-broadened transmission from the ENDF/B-IV total cross sections Doppler broadened to 300°K. The lower curve is the transmission similarly calculated from the Reich-Moore multilevel formalism with the ladder approximation to account for levels outside the resolved resonance region (from ref 16).

initial ^{235}U enrichment would have to be appropriately adjusted. It should also be noted that only 58% of the plutonium produced is ^{239}Pu. This is primarily because of the relatively high value of alpha (0.36) for ^{239}Pu.

PLUTONIUM - 239

The thermal cross sections of plutonium-239 are self consistent[6,7] and are known with reasonable accuracy. An interesting feature of the ^{239}Pu thermal parameters is the variation of $\overline{\nu}$ (number of neutrons per fission) with neutron energy as reported by Hockenbury et al.[23] and Gwin et al.[10] The experimental data show a drop of about 0.8% between 0.01 and 0.10 eV. This effect does not appear in reported data on the other fissile isotopes. Theoretically ^{239}Pu is more likely to show such a variation in $\overline{\nu}$ because of its low spin of 1/2, so that the total spin for s-wave resonances can be 0 or 1. Variation of $\overline{\nu}$ from resonance-to-resonance in the resonance region is well documented.[24-26] The effect on thermal reactors if these data are accepted will not necessarily be large because of compensations in an evaluation, however, there will be an effect on criticality and on temperature coefficients.

PLUTONIUM - 240

Plutonium-240 is an interesting isotope from the point of view of a thermal reactor because it looks like one resonance. The resonance at 1.058 eV dominates its cross section for thermal reactors. This resonance yields 99% of the 2200 m/sec capture cross section, 98% of the very small fission cross section (0.03 barns) and causes the scattering cross section to be small (1.54 barns) because of interference effects.

Plutonium-240 is important because it composes about 25% of the plutonium produced in a LWR, the capture cross section at thermal is large (290 barns) and the 1.058-eV resonance is very large and will self-shield at relatively low concentrations.

The data available on the 1.058 eV resonance of ^{240}Pu is not sufficient.[27] The radiation width, Γ_γ, is known to about 6% and the neutron width, Γ_n, is known to about 15%. The major constraint on these parameters is the 2200 m/sec capture cross section, 99% of which is determined by the product, $\Gamma_n\Gamma_\gamma$. The measurement of 289.5 ± 1.4 barns for the 2200 m/sec capture cross section by Lounsbury et al.[28] is the most accurate reported thermal cross section measurement. This measurement was an irradiation experiment in a Maxwellian neutron source. Additional measurements of the resonance parameters are needed because of

the importance to thermal reactors. Accurate thermal cross sections are not sufficient because of the unknown effect of negative energy resonances and because the shape of the resonance is needed.

There are problems in the benchmark calculations[29] concerning ^{240}Pu capture in a Pu fueled aqueous sphere. The more ^{240}Pu resonance capture a given critical assembly has, the more k_{eff} is over-predicted. Also, the lower the ratio of resonance capture in ^{240}Pu to that in ^{239}Pu, the higher the calculated k_{eff}. The fuel cycle cost sensitivity[5] to uncertainty in ^{240}Pu capture is small, however, an understanding of critical experiments containing ^{240}Pu is important.

The shape of the ^{240}Pu capture cross section is shown in Fig. 2. The ENDF/B-IV evaluation as well as the data of Weston and Todd[30] are shown.

PLUTONIUM - 241

Plutonium-241 accounts for about 12% of the plutonium produced in a LWR. It has a higher fission cross section and a lower capture-to-fission ratio than does ^{239}Pu. In a light water reactor it accounts for about 25% of the fissions in the plutonium isotopes. Except for the disadvantage of a relatively short half-life (15 years) ^{241}Pu is a better reactor fuel than ^{239}Pu. The beta decay of ^{241}Pu leads to ^{241}Am which has a small effective fission cross section for thermal reactors.

The cross sections of plutonium-241 are reasonably well known for thermal reactors.[6] There are no outstanding discrepancies in the thermal region except that the cross sections below 0.02 eV are poorly defined as they are for the other fissile isotopes.[7] Recently reported measurements[31] of the shape of the capture cross section may bring the experimental 2200 m/sec cross section and that for a 20° Maxwellian neutron source into better agreement. There are discrepancies of 5 to 10% amoung measurements of the average fission cross section in the resonance region,[31] however, this is not very serious in a thermal reactor because of the concentration of ^{241}Pu.

HIGHER ISOTOPES

There are no major problems with the other low concentration nuclides from the point of view of thermal reactors. It would be worthwhile to know some of these cross sections more accurately, i.e., the capture cross section of ^{238}Pu, the (n,2n) reactions, and the fission cross section of ^{241}Am, however, they are not priority I problems. If it becomes necessary to make precise predictions of the composition of the waste stream for a variety of conditions, the cross sections of the higher isotopes would assume greater importance.

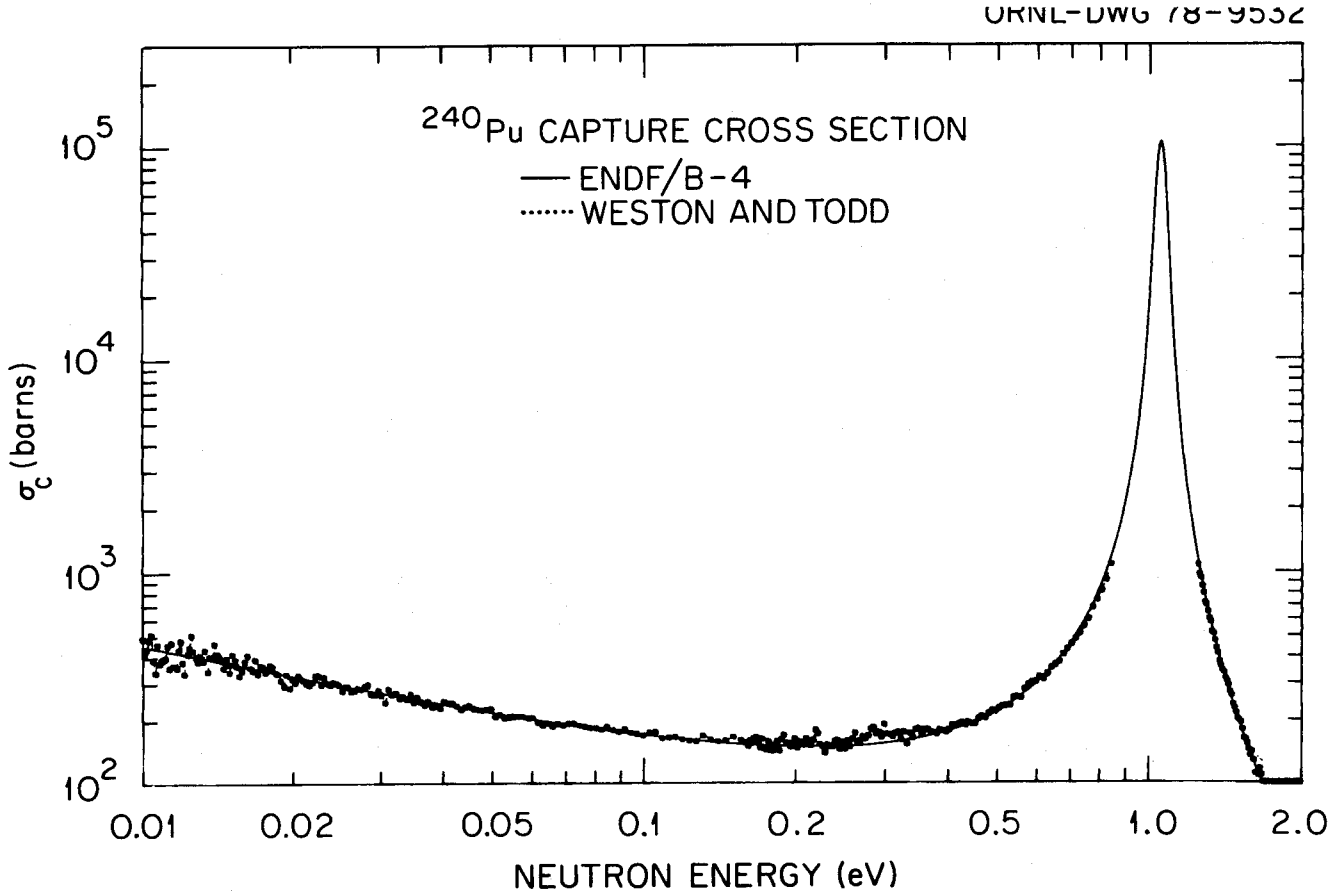

Fig. 2. The capture cross section of ^{240}Pu from 0.01 to 2.0 eV. The solid line is the ENDF/B-IV evaluation. The points are the data of Weston and Todd (ref 30).

DISCUSSION

This review has indicated that most cross-sections important to design of U-Pu fueled light water reactors with current fuel-water ratios are known with reasonable accuracy. There are discrepancies but with three exceptions they are not of overwhelming importance. There will always be discrepancies because an experimenter can usually reduce known uncertainties to less than unknown systematic uncertainties. The goal should be to reduce the uncertainties to an unimportant level. Integral experiments will continue to be necessary to suggest unknown systematic uncertainties in differential data and calculation methods and vice versa.

In the opinion of the author the three most serious remaining discrepancies are: (1) the resolution of the difference between integral measurements and differential calculations of ^{238}U resonance capture for highly self-shielded cases. This problem shows favorable progress towards solution, (2) the discrepancy between irradiation experiments and other measurements of the ratio of capture-to-fission in ^{235}U, and (3) the uncertainty in the parameters of the 1-eV resonance of ^{240}Pu.

REFERENCES

1. H. O. Haug, Calculations and Compilations of Composition, Radioactivity, Thermal Power, Gamma and Neutron Release Rates of Fission Products and Actinides of Spent Power Reactor Fuels and Their Reprocessing Wastes, Kernforschungszentrum, Karlsruhe, KFK-1945 (1974).
2. E. T. Tomlinson, G. de Saussure, and C. R. Weisbin, Sensitivity Analysis of TRX-2 Lattice Parameters with Emphasis on Epithermal ^{238}U Capture, Electric Power Research Institute, Palo Alto, CA, EPRI NP-346 (ENDF-252) (1977).
3. M. L. Williams and C. R. Weisbin, Sensitivity and Uncertainty Analysis for Functionals of the Time-Dependent Nuclide Density Field, Oak Ridge National Laboratory, Oak Ridge, TN, ORNL-5393 (ENDF-263) (1978).
4. R. D. Mcknight, Sensitivity Analysis for the Advanced Fuels Program Carbide Benchmark Critical Assembly, Proc. Advances in Reactor Physics, Gatlinburg, (1978) in press.
5. M. Becker et al., Sensitivity of LWR Fuel Cycle Costs to Uncertainties in Nuclear Data, Proc. Advances in Reactor Physics, Gatlinburg, TN (1978) in press.
6. H. D. Lemmel, Proc. Symp. Neutron Standards and Applications, p. 170, National Bureau of Standards, Washington, D. C., NBS-493 (1977).
7. B. R. Leonard, Jr., Proc. Conf. Nuclear Cross Sections and Technology, p. 281, National Bureau of Standards, Washington, D. C., NBS-425 (1975).

8. J. W. Boldeman, Proc. Symp. Neutron Standards and Applications, p. 182, National Bureau of Standards, Washington, D. C., NBS-493 (1977).
9. J. R. Smith, Proc. Conf. Nuclear Cross Sections and Technology, p. 262, National Bureau of Standards, Washington, D. C., NBS-425 (1975).
10. R. Gwin et al., Measurement of the Average Number of Prompt Neutrons Emitted per Fission of ^{239}Pu and ^{235}U, Oak Ridge National Laboratory, Oak Ridge, TN, ORNL/TM-6246 (1978).
11. R. R. Spencer, private communication (1978).
12. B. R. Leonard Jr., D. A. Kottwitz, and J. K. Thompson, Evaluation of the Neutron Cross Sections of ^{235}U in the Thermal Energy Region, Electric Power Research Institute, Palo Alto, CA, EPRI NP-167 (1976).
13. R. Gwin, E. G. Silver, R. W. Ingle, and H. Weaver, Nucl. Sci. Eng. 59, 79 (1976).
14. A. J. Deruytter and C. Wagemans, J. Nucl. Eng. 25, 263 (1971).
15. G. de Saussure et al., Nucl. Data for Reactors, Paris II, p. 233 (1966).
16. D. K. Olsen et al., Nucl. Sci. Eng. 62, 479 (1977).
17. H. I. Liou and R. E. Chrien, Nucl. Sci. Eng. 62, 463 (1977).
18. F. Poortmans et al., Neutron Resonance Parameters for ^{238}U, Int. Conf. on Neutron Physics, IV, Kiev (1977).
19. R. C. Block, D. R. Harris, and K. Kobayshi, Recent ^{238}U Self-Indication Measurements at RPI, private communication (1977).
20. G. de Saussure et al., Evaluation of the ^{238}U Neutron Cross Sections for Incident Neutron Energies up to 4 keV, Oak Ridge National Laboratory, Oak Ridge, TN, ORNL/TM-6152 (ENDF-257) (1978).
21. D. R. Harris, private communication (1978).
22. C. R. Weisbin, private communication (1978).
23. R. W. Hockenbury, R. L. Reed, and R. C. Block, Resonance and Thermal $\bar{\nu}$ Measurements on ^{239}Pu, Proc. Symp. Physics and Chemistry of Fission, Rochester, N. Y., Vol. II, p. 502, Int. Atomic Energy Agency, Vienna (1974).
24. D. Shackleton et al., Phys. Letters 42B, 344 (1972).
25. Yu Ryabov et al., Nucl. Phys. A216, 395 (1973).
26. L. W. Weston and J. H. Todd, Phys. Rev. C 10, 1402 (1974).
27. H. Weigmann, G. Rohr, and F. Poortmans, Proc. Conf. Resonance Parameters of Fertile Nuclei and ^{239}Pu, p. 219, Saclay, Commissariat a L'Energia Atomique, NEANDC(E) 163U (1974).
28. M. Lounsbury, R. W. Durham, and G. C. Hanna, Proc. Conf. on Nuclear Data for Reactors, Helsinki, Int. Atomic Energy Agency, Vienna (1970).
29. L. Levitt, B. Magurno, and P. Rose, Improvement of Reference Nuclear Data for Commercial Power Reactor Analysis and Design, p. 51-54, Electric Power Research Institute, Palo Alto, CA EPRI NP-556 (1977).
30. L. W. Weston and J. H. Todd, Nucl. Sci. Eng. 63, 143 (1977).
31. L. W. Weston and J. H. Todd, Nucl. Sci. Eng. 65, 460 (1978).

Section 3

THE ADEQUACY OF Th-232 AND U-233 ENDF/B DATA FOR HTGR DESIGN APPLICATIONS

The Adequacy of Th-232 and U-233 ENDF/B Data for HTGR Design Applications

D. R. Mathews and W. R. Davison

General Atomic Company
P.O. Box 81608
San Diego CA 92138

A paper prepared for publication in the proceedings of the symposium "Nuclear Data Problems for Thermal Reactor Applications" held at Brookhaven National Laboratory, Upton, New York, May 22-24, 1978

The work described in this paper was supported in part by the U.S. Department of Energy and its predecessor agencies.

1. INTRODUCTION

Th-232 and U-233 are two nuclides of great importance to the HTGR program because of their use in the reference HTGR fuel cycle. Consequently, we have spent a considerable amount of time over the years to identify data sets that are suitable for use in HTGR design applications.

In general, we are satisfied with the present status of the ENDF/B data for these nuclides. This is not to say that the data are perfect, nor even adequate for other applications - only that the bulk of the integral experiments we have analyzed are predicted with sufficient accuracy for our needs.

In this paper, we shall summarize the comparisons that have led us to this conclusion. In historical order, they include

- the HTGR critical experiments
- operating experience with the Peach Bottom reactor
- the HTLTR experiments and
- operating experience with the FSV reactor

Reference 1 contains a good summary of this experimental data base and we will quote from it extensively. It also contains a bibliography that can be used by anyone who desires more detail than will be presented here today.

2. HTGR CRITICAL EXPERIMENTS

The HTGR critical experiment program ran from 1966 to mid-1969 and was divided into two phases.

2.1 Reactivity Coefficients

In the first phase, five "clean" assemblies were constructed with varying ratios of carbon to uranium and reactivity coefficient measurements were made in each assembly for the principal nuclides of interest in HTGR design. Table 1 contains information characterizing the assmblies. The range of thermal energy spectra produced in these assemblies is wider than that resulting from the varying initial fuel loadings in HTGRs, depletion effects, or temperature variations. Thus any conclusions reached would be expected to apply to a wide variety of cases.

The experimental values for reactivity worths were obtained by inserting special elements into the central cell location and comparing their worth relative to that of a reference carbon block. The calculated values were obtained by straightforward eigenvalue difference techniques.

2.1.1 U-233

Three pairs of U-233 elements were used, They were loaded so that their thermal absorption would be similar to that of the surrounding regions and spectral perturbations would be minimized.

At the time these experiments were being analyzed, the nuclear data available were either ENDF/B Version I or earlier GA evaluations that yielded similar results. The ENDF/B-I U-233 data set is characterized in Table 2. The comparisons of calculations and experiments are shown in Figure 1. The calculated reactivity worth is typically 4% too high for all cores and uranium concentrations except for the C/U=5000 core where a 10% discrepancy was observed. This particular assembly gave similar anomalous discrepancies for boron and U-235 samples so this should not be taken to be an indictment of the U-233 cross section data.

Taken as a whole the experimental data indicate that the most likely source of the discrepancy is a general underestimation of the capture cross-section or an overestimation of either ν or $\nu\Sigma_f$ over a wide energy range.

TABLE 1
CHARACTERIZATION OF CRITICAL ASSEMBLIES USED IN
REACTIVITY COEFFICIENT PROGRAM

	Assembly Number				
	1*	2*	3	4	5
C/U ratio in core	5000	2500	1718	859	432
Mean fission energy (ev)	0.074	0.12	0.20	0.40	12.7
Most probable thermal energy (ev)	0.050	0.059	0.061	0.085	0.140
Average of a unit 1/v cross section ($0 \leq E \leq 2.38$ ev)	0.55	0.44	0.39	0.31	0.24
Core radius (cm)	71.5	64.0	59.0	56.5	54.7
Core length (cm)	183	183	183	183	183
Graphite reflector thickness (cm)					
Radial	15.1	7.5	8.4	7.5	6.8
Axial	0	0	0	0	0
Fast/thermal flux ratio (E_c = 2.38 ev)	2.15	3.40	4.62	12.07	15.33

* Assemblies 1 and 2 most closely resemble the large HTGR core.

TABLE 2

U-233 and Th-232 Cross Sections

	U-233 (ENDF/B-I)	Th-232 (GA Evaluation)
2200 meter/sec data		
$\sigma(n,\gamma)$, b	47.4	7.45
$\sigma(n,f)$, b	525	
α	0.0903	
η	2.293	
ν	2.500	
Cross section integrals		
(E > 0.5 ev)		
Capture integral, b	141	85.7
Fission integral, b	766	0.46
$\frac{\text{Capture integral}}{\text{Fission integral}}$	0.184	0.0054

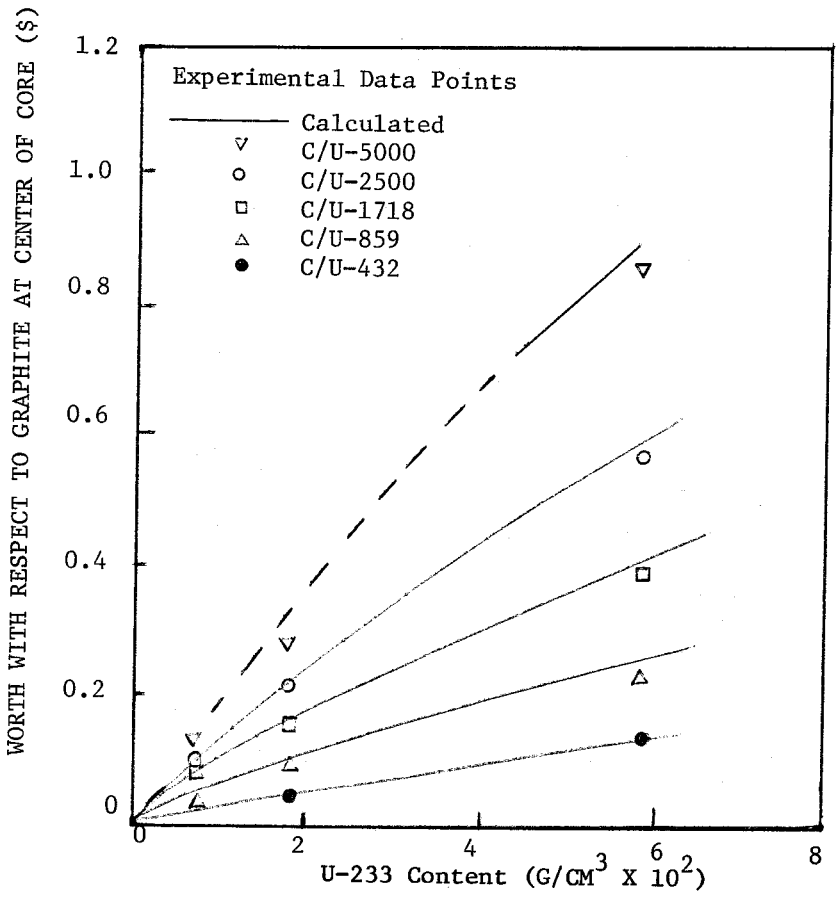

Figure 1- Calculated vs. experimental reactivity worth of special U-233 elements in five core assemblies

2.1.2 Thorium-232

Five pairs of thorium elements ranging in loading from 50 to 500 g/element were analyzed and the comparison is shown in Figure 2. From the comparison, it appears that the calculated worth is too high by 2-5% in most cases and by 5-10% in the C/U=5000 assembly. The Th-232 data set used in these calculations is characterized in Table 2.

2.2 Doppler Coefficient

The second phase of the experimental program was aimed at providing experimental data for the Doppler coefficient of Th-232. This was accomplished by heating the test element in an oven outside the core and measuring its reactivity worth relative to that of an identical element at room temperature. Table 3 contains the results which show a very good agreement.

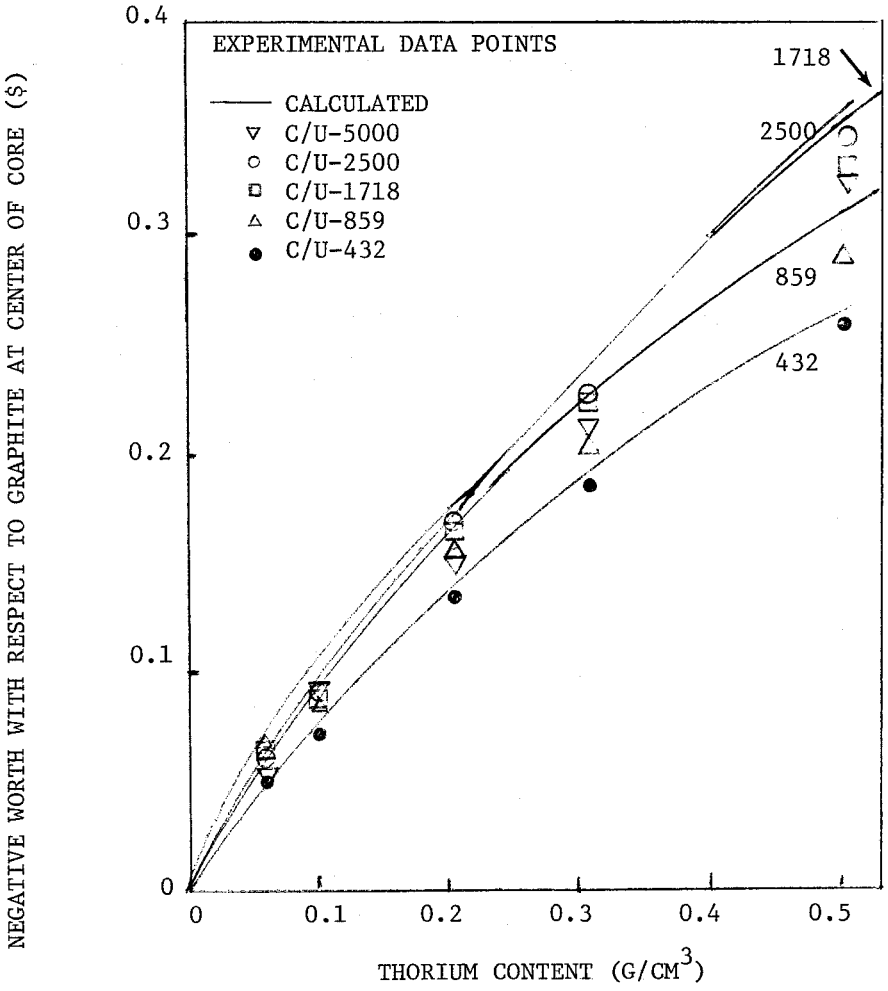

Figure 2- Calculated vs. experimental reactivity worth of special thorium elements in five core assemblies

TABLE 3
DOPPLER COEFFICIENT MEASUREMENTS IN THE HTGR CRITICAL ASSEMBLY LATTICE

Composition of Central Test Element	Reactivity Change (Dollars): 300°K to 600°K	
	Measured	Calculated
C/U = 2500, C/Th = ∞	-0.029	-0.028
C/U = 2500, C/Th = 300	-0.055	-0.053
C/U = 2500, C/Th = 200	-0.063	-0.062
C/U = 2500, C/Th = 100	-0.074	-0.074
C/U = 2500, Th-232 in C/Th = 100 lattice replaced by boron equivalent to the 1/v cross section of thorium	-0.0124	-0.0116

3.0 PEACH BOTTOM DATA

As the first HTGR operating in the United States, the Peach Bottom Reactor provided valuable information for the evaluation of HTGR physics design methods. Of particular relevance to this review are the initial reactivity measurements, which provide evidence of the worth of thorium, and the reactivity behavior with depletion, which provides evidence of our ability to treat U-233. Temperature defects also provide information of interest.

In each of these categories, the comparison was quite good. Specifically:

(1) The initial reactivities of cores 1 and 2 were calculated to within $0.007\Delta k$ and $0.003\Delta k$, respectively.

(2) The time behavior of the overall core 1 reactivity, as can be seen in Figure 3, was well predicted. Additionally, although no direct measurement of the reactivity worth of the transmutation from Pa-233 to U-233 was ever made, there is a large body of data that suggests that it can be predicted to within 5-10%. Since competing transmutations are present, it is difficult to be more precise than this. Peach Bottom core 2 was run for about 875 full power days. Toward the end of core 2 the reactivity decreased more rapidly than predicted due to higher than predicted fuel temperature increases and possibly some nuclear data problems.

(3) Table 4 presents a comparison of the calculated and measured temperature coefficients. It can be seen from the data in the table that the temperature coefficient is generally unpredicted, by amounts ranging up to 10%. Note, however, that the effect of core depletion upon the temperature coefficient appears to be well predicted.

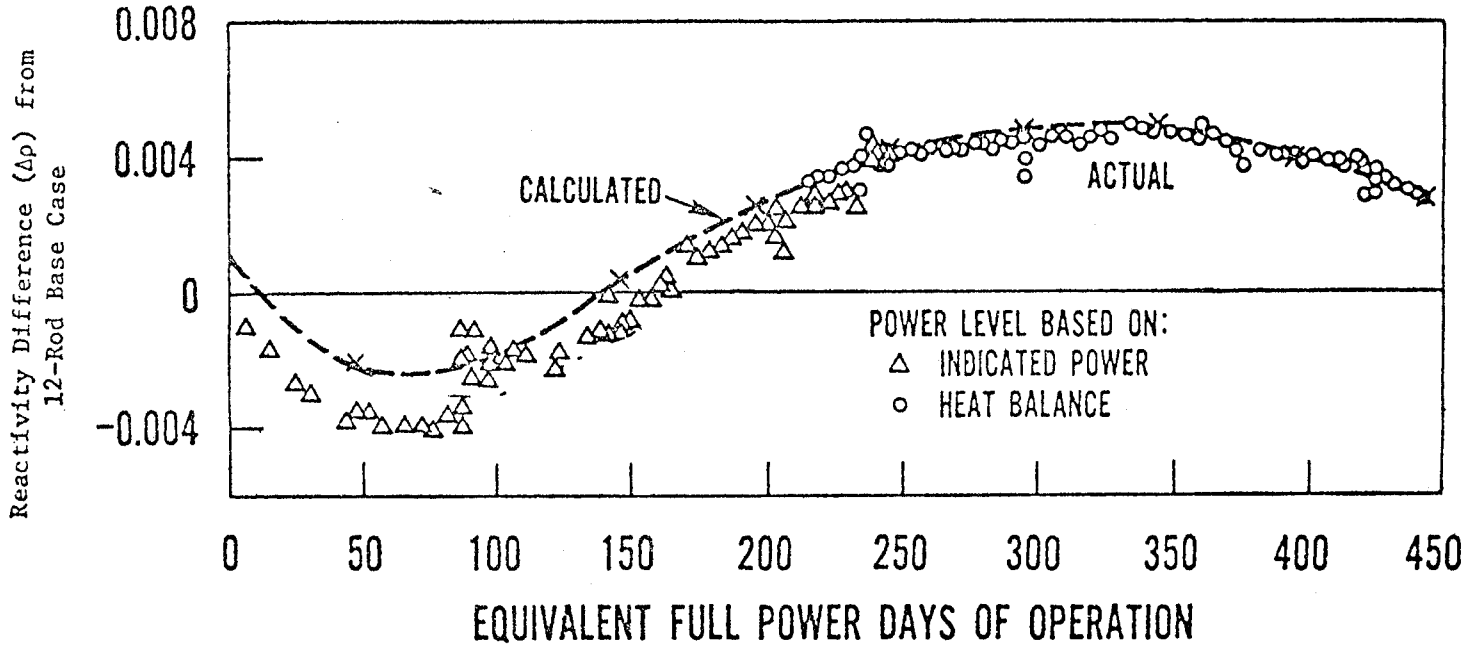

Figure 3 - Peach Bottom Core 1 reactivity difference vs. time
Note that the plotted reactivities are relative to full power, equilibrium Xe&Sm and a constant control rod configuration.

TABLE 4

TEMPERATURE COEFFICIENTS IN PEACH BOTTOM CORE 1

Type Measurement	Reactivity Effect	
	Measured	Calculated
Temperature defect [(a)] (isothermal)		
100°F to 600°F	-0.024 ± 0.002 Δρ	-0.022 Δρ
Temperature coefficient [(a)] (isothermal)		
Δρ/ΔT @ 100°F	-5.0×10^{-5}/°F	-4.8×10^{-5}/°F
Δρ/∇T @ 600°F	-4.5×10^{-5}/°F	-3.9×10^{-5}/°F
Temperature defect [(a)] 100°F to 1800°F	-0.070 Δρ	-0.063 Δρ
Temperature coefficient [(a)] @ operating temperature	-2.0×10^{-5}/°F	-2.7×10^{-5}/°F
Temperature defect 100°F to 1800°F		
168 EFPD	-0.066	-0.059
300 EFPD	-0.060	-0.054

(a) Measured at 0 EFPD.

4.0 HTLTR CRITICAL EXPERIMENTS

An experimental program to measure HTGR temperature coefficients was carried out from 1970-1971 in the High Temperature Lattice Test Reactor (HTLTR) at Battelle Northwest Laboratory (BNWL). The infinite multiplication constant k_∞ of a lattice of interest was determined by measuring the reactivity worth difference between a piece of that lattice material and a piece of copper absorber material placed in a voided region in the center of an appropriately designed critical assembly. The measurements were repeated at several temperatures and the temperature dependence of k_∞ thus determined. Several correction factors, both analytical and experimental, had to be applied to each measurement. These factors were of the same magnitude as the change in k_∞ between successive measurements, which made the analysis of the experiments quite complex.

The experimental program considered the five lattices described briefly in Table 5. Note that U-235/Th and Pu/Th lattices in addition to three U-233/Th lattices were built. The results of the final analysis are shown in Table 6. With the exception of Lattice 3, the results, especially for the overall temperature defect, are satisfactory and generally consistent with other experimental data. Newman, et al,[2,3] subsequently found unexpectedly high levels of neutron absorbing impurities in the graphite powder used in Lattices 3 and 5.

Discarding the Lattice 3 results, the final calculated results using ENDF/B-3 data[4] for the other two HTLTR lattices containing U-233 and Th-232 were ½ to 1% lower in room temperature k_∞ and 2 to 6% less negative in Δk_∞ over a 27 to 1000°C temperature range than the experimental results. Newman, et al, have obtained similar results.[2,3] It should be noted that the HTLTR experiments were designed to yield accurate values of the change in k_∞ with temperature and that accurate values of k_∞ itself cannot be expected because of the relatively small size of the HTGR test region.

TABLE 5

DEFINITION OF LATTICES USED IN THE HTLTR PROGRAM

Lattice Number	Fissle Material	Carbon to Fissle Atom Ratio	C/Th Ratio	Purpose of Experiments
1	U-235	6,400 (5,910)[a]	209 (193)[a]	Doppler coefficient
2	U-233	11,100 (10,300)	205 (189)	U-233 coefficient
3	U-233	14,900 (13,800)	301 (278)	Doppler and U-233 coefficients
4	Pu-239+ Pu-241	10,300 (9,850)	262 (250)	Pu coefficient, including particle effect
5	U-233	9,910 (9,470)	153 (146)	U-233 coefficient in MSBR lattice

[a] Without unfueled graphite end caps

TABLE 6

SUMMARY OF BNWL MEASURED AND GA CALCULATED

RESULTS FOR THE HTLTR EXPERIMENTS

Lattice	1	2	3	4	5
BNWL k_∞ (300)	1.111	1.0582	1.064	1.085	1.0287
Experiment Δk(1273)	0.078	0.0345	0.004	0.056	0.0250
GA k_∞(300)	1.1022	1.0471	1.1068	1.0809	1.0404
Calculation Δk(1273)	0.0622	0.0338	0.0181	0.0527	0.0267

5.0 OPERATING EXPERIENCE

The 330 Mw(e) Ft. St. Vrain Reactor, the first commercial size application of the HTGR concept, has provided data that substantiates the nuclear data used in its physics design. In general, the comparison between calculated and measured data is very good.[3] The discrepancy at the initial critical control rod position was only 0.001Δk and the temperature defect, as can be seen from Figure 4, has agreed very well with our predictions. It is, however, still too early to make any statements about U-233 worth.

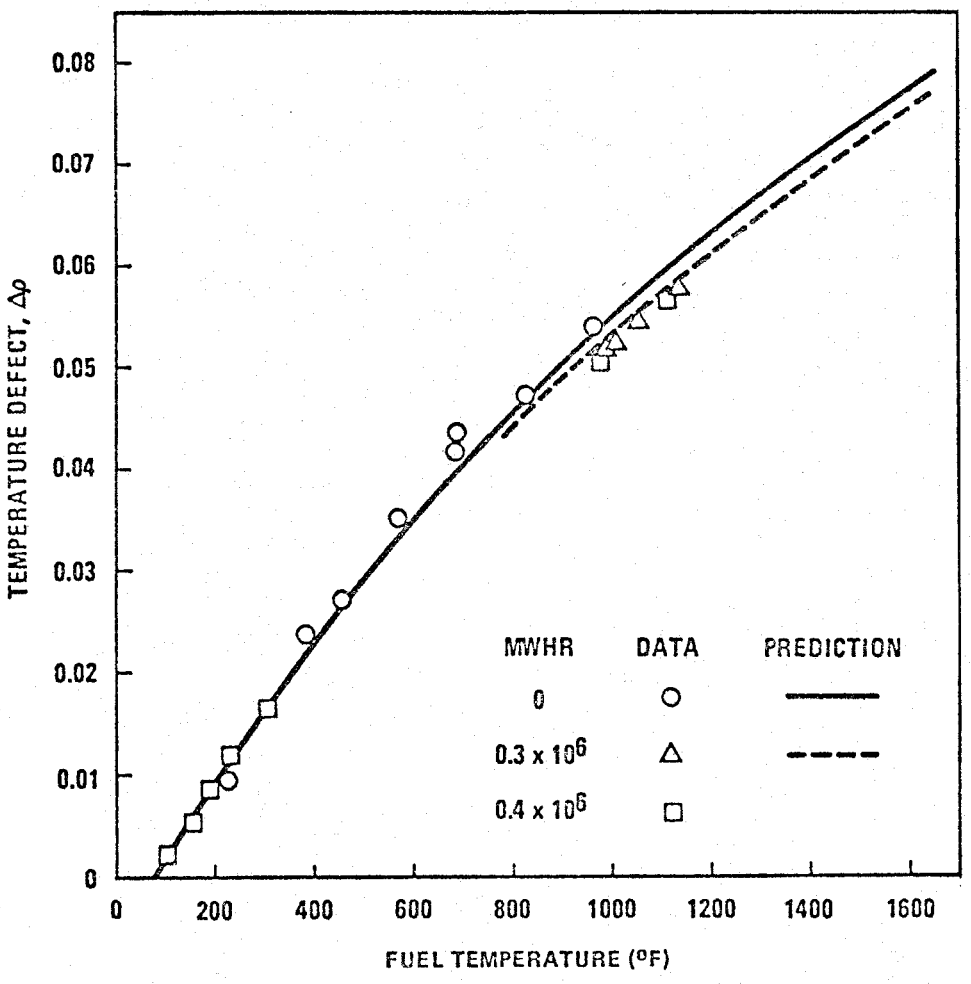

Fig. 4 FSV reactor temperature defect vs fuel temperature

6.0 SUMMARY

To summarize then, there is a considerable body of experimental evidence that suggests that when we use nuclear data consistent with the current ENDF/B library, we can predict the reactivity worths of Th-232 and U-233 and their temperature dependence with an acceptable degree of accuracy. To be sure, any one of the experiments is inadequate to permit a firm conclusion. This is an inherent weakness of integral comparisons. Nonetheless, the fact that we can predict all of the experimental data quite well gives us confidence in the validity of the data.

REFERENCES

1. Meldon H. Merrill, "Nuclear Design Methods and Experimental Data in Use at General Atomic", Gulf-GA-A12652, July, 1973.
2. D.F. Newman, et al, "Evaluation of Temperature Coefficients of Reactivity for ^{233}U-Thorium Fueled HTGR Lattices," EPRI NP-222, May, 1977.
3. D. McEachern, et al, "Fort St. Vrain Core Performance," GA-A14527, July, 1977.
4. K.R. Schultz and D.R. Mathews, "General Atomic Participation in the High Temperature Lattice Test Reactor Program," GA-A12710, June, 1975.
5. D.F. Newman and B.F. Gore, "Neutron Multiplication Factors as a Function of Temperature: A Comparison of Calculated and Measured Values for Lattices Using $^{233}UO_2$-ThO_2 Fuel in Graphite", Nucl. Tech. 37, 1978.

Section 4

CROSS SECTIONS AND YIELDS IMPORTANT FOR FISSION PRODUCT ABSORPTION IN THERMAL REACTORS

Cross Sections and Yields Important for Fission Product Absorption in Thermal Reactors

W.H. Walker
Atomic Energy of Canada Limited
Chalk River, Ontario, KOJ 1JO

INTRODUCTION

There is no scarcity of evaluations of fission product yields and cross sections. Both were reviewed for the 1973 panel on fission product nuclear data held at Bologna[1,2,3]. There have also been reviews of the sensitivity of reactor reactivity to fission product accumulation[4,5].

It is not at all clear that yet another is required. On the one hand, sensitivity studies for thermal reactors allow one to assign uncertainties to individual yields and cross sections which will ensure that absorption by fission products, both individually and collectively, introduces only a small uncertainty in reactor calculations. At the Bologna meeting a comparison of evaluated uncertainties with these requirements led to the conclusion that we knew, in 1973, all that we needed to know about fission products in thermal reactors. Thermal cross sections were not reviewed at all for the second panel on fission product nuclear data, held last fall at Petten.

On the other hand, there are quite large discrepancies when calculated and measured total fission product absorption are compared[6,7]. These discrepancies are in the ^{135}Xe transient as well as the long term absorption. Since these experiments and discrepancies will be reviewed later at this meeting by England and Wilson, it seems worthwhile to look closely at the data of the few fission products that have reactivity effects large enough that uncertainties in their yields or cross sections might possibly account for a significant part of the discrepancies. Only ^{135}Xe, ^{149}Sm, ^{143}Nd and ^{147}Pm satisfy this requirement.

Absorption by a particular fission product depends on both the number of atoms and the cross section of that nuclide. The cross section may be a function of neutron temperature and epithermal flux, while the number of atoms depends not only on its cumulative yield, but also on its own and its precursor's half-life and cross section. For the most part the decay data is well-established and will not be reviewed here, but will be referred to if it affects any of the measurements.

The cross section convention used will be that of Westcott[9]. That is, the flux is equal to nv_o where n is the total neutron density and v_o is 2200 m/s.

The Maxwellian cross section, σ_{th}, is $g_w \sigma_{2200}$. For the case of a 1/v absorber g_w=1.00 so that $\sigma_{th}=\sigma_{2200}$. The thermal reactor cross section is given by $\hat{\sigma}=\sigma_{2200}(g+rs)$ where r is the epithermal fraction and s is proportional to the reduced resonance integral above a temperature-dependent cut-off.

CROSS SECTIONS

^{135}Xe

The cross section used in ENDF/B(IV) is based on the work of Sumner[10]. Sumner's analysis assumes that the shape of the total cross section, f σ_t(E) say, is given by the results of Smith et al[11] and then uses additional experiments to obtain the normalization factor, f. The best fit to the renormalized data was obtained assuming g=5/8. The new parameters and those obtained originally by Smith et al are

	Sumner[10]	Smith et al[11]
Normalizing factor, f	0.96	1.0
g	5/8	5/8
E_r	0.08418 eV	0.08415±0.00028 eV
$\Gamma_n^o=\Gamma_n(E_r)/\sqrt{E_r}$	0.06788 eV	0.06067 eV
Γ_γ	0.09572 eV	0.09492 eV

The normalization used by Sumner is based on old data obtained under less than ideal conditions. Fortunately a more closely-controlled measurement of the effective cross section was made recently by Santry and Werner[12] at Chalk River. The ^{135}Xe was implanted in pure aluminum from a mix of rare gas fission products using a mass separator. The subsequent irradiation was in a well-thermalized neutron spectrum (r=.00355) at a neutron temperature of 318°K. Their effective cross section, $g_w(318^oK)\sigma_{2200}$, is 3.09±0.07 megabarns.

For this spectrum ENDF/B(IV) gives 3.11 megabarns. Thus the adequacy of data in current use appears to be well-established, at least for moderate neutron temperatures.

The effect of Doppler-broadening has been considered[13] and found to be negligible. At 20°C the difference between using the broadened and unbroadened peak is only 0.14% in the effective cross section, while a temperature increase to 800°C causes an additional change of only 0.35%. At higher temperatures, however, g_w(T) may deviate from the values predicted by the ENDF/B(IV) data.

^{149}Pm and ^{149}Sm

The mass 149 chain is the prime candidate to account for the discrepancy between calculated and measured long term fission product absorption. For example, if the absorption cross section of ^{149}Pm, the 53-d precursor of ^{149}Sm, were about 50 kilobarns its abundance would be reduced by a large factor and ^{149}Sm would not

Table 1

^{149}Sm Absorption Cross Section

Reference	Method	T_N (°C)	Epith. index r	Cross Section (kilobarns) Measured	$g_w(20°C)\sigma_{2200}$[a]	Comments
Bidinosti +[18]	mass spec	137	0.0098	83.8	70.16	Relative to σ_{2200}(Co) = 36.5b[b] and nat. abund. of 0.1384[c]
		120	0.018	80.5	69.43	
Tattersall +[19]	pile osc	20	<.001	68.2±0.7	68.59	Relative to σ_{2200} = 766.6b[b] for Harwell boron
		70	0.042	72.2±1.0	67.57	
Meadows, Whalen[20]	pulsed source	23	∿0	9.546	68.76[c]	Also measured σ_{2200} for ANL boron
Aitken, Cornish[21]	mass spec	130	0.0365	79.92±2.4	68.94	Relative to σ_{2200}(Co) = 36.6[b]
		80	0.0136	76.43±2.4	69.29	
		50	0.0015	73.62±2.4	69.96	
Sokolowski +[22]	pile osc	57	∿0	10.00±0.15	66.45[c]	Relative to σ_{2200} = 760.8b for ANL boron
Albert +[23]	pile osc	31.5	0.00075	9.608±0.10	67.74[c]	No standards listed
Mean					68.7±0.4	
ENDF/B(IV)					67.48	

[a] Values of g_w and s used in standardization

°C	20	40	60	80	100	120	140
g_w	1.638	1.719	1.793	1.861	1.923	1.979	2.029
s	-1.109	-1.322	-1.506	-1.665	-1.802	-1.919	-2.018

[b] Renormalized using σ_{2200}(Co)=37.24b(ENDF/B(IV)
σ_{2200}=771b for Harwell boro
σ_{2200}=759b for ANL boron

[c] Assuming a natural abundance of 0.1380

increase after irradiation as predicted. The resulting shortfall in absorption would be comparable to the observed discrepancy.

This is improbable for 2 reasons. Firstly, the mass 149 transient observed by Gunst et al[7] was as large as expected, and, secondly, there have been 3 measurements of the effective cross section giving values of 1000±400b[14], 1700±300b[15] and 1630±160b[16].

Gunst et al[7] observed a dependence of the magnitude of the mass 149 transient on the epithermal flux which they attributed to a large resonance absorption in ^{149}Pm. They estimated a resonance integral of ∿20 kilobarns.

A 20 kb resonance integral and a 1500b effective cross section requires a very large resonance close to, but above, the thermal region, i.e. near 0.5 eV. The reactor cross section would then be sensitive to neutron temperature as well as epithermal flux. This might explain the rather wide spread in measured values.

The ^{149}Sm cross section is readily measured since ^{149}Sm occurs naturally. Most measurements of $\sigma_T(E)$ were made in the 60's and are included in the ENDF/B evaluation[17] completed in 1967.

There have been several measurements of the effective reactor absorption cross section, $\hat{\sigma}_{ab}$, as well. Those which documented the neutron temperature and epithermal component are listed in Table 1. They have been standardized to a 20°C Maxwellian flux so that they can be compared. Values of g_w and s ($\hat{\sigma}_{ab}=\sigma_{2200}(g+r_s)$) were derived from ENDF/B(IV) and are listed in a footnote. Linear interpolation was used where necessary. Other renormalizations are noted in the comments column.

The mean value for 10 experiments is 68.7±0.4 where the uncertainty is the standard deviation in the average. The ENDF/B-(IV) value is 2% lower. See Appendix A for an analysis based on more recent differential data.

^{143}Nd

There has been only one measurement, by Lucas et al[24], since thermal cross sections were reviewed in 1969[25]. As part of the work aimed at interpreting the OKLA phenomenon, they measured the cross sections of several fission products, including ^{143}Nd, using separated isotopes.

The irradiations were done in different spectra in the TRITON-1 and TRITON-2 reactors so that the effective cross sections could be resolved into their thermal and epithermal components. Their results for ^{143}Nd are compared with AECL-3037[25] and ENDF/B(IV) values in Table 2. The reduced resonance integral is equal to $RI_{0.5}-0.45\ \sigma_{2200}$.

The results are not so discrepant as they seem. If σ_{2200} is derived from their measured cross sections assuming the ENDF/B(IV) reduced resonance integral (-15b) then a value of 330±5b is obtained as the weighted mean of 3 measurements.

Table 2

^{143}Nd Absorption Cross Sections

Reference	Method	σ_{2200}(b)	Resonance Integral(b) Reduced $RI_{0.5}$
Lucas +[24]	mass spect	338	-90
AECL-3037 [25]	evaluation	325	60
ENDF-B(IV)	evaluation	325	-15 131

Table 3

^{147}Pm Absorption Cross Sections

Reference	Method	Thermal cross section σ_{2200} - barns -	m/g	$\frac{RI_{0.5}}{\sigma_{2200}}$
Schuman,Berreth[26]	activation	235±17	0.895	13.7
Fenner,Large[27]	mass spect.	156±10	0.88	9.8
Mowatt,Walker[28]	activation	156±10	0.86	
Cabell[29]	activation	180±4*		13.7
Codding +[30]	time-of-flight	192^{+5}_{-1}		11.4
Kirouac +[31]	time-of-flight	181±10		12.6
ENDF/B(IV)		182		
Recommended		171±5	0.88±.02	13.7±0.3

*Only the partial cross section to the ground state was measured. This has been multiplied by 1.88±0.02 to obtain the absorption cross section.

^{147}Pm

Promethium-147 captures to form two isomers of ^{148}Pm. Of these the 41-day metastable state has such a large cross section that neutron capture competes significantly with β-decay. The capture product is ^{149}Pm which decays to ^{149}Sm and thus leads to a further neutron capture. By the end of the irradiation in a CANDU fuel bundle approximately 12% of all ^{149}Sm has come from the mass 147 chain. Figure 1 shows the various transmutations with probabilities typical of a CANDU reactor.

Table 3 list measured values of the absorption cross section[26-31] as well as associated data where available. The m/g values include both thermal and resonance data. Errors in m/g based on the individual cross sections are not applicable because the latter contain common normalization uncertainties. The spread in values suggests an uncertainty of about 2%, which seems reasonable.

The ratios of resonance integral to thermal cross section fall into 3 groups. The lowest value[27] is probably due to resonance self-shielding in the sample. The two time-of-flight values are suspect because of the appreciable corrections that had to be applied in the thermal region. The recommended value is therefore set equal to the two highest values, 13.7, with an assumed uncertainty of ∿2%.

The most significant discrepancies occur in the measured values of the absorption cross section. There is a spread of nearly 80 barns between the highest and lowest values while the two values claiming the highest accuracy differ by more than twice the sum of their uncertainties.

The simplest method of dealing with such discrepant data is to take a weighted mean. This gives a value approximately equal to the ENDF/B(IV) cross section.

An alternative, but not necessarily more valid, approach is to omit the high value and re-assess the time-of-flight cross sections on the assumption that they were not fully corrected. Since the problems requiring corrections in the thermal region are less important in the resonance region it is reasonable to assume that their resonance integrals are correct. The two agree, with an average value of 2240 ± 50b. If this is divided by the recommended $RI_{0.5}/\sigma_{2200}$ ratio, the thermal cross section is 163 ± 5b which is close to the average of the three integral measurements,[27,28,29]. Taking a weighted mean of the four then gives 171 ± 5. This value differs from all but the two highest values by the sum of their uncertainties, or less.

YIELDS

Mass 135 yields

The mass 135 decay chain is shown in figure 2 with major

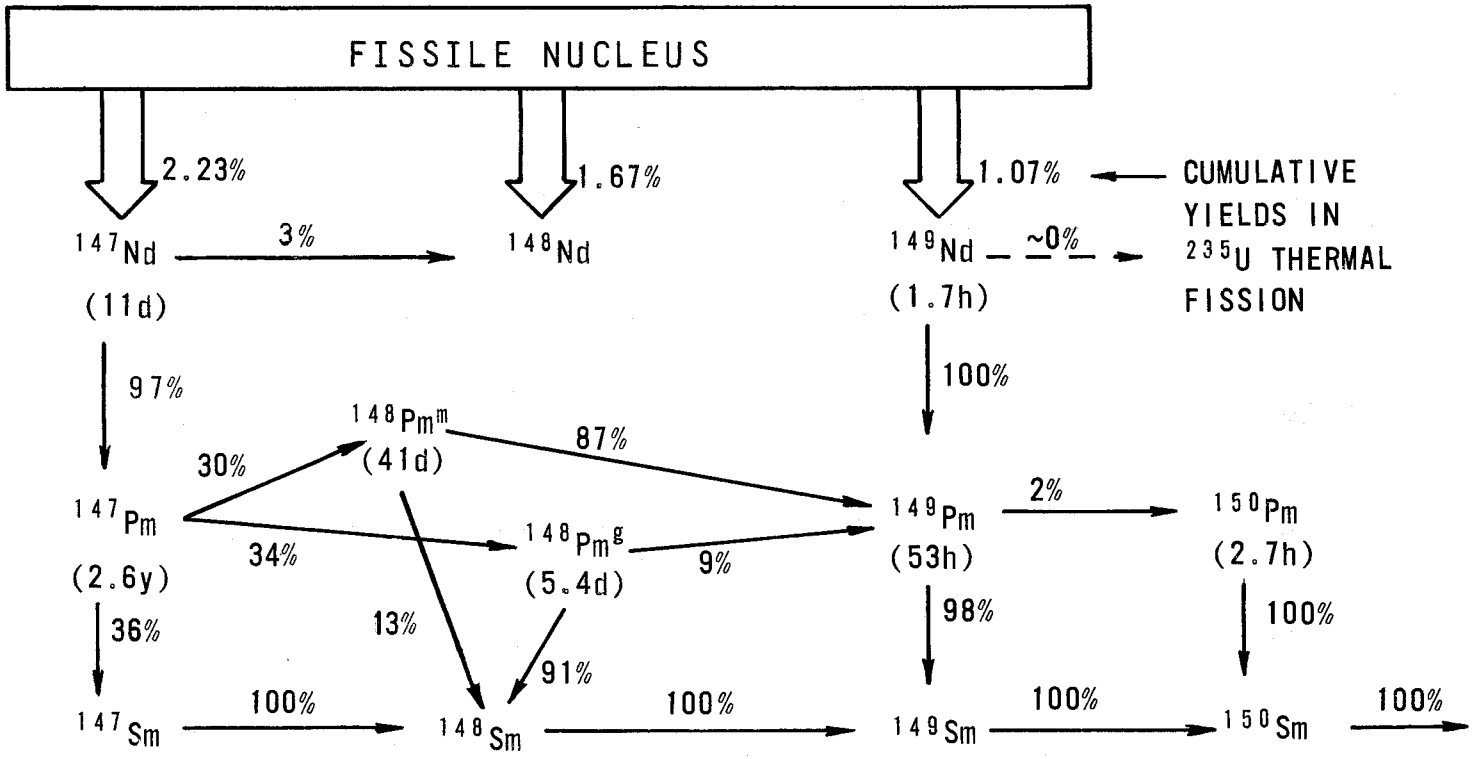

Figure 1 Fission product capture and decay in the 147-150 mass region.

A.E.C.L. Ref. # A-3171-D

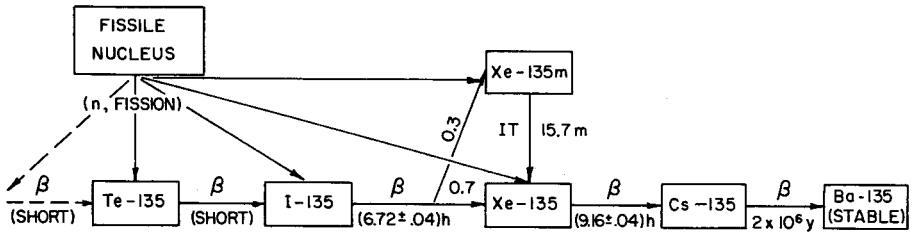

Figure 2 Mass 135 decay chain and direct yields.

direct yields indicated. At equilibrium in a power reactor, neutron absorption by ^{135}Xe depends to some extent on its cross-section since this affects relative capture and decay rates, but the major factor is the cumulative yield. Start-up and shut-down transient absorption is much more sensitive to the ^{135}Xe cross section, but also depends on the direct yield to ^{135}Xe (y_x), the cumulative yield to ^{135}I (y_I) and their respective half-lives. In a power reactor the shut-down transient approximates the $y_x=0$ curve of figure 3.

Mass 135 yields are uniquely difficult to measure not only because of the large ^{135}Xe cross section but also because it has a significant direct yield. Besides the usual methods of measurement, mass spectrometric and radiometric, the large ^{135}Xe cross section makes it possible to use reactivity measurements. The requirements and problems of each of these methods are discussed below.

Mass Spectrometry. In mass spectrometry it is usual to measure the stable or long-lived end product of the decay chain, in this case, Cs. However, if the radiation is done in a high flux most of the 135 chain ends up at ^{136}Xe instead of ^{135}Cs. Correcting for ^{135}Xe capture would be quite inaccurate since the capture to decay ratio is very sensitive to irradiation history. Thus the best that can be done is to add the ^{135}Cs and ^{136}Xe yields together, giving the sum of the two chain yields. This has been the case for the most extensive series of thermal fission measurements, those carried out at Idaho Falls over the last dozen years[65,66,67].

The ideal conditions for determining the mass 135 chain yield is a long irradiation at low flux so that ^{135}Xe captures are few or negligible compared to decay (say $\sim 10^{11}$ n/cm^{2}s). Measurements with these irradiation conditions were reported by various experimenters at McMaster University between 1955 and 1964[34,45,59,60,62]. These are the only direct mass spectrometric measurements of the mass 135 chain yields for the thermally-fissile nuclides, with the exception of one recent experiment the details of which have not yet been published[48], and two USSR measurements that give very different ratios for all 3 Cs isotopes and were discarded in an earlier evaluation[25].

It is disturbing to have the yield of such an important fission product based on a single set of old experiments. While the ^{133}Cs to ^{137}Cs ratios measured in the experiments agree well with those measured elsewhere[25] some indication that nothing has gone drastically wrong in determining mass 135 relative abundances would be reassuring.

It is possible to make such a check. Because ^{135}Xe capture is important only in the thermal region, the relative amounts of the 133, 135 and 137 Cs isotopes measured in a fast reactor will be proportional to the yields of these three chains. Recently a set of fast reactor yields has been published by Maeck and co-workers at Idaho Falls[68,69]. These are compared to the thermal measurements

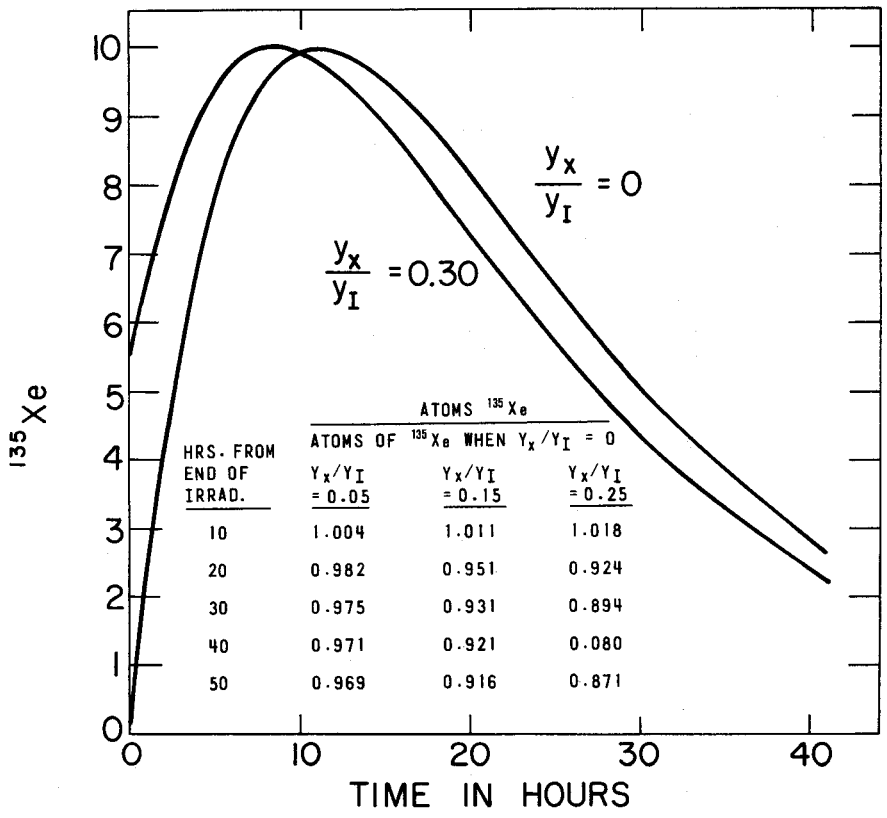

HRS. FROM END OF IRRAD.	Y_x/Y_I = 0.05	Y_x/Y_I = 0.15	Y_x/Y_I = 0.25
10	1.004	1.011	1.018
20	0.982	0.951	0.924
30	0.975	0.931	0.894
40	0.971	0.921	0.080
50	0.969	0.916	0.871

Figure 3 The ^{135}Xe transient as a function of its direct yield.

in Table 4. All measurements are normalized so that the abundances of ^{133}Cs and ^{135}Cs sum to 1.000.

There is good agreement between all ratios. The most divergent are for ^{241}Pu with differences of 1.6% at 133 and 137, and 2.7% at 135. Other differences are 1% or better except for ^{233}U where the thermal ^{135}Cs yield is low by 2.3%. Thus there do not appear to be any seriously discrepant ^{135}Cs yields in the McMaster measurements, but the yields for ^{233}U and ^{241}Pu fission may be 2-3% low.

Table 4

Relative Yields of Cs Isotopes

Fissile Nuclide	Neutron Energy	Reference	Relative yields (133+137=1.000) 133	135	137
^{233}U	thermal	Bidinosti et al[34]	0.467	0.487	0.533
	fast	Maeck[68]	0.471	0.499	0.529
^{235}U	thermal	Petruska et al[44]	0.519	0.505	0.481
	thermal	Wiles et al[45]	0.522	0.507	0.478
	fast	Maeck[68]	0.523	0.500	0.477
^{239}Pu	thermal	Wiles et al[59]	0.503	0.528 (±15%)	0.497
	thermal	Fickel et al[60]	0.516	0.556	0.484
	fast	Maeck[69]	0.514	0.557	0.486
^{241}Pu	thermal	Farrar et al[62]	0.498	0.537	0.502
	fast	Maeck[69]	0.506	0.552	0.494

It is also possible to measure mass spectrometrically the abundance of ^{135}Xe relative to the stable Xe isotopes as it is formed by ^{135}I decay following the end of a low flux irradiation. This has been done twice, for ^{241}Pu[62] and ^{235}U[48]. Yields determined in this way require correction if it was assumed in the analysis that the direct yield to ^{135}Xe was zero, as discussed in the next section.

Radiometric measurements. These can be either absolute or relative. The former may be based on absolute β-counting, usually in 4π geometry, or on γ-counting, in which case some knowledge of the intensity and internal conversion probability of the γ-ray used is required. In relative measurements the same counting method is applied to fission products from the fissile material and a reference fissile material, usually ^{235}U. Relative fission rates are determined by assuming, or by measuring separately, the absolute yield of one of the fission products being investigated, usually ^{99}Mo or ^{140}Ba.

For absolute determinations it is essential to know the shape of the decay curves for each nuclide, which may be a simple exponential if the precursor is relatively short-lived, as in the case of ^{135}I, or a function of both decay rates, as in the case of

^{135}Xe. In the latter case the decay rate will also depend on the direct yield to ^{135}Xe (y_X) as shown in fig. 3.

The irradiation conditions for the curves in fig. 3 are typical of those used in radiometric yield measurements. Here the flux is $10^{10}n/cm^2s$ and the irradiation period is 15 m. However, extending the irradiation to several hours makes little change in the relative amounts of ^{135}Xe.

If the direct yield is assumed to be zero in the analysis and the counting is mostly in the period from 15 hours after the end of the irradiation then the value obtained for the yield will be too low by the factors shown in the table. This will apply directly to absolute γ-counting or the mass spectrometer measurements. For relative measurements, using ^{233}U and ^{235}U say, both will be underestimated, but by different amounts, since the respective yields to ^{135}Xe are 30% and 3.5%.

Reactivity Measurements. To produce sufficient ^{135}Xe to give a measurable signal in a reactivity measuring facility such as a pile oscillator, fissile material ($\sim$1g) is irradiated for a day or longer at a high flux. In this case most direct yield ^{135}Xe is removed by capture so that the transient is close to the y = 0 curve and the quantity measured is the cumulative yield to iodine, y_I.

Both measurements of this type[41,42] were relative, using ^{235}U as reference. Difficulties in interpretation include: determining the relative fission rates, a flux depression correction that is time dependent, and possible changes in reactivity due to heating by β-decay of the water near the sample.

The measured yields are presented in Table 5. This is an updating of table 4 of ref. 1 with a number of corrections, several "flyers" omitted and renormalizations as listed in the footnotes.

Additional comments are:

^{233}U. The correction for the ^{135}Xe cumulative yield is more complicated than indicated in Fig. 3 because the irradiation was for several hours at a high flux ($\sim 2 \times 10^{13} n/cm^2s$)[35]. The corrections were calculated by simulating the irradiation in FISSPROD-2[70] assuming identical conditions for both ^{233}U and the ^{235}U reference standard. However, a comment in the text suggest that the fluxes were not identical.

The two measurements of the ^{135}Xe direct yield, based on the shape of the decay transient in an irradiated ^{233}U foil (as in Fig. 3)[37,38] agree and have a significantly lower average than the direct yield obtained by separating the ^{135}Xe from the sample[39]. For all other fissile nuclides the two methods agree.

^{235}U. There is agreement between all values except one absolute radiometric measurement of the ^{135}I yield[47]. Since the same author is in reasonable agreement for the ^{135}Xe yield it is possible that the γ-ray intensity used here is incorrect. To

Table 5

Mass 135 Thermal Fission Yields

Fissile Nuclide	Evaluated Chain Yield - % -	Percent Cumulative(C) and Fractional Direct(D) Yields by Isobar				
		Cs(Z=55) C	Xe(Z=54) C	Xe(Z=54) D	I(Z=53) C	I(Z=53) D
^{233}U	6.21±.15[32] 6.22[a] 6.22±.11[b]	6.25±.21[34,c]	5.64±.06[35,f] ↓ 6.31(30h)[ff]	.099±.013[36,x] .182±.016[37] .17±.02[38] .218±.005[39]	4.87±.45[40,d] 5.40±.45[41,e] 5.11±.10[42,e]	.606±.024[43]
LSF [g]		6.262±.104	6.243±.104	.213±.009	4.912±.084	.606±.024
^{235}U	6.60±.16[32] 6.61[a] 6.55±.06[b]	6.52±.15[44,c] 6.55±.2[45,c]	5.8±.6[46] 6.74±.18[47,h] 6.46±.20[48,i]	.025±.025[49] .041±.012[46] .027±.010[50] .035±.010[51] .025±.018[37] .019±.013[36] .036±.002[39]	6.5±.5[52] 5.31±.51[47,h,x] 5.90±.16[76,h,x]	.43±.10[53] .55±.09[54] .47±.02[55] .44±.07[56] .70±.17[57,x]
LSF [g]		6.504±.073	6.502±.073	.035±.002	6.272±.071	.467±.017
^{239}Pu	7.69±.26[26] 7.46[a] 7.42±.06[b]	7.21±1.00[59,c] 7.59±.17[60,c]	7.11±.20[61,f] ↓ 7.7(50h)[ff]	.148±.025[37] .151±.005[39]	6.67±.13[42,e] 6.59±.42[41,e]	.608±.017[43]
LSF [g]		7.623±.131	7.608±.131	.151±.005	6.460±.116	.608±.017
^{241}Pu	7.06±.24[32] 7.18[a] 7.30[b]	7.18±.24[62,c]	6.97±.24[62,j] 7.66±.23[78,f] 7.8±.2[63] ↓ 7.33(30h)[ff]	.052±.040[37] .032±.002[39]	6.8±.3[64,f] 7.95±.20[42,e,x] 8.00±.60[41,e,x] 6.68±.40[39,k]	
LSF [g]		7.200±.115	7.197±.116	.032±.002	6.966±.112	

a ENDF/B(IV)

b ENDF/B(5d)

c Renormalized using their isotopic ratios as given in ref. 32 and the sum of yields to ^{133}Cs and ^{137}Cs in ENDF/B(5d) (12.91% for ^{233}U, 13.09% for ^{235}U, 13.79% for ^{239}Pu and 13.60% for ^{241}Pu)

d Their measured yields, excluding ^{135}Xe, average 7% less than ENDF/B(5d) yields. Yield for ^{135}Xe is multiplied by 1.07±.09

e Relative yields, renormalized to 6.55% in ^{235}U. For ref. 42, the number of fissions was reestimated using measured ^{140}Ba yield ratios and ENDF/B(5d) yields (6.477 for ^{233}U, 6.339 for ^{235}U, 5.578 for ^{239}Pu, 6.355 for ^{241}Pu).

f Renormalized using ENDF/B(5d) yields. Use mass 99 as standard (4.904 for ^{233}U, 6.154 for ^{235}U, 6.190 for ^{239}Pu, 6.353 for ^{241}Pu)

ff Corrected to correct direct yield when $y_x=0$ is assumed. Correction factor used is for assumed time after the end of irradiation shown in brackets.

g Calculated fractional direct yields from ENDF/B(5d) are used to obtain differences between cumulative yields to Cs and Xe (.003 for ^{233}U, .002 for ^{239}Pu, negligible for ^{235}U, ^{241}Pu)

h Renormalized using γ-ray intensities of ENDF/B(IV)

i Renormalized using measured isotopic ratios and the sum of yields to ^{131}Xe, ^{132}Xe and ^{134}Xe from ENDF/B(5d) (14.98%). Uncertainty increased to value shown because experimental details are lacking.

j Renormalized using their isotopic ratios as given in ref. 32 and the sum of yields to ^{131}Xe, ^{132}Xe and ^{134}Xe in ENDF/B(5d) (14.02%)

k Relative to recommended ^{135}I yield in ^{239}Pu fission

x Omitted in least squares fit

obtain agreement with the remaining measurements, I for the 1260 keV should be decreased from 0.279 (ENDF/B(IV)) to 0.234, approximately the value used by the author. A similar absolute measurement[76] errs in the same direction.

^{239}Pu. The differences between the evaluated yields are due to inclusion in the ENDF/B(IV) and ENDF/B(5c) evaluation of two low values shown in the next two columns, the first[59] with a very low assigned error. With the correct error assignment to the first and the direct yield correction is made to the second, the ENDF/B(V) evaluation will increase so that there is no discrepancy.

^{241}Pu. The two reactivity measurements[41,42] are in good agreement with each other, but are about 12% higher than would be expected from the 7 remaining measurements. The discrepancy is difficult to understand. In one experiment[41] the relative number fissions in the ^{241}Pu and ^{235}U reference sample were calculated from the number of atoms and estimated cross section while in the other[42], as presented here, the relative number of fissions is based on evaluated ^{140}Ba yields (ENDF/B(5d) and measured relative ^{140}Ba activities. It is unlikely that the ^{140}Ba yield in ^{241}Pu and the calculated reaction rate are equally incorrect.

The recent measurements for fast reactor fission in ^{241}Pu[69] give a value of 7.35% for mass 135, in good agreement with the 7 lower values. For this reason the two reactivity results are omitted in the least squares fit.

LSF fits. LSF is a least squares fitting program[71] originally designed for the second IAEA[72] determination of a best set of 2200 m/s parameters for the four major fissile nuclides. It is therefore suitable for the analysis of interrelated data such as yields.

Yields were entered in a form representing the measurements as nearly as possible although normalizations other than those at mass 135 had to be omitted. In particular all ratio measurements were entered in that form (yields with superscripts for footnotes e,f, and k).

In addition to the yields shown in Table 5, cumulative yields to tellurium have been measured in ^{235}U thermal fission (3.4 ± 0.5%[56], and 3.3 ± 0.3%[58]). These were included in the LSF fit, which gave a best fit of 3.24 ± 0.12%. The fitted yields generally agree with those in ENDF/B(5d) with the exception of ^{239}Pu which was discussed above.

With the exception of the 2 reactivity measurements in ^{241}Pu fission[41,42] and the two low radiometric measurements of the ^{135}I yield in ^{235}U fission, which may be due to use of an incorrect γ-intensity all mass 135 yield measurements agree well and form a consistent set. There seems little possibility that the 9% difference between the calculated and measured ^{135}Xe transients[7] in ^{233}U fission is due to yield uncertainties to any significant degree.

Table 6

Mass 147 and 149 Chain Yields

	^{233}U		^{235}U		^{239}Pu		^{241}Pu	
	147	149	147	149	147	149	147	149
Input data								
Mass spect. isotopic ratios	.6882 ±.007	.3118 ±.007	.6787 ±.0060	.3213 ±.0060	.6261 ±.0032	.3739 ±.0032	.6054 ±.0043	.3946 ±.0043
Mass spect. abs. yields(%)								
-Maeck et al[67]			2.217 ±.022	1.023 ±.010				
-AECL-3037, part II[32,a]	1.70 ±.050	.766 ±.021	2.214 ±.040	1.061 ±.070	2.11 ±.07	1.27 ±.05	2.19 ±.06	1.43 ±.04
Radiometric yields[b]								
Bunney et al[74,c]	R.806 ±.04	R.726 ±.036	2.24 ±.11	1.06 ±.05				
Gordon et al[35,c]	R.815 ±.04							
McLaughlin[47,d]			2.18 ±.09	1.09 ±.06				
Bresesti et al[75,e]			2.14 ±.11					
Blachot et al[76,d]			2.30 ±.13					
DiIorio et al[73]			2.30 ±.05	0.97 ±.04				
Sorokina et al[77,f]					2.07 ±.08	1.11 ±.08 1.26 ±.05	2.52 ±.08	1.61 ±.05
Jain et al[61,c]					R.905 ±.03			
Chitambar et al[78,c]							R1.09 ±.03	
LSF output								
Ratios to ^{235}U	.776 ±.015	.749 ±.014	1.00	1.00	.932 ±.016	(1.256)	1.052 ±.015	(1.450)
Absolute yields	1.721 ±.033	.772 ±.015	2.215 ±.015	1.030 ±.009	2.065 ±.034	1.233 ±.021	2.330 ±.032	1.515 ±.022
ENDF/B(5d)	1.708	.757	2.227	1.075	2.048	1.244	2.391	1.551

a These yields have been corrected on the basis of more recent results. The ^{235}U and ^{239}Pu yields have been decreased 0.7% and 2.0% respectively to allow for higher Xe yields[66]. The "high ^{238}Ba" yields of tables 26 and 28[32] were used to take account of the higher ^{238}Ba yield measured for ^{239}Pu fission[66] (on the assumption that the higher yields will also be correct for ^{241}Pu).

b Radiometric yields are given either as percent absolute yields or as the ratio to the yield of the same fission product in ^{235}U thermal fission. The latter values are preceded by R.

c Renormalized to mass 99 yields in ENDF/B(5d) (see table 5, footnote f).

d Renormalized using ENDF/B(IV) γ-ray intensities.

e Renormalized using the ENDF/B(5d) yield for ^{141}Ce (5.843%).

f Renormalized using the ENDF/B(5d) yields for ^{144}Ce (4.389% in ^{235}U, 3.739% in ^{239}Pu).

Masses 147 and 149. Mass spectrometric measurements of Sm isotopic abundances are complicated by decay and burnup corrections. However, the fortunate circumstance that ^{150}Sm is a shielded isotope, i.e. without a significant cumulative yield, and has a low cross section means that virtually all the mass 149 yield appears either as ^{149}Sm or ^{150}Sm, even in high flux irradiations, so that the two isotopic abundances need only be added together.

The amount of ^{147}Sm formed depends on the length of post-irradiation cooling period and the half-life and cross-section of ^{147}Pm. Fortunately the half-life is known accurately, and the capture corrections are small enough that the uncertainties in the ^{147}Pm cross-section do not introduce significant errors. As a result both high flux and low flux measurements give consistent results for the relative yields of masses 147 and 149[32].

To take advantage of this correlation the two yields are considered together. The measurements are listed in table 6. The relative yields listed in the first line are based on 1,5,3 and 2 measurements respectively for ^{233}U, ^{235}U, ^{239}Pu and ^{241}Pu.

The corrections to the absolute yields from ref. 32 are based on the recent results of Maeck et al[66] who remeasured the relative yield of Xe to Nd in ^{235}U and ^{239}Pu fission. The new ratios are 2.5% and 8.6%, respectively, greater than the earlier Idaho Falls measurements[65]. When these new values are substituted for the earlier ones and the heavy mass yields renormalized to 100%, the remaining yields, including masses 147 and 149, decrease by 0.7% and 2% respectively.

The recent measurements[66] also determined a much higher Ba yield in ^{239}Pu fission. Since earlier McMaster measurements[60,62] were higher than other measurements for both ^{239}Pu and ^{241}Pu the AECL evaluation[32] had listed yields corresponding to both a high and low Ba yield. The values in table 6 correspond to the high Ba yield set for both fissile nuclides in the assumption that both McMaster results are correct.

The absolute yields given by DiIorio et al were measured with an on-line mass separator, not radiometrically.

All measurements relative to ^{235}U yields are listed as the measured rates $y_x(F)/y_x(^{235}U)$ where F refers to ^{233}U, ^{239}Pu or ^{241}Pu. The ratio is indicated by an R.

LSF was used to obtain a least squares fit to the listed measurements and the results are compared to ENDF/B(5d). For mass 147 both sets agree to better than 1% except for ^{241}Pu where the difference, 2½%, is within the sum of the assigned errors.

Although agreement for mass 149 is poorer, the differences only exceed the sum of errors of the two evaluations in the case of ^{235}U. This difference is due to the new Idaho Falls measurement[67] that has not yet been factored into ENDF/B. There appears to be no reason to suppose that either the 147 or 149 yield is in error by a large enough amount to account for the observed discrepancy in long-term fission product absorption. (Mass 149 would have to be $\sim$ 40% too high.)

Mass 143. Nd is the reference element in all mass spectrometric yield measurements and all measurements of relative yields agree, with a standard deviation from the mean of less than 1% for ^{143}Nd for all four thermally fissile nuclides. For ^{235}U fission the most recent measurement[67] agrees well with earlier results. Their value is 6.00 ± .032% compared to 5.96 ± .02% in ENDF/B(5d).

SUMMARY

The yields and cross sections affecting neutron absorption by ^{135}Xe, ^{149}Sm, ^{143}Nd and ^{147}Pm in a thermal reactor have been reviewed. A number of discrepancies have been noted but none are large enough to explain the differences between measured and calculated total fission product absorption[6,7].

The most significant discrepancies are:

^{149}Sm. Measured reactor cross sections give an average value of $g_w(20^oC)\sigma_{2200}$ that is about 2% greater than the ENDF/B(IV) value.

^{147}Pm. Measured values of the absorption cross section are so discrepant that new measurements are recommended.

Mass 135. Reactivity measurements of the ^{135}I cumulative yield in thermal neutron fission of ^{241}Pu are high compared to other measurements. A new measurement of the chain yield is recommended.

ACKNOWLEDGEMENTS

I am very grateful to W.J. Maeck for providing all the most recent Idaho Falls yield data and to A. Okazaki for useful discussions of the pile oscillator and radiometric measurements of mass 135 yields.

REFERENCES

1. W.H. Walker, review paper 11a, IAEA-169(I), 285 (1973).
2. J.G. Cuninghame, review paper 11b, IAEA(I), 353 (1973).
3. P. Ribon, J. Krebs, review paper 10, IAEA-169(I), 235 (1973).
4. W.H. Walker, Nuclear Data for Reactors (Paris) I, 521, (1966).
5. J.G. Tyror, review paper 3, IAEA-169(I), 51 (1973).
6. A. Okazaki, E.K. Sokolowski, Nuclear Data for Reactors (Helsinki)I, 703(1970).
7. S.B. Gunst, J.C. Connor, D.E. Conway, Nucl. Sci. Engng 58, 387 (1975).
8. T. England, W.Wilson - This meeting, review paper in section IV.
9. C.H. Westcott, W.H. Walker, T. Alexander, Can. J. Phys, 38 (1960).
10. H.M. Sumner, AEEW-R116 (1962).
11. E.C. Smith, G.S. Pawlicki, P.E.F. Thurlow, G.W. Parker, W.J. Martin, G.E. Creek, P.M. Lantz, S. Bernstein, Phys. Rev. 115, 1693 (1959).
12. D.C. Santry, R.D. Werner, J. Nucl. En. 27, 409 (1973).
13. J.B. Slater, private communication.
14. R.S. Mowatt, W.H. Walker, NBS Spec. Publ. 299, 1291 (1968).
15. I.A. Kondurov, L.M. Gracheva, A.I. Egorov, D.M. Kaminkev, A.M. Nikitin, Yu. V. Petrov, J. Nucl.En. 20, 814 (1966) translated from At.Energija 19, 188 (1965).
16. H. Gaggeler, H.R. von Gunten, H.S. Pruys, J. Inorg. Nucl. Chem. 38, 205 (1976).
17. B.R. Leonard, Jr., K.B. Stewart, Summary documentation in ENDF/B(IV) MAT-1027
18. D.R. Bidinosti, H.R. Fickel, R.H. Tomlinson, PIC-2,15, 459 (1958).
19. R.B. Tattersall, W.A. Cooper, D. Jowitt, S.K. Pattenden, AERE R/R 2459 (1958).
20. J.W. Meadows, J.F. Whalen, Nucl. Sci. Engng. 9, 132 (1961).
21. K.L. Aiken, F.W. Cornish, J. Inorg. Nucl. Chem. 17, 6 (1961).
22. E.K. Sokolowski, H. Pekarek, E. Jonsson, Nukleonik 6, 245 (1964).
23. D. Albert, J. Hagner, G. Hüttel, Kernenergie 10, 25 (1967).
24. M. Lucas, R. Hagemann, R. Naudet, C. Renson, C. Chevalier, Natural Reactor symposium paper AIEA/TC/119/114 Paris (Dec. 1977)
25. W.H. Walker, AECL-3039, part I (revised) (1972).
26. R.P. Schuman, J.R. Berreth, Nucl. Sci. Engng.12, 519 (1962).
27. N.C. Fenner, R. Large, J. Inorg. Nucl. Chem. 29, 2147 (1967).
28. R.S. Mowatt, W.H. Walker, Can. J. Phys 49, 108 (1971).
29. M. Cabell, J. Inorg. Nucl. Chem. 32, 3433 (1970).
30. J.W. Codding, R.L. Tromp, F.B. Simpson, Nucl. Sci. Eng. 43, 58 (1971).
31. G.J. Kirovac, H.M. Eiland, C.A. Conrad, R.E. Slovacek, K.W. Seeman, Nucl. Sci. Engng. 52, 310 (1973).
32. W.H. Walker, AECL-3037, part II (1973).
33. M.E. Meek, B.F. Rider, NEDO-12154-1 (1974).
34. D.R. Bidinosti, D.E. Irish, R.H. Tomlinson, Can. J. Phys. 39, 1391 (1961).

35. G.E. Gordon, J.W. Harvey, H. Nakahara, Nucleonics 24 (no. 12) 62 (1966).
36. H.A. Storms, C.D. Coryell, paper presented at 150th meeting of Am. Chem. Soc. (1965).
37. A. Okazaki, W.H. Walker, C.B. Bigham, Can. J. Phys. 44, 237 (1966); erratum Can. J. Phys. 49, 498 (1971).
38. R.M. Harbour, D.E. Troutner, K.W. MacMurdo, Phys. Rev. C10, 769 (1974).
39. R.C. Hawkings, W.J. Edwards, W.J. Olmstead, Can. J. Phys. 49, 785 (1971).
40. R. Ganapathy, T. Mo, J.L. Meason, J. Inorg. Nucl. Chem. 291, 257 (1967).
41. R.G. Nisle, I.E. Stepan, Nucl. Sci. Engng 31, 241.
42. A. Okazaki, W.H. Walker, Can. J. Phys. 43, 1036 (1965).
43. S.M. Qaim, H.O. Denschlag, J. Inorg. Nucl. Chem. 32, 1767 (1970).
44. J.A. Petruska, E.A. Melaika, R.H. Tomlinson, Can. J. Phys. 33, 640 (1955).
45. D.M. Wiles, B.W. Smith, R. Horsley, H.G. Thode, Can. J. Phys. 31, 419 (1953).
46. E.J. Hoagland, N. Sugarman, NNES, Div. IV. vol. 9 part V, 1035 (1951).
47. T.P. McLaughlin, Dissertation, University of Arizona, (1971).
48. F.C. Schoenig, W.E. Moore, submitted to Nucl. Sci. Engng.
49. L.E. Glendenin, M.I.T. report no. 35 (1949).
50. F. Brown, L. Yaffe, Can. J. Chem. 31, 242 (1953).
51. S. Katcoff, W. Rubinson, Phys. Rev. 91, 1458 (1953).
52. A.C. Pappas, AECU-2806 (1953).
53. H. Yoshida, Y. Paiss, S. Amiel, IA-1128, 63 (1966).
54. F. Wunderlich, Radiochim Acta 7, 105 (1967).
55. H.O. Denschlag, J. Inorg. Nucl. Chem. 31, 1873 (1969).
56. A.A. Delucchi, A.E. Greendale, Phys. Rev. C1. 1491 (1970).
57. F.H. Frohner, Z. Physik 170, 62 (1962).
58. R. Naeumann, H. Folger, H.O. Denschlag, J. Inorg. Nucl. Chem. 34, 1785 (1972).
59. D.M. Wiles, J.A. Petruska, R.H. Tomlinson, Can. J. Chem. 34 227 (1956).
60. H.R. Fickel, R.H. Tomlinson, Can. J. Phys. 37, 926 (1959).
61. H.C. Jain, K. Rengan, M.V. Ramanish, B.A.R.C./I-62 (1970).
62. H. Farrar, W.B. Clarke, H.G. Thode, R.H. Tomlinson, Can. J. Phys. 42, 2063 (1964).
63. Skovorodkin, A.V. Sorokina, K.A. Petrzhak, A.S. Krivokhatskii Sov. At. En 35, 1109 (1973). (translated from At. Energiya 35, 409 (1973). Normalization date not given.
64. J.L. Kirby, HW-77609, 3.1 (1963).
65. F.L. Lisman, R.M. Abernathey, W.J. Maeck, J.E. Rein, Nucl. Sci. Engng. 42, 191 (1970).
66. W.J. Maeck, F.A. Duce, L.L. Dickerson, J.H. Keller, R.L. Tromp, ICP-1092 (1976).
67. W.J. Maeck, W.A. Emal, F.A. Duce, R.L. Tromp, J.W. Meteer, ICP-1142, in preparation.
68. W.J. Maeck, UC-79c (1975).

69. W.J. Maeck, ICP-1050-II (1977).
70. W.H. Walker, AECL-5105 (1975).
71. D. McPherson, J.H. Johnson, AECL-3415 (1973).
72. G.C. Hanna, C.H. Westcott, H.D. Lemmel, B.R. Leonard, Jr., J.S. Story, P.M. Atree Atomic En. Rev. VII,#4 (1969).
73. G. DiIorio, B.W. Wehring, Trans. Am. Nucl. Soc. 23, 523 (1976) and private communication.
74. L.R. Bunney, E.M. Scadden, J. Inorg. Nucl. Chem. 27, 273 (1965).
75. M. Bresesti, G. Burei, P. Ferrari, L. Moretto, J. Inorg. Nucl. Chem. 29, 1189 (1967).
76. J. Blachot, L.C. Carroz, P. Cavallini, C. Chauvin, A. Ferrieu, A. Moussa, J. Inorg. Nucl. Chem. 36, 495 (1974).
77. A.V. Sorokina, N.V. Skovorodkin, S.S. Bugorkov, A.S. Krivokhatskii, K.A. Petrzhak, Sov. At. En. 31, 806 (1971). Translated from At. Energiya 31, 99.
78. S.A. Chitambar, H.C. Jain, V.D. Kavimandan, C.K. Mathews B.A.R.C. 690, 134 (1973).

APPENDIX A

^{149}Sm - The shape of the cross section near thermal energies

Two differential measurements[1,2] over the 0.1 eV resonance have been reported since the ENDF/B evaluation, but only one of these extends through the critical thermal region.

Subsequent to presentation of the main text a plot of the Japanese results was obtained from the National Nuclear Data Center (NNDC) at BNL showing the ENDF/B(IV) data for comparison (Fig. A1). The two differ by about 8% near 0.025 eV and 5% near the resonance maximum.

In this appendix the integral-differential comparison of Table 1 is repeated using g_w and s values obtained from a curve fitted to the experimental points shown in Fig. A1.

The resonance parameters given in the original paper[1] were from a fit to the data that took no account of the contribution from other levels. These are sufficiently remote that this contribution is essentially 1/v. The appropriate equation to be fitted is, therefore,

$$\sigma_t(E) = \left(\frac{A+1}{A} \right)^2 \frac{6.5095\times10^5 \; g\Gamma_n\Gamma}{\sqrt{E.E_r}\left[(E-E_r)^2+\Gamma^2/4\right]} + P/\sqrt{E}$$

where A=149, g=0.5625 and E_r, Γ_n, Γ and P are variable parameters.

A non-linear least squares fitting program was used to fit this equation to the data set provided from the SCISRS library by NNDC. Since uncertainties were not included in the data set, these had to be estimated from error bars shown on the plotted experimental data of ref. 1. Table A1 shows the experimental cross sections, their assigned uncertainties, the cross sections obtained from the best fit and the percent differences, given by

$$100 \times \left(\frac{\sigma_{calc}}{\sigma_{meas}} - 1 \right)$$

The parameters obtained from this fit are compared in Table A2 with those given by Asami et al from their fit to the same data and the ENDF/B(IV) values.

Since the contribution from higher energy levels to σ_t at .0253 eV is 160b only 255b needs to come from a bound level. Parameters for this level can be quite arbitrary. If the spin and resonance energy used in ENDF/B(IV) are retained (3 and -0.285 eV respectively) and Γ=62 meV, then Γ_n = 0.118 meV, just over 10% of the value in ENDF/B(IV).

To obtain new g_w and s values for use in standardizing the integral experiments the ^{149}Sm file (MAT1027) in ENDF/B(IV) was modified by substituting revised parameters for the first two levels and run through RESEND. As a check RESEND values of σ_T were compared with the fitted cross section in Table A1. Differences were less than $\sim$0.3%

Table A1

^{149}Sm Total Cross Section - A Comparison of Measured and Fitted Data

ENERGY (EV)	TOTAL CROSS SECTION(KILOB) MEASURED	CALCULATED	PERCENT UNCERTAINTY	PERCENT DIFFERENCE (CALC-MEAS)	ENERGY (EV)	TOTAL CROSS SECTION(KILOB) MEASURED	CALCULATED	PERCENT UNCERTAINTY	PERCENT DIFFERENCE (CALC-MEAS)
.6473E-03	139.900	149.086	28.592	6.566	.7633E-01	98.400	98.013	1.016	-.393
.8454E-03	138.800	130.928	14.409	-5.671	.7731E-01	100.500	100.282	.995	-.217
.1070E-02	110.100	116.859	6.358	6.139	.7830E-01	105.200	102.581	.951	-2.489
.1321E-02	106.300	105.659	2.352	-.603	.7932E-01	106.200	104.948	.942	-1.179
.1598E-02	95.800	96.557	1.044	.790	.8036E-01	110.300	107.345	.907	-2.679
.1902E-02	96.180	89.003	1.040	-7.462	.8142E-01	110.000	109.759	.909	-.220
.2232E-02	84.130	82.664	1.189	-1.742	.8249E-01	112.200	112.146	.891	-.048
.2589E-02	77.830	77.264	1.285	-.727	.8360E-01	114.700	114.552	.872	-.129
.2972E-02	70.430	72.631	1.420	3.124	.8472E-01	117.700	116.883	.850	-.694
.3382E-02	66.770	68.610	1.498	2.755	.8587E-01	120.000	119.152	.833	-.707
.3818E-02	65.440	65.104	1.528	-.513	.8704E-01	121.000	121.301	.826	.249
.4280E-02	60.820	62.028	1.644	1.986	.8823E-01	122.800	123.293	.814	.402
.4768E-02	60.750	59.313	1.646	-2.365	.8945E-01	124.800	125.100	.801	.240
.5284E-02	54.990	56.898	1.819	3.470	.9070E-01	126.400	126.671	.791	.214
.6393E-02	52.590	52.838	1.902	.472	.9197E-01	125.800	127.943	.795	1.703
.7609E-02	49.650	49.585	2.014	-.131	.9327E-01	128.000	128.876	.781	.684
.8930E-02	47.160	46.970	2.120	-.404	.9460E-01	130.000	129.417	.769	-.449
.1036E-01	43.500	44.861	2.299	3.129	.9559E-01	126.700	129.535	.789	2.238
1189E-01	43.970	43.182	2.274	-1.792	.9734E-01	128.300	129.133	.779	.649
.1353E-01	41.600	41.856	2.404	.616	.9876E-01	128.800	128.229	.776	-.443
.1527E-01	38.330	40.845	2.609	6.560	.1002	125.200	126.795	.799	1.274
.1712E-01	40.230	40.107	2.486	-.306	.1017	123.800	124.772	.808	.785
.1907E-01	37.000	39.623	2.703	7.089	.1032	123.500	122.250	.810	-1.013
.2114E-01	38.070	39.374	2.627	3.426	.1048	119.200	119.067	.839	-.111
.2330E-01	36.300	39.355	2.755	8.417	.1063	116.200	115.687	.861	-.441
.2557E-01	38.380	39.562	2.606	3.078	.1080	111.500	111.478	.897	-.020
.2795E-01	37.670	39.998	2.655	6.179	.1096	108.200	107.235	.924	-.892
.3044E-01	38.840	40.673	2.575	4.720	.1201	76.580	77.713	1.306	1.479
.3302E-01	39.750	41.597	2.516	4.646	.1303	55.320	54.104	1.808	-2.198
.3500E-01	41.550	42.455	2.407	2.179	.1400	40.750	38.475	2.454	-5.584
.4001E-01	42.740	45.210	2.340	5.780	.1502	29.700	27.521	3.367	-7.338
.4500E-01	46.610	48.825	2.145	4.751	.1599	23.020	20.556	4.344	-10.702
.5010E-01	53.670	53.513	1.863	-.293	.1699	16.510	15.627	6.057	-5.351
.5501E-01	57.410	59.104	1.742	2.950	.1801	13.700	12.114	7.299	-11.574
.6003E-01	64.040	66.061	1.562	3.156	.1898	10.500	9.708	9.524	-7.545
.6498E-01	74.660	74.277	1.339	-.513	.2002	8.722	7.806	9.172	-10.498
.6999E-01	84.710	84.003	1.180	-.835	.2209	5.117	5.317	9.771	3.906
.7353E-01	94.300	91.643	1.060	-2.817	.2395	3.388	3.941	10.331	16.326
.7443E-01	94.170	93.666	1.062	-.535	.2605	3.492	2.928	8.591	-16.160
.7537E-01	96.470	95.806	1.037	-.688	.2802	2.368	2.287	8.446	-3.436

Table A2

Parameters for the 0.09 eV resonance

Source	E_r (eV)	Γ (meV)	Γ_n (meV)	1/v contribution to σ_t (.0253 eV) (barns)
This work	0.0981±0.0001	62.27±0.36	0.529±0.003	415±268
Asami et al	0.0989± .0008	59.5 ±0.8	0.538±0.010	0
ENDF/B(IV)	0.0976	64.1	0.513	2416

The new g_w and s values are given in Table A3. This table repeats some of the information from Table 1 of the main text, but the last column, showing the derived values of $g_w(20^\circ C)\sigma_{2200}$, is based on the new g_w and s values.

The values of $g_w(20^\circ C)\sigma_{2200}$ in Table A3 average about 1% lower than those in Table 1. The average has a somewhat smaller standard deviation and is in better agreement with the value derived from the modified differential data shown in the last line.

It is concluded that there is no major uncertainty in the ^{149}Sm cross section but that the parameters of the first two levels listed in ENDF/B should be modified as indicated here to obtain a better representation of the cross section in the region below 0.25 eV.

REFERENCES

1. T. Asami, K. Okamoto, K. Ideno, Y. Ohno, J. Phys. Soc. Jap 26,225(1969).
2. O.R. Akyuez, C. Cansoy, F. Domanic, Y. Oergeevren, CNAEM 52 (1968).

Table A3

^{149}Sm Absorption Cross Section

Reference	T_N(°C)	r	Cross section (kilobarns) Measured	$g_w(20°C)\sigma_{2200}$[a]
Bidinosti	137	0.0098	83.8	68.37
	120	0.018	80.5	68.32
Tattersall	20	<0.001	68.2±0.7	68.59
	70	0.042	72.2±1.0	66.64
Meadows	23	∿0	69.30	68.63
Aitken	130	0.0365	79.91±2.4	68.02
	80	0.0136	76.41±2.4	68.66
	50	0.0015	73.6 ±2.4	69.60
Sokolowski	57	∿0	72.5±1.1	66.04
Albert	31.5	0.00075	69.6±0.7	67.59
Mean				68.04±0.35
ENDF/B(IV) with new parameters				67.47

[a] Values of g_w and s used to standardize data

°C	20	40	60	80	100	120	140
g_w	1.7125	1.8036	1.8871	1.9634	2.0327	2.0953	2.1515
s	-1.1308	-1.3680	-1.5738	-1.7516	-1.9049	-2.0364	-2.1488

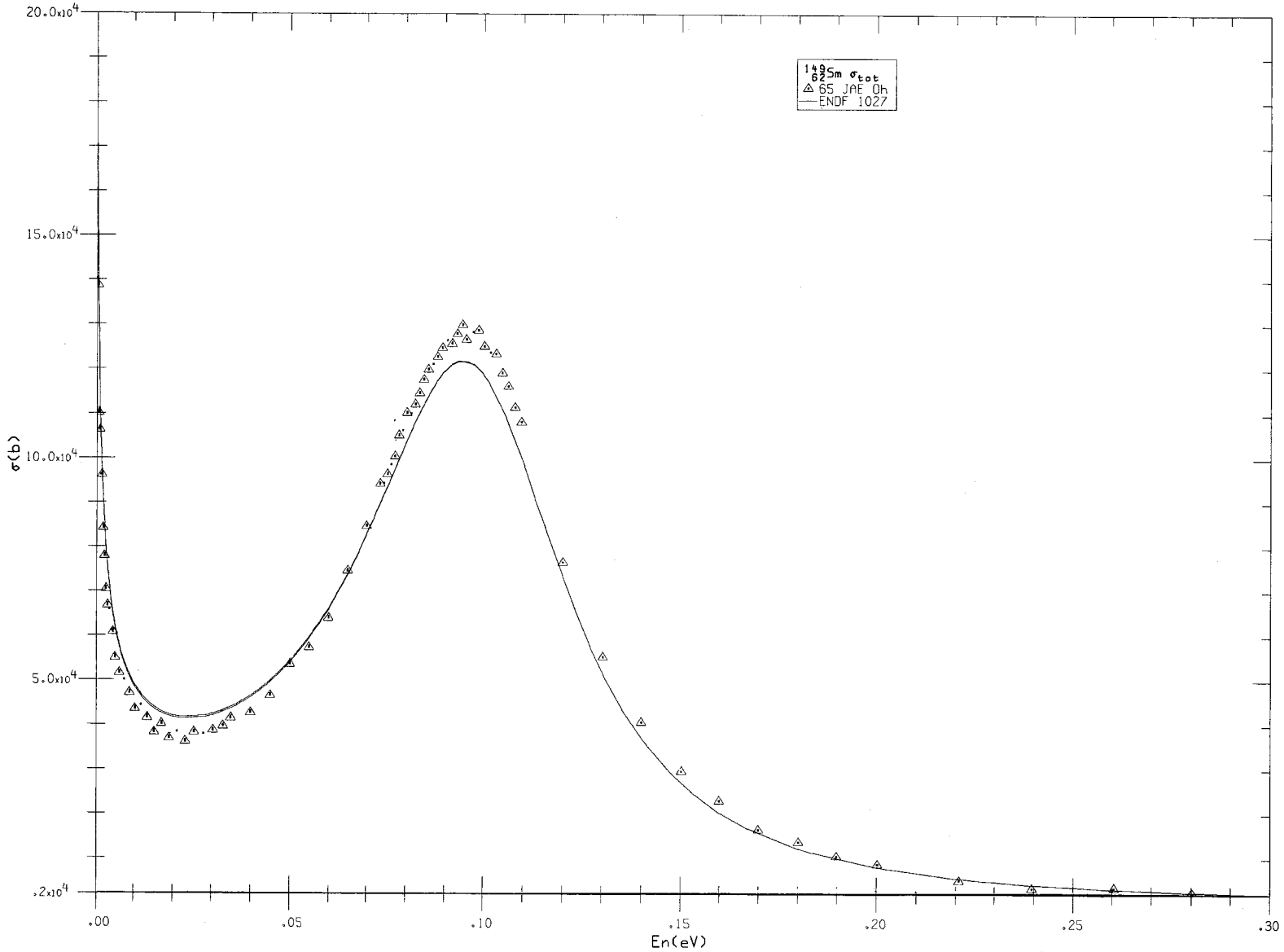

Fig. A1 ^{149}Sm Total Cross Section - A Comparison of ENDF/B(IV) with Measurement.

Section 5

STATUS OF ^{252}Cf $\overline{\nu}$ AND ITS IMPACT ON THERMAL REACTOR PARAMETERS

Status of ^{252}Cf $\bar{\nu}$ and its Impact on Thermal Reactor Parameters

J. R. Smith
Idaho National Engineering Laboratory, EG&G Idaho, Inc.
Idaho Falls, Idaho

INTRODUCTION

No discussion of nuclear reactor data problems would be complete without dealing with that most venerable of data discrepancies, $\bar{\nu}$ for ^{252}Cf. $\bar{\nu}$, the number of neutrons produced in a fission event, is of commanding importance in the design and operation of any fission reactor. The neutron multiplicities of the fissile materials are commonly measured relative to $\bar{\nu}$ for ^{252}Cf, so the accuracy with which they are known cannot be greater than the accuracy with which $\bar{\nu}$ for ^{252}Cf is determined. Reactor designers have requested accuracies of 1/4% to 1/2% for the multiplicities. The existence of a spread of as much as 3% in the results from experiments claiming accuracies of the order of half a percent has represented a rather frustrating situation that was called a "scandal" by Herbert Kouts, keynoting the 1975 Nuclear Data Conference at Washington. A number of developments since then have helped to clarify the picture and make the discrepancies somewhat less scandalous than they then appeared to be. Nevertheless there continue to be some perplexing problems.

There are two aspects to the ^{252}Cf $\bar{\nu}$ discrepancy. The obvious problem is that the disagreement between measurements makes it difficult to extract with confidence a best value from the array of measured values that have been produced. Then there is the more important problem, so far as reactor applications go, of fitting the ^{252}Cf $\bar{\nu}$ value into the general reactor picture so that the completed data file may be used with confidence. The relation connecting the thermal fission parameters appears deceptively simple:

$$\eta = \frac{\bar{\nu}}{1+\alpha} = \frac{\bar{\nu}\sigma_f}{\sigma_a} \qquad (1)$$

Here η is the average number of fission neutrons produced per absorption event, $\bar{\nu}$ is the average number of neutrons produced per fission event, σ_f and σ_a are the microscopic fission and absorption cross sections, and α is the ratio of the capture and fission cross sections. To include ^{252}Cf in the picture, we note that when the $\bar{\nu}$ ratios are measured, it is the ratio of prompt neutrons that is measured. Therefore Eq. 1 becomes

*Work performed under the auspices of the U.S. Department of Energy.

$$\eta = [(\bar{\nu}_p)C_f R_p + (\bar{\nu}_d)_x]\frac{\sigma_f}{\sigma_t - \sigma_s} \approx \frac{(\bar{\nu}_t)C_f R_p\ [1 + (\frac{\bar{\nu}_d}{\bar{\nu}_p})_x - (\frac{\bar{\nu}_d}{\bar{\nu}_p})C_f]}{1 + \alpha}. \quad (2)$$

R_p is the prompt $\bar{\nu}$ ratio, $\nu px/\nu pC_f$ where the subscript x refers to the fissile nucleus in question.

Eq. (2) represents the complexity of the problem somewhat better than does Eq. (1). There are, however, several more complications that are still not represented. The "gated" $\bar{\nu}$ measurements (large liquid scintillators and the boron pile) measure $\bar{\nu}p$ and Rp. The "ungated" measurements (manganese baths) measure $\bar{\nu}_t$. The delayed neutron fractions are determined in separate experiments. Measurements of $\eta, \sigma f, \sigma t$, and σs have been made with monochromatic neutrons, while reactor spectra have been used in measurements of η, α, and fission cross sections and ratios. It is therefore necessary to take into account the relation between "effective" cross sections and the monochromatic quantitites. By the Westcott formalism[2] the relations are defined as

$$\hat{\sigma} = \sigma_{2200}(g + rs)$$

and

$$\hat{\alpha} = \alpha_{2200}\frac{(g + rs)_c}{(g + rs)_f} \quad (3)$$

In implementing the Westcott formalism, it is necessary to know both the shape of the neutron spectrum and the shape of the cross section dependence. The half lives of α- particle emitters plays a role in the fission cross section measurements, if α-particle counting is used to assay the foil. Each experiment has its own peculiar set of systematic problems that must be understood and accurately evaluated.

In view of the complexity of the picture, one might be justified in asking how we know when we have a discrepancy. For example, how do we know there is a discrepancy between $\bar{\nu}$ and η? A high degree of confidence must be established in all of the other parameters in the picture in order to state that there is a discrepancy between these two quantities.

Several attempts have been made to find a "best set" of the thermal fission parameters on the basis of least squares[3-5]. It has usually turned out that a satisfactory fit can be made to most of the data, with the residual error for the whole system assigned to one area that is thereupon declared to be discrepant. When the low $\bar{\nu}$ value from the Boron Pile[6] first appeared, it was at first considered suspect. After two manganese bath measurements[7-8] produced $\bar{\nu}$ values supporting the Boron Pile, the low values became respectable, and the η values were declared discrepant.[9] Intensive reexamination[10-13] of two η experiments[14,15] left the original values essentially unchanged. Suspicions have been cast successively on the α values,[16] the g-values,[5] and the $\bar{\nu}$ ratios.

This game of musical chairs indicates that systematic errors are still present. In that case the least squares approach is of questionable validity. Both the disagreement among measured ^{252}Cf $\bar{\nu}$ values and the difficulties in obtaining a satisfactory least-squares adjustment of the fissile parameters suggest that the $\bar{\nu}$ discrepancy itself is not yet satisfactorily resolved.

CONSEQUENCES OF DATA UNCERTAINTIES

Despite the existence of discrepancies, it is necessary to fit together some sort of data file for use in reactor applications. Difficult decisions must sometimes be made to impose an adequate state of agreement amongst the fission parameters. If calculations with the assembled data set still do not match the performance of a benchmark experiment, adjustments may be made to force agreement. Such adjustments are not without their hazards. An adjustment that matches one critical assembly may not be suitable for another type of reactor, or even for an operating reactor of the same type. Becker et al.[17] have developed a sensitivity analysis system to assess the economic implications of uncertainties in nuclear data and methods for light-water reactors. Their studies indicate that $\bar{\nu}$ is clearly the most sensitive nuclear datum in determining fuel cycle costs. Don Harris[18] has calculated fuel cost sensitivity coefficients for $\bar{\nu}$ in a BWR. In Table I are shown coefficients in terms of fractional cost per fractional change in $\bar{\nu}$ for a single reload at anticipated 1985 costs. At an anticipated cost of $37.8 million per core reload, the investment in $\bar{\nu}$ uncertainty is substantial. Since all $\bar{\nu}$ values are normalized to ^{252}Cf $\bar{\nu}$, the "All $\bar{\nu}$" sensitivity line represents ^{252}Cf $\bar{\nu}$. Becker et al[17] show that even when changes in $\bar{\nu}$ and the fission cross section compensate each other in terms of reproducing k_{eff} for a clean critical experiment, the actual fuel costs for a PWR can be seriously impacted by an uncertainty in $\bar{\nu}$. It is therefore important to obtain the most accurate asssessment possible of $\bar{\nu}$ for all fuel components of a reactor.

PRESENT STATUS OF ^{252}Cf $\bar{\nu}$

At the request of the DOE Nuclear Data Committee, those investigators working on the $\bar{\nu}$ problem in this country have been holding workshops, to exchange information and compare results. A Workshop held Dec. 6, 1977, prior to the last CSEWG meeting, evolved a picture of the current status of $\bar{\nu}$. The descriptions that follow are drawn largely from material presented there. Since this was in fact a Workshop, many of the results were preliminary, and intended only for review and discussion. Therefore the present summary and conclusions must be considered preliminary and subject to change.

Table I

Sensitivity of 1985 BWR Fuel Cycle Cost to $\bar{\nu}$ Value

	Cost Coefficient $\frac{\delta c/c}{\delta\bar{\nu}/\bar{\nu}}$	
Parameter	Assuming Recycle	Assuming throwaway cycle
^{235}U $\bar{\nu}$	-1.41	-1.76
^{238}U $\bar{\nu}$	- .14	- .18
^{239}Pu $\bar{\nu}$	-1.35	-1.70
^{241}Pu $\bar{\nu}$	- .27	- .34
All $\bar{\nu}$	-3.17	-3.95

The value of $\bar{\nu}$ for ^{252}Cf now appears to be on the upswing, with upward revaluations found appropriate for the manganese bath results[7-8], as well as for the Boron Pile. Gwin has obtained a higher $\bar{\nu}$ ratio for ^{255}U than those previously reported. The big news at the $\bar{\nu}$ Workshop, though, was the new large liquid scintillator measurement of ^{252}Cf $\bar{\nu}$ by Spencer at ORNL.

Manganese Bath $\bar{\nu}$ Measurements

The revaluations of the manganese bath $\bar{\nu}$ values are a consequence of an investigation into the systematics of the manganese bath by the present author and others three years ago. To explain the rationale and subsequent developments associated with this investigation, it is necessary to begin with a description of the response of a manganese bath. If a constant-strength neutron source irradiates a manganese bath, the resulting saturated activity produced is given by

$$A_s = Qf\varepsilon(1-L)\ (1-S)\ (1-F) \qquad (4)$$

where A = the saturated activity
Q = the source strength
f = the fraction of neutrons absorbed in the manganese of the bath
ε = the efficiency of the ^{56}Mn detector, in terms of counting rate observed per disintegration in the bath.

L, S, and F are corrections for neutron losses due to leakage, absorption in the source itself and its surroundings, and high-energy (n,p) and (n,α) reactions that may not already be accounted for in the f term.

The fraction absorbed in manganese is given as the ratio of the macroscopic absorption cross section of manganese to that of the whole bath

$$f = \frac{N_{Mn}\ \sigma_{Mn}\ (1 + Grs)_{Mn}}{N_{Mn}\sigma_{Mn}(1 + Grs)_{Mn} + N_H\ \sigma_H + N_S\ \sigma s(1 + Grs) + N_o\sigma_o + \Sigma N_i\sigma_i} \qquad (5)$$

This formulation, originally due to Axton[21], uses the Westcott formalism to correct for the epithermal departures from I/V behavior, principally of manganese. In Eq (5) the Westcott "g" value is unity. The "G" shown is a factor introduced by Axton to take into account the decrease in the effective resonance integral due to resonance self-shielding. The last term in the denominator represents absorption due to impurities in the bath.

The problem with using Eq. 5 directly in deducing neutron source strengths is that the accuracy is limited by the accuracy with which the absorption cross sections are known. Axton further rearranged Eqs. 4 and 5 to give:

$$\frac{\varepsilon(1-L)(1-S)(1-F)}{A_S} = \frac{\sigma_H}{\sigma_{Mn}}\frac{1}{Q}\quad\frac{N_H}{N_{Mn}(1+Grs)} + \frac{1}{Q}\left[1+\frac{\sigma_s}{\sigma_{Mn}(1+Grs)}\right]. \quad (6)$$

In Eq. 6, advantage has been taken of the fact that the oxygen thermal absorption is negligibly small compared to the other absorption terms, and that $N_S = N_{Mn}$. Also at this point the bath impurity content was presumed to be negligible.

Eq. 6 represents a straight line, of slope $\frac{\sigma_H}{\sigma_{Mn}} = \frac{1}{Q}$ and intercept $\frac{1}{Q}\left(1+\frac{\sigma_s}{\sigma_{Mn}(1+Grs)}\right)$. Axton pointed out that varying the concentration of the bath and fitting the data to Eq. 6 allows the source strength to be deduced from the intercept. Fig. 1 shows the operation of this principle in the measurement of the NPL standard Ra-γ-Be source.[21] The use of the intercept is equivalent to extrapolation to zero hydrogen content of the bath, and allows extraction of the source strength without explicitly using the hydrogen-to-manganese cross-section ratio. This ratio can, however, be extracted from the same concentration-dependent data, by dividing the slope by the intercept. In Axton's measurement, he derived a cross-section ratio $\frac{\sigma_H}{\sigma_{Mn}} = 0.024965$.

DeVolpi[22] also used the extrapolation method in determining source strengths, including the ^{252}Cf sources involved in his measurement of $\bar{\nu}$. The effective cross-section ratio derived from his data was 0.02531, which is 1.4% above Axton's value. Another disagreement came in measurements on the standard Ra-γ-Be source NBS-II. DeVolpi's value was about 0.5% higher than Axton's. Moreover, the two experimenters used quite different estimates for the effects of leakage and high energy parasitic absorption in the Mn bath. In view of these points of disagreement, it seemed that there was more than meets the eye in the apparently excellent agreement on the value of $^{252}Cf\,\bar{\nu}$. Axton obtained 3.725 + 0.019,[9] while DeVolpi measured 3.729 + 0.017.[7]

As a tool in sorting out these internal discrepancies in manganese bath measurements we used the concentration-variation technique to determine σ_H/σ_{Mn} for a Bragg beam of energy near 0.018 eV. At this energy leakage is minimized, and the manganese resonance absorption and (n,p) and (n,α) reactions in oxygen and sulphur do not play a part. Bath concentrations were determined by three methods. The gravimetric method consisted of evaporating a sample of the solution to dryness and weighing the dried salt. This is the method Axton had used.[21] The densimetric method consisted of measuring the density of the solution and comparing with a previously prepared density-concentration curve. DeVolpi[24] had used

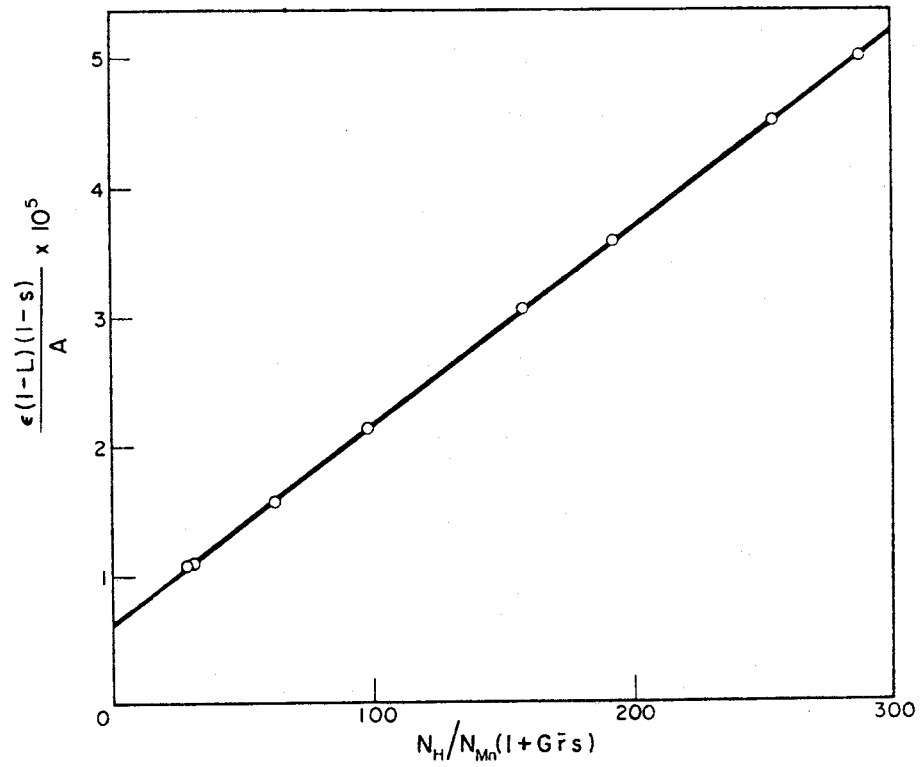

Figure 1. Response of a manganese bath in terms of corrected inverse activity as a function of concentration. From Axton et al.[21]

this method, which Darrell Reeder had originally worked out to monitor the concentration of our bath during the η measurements. The third method was volumetric, and consisted of titrating samples of the solution with an EDTA solution that had previously been calibrated by titrating a standard solution prepared from high purity metallic manganese or indium. We found a systematic difference of roughly 0.2% between the volumetric and gravimetric determinations that appeared to represent the impurity content of the solution. Chemical analyses of the solution confirmed that no titratable ions were present in amounts adequate to disturb the volumetric determination, and that other impurities were present in the amount indicated by the gravimetric-volumetric difference.

The experiment produced a ratio $\sigma_H/\sigma_{Mn} = 0.02503$, a figure later revised to 0.02486 after more detailed consideration of leakage effects. This value agrees better with Axton than with DeVolpi's result. It was suspected that DeVolpi's higher value might have been due to the presence of contaminants in his solution. To a first approximation, a source strength based on the intercept might be relatively unaffected by the presence of impurities, provided the impurity content is a constant fraction of the $MnSO_4$ content. Departure from such linearity could introduce a curvature in the fit, and affect the source strength deduced.

Examination of DeVolpi's data, received by private communication, showed no obvious evidence of such curvature. This need not be too surprising, since DeVolpi's method of evaluating some systematic corrections involved forcing linearity of this curve. Nevertheless there appears to be a substantial degree of compensation among the systematic corrections when the source strength is derived from the intercept of the fitted curve. The σ_H/σ_{Mn} ratio, however,is very sensitive to changes in the estimates of systematic corrections and to errors in the $MnSO_4$ concentration, which might be due to the presence of impurities in the bath. When DeVolpi described his measurements of source strength in his Metrologia article,[22] he correctly derived all the source strengths from the intercepts of the fitted curves as a function of concentration. He also derived an average value of σ_H/σ_{Mn}, and thereafter appears to have used this value in deriving source strengths from weighted averages of measurements (corresponding to the direct use of Eqs. 4 and 5), applying corrections individually, rather than using the intercept from the refitted curve, as in Eq. 6. Between the times of the Metrologia[22] and Physical Review[7] publications, DeVolpi modified his estimates of some of the individual corrections. The changes had only modest effects

on the source strength derived from the intercept of fits to the revised data, but the calculations using σ_H/σ_{Mn} = .02531 showed appreciable fluctuations, because the "effective" value of σ_H/σ_{Mn} had also changed. It was suggested to DeVolpi that his $^{252}Cf\ \bar{\nu}$ value should be based on the source strengths derived from the intercepts of the refitted curves. This would raise his $\bar{\nu}$ value by about half a percent.

DeVolpi responded that this analysis was correct. In a note submitted to the Normalization and Standards Subcommittee of CSEWG, he states that we would be justified in raising his value to 3.747.

It should be emphasized that the only thing involved in this revision of DeVolpi's $\bar{\nu}$ value is a return to the principle of source strength determination from extrapolation to zero hydrogen content, as described in his Metrologia article. A corollary note of interest in that DeVolpi's value for the NBS-II source strength, as derived from the intercept term of Eq. 6, remained essentially unchanged through three iterations in some of the corrections applied.

The reason for the relative invariance of the intercept method is that it is really the ratio of the macroscopic cross-sections, $N_H\sigma_H/N_{Mn}\sigma_{Mn}$, that is important to the analysis. If an error in determining the concentration ratio N_H/N_{Mn} leads to a compensating error in the effective cross section ratio, the derived source strength should be unchanged.

Some of the foregoing comments are pertinent also in considering the Axton measurements. The agreement between his σ_H/σ_{Mn} value and ours appear pretty good at first glance. However, correspondence with Axton concerning the method we devised for monitoring the impurity content of the manganese bath has led to similar studies of his solution. Although he had previously had a spectrographic analysis of his bath indicating the presence of no impurities at greater than 0.01% level,[25] a diffuse end-point in the volumetric analysis indicated the presence of a substantial contaminant content. Axton sent a sample of his solution to us, and Darrell Reeder produced the analysis shown in Table II. Axton countered with the analysis that George H. Risebrow-Smith had produced at NPL. There is rather remarkable agreement between the analyses. Axton continued the analysis to include 32 of the natural elements. He found that small amounts of neutron absorbers, particularly Li, were playing a role. With the new information on contaminants, he reanalyzed the NPL manganese bath source strength measurement, including the Cf-252 data on which the NPL Cf-252 nu-bar value is based. The resulting nu-bar value, according to a recent communication, is 3.743 neuts/fission. This brings Axton into good agreement with DeVolpi's revised value, and with the newer value by Bozorgmanesh. Since all of Axton's source strength measurements share the same manganese bath systematics, this revaluation also implies a rise in the White-Axton value to 3.815.

Table II

Analysis of NPL Manganese Bath

	INEL Analysis		NPL Analysis	
Element	PPM	PPM as Sulfate	PPM	PPM as Sulfate
Mg	1662	8228 *	1653	8188*
Ca	340	1156 *	337	1143*
Zn	205	506 *	117	289*
Na	184	568 +	164	508+
K	45	100 @	274	611++
Co	59	155 *	58.4	154*
Ni	47	124 *	46.7	123*
Cr	13.6	51 @	7.8	29.4*
Cd	3	5.6 @	3.1	5.8*
Fe	50	136 @	80	212 *
Al			27	172.8%
Li			18.7	148 +
B			1	3.2 %
Others				140
Total		11030 PPM		11736 PPM

Impurities from grav/vol ratio: 1.1%

*Atomic absorption
+Flame emission
++Gravimetric
%Colormetric
@Spark source mass spectrometry (semi-quantitative)

In Table III the Axton and DeVolpi results are somewhat arbitrarily given equal weights by assigning equal errors of 0.019, the error Axton quotes[9].

Another measurement of ^{252}Cf $\bar{\nu}$ by the manganese bath method is now in the picture. Hadi Bozorgmanesh[28] used defined solid angle counting, using a solid state detector, to determine the fission rate of a ^{252}Cf source, whose neutron yield was then measured in the U. of Michigan manganese bath. The source strength was not measured directly, but was normalized to an average of the measured values for the source strength of NBS-II.

It is the defined solid angle counting that is the major contribution of this experiment. A previous use of this technique in the White and Axton experiment[27] was attendant with difficulties that led the authors to down-weight the result. Bozorgmanesh took great care to determine the solid angle, and parameterized it by varying both the aperture and the source-aperture distance. Fig. 2 reproduces a diagram from the Bozorgmanesh dissertation,[28] illustrating the consistency in results as the aperture and distance are varied. The Bozorgmanesh result is $\bar{\nu}$ = 3.744 ± 0.023 neuts per fission.

A manganese bath measurement of ^{252}Cf $\bar{\nu}$ by Aleksandrov[29] also used defined solid angle counting. This value does not claim the accuracy of the Bozorgmanesh, Axton, and DeVolpi measurements, but is in excellent agreement with them at 3.747 ± 0.038 neuts/fission.

We have also a manganese bath $\bar{\nu}$ measurement in progress at INEL. The NBS-designed double fission chamber[44] is being used. Calibration of the fission rate is being performed by neutron-fission and fission-fission coincidences, and the neutron yield is measured in the manganese bath used in the measurements. Since concentration variations have not yet begun, results are too preliminary even to quote here. Early indications are that the value may be near the other manganese bath results.

Because of the central role played by standard Ra-γ-Be neutron sources in the Axton and Bozorgmanesh ^{252}Cf $\bar{\nu}$ measurements, and in view of the importance of manganese bath chemistry in these absolute source strength determinations, the ^{252}Cf $\bar{\nu}$ Workshop recommended that NBS-II be remeasured, employing concentration variations and comprehensive determination of the manganese bath chemistry.

Table III

$^{252}Cf\ \bar{\nu}_t$ Summary

	1972 Status[9]	Current Status	Group Ave.
Liquid Scintillator			
Spencer [34]		3.802±0.013	
Boldeman [33,19]	3.744±0.014	3.755±0.016*	
Asplund-Nilsson [37]	3.778±0.060	3.792±0.040*	
Hopkins-Diven [36]	3.770±0.031	3.777±0.031*	3.783±.009
Manganese Bath			
Axton [9]	3.725±0.019	3.743±0.019	
DeVolpi [7]	3.729±0.030	3.747±0.019	
Bozorgmanesh [28]		3.744±0.023	
White, Axton [27]	3.797±0.040	3.815±0.040	
Aleksandrov [29]		3.747±0.036	3.750±.011
Boron Pile			
Colvin [30]	3.713±0.015	3.739±0.021	
Overall Wtd. Ave:	3.735±0.008	3.766±0.007	
Ave:		3.766±0.009	
Without Spencer:			
Wtd. Ave:		3.753±0.008	
Ave:		3.762±0.009	

*Values and errors assigned by Boldeman[19]

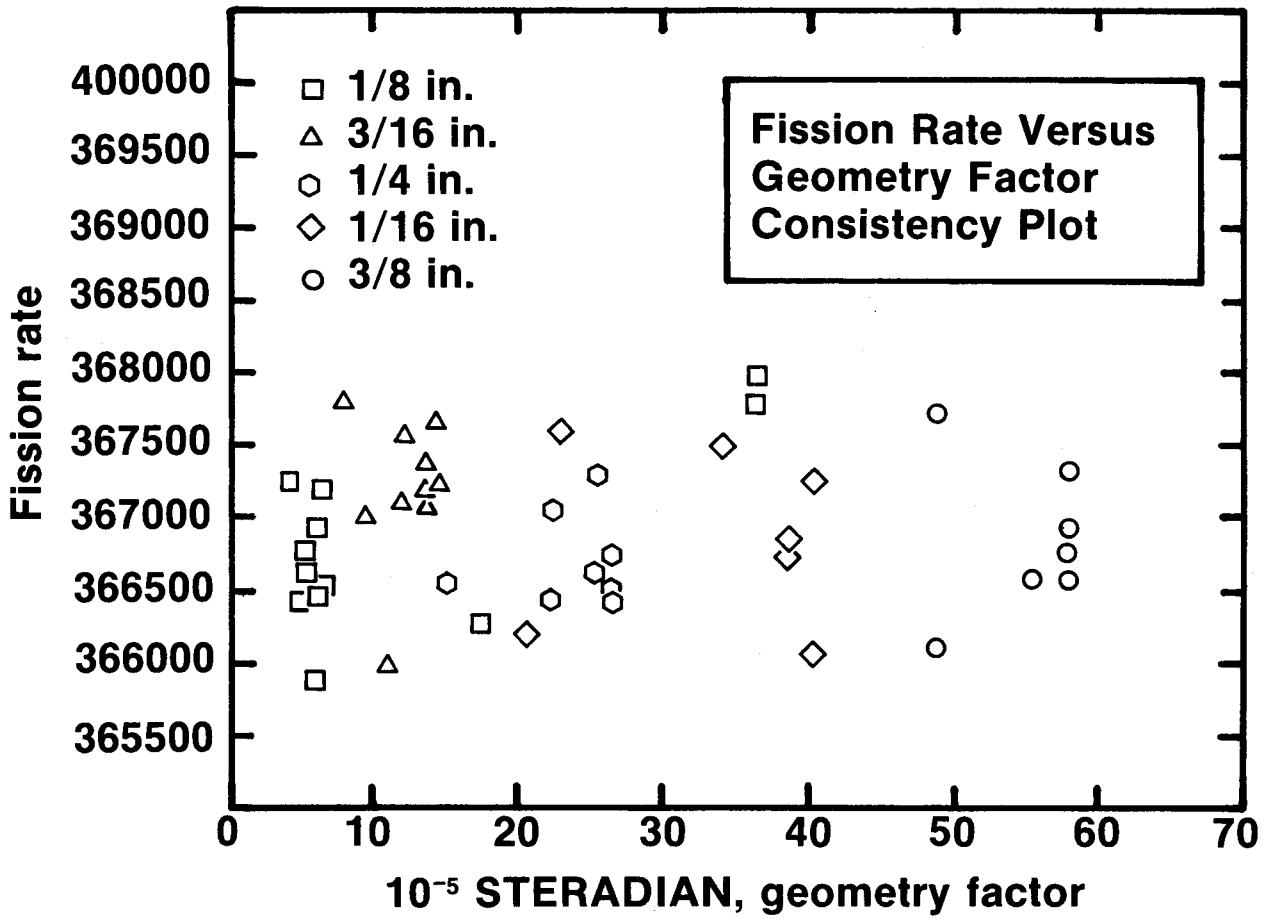

Figure 2. Fission rate versus geometry factor observed by Bozorgmanesh.[28]

Boron Pile

Notable among the evaluational efforts to resolve the $\bar{\nu}$-η discrepancy is the work of the Bettis Atomic Power Laboratory. Using their versatile Monte Carlo code RECAP, Bettis investigators have subjected the manganese bath η measurements of Macklin-DeSaussure[15] and Smith et al[14] to thorough analyses.[11-13] These calculations largely confirmed the original analyses in detail, at least to the extent that no systematic problem was identified to change the η values substantially. In addition to the η analyses, Ullo has modelled three $\bar{\nu}$ experiments with RECAP.[30-31] These are the Boron Pile measurement of Colvin and Sowerby [6] and the liquid scintillator measurements of both Boldeman[33] and Spencer.[34]

For the Boron Pile calculation Ullo obtained from the original authors as complete a description as possible of the experiment, and included great detail in the Monte Carlo model. In particular, the BF_3 counters were correctly described as being made of copper, whereas the transport calculation that was part of the original analysis used aluminum cross-sections to simulate the copper. ENDF/B Version IV cross sections were used throughout the analysis. The Boron Pile efficiency calculated by RECAP is illustrated in Fig. 3. Also shown are the Sn calculation by Carlsen, the experimental calibration points, and the efficiency curve adopted in the original analysis.[6] Axton[9] has also made a Monte Carlo calculation. His curve, as displayed by Boldeman,[19] is also shown in Fig. 3. Agreement in shape is good between the Ullo and Axton calculations, except for the dip in the 8-10 MeV region shown by Ullo. The dip is due to (n,α) reactions in carbon, and has only a modest effect on the Boron Pile measurement. The major difference appears to be in the normalization of the calculated curve to the measured points. Ullo used two different methods of normalization. The first method[30] consisted of normalizing the calculated curve to the calibration measurements at 265 keV and 2.0 MeV. In Fig. 1 the Ullo calculations are shown normalized to the 265 keV point. A weighted average of the two resulting values, $\bar{\nu}_p = 3.733 \pm 0.022$, was then judged to be the best value. Ullo described to the Workshop the use of a second normalization technique, using an overall normalization factor which was a weighted average of the values obtained by comparing calculations to experimental measurements of the efficiency at 0.190, 0.265, and 2.0 MeV. The second method produced a value $\bar{\nu}_p = 3.727 \pm 0.020$. Since the second method represents the more thorough analysis, its result is adopted as the Boron Pile result in the summary of Table III.

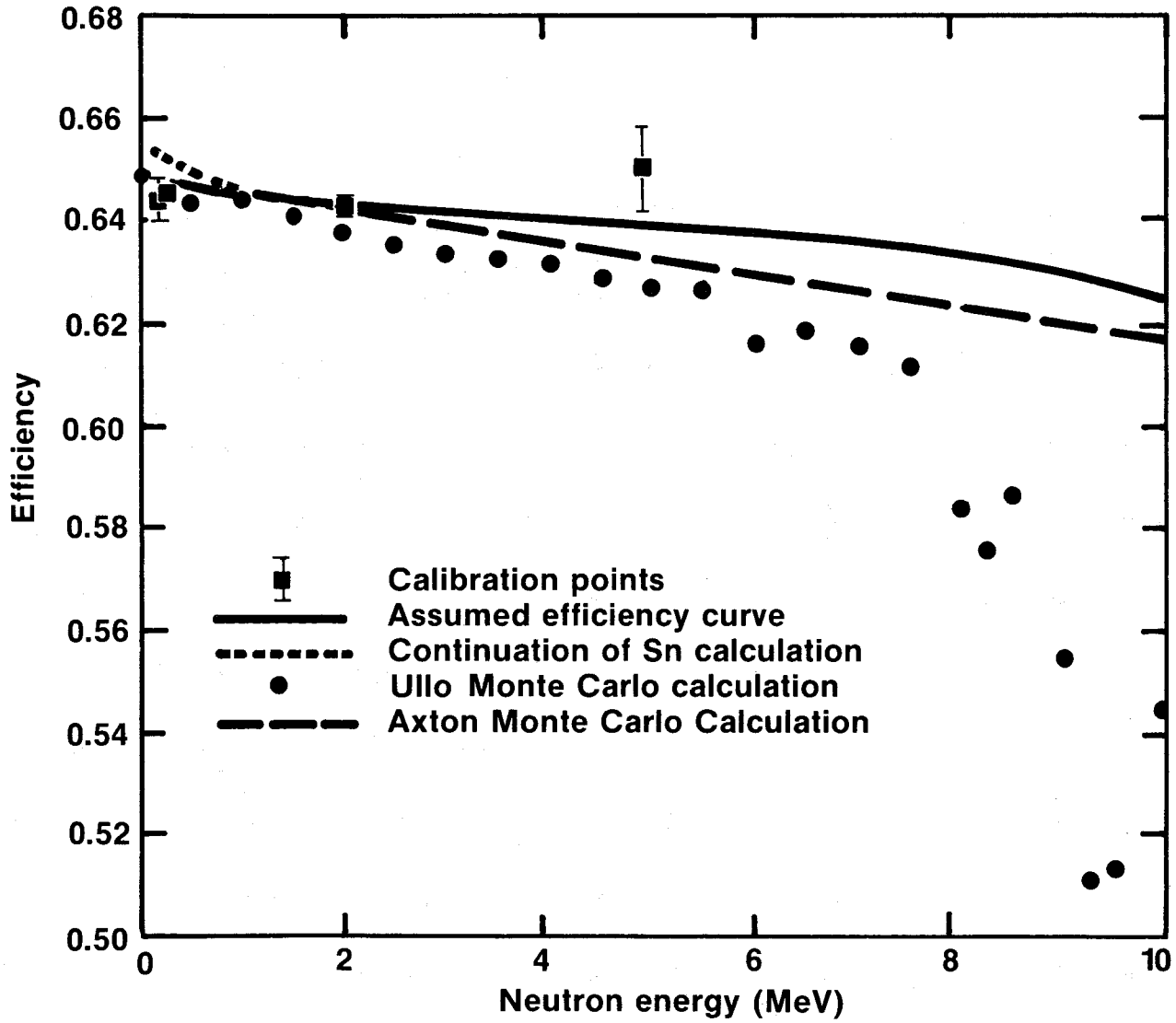

Figure 3. Boron Pile efficiency, comparing the Ullo calculations with the calibration points and the original calculation. The Ullo calculations are normalized to the calibration point at 265 KeV.

LIQUID SCINTILLATOR $\bar{\nu}$ MEASUREMENTS

The big news of the ^{252}Cf $\bar{\nu}$ Workshop was Robert Spencer's description of his measurements of the $\bar{\nu}$ using a large liquid scintillator. Even though the value he presented was preliminary and subject to further investigations, at $\bar{\nu}_p = 3.789 \pm 0.007$ it represents at once the highest value (except for the White-Axton results) and the lowest error assignment of all the $\bar{\nu}$ values. We are faced with something of a paradox here. The "preliminary" nature of the Spencer result suggests that the value is subject to change, while the small error quotation suggests that not much change is to be expected. Despite this ambiguity, one is forced to recognize that this value will dominate any weighted average of $\bar{\nu}$ values in which it is included. Treating the Spencer value is a little like sleeping with a grizzly bear. He tends to take up the whole bed, but he commands enough respect that one hesitates to complain. Moreover, once having noticed him, it is difficult to ignore him.

Spencer's analysis of his scintillator response was performed using the Monte Carlo code DENIS of Poitou and Signarbieux.[35] Ullo has been working closely with Spencer, and has provided a second Monte Carlo analysis using the RECAP code. Ullo's analysis yielded $\bar{\nu}_p = 3.797 \pm 0.010$. The difference between the two values is probably due to differences in the Monte Carlo models used. For example, the RECAP model used ENDF/B-IV cross sections and modeled the photomultiplier tube explicitly. Spencer's analysis used cross sections that came with the DENIS code, and made a separate correction for the effect of the photomultiplier tube. The principal reason for the difference in error estimates is that Spencer ran his Monte Carlo calculation for more histories to obtain better Monte Carlo statistics. In recognition of the difference between the two Monte Carlo calculations, I have entered the Spencer value into the summary of Table III as the average from the two analyses, with the Ullo error estimates combined in quadrature with the difference in the two calculations. The resulting value, with delayed neutrons added, is $\bar{\nu}_t = 3.802 \pm 0.013$. This still leaves the measurement with weight equal to that of all the other three scintillator measurements combined.

The Spencer and Boldeman $\bar{\nu}$ values each overlap errors with the Hopkins-Diven[36] and Asplund-Nilsson[37] values, but do not overlap errors with each other. There thus needs to be a rigorous scrutiny of both experiments to determine whether one or the other is burdened with a latent systematic effect. Such an examination is not in store for this presentation, but a brief comparison of the experiments may be of interest.

Figure 4 shows the Spencer scintillator tank, which has the form of a central cylinder flanked by two truncated cone end sections. The central hole is 13.7 cm in diameter, which allows a fairly large chance for neutron escape. To restrict such escape, Spencer has installed carbon plugs in each end, reducing the escape aperture to 3.8 cm. The overall length of the tank is 114.3 cm. The Boldeman tank is a sphere 76 cm in diameter, with a 7.62 cm through hole. The Boldeman chamber is thus substantially smaller. The central hole is also smaller, but with the smaller tank diameter, the solid angle for escape is similar to that of the Spencer tank before insertion of the graphite plugs. Both scintillators contain gadolinium for neutron absorption, but Spencer's solution has only .22% by weight Gd compared to 0.5% for Boldeman.

Both experiments use accelerator neutrons scattered from hydrogen to calibrate the scintillators. Boldeman used 2 MeV and 16 MeV neutrons, which struck a gaseous hydrogen target, the recoil protons from which were counted by a solid state detector. Spencer uses a scintillator of NE 213 as both scatterer and proton detector. Both experiments utilize the size of the proton pulse, along with knowledge of the incident neutron energy, to deduce the angle and energy of the scattered neutron, which is then detected by the scintillator with its characteristic efficiency. The experimental calibrations cannot cover all possible angles and energies, so they are used to test and normalize the Monte Carlo calculations, which are used to complete the picture of the tank's response. The overall efficiency curves from the Spencer and Boldeman tanks, as a function of neutron energy, are shown in Fig. 5. The difference in high energy response, due to the larger size of the Spencer tank, is readily apparent. The really intriguing feature, though is the falloff in detection efficiency for the Spencer scintillator at low energies. This is due to the finite length of the counting time. Neutrons are counted for 50 μsec after a 500 nsec delay following a fission pulse. The falloff is apparently due to prolonged multiple scattering of the lower energy neutrons in the vicinity of the central hole. They are not captured until after the end of the 50 μsec counting period. This falloff in efficiency, and the question of whether Boldeman's tank should have a similar response, should be the subject of future investigations.

A second difference between the Spencer and Boldeman results is in the assessment of the effects of delayed γ-rays. Spencer has attacked this problem by calculating the invariant "shape parameter" $R = \frac{\sigma_{\bar{\nu}}^2}{\bar{\nu}^2} - \frac{1}{\bar{\nu}}$, [42,43] as a function of scintillator tank efficiency. He observed the behavior depicted in Fig 6. Departures of R from constancy above 82% efficiency were believed to

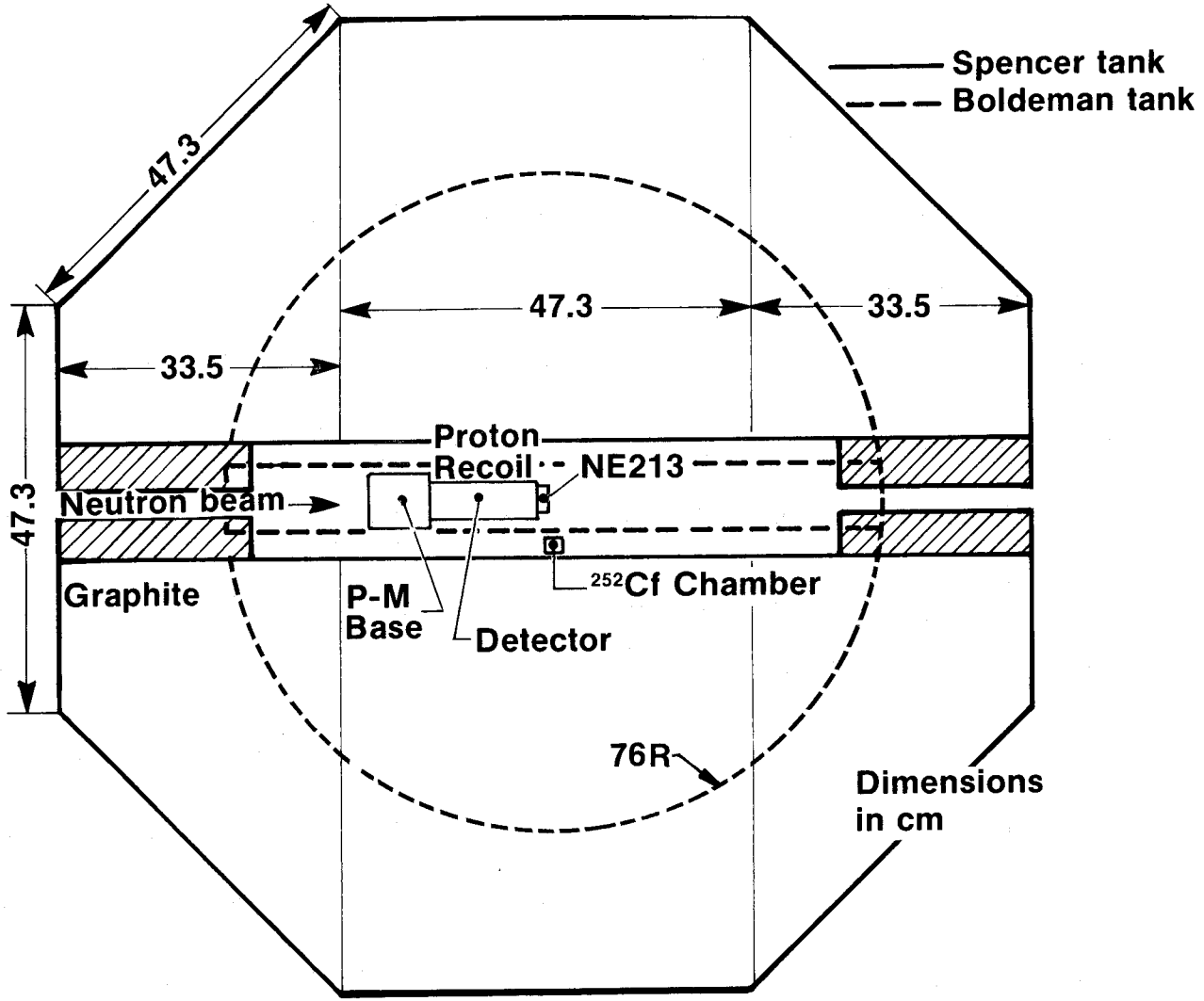

Figure 4. Diagram of the ORNL liquid scintillator tank (solid curve) as in Spencer's ^{252}Cf $\bar{\nu}$ measurement. For comparison of geometries the Boldeman scintillator is shown by dashed lines.

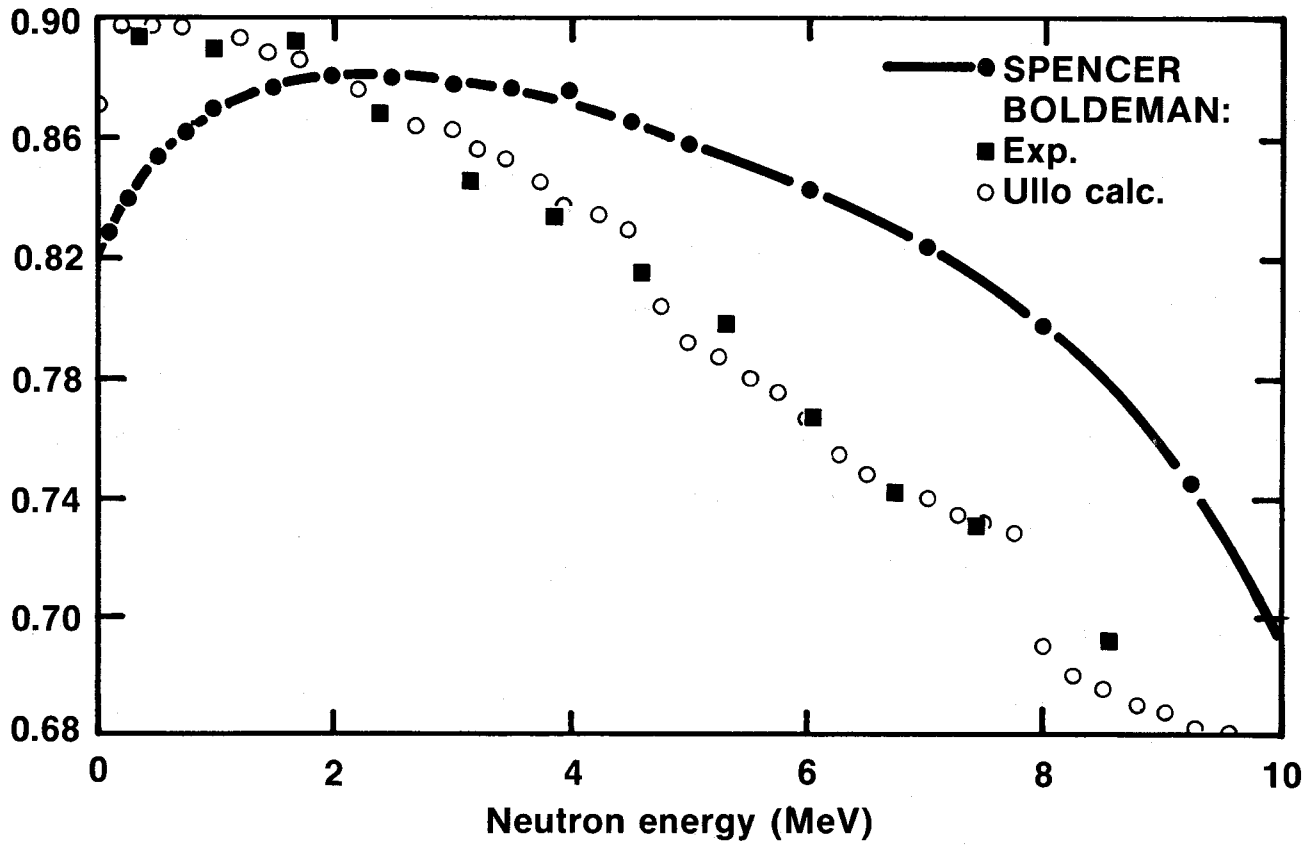

Figure 5. Comparison of the efficiencies of the Spencer and Boldeman scintillator tanks, as calculated by Ullo. The Boldeman experimental normalization points are also shown.

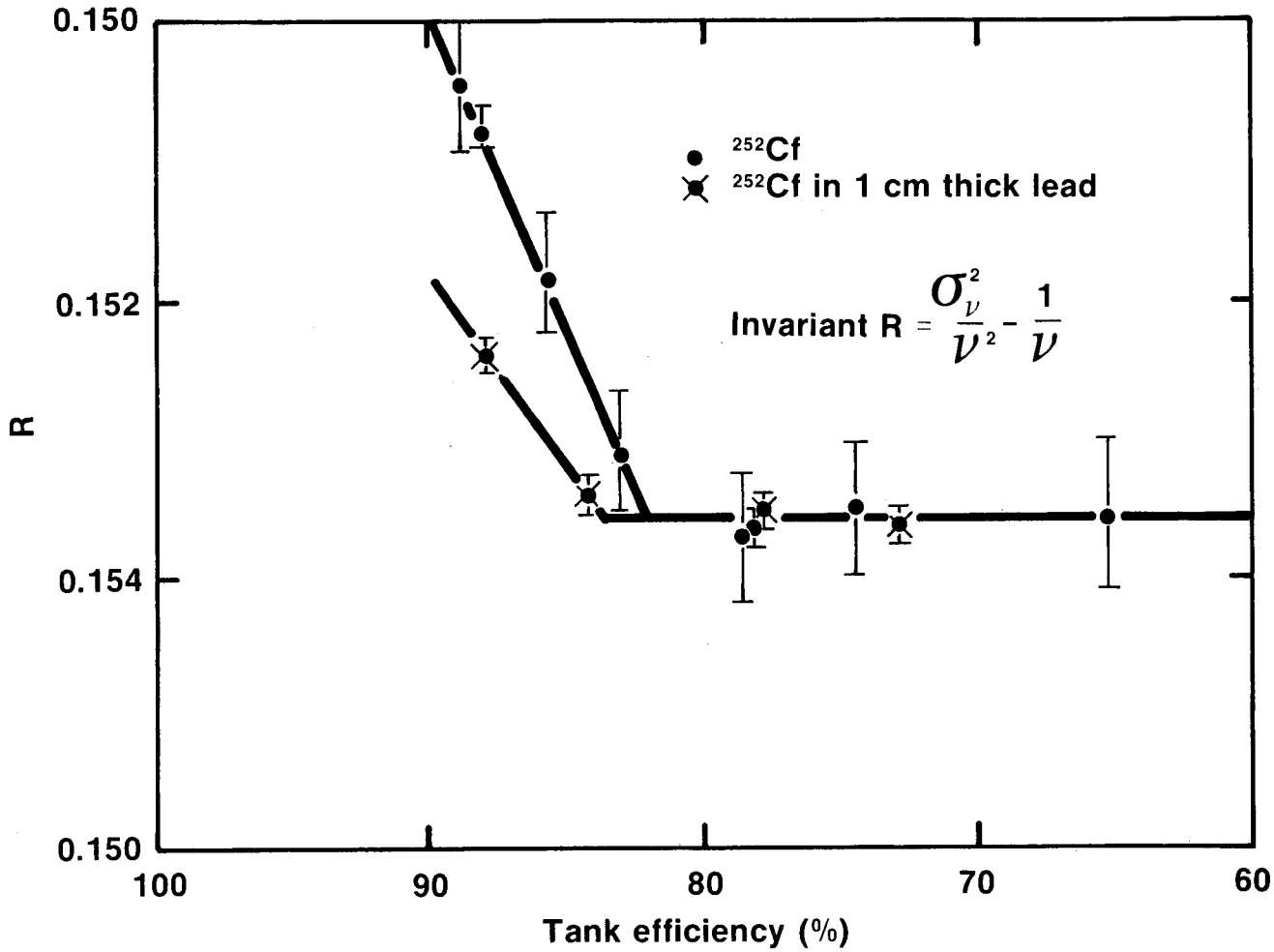

Figure 6. The shape parameter R vs. scintillator efficiency as determined in Spencer's experiment.

represent the effects of the delayed gamma rays. Support for this belief was obtained by repeating the experiment with a lead shield surrounding the fission chamber to suppress the delayed gamma rays. The parameter R dropped sharply in the region of its departure from constancy. Spencer then based his correction for delayed gamma ray effects on the value of the parameter R at his operating point. This gave a correction that was about one-fifth of the value derived by Boldeman's method of measuring the tank γ-ray efficiency with calibrated sources and folding in the characteristics of the delayed gamma rays as compiled by Boldeman.[33] Thus a small part of the difference between the Spencer and Boldeman values may be due to different methods of assessing the effects of delayed gamma rays.

$\bar{\nu}$ Ratio Measurements

Finally I want to mention the $\bar{\nu}_p$ ratio measurements of Gwin. He has measured $\bar{\nu}_p(E)$ for ^{235}U and ^{239}Pu relative to $\bar{\nu}_p$ for ^{252}Cf over the energy range 0.005 eV to 10 MeV, using a multi-section fission chamber in a large liquid scintillator. It is the thermal region we are interested in at the moment. His $\bar{\nu}_p$ ratio for ^{239}Pu agrees with that of Boldeman;[39] but for ^{235}U the $\bar{\nu}_p$ ratio is about 0.8% higher than that of Boldeman. The Boldeman ratios carry the lowest error estimates of all the measurements, and have long dominated the field. In fact Boldeman quotes smaller errors than does Gwin. In terms of error bars and the preponderance of measured values, the odds would seem to be against Gwin. However, Gwin has suggested the possibility of a systematic error in $\bar{\nu}_p$ ratio measurements. In comparing his experiment with Boldeman's, Gwin has noted that in the case of ^{239}Pu, where they agree, they used about the same thickness fission foils, about 0.1 mg/cm^2. For ^{235}U, Gwin again used a foil about 0.1 mg/cm^2. Boldeman used a much thicker foil, whose exact thickness is not clear from his paper, but which may have been near 0.8 mg/cm.^{2} Mather[40] and Asplund-Nilsson[40] have observed a foil thickness effect, but Diven[32] has reportedly looked for such an effect and found none, at least with his experimental setup.

To illustrate how use of a thick foil might affect the $\bar{\nu}_p$ ratio measurements, I will draw on experience with the chamber we are using in our measurement of $\bar{\nu}_t$ for ^{252}Cf. The solid line in Fig. 7 shows the pulse height spectrum observed. Since the fission fragments are not stopped in the chamber, this pulse height distribution is determined mainly by geometrical effects. The peak is due principally to those fragments traveling straight across the chamber, while the shoulder on the high pulse height side is due to those fragments going towards the corners or sides and thus having a longer path length in the gas. The small pulses are due mainly to fragments barely escaping from the deposit, with some contribution from material self-transferred

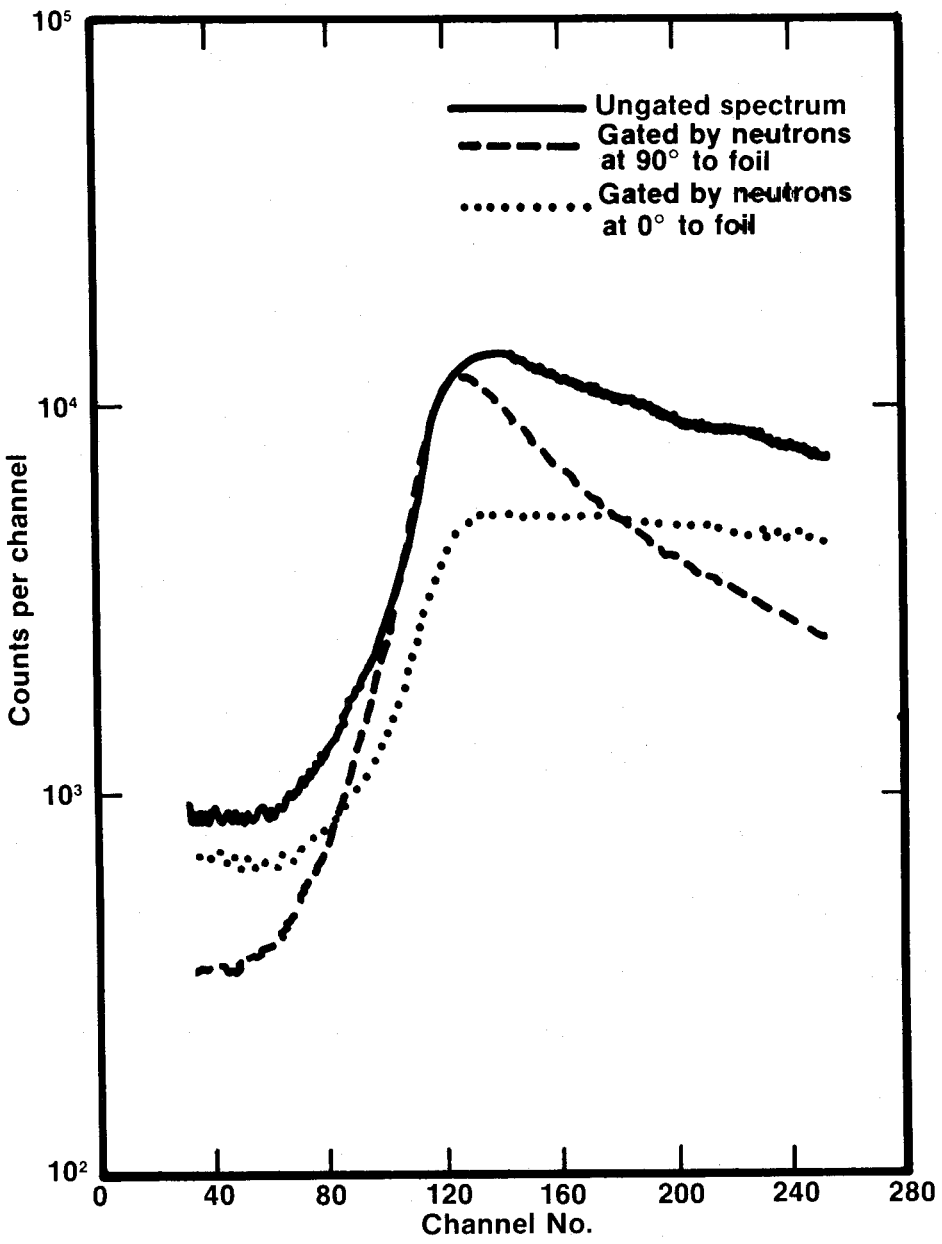

Figure 7. Comparison of ungated fission pulse height spectrum (solid curve) with spectra gated by neutrons observed normal to the foil (dashed curve) and in the plane of the foil (dotted curve).

around the chamber. The fission neutrons are emitted mainly in the direction of fission fragment travel. Thus a spectrum gated by neutrons observed normal to the fission foil appears as the dashed line in Fig. 7. The central peak is predominant, the shoulder is lower, and the valley is deeper. A spectrum gated by neutrons observed in the plane of the foil appears as the dotted curve in Fig. 7. The central peak is attenuated, the shoulder is accentuated, and the valley is higher. This corresponds to fragments travelling at small angles to the plane of the foil, and higher. This is because the small pulses are due mainly to fragments travelling at small angles to the plane of the foil, and barely escaping. A fission chamber biased on the plateau will discriminate against the small pulses below the bias setting, and so against those neutrons emitted in the plane of the foil. It is just those neutrons for which the efficiency of the tank is greatest, as those neutrons emitted normal to the foil have a greater chance of escaping via the through hole. Thus, despite the large solid angle subtended by the scintillator tank, there is a chance for an angular correlation problem in such experiments. Analyses of experiments of the type should include an appraisal of the angular correlation effects, and appropriate corrections should be applied.

Because of the key role played by the $\bar{\nu}$ ratios in the overall $\bar{\nu}$ picture, the Workshop recommended that the Gwin measurements at low energies be repeated, to confirm the existence and magnitude of the foil thickness effect, and extend the measurement to include ^{233}U. They should also include ^{241}Pu.

SUMMARY

With the revaluation of the Boron Pile, the Axton and DeVolpi values, and the addition of the Spencer, Bozorgmanesh, and Aleksandrov results, the ^{252}Cf $\bar{\nu}$ picture currently appears as shown in Table III. For comparison the status as of the 1972 survey[9] is also shown.

An obvious feature of Table III is the excellent agreement existing among the manganese bath values, with the exception of the White-Axton result. The interesting thing about this agreement is the variety of techniques used in the fission assay side of the experiment. DeVolpi used neutron-fission coincidence counting, Axton used a fission-fission coincidence technique, while Bozorgmanesh and Aleksandrov, as well as White, used defined solid angle counting. One is temped to conclude that if a systematic error remains in this group, it is probably in the neutron yeild measurements using the manganese bath. However, a systematic effect that would raise the manganese bath $\bar{\nu}$ values would preferably be one that would not also raise the η values. It

would truly be a reversal of form if the η values were now suddenly to be considered low. Such a prospect could develop, if Spencer's high $\bar{\nu}$ value and Gwin's high $\bar{\nu}$ ratios are both confirmed.

A weighted average of all $\bar{\nu}$ values now yields $\bar{\nu}_t$=3.766±0.008. The weight of the Spencer value, even with the expanded errors given it for Table III, is evident in a comparison with a weighted average without the Spencer value included. This is $\bar{\nu}_t$=3.753+0.009, a shade above the 3.750 value to which Version V* is normalized. Even the higher value is nearly a percent lower than Spencer's value. This is more than two standard deviations, even in terms of the expanded error we have assigned. Thus we still have a ^{252}Cf $\bar{\nu}$ discrepancy to deal with.

Current $\bar{\nu}$ For The Fissile Nuclei

The connection of the current ^{252}Cf $\bar{\nu}$ picture with thermal fissile parameters is illustrated in Table IV. Three values of ^{252}Cf $\bar{\nu}$, the Vintage 1972 weighted average 3.734, the ENDF/B-V value 3.750,* and the overall average from Table III, are combined with different values of the $\bar{\nu}_p$ ratios to produce $\bar{\nu}_t$ values for the fissile nuclei. The $\bar{\nu}_p$ ratios are those of Boldeman's evaluation, Gwin's measurements, and the ENDF/B-V values. These are compared with ν_t values derived from the Smith η values and α from ENDF/B-V. For ^{235}U the η-ν discrepancy appears to have shrunk to tolerable dimensions if Gwin's $\bar{\nu}_p$ ratio is used, along with a ^{252}Cf $\bar{\nu}$ value near 3.750. The same can be said of ^{239}Pu. ^{233}U and ^{241}Pu require either a higher $\bar{\nu}$ ratio or a higher value of ^{252}Cf $\bar{\nu}$. If the foil thickness effect described above is a determining factor, higher $\bar{\nu}$ ratios may be in order for these nuclei. Boldeman's foils in these cases were three to four times thicker than his ^{239}Pu foil, though not as thick as the his ^{235}U foil.

CONCLUSIONS

Substantial progress has been made in the resolution of the $\bar{\nu}$-η discrepancy. The revaluation of manganese bath values, along with the appearance of a new high ^{252}Cf $\bar{\nu}$ value and the prospect of higher $\bar{\nu}$ ratios, now allow estimates of $\bar{\nu}$ for the fissile nuclei in comfortable agreement with those derived from η and α values. The Spencer $\bar{\nu}$ measurement should be vigorously pursued to produce a final value, and identify the reason for the difference between the Spencer and Boldeman values. Of equal importance is the need to confirm the existence of a foil thickness effect in the ratio measurements, and extend the study of this effect to

*The ENDF/B-V values used in this paper were from a preliminary, unreleased file. At the CSEWG meeting which followed this Seminar, the decision was made to base the ENDF/B-V $\bar{\nu}$ values on ^{252}Cf $\bar{\nu}_t$=3.766.

Table IV

Status of $\bar{\nu}$ for the Fissile Nuclei

Nucleus	R_p	R_t	$\bar{\nu}_t$, assuming ^{252}Cf $\bar{\nu}$ =: 3.734	3.750	3.766	$\bar{\nu}_t$ from $\bar{\nu}_t = \eta(S)^{(1+\alpha)}(V)$
^{233}U	0.6587 ± 0.0013 (B)	.6590	2.461	2.471	2.482	2.295 x 1.0866 = 2.494
	0.6666 (V)	.6669	2.474	2.501	2.512	
^{235}U	0.6386 ± 0.0010 (B)	.6415	2.395	2.406	2.416	
	0.6428 (V)	.6458	2.411	2.422	2.432	2.081 x 1.1686 = 2.432
	0.6441 ± 0.0019 (G)	.6471	2.416	2.427	2.437	
^{239}Pu	0.7647 ± 0.0018 (B)	.7647	2.855	2.868	2.880	
	0.7680 (V)	.7680	2.868	2.880	2.892	2.110 x 1.3643 = 2.879
	0.765 ± 0.003 (G)	.7650	2.857	2.869	2.881	
^{241}Pu	0.7769 ± 0.0018 (B)	.7794	2.910	2.923	2.935	2.165 x 1.3635 = 2.952
	0.7623 (V)	.7647	2.855	2.868	2.880	

(B) Boldeman [39]
(G) Gwin [38]
(V) ENDF/B, Vers. V (Preliminary)
(S) Smith [14]

^{233}U and ^{241}Pu, as well as ^{235}U. These results, together with a final value from the INEL manganese bath measurement, should allow the $\bar{\nu}$-n discrepancy to be laid comfortably to rest --perhaps -- until reactor designers begin to demand accuracies to 0.1%.

ACKNOWLEDGMENT

The author is indebted to the participants of the ^{252}Cf $\bar{\nu}$ Workshop for their contributions to this summary, and for their permission to use unpublished data. Those contributing descriptions of recent work to the Workshop included, in addition to the present author, V. Spiegel, G. F. Knoll, J. J. Ullo, R. R. Spencer, R. Gwin, and A. DeVolpi (who submitted his contribution in absentia.) In addition, special acknowledgment is due to E. J. Axton, for a large volume of correspondence relative to manganese bath effects.

REFERENCES

1. H.J.C. Kouts, Proc. Conf. Nuclear Cross Sections and Technology, Vol. 1, p.3, NBS Special Publication 425. Vol. 1 (1975).
2. C.H. Westcott, Effective Cross Section Values for Well-Moderated Thermal Reactor Spectra, CRRP-960 (1960).
3. C.H. Westcott et al, Atomic Energy Review 3, 2 (1965)
4. G.C. Hanna et al, Atomic Energy Review 7, No. 4, 2 (1969)
5. H.D. Lemmel, Proc. Conf. Nuclear Cross Section and Technology Vol. 1, 286 (1975).
6. D.W. Colvin and M.G. Sowerby, in Physics and Chemistry of Fission (Proc. Symp. Salzberg, 1965) Vol 2, p.25, IAEA, Vienna (1965).
7. A. Devolpi and K.G. Porges, Phys Rev C1, 683 (1970).
8. E. J. Axton et, J. Nucl. Energy A/B 23, 457 (1969).
9. E.J. Axton, Proc. IAEA Panel Neutron Standard Reference Data, p. 261, (1972).
10. J.R. Smith, Proc. Conf. Nuclear Cross Sections and Technology, Vol 1, p. 262 (1975.
11. J.A. Mitchell and C.J. Emert, Proc. 3rd Conf. Neutron Cross Sections and Technology, Vol 2, 605 (1971).
12. J.J. Ullo and M. Goldsmith, Nucl Sci and Eng. 60, 239 (1976)
13. M. Goldsmith and J.J. Ullo, Nucl Sci and Eng. 60, 251 (1976)
14. J.R. Smith, S.D. Reeder and R.G. Fluharty, AEC Report IDO-17083 (1966). Also Proc. Conf. Nuclear Cross Sections and Technology, Vol. 1 262 (1975).
15. R.L. Macklin et al, Nucl Sci and Eng 8, 210 (1976).

16. B.R. Leonard, Jr., Proc. Conf. Nuclear Cross Section and Technology, Vol 1, 281 (1975).
17. M. Becker et al, Trans. Am. Nucl. Soc. 24, 216 (1976).
18. D.R. Harris, private communication.
19. J.W. Boldeman, in Neutron Standards and Applications, p.182, NBS Special Publication 493 (1977).
20. J.R. Smith et al., in Report TREE-1116, p. 158 (1977)
21. E.J. Axton, P.Cross, and J.C. Robertson, J. Nucl Energy Parts A/B, 19, 409 (1965).
22. A. DeVolpi and K.G. Porges, Metrologia 5, 128 (1969).
23. A. DeVolpi, J. Nucl. Energy 26, 75 (1972).
24. A. DeVolpi, R.J. Armani, and K.G. Porges, J. Nucl Energy Parts A/B, 19, 597 (1965).
25. E.J. Axton, Private Communication.
26. R.H. Noyce et al, J. Nucl. Energy A/B 17, 213 (1963).
27. P.H. White and E.J. Axton, J. Nucl. Energy 22, 73 (1968).
28. H. Bozorgmanesh, Absolute Measurement of the Number of Neutrons per Spontaneous Fission of Californium-252, Ph.D. Dissertation, U. Michigan (1977).
29. B.M. Aleksandrov et al, 1975 Kiev Conf. Vol 5, p. 166.
30. J. J. Ullo, Report WAPD-TM-1287, (Aug 1977).
31. J.J. Ullo, Report WAPD-TM-1232 (Nov 1976).
32. B. C. Diven, Private Communication to J.W. Boldeman.
33. J.W. Boldeman, Nucl Sci and Eng 55, 188 (1974).
34. R.R. Spencer, private communication to ^{252}Cf $\bar{\nu}$ Workshop, Dec 1977.
35. J. Poitou and C. Signarbieux, Nucl. Inst. Meth 114, 113 (1974)
36. J.C. Hopkins and B.C. Diven, Nucl Phys. 48, 433 (1963).
37. I. Asplund-Nilsson, H. Condé, and N. Starfelt, Nucl Sci and Eng. 16, 124 (1963).
38. R. Gwin et al, Measurements of the Average Number of Prompt Neutrons Per Fission of ^{239}Pu and ^{235}U, Report ORNL/TM-6246 (1978)
39. J.W. Boldeman and A.W. Dalton, AAEC/E172 (1967).
40. P.S. Mather, P. Fieldhouse, and A. Moat, Phys Rev 133, B1403 (1964).
41. I. Asplund-Nilsson, H. Conde, and N. Starfelt, Nucl. Sci. and Eng. 20, 527 (1964).
42. B.C. Diven et al, Phys Rev 101, 1012 (1956).
43. C. Signarbieux et al, Nucl Instr Meth 95, (1971).
44. J.A. Grundl et al, Nucl. Tech. 25, 237 (1975).

Section 6

A REVIEW OF PLUTONIUM EXPERIMENTS

A Review of Plutonium Experiments

R. Sher and J. Adir*
Department of Mechanical Engineering
Stanford University

I. INTRODUCTION

This paper reviews a number of thermal plutonium-fueled experiments, many of which are being proposed as benchmarks. Recently, U. Jenquin (BNWL) has supplied the data-testing subcommittee of CSEWG with detailed descriptions of 41 plutonium experiments [1], referred to hereafter as CSEWG benchmarks. Many of these are taken from larger sets of measurements, and in addition there exist some other experiments not included in his compilation. The experiments include homogeneous solutions of plutonium nitrate in water, homogeneous mixtures of PuO_2 and polystyrene, H_2O-moderated lattices of Aℓ-Pu rods with three different Pu contents, and two extensive sets of H_2O-moderated lattices with mixed-oxide fuel rods, one done at BNWL and the other at Belgonucléaire.

In contrast with uranium benchmarks, comparatively few of these plutonium experiments have measured reaction rate parameters, so the main emphasis will be on measurements of criticality and calculations of the eigenvalue. We have chosen to restrict ourselves to bare or completely reflected systems, so that we do not include, for example, many experiments in which critical loadings of partially reflected cylinders were obtained. We also restrict ourselves to reasonably well-thermalized systems. Tables 1-13 summarize the experiments covered in this paper.

II. EXPERIMENTAL DESCRIPTIONS

1. Homogeneous Plutonium Nitrate Solutions

References [2] and [3] describe a series of homogeneous plutonium nitrate solution experiments in partially reflected cylinders and bare and completely reflected 0.05"-thick stainless steel spheres. The main purpose of these experiments was to determine critical safety. Diameters ranged from 11 to 15 inches for the reflected spheres (water reflection at least 30 cm (12")), and were 16 or 18 inches for the bare spheres. ^{240}Pu weight percentages ranged from 0.54 to 4.6% (with uncertainties of ± 7% of these values). Critical concentrations were obtained as functions of size, ^{240}Pu percentage and nitrate ion concentration. CSEWG benchmark experiments 2, 3, 4, 14 and 15 are taken from these measurements [1]. Table 1 gives pertinent details on these experiments. It should be noted

*Permanent address: Dept. of Theoretical Physics, Hebrew University, Jerusalem, Israel.

Table 1

$(PuNO_3)_4$ Solutions

Composition of Solution (atoms/cm^3)	Benchmark				
	2	3	4	14	15
^{239}Pu x 10^{19} at./cm^3	41.307	6.6004	8.2232	5.848	6.038
^{240}Pu x 10^{18} "	19.752	0.35692	3.9321	2.79	2.90
^{241}Pu x 10^{17} "	13.251	--	2.6356	1.9	1.9
^{242}Pu x 10^{15} "	24.899	--	5.3567	5.0	5.0
N x 10^{20} "	47.224	7.5114	6.4132	5.633	5.824
O x 10^{22} "	3.9764	3.4514	3.4536	3.435	3.432
H x 10^{22} "	5.4182	6.5006	6.5520	6.561	6.542
Fe x 10^{17} "	35.612	15.457	6.9650	5.0	5.1
Solution Density (kg/m^3)	1429±5.72	1069.2±0.3	1076±4.3	1060±4	1060±4
Plutonium Density "	172.3±0.86	26.3±0.3	34.3±0.2	24.4±0.1	25.2±0.1
Excess Nitrate Molarity	4.96±0.12	0.806±0.009	0.49±0.02	0.53±0.01	0.55±0.02
H/Pu Atom Ratio	124.8±0.9	979.6±9.9	758.0±0.2	1067±7	1031±7
Thickness of Vessel Wall, mm	1.22	1.27	1.22	1.22	3.25
Composition of Vessel Wall					
Fe x 10^{22} at/cm^3	6.331	6.175	6.331	6.331	6.331
Cr x 10^{22} "	1.654	1.658	1.654	1.654	1.654
Ni x 10^{21} "	6.510	8.158	6.510	6.510	6.510
Composition of Reflector	(none)	(H_2O)	(same as vessel wall)	(H_2O)	(H_2O)
H x 10^{22} at/cm^3	0	6.663	0	6.668	6.668
O x 10^{22} "	0	3.332	0	3.334	3.334
Thickness of reflector, mm	0	$\geq$ 300 mm	6.604	$\sim$ 300 mm	$\sim$ 300 mm
Critical radius, cm	19.32	17.78	19.32	19.32	19.32

that experiments 2 and 4 are identical except that experiment 4 has an extra 6.6 mm of steel added to the vessel wall; a similar situation holds for experiments 14 and 15 (both are water reflected, but 15 has an extra-thick steel wall).

The experiments reported in reference [2] do not include data for ^{241}Pu concentrations. The 4.6% ^{240}Pu used in reference [3] contains about 0.3% ^{241}Pu. The ^{241}Pu content in Benchmark 3 (0.54% ^{240}Pu) is presumably negligible, but for the higher ^{240}Pu experiments in ref. [1], it is unaccounted for.

The stated error in critical masses in the experiments of ref. [2] is about 1.5%. The volume was measured to about 0.3%, so that the critical plutonium concentrations are also known to about 1.5%. The stated uncertainties in the experiments of ref. [3] are slightly smaller, of the order of 1%. It should be noted that the water concentration in both cases was obtained by measuring the specific gravity of the solution and subtracting all other components; it was therefore originally stated with an error of ± 5%. The atomic densities given in the CSEWG benchmark descriptions of these experiments, however, show somewhat smaller uncertainties, generally of the order of 0.5% or less.

Benchmark 7 [1] is an unreflected cylinder (except for the tank wall) done in the U. K. The fuel was $Pu(NO_3)_4$ in aqueous solution; the ^{240}Pu content was 13.8%. There was an air space of unknown height above the solution.

2. Homogeneous PuO_2 - Polystyrene Assemblies

References [4] and [5] report experiments with homogeneous mixtures of PuO_2 and polystyrene $(C_8H_8)_n$, bare and completely reflected with Plexiglas. ^{240}Pu enrichments were 2.2%, 8%, and 18.35%. H/Pu ratios were 15.1 and 49.6. One bare and one reflected assembly are listed together in ref. [1] as CSEWG Benchmark #5; other assemblies are listed as Benchmark #8.

For these experiments, rectangular parallelepiped compacts of the PuO_2 - polystyrene mixture were fabricated and stacked into rectangular prisms. The compacts were fabricated by pressing 100-mesh polystyrene and PuO_2; maximum particle sizes for both are stated to be 150 microns, but most particles were considerably smaller. The compacts were coated with 0.001-inch-thick aluminum paint and covered with 0.010-inch-thick rubberized plastic. The effects of the plastic were determined in one bare assembly of each series by inserting rubberized plastic shims between the compacts and extrapolating the results to zero thickness.

Table 2 gives details of composition and sizes for these experiments. It should be noted that the bare assembly with H/Pu = 49.6, ^{240}Pu = 18.35%, included some compacts with H/Pu = 5, which probably makes it a somewhat less desirable candidate as a benchmark experiment.

Table 2

Homogeneous PuO_2-Polystyrene Assemblies

	Benchmark						
	5		8				
Fuel composition:							
^{238}Pu x 10^{18} at/cm^3	---		2.123				
^{239}Pu x 10^{21} "	2.756		0.6996				
^{240}Pu x 10^{20} "	0.6172		1.700				
^{241}Pu x 10^{18} "	3.010		39.36				
^{242}Pu x 10^{19} "	---		1.044				
^{241}Am x 10^{18} "	---		7.272				
H x 10^{22} "	4.260		4.573				
O x 10^{22} "	0.5642		0.2095				
C x 10^{22} "	4.260		4.502				
Fuel density, kg/m^3	2190.9 ± 26.4		1399.4 ± 12.9				
Plutonium density, kg/m^3	1120 ± 20		366.3 ± 3.8				
H/Pu atom ratio	15.1		49.62 ± 0.65				49.62*
Particle sizes, μm, max:							
PuO_2	150		1.2				1.2
Polystyrene	150		150				150
Composition of reflector (plexiglas)		(Bare)					(Bare)
H x 10^{22} at/cm^3	5.666		5.666				
C x 10^{22} "	3.570		3.570				
O x 10^{22} "	1.428		1.428				
Reflector density, kg/m^3	1185	0	1185				0
Reflector thickness, cm	15	0	15				0
Critical dimensions, mm:							
L	230.1	306.8	407.2	509.0	610.8	610.8	458.1*
W	230.1	306.8	407.2	509.0	509.0	610.8	407.12*
H	201.2 ± 1.8	344.9 ± 5.1	235.8	186.8	174.8	163.5	491.19*
Composition of clad							
H 4.489 x 10^{22} at/cm^3							
C 3.111 x 10^{22} "							
Cl 7.240 x 10^{21} "							
Clad density 1120 kg/m^3							
Clad thickness 0.18 mm							

*Bare assembly had some H/Pu = 5 material.

3. Heterogeneous Lattices - Pu-Aℓ Fuel Elements

References [6-11] describe a series of experiments utilizing Aℓ-Pu fuel rods with diameters 1.4 cm, H_2O moderated. The clad was Zircaloy-2. The first series of measurements used 1.8% Pu (6% ^{240}Pu) with active fuel length 111.33 cm; the second series used 2% Pu (16% ^{240}Pu) with active fuel length 91.44 cm, and the third series utilized 5% Pu (5% ^{240}Pu), active length 61 cm. Various triangular lattice spacings were employed. The lattices were fully reflected with H_2O. One of the 5% Pu lattices was also measured with borated H_2O (100 and 285 ppm). Critical loadings were measured by critical approach techniques, with up to 96% of the critical mass loaded in as nearly a cylindrical core shape as possible. The critical loadings were determined to about ± 1%. Reflector savings and material bucklings were obtained from exponential experiments at about 50% critical loading. These lattices consitute Benchmarks 16-26 [1]. Tables 3-5 give pertinent details.

It should be noted that in the original measurements on these systems, the rods were surrounded with lucite sleeves. It was originally assumed that the lucite was equivalent to the water it displaced. At a later date, some of the lattices were remeasured without the lucite and the critical loadings were found to change [6]. Some of this change was attributed to possible voids between the lucite sleeves and the rods, while part of it may also have been due to the decay of ^{241}Pu between the original measurements and the later ones. The more recent data are used where available; it would probably be best not to use any of the experiments in which the lucite was present for benchmark purposes.

4. PuO_2 - H_2O Moderated Lattices

Two sets of lattice measurements employing mixed-oxide fuel rods in water-moderated lattices are reported in references [12-15]. One is a series done at BNWL [12-14] and is listed in the Benchmark Compilation as #27-41. The other set was done by Belgonucléaire at the Venus critical facility at Mol [15].

BNWL Lattices. Benchmarks 27-41 used three fuel compositions. They were UO_2 - 2 w/o PuO_2 with 8% ^{240}Pu; UO_2 - 2 w/o PuO_2 with 24% ^{240}Pu; and UO_2 - 4 w/o PuO_2 with 18% ^{240}Pu. All fuel rods were 1.4 cm diameter. For each fuel, critical loadings at three different lattice spacings were determined; in some cases the water was borated. With the first of the above-mentioned fuels, both critical approach and critical experiments were performed, but with different lattice spacings in the two cases. The 18% ^{240}Pu and 24% ^{240}Pu lattices were measured only by critical approach techniques. Other fuel compositions were also utilized, containing 1.5% PuO_2 in depleted uranium (0.16 at. % ^{235}U, $\sim$ 8% ^{240}Pu) and 2% PuO_2 in natural uranium (16% ^{240}Pu); Tables 6-11 show the critical loadings of these lattices.

Table 3

1.8% Pu-Aℓ Rod Lattices

Fuel length 111.33 cm			
Fuel Composition:			
^{238}Pu	x 10^{16}	at/cm^3	1.4
^{239}Pu	x 10^{20}	"	1.195
^{240}Pu	x 10^{18}	"	7.07
^{241}Pu	x 10^{17}	"	3.58
^{242}Pu	x 10^{16}	"	1.8
^{241}Am	x 10^{17}	"	2.72
Aℓ	x 10^{22}	"	5.876
Ni	x 10^{20}	"	4.48
Fe	x 10^{20}	"	1.43
Si	x 10^{20}	"	4.01
Void thickness, cm			0.0064
Clad thickness, cm			0.0762
Clad composition (Zircaloy-2):			
Zr	x 10^{22}	at/cm^3	4.226
Sn	x 10^{20}	"	4.465
Fe	x 10^{19}	"	9.138
Cr	x 10^{19}	"	6.795
Ni	x 10^{19}	"	3.343
Moderator composition:			
H	x 10^{22}	"	6.671
O	x 10^{22}	"	3.336

	Benchmark		
	16	17	18
Lattice pitch, cm	1.905	2.159	2.362
H/Pu atom ratio	632	1003	1333
Critical number of rods	541 ± 1	486 ± 2	560 ± 2

Table 4

2% Pu-Aℓ Rod Lattices

Fuel length 91.44 cm			
Fuel composition:			
^{238}Pu	x 10^{16} at/cm^3	2	
^{239}Pu	x 10^{20} "	1.125	
^{240}Pu	x 10^{19} "	2.276	
^{241}Pu	x 10^{18} "	2.11	
^{242}Pu	x 10^{17} "	2.7	
^{241}Am	x 10^{18} "	1.21	
Aℓ	x 10^{22} "	5.86	
Ni	x 10^{20} "	4.50	
Fe	x 10^{19} "	8.71	
Void thickness, cm		0.0064	
Clad thickness, cm		0.0762	
Clad composition (Zircaloy-2)		See Table 3	
Moderator composition:			
H	x 10^{22} at/cm^3	6.671	
O	x 10^{22} "	3.336	
		Benchmark	
		19	20	21
Lattice pitch, cm		1.905	2.159	2.362
H/Pu atom ratio		583	926	1230
Critical number of rods		861 ± 1	826 ± 1	1115 ± 5

Table 5

5% Pu-Aℓ Rod Lattices

Fuel length 61 cm					
Fuel composition:					
^{239}Pu x 10^{20} at/cm^3	3.384				
^{240}Pu x 10^{19} "	1.96				
^{241}Pu x 10^{17} "	8.8				
^{242}Pu x 10^{17} "	1.0				
^{241}Am x 10^{17} "	5.8				
Aℓ x 10^{22} "	5.87				
Ni x 10^{20} "	4.47				
Fe x 10^{20} "	1.40				
Si x 10^{20} "	4.02				
Void thickness, cm	0.0064				
Clad thickness, cm	0.0762				
Clad composition (Zircaloy-2)	See Table 3				
	Benchmark				
Moderator composition:	22	23	24	25	26
H x 10^{22} "	6.671	6.671	6.671	6.671	6.671
O x 10^{22} "	3.336	3.336	3.336	3.336	3.336
B x 10^{18} "	0	0	0	5.558	15.84
Lattice pitch, cm	2.159	2.667	3.302	2.667	2.667
H/Pu atom ratio	355	666	1148	666	666
Critical No. of rods	220.7±0.2	167.3±0.1	214.9±0.4	209.0±0.2	288.0±1.2

Table 6

UO_2-2% PuO_2 Rod Lattices

Fuel length 91.4 cm			
Fuel diameter 1.4 cm			
T_{H_2O} = 22°C			
Fuel composition:			
^{235}U	x 10^{20} at/cm^3	1.504	
^{238}U	x 10^{22} "	2.073	
^{238}Pu	x 10^{16} "	4	
^{239}Pu	x 10^{20} "	3.974	
^{240}Pu	x 10^{19} "	3.344	
^{241}Pu	x 10^{18} "	2.64	
^{242}Pu	x 10^{17} "	1.2	
^{241}Am	x 10^{17} "	4.7	
O	x 10^{22} "	4.401	
Clad thickness, cm		0.0762	
Clad composition (Zircaloy-2)		See Table 3	
Moderator composition:			
H	x 10^{22} at/cm^3	6.671	
O	x 10^{22} "	3.336	
		Benchmark	
		27	28	29
Lattice pitch, cm		2.032	2.667	3.520
H/Pu atom ratio		238	554	1113
Critical no. of rods		319.7 ± 0.1	152.1 ± 0.2	179.5 ± 0.2

Mean PuO_2 particle diameter, 25 μm.

Table 7

UO_2-2% PuO_2 Rod Lattices

(See Table 6 for fuel rod dimensions and composition of fuel* and clad.)

	Benchmark					
Moderator composition	30	31	32	33	34	35
H x 10^{22} at/cm^3	6.671	6.671	6.671	6.671	6.671	6.671
O x 10^{22} "	3.336	3.336	3.336	3.336	3.336	3.336
B x 10^{16} "	195 ± 0.6	3826.7 ± 11	22.79 ± 1.2	6077.7 ± 11	33.35 ± 0.55	4268.5 ± 11
Lattice pitch, cm	1.778	1.778	2.209	2.209	2.514	2.514
H/Pu atom ratio	185	185	391	391	564	564
Critical number of rods	469	761	195	761	160	689

* ^{241}Pu 1.60×10^{18} atoms/cm^3.
^{242}Pu 1.2×10^{17} "
^{241}Am 1.51×10^{18} "

Other atom densities same as in Table 6.

Table 8

UO_2-2% PuO_2 Rod Lattices

Fuel length 91.4 cm Fuel diameter 1.4 cm T_{H_2O} = 24 °C Fuel composition			
^{235}U	x 10^{20} at/cm^3	1.503	
^{238}U	x 10^{22} "	2.071	
^{239}Pu	x 10^{20} "	3.044	
^{240}Pu	x 10^{19} "	9.94	
^{241}Pu	x 10^{19} "	1.68	
^{242}Pu	x 10^{18} "	2.7	
^{241}Am	x 10^{18} "	1.7	
O	x 10^{22} "	4.258	
Clad dimensions and composition		See Table 3	
Moderator composition:			
H	x 10^{22} at/cm^3	6.668	
O	x 10^{22} "	3.334	
		Benchmark	
		36	37	38
Lattice pitch, cm		2.032	2.667	3.520
H/Pu atom ratio		238	554	1113
Critical number of rods		519.5 ± 0.1	233.2 ± 0.1	365 ± 0.1

Mean PuO_2 particle diameter 25 μm.

Table 9

UO_2-4% PuO_2 Rod Lattices

Fuel length 91.4 cm			
Fuel diameter 1.4 cm			
T_{H_2O} = 25°C			
Fuel composition:			
^{235}U	x 10^{20} at/cm^3	1.458	
^{238}U	x 10^{22} "	2.011	
^{238}Pu	x 10^{18} "	2.3	
^{239}Pu	x 10^{20} "	6.300	
^{240}Pu	x 10^{20} "	1.513	
^{241}Pu	x 10^{19} "	3.95	
^{242}Pu	x 10^{18} "	9.6	
^{241}Am	x 10^{18} "	3.6	
O	x 10^{22} "	4.220	
Clad thickness, cm		0.0858	
Clad composition (Zircaloy-2)		See Table 3	
Moderator composition:			
H	x 10^{22} "	6.666	
O	x 10^{22} "	3.333	
		Benchmark	
		39	40	41
Lattice pitch, cm		2.159	2.667	4.318
H/Pu atom ratio		153	289	922
Critical number of rods		252.6 ± 0.5	138.9 ± 0.4	271.9 ± 0.5

Mean PuO_2 particle diameter, 25 μm.
The bottom 0.5 cm of each rod was (natural) UO_2.

Table 10

(Depleted) UO_2-1.5% PuO_2 Rod Lattices

Fuel length 123.2 cm						
Fuel diameter 0.945 cm						
T_{H_2O} = 25°C						
Fuel composition*:						
^{235}U x 10^{19} at/cm^3	3.371					
^{238}U x 10^{22} "	2.104					
^{239}Pu x 10^{20} "	2.921					
^{240}Pu x 10^{19} "	2.502					
^{241}Pu x 10^{18} "	2.333					
^{242}Pu x 10^{16} "	9.586					
O x 10^{22} "	4.278					
Clad thickness, cm	0.0686					
Clad composition (Zircaloy-2)	See Table 3					
Moderator composition:						
H x 10^{22} at/cm^3	6.666					
O x 10^{22} "	3.333					
Lattice pitch, cm	1.397	1.524	1.8034	2.032	2.286	2.3622
H/Pu atom ratio	230	326	567	794	1077	1169
Critical number of rods	1487 ± 3	829 ± 7	484 ± 1	420 ± 1	452 ± 2	488 ± 2

Mean PuO_2 particle size 25 μm.

*Approximate, based on data in Ref. 10.

Table 11

UO_2-2% PuO_2 Rod Lattices

Fuel length 91.4 cm Fuel diameter 1.4 cm T_{H_2O} = 23°C Fuel composition*:					
^{235}U x 10^{20} at/cm^3	1.503				
^{238}U x 10^{22} "	2.072				
^{239}Pu x 10^{20} "	3.482				
^{240}Pu x 10^{19} "	5.758				
^{241}Pu x 10^{18} "	9.230				
^{242}Pu x 10^{17} "	8.586				
O x 10^{22} "	4.256				
Clad thickness, cm	0.0762				
Clad composition (Zircaloy-2)	See Table 3				
Moderator composition:					
H x 10^{22} at/cm^3	6.670				
O x 10^{22} "	3.335				
Lattice pitch, cm	2.3622	2.667	2.903	3.353	3.520
H/Pu atom ratio	391	554	693	991	1113
Critical number of rods	245.6 ± 0.1	194.3 ± 0.1	187.5 ± 0.1	221.1 ± 0.1	254.6 ± 0.1

Mean PuO_2 particle diameter 25 μm.

* Approximate, based on data in Ref. 10.

We should also mention another set of measurements at Hanford in the PCTR reactor [16], in which k_∞ of lattices fueled with mixed-oxide rods was measured. These rods were similar in construction to the ones mentioned above. Some were 2% PuO_2 in natural uranium oxide ($\sim$8% ^{240}Pu); others were 0.9% PuO_2 in depleted UO_2. The mean particle size in these rods was 25 μm. Other fuels were used that were either essentially homogeneous or had larger particle diameters ranging from 52 μm to 328 μm. Table 12 shows the measured k_∞'s for all of these. The lattice pitch in all cases was 1 inch (square lattice). These experiments are of particular interest in determining the effect of particle size on k, although other parameters and reaction rates were also measured.

Belgian Lattices. The Belgonucleaire experiments [15] utilized mixed-oxide fuels of six compositions, including pure UO_2. The ^{235}U enrichment was varied as well as the PuO_2 content. These lattices were fully reflected and moderated by H_2O; various lattice spacings were used for each fuel type in a square lattice. Some of the cores were near-cylindrical; others were square. Critical loadings were determined, although in some cases there was an insufficient number of rods to achieve criticality, and some rods of a different fuel were used to obtain a critical mass. Table 13 gives the pertinent data for some of these experiments. It should be noted that there are a few minor inconsistencies in the reported data, e.g., reported moderator-to-fuel ratios do not agree with values inferred from the given lattice dimensions.

III. CALCULATIONS

1. Calculations on Plutonium Nitrate Experiments

Calculated values of k_{eff} on the plutonium nitrate experiments are reported in refs. [3] and [17]. These calculations used multigroup S_4 and diffusion theory with 18 energy groups. The best agreements with the experimental values ($k_{eff} = 1$) were obtained with GAMTEC-II group constants and ^{239}Pu cross sections normalized to the Sher-Felberbaum 2200 m/sec values [18]; the mean calculated value for k_{eff} was 1.000 ± 0.003, using diffusion theory, but this good agreement is undoubtedly fortuitous. The transport theory calculations yielded a mean k_{eff} of 1.015 ± 0.005. Table 14 shows these results.

A recent Monte Carlo calculation [19] on one of these experiments (Benchmark # 3) with the RECAP code using ENDF/B-4 cross sections yielded $k_{eff} = 1.011 \pm .0022$; the authors suspect that this may mean that there is an error in the specifications of these experiments.

Liikala et al. [20] calculated two of the $Pu(NO_3)_4$ experiments. These were 15.2 in. diameter spheres, one H_2O reflected with H/Pu = 553, and the other bare with H/Pu = 668. The calculated k_{eff}'s were 1.0135 and 1.0127, respectively. These

Table 12

Effect of Particle Size on k_∞ in 2% PuO_2-UO_2 Fuel Rods

PuO_2 Particle Diameter, μm	k_∞ (exp.)	k_∞ (calc.)	C/E
0	1.316 ± 0.005	1.348	1.024
0	1.315 ± 0.005	1.348	1.025
0	1.313 ± 0.005	1.348	1.027
52	1.303 ± 0.006	1.339	1.028
107	1.286 ± 0.007	1.331	1.035
107	1.278 ± 0.006	1.331	1.041
107	1.274 ± 0.007	1.331	1.045
195	1.286 ± 0.006	1.317	1.024
195	1.278 ± 0.006	1.317	1.031
328	1.261 ± 0.006	1.296	1.028
328	1.265 ± 0.007	1.296	1.025
		Average =	1.030 ± 0.007

Table 13

(3%) UO_2-1% PuO_2 Rod Lattices

Fuel length 50.0 cm Fuel diameter 0.89 cm Fuel composition: ^{235}U x 10^{20} at/cm^3 ^{238}U x 10^{22} " ^{239}Pu x 10^{20} " ^{240}Pu x 10^{19} " ^{241}Pu x 10^{18} " ^{242}Pu x 10^{16} " O x 10^{22} "	 7.024 2.271 2.343 1.855 1.527 7.635 4.734			
Clad thickness, cm Clad composition (assumed s.s. 347): Fe x 10^{22} at/cm^3 Cr x 10^{22} " Ni x 10^{21} " Mn x 10^{21} " C x 10^{20} "	0.045 5.926 1.638 8.063 1.723 3.153			
Moderator composition: H x 10^{22} at/cm^3 O x 10^{22} "	 6.670 3.335			
Lattice pitch, cm	2.606	2.606	1.843	1.843
H/Pu atom ratio	2542	2542	1114	1114
Critical number of rods	363 (cyl.)	400 (square)	299 (cyl.)	315 (square)

Table 14
Computed Eigenvalues for Critical Assemblies

Sphere Diameter in.	Reflector	Pu g/liter	NO_3 g/liter	H_2O g/liter	k_{eff} (Diffusion Theory) GAMTEC-II Sher Data	k_{eff} (Diffusion Theory) GAMTEC-II Leonard Data	k_{eff} (Transport Theory) GAMTEC-II Sher Data	k_{eff} (Transport Theory) Hansen-Roach Data
Aqueous $Pu(NO_3)_4$ Solutions (4.6% ^{240}Pu)								
14	Full water	33.0	162	924.9	0.999	1.025	1.015	1.027
14	Full water	47.9	465	774.4	1.005	1.031	1.019	1.027
11.5	Full water	73.0	86	970.9	1.001	1.028	1.021	1.025
11.5	Full water	268.7	346	868.0	1.001	1.030	1.018	1.042
15.2	Full water	24.4	58	976.9	1.000	1.023	1.014	1.030
15.2	Full water	38.7	517	736.6	1.007	1.034	1.013	1.029
15.2	0.048-in. Stainless steel	39.0	64	977.8	0.997	1.024	1.006	1.011
15.2	0.048-in. Stainless steel	172.8	483	765.8	0.993	1.029	1.010	1.017
Mean Value for k_{eff}[a]					1.000 ±0.004	1.028 ±0.004	1.015 ±0.005	1.026 ±0.009
PuO_2-Polystyrene Assemblies (H/Pu = 15)								
Infinite Slab Thickness in.	Reflector	% ^{240}Pu						
6.33 ± 0.16	Unreflected	2.2			0.994	---	1.004	1.043
2.36 ± 0.04	Full Plexiglas	2.2			0.993	---	0.991	1.069
7.28 ± 0.16	Unreflected	8.0			0.984	---	0.988	1.011
2.91 ± 0.04	Full Plexiglas	8.0			0.982	---	0.979	1.046

[a] Uncertainties denote standard deviation from the mean value.

calculations used the same diffusion theory code (HFN) as in ref. [17]; the group gross sections, however, were obtained from HGR3/BRT-1. The basic difference is that the ^{239}Pu cross sections were normalized to the 1965 IAEA evaluation [21], which leads to a ^{239}Pu η value about 1% higher than the Sher-Felberbaum value. The ratio of the η values is about the same as the ratio of the calculated k_{eff}'s.

In summary, calculations with recent cross sections seem to overestimate k_{eff} in these systems by about 1%.

2. Homogeneous PuO_2- Polystyrene Assemblies

Calculations on the experiments with H/Pu = 15, 2% and 8% ^{240}Pu were done by multigroup diffusion and S_4 methods, using GAMTEC-2 group constants [17]. The calculations were for infinite slabs; the "experimental" values of the critical dimensions were obtained from the measured rectangular parellelepiped assemblies, using a constant buckling conversion scheme [4]. As with the $Pu(NO_3)_4$ solutions, the best agreement was obtained with diffusion theory and the Sher-Felberbaum normalizations. These results are also shown in Table 14.

For the 18.35% ^{240}Pu systems, critical thicknesses of infinite slabs were also inferred from the measurements [5]. Two cases were then calculated, using diffusion theory and transport theory with group cross sections based on the Sher-Felberbaum normalizations and on ENDF/B-2 cross sections. The results are shown in Table 15 [5]. The authors point out that the inferred critical thickness of 23.85 cm for the bare system is made suspect by the high values of k_{eff} in all the calculations.

Table 15

Calculated k_{eff}

	Infinite-slab thickness, cm.	DTF-IV		HFN	
		Orig. σ's	ENDF/B-2	Orig. σ's	ENDF/B-2
Bare	23.85 ± 0.29	1.028	1.049	1.014	1.041
Plexiglas-reflected	10.87 ± 0.14	.998	.999	.998	1.004

3. Pu-Aℓ Lattices

Liikala et al. [20] calculated the Aℓ-Pu (1.8%) systems, using the original data, which included the lucite sleeves around the fuel elements. As has been noted, these data were superseded by later experiments without the lucite. The mean value of k_{eff} calculated was 1.0076 ± 0.002. A similar situation exists with

the 2% Pu-Aℓ lattices -- the calculations were apparently done on the older systems, but the experimental values were superseded. The mean calculated k_{eff} was 1.0204 ± 0.0026. The 5% Pu-Aℓ lattices, however, were not remeasured. For these, the mean calculated k_{eff} was 1.0056 ± 0.0032.

All of these calculations used the one-dimensional diffusion theory code HFN, with group cross sections obtained from cell calculations using HRG-3 and BRT-I. Basic cross section data were eseentially ENDF/B-1, normalized to the 1965 IAEA 2200/m/sec values [21]. Liikala et al. did a detailed study of the sensitivity of these (and other) calculations to many of the areas of calculational uncertainty; in general, any particular assumption led to an estimated bias ranging from -0.5% to +0.5% in k_{eff}. One noteworthy exception was that for one of the Aℓ-5% Pu lattices, k_{eff} increased by about 3.6% when transport theory was used instead of diffusion theory. Uncertainties in cross sections led to estimated uncertainties in k_{eff} of ± 1%.

4. PuO_2-UO_2 Lattices (BNWL)

Table 16 [20] shows calculated k_{eff}'s for the BNWL PuO_2-UO_2 lattices, including Benchmarks 27-29, 36-41, and the lattices with 1.5% PuO_2 (8% ^{240}Pu) and 2% PuO_2 (16% ^{240}Pu). These were calculated in the same manner as the Pu-Aℓ lattices.

In these calculations the fuel was assumed to be homogeneous. The mean size of the PuO_2 particles was approximately 25 μm. The self-shielding effect of this finite particle size was evaluated and was found to lower k_{eff} by 0.1 to 0.7% (that is, the calculated k_{eff}'s based on homogeneity were too high). The smallest bias is in the tightest lattices.

Ozer and Fiarman [22,23] have recently calculated the UO_2-2% PuO_2 (8% ^{240}Pu) lattices (Benchmarks 30-35). These calculations were based on ENDF/B-4 cross sections processed into multi-group form by ETOG-III and FLANGE-II. Hydrogen cross sections were adjusted to account for proton binding effects and upscattering into the ^{240}Pu low-energy resonance. Four-group cross sections were generated by the BNL version of HAMMER. The 4-group constants were then used as input into a two-region, one-dimensional, discrete ordinates transport calculation using the code ANISN. This was done to obtain an explicit radial representation of the core and reflector regions, since the eigenvalues calculated with HAMMER were strongly sensitive to the input bucklings. Axial leakage was accounted for by a DB_z^2 term added to the absorption cross section.

The results for the PuO_2-UO_2 lattices given in ref. [22] were preliminary and did not include an important correction to the HAMMER resonance absorption rates. The final results, given in ref. [23] and Table 17, do include this correction. The correction is obtained by comparing the zero-buckling resonance absorption rate calculated with HAMMER with that calculated with a fine-group code (RABBLE). For UO_2 lattices, the correction is obtained by a Monte Carlo calculation (REPC). For the mixed-oxide lattices,

Table 16

Calculated k_{eff}, UO_2-PuO_2 Rod Lattices
(Measured k_{eff} = 1.0000)

Lattice Spacing[a] (in.)	H/Pu Atom Ratio	UO_2-2 wt% PuO_2 k_{eff} 8% ^{240}Pu	UO_2-2 wt% PuO_2 k_{eff} 16% ^{240}Pu	UO_2-2 wt% PuO_2 k_{eff} 24% ^{240}Pu
0.80	238	0.9920	--	0.9942
0.93	391	0.9979	0.9982	0.9963
1.05	554	0.9913	0.9931	0.9981
1.143	693	0.9992	1.0000	1.0007
1.32	991	0.9999	0.9995	0.9985
1.386	1113	0.9979	0.9964	0.9971
	Mean =	0.9964 ±0.0043	0.9974 ±0.0024	0.9975 ±0.0022

UO_2-4 wt% PuO_2			UO_2-1.5 wt% PuO_2		
Lattice Spacing[a] (in.)	H/Pu Atom Ratio	k_{eff}	Lattice Spacing[a] (in.)	H/Pu Atom Ratio	k_{eff}
0.85	153	0.9964	0.55	230	1.0035
0.93	203	0.9940	0.60	326	0.9988
1.05	289	1.0035	0.71	567	0.9988
1.143	414	1.0024	0.80	794	0.9968
1.386	578	1.0062	0.90	1077	0.9971
1.60	805	1.0047	0.93	1169	0.9989
1.70	922	1.0031			
Mean =		1.0015 ±0.0045	Mean =		0.9990 ±0.0013

Note: The uncertainties assigned to the mean values are standard deviations for a typical value rather than for the mean value.

[a]These are all triangular pitch lattices.

REPC could not be used, since it could not handle four resonance nuclides. For one UO_2 lattice, the RABBLE correction factor was only half of the REPC correction factor for ^{238}U absorption, but since there was no other choice, the RABBLE correction factors were used for the mixed-oxide lattices despite this uncertainty.

Table 17

Calculated k_{eff}, Benchmarks 30-35

Benchmark	H/Pu	Boron Conc. (ppm)	k_{eff} HAMMER No Res. Corr.	k_{eff} HAMMER Res. Corr.	ANISN*
30	185	1.7 ± 0.1	0.9935	0.9974	0.9827
31	185	680.9 ± 2	0.9843	0.9871	0.9934
32	391	0.9 ± 0.2	0.9894	0.9961	1.0012
33	391	1090.4 ± 2	0.9976	1.0049	1.0034
34	564	1.6 ± 0.1	1.0109	1.0178	1.0059
35	564	767.2 ± 2	0.9963	1.0042	1.0000

*4-group cross sections generated by HAMMER, including resonance correction factors.

5. Belgonucléaire Lattices

Calculations on some of the Belgian lattices are in progress at Stanford. Two input uncertainties are the discrepancy in moderator-to-fuel ratios mentioned previously, and an uncertainty as to the type of stainless steel used for the cladding; we assume it is SS-347. In these calculations, 4-group cross sections are obtained from a HAMMER cell calculation with ENDF/B-4 cross sections; these are then used in an ANISN (P_1-S_4) calculation. The axial buckling is known to be $B_z^2 = 26\ m^{-1}$. The group cross sections for the water reflector are calculated in three ways: (1) cross sections for the reflector water are taken from the actual cell calculation, averaging is performed with core fluxes; (2) water cross sections are calculated for a larger cell (radius = 5 inches); (3) water cross sections are calculated for a still larger cell (radius = 15 inches); this means that averaging is done with an asymptotic flux rather than the core flux.

Several different schemes for treating the radial and axial buckling are under investigation. These include:

- B_r^2 is obtained from a fit to the radial fission density, as calculated by ANISN.
- The extrapolation distance, λ, is calculated from

$$B_r^2 = \left(\frac{2.405}{R_o + \lambda}\right)^2$$

(1) The axial buckling is calculated from

$$B_z^2 = \left(\frac{\pi}{50+2\lambda}\right)^2$$

- B_g^2 is then $B_r^2 + B_z^2$.
- The material buckling, B_m^2, is obtained from the HAMMER cell calculation.
- A HAMMER calculation in which the input buckling, B_{in}^2, equals B_g^2 is then used to obtain k_{eff} (if $B_{in}^2 = B_m^2$, $k_{eff} = 1$).

(2) The axial buckling is obtained from

$$B_z^2 = \left(\frac{\pi}{H + \frac{2C}{\Sigma_{tr}}}\right)^2 ,$$

where Σ_{tr} is the transport cross section and C is a constant; since Σ_{tr} is energy-dependent, B_z^2 is also energy-dependent. $C = 0$ makes B_z^2 energy-independent and with $H = 61.612$ cm, $B_z^2 = 26\ m^{-2}$. $H = 61.612$, $C = 0.71$ introduces a weak energy dependence.

The results for some of the lattices are shown in Table 18. Preliminary conclusions are:

- k_{eff} as calculated by ANISN (with $H = 61.612$ cm, $C = 0$ and the asymptotic reflector spectrum) gives a result consistent with k_{eff} calculated by HAMMER, when the actual geometric buckling is used.
- Overall best results seem to be obtained with $H = 61.612$ and $C = 0.71$.

It should be noted that the correction made by Fiarman and Ozer to HAMMER to improve the resonance capture part of the calculation has not been applied in these calculations.

Table 18

Calculated Results, Belgonucléaire Lattices

	Case 1	Case 2	Case 3	Case 4	Core Height H, cm	Extrapolation Constant	Code Used
^{235}U Enrich.	4%	4%	3%	3%			
$PuO_2/(PuO_2+UO_2)$	0	0	1%	1%			
R_F, cm	0.445	0.445	0.445	0.445			
R_C, cm	0.490	0.490	0.490	0.490			
R_M, cm	0.735	1.040	1.040	1.470			
Pitch, cm	P = 1.303	$\sqrt{2}P$	$\sqrt{2}P$	2P			
V_M/V_F	1.517	4.245	4.245	9.704			
H/Pu			1115	2549			
N (No. of rods)	864	374	315	400			
R_o (Reactor radius, cm)	21.61	20.11	18.45	29.41			
	k_{eff}						
$Refl_1$ (Cell water)	0.99006	1.00557	1.01016	0.987486	61.612	0	ANISN
	1.00011				61.612	1.42	"
$Refl_2$ (5" water)	0.977153	0.99975	1.00271	0.986337	61.612	0	"
$Refl_3$ (15" water)	0.974957	0.99831	1.00107	0.985711	61.612	0	"
	0.981052	0.99987	1.00277	0.986022	$50+2\lambda$	0	"
	0.984829	1.00735	1.00976	0.995147	61.612	1.42	"
B_r^2, m^{-2}	69.53	83.59	94.90	46.44	61.612	0	"
B_z^2, m^{-2}	23.75	25.36	25.28	25.88	61.612	0	"
$B_g^2 = B_r^2 + B_z^2$, m^{-2}	93.28	108.95	120.18	72.32	61.612	0	"
B_m^2, m^{-2}	84.38	105.59	117.41	65.37	61.612		HAMMER
$k_{eff}\left(B_{in}^2 = B_g^2\right)$	0.974890	0.99186	0.99355	0.98277			HAMMER
λ, cm	7.23	6.19	6.24	5.88			ANISN

REFERENCES

1. U. P. Jenquin, Compilation of Plutonium Benchmark Experiments (1976).
2. F. F. Kruesi, J. O. Erkman, and D. D. Lanning, HW-24514 DEL, p. 67 (1952).
3. R. C. Lloyd, C. R. Richey, E. D. Clayton, and D. R. Skeen, N.S.E. 25, 165 (1966).
4. C. R. Richey, J. D. White, E. D. Clayton, and R. C. Lloyd, N.S.E. 23, 150 (1965).
5. S. R. Bierman and E. D. Clayton, Nucl. Tech. 15, 5 (1972).
6. J. H. Lauby, BNWL-1381-2 (1970).
7. W. P. Stinson and V. O. Uotinen, BNWL-1627 (1971).
8. W. P. Stinson and L. C. Schmid, HW-74190 (1962).
9. W. P. Stinson et al., HW-79054 (1963).
10. V. U. Uotinen et al., Nucl. Tech. 15, 257 (1972).
11. W. P. Stinson and J. H. Lauby, BNWL-907 (1968).
12. R. I. Smith and G. J. Konzek, EPRI NP-196, Vol. I (1976).
13. R. I. Smith and G. J. Konzek, EPRI NP-196, Vol. II (1978).
14. W. P. Stinson and J. H. Lauby, BNWL-739 (1968); BNWL-985 (1969).
15. L. Bindler et al., Belgonucléaire Report BN-7211-01 (1972); also Trans. A.N.S. 15, 954 (1972).
16. D. F. Newman, Nucl. Tech. 15, 1972 (1972).
17. C. R. Richey, N.S.E. 31, 32 (1968).
18. R. Sher and J. Felberbaum, BNL-722 (1962).
19. L. Levitt et al., Interim Report to EPRI, Dec. 1977.
20. R. C. Liikala, V. O. Uotinen, and U. P. Jenquin, Nucl. Tech. 15, 272 (1972).
21. C. H. Westcott et al., At. Energy Rev. 3, 2 (1965).
22. O. Ozer and S. Fiarman, Trans. A.N.S. 26, 596 (1977).
23. R. Sher and S. Fiarman, EPRI Report NP-691 (1978).

Section 7

ANALYSIS OF U235-U238 THERMAL REACTOR BENCHMARKS--CONSISTENCY AND INTERPRETATION

Analysis of U235-U238 Thermal Reactor Benchmarks - Consistency and Interpretation

J. Hardy, Jr.
Bettis Atomic Power Laboratory, West Mifflin, Pennsylvania*

D. R. Finch
Savannah River Laboratory, Aiken, South Carolina

ABSTRACT

The thermal-reactor benchmark testing of ENDF/B-IV data for U235 and U238 is reviewed. Criticality and integral parameter results obtained by different calculational methods are compared and consistency of the measured integral parameters is discussed. The major deficiencies observed are an underprediction of leakage in homogeneous critical assemblies, and an overprediction of U238 resonance capture in lattices. The major difference among calculational methods is in the prediction of resonance capture in lattices. A new harder U235 fission spectrum significantly improves K_{eff} vs leakage. New resonance parameters for U238 remove about half of the disagreement with integral experiment.

I. INTRODUCTION

This paper surveys the results of integral testing of ENDF/B data for application to U235-U238 thermal reactors. There has been a fairly extensive effort to test ENDF/B-IV, and these results will be summarized. The expected effects of some data changes in prospect for the forthcoming ENDF/B-V will be mentioned.

Before one can draw conclusions about adequacy of differential data, there are two prior questions which must be considered:

(1) How good are the integral experiments? This includes questions of self- and mutual consistency, as well as scope and detail of testing.

(2) How good are the calculational methods used in analyzing the integral experiments?

Examining a number of integral experiments with the same data set and method offers the possibility of drawing conclusions about consistency among the experiments. And of course the analysis of one experiment with a given data set and different methods shows up clearly the methods differences, and these can be significant even among the presumed best methods. Although such comparisons cannot eliminate the possibility of methods errors, it is only through such detailed studies that some order can be obtained in addressing the threefold question of adequacy of differential data, methods, and integral experiments.

* Work performed under the AWBA Development Program.

II. SURVEY OF RESULTS WITH ENDF/B-IV

Seven laboratories participated in the initial CSEWG thermal reactor data testing of ENDF/B-IV, under the leadership of F. J. McCrosson. Effort was concentrated on the homogeneous aqueous U235 ORNL spheres, the H_2O-moderated TRX-1 and 2 simple rod-lattices of slightly-enriched uranium, and the D_2O-moderated MIT-1, 2, and 3 exponential lattices[1]. There was, in addition, a comparison of the more important few-group processed cross sections and of few-group reaction rates. Results are collected in ENDF-230[2]. More recent studies in this area include:

(1) Full core Monte Carlo analyses of TRX-1 and TRX-2 at Brookhaven[3] and at Bettis[4].

(2) Analysis of an extended set of aqueous homogeneous U235 criticals spanning a wide range of hydrogen/uranium ratio and leakage[5].

(3) The Oak Ridge sensitivity analysis of TRX-2[6].

(4) Consistency analysis of integral parameters in TRX and MIT benchmarks[7].

This section summarizes the status of results obtained for these systems.

A. Aqueous Homogeneous U235 Criticals

1. CSEWG Analyses. The Gwin-Magnuson U235-H_2O spheres (No. 1-4 and 10) were analyzed by five laboratories. K_{eff} results[2] shown in Table 1 are reasonably consistent. There are systematic differences among the methods of as much as 0.4%.

2. Analyses of Homogeneous Assemblies. In connection with studies of homogeneous U233 criticals, a set of seventeen U235 homogeneous criticals was also analyzed, for comparison purposes[5]. These included all the Gwin-Magnuson criticals[8] plus five smaller assemblies with hydrogen/uranium ratios as low as 27.1[9,10]. The purpose of this study was to examine in detail the ability of ENDF/B-IV data to predict criticality of such systems over a wide range of H/U, with the intent of drawing specific conclusions about the data set. These systems span a wide range of spectrum hardness (with as much as 50% epithermal fission) and of leakage (from 1%-50%). Criticality and detailed reaction rates were calculated and sensitivity of k_{eff} to certain major data changes was determined.

(a) Calculational Methods. For the calculations in Ref. 5, nuclear data were from ENDF/B-IV, multigroup processed with the ETOMX and ETOTX programs (Bettis versions of ETOG[11] and ETOT[12], respectively.) Thermal scattering kernels were generated with FLAN2 (a Bettis version of FLANGEII[13]) from the ENDF/B $S(\alpha,\beta)$ files based on the Haywood kernel.

Table 1

K_{eff} of ORNL U235 Spheres Obtained with ENDF/B-IV Data

ORNL	BNL	ANC	BAPL	GA	SRL	Average	Range
1	1.0007 ± .0026	1.0025	.9983	1.0012	.9996	1.0004	.0042
2	.9993 ± .0036	1.0018	.9980	1.0007	--	1.0002	.0038
3		.9984	.9949	.9978	--	.9970	.0035
4		.9998	.9963	.9989	.9976	.9982	.0035
10		.9988	.9957	.9982	.9951	.9970	.0037

NOTE: All results are from Ref. 2, except BNL is from Ref. 3. Uncertainties are one standard deviation. See Table 15 for a guide to the calculational methods.

The criticals were analyzed with the Monte Carlo program RCP01, an extension of RECAP[14], and with P7MG, an extension of P3MG[15], a one-dimensional, multigroup P_ℓ program. RCP01, which employed a very detailed representation of cross sections and geometry, was used for the overall study of criticality versus H/U ratio. Cross section sensitivities were derived from P7MG, which was also used for the analysis of the Gwin-Magnuson criticals to infer constraints on the 2200 m/s parameters for U235. The agreement between RCP01 and P7MG was checked for five specific experiments and found to be very good.

(b) Criticality Versus Hydrogen/Uranium Ratio. Calculated K_{eff} values are shown in Table 2 and in Figure 1 plotted against leakage. They increase from 0.994 at zero leakage to 1.01 at 45% leakage. Similar behavior was observed for the U233 systems[5] (as shown in Figure 1).

Although there remain questions of interpretation about individual experiments, these are judged not to be significant for the overall pattern.

Errors in calculated K_{eff} can stem from energy-dependent errors of eta which are emphasized as the spectrum hardens (for example, uranium capture and fission resonance integrals, and thermal capture and fission cross sections.) The hydrogen thermal σ_A affects the very thermalized assemblies and nubar affects all assemblies equally. The other major source of error in K_{eff} is underprediction of leakage, which is emphasized in the smaller cores (see Figure 1). The most significant factors potentially affecting leakage are considered to be:

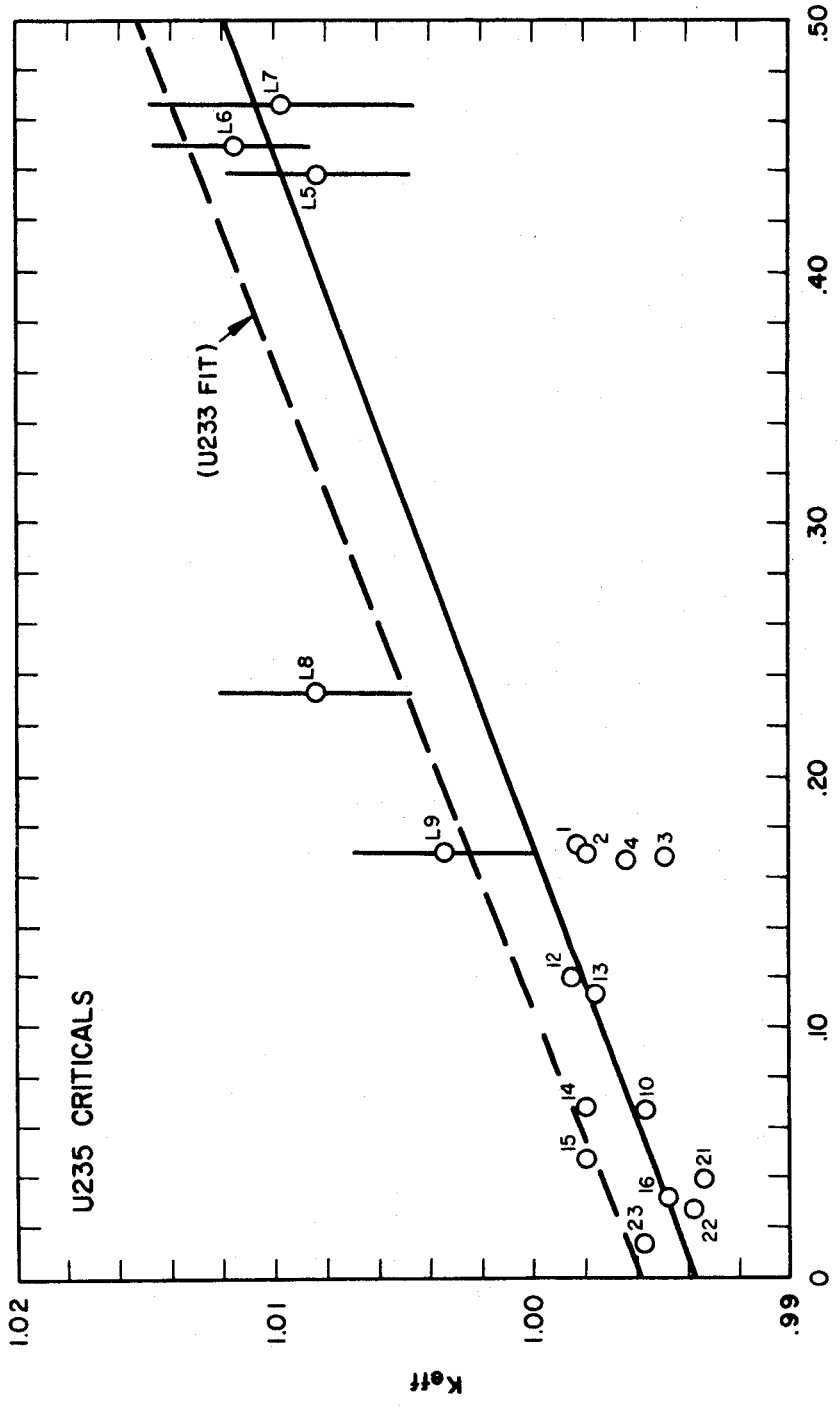

Figure 1 - Calculated Keff Versus Total Leakage Fraction for U235 Criticals

(1) multigroup averaging and limited P_ℓ treatment of scattering in RCP01

(2) oxygen scattering cross section and angular pattern (MeV range)

(3) fission spectrum.

Table 2

Results for Homogeneous U235 Critical Experiments Calculated with ENDF/B-IV Data

Experiment	H/U235	Calculated Results		
		Total Leakage	δ^{25}	$K_{eff} \pm 2\sigma$
L5	27.1	.4380	.8175	1.0085 ± .0036
L6	44.3	.4501	.4722	1.0117 ± .0030
L7	76.1	.4661	.1962	1.0098 ± .0051
4	972	.1669	.0306	.9964
3	1033	.1678	.0288	.9949
L8	1112	.2333	.0251	1.0085 ± .0037
2	1177	.1678	.0255	1.0007 ± .0035
		.1699	.0252	.9980
1	1378	.1729	.0215	.9983
L9	1393	.1703	.0214	1.0035 ± .0035
12	1604	.1197	.0194	.9985
13	1634	.1126	.0192	.9976
14	1821	.0679	.0178	.9980
10	1835	.0663	.0179	.9936 ± .0031
		.0670	.0177	.9957
15	1905	.0475	.0173	.9980
21	1955	.0388	.0170	.9934
16	1981	.0329	.0169	.9939 ± .0008
22	2004	.0269	.0167	.9938
23	2052	.0141	.0165	.9949 ± .0003
		.0134	.0165	.9957

NOTE: Experiments labeled by numbers are the Gwin-Magnuson criticals (Ref. 8); others are labeled as in Ref. 5.

δ^{25} is the ratio of epithermal/thermal U235 fission.

Uncertainty is two standard deviations for RCP01 results. K_{eff} values without uncertainties are from P7MG.

Since almost the same trend in calculated K_{eff} error is found for U233 systems[5], it is tempting to seek a common source of difficulty (e.g., items (1) and (2) above) but this has not proved fruitful.

It seems unlikely that the trend is due to energy-dependent errors of eta within the thermal range (which are emphasized as the flux spectrum hardens) since substantial errors would be required.

Furthermore, calculational approximations (including data processing) were deemed to be relatively unimportant. This was supported by a comparison of RCP01-calculated leakage with results obtained with the VIM Monte Carlo Program[16]. The comparison, using ENDF/B-IV data, was made for a small cylinder of U235-H_2O in vacuum, with a spatially flat fission source. RCP01 employed multigroup averaged scattering cross sections with a P_3 angular treatment. VIM employed a strictly pointwise representation of the ENDF-tabulated data and a detailed elastic scattering angular treatment (20 equal cosθ intervals). Results for total leakage (10 MeV - 1.12 eV) were:

RCP01:	0.5285 ± 0.0006
VIM:	0.5267 ± 0.0007
RCP01-VIM:	0.0018 ± 0.0009

Agreement was very good, allowing for statistics (uncertainties are one standard deviation), and if anything RCP01 slightly overestimates leakage relative to VIM.

(c) Sensitivities of Calculated K_{eff} to Nuclear Data.

Sensitivities of the calculated K_{eff} to several nuclear data changes were determined for selected assemblies. These changes include the hydrogen thermal absorption cross section, the uranium capture and fission resonance integrals, the uranium inelastic cross sections, the ENDF/B version of oxygen, and representations of the fission neutron spectrum.

A reference K_{eff} was computed for each assembly with P7MG and ENDF/B-IV data. Then for each change in data a δK_{eff} was determined relative to this reference value. The sensitivities of K_{eff} to the various parameters are summarized in Tables 3-5. The following points are noteworthy:

(1) The uranium capture and fission resonance integrals were varied as shown in Table 3. In each case this was achieved by a uniform percentage change of the smooth multigroup cross sections. For these U235 systems, the sensitivities are significant and their relative importance can be seen from the resonance integrals shown in Table 4. Compared to the integral measurements, the ENDF/B-IV U235 fission integral is too large and the capture integral is low. Each of these factors

Table 3

Sensitivities of K_{eff} to Uranium Capture and Fission Resonance Integrals

U235	Experiment: H/U235:	Change in K_{eff} L5 27.1	L6 44.3	L7 76.1	L8 1112	23 2052
Smooth capture integral increased 6.0 b		-.0077	-.0053	-.0028	-.0003	-.0002
Smooth fission integral increased 10.0 b		+.0080	+.0053	+.0027	+.0005	+.0004

Table 4

U235 Resonance Capture and Fission Integrals

	Resonance Integral Above 0.625 eV (barns) Fission	Capture
ENDF/B-IV (Mat. 1261)	267.6	135.7
BNL-325, 3rd ed. (Ref. 17)*	259 ± 5	142 ± 6

*Inferred using ΔI(0.5 eV - 0.625 eV) = 16 b for fission and 2 b for capture.

could account for as much as 0.5% of the K_{eff} difference between small and large cores.

(2) Reducing the hydrogen 2200 m/sec absorption cross section from 0.332 b to 0.330 b increases the reactivity of the thermal assemblies by 0.3% with negligible effect on the high-leakage assemblies (Table 5).

Table 5

Sensitivities of U235 Critical Assemblies to Changes in Nuclear Data

Data Component	Change in Data Component	Change in K_{eff} H/U235-27.1(L5)	44.3(L6)	1112(L8)	1177(2)	1835(10)
Hydrogen Cross Sections	Reduced thermal absorption cross section from 0.332 b to 0.330 b	+0.0001	+0.0001	+0.0021	+0.0020	+0.0028
Uranium-235 Scattering Cross Sections	Reduced the inelastic cross section by 20%	-0.0016	-0.0011	0.0000	0.0000	0.0000
	Inelastic cross section reduced by 20% and the elastic cross section increased by an equivalent amount	-0.0009	-0.0006	0.0000	0.0000	0.0000
Oxygen Cross Sections	ENDF/B-IV → ENDF/B-III	-0.0033	-0.0034	-0.0013	-0.0008	-0.0001
	ENDF/B-IV → ENDF/B-I	-0.0049	-0.0050	-0.0018	-0.0012	-0.0002
Fission Spectrum *	Maxwellian spectrum $\bar{E}$=2.0 MeV	-0.0022	-0.0023	-0.0012	-0.0009	-0.0004
	Maxwellian spectrum $\bar{E}$=2.1 MeV	-0.0157	-0.0165	-0.0087	-0.0067	-0.0031
	Watt spectrum ($\bar{E}$=2.0 MeV)	-0.0053	-0.0054	-0.0020	-0.0015	-0.0004

* All are relative to the ENDF/B-IV fission neutron spectrum for U235, a Maxwellian with $\bar{E}$ = 1.985 MeV.

(3) A 20% reduction of the uranium inelastic cross sections produced negligible changes of reactivity.

(4) Sensitivities to the ENDF/B version of oxygen are worth as much as 0.6% in K_{eff} for the high-leakage assemblies and are negligible for the large assemblies. The successive versions of oxygen (ENDF/B-I to ENDF/B-IV) show an increase in backscattering, which tends to reduce leakage.

(5) The fission neutron spectrum significantly affects fast neutron leakage. Sensitivity of K_{eff} to mean energy (for a Maxwellian shape) and to the difference between Watt and Maxwellian shapes (for the same mean energy) is shown in Table 5.

(d) U235 Fission Spectrum. Four recent differential experiments show that the prompt neutron spectrum for low-energy U235 fission is significantly harder than that of ENDF/B-IV, a Maxwellian with $\bar{E}$ = 1.985 MeV. A description of the experiments and an analysis of them by J. M. Adams appear in the Proceedings of the Specialists Meeting on Inelastic Scattering and Fission Neutron Spectra, which was held at Harwell in April 1975. Although it did not provide an exact fit to the data, the Watt model fit quite well and was clearly better than a Maxwellian. The Adams best-fit Watt spectrum had a mean energy of 2.016 MeV.

In a recent study, N. M. Steen[20] performed a least-squares adjustment of data for U235 and U233 systems. Among the data included in the fit were thermal criticality parameters (including Cf252 $\bar{\nu}$, thermal $\bar{\nu}$ ratios and η for U233 and U235, K2 values* from the Gwin-Magnuson criticals), K_{eff} values of small homogeneous criticals, and differential prompt fission spectra. For U235, a good fit was obtained with a Watt shape ($\bar{E}$ = 2.027 $\pm$ .004 MeV). This is based on the same four differential experiments as the Adams spectrum and is somewhat harder. A more complex prompt spectrum model (two fully accelerated fragments plus a stationary source) also gives a good fit to the differential data and a mean energy of 2.073 $\pm$ .005 MeV. This is denoted the Standard 2 model.

The effects of alternative spectra on K_{eff} of the homogeneous criticals, as calculated by P7MG, are shown in Figure 2. In part A of this figure, the effect of a 10 b reduction of the ENDF/B-IV U235 fission resonance integral is shown by black dots for the three high-leakage criticals. (For the others, the effect is negligible). Part B shows the effect of the reduced fission integral plus use of an equilibrium spectrum based on a Watt prompt spectrum with $\bar{E}$ = 2.027 MeV. This combination removes most of the K_{eff} variation with leakage. Finally, part C shows the effect of changing to an equilibrium spectrum based on the much harder Steen Standard 2 model.

---

*K2 is described in section (f) below.

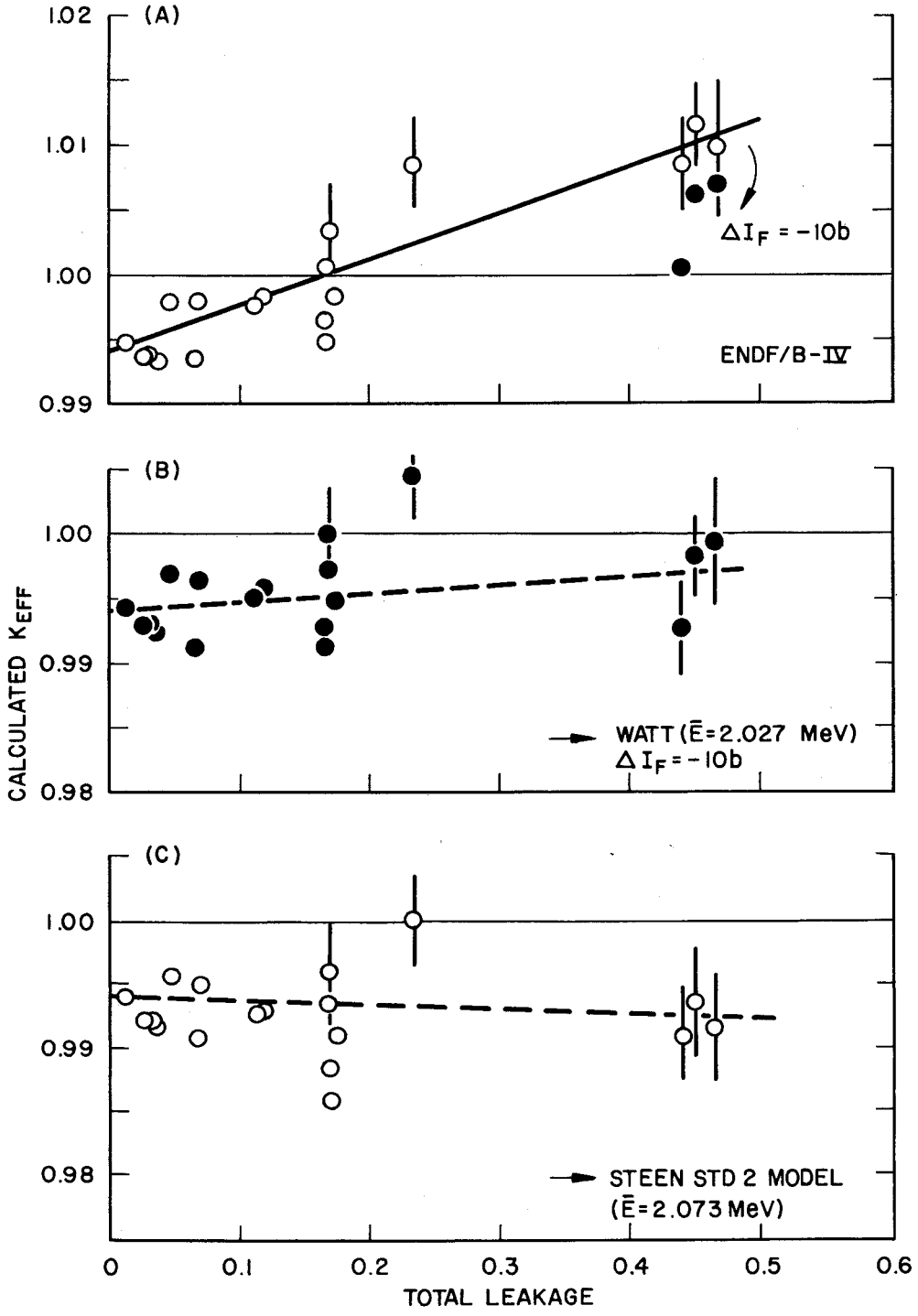

Figure 2 - Effects of Alternative Fission Spectra on K_{eff} of U235 Criticals

It is clear that the trend of K_{eff} with leakage can be eliminated by use of either of these hardened fission spectra along with a suitable choice of U235 capture and fission resonance integrals. In either case, there remains a residual defect of K_{eff} which could most readily be removed by a $\bar{\nu}$ increase of ~0.6%. The combinations of criticality parameters obtained in the least squares fit[20] are shown in Table 6.

(e) Age in H_2O. With ENDF/B-IV data, the calculated age to indium resonance (1.47 eV) for a U235 fission source in H_2O is well below experiment (see Table 7). The equilibrium spectrum based on the Watt prompt spectrum with $\bar{E}$ = 2.027 MeV provides only slightly better agreement. The harder Steen Standard 2 spectrum, with $\bar{E}$ = 2.073 MeV, leads to very good agreement.

Table 7

Flux Age to 1.47 eV in H_2O (U235 Fission Source)

	Age (cm^2)
Experiment (Ref. 18, 19)	26.4 ± 0.3
ENDF/B-IV Calculation	25.49
ENDF/B-IV (except Watt model, $\bar{E}$ = 2.027 MeV)	25.88
ENDF/B-IV (except Steen Std. 2 model, $\bar{E}$ = 2.073 MeV)	26.33

(f) Spectrum Averaged Cross Sections. In another paper at the 1975 Harwell Specialists Meeting, A Fabry reviewed current evidence on fission spectra derived from integral experiments. The spectrum mean energy derived from dosimetry measurements is now 2.00 - 2.05 MeV, and this is consistent with the mean energy implied by the fission age-to-indium resonance in H_2O. He also emphasized the importance of integral spectrum-average cross sections, particularly $\bar{\sigma}_f^{U235}$, $\bar{\sigma}_f^{U238}$ and their ratio.

Table 8 shows integral experimental values recommended by A. Fabry along with calculated values. The ENDF/B-IV calculation produces a low value of $\bar{\sigma}_f^{U238}$. Some improvement is obtained with the Watt shape, and very good agreement is shown by the Standard 2 spectrum. It should be mentioned that $\bar{\sigma}_f^{U238}$ was not used in the fit so that this is an independent test of the spectrum.

Table 6

Comparison of Fission Spectra and Other Parameters
Affecting Criticality of U235 Assemblies

	Experimental Value	Calculation		
		ENDF/B-IV	L. S. Fit Results	
Fission Spectrum Model		Maxwellian $\bar{E}_p$ = 1.985 MeV	Watt $\bar{E}_p$ = 2.027 MeV	Standard $\bar{E}_p$ = 2.073 MeV
I_F(>.625 eV), b	259 ± 5	267.6	259.3	259.7
I_c(>.625 eV), b		135.7	136.3	131.0
α(>.625 eV)	0.548 ± .025	.5071	0.5257	0.5043
σ_f(.0253 eV), b	581.6 ± 4.7	585.4	582.3	581.8
σ_c(.0253 eV), b		97.7	98.7	98.8
α(.0253 eV)	0.1689 ± .0021	0.1669	0.1695	0.1699
ν_t(.0253 eV)		2.4188	2.4289	2.4334
K_{eff}, 0% leakage	1.000	.9957	.9961	.9973
K_{eff}, 45% leakage	1.000	1.0096	1.0011	.9993

Note: Results from Ref. 20.

Table 8

Spectrum Averaged Cross Sections

	$\bar{\sigma}_f^{U235}$ (mb)	$\bar{\sigma}_f^{U238}$ (mb)	$\bar{\sigma}_f^{U235} / \bar{\sigma}_f^{U238}$
Integral Experiment (A. Fabry)	1220 ± 31	313.5 ± 10	3.89 ± .08
ENDF/B-IV Calculation	1244	294	4.23
ENDF/B-IV (except Watt spec., $\bar{E}$ = 2.027 MeV)	1242	304	4.08
ENDF/B-IV (except Std. 2 spec., $\bar{E}$ = 2.073 MeV)	1235	312	3.96

(g) Evaluation of the Thermal Criticality Parameter K2. A constraint on the thermal criticality parameters of U235 has been derived by Gwin[21] from the Gwin-Magnuson homogeneous criticals near the zero-leakage limit. This is $K2 \equiv (\bar{\eta}_U - 1) \frac{\bar{\sigma}_a^U}{\bar{\sigma}_a^H}$, relating the thermal-average eta for U235, and the U235 and hydrogen thermal absorption cross sections (Table 9). Also shown are K2 values obtained in Ref. 5 and corresponding "g" factors. The uncertainty on K2 is meant to account for all sources of error in the analysis (mainly fissile inventory, calculated epithermal multiplication and absorption, and calculated leakage).

It is essential to determine K2 near the zero-leakage limit since inferences about thermal eta, derived from analysis of critical systems, must not be influenced by criticality errors stemming from inability to calculate leakage. This is illustrated by Figures 3 and 4* which show K2 values calculated for the Gwin-Magnuson Criticals with ENDF/B-IV and with artificially enhanced fast leakage. Errors in calculated leakage can be caused by high-energy data inadequacies (as is evident for ENDF/B-IV) and calculational approximation, and by systematic errors in interpreting the experiments.

*In Figures 3 and 4, K2 is plotted versus the quantity FP. F can be viewed as the product of fast multiplication factor and resonance escape probability (ϵp), and P is the nonleakage probability. At FP = 1.0, fast multiplication just balances the small fast absorption and leakage.

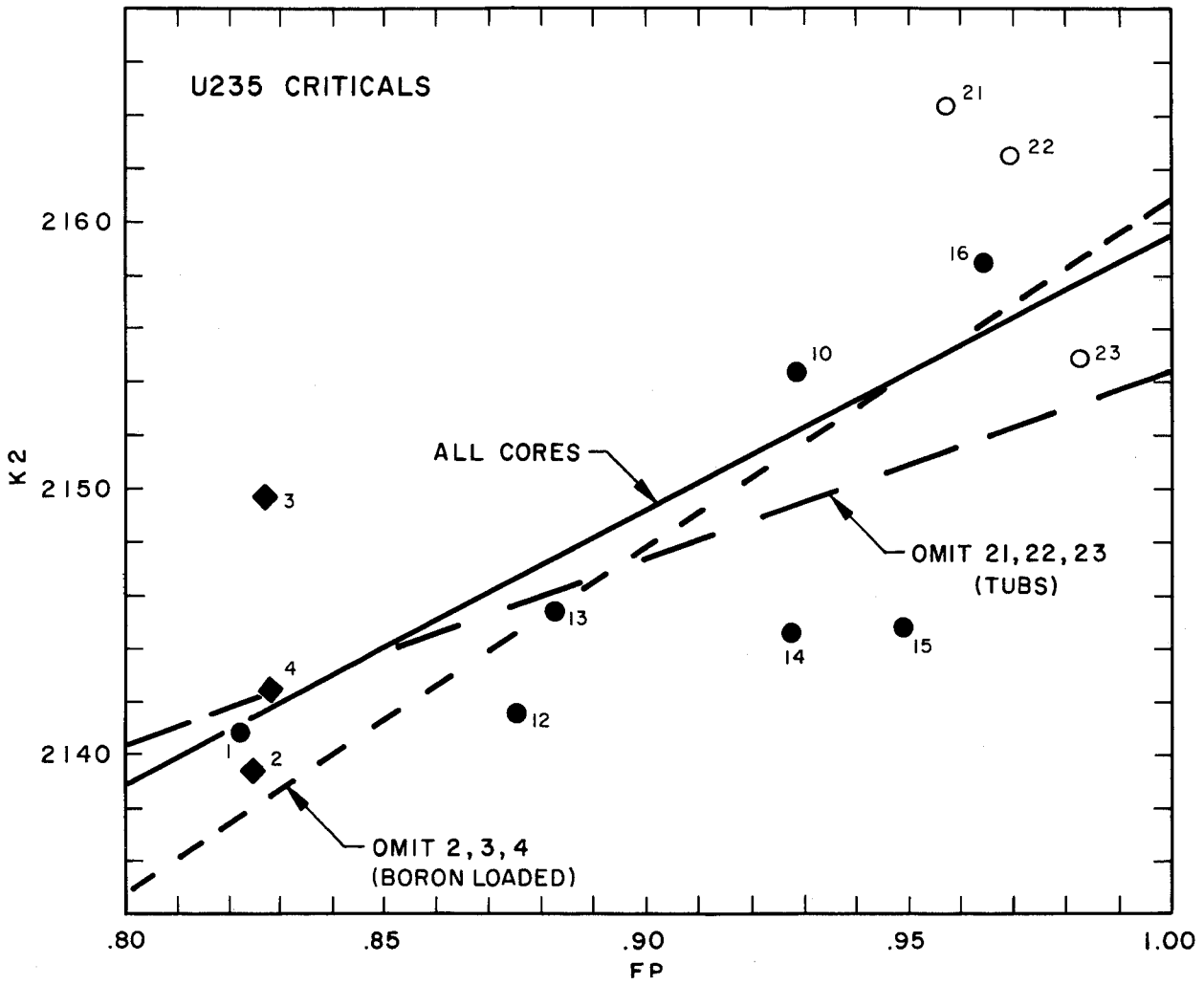

Figure 3 - Thermal Criticality Parameter K2 Versus FP Calculated with ENDF/B-IV for U235 Criticals

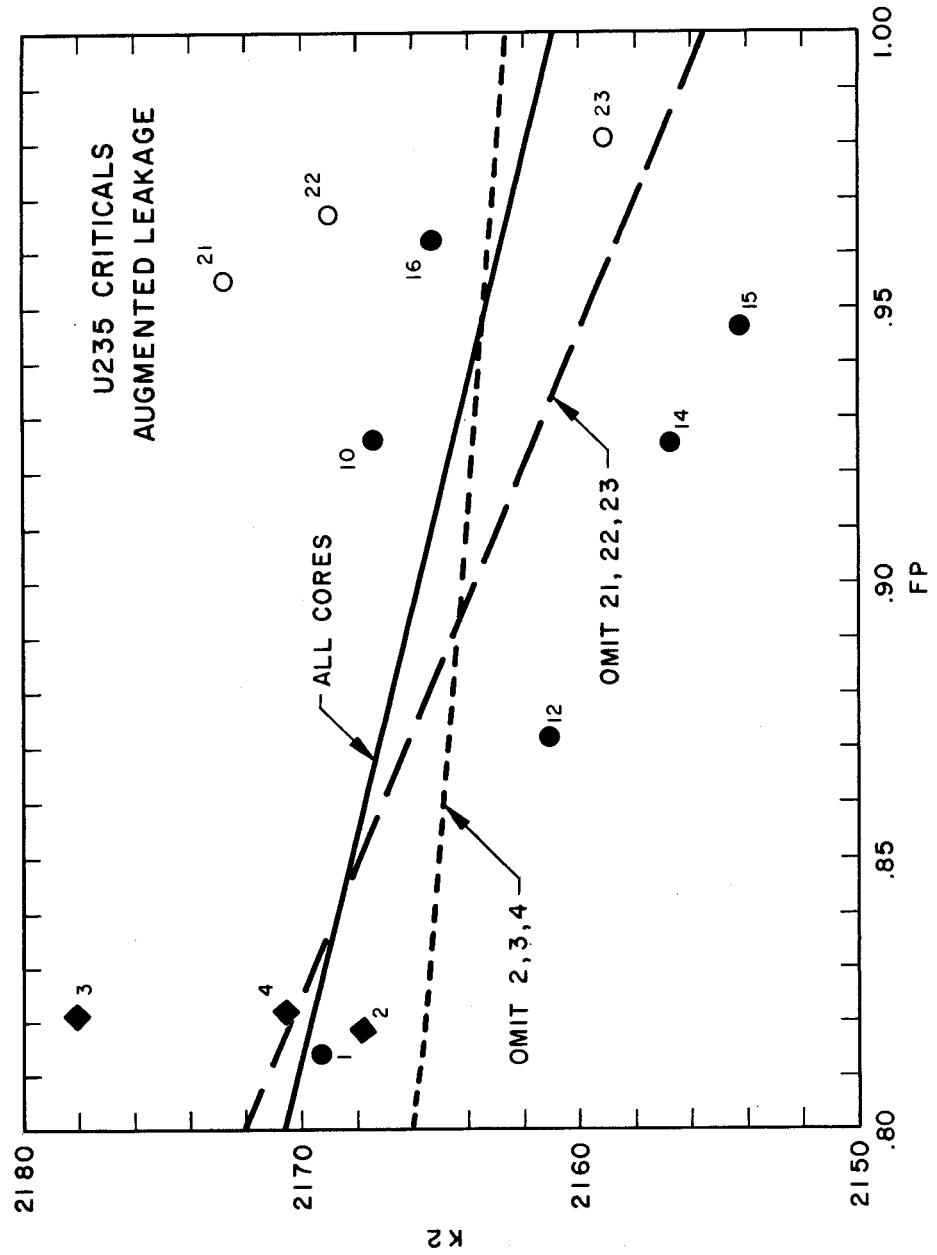

Figure 4 - Thermal Criticality Parameter K2 Versus FP Calculated With Augmented Leakage for U235 Criticals

Table 9

Thermal Criticality Parameter Constraint
K2 Derived from the Gwin-Magnuson Criticals

	(Ref. 5)	(Ref. 21)
K2	2155 ± 11	2148
g_f^u	.97065	
g_a^u	.97326	

Note: $K2 \equiv (\bar{\eta}_U - 1) \frac{\bar{\sigma}_a^U}{\bar{\sigma}_a^H}$

where $\bar{\sigma}_f^U = g_f^U \sigma_f^U$ (.0253 eV)

$\bar{\sigma}_a^U = g_a^U \sigma_a^U$ (.0253 eV)

It should be mentioned that the spread of K_{eff} values observed in different analyses (Table 1) does not imply a significant calculational method error in determining the K2 constraint.

ENDF/B-IV U235 (mat 1261), with the "g" factors of Table 9, gives K2 = 2137. This is 0.8% below the experimental value of 2155 ± 11 (0.5%).

B. TRX-1 and TRX-2 Lattices

The TRX Criticals were H_2O-moderated, fully reflected simple lattices operated at room temperature. The fuel rods were of uranium (enriched to 1.3% U235) clad in aluminum. They were 48 inches long and of 0.387 inch diameter, arranged in hexagonal arrays. TRX-1 and TRX-2 were full lattices, with moderator/fuel volume ratios of 2.35 and 4.02, respectively.

The following parameters were measured at the center of each lattice: the epi-thermal/thermal ratio of U238 capture (ρ^{28}) and of U235 fission (δ^{25}), the ratio of U238 capture to U235 fission (CR*), and the ratio of U238 fission to U235 fission (δ^{28}). Axial and radial bucklings were also measured.

1. Comparison of Full-Core and Leakage-Corrected Cell Monte Carlo Results. The integral parameters were calculated[4] by a method which has been used for several years. First, a full-energy-range cell calculation (zero leakage) was done with the

RCP01 Monte Carlo program. Relatively small leakage corrections to the cell reaction rates were then obtained from a full-core analysis with the multigroup P$_\ell$ program P7MG, which treated a homogenized lattice. Intracell flux weighting factors in P7MG were chosen to match Monte Carlo reaction rates in the zero-leakage cell.

Table 10 shows calculated lattice parameters obtained by the RCP01/P7MG method with ENDF/B-IV data. Also shown are measured parameters incorporating the systematic corrections evaluated by Sher and Fiarman[22].

Table 10

TRX Lattice Parameters, Measured and Calculated with ENDF/B-IV Data

	TRX-1 V_w/V_u = 2.35		TRX-2 V_w/V_u = 4.02	
	Exp.	Calc.	Exp.	Calc.
ρ^{28}(epi/thermal U238 capture)	1.320 ±.021	1.396 ±.004	.837 ±.016	.867 ±.004
δ^{25}(epi/thermal U235 fission)	.0987 ±.0010	.1009 ±.0004	.0614 ±.0008	.0614 ±.0003
δ^{28}(U238 fission/ U235 fission)	.0946 ±.0041	.0964 ±.0003	.0693 ±.0035	.0686 ±.0003
CR*(U238 capture/ U235 fission)	.797 ±.008	.809 ±.001	.647 ±.006	.648 ±.001
K_{eff}	1.000	.9837 ±.0010	1.000	.9894 ±.0013

Table 11 shows the calculation/experiment ratios for ENDF/B-IV in comparison with similar results for earlier versions. The following points are noteworthy:

(1) U238 epithermal capture is down 3-4% from Version III, with a corresponding reduction of ρ^{28}, which is now about 5% high relative to experiment.

(2) U238 fission is 6-9% above Version III depending on lattice pitch. This is due to the harder fission spectrum and reduced U238 inelastic scattering of Version IV.

(3) U235 epithermal fission is down 2% from Version III; thermal fission is up 1-2%.

(4) Total U238 capture is down ~2% from Version III; total U235 fission is up ~1%. CR* is much improved.

The RCPO1/P7MG method has been considered adequate because, except for K_{eff}, leakage affects the integral parameters only in a secondary way and parameter leakage corrections are modest (usually < 5%). On the other hand, K_{eff} is directly sensitive to the full-core leakage rates, which are determined by P7MG. In TRX-1 and TRX-2, the leakage is about 15%.

Table 11

Summary of Parameter Results (ENDF/B-II, III, IV)

Parameter	ENDF/B Version	Calculation/Experiment TRX-1	TRX-2
ρ^{28}	IV	1.058 ± .017	1.036 ± .020
	III	1.077	1.074
	II	1.079	1.071
δ^{25}	IV	1.022 ± .011	1.000 ± .014
	III	1.045	1.057 (?)
	II	1.034	1.023
δ^{28}	IV	1.019 ± .044	.990 ± .050
	III	.944	.943
	II	.904	.894
CR*	IV	1.015 ± .010	1.002 ± .010
	III	1.040	1.031
	II	1.043	1.031

In order to obtain an overall calculation of consistent accuracy, Monte Carlo analyses of the uniform TRX lattices were done with each core represented explicitly in three dimensions[4]. Figs. 5 and 6 show the radial RCPO1 representation of the lattices, with each clad rod described explicitly. In each case, the lattice was surrounded by a thick water reflector. The axial description of the cores is shown schematically in Figure 7.

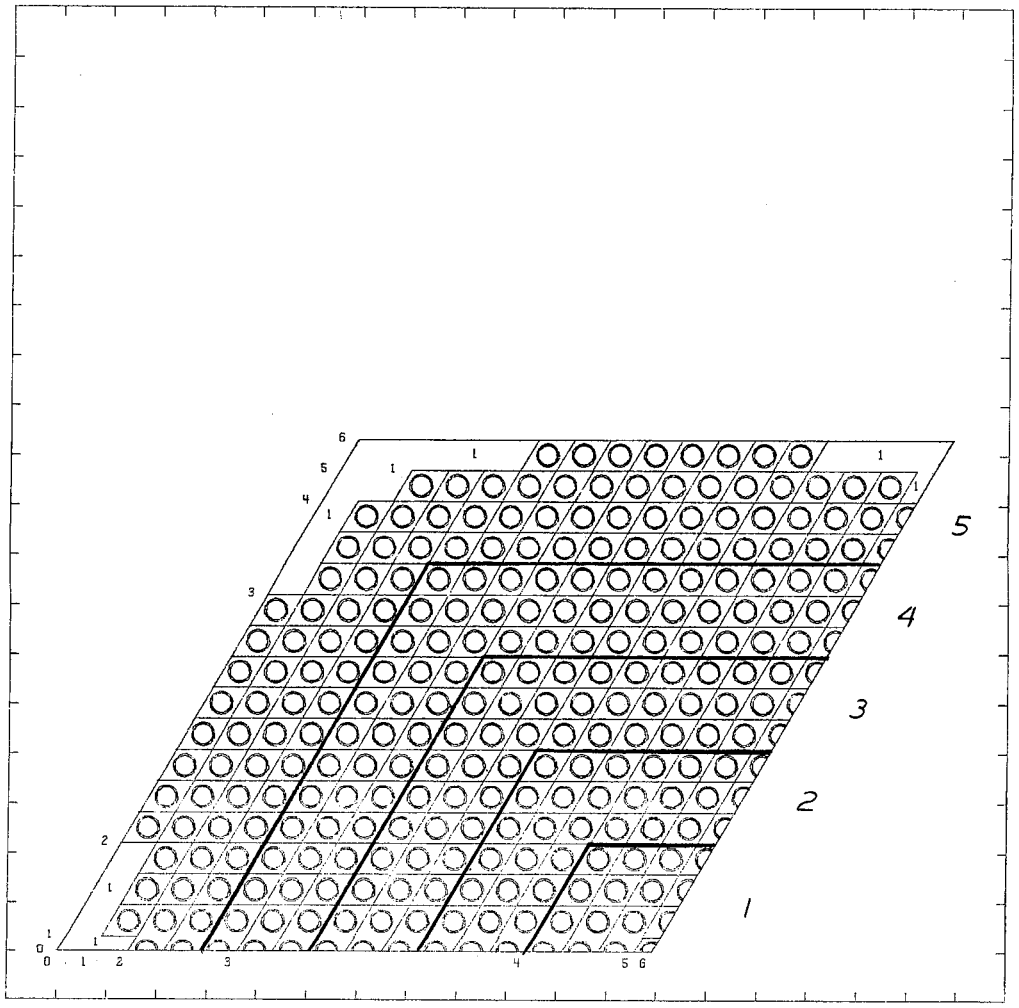

Figure 5 - RCP01 Radial Representation of TRX-1 (1/3 Core)

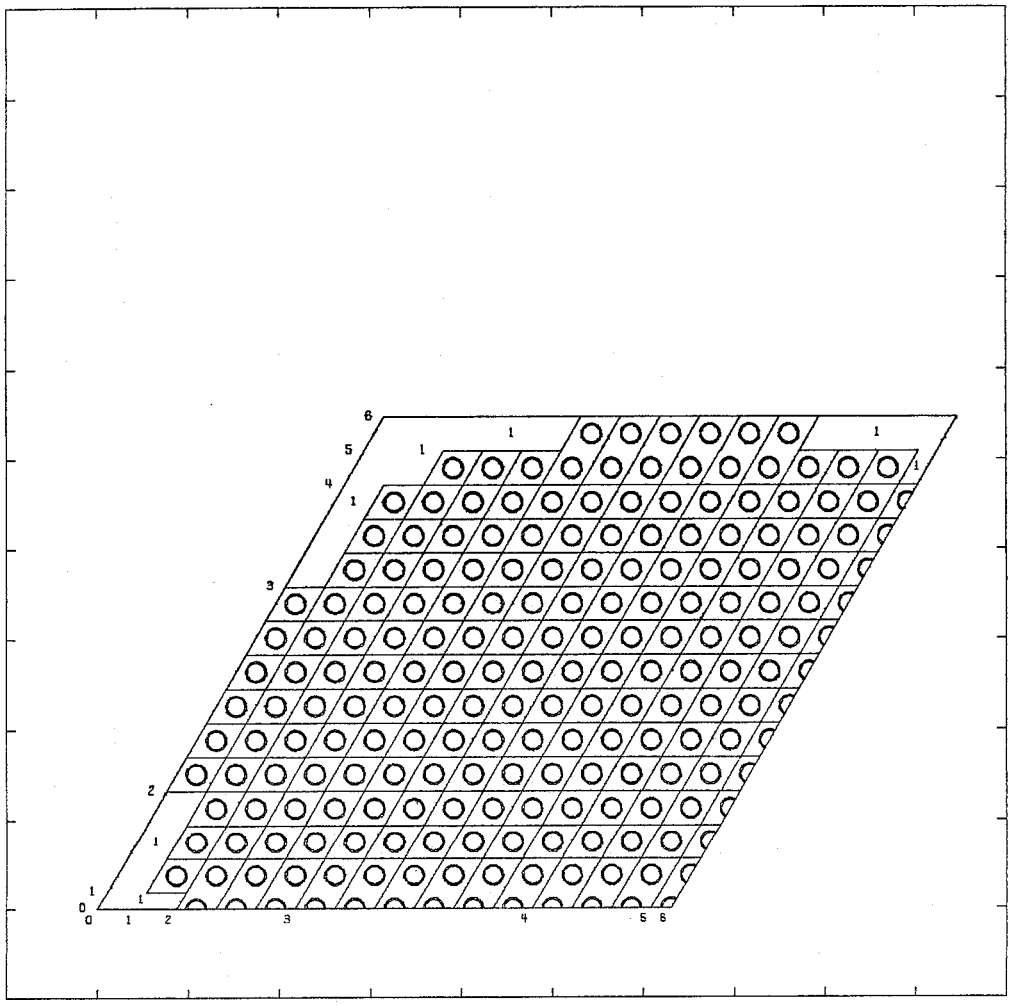

Figure 6 - RCP01 Radial Representation of TRX-2

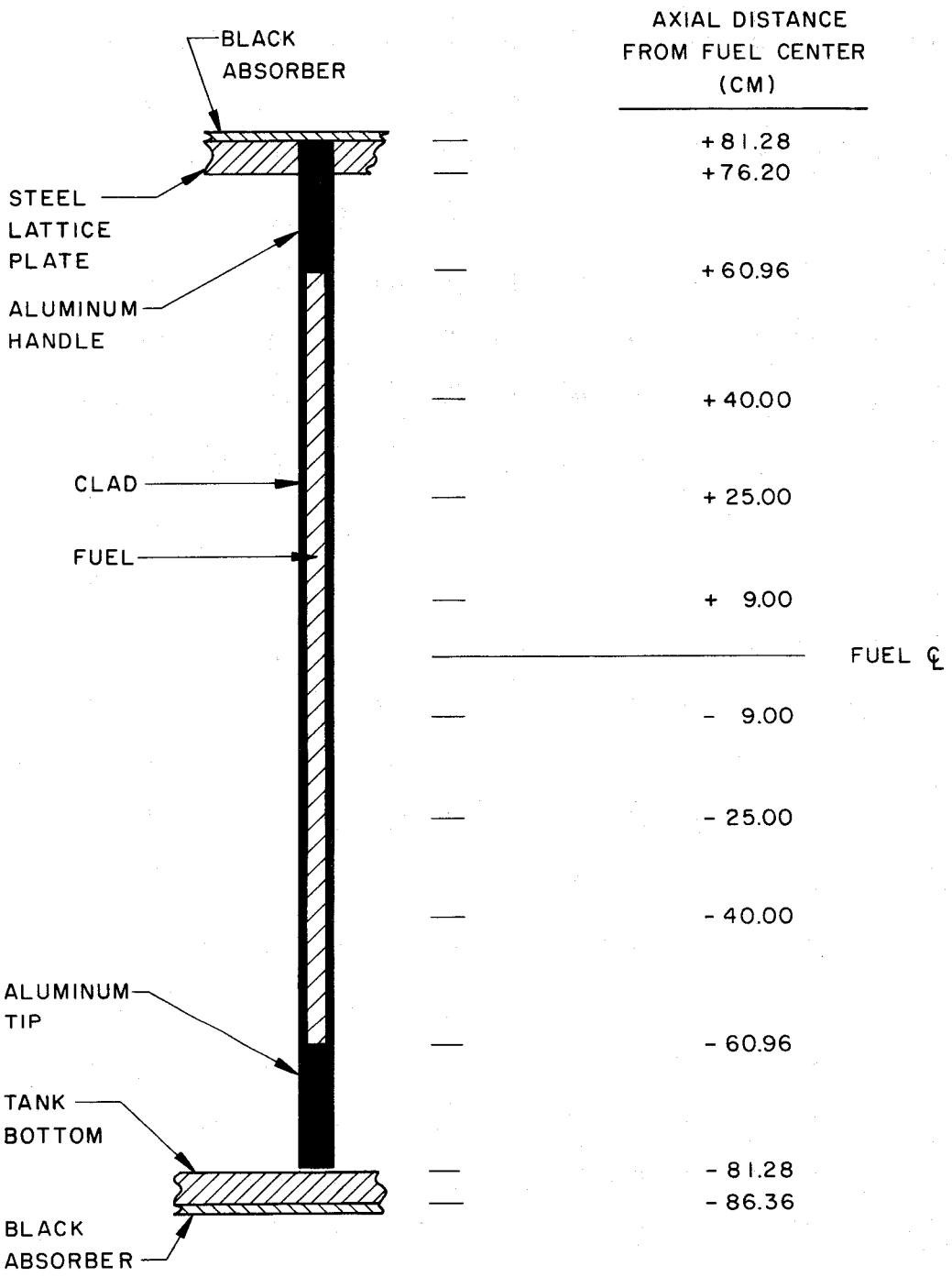

Figure 7 - RCP01 Axial Representation (Schematic)

Several independent 100-iteration calculations were run for each core. There were 500 histories in the first iteration; this was increased by 10 histories in each succeeding iteration, for a total of 100,500 histories. The first calculation started with a flat source guess. In subsequent calculations, the initial-source guess was obtained from the final spatially-converged source for the first calculation.

Because of the large central asymptotic regions in TRX-1 and TRX-2, it was possible to obtain good statistics for central core reaction rates and integral parameters. These are directly comparable with the measurements, which were made at (or very near) core center. The best central-core parameter values are taken to be those obtained over hexes 0-6, and within 40 cm of axial center. In Tables 12 and 13, these are compared with corresponding parameters obtained from the RCP01/P7MG method. Agreement is excellent for both lattices. This is fortunate because such full-core Monte Carlo calculations are expensive (due to the added spatial variables) and cannot be applied to parameters measured in marginally asymptotic situations.

Table 12

Comparison of TRX-1 Integral Parameters Obtained by the Full-Core-RCP01 and RCP01/P7MG Methods

Integral Parameter	Zero-Leakage Cell (RCP01)	Center of Actual Core	
		RCP01/P7MG	Direct RCP01
ρ^{28}	1.334 ± .004	1.396 ± .004	1.396 ± .004
δ^{25}	.0970 ± .0004	.1009 ± .0004	.1009 ± .0005
δ^{28}	.0896 ± .0003	.0964 ± .0003	.0972 ± .0003
CR*	.793 ± .001	.809 ± .001	.809 ± .001
K_{eff}	1.1696 ± .0009	.9837 ± .0008	.9839 ± .0006

Similar full-core Monte Carlo analyses of these lattices were done at BNL[3] with the RECAP program. A fairly detailed comparison showed good agreement between the two Monte Carlo cross section libraries, and major reaction rates in the zero-leakage cell showed excellent agreement with the RCP01 results. Differences in the full-core central parameter results appear to be due to statistics. (See Figures 8-10.)

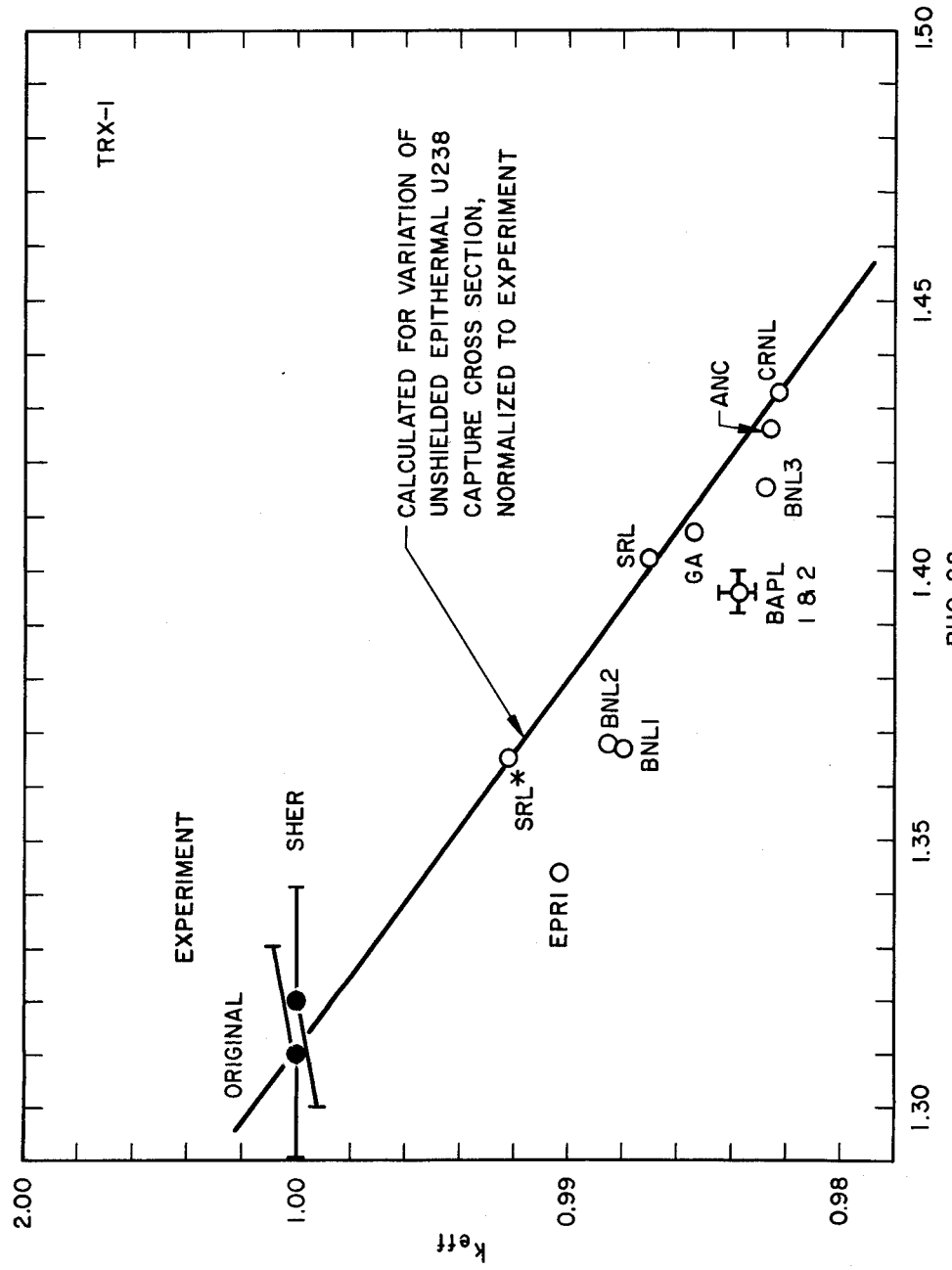

Figure 8A - Keff Versus Rho 28 for TRX-1

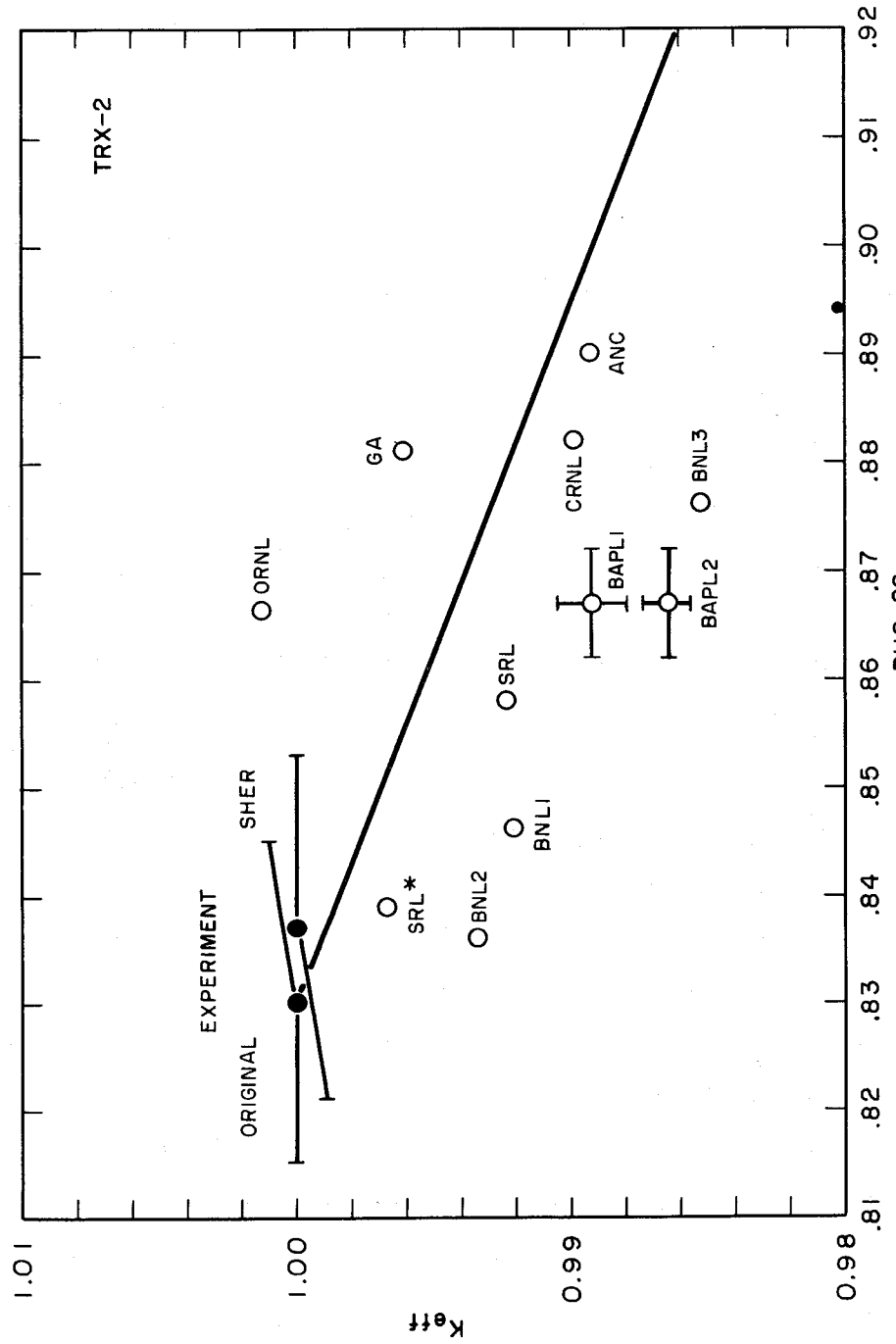

Figure 8B - Keff Versus Rho 28 for TRX-2

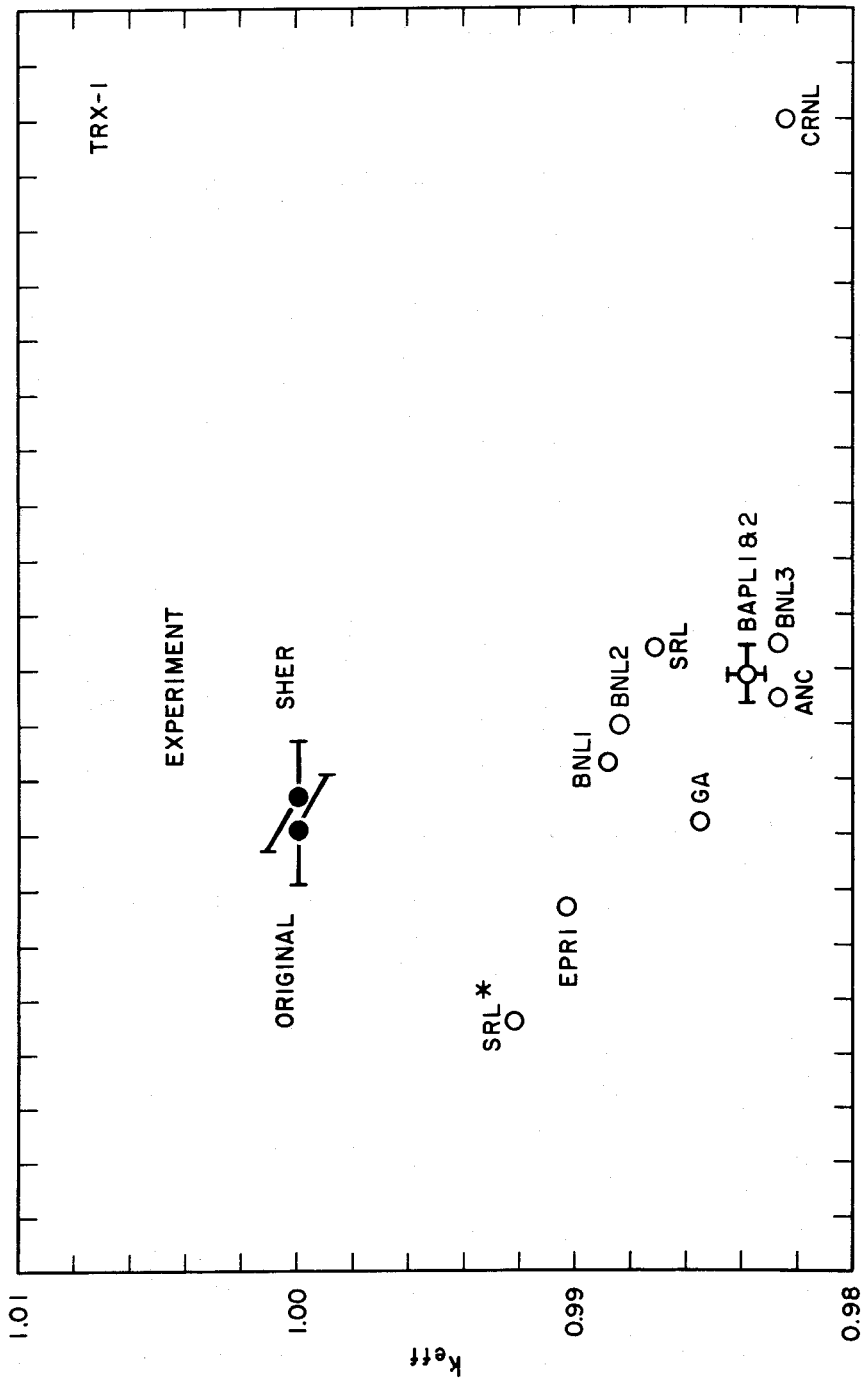

Figure 9A - K_{eff} Versus Delta 25 for TRX-1

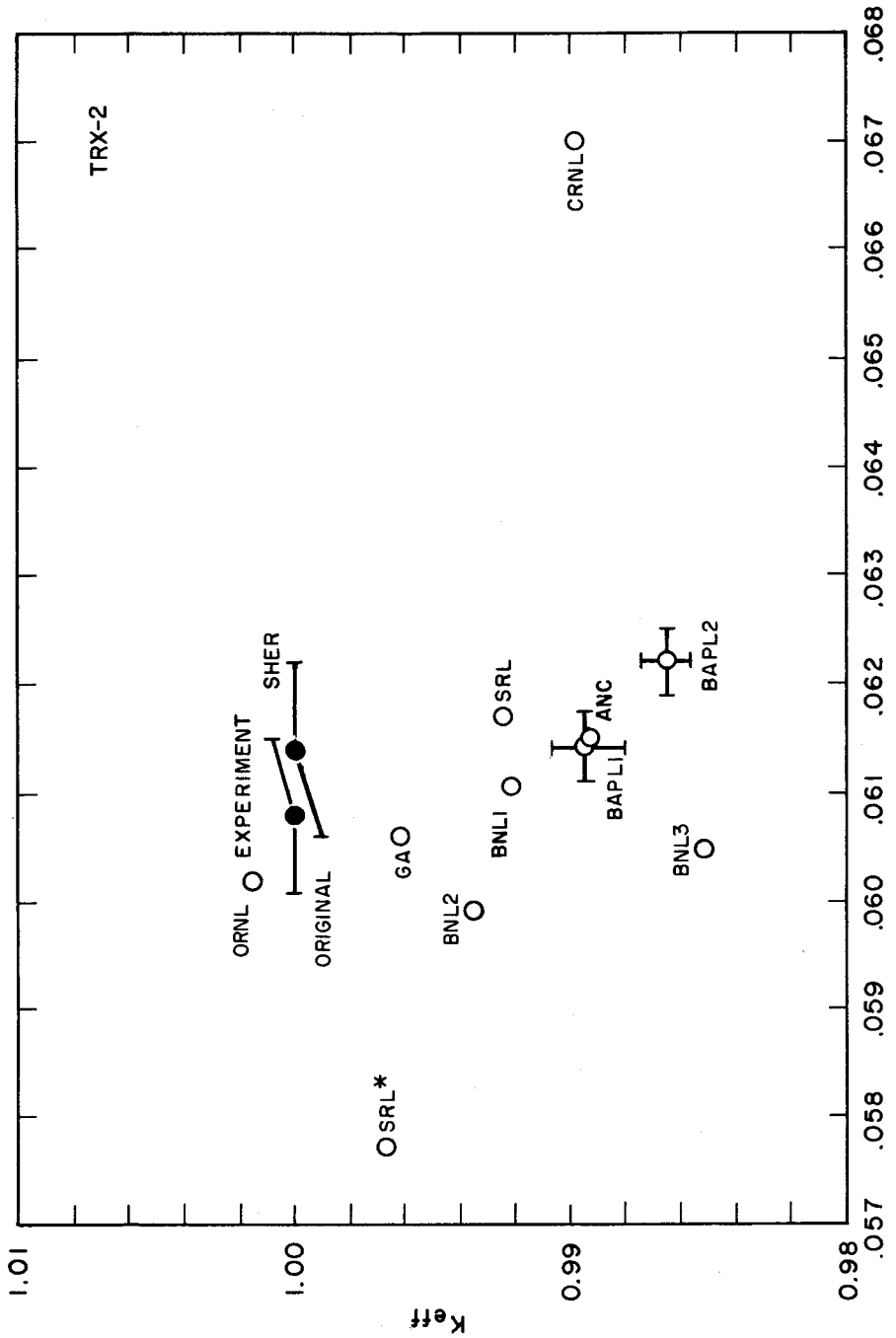

Figure 9B - K_{eff} Versus Delta 25 for TRX-2

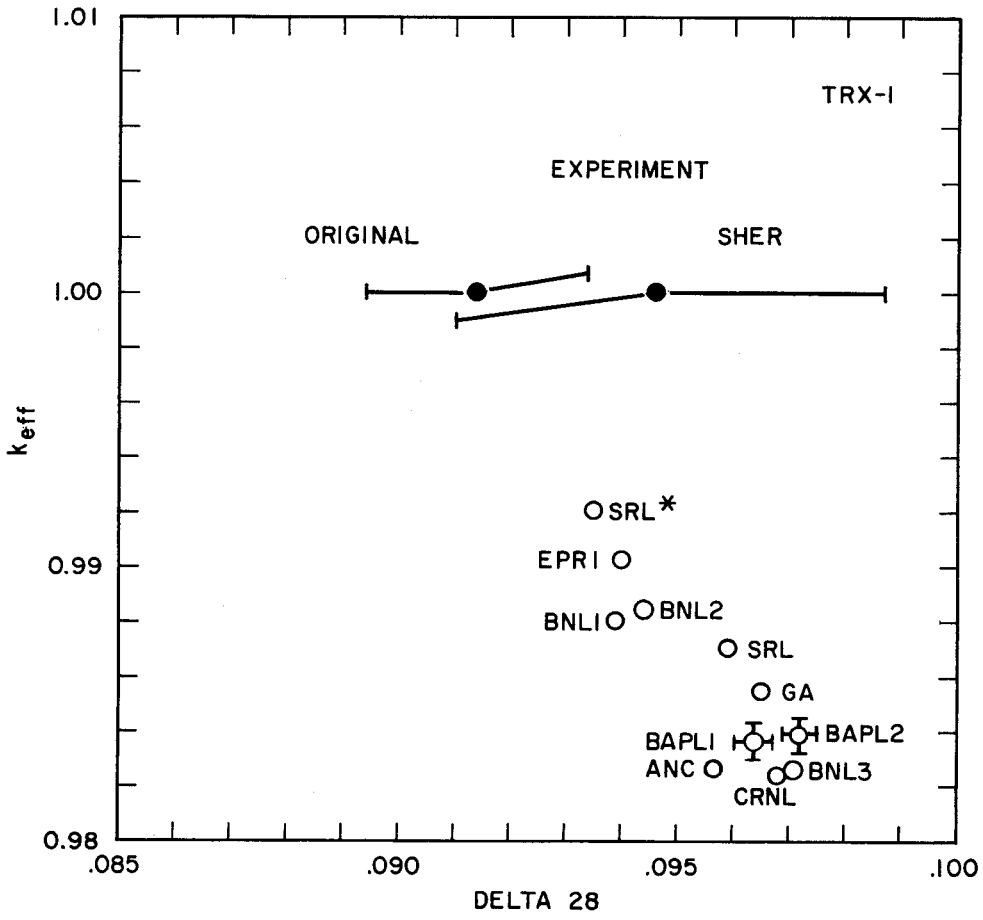

Figure 10A - K_{eff} Versus Delta 28 for TRX-1

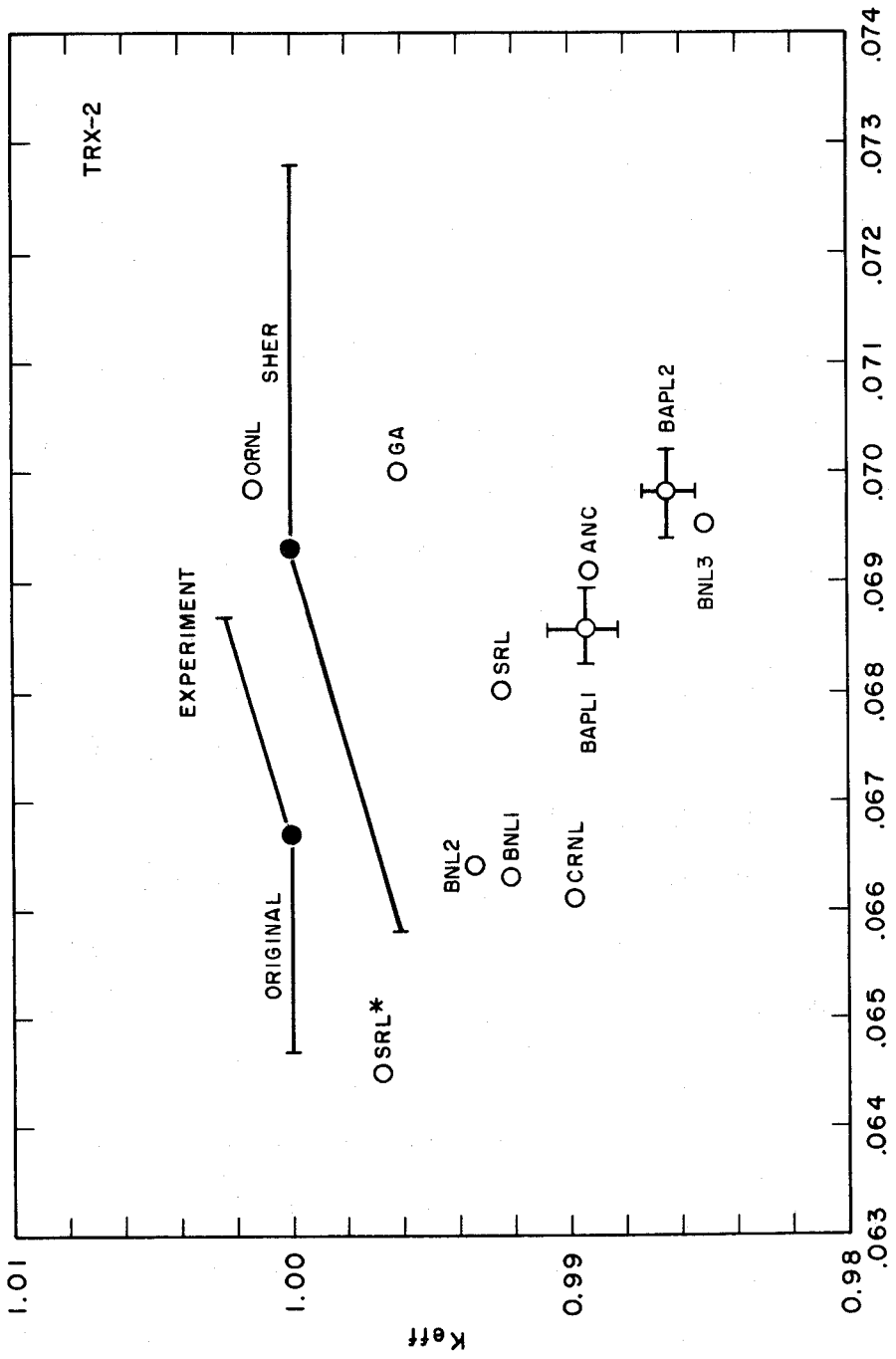

Figure 10B - K_{eff} Versus Delta 28 for TRX-2

Table 13

Comparison of TRX-2 Integral Parameters Obtained by the Full-Core-RCP01 and RCP01/P7MG Methods

Integral Parameter	Zero-Leakage Cell (RCP01)	Center of Actual Core	
		RCP01/P7MG	Direct RCP01
ρ^{28}	.839 ± .003	.867 ± .004	.867 ± .005
δ^{25}	.0596 ± .0003	.0614 ± .0003	.0622 ± .0003
δ^{28}	.0651 ± .0003	.0686 ± .0003	.0698 ± .0004
CR*	.639 ± .001	.648 ± .001	.648 ± .002
K_{eff}	1.1586 ± .0013	.9894 ± .0013	.9865 ± .0008

2. Nuclear Data Sensitivities. The important data-sensitivities of integral parameters in these lattices can be summarized qualitatively as follows:

ρ^{28} is sensitive to the U238 thermal σ_c and the shielded capture resonance integral. Since this integral is only about 15b, unshielded components of the capture, which are small compared to the dilute capture integral, become very important in the lattice.

δ^{25} is sensitive to the U235 thermal σ_f and the dilute fission resonance integral.

Both ρ^{28} and δ^{25} are sensitive to the moderator σ_s (since slowing down competes directly with resonance absorption). For hydrogen, the uncertainty of σ_s is not important for ρ^{28} and δ^{25}. However, for deuterium the uncertainty may be significant. Slowing down and leakage act as buffers, which decouple U238 and U235 resonance absorption.

δ^{28} is primarily sensitive to the U238 fission cross section, the U238 inelastic scattering (by level), and the U235 fission spectrum. It is relatively insensitive to U235 fission cross sections (insofar as these are able to give reasonable K_{eff}).

K_{eff} is sensitive to the above data, plus leakage. The other parameters do not show a very significant leakage sensitivity.

Tomlinson, et al[6] have performed a systematic sensitivity analysis of TRX-2, obtaining detailed sensitivity profiles for each integral parameter in terms of the most important cross sections, by multigroup. They have also unfolded integral parameter uncertainties stemming from uncertainties of differential data. These are shown in Table 14 along with uncertainties assigned to the

integral measurements[22]. The 0.4% uncertainty of δ^{28} calculated in Ref. 6 seems rather small in view of the fact that δ^{28} in TRX-2 increased 5% from ENDF/B Version II to III and another 5% from Version III to IV.

Table 14

Uncertainties of TRX-2 Integral Parameters (1σ)

	Integral Experiment (Ref. 22) %	Calculated Value, from Differential Data Alone (Ref. 6) %
ρ^{28}	1.9	0.9
δ^{25}	1.3	2.0
δ^{28}	5.1	0.4
CR*	0.9	0.8
K_{eff}	--	0.4

3. Comparison of Calculations and Experiment.

(a) Rho 28 (Figure 8). In CSEWG data testing, the chief problem in analyzing these lattices, both from a data and methods point of view, has been to properly calculate U238 resonance capture. The situation with ENDF/B-IV data is best illustrated by a plot of ρ^{28} versus K_{eff}, as shown in Figure 8A for TRX-1. The line in this figure is a calculated sensitivity[23] obtained by varying the unshielded U238 epithermal capture cross section, normalized to the experimental value. The other data points are ENDF/B-IV results obtained in CSEWG data testing[2,3,4,6*].

In Figure 8A, the strong correlation between calculated K_{eff} and ρ^{28} results suggests that differences of calculated U238 resonance capture are the chief source of the K_{eff} differences. Furthermore the spread of calculated ρ^{28} values is as large as the difference of the best results from experiment. Leakage calculations by the different data testers appear to be generally consistent, since individual leakage errors would tend to disperse K_{eff} while having little effect on ρ^{28}.

*A key to the calculations in Figures 8-13 can be found in Table 15.

Table 15

Guide to Benchmark Calculation Results

Designation	Laboratory	Method
ANC	Aerojet Nuclear Co.	S_N with RABBLE resonance treatment (Ref. 2)
BAPL1	Bettis Atomic Power Lab	Cell Monte Carlo with B_1 leakage correction (RCP01/P7MG) (Ref. 4) (Supersedes Ref. 2)
BAPL2	Bettis Atomic Power Lab	Full core Monte Carlo (RCP01) (Ref. 4)
BNL1	Brookhaven National Lab	HAMMER with REPC Monte Carlo resonance absorption (Ref. 24)
BNL2	Brookhaven National Lab	HAMMER with RECAP-12 Monte Carlo cell rates (Ref. 3)
BNL3	Brookhaven National Lab	Full core Monte Carlo (RECAP-12) (Ref. 3)
CRNL	Chalk River Nuclear Laboratories	HAMMER with Nordheim resonance treatment (Ref.2)
EPRI	Electric Power Research Institute	HAMMER with RABBLE resonance treatment (Ref.2)
GA	General Atomic Company	S_N with GAND3 and MICROX resonance treatment (Ref.2)
SRL	Savannah River Laboratory	Integral transport theory with Nordheim resonance treatment. B_1 leakage correction (Ref. 2)
SRL*	Savannah River Laboratory	Same as SRL except improved resonance absorption (Ref. 2)

The correlation of K_{eff} with ρ^{28} shown in Figure 8A also tends to support the measured ρ^{28}. That is, a calculation which reproduces the measured ρ^{28} can be expected to give a correct K_{eff}. In this connection, however, recall that the harder fission spectra previously discussed will, at 15% leakage, give K_{eff} around .994 for the homogeneous U235 criticals. These same spectra do not change K_{eff} in TRX-1 because the increased leakage is almost

exactly compensated by increased U238 fission. Thus, with these spectra, the TRX-1 K_{eff} of 0.985 is to be compared not with 1.00 but with 0.994. Whatever change is made to U235 to bring the homogeneous critical K_{eff} to 1.00 will bring the TRX-1 K_{eff} up by about the same amount. Hence the defect of K_{eff} attributable to excess U238 capture is approximately 0.9%.

The U238 capture situation is similar for TRX-2, as shown in Figure 8B. The ORNL analysis[6] obtains a 0.9% standard deviation of ρ^{28} from all differential data uncertainties. Once again the calculated ρ^{28} and K_{eff} results are highly correlated. For this lattice, they fall about 0.5% below the calculated sensitivity line.

The high eigenvalues obtained by GA and ORNL for TRX-2 appear to be due to leakage under-prediction (as happened in the earlier BAPL calculations[2]). Overall, compared to TRX-1, there seems to be a somewhat greater spread in calculated leakage for this looser (i.e. more heterogeneous) lattice.

In summary, with ENDF/B-IV, the RCP01/P7MG values of ρ^{28} are 3.5% - 5.5% above experiment, and a ~2.5% reduction of calculated ρ^{28} can be expected by use of new resonance parameters[4], which leaves ρ^{28} 1% - 3% above experiment, if there are no other significant changes in capture data. At this level, many factors can be important and some additional improvement may be obtainable - from a multilevel resonance representation, for example (see Ref. 23). The uncertainty of ρ^{28} from differential data is 0.9%[6] and an overall uncertainty of 2% is assigned to the integral measurements. Differences among the calculational methods, even among the presumed best methods, are 2-3% and now constitute the most important area of uncertainty.

(b) Delta 25 (Figure 9). SRL*, EPRI and CRNL are outliers; other calculations show reasonable agreement among themselves and with experiment. The ENDF/B-IV U235 fission resonance integral is about 284b (above 0.5 eV), while the best integral result is near the value 275 + 5 of Ref. 17. Change to the lower value would reduce δ^{25} by slightly more than 3%.

(c) Delta 28 (Figure 10). Agreement is within about 3% among calculations for TRX-1, but much worse in the looser (and more heterogeneous) TRX-2. For both lattices, the large experimental uncertainties cover the calculated results. δ^{28} increased by 10% from ENDF/B Version II to Version IV. Further increases are expected with ENDF/B-V due to changes of the U238 inelastic scattering cross section. Use of an equilibrium spectrum based on a Watt prompt fission spectrum with $\bar{E}$ = 2.027 MeV will raise δ^{28} by 3%. The Steen Standard 2 prompt spectrum raises it by 6%.

C. MIT-1, 2, and 3 Lattices

The MIT experiments were D_2O-moderated exponential lattices of natural uranium rods in a triangular lattice pattern. The rods were

of 2.565 cm diameter with spacings of 11.43, 12.70 and 14.605 cm, respectively, in MIT-1, 2, and 3. Measured lattice integral parameters included B^2, ρ^{28}, δ^{25}, δ^{28} and CR*.

MIT-1 and 2 were analyzed by five laboratories and MIT-3 was analyzed by three laboratories, with results shown in ENDF-230[2].

A comparison of calculated and measured integral parameters is shown in Figures 11-13. In comparison to the TRX results, the following observations can be made.

ρ^{28} is calculated a few percent high, in qualitative agreement with TRX-1, 2.

δ^{25} is calculated much higher but the spread is so great that little can be said.

δ^{28} shows agreement, within large experimental uncertainties, but is on the low side relative to the TRX comparison.

The integral parameter results for these lattices are not inconsistent with those for the TRX series. However, due to the scatter of calculation/experiment comparisons, and among the calculations themselves, it is not possible to draw any more specific conclusions.

III. CONSISTENCY ANALYSIS OF THERMAL BENCHMARK EXPERIMENTS

In Section II results of lattice calculations using ENDF/B-IV cross sections have been compared to experimental results for the TRX-1, 2 and MIT-1, 2, 3 lattices. The quality of measurement in these experiments was not considered, but should be given careful attention to put the calculated results in proper perspective. The objective of this section is to examine the benchmark experiments to determine if the measured integral parameters are consistent among themselves.

It is instructive to examine how a thermal "benchmark" lattice experiment is chosen. Historically it appears that consensus was the primary criterion; that is, a geometrically simple lattice having good, widely distributed documentation could achieve "benchmark" status easily. There is no evidence that another criterion was used in the selection of the TRX or MIT benchmarks in Section II. For cross section testing purposes a benchmark experiment should meet a strict quantitative criterion rather than a purely qualitative one.

Consistency analysis provides this quantitative criterion to select thermal benchmarks, and has additional applications in other contexts. It can provide information on required integral parameter measurements to assure consistency. It can be used during an experiment to assess the quality of results prior to dismantling the experiment. And, to a limited extent, it can be used to assess the adequacy of experimental methods used in integral parameter measurements.

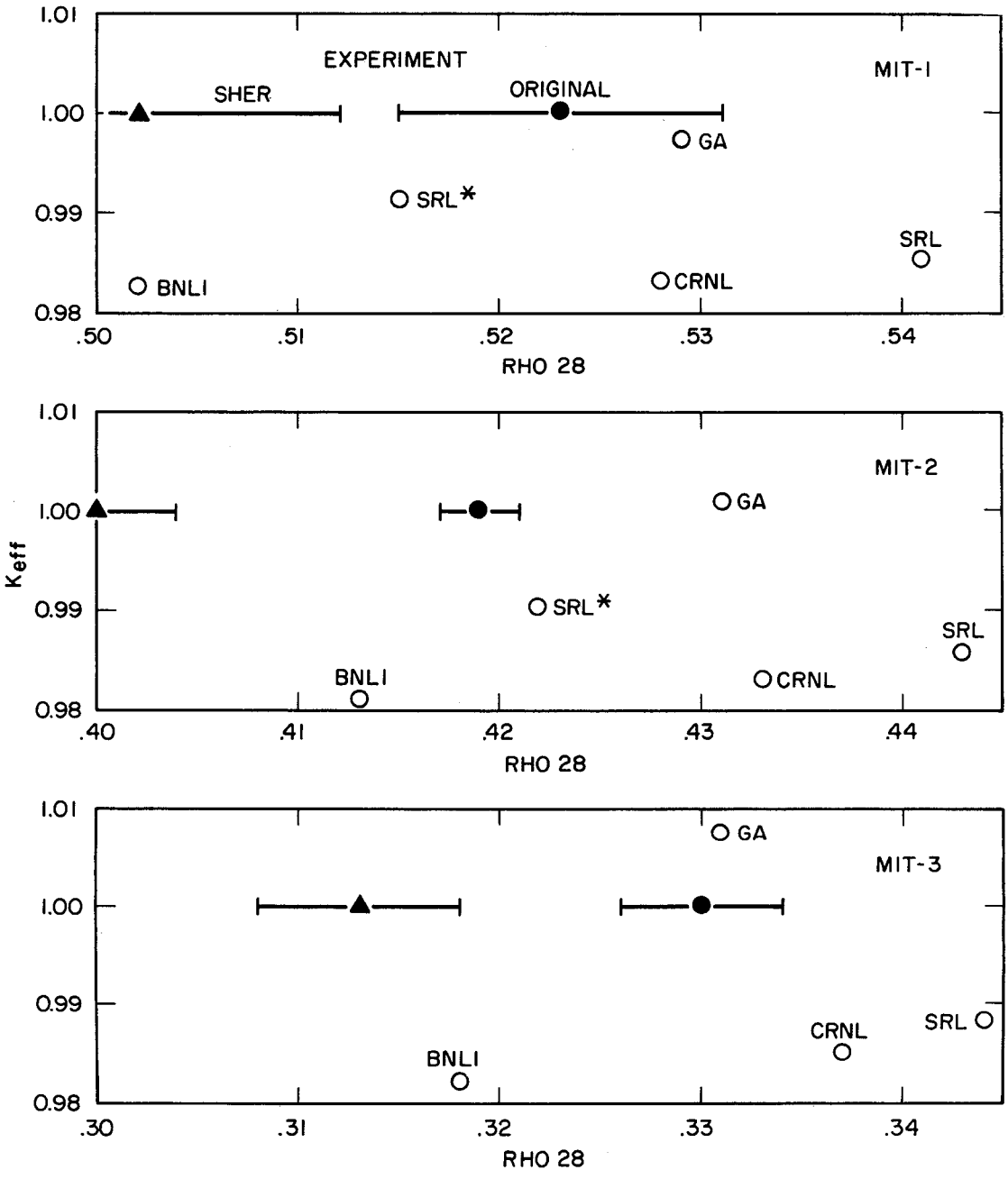

Figure 11 - K_{eff} Versus Rho 28 for MIT-1, 2, 3

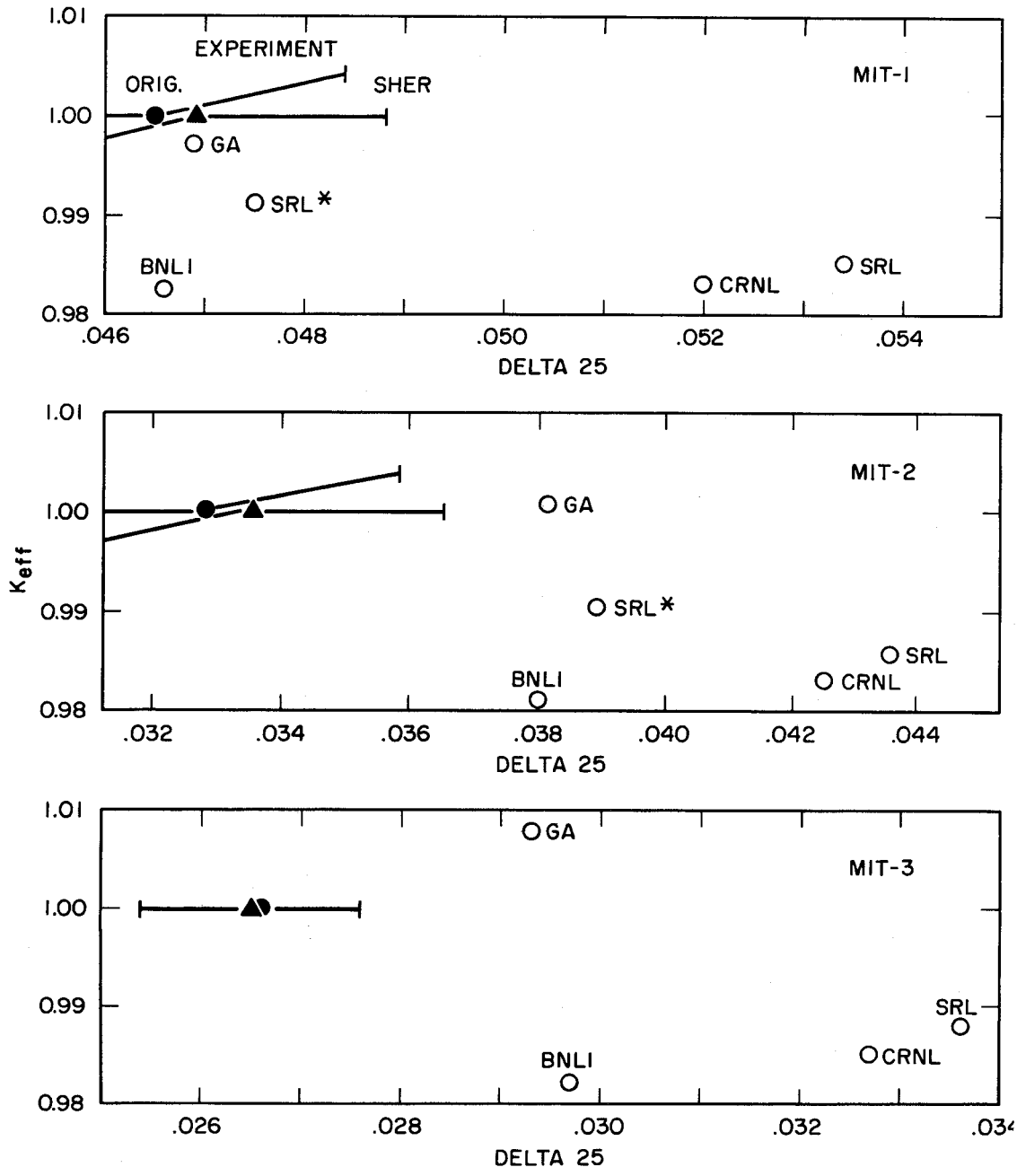

Figure 12 - K_{eff} Versus Delta 25 for MIT-1, 2, 3

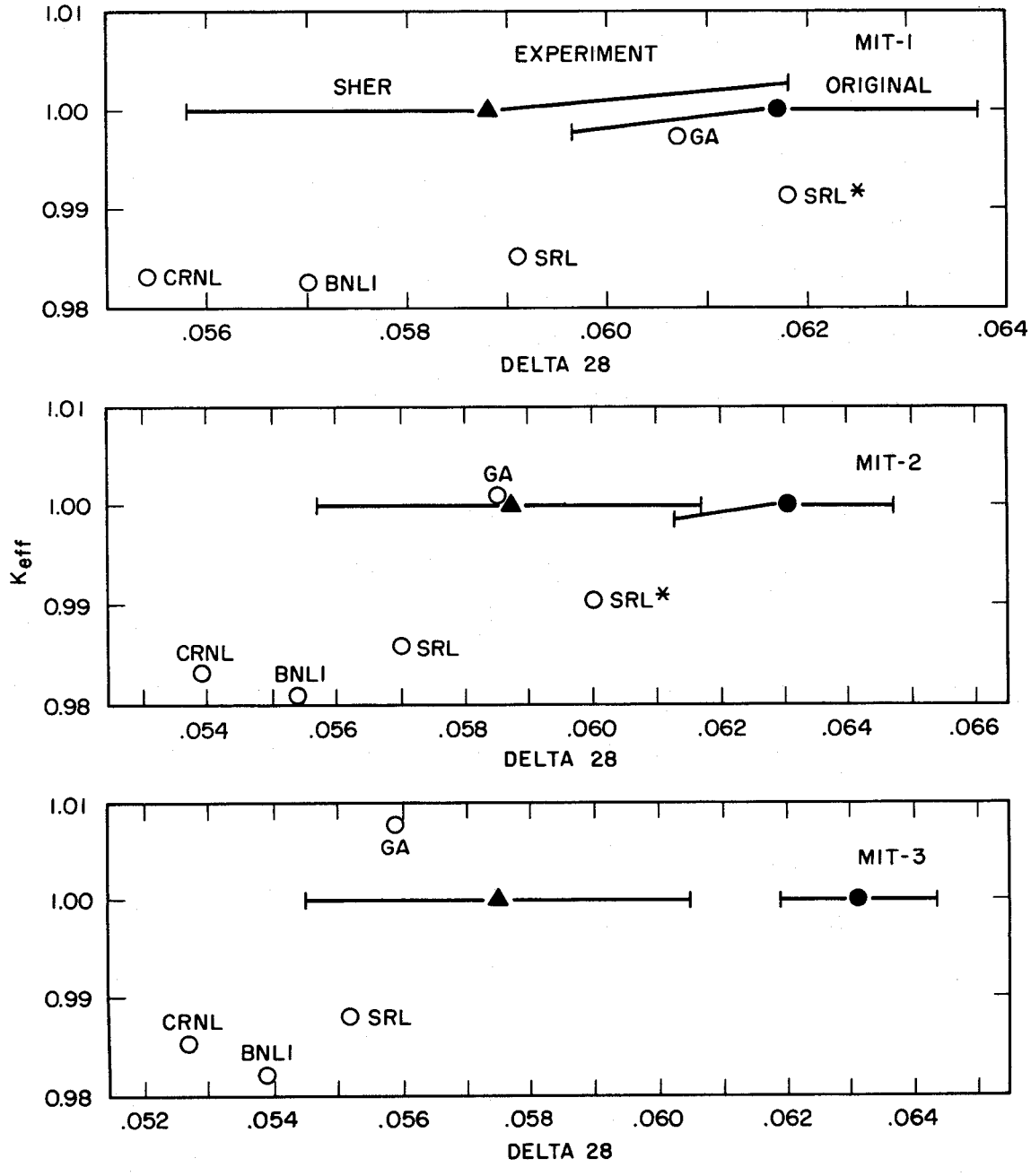

Figure 13 - K_{eff} Versus Delta 28 for MIT-1, 2, 3

The general approach of consistency analysis of thermal benchmarks is to write down the equations relating measured integral activation parameters to reactivity. These quantities are related by cross section and spectrum dependent coefficients. The coefficient terms are evaluated by calculation with a state-of-the-art lattice analysis code using the best cross section data available (here ENDF/B-IV). One integral parameter is then written in terms of the other measured integral parameters and the coefficients from calculation to predict a value for the parameter of interest. In a consistent benchmark experiment the predicted and experimental value of the parameter will agree within the calculated and experimental uncertainties.

The emphasis here will be on the TRX-1, 2 and MIT-1, 2, and 3 benchmark experiments. Application of consistency analysis to a wider range of benchmark experiments appears in Ref. 7.

A. Consistency Equations for U235-U238 Lattices

This section will derive an expression for lattice material buckling in terms of the experimentally measured activation parameters and cross section dependent constants.

For a uniform lattice with U235 and U238 the only fissionable materials present, the two-group neutron balance equation that must hold at critical (or steady state sub-critical with constant source) is

$$\text{LEAKAGE} + \text{ABSORPTION} = \text{PRODUCTION} \tag{1}$$

$$(D_1\varphi_1+D_2\varphi_2)B_m^2 + \Sigma_{a_1}\varphi_1 + \Sigma_{a_2}\varphi_2 = \nu\Sigma_{f_1}\varphi_1 + \nu\Sigma_{f_2}\varphi_2 \tag{1a}$$

Dividing Equation 1a by $\Sigma_{f_2}\varphi_2$ and rewriting slightly yields

$$\left\{\frac{D_1\varphi_1/\varphi_2+D_2}{\Sigma_{f_2}}\right\}B_m^2 = \frac{\left\{\nu\Sigma_{f_1}^{25}\varphi_1+\nu\Sigma_{f_1}^{28}\varphi_1+\nu\Sigma_{f_2}^{25}\varphi_2-\Sigma_{C_1}^{25}\varphi_1-\Sigma_{C_1}^{28}\varphi_1-\Sigma_{C_1}^{0}\varphi_1-\Sigma_{f_1}^{25}\varphi_1-\Sigma_{f_1}^{28}\varphi_1\right\}}{\Sigma_{f_2}\varphi_2}$$

$$- \frac{\Sigma_{C_2}^{25}\varphi_2 + \Sigma_{C_2}^{28}\varphi_2 + \Sigma_{C_2}^{0}\varphi_2 + \Sigma_{f_2}^{25}\varphi_2}{\Sigma_{f_2}\varphi_2} \tag{1b}$$

where $\Sigma_{C_n}^{0}$ represents capture in all materials other than U235 and U238.

The experimentally measured activation parameters are defined as follows.

U238 capture ratio $$\rho^{28} = \frac{\text{Epithermal U238 captures}^{\dagger}}{\text{Thermal U238 captures}} = \frac{\Sigma_{C_1}^{28}\varphi_1}{\Sigma_{C_2}^{28}\varphi_2}$$

U235 fission ratio $$\delta^{25} = \frac{\text{Epithermal U235 fissions}^{\dagger}}{\text{Thermal U235 fissions}} = \frac{\Sigma_{f_1}^{25}\varphi_1}{\Sigma_{f_2}^{25}\varphi_2}$$

U238 fast fission ratio $$\delta^{28} = \frac{\text{Total fission in U238}}{\text{Total fissions in U235}} = \frac{\Sigma_{f_1}^{28}\varphi_1}{\Sigma_{f_1}^{25}\varphi_1 + \Sigma_{f_2}^{25}\varphi_2}$$

Modified conversion ratio $$C^* = \frac{\text{Total U238 captures}}{\text{Total U235 fissions}} = \frac{\Sigma_{C_1}^{28}\varphi_1 + \Sigma_{C_2}^{28}\varphi_2}{\Sigma_{f_1}^{25}\varphi_1 + \Sigma_{f_2}^{25}\varphi_2} \qquad (2)$$

Define in addition the quantity

$$\xi \equiv \frac{\text{Total captures in materials other than U235 or U238}}{\text{Total fission in U235}}$$

$$= \frac{\Sigma_{C_1}^{0}\varphi_1 + \Sigma_{C_2}^{0}\varphi_2}{\Sigma_{f_1}^{25}\varphi_1 + \Sigma_{f_2}^{25}\varphi_2} \qquad (3)$$

The (n,2n) reactions can be included in the numerator of ξ as negative capture events. Also define

$$\bar{\nu}_n = \frac{\overline{\nu\Sigma}_{f_n}}{\overline{\Sigma}_{f_n}} \text{ and } \bar{\alpha}_n = \frac{\overline{\Sigma}_{c_n}}{\overline{\Sigma}_{f_n}} \qquad (4)$$

Using the definitions in Equations 2, 3, and 4 allows Equation 1b to be written

$$\left\{\frac{D_1\varphi_1/\varphi_2 + D_2}{\Sigma_{f_2}}\right\} B_m^2 = (\bar{\nu}_2^{25}-1) + (\bar{\nu}_1^{25}-1)\,\delta^{25} - \bar{\alpha}_2^{25} - \bar{\alpha}_1^{25}\delta^{25} + (1+\delta^{25})\left\{(\bar{\nu}_1^{28}-1)\,\delta^{28} - C^* - \xi\right\}. \qquad (5)$$

---

†Relative to a Cd cut-off defining the group 1 - group 2 break.

The φ_1/φ_2 flux ratio is eliminated using the group 2 balance equation

$$(\Sigma_{a_2} + \Sigma_{r_{2\to1}} + D_2 B_m^2)\varphi_2 = \Sigma_{r_{1\to2}} \varphi_1 \tag{6}$$

Substitution of Equation 6 into Equation 5 yields the final expression

$$B_m^2 \left\{ \frac{D_1(\Sigma_{a_2} + \Sigma_{r_{2\to1}} + D_2 B_m^2}{\Sigma_{f_2} \Sigma_{r_{1\to2}}} + \frac{D_2}{\Sigma_{f_2}} \right\} = (\bar{\nu}_1^{25}-1)$$

$$+ (\bar{\nu}_1^{25}-1)\delta^{25} - \bar{\alpha}_2^{25} - \bar{\alpha}_1^{25}\delta^{25}$$

$$+ (1+\delta^{25}) \left\{ (\bar{\nu}_1^{28}-1)\delta^{28} - C^* - \xi \right\} . \tag{7}$$

Equation 7 could be expressed in terms of ρ^{28} rather than C* using

$$C^* = \frac{\Sigma_{c_2}^{28}\varphi_2 \ (1 + \rho^{28})}{\Sigma_{f_2}^{25}\varphi_2 \ (1 + \delta^{25})} = \frac{C^{28}}{F^{25}} \frac{(1 + \rho^{28})}{(1 + \delta^{25})} \tag{8}$$

C^{28}/F^{25} is a commonly used symbol for this thermal cross section ratio. Equation 8 can also be rewritten to predict C^{28}/F^{25} as

$$C^{28}/F^{25} = C^* \frac{(1 + \delta^{25})}{(1 + \rho^{28})} = \frac{\Sigma_{c_2}^{28}}{\Sigma_{f_2}^{25}} \tag{8a}$$

C^{28}/F^{25} is also calculated to high accuracy by state-of-the-art lattice analysis codes.

The definition of C* in Equation 8 has been designated[4] the "indirect" C*, and the experimentally determined C* the "direct" C*. These definitions will be used throughout the following discussion.

Equation 7 is a relationship linking material buckling to measured activation parameters. It is an exact neutron balance equation at $K_{eff} = 1$ and should be satisfied by all transport theory lattice analysis codes even if they are inaccurate.

The quantities in Equation 7 fall into three categories:

Quantities that are the most difficult to calculate, hence are measured. (B_m^2, δ^{25}, δ^{28}, C* or ρ^{28})

Quantities that involve basic nuclear data that may be calculated within the uncertainties of the basic data.

$$(\bar{\nu}_1^{25}, \bar{\nu}_2^{25}, \bar{\nu}_1^{28}, \bar{\alpha}_2^{25}, \bar{\alpha}_2^{28}, \Sigma_{c_2}^{28}/\Sigma_{f_2}^{25})$$

Quantities that are truly cell dependent, but which present state-of-the art lattice analysis codes should be able to calculate satisfactorily.

$$(D_1, D_2, \Sigma_{r_{1\to2}}, \Sigma_{r_{2\to1}}, \Sigma_{f_2}, \Sigma_{c_2}, \text{ and } \xi)$$

The parameter ξ is an important one in that it plays an equivalent role to C* in Equation 7. For H_2O moderated lattices ξ is of magnitude ~0.4 and for D_2O moderated lattices ξ is of magnitude ~0.03. One expects, therefore, that H_2O moderated lattices will be much more sensitive to the ξ parameter.

B. Methods of Consistency Analysis

Equation 7 is the fundamental equation that relates the experimental integral activation and reactivity parameters. It predicts a material buckling (B_m^2) from the integral activation parameters δ^{25}, δ^{28}, and C* (or ρ^{28}), but could be used to predict a C* (or δ^{25}, or δ^{28}) using experimental values of B_m^2, δ^{25}, and δ^{28}. Because the material buckling is measured independent of the activation parameters, Equation 7 has almost always been used to predict material buckling. This procedure will be used in all that follows.

Three quantitative consistency tests can be defined from Equations 7 and 8a. Assume that all cross section and spectrum dependent coefficients in Equation 7 and 8 have been determined by a state-of-the-art lattice analysis calculation. The three tests are:

1. The experimental B_m^2 is compared to the B_m^2 from Equation 7 using experimental values of δ^{25}, δ^{28}, and C*.
2. The experimental B_m^2 is compared to the B_m^2 from Equation 7 using experimental values of δ^{25} and δ^{28}, and C* from Equation 8.
3. The C^{28}/F^{25} calculated by the lattice analysis code is compared to C^{28}/F^{25} from equation 8a using the experimental values of ρ^{28}, δ^{25}, and C*.

In each of these tests the consistency (or inconsistency) of the experimental parameters is determined from comparison of the indicated parameters and their associated uncertainties. A consistent experiment will demonstrate reasonable agreement between the calculated and measured quantities in all tests.

C. Application of Consistency Analysis to Thermal Benchmarks

Results from applying the consistency tests defined above have been reported for a wide selection of thermal benchmarks in Ref. 7. Here the results for TRX-1, 2 and MIT-1, 2, 3 will be reviewed. Results for three other MIT lattices (identified as MIT-4, 5, and 6) will also be reviewed to document their implementation as thermal benchmarks.

Lattice Analysis calculations for all benchmarks reviewed here were done with the RAHABR[25] lattice analysis module of the JOSHUA System[26] using ENDF/B-IV cross sections. These calculation results are reported in the comparisons in Section II as the SRL* results.

The uncertainties quoted for these consistency results are minimum uncertainties as no cross section uncertainties were included in the consistency calculations. It is possible to include cross section uncertainties with considerable effort from the ENDF/B error files; however, their inclusion does not alter the consistency results so were omitted for simplicity.

The results from applying the three consistency tests defined above to the TRX-1, 2 and MIT-1, 2, 3 lattices are summarized in Table 16. This table reveals that the TRX lattices demonstrate good consistency while the MIT lattices demonstrate poor consistency. It is not evident from the data in this table why this is true, thus each set of lattices will be examined individually.

TRX Lattices. A detailed comparison of experimental, calculated, and consistency analysis results for TRX-1, and 2 appears in Table 17. The agreement between calculation and experiment is within the experimental uncertainty except for δ^{25} which is calculated 5% low for both lattices.

The material buckling calculated from Equation 7 overlaps the experimental value in uncertainty for both the direct and indirect C* parameters. The uncertainty in the material buckling calculated from Equation 7 is much larger than the experimental uncertainty and arises from the large relative uncertainties assigned to the experimental ρ^{28} and C* parameters.

The C^{28}/F^{25} values calculated from Equation 8a do not agree with the lattice analysis calculation within the experimental uncertainty. This arises because the thermal cross sections used in the analysis of the experiment were different from the ENDF/B-IV cross sections used in the calculation. Table 18 compares calculated C^{28}/F^{25} values obtained from cross sections used in the original experimental analysis[4] with values obtained by RCP01 and by RAHABR using ENDF/B-IV cross sections. The ENDF/B-IV results from RCP01 and RAHABR agree to within $\frac{1}{4}$% for both lattices while the original lattice analysis was 1-2% higher. The C^{28}/F^{25} values calculated with the cross sections from the original experimental analysis agree well with values from Equation 8a. Had ENDF/B-IV cross sections been used in the experimental analysis the ρ^{28} and C* results would shift toward the indirect C* results in Table 17 and consistency analysis would give better agreement.

Table 16

Results of Consistency Analysis of TRX-1, 2 and MIT-1, 2, 3 Benchmarks

Lattice Name	Material Buckling (B_m^2) m^{-2}			C^{28}/F^{25}		Consistency of Experiment
	Experiment[22]	Equation 7 Direct C*	Equation 7 Indirect C*	RAHABR[25]	Equation 8a	
TRX-1	57.00 ± 1.00	55.84 ± 1.55	58.06 ± 1.46	.370	.377 ± 0.005	Good
TRX-2	54.69 ± 0.36	53.96 ± 1.32	55.66 ± 1.28	.367	.374 ± 0.005	Good
MIT-1	8.48 ± 0.10	6.69 ± 0.54	8.04 ± 0.20	.665	.709 ± 0.016	Poor
MIT-2	8.65 ± 0.10	7.33 ± 0.42	8.28 ± 0.15	.663	.700 ± 0.015	Poor
MIT-3	8.15 ± 0.08	7.65 ± 0.29	7.86 ± 0.11	.661	.672 ± 0.013	Poor

Table 17

Experimental, Calculated, and Consistency Analysis Results for TRX-1 and TRX-2

Parameter	TRX-1		TRX-2	
	Experiment[22]	Calculation[25]	Experiment[22]	Calculation[25]
		Parameters		
$B_m^2(m^{-2})$	57.00 ± 1.00	56.09	54.69 ± 0.36	53.84
ρ^{28}	1.320 ± .021	1.3389	0.837 ± .016	.83829
δ^{25}	.0987 ± .001	.093657	.0614 ± .0008	.057629
δ^{28}	.0945 ± .008	.092623	.0693 ± .0035	.064200
C*(Direct)	.797 ± .008	.79110	.647 ± .006	.63821
K_{eff} at Expt. B_m^2	1.0	.99505	1.0	.99663
		Consistency Analysis		
Direct C*				
$B_m^2(m^{-2})$	55.84 ± 1.55	56.09	53.96 ± 1.32	53.84
C^{28}/F^{25}	.377 ± .005	.36991	.374 ± .005	.36718
Indirect C*				
$B_m^2(m^{-2})$	58.06 ± 1.46	56.09	55.66 ± 1.28	53.84
C^{28}/F^{25}	.36991	.36991	.36718	.36718
C*(Indirect)	.781 ± .007	.79110	.636 ± .006	.63821

Table 18

TRX Lattice C^{28}/F^{25} Values from Different Cross Section Sets

	Ref. 4	RCP01-ENDF/B-IV	RAHABR-ENDF/B-IV
TRX-1	.37620	.37147	.36991
TRX-2	.37314	.36853	.36718

MIT-1, 2, 3 Lattices. A detailed comparison between experiment, calculated, and consistency analysis results is shown in Table 19 for MIT-1, 2, and 3 thermal benchmarks. This table shows only a few instances of agreement between calculation and experiment.

The consistency analysis results for direct C* show large discrepancies in material buckling and C^{28}/F^{25} compared to both experimental and calculated results. The consistency analysis results for the indirect C* show good agreement in material buckling with calculation but not experiment.

The B_m^2, C* (direct), and C* (indirect) results from experiment, calculation, and consistency analysis have been plotted as a function of lattice pitch in Figure 14. This figure shows that C* (direct) and the consistency material buckling from Equation 7 derived from C* (direct) lie far away from all other results. The documentation of the parameter measurements for these experiments[27] reveals that C* (direct) and ρ^{28} were obtained from separate foil irradiations. One explanation of the results in Figure 14 is that the C* (direct) measurement was in error while the ρ^{28} measurement was correct. Even with this explanation the consistency material bucklings for C* (indirect) do not agree with experiment.

Comparison of material bucklings of lattices measured in both a D_2O critical experiment and a D_2O sub-critical experiment has shown systematic differences in the measured bucklings.[28] In Reference 7 fourteen lattice experiments of four different fuel assemblies and U235 enrichments, all measured in D_2O sub-critical experiments, were examined. Consistency analysis and calculations predicted significantly lower material bucklings than experiment for all fourteen lattices. A recently performed benchmark experiment[29] in the SRL Lattice Test Reactor critical facility on a lattice previously measured[30] in the SRL Sub-Critical Exponential facility gave a material buckling 0.50 m^{-2} lower and in excellent agreement with calculation. These results collectively cast doubt on material bucklings measured in a D_2O sub-critical experiment.

Because of the probable errors in the C* (direct) measurement and the disagreement in material buckling these lattices are classified as inconsistent. They are not recommended for further testing of ENDF/B data.

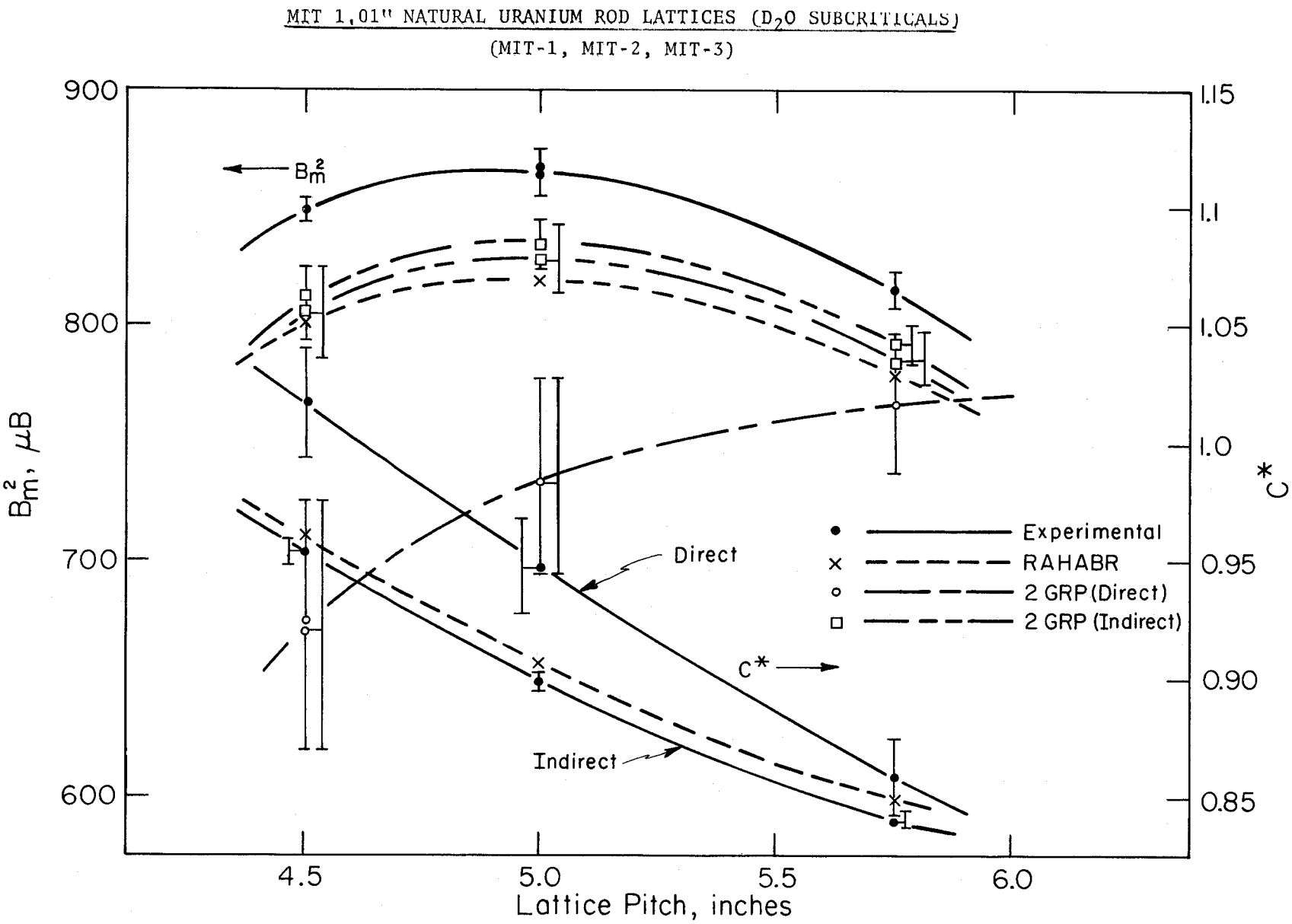

Figure 14 - Results for MIT 1, 2, 3 Thermal Benchmarks

Table 19

Experimental, Calculated, and Consistency Analysis Results for MIT 1, 2, 3

Parameter	MIT-1		MIT-2		MIT-3	
	Experiment[22]	Calculation[25]	Experiment[22]	Calculation[25]	Experiment[22]	Calculation[25]
	Parameters					
$B_m^2(m^{-2})$	8.48 ± 0.10	8.01	8.65 ± 0.10	8.18	8.15 ± 0.08	7.81
ρ^{28}	0.502 ± 0.01	0.51323	0.400 ± 0.004	0.42262	0.313 ± 0.005	0.32372
δ^{25}	0.0469 ± 0.0019	0.047291	0.0335 ± 0.003	0.038874	0.0265 ± 0.0011	0.029820
δ^{28}	0.0588 ± 0.003	0.061535	0.0587 ± 0.003	0.06001	0.0575 ± 0.003	0.057826
C*(direct)	1.017 ± 0.023	0.96084	0.948 ± 0.020	0.90830	0.859 ± 0.016	0.85018
K_{eff} at Expt. B_m^2	1.0	.99105	1.0	.98919	1.0	.99088
	Consistency Analysis					
Direct C*						
$B_m^2(m^{-2})$	6.69 ± 0.54	8.01	7.33 ± 0.42	8.18	7.65 ± 0.29	7.81
C^{28}/F^{25}	0.709 ± 0.016	0.66499	0.700 ± 0.015	0.66329	0.672 ± .013	0.66143
Indirect C*						
$B_m^2(m^{-2})$	8.04 ± 0.20	8.01	8.28 ± 0.15	8.18	7.86 ± 0.11	7.81
C^{28}/F^{25}	0.66499	0.66499	0.66329	0.66329	0.66143	0.66143
C*(indirect)	0.954 ± 0.007	.96084	0.899 ± 0.004	0.90830	0.846 ± 0.003	0.85018

In place of these lattices three new benchmarks (MIT-4, 5, and 6) have been proposed which appear to give better, but not perfect consistency agreement.

MIT-4, 5, 6 Lattices. These three lattices were measured later in the MIT heavy Water Lattice Project than the MIT-1, 2, 3 lattices. These lattices consisted[31] of Aluminum clad 0.387 inch dia. U-metal rods enriched to 0.947 wt. % U235 and triangular lattice pitches of 1.5, 2.25, and 3.0 inches. These lattices are of more practical interest than MIT-1, 2, and 3 because they span a wider range of moderator-to-fuel ratios and give a wider range of ρ^{28} values for calculational comparison.

Table 20 shows a detailed comparison of the experimental, calculated, and consistency analysis results. Figure 15 plots the C* and material buckling results as a function of lattice pitch. The material buckling from calculation and consistency analysis show good agreement, but both are lower than experiment. Here, as for MIT-1, 2, 3, it is believed that the material bucklings from the sub-critical experiment are in error toward high experimental values of B_m^2.

The ρ^{28} and C* (direct) measurements are presumed done in the same manner as for MIT-1, 2, 3, but here the results show excellent agreement. The precision of these measurements are quoted as almost an order of magnitude better than the MIT-1, 2, 3 (see Tables 19 and 20). It is doubtful that the uncertainties on ρ^{28} and C* (direct) in Table 20 are realistic. More realistic estimates of the ρ^{28} and C* (direct) uncertainties would improve the agreement between experiment, calculation, and consistency analysis.

The CSEWG thermal data testing subcommittee has proposed that these experiments, with the material buckling modified to the consistency analysis material buckling, be utilized as benchmarks for ENDF/B-V data testing. This procedure fills the void of having no consistent D_2O moderated benchmark lattice experiments, but does not provide benchmarks that are definitive or defensible. What is needed are new critical experiments on D_2O moderated, single rod lattices to provide good cross section testing benchmarks.

IV. SUMMARY AND CONCLUSIONS

1. With ENDF/B-IV, aqueous homogeneous U235 criticals show calculated K_{eff} values ranging from 0.994 for large thermal systems to 1.01 at 45% leakage. Although a number of factors could play a role, this trend is thought to be due mostly to an underprediction of leakage, resulting from a too-soft fission spectrum. The U235 capture and fission resonance integrals are also important.

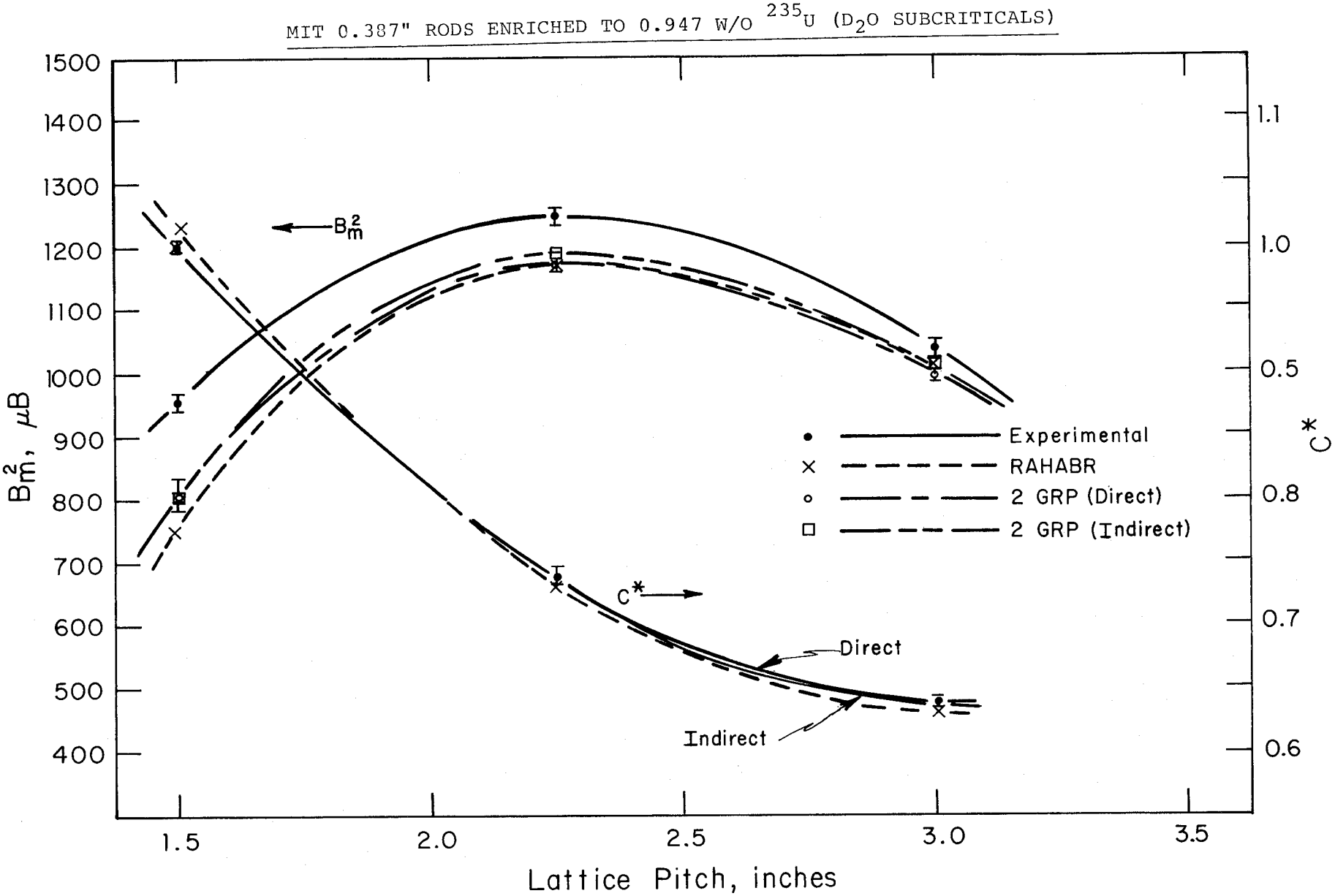

Figure 15 - Results for MIT 4, 5, 6 Benchmarks

Table 20

Experimental, Calculated, and Consistency Analysis Results for MIT 4,5,6

Parameter	MIT-4		MIT-5		MIT-6	
	Experiment[31]	Calculation[25]	Experiment[31]	Calculation[25]	Experiment[31]	Calculation[25]
	Parameters					
$B_m^2(m^{-2})$	9.55 ± 0.10	7.55	12.44 ± .11	11.73	10.41 ± .14	10.08
ρ^{28}	1.155 ± .001	1.16808	0.525 ± .002	.52469	0.317 ± .002	0.30572
δ^{25}	0.0865 ± .0016	0.082602	0.0371 ± .0012	0.036587	0.0222 ± .0024	0.021410
δ^{28}	0.0459 ± .0013	0.041659	0.0326 ± .001	0.030053	0.0291 ± .0018	0.026596
C*(direct)	1.007 ± .008	1.0164	0.740 ± .007	0.73578	0.647 ± .002	0.63598
K_{eff} at Expt. B_m^2	1.0	.97012	1.0	.98595	1.0	.99141
	Consistency Analysis					
Direct C*						
$B_m^2(m^{-2})$	8.05 ± .26	7.55	11.74 ± .17	11.73	9.97 ± .08	10.08
C^{28}/F^{25}	.507 ± .004	.50762	.503 ± .005	.50024	.502 ± .002	.49750
Indirect C*						
$B_m^2(m^{-2})$	8.06 ± .10	7.55	11.83 ± .06	11.73	10.07 ± .08	10.08
C^{28}/F^{25}	.50762	.50762	.50024	.50024	.49750	.49750
C*(indirect)	1.007 ± .002	1.0164	0.736 ± .001	.73578	.641 ± .002	.63598

2. New differential fission spectrum measurements clearly indicate that the Maxwellian model is inadequate and a more complex representation is required. Furthermore, the ENDF/B-IV mean energy ($\bar{E}$ = 1.985 MeV) is too low. The recent measurements support a mean energy in the range 2.02-2.08 MeV, depending on model representation. An equilibrium spectrum based on a Watt shape with $\bar{E}$ = 2.027 MeV (which fits the differential data reasonably well), plus a 10 barn reduction of the ENDF/B-IV U235 fission resonance integral, can remove most of the K_{eff} trend observed for the homogeneous criticals. The more complex Steen Standard 2 model, with $\bar{E}$ = 2.073 MeV, also gives a good fit to the differential data and eliminates the K_{eff} leakage trend (with suitable choices for U235 resonance capture and fission integrals). In either case, further measures, such as an ~0.5% increase of $\bar{\nu}$, are required to eliminate the K_{eff} bias.

3. ENDF/B-IV gives a fission age in H_2O of 25.5 cm^2, significantly below the measured value of 26.4 $\pm$ 0.3 cm^2. An equilibrium spectrum based on the Watt prompt spectrum with $\bar{E}$ = 2.027 MeV provides only slightly better agreement. The Steen Standard 2 model, with $\bar{E}$ = 2.073 MeV, leads to very good agreement. It also produces excellent agreement with integral measurements of $\bar{\sigma}_f^{U238}$ and $\bar{\sigma}_f^{U235}/\bar{\sigma}_f^{U238}$ (fission spectrum averages).

4. The Gwin-Magnuson critical experiments imply a constraint $K2 = (\bar{\eta}^U - 1)\,\bar{\sigma}_A^U/\bar{\sigma}_A^H$ on the thermal criticality parameters of U235. According to the analysis of Ref. 5, the experiments imply that K2 = 2155 $\pm$ 11 (0.5%), whereas ENDF/B-IV is 0.8% below this.

5. Analyses of the TRX-1 and 2 H_2O-moderated critical lattices give a reasonably coherent picture of nuclear data performance and of consistency among different calculational methods. The picture is much less clear for the D_2O-moderated MIT exponential lattices.

6. For TRX-1 and 2, the strong correlation of calculated K_{eff} and ρ^{28} suggests that U238 resonance capture is the principal difference among the calculational methods. In particular, it implies that the different leakage calculations are, with a couple of exceptions, consistent with each other. It also tends to support the measured ρ^{28}, inasmuch as a calculation which reproduces ρ^{28} will give K_{eff} close to unity. The best methods give ρ^{28} about 5% high, of which half (2.5%) is removed by new parameters for the low energy U238 resonances. ENDF/B-V is expected to produce better agreement provided there are no other significant changes in U238 capture data.

7. Calculations of δ^{25} show a fairly good consistency, with two or three exceptions. The best values are in good agreement with experiment.

8. The calculations of δ^{28} show amazing consistency in TRX-1 and fair consistency in the looser TRX-2. Calculated values are in good agreement with experiment. δ^{28} is expected to increase by a few percent with ENDF/B-V data, due to a harder fission spectrum and to changes of the U238 inelastic scattering.

9. Full core Monte Carlo analyses of TRX-1 and 2 give good agreement with corresponding cell Monte Carlo - plus - B_1 leakage corrections for integral parameters. This is expected for reaction rate ratios, which are subject to relatively small (< 5%) leakage corrections. Even for K_{eff}, for which the 15% leakage is directly important, the homogenized lattice B_1 analysis shows quite good agreement with the full core Monte Carlo calculation.

10. Consistency analysis of the TRX-1 and 2 lattices show the experimental results reported in Ref. 22 to be consistent. If the original experiment had been analyzed using ENDF/B-IV data the results would be even more consistent.

11. Consistency analysis of the MIT-1, 2, and 3 lattices show the experimental results reported in Ref. 22 are inconsistent. It is suspected that errors were made in the measurement of C* (direct). Material bucklings from these sub-critical experiments are significantly higher than predicted by consistency analysis or calculation. This material buckling discrepancy is a problem common to all D_2O sub-critical experiments. It is recommended that MIT-1, 2, and 3 no longer be used as cross section testing benchmarks.

12. Three new D_2O sub-critical experiments have been proposed as thermal benchmark experiments, and designated MIT-4, 5, and 6. These experiments are later experiments in the MIT Heavy Water Lattice Project than MIT-1, 2, and 3, and appear to have a greater consistency between the measured activation parameters. The material buckling discrepancy observed for MIT-1, 2, and 3 is also observed for these lattices. The final MIT-4, 5, and 6 benchmarks define the material buckling to be that predicted by consistency analysis.

13. All of the "benchmark quality" D_2O lattice experiments that appear in the literature have been sub-critical experiments. Because of the material buckling discrepancies that exist in all of these experiments new measurements in critical experiments are needed for cross section testing purposes. Any such experiments should utilize simple single rod assemblies at, or near, natural U235 enrichment, and should measure a complete set of activation and reactivity parameters. The results of these experiments should satisfy the consistency analysis equations before acceptance as a cross section testing benchmark.

REFERENCES

1. Cross Section Evaluation Working Group Benchmark Specifications, ENDF-202, November 1974.
2. Benchmark Testing of ENDF/B-IV, ENDF-230, March 1976.
3. L. Levitt and P. Rose in "Improvement of Reference Nuclear Data for Commercial Power Reactor Analysis and Design," EPRI NP-556, October 1977.
4. J. Hardy, Jr., "Monte Carlo Analyses of TRX Slightly Enriched Uranium-H_2O Critical Experiments with ENDF/B-IV and Related Data Sets," WAPD-TM-1307, December 1977.
5. J.J. Ullo and J. Hardy, Jr., "Analysis of Homogeneous U^{233} and U^{235} Critical Assemblies with ENDF/B-IV Data," WAPD-TM-1299, October 1977.
6. E.T. Tomlinson, G. deSaussure, and C.R. Weisbin, "Sensitivity Analysis of TRX-2 Lattice Parameters with Emphasis on Epithermal ^{238}U Capture," EPRI NP-346 (ENDF 252), March 1977.
7. D.R. Finch and W.E. Graves, "Quantitative Consistency Testing of Thermal Benchmark Lattice Experiments," Trans. Am. Nucl. Soc. 27, 888, November 1977.
8. R. Gwin and D.W. Magnuson, Nucl. Sci. Eng., 12, 364 (1962).
9. J.K. Fox, L.W. Gilley, and D. Callihan, "Critical Mass Studies, Part IX, Aqueous U^{235} Solutions," ORNL-2367, 22 (1958).
10. J.K. Fox, L.W. Gilley, R. Gwin, and J.T. Thomas, "Critical Parameters of Uranium Solutions in Simple Geometry," in "Neutron Physics Division Annual Progress Report for Period Ending September 1, 1958," ORNL-2609, Oak Ridge National Laboratory (1958).
11. D.E. Kusner, S. Kellman, and R.A. Dannels, "ETOG-1, A Fortran IV Program to Process Data from the ENDF/B File to the MUFT, GAM and ANISN Formats," WCAP-3845-1 (ENDF 114), December 1969.
12. C.L. Beard and R.A. Dannels, "ETOT, A Fortran IV Program to Process Data from the ENDF/B File to Thermal Library Format," WCAP-7363, March 1971.
13. H.C. Honeck and D.R. Finch, "FLANGEII (Version 71-1). A Code to Process Thermal Neutron Data from an ENDF/B Tape," DP-1278, October 1971.
14. N.R. Candelore and R.C. Gast, "RECAP-3, A Monte Carlo Program for Estimating Epithermal Capture Rates in Rectangular or 60° Parallelogram Geometry," WAPD-TM-437, 1964.
15. H. Bohl, Jr., et al., "P3MG-1, A One-Dimensional Multigroup P-3 Program for the Philco-2000 Computer," WAPD-TM-272, 1963.
16. E.M. Gelbard and R.E. Prael, "Monte Carlo Work at Argonne National Laboratory," Proc. NEACRP Meeting of a Monte Carlo Study Group, July 1-3, 1974, ANL-75-2 (NEA-CRP-118), Argonne National Laboratory (1975), p. 201.
17. S.F. Mughabghab and D.I. Garber, "Neutron Cross Sections," BNL 325, Third Edition, June 1973.
18. R.K. Paschall, Nucl. Sci. Eng., 20, 436-444 (1964); also 23, 256-263 (1965).

19. J.D. Spencer, "An Experimental Determination of the Neutron Age to Indium Resonance Energy in Aluminum-Water Mixtures," Ph.D. Thesis, University of Virginia (1966).
20. N.M. Steen, "Status of Nuclear Data for Th232 and U233," to be presented at the June 1978 Meeting of the American Nuclear Society.
21. R. Gwin, "Critical Experiments and the 2200 m/sec Neutron Parameters," ORNL-TM-4550, January 1975.
22. R. Sher and S. Fiarman, "Studies of Thermal Reactor Benchmark Data Interpretation: Experimental Corrections," EPRI NP-209, October 1976.
23. S. Pearlstein, Editor, "Seminar on ^{238}U Resonance Capture," ENDF-217, March 1975.
24. W. Rothenstein, "Thermal Reactor Lattice Analysis Using ENDF/B-IV Data with Monte Carlo Resonance Reaction Rates," Nuclear Science Eng. 59, 337 (1976).
25. RAHABR is a modification of the JOSHUA module RAHAB2 and contains the RRR1D resonance region calculation. RAHAB2 is documented in USAEC report DPSTM-500, Vol. 4, RRR1D is described in the Savannah River Laboratory monthly report for August 1976.
26. H.C. Honeck, The JOSHUA System, USERDA report DP-1380, E. I. duPont de Nemours & Co., Savannah River Laboratory, Aiken, S. C. (1975).
27. T.J. Thompson, et al., Heavy Water Lattice Project Annual Report, September 30, 1966, USAEC report MIT-2344-09, Massachusetts Institute of Technology (1966).
28. W.E. Graves and E.J. Hennelly, "Comparison of the Worth of Critical and Exponential Measurements for Heavy Water-Moderated Reactors," Proceedings of Symposium on Exponential and Critical Experiments, Amsterdam, IAEA, Vienna (1964).
29. C.E. Ahlfeld, et al., "Coaxial Fuel SRL Benchmark Experiments," paper #3, session II, this meeting.
30. D.J. Pellarin and B.M. Morris, Reactivity and Reaction Rate Measurements in U-D_2O Lattices With Coaxial Fuel, USERDA report DP-1409, E. I. duPont de Nemours & Co., Savannah River Laboratory, Aiken, S. C. (1976).
31. T.J. Thompson, et al., Heavy Water Lattice Project Final Report, USAEC report MIT-2344-12, Massachusetts Institute of Technology (1967).

Section 8

REACTIVITY AND PARAMETER MEASUREMENTS IN A COAXIAL URANIUM FUEL-D_2O MODERATED CRITICAL LATTICE

Reactivity and Parameter Measurements in a Coaxial Uranium Fuel-D_2O Moderated Critical Lattice*

D. J. Pellarin, C. E. Ahlfeld and N. P. Baumann
Savannah River Laboratory, E. I. du Pont de Nemours & Co.,
Aiken, South Carolina 29801

ABSTRACT

Reactivity and reaction rate parameters were measured for a 7-inch triangular pitch lattice of coaxial uranium fuel in a critical, D_2O-moderated reactor. The results were compared with RAHABR computations using ENDF/B-IV cross sections and with an earlier subcritical exponential measurement of the same lattice. Measured and calculated reactivity are in good agreement, however, the calculated ratio of epicadmium ^{238}U captures to subcadmium ^{238}U captures (ρ^{28}) was 10% lower than measured. Indirect verification of the ρ^{28} measurement was obtained by measurement of a new conversion ratio parameter (C^+) defined as the ratio of ^{238}U captures to total fissions. Agreement between measured and calculated inner-to-outer fuel activation ratios suggests that the discrepancy is caused by underprediction of epicadmium captures in ^{238}U or by erroneously high measured values of ρ^{28} and C^+. However, any adjustment of ^{238}U captures to match the measured ρ^{28} will cause the calculated reactivity to be underpredicted. An unresolved concern is that the experimental results do not satisfy an internal consistency criterion based on the two group neutron balance equation even though all known systematic errors have been accounted for and well known experimental techniques are used. Reaction rate parameters from the critical experiment agree with the exponential measurements indicating that the neutron spectra in the measurement regions were closely identical. The measured buckling in the critical facility is 0.52 m^{-2} lower than in the exponential. Other studies have shown systematic differences in reactivity between D_2O critical and exponential measurements.

INTRODUCTION

A fundamental goal of the calculational program at Savannah River Laboratory is to provide accurate representation of reactivity and reaction rates over a wide range of D_2O-thermal reactor lattices. A broad base of experimental evidence is required to evaluate the theoretical methods and differential cross sections

---

*The information contained in this article was developed during the course of work under Contract No. AT(07-2)-1 with the U. S. Department of Energy.

used for predicting these integral reactor properties. (The most meaningful evaluations occur for lattices with simple geometry and composition so that errors of representation in the theoretical methods are minimized.) Several years ago two different, slightly enriched, coaxial fuel assemblies (Type I and Type II) each were studied in uniform lattices over a range of pitches in the exponential facility (SE) at SRL.[1] The purpose of these experiments was to provide information to assess the performance of the RAHAB[2] code with ENDF/B-IV cross sections. The calculated k_{eff}'s were 4 to 8% low and resonance capture in ^{238}U was consistently overpredicted by as much as 22%. Development later of an improved resonance treatment calculation in the RAHAB code improved agreement with the SE coaxial fuel experiments but significant discrepancies remained. In early 1977, analyses of the SE experiments by use of equations that tested the internal consistency of the data indicated that they may not be valid SRL benchmarks.[3] Possible distortion of the neutron energy spectrum by anisotropic leakage in the small exponential lattice and concern about the accuracy of the reactivity measurement in an exponential suggested the need to repeat several of the experiments in the critical LTR facility at SRL. Accordingly, reactivity and activation parameters have been remeasured for the Mark 15 (Type II) coaxial fuel at a 7-inch triangular pitch in the LTR and preparations are being made to remeasure the Mark 5R (Type I) coaxial fuel at a 7-inch triangular pitch.

In this paper:

- The results of the Mark 15-LTR experiments are reported and compared both with the earlier SE experiments and with computations by the transport theory code RAHABR[4] using ENDF/B-IV cross sections.
- The internal consistency of the Mark 15-LTR data is investigated.
- Measurement of a useful new conversion ratio parameter is described.
- Measurement techniques, corrections to the data, and systematic errors are discussed to illustrate experimental methods and justify the assigned error flags.
- The preliminary results of an experimental investigation of the energy dependence of the ^{238}U subcadmium cross section are presented in the Appendix.

LATTICE DESCRIPTION

The Mark 15 fuel assembly consisted of six stacked, unclad, nickel-plated inner and outer fuel pairs supported by aluminum

housing tubes to produce a uniform, continuous, coaxial fuel column 66.7-inches long. The fuel assembly geometry and composition are summarized in Table 1.

127 Mark 15 assemblies were placed on a 7-inch triangular pitch in the LTR. An outer poison boundary consisting of 1-inch diameter 4.9 wt % Li-Al rods surrounded the lattice to reduce reflector effects and improve the definition of the radial buckling. The lattice arrangement is shown in Figure 1.

The LTR is a stainless steel cylindrical vessel, 10 ft in diameter and 11 ft high with walls 1/4-inch thick. The lattice was supported and spaced on a precision made 1-inch thick aluminum bottom plate positioned about 4-inches above the tank bottom. A bottom poison boundary consisting of two layers of 1/8-inch boral sheet is located 1-1/2-inches beneath the fuel support plate. Top support and spacing was provided by a combination of grid support beams and interlocking spacers. A moderator supply system provides for filling and level control of the D_2O to ± 0.005 cm.

MEASUREMENT PROCEDURES

The satisfactory prediction of reactivity (B_m^2) is taken as the most important criterion in testing a reactor physics code and its associated nuclear data library. Integral reaction rate parameters provide detailed diagnostic information to assist the evaluation. In the Mark 15-LTR experiment integral parameters representative of important reaction rate ratios in the fuel were measured separately for the inner and outer fuel by activation of foil detectors placed within the fuel. Parameters that were derived from experimental data are summarized as follows:

^{238}U (n,γ) Capture Ratio $\rho^{28} = \dfrac{\text{Epicadmium } ^{238}U \text{ Captures}}{\text{Subcadmium } ^{238}U \text{ Captures}}$

^{235}U Fission Capture Ratio $\delta^{25} = \dfrac{\text{Epicadmium } ^{235}U \text{ Fissions}}{\text{Subcadmium } ^{235}U \text{ Fissions}}$

^{238}U Fast Fissions $\delta^{28} = \dfrac{^{238}U \text{ Fissions}}{^{235}U \text{ Fissions}}$

Conversion Ratio Index $C^{+} = \dfrac{^{238}U \text{ Captures}}{\text{Total Fissions}}$

Thermal Neutron Spectral Index $R = \dfrac{[^{176}Lu/^{63}Cu]^{\text{Subcadmium}}_{\text{Fuel}}}{[^{176}Lu/^{63}Cu]^{\text{Subcadmium}}_{\text{Thermal Ref.}}}$

Table 1

Mark 15 Assembly Geometry and Fuel Compositions

Al Inner Housing, inches	
O.D.	2.004
I.D.	1.748
Inner Fuel Slug[a]	
O.D.	2.606
I.D.	2.017
Outer Fuel Slug[a]	
O.D.	3.641
I.D.	3.164
Al Outer Housing	
O.D.	4.050
I.D.	3.950
Fuel Composition, wt %	
^{235}U	1.100
^{238}U	98.877
^{236}U	0.023

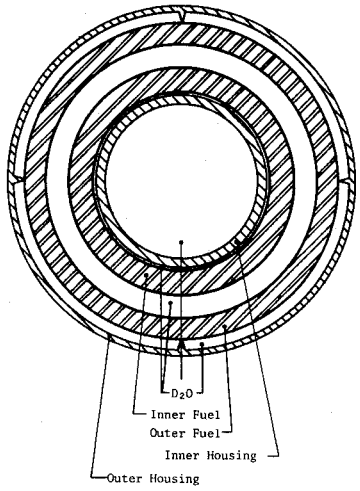

a. Dimensions include a 0.0015-inch thick nickel plating on the fuel surfaces.

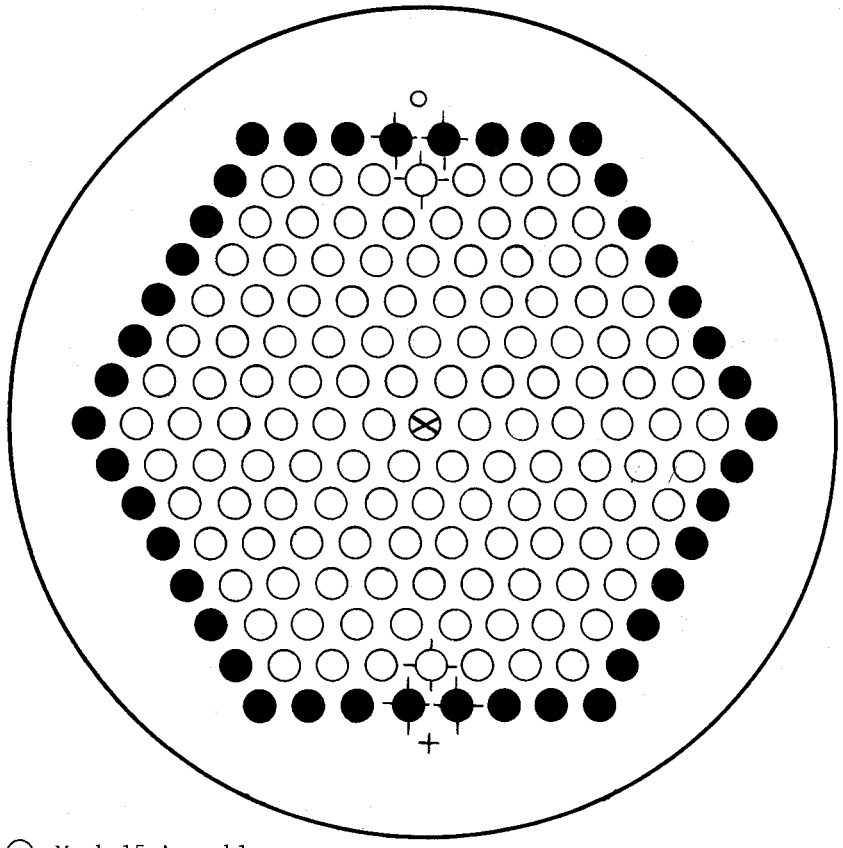

○ Mark 15 Assembly

● 4.9 wt % Li-Al Poison Rod

⊗ Foil Bearing Mark 15 Assembly

-|- Assembly Removed for Reference Environment

o δ^{28} Reference

\+ Reference Foil Spinner

FIGURE 1. Mark 15 Lattice at 7" Δ Pitch in LTR

Material Buckling, B_m^2

The material buckling was obtained by measuring flux profiles in the critical reactor. Radial and axial curvatures were determined independently and combined to obtain $B_m^2 = B_r^2 + B_z^2$. Flux shape data were obtained from activation of both brass (Cu) bead chains and gold pins placed on the axial center line in the central D_2O region of the fuel assemblies. Extensive flux energy-spectrum mapping of the Mark 15 core was done by bare and cadmium-covered gold pin activations to avoid use of data from regions where the flux curvature was energy dependent (i.e. non-asymptotic). The radial activation data were fitted by a least squares procedure to a J_o function and the vertical data to a cosine function. The data that were used in the fit were examined to eliminate errors due to edge effects. This was accomplished by dropping outermost data points until the effects on the curve fitting were random. In practice this amounted to eliminating only the outermost ring of fuel cells for the radial fit. A check of the lattice uniformity was performed by activation of gold pins at five axial levels in the center of all 127 fuel assemblies. Less than 2% variation was found among equivalent positions indicating that no severe radial or axial flux asymmetry existed in the reactor.

Lattice Parameters

Experimental Arrangement. The foil bearing assembly for the activation experiment was placed at the center of the lattice. It was identical to the other lattice fuel assemblies except that inner and outer fuel pieces with accurately machined central angle slots to accommodate thin, bare, arc shaped foils and 1/2-inch thick filler pieces were located at the center of the fuel column. The shaped foils were fabricated to fit accurately in the slots so the specific activity of the foil represented the average reaction rate in the fuel. Epicadmium activations were obtained from foils placed inside a small (0.375-inch diameter x 0.100-inch thick) cadmium pill box contained in a recess in the lower filler piece about 3-inches from the nearest bare foil. The foil bearing assembly was rotated during irradiation to average any radial flux asymmetry.

Reference foils used in the ρ^{28} and spectral index measurements were located on a rotating disc in the reflector region of the reactor and were irradiated simultaneously with the foils in the lattice. The measured cadmium ratio (0.032-inch cadmium) for 0.0105-inch thick copper (^{63}Cu) at the reference position was 195. Paired natural and depleted uranium reference foils for the δ^{28} measurement were placed in an isolated 1-inch natural uranium rod also located in the reflector. Fuel assemblies and poison boundary rods were removed in the immediate proximity of these reference positions to increase the thermal-to-fast flux ratio. Refer to Figure 1.

ρ^{28} Measurement. Measurement of the ^{238}U (n,γ) capture ratio (ρ^{28}) was made by the "copper subtraction" method that permits the epicadmium component of the ^{238}U captures in the fuel to be determined without cadmium-covered ^{238}U foils. Bare and cadmium covered 0.0105-inch thick copper foils were used to determine the subcadmium ^{63}Cu captures in the fuel. Thin (0.003 to 0.004-inch thick) bare natural and depleted (0.019 wt % ^{235}U) uranium foils were used to determine the total ^{238}U captures in the fuel. Bare and cadmium covered copper, natural and depleted uranium foils were irradiated in a reference thermal flux to provide a normalization for subcadmium captures. The subcadmium ^{238}U captures in the fuel were obtained by:

$$^{238}U^{\text{Fuel}}_{\text{Subcd}} = {}^{63}Cu^{\text{Fuel}}_{\text{Subcd}} \cdot \frac{^{238}U^{\text{Th Ref}}_{\text{Subcd}}}{^{63}Cu^{\text{Th Ref}}_{\text{Subcd}}}$$

The epicadmium component of the ^{238}U captures was obtained as the difference between the total capture and the thermal capture. Good agreement was obtained by J. Hardy, Jr. et al[5,6] in a comparison of ρ^{28} values measured by the subtraction method and by the direct measurement of the ^{238}U capture cadmium ratio.

Inherent in the subtraction measurement method is the assumption that copper and ^{238}U thermal cross sections are 1/v below 0.625 eV. ENDF/B-IV evaluations show the ^{238}U subcadmium capture cross section departing slightly from 1/v behavior in the upper end of the thermal region (refer to Figure 2 in the Appendix). The cross section in this region is above that given by the 1/v dependence. Calculations show that the effect is to yield ρ^{28} values by the subtraction method that may be about 1-1/2% high for the Mark 15 lattice in this report. Preliminary results of an investigation of the ^{238}U subcadmium cross section are given in the Appendix.

The ^{239}Np decay from ^{238}U capture was counted in the time interval from 2 to 4 days after irradiation to maximize the 2.3-day decay activity of ^{239}Np relative to background fission product activity. The data were obtained with NaI scintillation counters biased to accept gamma energies in the interval from 90 to 116 keV. A simultaneous count representative of fission product decay activity, obtained at an integral bias of 500 keV, was used to correct for the fission product contribution to the counting rate in the window. The ratio of the ^{235}U fission product counting rate in the 90 to 116 keV window to the ^{235}U fission product counting rate at the 500 keV bias was determined from the natural and depleted uranium foils in the thermal reference that were counted with the foils from the lattice. (The ratio for the small contribution from ^{238}U fission products is assumed to be identical to that for ^{235}U.) The fission product corrections for the

depleted and natural uranium foils were about 0.7% and 5% respectively. No systematic differences were noted in the ρ^{28} values between the natural and depleted foil types. Additional confirmation that the fission product correction was treated properly was obtained by counting the 278 keV γ-ray peak of ^{239}Np using a Ge-Li detector. This peak is nearly free of fission product contamination and gamma self-shielding is less important. Normalized ^{239}Np activations agreed within ±1% for the two methods.

An experimentally determined correction factor of 1.0882 was used to convert the average epicadmium specific activity of the two 0.272-inch diameter x 0.0105-inch thick copper foils used in the cadmium pill box in the fuel to the equivalent epicadmium specific activity for a single 0.500-inch diameter x 0.0105-inch thick copper foil under 30 mils of cadmium (dimensionally similar to the arc-shaped bare copper foils contained in the foil). The factor was measured by irradiating copper foils in both geometries under cadmium on a spinner in the center of the SP[1] reactor. The correction simultaneously establishes the effective cadmium energy for the ρ^{28} measurement at 0.625 eV corresponding to 0.030-inch thick cadmium in slab geometry and isotropic flux incident with a 1/E energy dependence; conditions closely approximated in the SP experiment.

An analytical investigation of the sensitivity of ρ^{28} to the cadmium cutoff energy was made for the Mark 15 lattice using RAHABR. A 10% change in the effective cadmium cutoff energy from a reference energy of 0.6325 eV produced only a 1.07% change in the assembly average value of ρ^{28}.

Small corrections of 1% for the inner fuel and 2% for the outer fuel accounted for the increase in ^{238}U resonance capture caused by neutron streaming through the 0.001-inch gap at the interface between foils and fuel where aluminum was placed to prevent fission product contamination of the foils. These corrections were derived from an auxiliary experiment with coaxial fuel in which known gaps of from 0.001 to 0.021 inch were introduced at the foil sites for the ρ^{28} measurement. The normalized epicadmium activation component of each foil was plotted against foil gap thickness and extrapolated to zero gap to obtain the correction. The magnitudes of these corrections are in quantitative agreement with values derived for rods in a study made by R. Sher and S. Fiarman in which they modeled the streaming of resonance neutrons with a Monte Carlo calculation.[6]

Small calculated corrections of about 2% were applied to the measured subcadmium copper and uranium foil activities in the lattice to account for the thermal flux peaking at the foil sites in the fuel. Calculated thermal flux depression factors were used to derive these corrections.[1] The calculational model assumed an isotropic, monoenergetic flux incident on a slab absorber within a cavity.

Other corrections to the experimental data accounted for:

- Differences (~4%) in gamma attenuation in the 90 to 116 keV window count caused by the difference in foil thickness between the natural and depleted uranium foils used in the measurements. (No systematic differences were noted between the 4 depleted uranium and 2 natural uranium foil detectors used to derive ρ^{28} for each of the coaxial fuel tubes.)

- Differences in the axial elevation of the foils in the experiment. This correction was obtained from a smooth fit of the axial flux derived from bare gold pin activations. With the foil loading centered near the peak of the cosine flux distribution, this correction was less than 1%.

- Small (<1%) differences in foil-to-counter geometry.

Small adjustments obtained from RAHABR calculations were used to convert the measured parameters at 99.61 mol % D_2O to values for 99.75 mol % D_2O.

δ^{25} Measurement. The ^{235}U fission capture ratio (δ^{25}) was measured by activating thin bare and cadmium-covered, dilute ^{235}U-Al foils in the fuel. The fission product gamma activity was measured during the interval from 2 to 4 hours after irradiation by NaI scintillation counters biased at 200 keV. Corrections were made for differences in the axial elevations of the foils, flux peaking at the foil sites in the fuel, foil weight (based on activation calibration) and for counting conditions (i.e., background, deadtime and foil-to-counter geometry differences).

δ^{28} Measurement. The ratio of fissions in ^{238}U to fissions in ^{235}U (δ^{28}) was measured using paired natural and depleted uranium foils in the fuel; 1/2-inch diameter foils of identical composition and thickness were simultaneously irradiated in the δ^{28} reference. The reference was taken as a 1/2-inch recess in the isolated 1-inch natural uranium rod in D_2O. The δ^{28} values for the lattice are based on a δ^{28} reference value of 0.076. This value was obtained by direct measurement using the double fission chamber method for an isolated 1-inch diameter natural uranium rod imbedded in graphite as described in Reference 1. A 7.7% reduction obtained RAHAB cell calculations has been applied to the 0.076 reference value to account for the difference in backscatter between D_2O and graphite.

R Measurement. Bare and cadmium covered lutetium and copper foils were irradiated in the fuel and in the thermal reference. The activation ratio of subcadmium captures in ^{176}Lu (0.14 eV resonance) to subcadmium captures in ^{63}Cu (1/v) within the fuel is a parameter related to the energy distribution of the thermal neutrons. Normalization to the same ratio in the undistorted

Maxwellian spectrum at the thermal reference position provides a spectral index, R, that is a measure of the spectrum hardening in the fuel.

C^+ Measurement. A new procedure was derived for the determination of an important reaction rate parameter (C^+) defined as the ratio of ^{238}U (n,γ) captures to total (^{235}U + ^{238}U) fissions. This parameter is closely related to the modified conversion ratio (C^*) defined as the ratio of ^{238}U (n,γ) captures to ^{235}U fissions. The procedure requires irradiation in the lattice of thick, full ring segments of the actual Mark 15 fuel rather than small sectored foils. The advantages of this measurement over the foil method of measuring the C^* parameter are:

- Positional inaccuracies are minimized
- Azimuthal variations are automatically averaged
- Errors from differential fission product escape are reduced
- No perturbations are introduced from use of foils in the lattice.

C^+ was determined from the relative fission rates and the relative ^{238}U capture rates in "foils" of Mark 15 fuel irradiated simultaneously in the LTR lattice and in the SP thermal column. The "foils"in the lattice consisted of 1/2-inch-long ring sections irradiated as an integral part of the Mark 15 coaxial fuel near the center of the LTR. The "foils" in the thermal reference were 1/2-inch-long (30°-inner; 18°- outer) ring sectors of Mark 15 fuel. These were stacked in linear columns with identical guard pieces at both ends. Following irradiation the relative total fission rate between the lattice and reference "foils" was determined by counting with a Ge-Li detector the 1596-keV photopeak from ^{140}La. The relative ^{239}Np capture rate was measured by counting the photopeak at 278 keV. The full ring segments were placed symmetrically on the axis of the cylindrical Ge-Li detector for counting. The ring sectors were assembled on the same arc as the full rings. Lead rings were placed on the inside and outside of the Mark 15 rings and similarly around the ring sectors to minimize counting of circumferential surface activation. In addition, unirradiated sectors were placed at both ends of the ring sector arc. Counting was done in the interval from 3-8 days after irradiation. The value of C^+ is related to the counting ratios by the expression

$$C^+ = \left[\frac{\Sigma_a^{238}}{\Sigma_f^{235}}\right]_{\text{Th Ref}} \cdot \frac{[^{239}\text{Np Prod}]_{\text{Lattice}}}{[^{239}\text{Np Prod}]_{\text{Th Ref}}} \cdot \frac{[^{140}\text{La Prod}]_{\text{Th Ref}}}{[^{140}\text{La Prod}]_{\text{Lattice}}}$$

$$\cdot \frac{(1 + f\,\delta^{28})}{(1 + \delta^{28})}$$

Here the right hand ratio which includes the f factor corrects for the difference in fission product yield of ^{140}La between ^{235}U and ^{238}U fission. The δ^{28} value is that measured for each tube (see Table 4). Values of f, σ_a^{238}, σ_f^{235}, g^{235}, and g^{238} used in the determination of C^+ are given in Table 2. Inherent in the measurement is the assumption that the ^{132}Te and ^{140}La fission product yields are independent of neutron energy. A small (<1%) correction for ^{238}U epithermal neutron capture in the thermal reference was measured using bare and cadmium covered depleted uranium foils. A calculated correction of ∿2% also was applied to account for ^{238}U fast fission in the thermal reference.

Inner-to-Outer Fuel Activation Rate Ratios. Inner-to-outer fuel activation rate ratios per unit volume were obtained for ^{238}U epicadmium capture, ^{238}U subcadmium capture, ^{238}U fission, ^{235}U subcadmium fission, ^{235}U epicadmium fission and ^{235}U fission. These ratios were derived as a byproduct of the foil activations for the ρ^{28}, δ^{28}, and δ^{25} measurements.

The inner-to-outer fuel total fission ratio per unit volume was obtained as a byproduct of the C^+ measurement. Approximately two weeks after irradiation, with the ^{140}La activity dominant, a measurement of the ratio of the total ^{140}La yield of the inner-to-outer ring was made by monitoring the 1596 keV photopeak with a Ge-Li detector. The measurements were made at different elevations above the detector to study the geometry dependent counting efficiencies between the inner and outer rings. The ^{140}La activity is closely proportional to the fission product yield with only a small correction for the different yield in ^{238}U and ^{235}U fission. The ratio of ^{238}U fissions to ^{235}U fissions used for this correction was obtained from the δ^{28} measurement. The activity ratio was corrected for the difference in volume between the inner and outer fuel rings.

COMPARISON OF RESULTS

LTR and SE Experiments

Material Buckling. A measured value of 7.29 ± 0.06 m^{-2} was obtained for the material buckling from the LTR experiment compared to 7.81 ± 0.30 in the SE after adjustment to comparable conditions (see Table 3). The large (0.51 m^{-2}) discrepancy is outside of experimental uncertainties. Systematic differences in the

Table 2

Constants Used in C^+ Measurements

Decay Chain		$^{140}Ba \rightarrow ^{140}La$
^{235}U Fission Product Yield		0.0636
^{238}U Fission Product Yield		0.0605
f		0.951
	^{235}U	^{238}U
σ_a, b	-	2.70
σ_f, b	582.2	-
g	0.9759	1.000[a]

a. Refer to the section on the energy dependent of the ^{238}U subcadmium capture cross section in the Appendix.

Table 3

Mark 15 Lattice Reactivity at 7-inch Δ Pitch & 99.75 mol % D_2O

	Material Buckling, m^{-2}
LTR Measurement	7.29 ± 0.06[a]
SE Measurement (Ref. 2)	7.81 ± 0.30[b]
RAHABR Computation	7.12 ± 0.20

a. The material buckling measured at 99.61 mol % D_2O has been reduced by 0.16 m^{-2} (based on calculation) to correct to conditions at 99.75 mol % D_2O. Corrections have been applied for the reactivity effects of the activation detectors (estimated to be worth -0.01 m^{-2}) and for the presence of 29 highly perforated, thin wall aluminum guide tubes (for safety and control rods) located at interstitial positions in the lattice (estimated to be worth -0.01 m^{-2}).

b. A small (+0.11 m^{-2}) calculated correction has been applied to convert the SE measurement to the same geometrical lattice conditions as the LTR measurement.

The Mark 15 fuel in the SE measurement was clad with 30 mil thick aluminum and the outside surface of the inner fuel contained 4 thin aluminum ribs. Minor differences in the support tube housing arrangement also existed. The SE geometry is detailed in Reference 1.

Table 4

Mark 15 Lattice Parameters at 7-inch Δ Pitch & 99.75 mol % D_2O

Parameter	Inner Tube			Outer Tube			Assembly Avg.		
	Measurement		RAHABR Calc	Measurement		RAHABR Calc	Measurement		RAHABR Calc
	LTR[a]	SE[b]		LTR[a]	SE[b]		LTR[a]	SE[b]	
ρ^{28}	2.23 ± .04	2.14 ± .04	1.985	1.98 ± .08	1.86 ± .05	1.777	2.05 ± .09	1.97 ± .06	1.856
δ^{25}	0.193 ± .002	0.194 ± .002	0.1936	0.150 ± .003	0.152 ± .003	0.1458	0.168 ± .004	0.168 ± .004	0.1636
δ^{28}	0.107 ± .004	0.103 ± .004	0.0940	0.073 ± .003	0.070 ± .003	0.0660	0.086 ± .005	0.083 ± .005	0.0767
C^{+c}	1.087 ± .009	---	1.031	1.036 ± .008	---	1.009	1.056 ± .007	---	1.017
	(1.094 ± .014)	(1.074 ± .015)		(1.066 ± .029)	(1.030 ± .018)		(1.067 ± .033)	(1.049 ± .022)	
R	1.621 ± .020	1.644 ± .016	---	1.493 ± .030	1.539 ± .023	---	---	---	---

a. Small calculated corrections from RAHABR have been applied to convert the parameters measured in the LTR at 99.61 mol % D_2O to values that would be obtained at 99.75 mol % D_2O.

b. Small calculated corrections from RAHABR have been applied to convert the ρ^{28}, δ^{25} and δ^{28} parameters measured in the SE to the same geometrical lattice conditions as the LTR measurement. (See footnote in Table 3.)

c. Values in parentheses were derived from the expression $C^{+} = \frac{C^{28}}{F^{25}} \cdot \frac{(1 + \rho^{28})}{(1 + \delta^{25})(1 + \delta^{25})}$.

reactivity measured in an exponential facility and those obtained from critical measurements were reported for the simple case of 1-inch diameter natural uranium rods and rod clusters in D_2O.[7] The differences were found to be dependent on fuel assembly size and the moderator-to-fuel ratio. An extrapolated value of about 0.30 m^{-2} (exponential measurement higher) is obtained for single rods with the same moderator-to-fuel ratio as the Mark 15 at the 7-inch pitch. Efforts to determine the source of systematic error in exponential reactivity measurements have not been successful. The use of reactivity data from D_2O exponential experiments as benchmarks to test analytical methods used in lattice analysis and to evaluate cross section data may no longer be justified with the current state of calculational sophistication.

Lattice Parameters. Parameters measured in the critical LTR reactor are compared with the SE exponential measurements in Table 4. Parameters measured in the SE and LTR agree within the assigned errors. The results indicate that the neutron spectrum is closely identical in the asymptotic regions of the critical and exponential facilities where the measurements were made.

LTR Experiment and RAHABR Computations

Material Buckling. The measured material buckling (7.29 ± 0.06 m^{-2}) in the LTR is in good agreement with the 7.12 ± 0.20 m^{-2} value calculated by RAHABR using ENDF/B-IV cross sections (see Table 3).

Lattice Parameters. Parameters measured in the LTR are compared with RAHABR (ENDF/B-IV) calculations in Table 4.

The major discrepancies between measured and calculated parameters occur in ρ^{28} and δ^{28} which are calculated about 10% low in both the inner and outer fuel. The discrepancy between measured and calculated δ^{28} will be reduced by ENDF/B-V data as a result of a harder fission spectrum and changes in ^{238}U inelastic scattering. Independent confirmation of the measured values of ρ^{28} was obtained via the C^+ measurement. The C^+ parameter is related to ρ^{28}, δ^{25} and δ^{28} by the expression

$$C^+ = \frac{C^{28}}{F^{25}} \cdot \frac{(1 + \rho^{28})}{(1 + \delta^{25})(1 + \delta^{28})}$$

where

$C^{28} \equiv$ Subcadmium ^{238}U captures in the fuel

$F^{25} \equiv$ Subcadmium ^{235}U fissions in the fuel

Since $\rho^{28} \approx 2.0$ in the Mark 15 lattice, C^+ is sensitive to small percentage changes in ρ^{28}. Therefore the C^+ measurement within 1% accuracy becomes an independent means of verifying the ρ^{28}

measurement. The C^{28} to F^{25} ratio is calculated quite well by RAHABR for this purpose. Values of C^+ derived from parameters by this method are given in Table 4. Agreement with the direct measurement of C^+ is good providing additional confidence in the value of ρ^{28} derived by the foil activation technique.

A comparison of measured and calculated inner-to-outer fuel reaction rate ratios are given in Table 5. The good agreement indicates that the spatial distribution of the neutron energy spectrum is calculated properly in the coaxial fuel by RAHABR. With the inner-to-outer ratios of epicadmium ^{238}U captures and subcadmium ^{238}U captures predicted properly, the 10% discrepancy of ρ^{28} in both the inner and outer fuel suggests either that the resonance capture in ^{238}U is uniformly underpredicted or that the measured ρ^{28} is erroneously high.

The inner-to-outer fuel total fission ratio is related to foil parameters by the expression:

$$(I/0)_{\substack{\text{Total}\\\text{Fission}}} = (I/0)_{^{235}U\ \substack{\text{Subcd}\\\text{Fission}}} \cdot \frac{[(1+\delta^{28})(1+\delta^{25})]_{\text{inner}}}{[(1+\delta^{28})(1+\delta^{25})]_{\text{outer}}}$$

The ratio obtained from this expression is compared with that from the ^{140}La measurement in Table 5. No explanation is available to account for the 5.8% difference between the two values.

CONSISTENCY ANALYSIS

The consistency of the Mark 15 data from the LTR experiment has been tested using a two-energy-group, neutron balance equation[3] that expresses the material buckling (B_m^2) as a function of the integral parameters and calculable cross-section dependent terms. The expression is

$$B_m^2 \left\{ \frac{D_1 \ (\Sigma_{a2} + \Sigma_{r2\to1} + D_2 \ B_m^2)}{\Sigma_{f2} \ \Sigma_{r1\to2}} + \frac{D_2}{\Sigma_{f2}} \right\} = (\bar{\nu}_a^{25} - 1) +$$

$$(\bar{\nu}_1^{25} - 1)\ \delta^{25} - \bar{\alpha}_2^{25} - \bar{\alpha}_1^{25}\ \delta^{25} +$$

$$(1+\delta^{25})\ [(\bar{\nu}_1^{28} - 1)\ \delta^{28} - (1+\delta^{28})\ C^+ - \zeta]$$

where δ^{25}, δ^{28} and C^+ are the experimentally determined activation parameters. (The equation can be cast in terms of ρ^{28} using the relation given earlier for C^+.)

and

Table 5

Comparison of Measured and Calculated
Inner-to-Outer Fuel Reaction Rate Ratios, 99.61 mol % D_2O

Reaction Rates	Inner-to-Outer Ratio (per unit volume) Measured	Calculated (RAHABR)
epi Cd ^{238}U captures	0.809 ± .018	0.803
sub Cd ^{238}U captures	0.719 ± .007	0.718
^{238}U fissions	1.048 ± .011	1.050
epi Cd ^{235}U fissions	0.911 ± .012	0.940
sub Cd ^{235}U fissions	0.706 ± .010	0.707
^{235}U fissions	0.732 ± .007	0.737
Total fissions	0.801 ± .012[a]	0.756
	0.757 ± .02[b]	

a. Measured by ^{140}La signal from Mark 15 fuel ring pieces.

b. Derived from foil activations by use of the expression:

$$\text{Total Fission} = (I/O)_{\substack{\text{sub Cd } ^{235}U \\ \text{fissions}}} \cdot \frac{(1+\delta^{28})_{\text{inner}}}{(1+\delta^{25})_{\text{outer}}} \cdot \frac{(1+\delta^{25})_{\text{inner}}}{(1+\delta^{25})_{\text{outer}}}$$

$$\zeta = \frac{\text{Total Captures in Materials Other than } ^{235}U \text{ and } ^{238}U}{\text{Total } ^{235}U \text{ Fissions}}$$

$$\overline{\nu}_n = \frac{\overline{\nu\Sigma_f}_n}{\Sigma_{f_n}}$$

$$\overline{\alpha}_n = \frac{\Sigma_{c_n}}{\Sigma_{f_n}}$$

The consistency buckling obtained from this expression using RAHABR (ENDF/B-IV) to generate the cross section dependent terms was 5.42 ± 1.18 m^{-2} compared to the measured buckling of 7.29 ± 0.06 m^{-2}. Assuming that the measured buckling is correct, that the two-group neutron balance expression relating measured parameters to B_m^2 is valid, and that the cross sections are correct, then the discrepancy between the measured buckling and the consistency buckling would be attributed to erroneous experimental parameter(s).

The sensitivity of B_m^2 to small variations in the Mark 15 reaction rate parameters has been investigated using the consistency equation in the form:

$$C_1 (B_m^2)^2 + C_2 B_m^2 - C_2 = 0$$

where

$$C_1 = \frac{D_1 D_2}{\Sigma_{f2} \Sigma_{r1\to2}}$$

$$C_2 = \frac{D_1 (\Sigma_{a2} + \Sigma_{r2\to1})}{\Sigma_{f2} \Sigma_{r1\to2}} + \frac{D_2}{\Sigma_{f2}}$$

$$C_3 = (\overline{\nu}_2^{25} - 1) + \delta^{25} (\overline{\nu}_1^{25} - 1 - \overline{\alpha}_1^{25}) - \overline{\alpha}_2^{25} +$$

$$(1 + \delta^{25}) \left[(\overline{\nu}_1^{28} - 1) \delta^{28} - \frac{C^{28}}{F^{25}} \frac{(1 + \rho^{28})}{(1 + \delta^{25})} - \zeta \right]$$

here

$\frac{C^{28}}{F^{25}}$ is the ratio of ^{238}U thermal captures to ^{235}U thermal fissions

Sensitivity coefficients are summarized in Table 6. Also shown in Table 6 is the percent change required to force internal consistency for each of several variables. Small changes in ρ^{28}

Table 6

Sensitivity Analysis of Consistency Equation
for Mark 15 Lattice at 7-Inch Δ Pitch

Variable	Change in B_m^2, m^{-2} / 1% Change in Variable	% Change in Variable To Force Consistency
ρ^{28}	-0.21	-8.8
δ^{25}	0.043	43.0
δ^{28}	0.035	52.9
C_1	-0.011	-168.0
C_2	-0.053	-34.9
C_3	-0.053	34.9

have a significant effect on B_m^2 while other variables are much less important. In fact most of the 25% discrepancy between the measured buckling and the consistency buckling could be resolved by a 6.5% decrease in the measured ρ^{28}. Not only would this satisfy the consistency criteria but it would also improve agreement between the measured and calculated values of ρ^{28}. However, corrections have been applied for all known systematic errors in the ρ^{28} measurement. A conservative 2% error flag is assigned to ρ^{28}_{inner} where the standard deviation of the mean for the six foils used in the measurement was ±0.3% and a 4% error flag is assigned to ρ^{28}_{outer} where the standard deviation of the mean for the five foils used in the measurement was ±2.0%. The most likely source of error, reflected in the count rate variation for the foil detectors in the fuel, is the accuracy of the geometrical fit of the foil and fuel segments in the machined window slot of the fuel. Some measure of this error is obtained from an earlier study[8] using foils in a 1/2-inch diameter natural uranium rod to investigate the effect of radial misalignment. As expected, the activations lost due to indentation were nearly offset by those gained in the protruding section. The net effect was to give activation results ∿0.2% lower than the correct values for a 0.005-inch radial misalignment. The effect of foil misalignment is more severe in coaxial fuel, particularly in the outer fuel where the thermal flux gradient is steep, and this probably accounts for the larger spread in activation results for the foils in the outer fuel.

The overall consistency of results with the independent C^+ measurement technique and the general agreement in results from experiments at different laboratories suggests that there are no serious systematic errors in the measurement and correction techniques for the determination of ρ^{28} (Reference 9). However, any adjustment of the calculated ρ^{28} would destroy the good agreement between measured and calculated reactivity.

SUMMARY AND CONCLUSIONS

- Although measured and calculated buckling for the Mark 15-LTR critical is in good agreement, a significant discrepancy exists in ρ^{28} that cannot be resolved within experimental errors.

- Agreement between measured and calculated inner-to-outer fuel activation ratios suggests that the ρ^{28} discrepancy is most likely a result of the underprediction of epicadmium captures in ^{238}U. However, adjustment of ^{238}U captures to correct ρ^{28} will cause the buckling to be underestimated.

- The Mark 15-LTR experiment does not meet the internal consistency criterion using RAHABR with ENDF/B-IV cross sections to generate the cross section dependent terms.

- The use of D_2O exponential experiments as valid benchmarks is compromised by systematic error in B_m^2 although nuclear parameters are in agreement with critical experiments.

REFERENCES

1. D. J. Pellarin and B. M. Morris. "Reactivity and Reactor Rate Measurements in U-D_2O Lattices with Coaxial Fuel." USERDA Report DP-1409, E. I. du Pont de Nemours & Co., Savannah River Laboratory, Aiken, S. C. (1976).
2. H. C. Honeck. "The JOSHUA System." USAEC Report DP-1380, E. I. du Pont de Nemours & Co., Savannah River Laboratory, Aiken, S. C. (1975).
3. D. R. Finch and W. E. Graves. "Quantitative Consistency Testing of Thermal Benchmark Lattice Experiments." Trans. Am. Nucl. Soc. 27, 888 (1977).
4. "JOSHUA Manual." USAEC Report DPSTM-500, Vol. 4, E. I. du Pont de Nemours & Co., Savannah River Laboratory, Aiken, S. C. (1970).
5. J. Hardy, Jr., D. Klein, and J. J. Volpe. "A Study of Physics Parameters in Several Water-Moderated Lattices of Slightly Enriched and Natural Uranium." Report WAPD-TM-931, Bettis Atomic Power Laboratory, Pittsburgh, Pa. (1970).
6. R. Sher and S. Fiarman. "Studies of Thermal Benchmark Data Interpretation: Experimental Corrections." Report EPRI NP-209 Project 247, Electric Power Research Institute, Palo Alto, CA. (1976).
7. E. C. Wingfield and E. J. Hennelly. "Exponential Measurements of Natural Uranium Rods in Heavy Water and Comparisons with Critical Experiments." Nucl. Sci. Eng. 12, 348-358 (1962).
8. D. J. Pellarin and N. P. Baumann. "^{238}U Resonance Capture Integrals for Rods of UO_2, UC and U-Metal." USAEC Report DP-1203, E. I. du Pont de Nemours & Co., Savannah River Laboratory, Aiken, S. C. (1970).
9. "Seminar on ^{238}U Resonance Capture." Report BNL-NCS-50451 (ENDF-217), Brookhaven National Laboratory, Upton, NY (March 1975).

APPENDIX

Energy Dependence of ^{238}U Subcadmium Capture Cross Section

The energy dependence of the ^{238}U capture cross section in the thermal and near thermal energy region is important since it enters into the basic computation of lattice bucklings and reactivities. It is particularly important for massive ^{238}U bearing assemblies at low moderator-to-fuel ratios. Absorption hardening and a hard spectrum combine to shift a larger fraction of the neutron induced reactions to the upper end of the thermal region where this cross section is most uncertain. Knowledge of the

energy dependence of the cross section is also essential to compare conversion ratio (C^* or C^+) measurements to direct cadmium ratio (ρ^{28}) measurements. Such comparisons rely on calculations of the subcadmium ratio of ^{238}U fissions both in the thermal reference and in the lattice. Measurements of the ^{238}U cadmium ratio (ρ^{28}) by the indirect method also depend sensitively on the ^{238}U cross section shape. A computation must be made of the ratio of ^{238}U to 1/v activations in the thermal reference flux to the same ratio for subcadmium neutrons in the lattice. For this application it has generally been assumed (including values in this report) that ^{238}U is closely 1/v and that the two ratios are the same.

Figure 2 shows three shape dependences that have been used at SRL. The 1/v dependence has been assumed for analysis of various activation experiments. The values listed as SRL "STANDARD" assumes a low lying negative energy resonance. The choice of energy and partial widths is such as to give good agreement with D_2O-Uranium lattice buckling measurements at SRL. The ENDF/B-IV values assume negative energy levels so far removed from thermal energies that they have essentially no effect on the shape.

An experimental program has been devised to investigate this energy dependence. The experimental technique utilizes a well-thermalized neutron flux which is thermally heated to selected temperatures. Pairs of multilayer packets of alternating copper and ^{238}U foils are simultaneously irradiated under thin gadolinium filters in the heated flux and irradiated bare in a well-thermalized flux at room temperature. Cadmium covered foils provide corrections for the small epicadmium component in both cases. The relative copper and ^{238}U activations are counted in a Ge-Li detector under conditions designed to minimize errors in the activation ratios.

Figure 3 shows the ENDF/B-IV normalized activation ratios for a range of neutron temperatures and gadolinium thicknesses. The calculations assume isotropic flux incident on infinite slabs. (Thin detectors are used for these illustrations, but the actual foil packet conditions are included in the analysis of the experiments.) A preliminary experiment has been completed with the "heated" flux at room temperature and with a gadolinium filter surface density of 0.000145 atoms/barn. The experimental ratio of ^{238}U to Cu activations in the "heated" flux to the bare foil activations in the reference flux was 1.012 ± 0.004 compared to 1.0148 calculated from ENDF/B-IV, 1.000 for a 1/v dependence, and a quantity less than unity for the SRL "STANDARD" cross sections. These preliminary results agree with the ENDF/B-IV structure within the experimental errors.

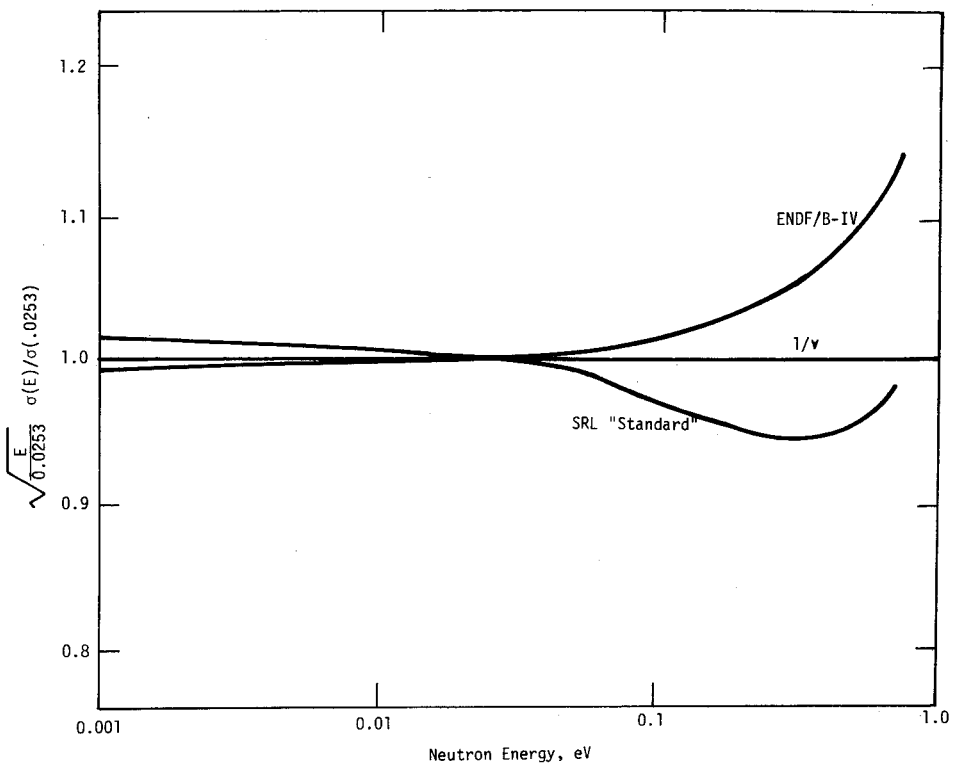

FIGURE 2. Energy Dependence of ^{238}U Capture Cross Section

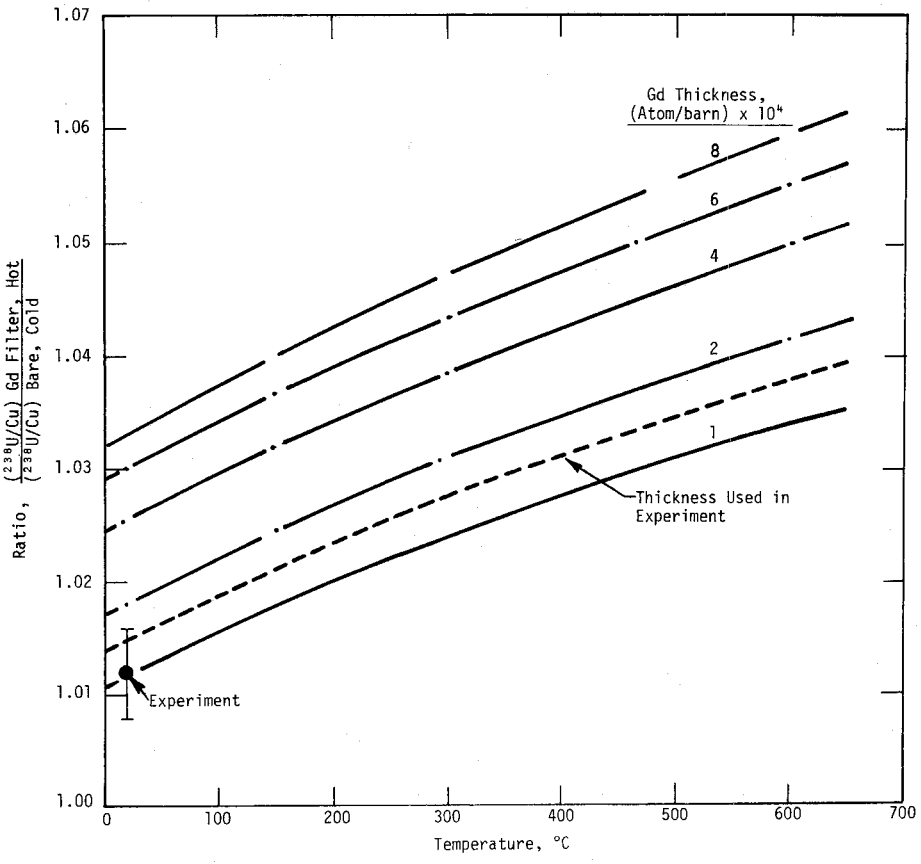

FIGURE 3. Activation Ratios for ^{238}U/Cu Using ENDF/B-IV

Section 9

REVIEW OF THORIUM-U233 CYCLE THERMAL REACTOR BENCHMARK STUDIES

Review of Thorium-U233 Cycle Thermal Reactor Benchmark Studies

J. J. Ullo, J. Hardy, Jr., and N. M. Steen
Bettis Atomic Power Laboratory, West Mifflin, Pennsylvania

ABSTRACT

A survey is made of many existing integral experiments for U233 systems and thorium-uranium based fuel systems. The aim is to understand to what extent they give a consistent test of ENDF/B-IV nuclear data. A principal result is that ENDF/B-IV leads to an underprediction of leakage. Extensive results from testing alternate thorium data sets are presented. For one evaluation due to Leonard they depict a possibly growing discrepancy between measured integral parameters such as ρ^{02} and I'^{232} and the differential data, which underpredicts them. Sensitivities to other nuclear data components, notably the fission neutron spectrum, were determined. A new harder U233 spectrum significantly reduces a bias trend in K_{eff} vs. leakage.

INTRODUCTION

Not unexpected due to the renewed interest in the U233-thorium fuel cycle is the desire to establish the adequacy of existing clean thorium-U233 experiments to provide a test of theoretical techniques and nuclear data. This paper summarizes the results of a survey of U233 and thorium-uranium critical experiments which may be of potential use as thermal reactor benchmarks.

The presentation has been divided into two parts. In the first, we describe analyses of existing thorium-uranium experiments in order to assess their reliability as benchmarks. ENDF/B-IV data were used throughout. Experiments studied included homogeneous U233 criticals[1], simple thorium-U235 critical lattices moderated with H_2O (TUPE[2]) and D_2O (THUD[3]), the BNL thorium-U233 exponential lattices[4,5], and critical experiments in support of LWBR including ETA-I and ETA-II[6,7], the BMU series[8] and the detailed cells[9].

In the second part, the sensitivities of the integral parameters for selected experiments to various thorium data sets are summarized and discussed. The alternate thorium sets tested included the Leonard evaluation[10], the Derrien evaluation[11], and the LWBR data set based on the Steen evaluation[12]. Sensitivities to several other data changes were also determined with the representation of the fission neutron spectrum for U233 and U235 being the most significant.

---

*Work performed under the auspices of U.S. Department of Energy under Contract No. EY-76-C-11-0014

I. Calculation of Uranium-Thorium Experiments With ENDF/B-IV Data

In this section, our analyses of homogeneous U233 criticals and thorium-uranium lattice critical and exponential experiments which are potentially useful for data testing are discussed. In addition, related analyses performed at other laboratories using ENDF/B-IV data are summarized for comparison.

A. Analyses of Homogeneous U233 Critical Experiments. In a study done at Oak Ridge[13] to compare Hanson-Roach and ENDF/B-IV data sets, McNeany and Jenkins reported that ENDF/B-IV produced errors of several percent in calculated neutron multiplication factors for homogeneous U233 assemblies with low hydrogen/uranium atom ratios (H/U). It was concluded that the ENDF/B-IV data file was not satisfactory for calculating criticality of such assemblies.

More recently, a set of fourteen U233 criticals (including several of those considered in the Oak Ridge study) was analyzed at Bettis[1], and a corresponding set of seventeen U235 criticals was analyzed for comparison. The purpose was to examine in detail the ability of ENDF/B-IV data to predict criticality of such systems over a wide range of H/U, with the intent of drawing specific conclusions about the data set. These systems span a wide range of spectrum hardness (with as much as 50% epithermal fission) and of leakage (from 1%-50%). The critical eigenvalue and detailed reaction rates were calculated, and eigenvalue sensitivities to certain major data changes were determined.

The criticals were analyzed with the Monte Carlo program RCP01, an extension of RECAP[14], and with P7MG, an extension of P3MG[15], a one-dimensional, multigroup P_ℓ program. RCP01 was used for the overall study of criticality versus H/U ratio. Cross section sensitivities were derived from P7MG and are presented in Part II of this paper. The agreement between RCP01 and P7MG was checked for five specific experiments and found to be very good.

1. Criticality Versus Hydrogen/Uranium Ratio. Eigenvalues for the U233 criticals (Table I) show generally good agreement with the Oak Ridge calculations. This suggests that the use of different analysis programs and nuclear data processing procedures has little effect on the calculated results. For both U233 and U235, the ENDF/B-IV-calculated eigenvalues[1] become increasingly high relative to experiment as the H/U ratio is decreased from well thermalized systems (Figure 1).

Table I - Results for Homogeneous U233 Critical Experiments Calculated with ENDF/B-IV Data

Experiment	H/U233	Calculated Total Leakage	Calculated δ^{23}	Calculated K_{eff} Ref. (1)*	Calculated K_{eff} Ref. (13)**
L1	119	.5149	.4493	1.0116±.0034	
L2	154	.5081	.3466	1.0226±.0027	1.027±.007
L3	381	.4617	.1526	1.0110±.0035	1.026±.006
L4	581	.4081	.1094	1.0111±.0034	
9	1324	.1742	.0635	1.0007±.0037	
		.1736	.0655	1.0029	
8	1369	.1743	.0633	1.0035	
7	1417	.1751	.0610	1.0035	
6	1470	.1759	.0588	1.0037	
5	1533	.1776	.0548	1.0017±.0016	1.005±.003
		.1769	.0563	1.0032	
17	1820	.1094	.0505	.9990	
18	1901	.0880	.0491	1.0002	
11	1986	.0683	.0463	.9974±.0031	.994
		.0686	.0477	.9981	
19	1997	.0649	.0476	.9991	
20	2106	.0402	.0461	.9956±.0008	
		.0398	.0461	.9967	

* Uncertainty is two standard deviations for RCP01 results. Eigenvalues without uncertainties are from P7MG.

** Uncertainty is one standard deviation.

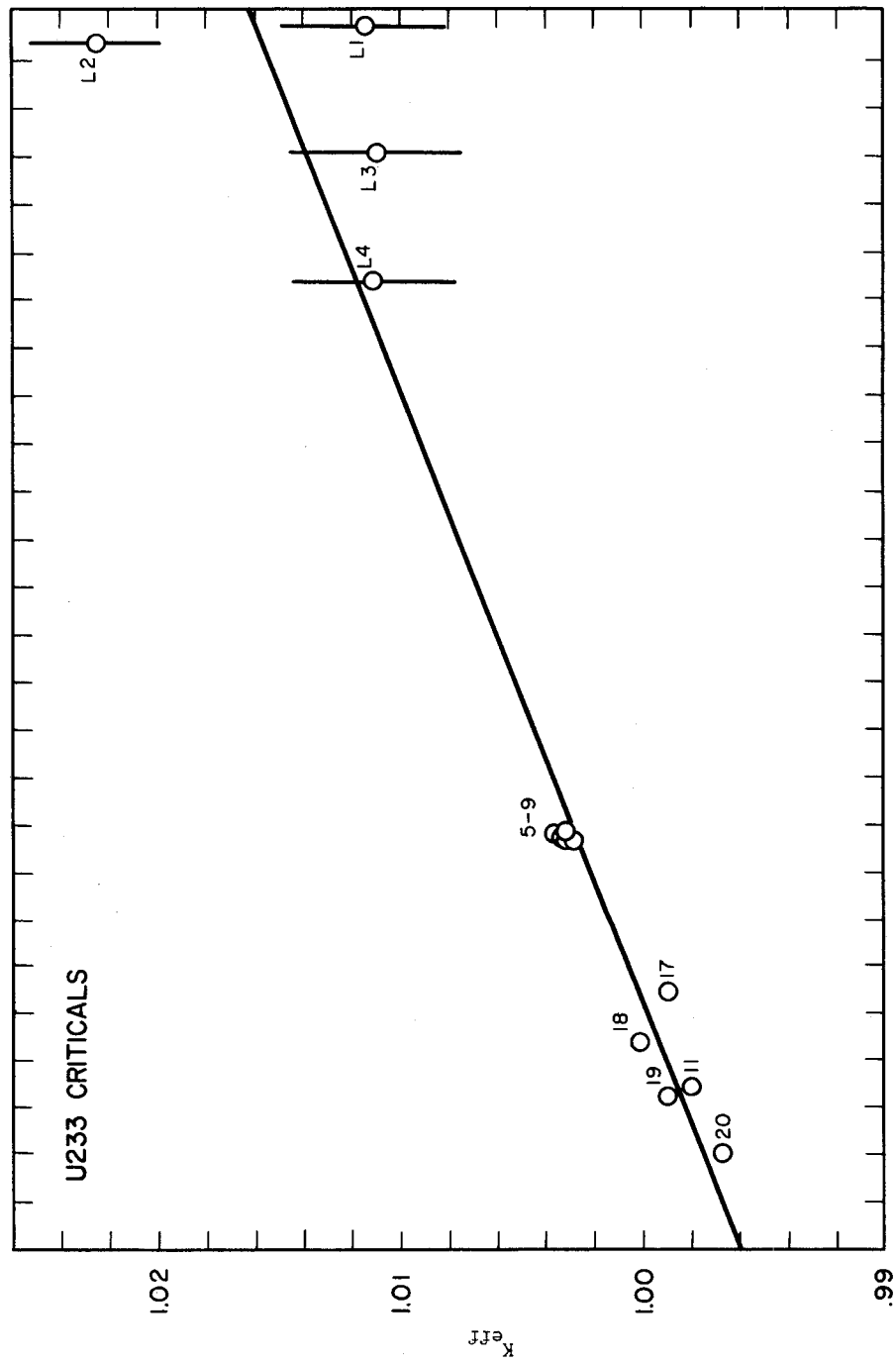

Figure 1 - U233 Homogeneous Criticals, Calculated Eigenvalue vs. Total Leakage Fraction

Although there remain questions of interpretation about individual experiments, these are judged not to be significant for the overall pattern. Errors in calculated eigenvalue can stem from energy-dependent errors of η which are emphasized as the spectrum hardens, but arguments were presented in Reference 1 which tended to discount this possibility. The other source of eigenvalue error is under-prediction of leakage which is emphasized in the smaller cores. The most significant factors potentially affecting leakage are considered to be:

(1) multigroup averaging and limited P_ℓ treatment in RCP01
(2) oxygen scattering cross section and angular pattern (meV)
(3) fission spectrum of U233 and of U235.

Since the trend in calculated eigenvalue error is nearly the same for U233 and for U235 systems, it is tempting to seek a common source of difficulty (e.g., items (1) and (2) above), but this has not proved fruitful. Furthermore, calculational approximations (including data processing) were deemed to be relatively unimportant. Sensitivities to the fission spectrum mean energy and shape were significant and are further examined in Part II.

B. TUPE Lattices (Th-U235-H_2O). The TUPE (Thorium-Uranium-Physics-Experiment) criticals were operated at Babcock and Wilcox in the late 1950's[2]. There were five H_2O-moderated simple lattices constructed from $U235O_2$-ThO_2 rods having Th/U235 atom ratios of 15/1 and 25/1. The lattices were square arrays of four pitches, with moderator/fuel volume ratios ranging from 1.38 to 5.79.

The five uniform lattices have been analyzed with ENDF/B-IV data and the RCP01 Monte Carlo program. The cores were described explicitly in three dimensions, including the lattice plates, core support structure and tank, with a black absorbing boundary placed outside the tank.

Table II and Figure 2 present eigenvalues obtained in the full-core analyses with ENDF/B-IV data. These show relatively good agreement with experiment, although there is a distinct downward trend in the tighter lattices.

Material bucklings were reported[2], inferred from careful measurements of radial and axial activation shapes. For comparison with the full-core Monte Carlo results, eigenvalues have been calculated from a zero-leakage cell Monte Carlo, with leakage correction obtained from MUFT7, an extension of MUFT5[16], using the measured material buckling. Fast advantage factors and thermal disadvantage factors were obtained from the RCP01 cell region fluxes for the fast (10 meV - 820 keV) and thermal (0 - 0.625 eV) groups. The MUFT7 calculation used a recently

Table II - Calculated Criticality of TUPE Lattices
(Full Core RCP01)

Lattice Ident. (Ref. 2)	Mod./Fuel Volume Ratio	Number of Rods	Moderator Height (cm)	Calculated Net Leakage	Calculated $K_{eff} \pm \sigma$*
15A	1.379	1108	127.21	0.313	1.0002±.0014
15B	1.642	880	133.44	0.325	.9947±.0013
15D	2.945	514	135.05	0.317	1.0056±.0014
25D	3.636	1176	140.50	0.206	1.0075±.0013
$25\sqrt{2}$B	5.794	1146	135.27	0.165	1.0060±.0013

*Monte Carlo statistical error at one standard deviation.

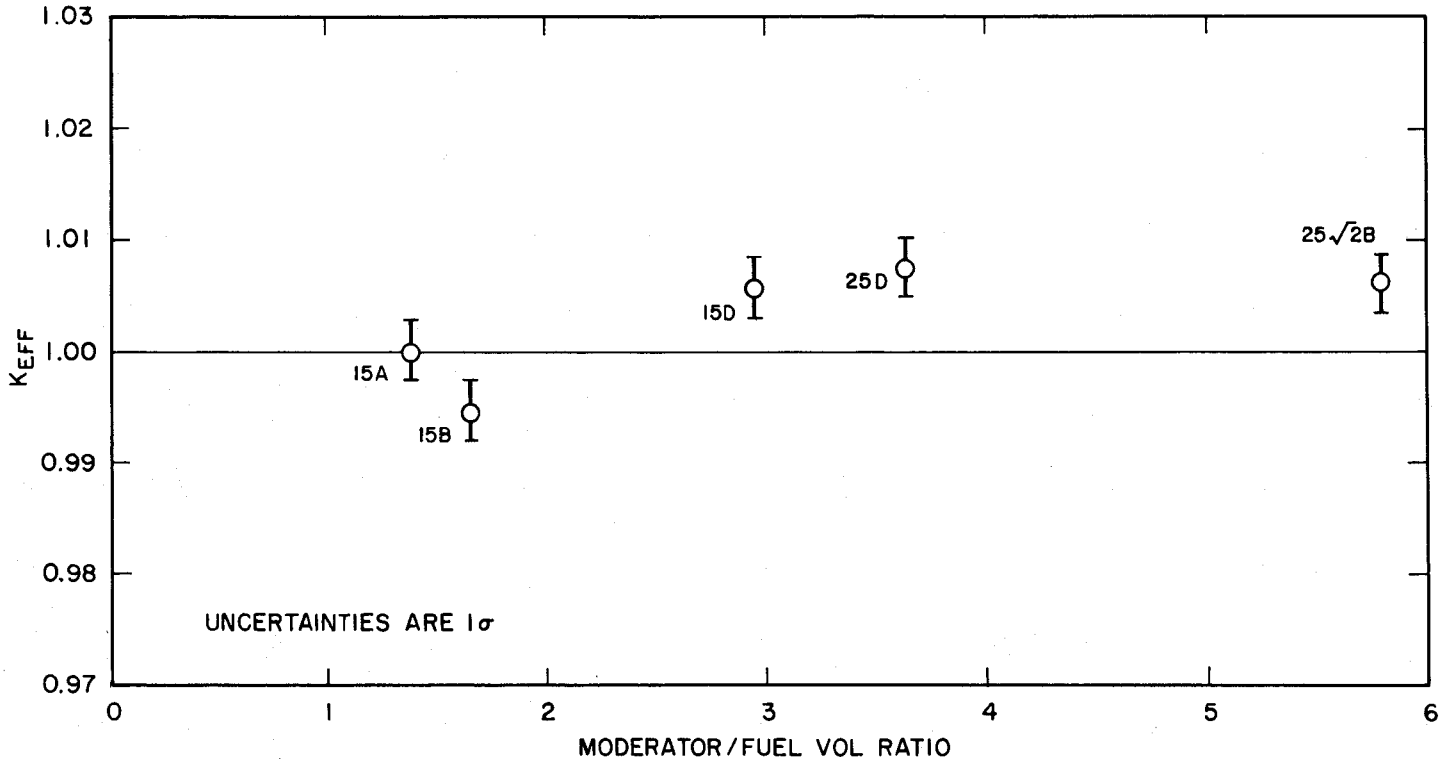

Figure 2 - TUPE U235-ThO_2-H_2O Lattices, Full Core RCP01
Calculated K_{eff} vs. (M/F) Volume Ratio

developed resonance absorption treatment, based on integral transport theory, with the same detailed cross section profile as used in RCP01. This produced reaction rates in good agreement with the cell RCP01 over the range 0.625 eV - 5530 eV in which it was applied. An alternative calculation was done with the P7MG program. This used the small measured axial buckling (~0.0004 cm^2) and did an explicit radial traverse of the homogenized core out through the reflector. The calculation was otherwise similar to MUFT7.

Results are shown in Table III and in Figure 3. Two points are noteworthy:

(1) The P7MG leakage-corrected eigenvalues are somewhat higher than the full-core RCP01 but in reasonable agreement in view of the approximations (homogenization, few-group flux weighting) in P7MG.

(2) For the 15/1-fueled lattices, use of the measured B_m^2 values in MUFT7 produces eigenvalues significantly below those calculated with the explicit radial traverse by P7MG or by the full-core RCP01. Since MUFT7 and P7MG contain basically similar approximations, except for the explicit spatial treatment in P7MG, this suggests that the measured bucklings are too large. It is clear from the P7MG results that this is due to nonasymptotic spectra in the smaller cores[2] - that is, the calculated radial flux shapes agree reasonably well with measurement, but these are not the correct asymptotic shapes. For the 25/1-fueled lattices, which have smaller bucklings, agreement is satisfactory.

Other analyses of lattices 15A and 15B using ENDF/B-IV data have been reported. These were done at GE San Jose[17] and Combustion Engineering[18]. Eigenvalue results are compared in Table III. These show good agreement for the spatially dependent calculations. For the point calculations with measured B_m^2, the CEPAK result is not as low as obtained with MUFT7.

Cadmium ratios of Th232 capture and U235 fission activations were measured with thorium metal foils and U235-Al foils, respectively. Statistics, from reproducibility, appear to be good for U235 (~1% in δ^{25}); for thorium capture, uncertainties of ρ^{02} range from 2% (for core $25\sqrt{2}B$) to nearly 6% (for core 15B). Interpretation of these measurements would require detailed study of experimental effects - mainly cadmium cutoff energy and flux perturbation by the detector foils and cadmium sleeves. No attempt has been made to analyze these measurements, and such an effort is judged to be unfruitful.

This conclusion is supported by the calculated ρ^{02} values shown in Table IV. The GE-San Jose and BAPL results agree well, but are far below experiment. Since it seems unlikely that the calculations are in error by anywhere near this amount (in view of the good eigenvalues), much of the differences must be attributed to problems with the measurements or their interpretation.

Table III - Comparison of Eigenvalues for the TUPE Lattices

Lattice Ident.	Measured Material B^2 $(cm^{-2}) \times 10^4$	$K_{eff} \pm \sigma$*		K_{eff} (MUFT7) / K_{eff} (Full Core RCP01)	K_{eff} (P7MG) / K_{eff} (Full Core RCP01)	K_{eff}** (GE-San Jose)	K_{eff}*** (Combustion Engineering)
		MUFT7	P7MG				
15A	85.31±.26	.9756±.0014	1.0044±.0014	.9754±.0020	1.0042±.0020	1.006	--
15B	94.25±.29	.9758±.0018	1.0010±.0018	.9810±.0022	1.0063±.0022	1.005	0.9873, 1.0023
15D	114.20±.70	.9883±.0019	1.0137±.0019	.9828±.0024	1.0081±.0024	--	--
25D	64.01±.46	1.0046±.0033	1.0117±.0033	.9971±.0035	1.0042±.0035	--	--
$25\sqrt{2}$B	53.55±.11	1.0060±.0029	1.0129±.0029	1.0000±.0032	1.0069±.0032	--	--

* Both normalized to the same cell RCP01. Uncertainties stem from Monte Carlo statistics at one standard deviation. The MUFT7 calculations used measured material B^2_m.

** Work reported[17] used BWR lattice methods.

*** Work reported[18] consisted of a point CEPAK calculation (low eigenvalue) and a 2D PDQ spatial calculation.

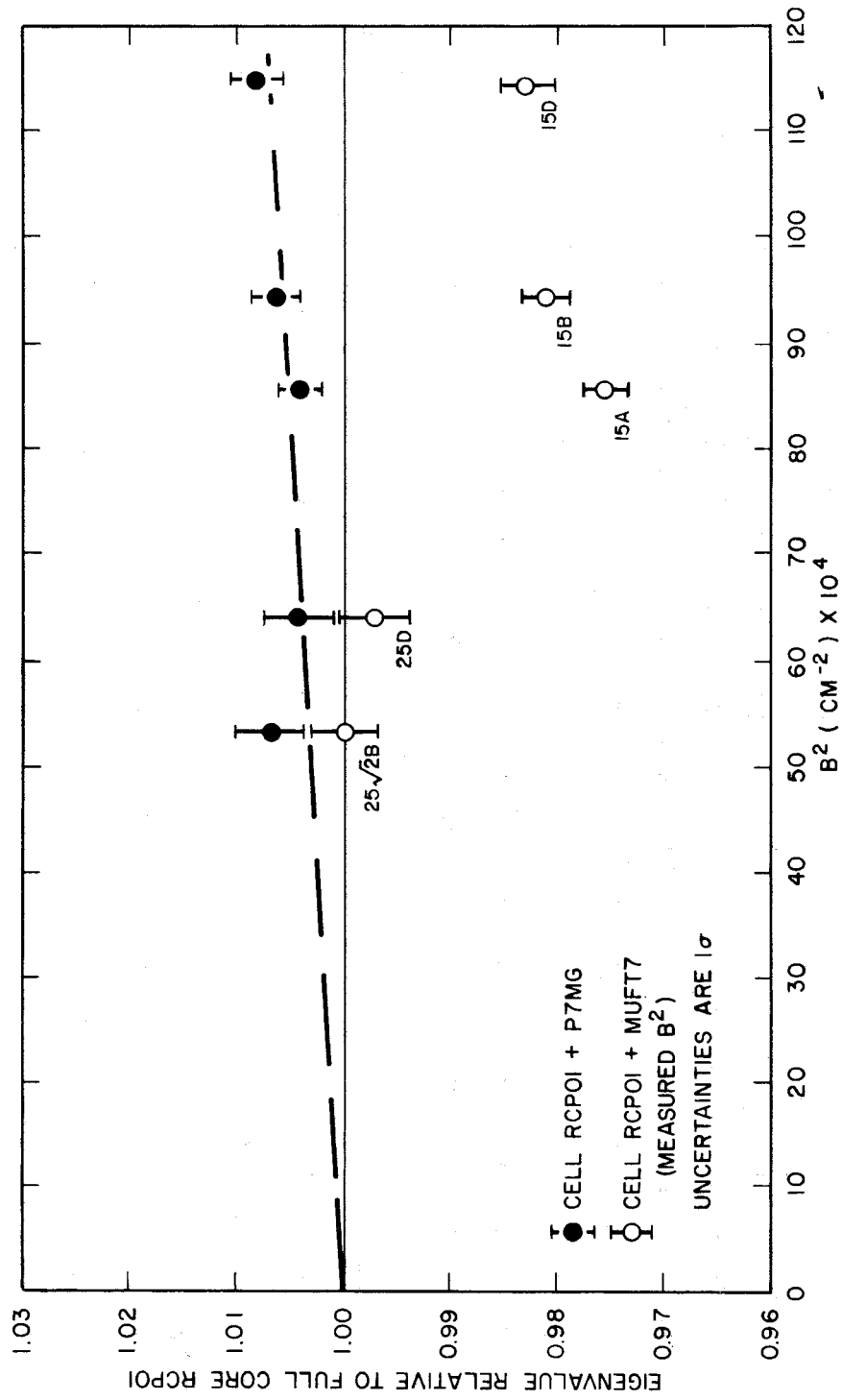

Figure 3 - TUPE Lattices, Alternate Calculated K_{eff}

This suggests that useful information about thorium resonance capture is not likely to be gained by analysis of these measurements.

Table IV - Comparison of Calculated and Measured Values of ρ^{02} for TUPE Cores

Core:	15A	15B	Cutoff Energy
Experiment	2.70±.09	2.09±.12	
Calculation:			
GE-San Jose[17]	1.65	1.42	0.4 eV
BAPL RCP01/P7MG	1.69	1.43	0.4 eV
	1.56	1.33	0.625 eV

ρ^{02} = epithermal thorium capture/thermal thorium capture.

C. THUD Lattices (Th-U235-D_2O). The THUD (Thorium-Uranium-Deuterium) lattice critical experiments were run at the Argonne National Laboratory in the late 1950's[3]. There were 45 uniform single-rod lattices with two types of fuel: $U235O_2$-ThO_2 rods with Th/U235 atom ratios of 15/1 and 25/1 (the same rods used in the TUPE criticals run at Babcock and Wilcox). The lattices were triangular arrays at four pitches (of 2, 3, 4, and 6 X 0.953 cm). At each pitch several lattices were run, differing in number of fuel rods and moderator critical height.

The D_2O purity, initially better than 99%, decreased by 2% over the 2 1/2 year duration of the program. At the end, an independent analysis obtained a purity 1.6% below the last ANL determination, and this discrepancy was not explained.

To test overall consistency of interpretation, we chose initially to analyze a specific lattice for which measurements were made at the beginning, middle, and end of the program (designated core 91, 233, and 456, respectively). This lattice had 745 fuel rods with Th/U235 of 25/1 at the 2 X 0.953 cm pitch. Core 456 was also analyzed with a D_2O purity 1.6% below the ANL determination. Composition data for the fuel were those used in the analysis of the TUPE lattices[2].

The lattice was described explicitly in three dimensions by the RCP01 Monte Carlo program, including corner posts, grid sheets, cross shaped control rod guides and the tank.

Table V shows eigenvalues obtained from the full core analyses with ENDF/B-IV data. Within statistics, the three

cores have consistent eigenvalues, averaging 1.0010±.0013 (σ). For core 456, a 1.6% reduction of D_2O purity reduced the calculated eigenvalue by 0.22±0.31%. It is noteworthy that neutron leakage out of the reactor tank was calculated to be ~10%. This suggests that questions of room return could be significant for these lattices.

In order to do sensitivity studies, core 456 was analyzed with P7MG, which performed an explicit radial traverse of the homogenized lattice out through the reflector. Zero-leakage cell reaction rates were normalized to a Monte Carlo cell calculation.

For THUD 456, P7MG showed a small (0.17%) decrease in eigenvalue due to the 1.6% reduction of D_2O purity, in good agreement with RCP01. Epithermal/thermal reaction ratios were reduced by 9%, however. Thus, the D_2O purity ambiguity is quite significant for such quantities as ρ^{02} (ratio of epithermal/thermal thorium captures) and δ^{25} (ratio of epithermal/thermal U235 fissions) although it has little effect on eigenvalue.

Table V - Calculated Criticality of THUD Lattices (Full Core RCP01)

Lattice Ident.	Date of Run	D_2O Purity (%)	Moderator Height (cm)	Calculated Net Leakage	Calculated $K_{eff}\pm\sigma$*
91	3/58	98.5	132.84	.269	1.0024±.0023
233	11/58	97.9	135.08	.268	1.0018±.0024
456	12/59	97.2	139.09	.267	0.9987±.0021
				Average	1.0010±.0013
456	12/59	95.6(?)	139.09	.271	0.9965±.0023

*One standard deviation.

There is another ambiguity, which has to do with the composition of the 25/1 fuel. Different chemical analyses obtained values for the Th/U atom ratio of 25.33 and 24.65, as shown in Tables XLII and XLVI of Ref. 3. Although the former value seems to be preferred and has been used by B&W (Ref. 2 and private communication from Warren Wittkopf), there remains a significant uncertainty in this regard. K_{eff} results quoted here are for

Th/U = 25.33. Use of the 24.65 value would raise K_{eff} by 0.75% for these THUD lattices. It would raise K_{eff} for the $25\sqrt{2}B$ and 25D TUPE lattices by 0.9%, worsening agreement with the 15/1-fueled TUPE lattices.

There were a limited number of integral parameter measurements for these cores - specifically, Th232 capture cadmium ratios obtained with metal foils. Interpretation of these measurements as in the case of the TUPE lattices would require detailed study of experimental effects such as cadmium cutoff. Since, in most cases, only one irradiation was made and uncertainties are not quoted, it is judged that such an undertaking is not warranted.

D. BNL U233-ThO_2 Exponential Experiments. To provide an extensive set of data for lattice parameters for the evaluation of various theoretical techniques and nuclear data, a series of exponential experiments were carried out at the Brookhaven National Laboratory. The assemblies were fueled with U233-ThO_2 elements, which were arranged in uniform lattices having a triangular pitch in light and heavy water. Measurements were made of the material buckling B_m^2, reflector savings, dysprosium disadvantage factor, ratio of epicadmium to subcadmium capture in thorium (ρ^{02}), and the ratio of Th232 fission to U233 fission (δ^{02}). Much of the basic data for the BNL experiments has been compiled by Price[4], and the most recent survey of the data is presented in the paper by Windsor et al.[5]

Recent calculations of the light water lattices having moderator-to-fuel (M/F) volume ratios ranging from 0.997:1 to 3.004:1 have been reported by Sehgal et al.[19] This analysis, which used ENDF/B-IV cross sections in RABBLE/HAMMER cell calculations, produced values of K_{eff} shown in the third column of Table VI. Another set of calculations were reported by Shapiro et al.[18] for the lattices whose volume ratios ranged from 0.997:1 to 4.2722:1. The analytic model used in this study was based on the CEPAK code and used ENDF/B-IV data and L factors for Th232 and U233 resonance reaction rates which were corrected for resonance interference between Th232 and U233. These results are shown in the fourth column of Table VI. They typically are 0.5-1% higher than the corresponding results of Sehgal, but they also exhibit the same upward trend with increasing moderator-to-fuel volume ratio (Figure 4).

Other recent studies of the light water lattices have yielded differing results. Weiss and Malaviya[20] have analyzed all eight unpoisoned light water lattices using the HAMMER computer code and ENDF/B-IV cross sections. Resonance self-shielding was accounted for using the Nordheim approximation. The results, which are seen in column five of Table VI, show that criticality was underpredicted by an amount varying from 0.1-1.3%. However, the trend in the calculated K_{eff} vs.

Table VI - Calculated Values of K_{eff} for the BNL U233-Th232-H_2O Exponential Experiments Using ENDF/B-IV

V(Moderator) / V(Fuel)	$B_m^2(m^{-2})$ (Experimental)	Calculated K_{eff} (Ref. 19)	(Ref. 18)	(Ref. 20)	(Ref. 17)
0.997	75.88	0.9823	0.9918	0.9994	1.005
1.384	86.06	0.9895	0.9957	0.9915	1.005
1.7134	89.34	0.9962	1.0013	0.9907	1.006
2.1943	90.35	1.0005	1.0054	0.9889	1.002
3.0043	85.54	1.0037	1.0087	0.9871	0.994
4.2722	69.8	--	1.0117	0.9886	--
6.8449	32.2	--	--	0.9928	--
9.2747	-1.22	--	--	0.9970	--

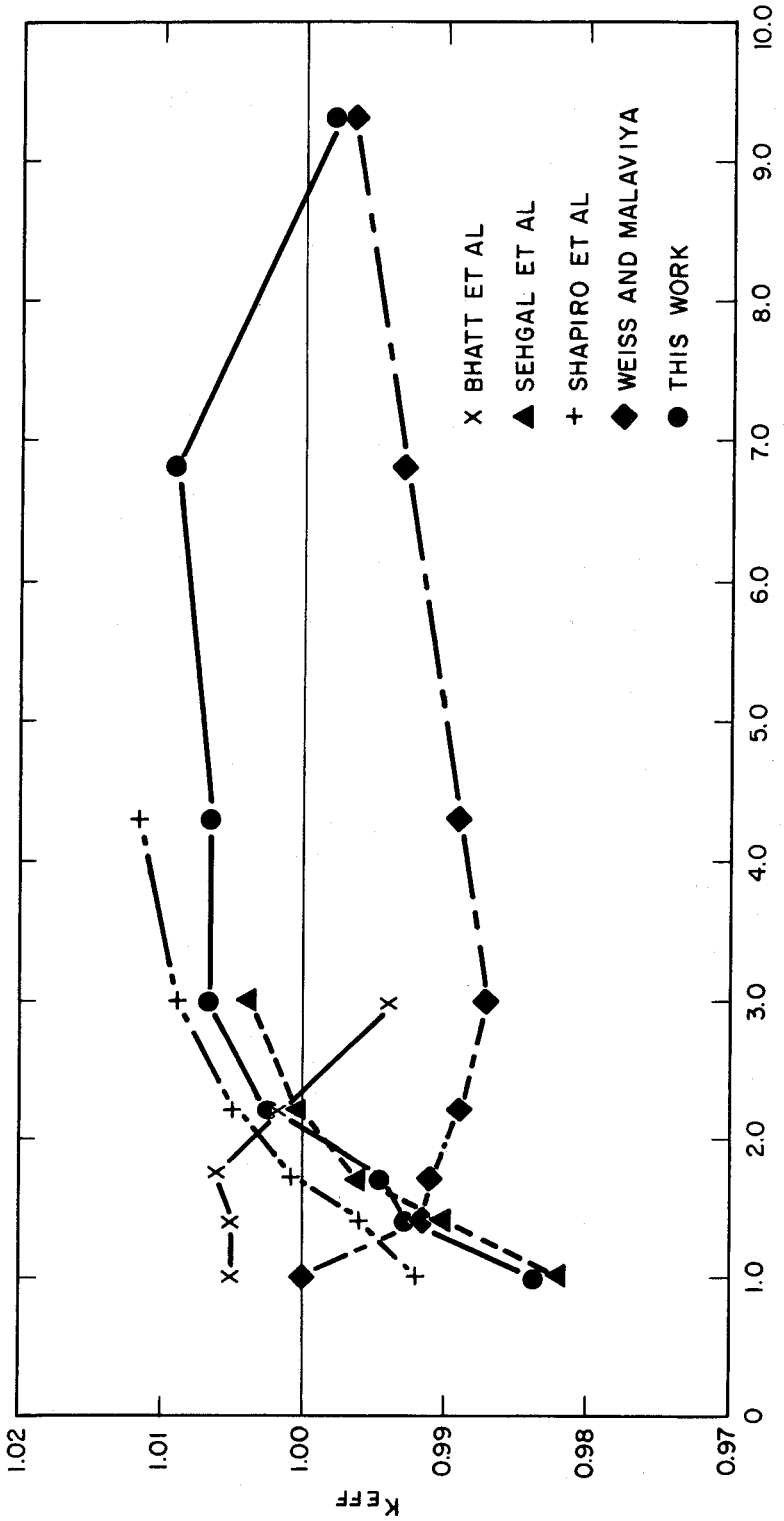

Figure 4 - BNL U233-ThO_2-H_2O Exponential Lattices, Comparison of Keff Calculations Based on ENDF/B-IV

moderator-to-fuel volume ratio is opposite to that of References 18 and 19. The causes for this difference were not discussed.

Bhatt et al.[17] have reported an analysis of those BNL exponential lattices with (M/F) ≤ 3.0043. These calculations used BWR lattice physics methods similar to those applied to the TUPE lattices (Table III). The calculated critical eigenvalues, listed in column six of Table VI, are overpredicted by ~0.5% for (M/F) ≤ 2.0. For the (M/F) = 3.004 lattice, the bias changes sign.

Another key comparison of the results reported from several of the studies mentioned above can be made of the predicted epicadmium-to-subcadmium capture ratios (ρ^{02}) for Th232. These calculations of ρ^{02} are compared with the measured values in Table VII. Generally, the calculations of ρ^{02} are in good agreement with each other, but they consistently underpredict the measured values.

The above comparison of K_{eff} values, which were calculated for the BNL light water U233-thorium lattices, depicts a method dependence which tends to confound the interpretation of these experiments for nuclear data testing purposes. In an attempt to clear up some of these discrepancies, we have analyzed the unpoisoned light water lattices and all of the heavy water lattices. Three methods to compute K_{eff} were compared. In increasing order of sophistication, they were:

(1) Single lattice cell Monte Carlo (using the RCP01 program) calculations which were corrected for neutron leakage using the MUFT7 program and the measured material bucklings. Resonance absorption in MUFT7 was handled by a heterogeneous collision probabilistic method. Computed reaction rates in the resonance range and other energy ranges for the unbuckled MUFT7 calculations generally were in good agreement with the corresponding Monte Carlo cell results.

(2) Same as Method 1 except that one-dimensional, homogenized P7MG transport calculations with a small negative transverse buckling given by $B_z^2 = -\frac{1}{\ell_z^2}$, where ℓ_z was the measured relaxation length, were used to correct for neutron leakage. This avoided the use of the measured radial bucklings. (Resonance absorption in P7MG was treated in a manner similar to MUFT7.)

(3) Monte Carlo calculations (using the RCP01 program) which represented the entire lattice explicitly in two dimensions. The final K_{eff} values included a small correction for axial inleakage which was obtained from the P7MG transport program.

Table VII - Comparison of Calculated and Measured Values of ρ^{02} for the Unpoisoned BNL U233-Th232-H_2O Lattices

V(Moderator) / V(Fuel)	B_m^2 (m^{-2})	Measured ρ^{02}	Calculated Results			
			Ref. (19)	Ref. (18)	Ref. (17)	This Work
0.997	75.88	1.380±0.042	1.308	1.307	1.283	1.271
1.384	86.06	0.928±0.038	0.901	0.906	0.904	0.865
1.713	89.34	0.754±0.024	0.716	0.720	0.729	0.698
2.194	90.35	0.607±0.026	0.553	0.561	0.575	0.543
3.004	85.54	0.435±0.013	0.406	0.411	0.431	0.396
4.2722	69.8	--	--	--	--	--
6.8449	32.2	0.218±0.008	--	--	--	0.201
0.2747	-1.22	0.170±0.007	--	--	--	0.158

The results for the light water lattices using Method 1 (Table VIII, column 2) are in good agreement with [19] and once again exhibit an upward trend with (M/F) volume ratio for values of (M/F) below 3.0. The results for the lattices with (M/F) ≥ 3.0 become more uniform with the exception of the 9.27:1.0 lattice, which has a negative material buckling. The Method 2 (RCP Cell + P7MG) results appear to be nominally 0.8% higher than the corresponding Method 1 values of K_{eff} and appear to form a more consistent set. They also exhibit a slight rising trend in K_{eff} for (M/F) values below 3.0. With perhaps the exception of the 1.38:1.0 lattice, the 2D Monte Carlo calculations (Method 3) yield the most consistent set of K_{eff} values (Figure 5).

Table VIII - Comparison of Several Methods for Computing K_{eff} for the BNL U233-Th232-H_2O Exponential Experiments

V(Moderator)/V(Fuel)	Calculated K_{eff}*		
	Cell RCP01+ MUFT7 (Method 1)	Cell RCP01+ P7MG** (Method 2)	2D Full Core RCP01+P7MG (Method 3)
0.997	0.9835±0.0021	0.9993	0.9986±0.0020
1.384	0.9926±0.0018	0.9984	0.9907±0.0022
1.7134	0.9944±0.0018	1.0038	1.0077±0.0028
2.1943	1.0025±0.0021	1.0104	1.0040±0.0019
3.0043	1.0068±0.0022	1.0106	1.0028±0.0024
4.2722	1.0066±0.0023	1.0074	1.0055±0.0025
6.8449	1.0091±0.0026	1.0049	1.0015±0.0025
9.2747	0.9976±0.0029	1.0026	0.9969±0.0023

* Monte Carlo statistical errors are one standard deviation.

** Statistical errors (not shown) are the same as for Method 1.

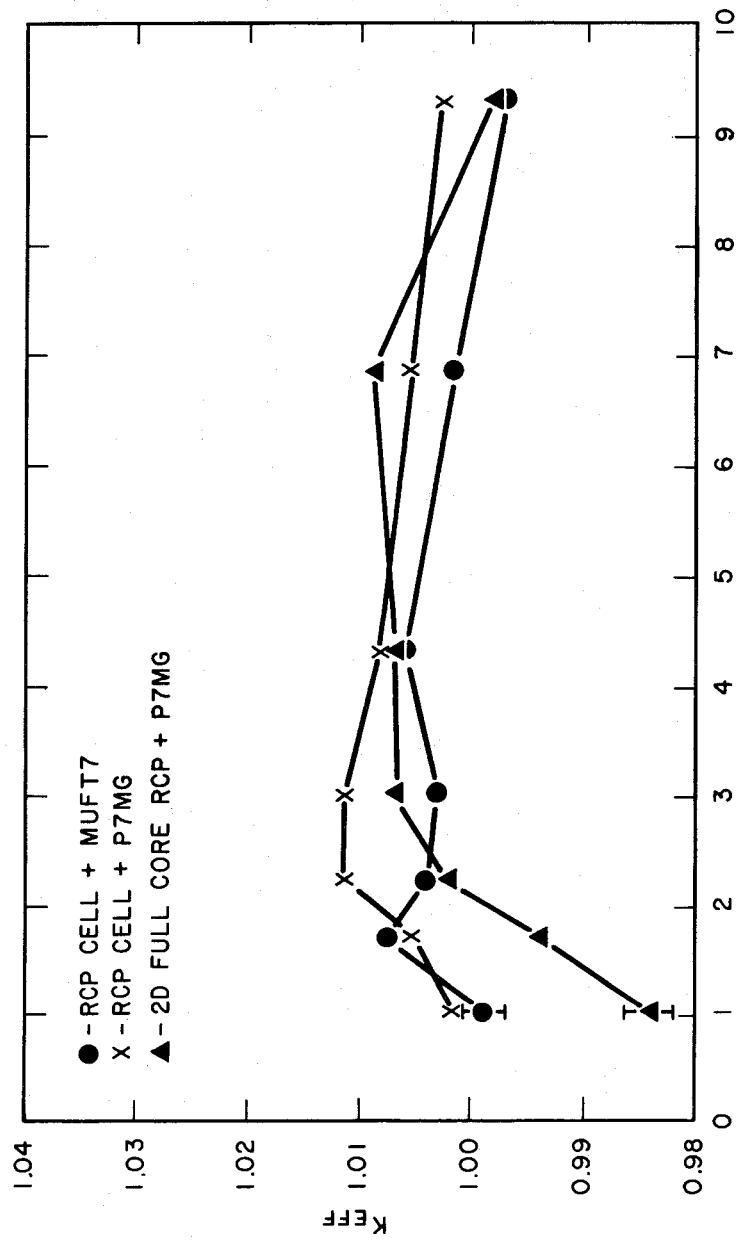

Figure 5 - BNL U233-ThO_2-H_2O Exponential Lattices, Comparison of Three Methods (see text) to Calculate K_{eff}. ENDF/B-IV Data Were Used Throughout.

It appears that the greater overall consistency of interpretation that is achieved with the 2D Monte Carlo results as compared with those based on Methods 1 and 2 may be due to the elimination of approximations involved in the homogenization of the lattices. Since the tight lattices have the smallest fueled radii, it is supposed that errors in effective resonance cross sections that occur near the core-reflector interface can significantly affect calculated results. Note that for the larger lattices ($M/F > 3.0$) the rising trend in K_{eff} vs. M/F does not persist for Methods 1 and 2.

Our calculated values of ρ^{02} are compared with experiment and those yielded by other analyses in Table VII. Once again, ρ^{02} is underpredicted by ~8% which is consistent with the other studies. Sensitivities of the calculated ρ^{02} values to alternate thorium evaluations will be discussed in Section II.A.

The BNL U233-thorium-D_2O exponential lattices were also analyzed in a similar manner as described for the light water lattices above. Results are shown in Table IX and Figure 6. Using Method 1 (RCP01 Cell + MUFT7) the calculated values of K_{eff} form a nearly consistent set. However, criticality is nominally underpredicted by 1.5%. Those results based on Method 2 (Cell RCP01 + P7MG) and Method 3 (2D full core RCP + P7MG) also underpredict criticality by 1-2%. For $(M/F) \leq 55.2$, the full core Monte Carlo results depict a slight downward trend in K_{eff} vs the (M/F) volume ratio.

The calculated values of ρ^{02} for the D_2O lattices are compared with experiment in Table X. These predictions of ρ^{02} based on ENDF/B-IV generally are in good agreement with experiment in contrast to the ρ^{02} results for the H_2O lattices which fell 8% below experiment. For the $(M/F) = 81.2$ and 120.5 lattices, the ρ^{02} results appear to be out of line with the others. This again may be due to a problem of interpretation of those experiments.

E. ETA-I and ETA-II Lattices. The ETA-I and ETA-II critical experiments were carried out at the Bettis Atomic Power Laboratory in 1969 and 1970. These were D_2O-moderated tight lattices designed to test thorium and U233 cross sections in very hard neutron flux spectra. For ETA-I, the 26 inch diameter test lattice contained 2304 $U235O_2$-ThO_2 fuel rods, with Th/U235 atom ratio of 15/1. (These were the same rods that had been used ten years earlier in the TUPE and THUD experiments.) For ETA-II, there were 864 $U233O_2$-ThO_2 rods which had been used previously in the BNL exponential lattices. In both experiments it was necessary to use an H_2O-moderated driver lattice of TRX UO_2 fuel rods in order to achieve criticality. At core center,

Table IX - Comparison of Several Methods for Computing K_{eff} for the BNL U233-Th232-D_2O Exponential Experiments

V(Moderator) / V(Fuel)	Calculated K_{eff}*		
	Cell RCPO1+ MUFT7 (Method 1)	Cell RCPO1+ P7MG** (Method 2)	2D Full Core RCPO1+P7MG (Method 3)
3.005	0.9857±0.0032	--	--
11.716	0.9806±0.0020	0.9911	0.9906±0.0029
16.051	0.9821±0.0020	--	--
29.113	0.9822±0.0019	0.9868	0.9846±0.0028
37.828	0.9890±0.0020	--	--
55.226	0.9792±0.0020	0.9905	0.9795±0.0025
81.212	0.9913±0.0027	--	--
120.491	0.9892±0.0033	--	--

* Monte Carlo statistical errors are one standard deviation.

** Statistical errors (not shown) are the same as for Method 1.

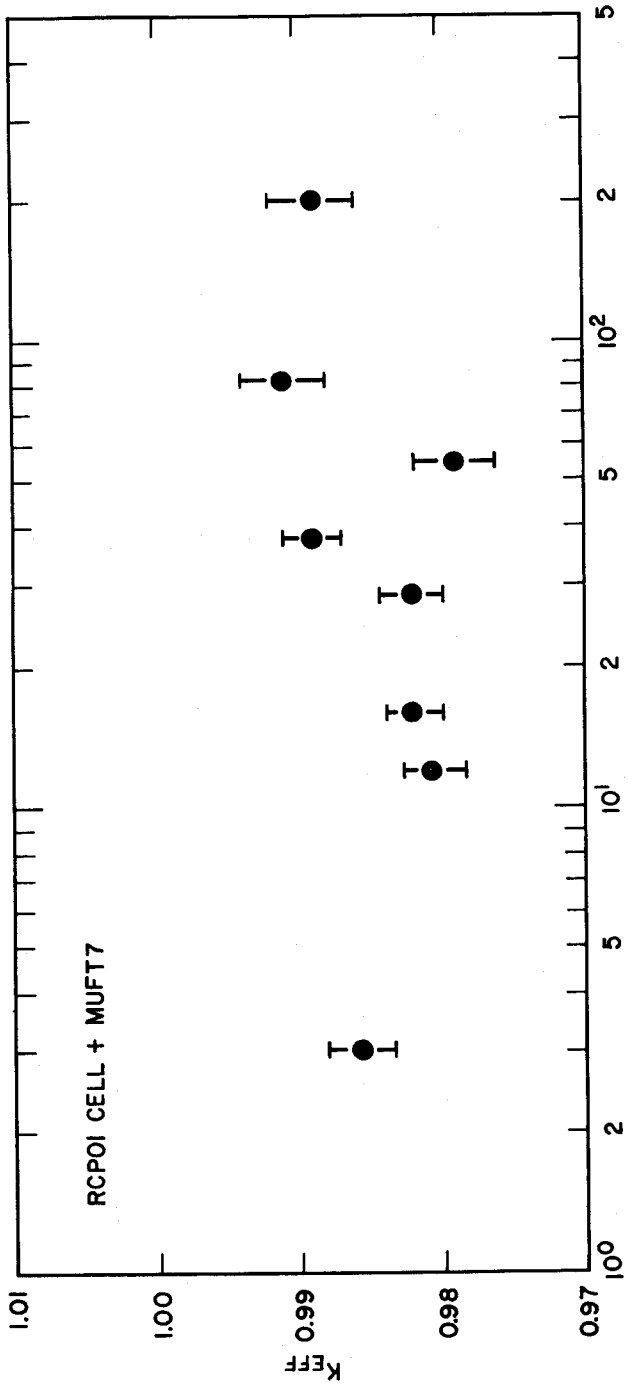

Figure 6 - BNL U233-ThO_2-D_2O Exponential Lattices, Calculated K_{eff} (Method 1) vs. M/F Volume Ratio

Table X - Comparison Between Calculated and Measured ρ^{02} Values for the BNL U233-Th232-D_2O Lattices

$\frac{V(Moderator)}{V(Fuel)}$	Measured ρ^{02}	Calculated ρ^{02}	$\frac{\rho^{02}_{(calc.)}}{\rho^{02}_{(meas.)}}$
3.005	4.71±0.18*	4.377	0.929±0.038
11.716	0.794±0.028*	0.759	0.956±0.035
16.051	0.565±0.017*	0.555	0.982±0.030
29.113	0.297±0.011	0.297	1.000±0.037
37.828	0.234±0.008	0.230	0.983±0.034
55.226	0.166±0.006	0.164	0.987±0.036
81.312	0.104±0.005	0.111	1.066±0.048
120.491	0.089±0.005	0.079	0.888±0.056

* Weighted average of ρ^{02} determined by the cadmium ratio and thermal activation methods. All other values are based on the Cd ratio method.

where integral parameters were measured, the flux spectrum was nearly asymptotic, despite the strong spectrum shift between the test and driver lattices. Parameters were measured by activation techniques, as follows[6]:

$\delta^{23}(\delta^{25})$	(a) cadmium ratio; U233(U235)-Al detector foil. (b) thermal subtraction method, relative to Dy164-Al detector foil, normalized in reflector.
ρ^{02}	Thermal subtraction method, relative to Dy164-Al detector, normalized in reflector. Ge(Li) count of 312 keV γ from fuel and ThO_2 pellets.
CR*	(a) From same thorium and U233(U235) activations. (b) Indirect, from ρ^{02} and $\delta^{23}(\delta^{25})$ as a check.
δ^{02}	Fuel and ThO_2 detector pellets. Ge(Li) counting of selected fission product γ's.

Interpretation of the parameters requires an explicit radial analysis of the full core to obtain leakage corrections. Since spatial activation shapes were not measured, K_{eff} depends significantly on the calculated leakage to the driver and hence on the driver itself. Other integral parameters are relatively insensitive to the driver, however. Due to the tightness of the inner lattice, interaction between thorium and uranium is strongly emphasized as compared to a more thermalized lattice.

Integral parameters at core center were calculated for a cell using RCP01, with leakage corrections from P7MG, which performed a homogenized multigroup P_ℓ radial traverse. Results from the original analyses are compared with experiment in Table XI. For both lattices agreement with experiment is reasonably good, with ρ^{02} approximately 3% high. These analyses used the LWBR thorium cross sections[12] which differ in several significant respects from the ENDF/B-IV file. The most notable differences affecting integral parameters are a thermal σ_a of 7.34b (versus 7.40b in ENDF/B-IV) and a fission cross section about 10% higher than ENDF/B-IV. The U235 deck had a fission resonance integral of 259b above 0.625 eV, compared to 268b for ENDF/B-IV material 1261. Its thermal fission cross section was 0.8% below ENDF/B-IV. Other important data (for U233, deuterium and oxygen) were not significantly different from the ENDF/B-IV set.

The ETA lattices have been reanalyzed with the same calculational methods and ENDF/B-IV data. These integral parameter results are also shown in Table XI. The major differences from the calculated parameters of [6] are:

(1) Slightly reduced (1.5%) Th232 resonance capture (reflected in ρ^{02} and CR*).

(2) 4.5% higher δ^{25}, of which 3.5% can be attributed to the higher U235 resonance fission integral of ENDF/B-IV. (This also lowers calculated CR* by about 1%

Table XI - Comparison of Measured and Calculated Integral Parameters for ETA-I (U^{235}-Th-D_2O) and ETA-II (U^{233}-Th-D_2O)

Integral Parameter	ETA-I Experiment	Calculation*		ETA-II Experiment	Calculation*	
		Original (Ref. 6)	ENDF/B-IV		Original (Ref. 6)	ENDF/B-IV
ρ^{02}	10.54±.15	10.92±.06	10.9±.06	8.89±.15	9.16±.05	8.71±.05
δ^{25}	1.74±.02	1.78±.01	1.86±.01	2.96±.08	2.99±.02	2.90±.02
δ^{02}	.0166±.0009**	.0155±.0002	.0141±.0001	.0181±.0014	.0185±.0001	.0165±.0002
CR*	.867±.009	.882±.003	.857±.003	1.047±.02	1.050±.003	1.034±.004

* Uncertainties on calculated results are from Monte Carlo statistics.

** Measured and calculated for the central rod of the nine-rod cell. Other parameter results are for the entire cell.

and raises ρ^{02} by 1%.)

(3) Approximately 10% lower δ^{02} is due mostly to the difference of σ_f^{Th232}.

Additional studies to examine alternative thorium data sets have been undertaken and are discussed in Part II of this paper.

F. LWBR Criticals. Of those critical assemblies constructed in support of the LWBR program, the detailed cell[9] and one BMU[8] core were analyzed with RCP01 and ENDF/B-IV data. For these calculations the cores were represented explicitly in three dimensions including all fuel rods and lattice structural components. There was some homogenization of peripheral structure.

The BMU-1B core consisted of a symmetric hexagonal seed with 810 ThO_2 blanket rods. These were approximately 0.25-inch diameter on a 0.32-inch triangular pitch. The upper 14-inch of each rod was 5 w/o $^{233}UO_2$-ThO_2, the remainder was 9 w/o. The seed rods rested on an equal number of 14-inch-long ThO_2 rods. The center seven lattice positions were occupied by a Zircaloy can. The 1/8-inch water gap between the walls provided channels for six hafnium control blades. The surrounding blanket contained 811 42-inch-long ThO_2 rods and 360 2 w/o $^{233}UO_2$-ThO_2 rods. These were of approximately 0.625-inch diameter, on a 0.70-inch triangular pitch.

The detailed cell was a single seed and blanket core, approximately 105 inches high, with a movable central seed region. The seed was a symmetric hexagon containing 15 rows of 0.305-inch diameter fuel rods on a 0.368-inch triangular pitch. An inner blanket region surrounded the seed, separated from it by a double-walled hexagonal Zircaloy can. The 1/8-inch water gap between the walls provided channels for six hafnium control blades. The inner blanket was a nonsymmetric hexagon comprising ordinary and power-flattening regions. The outer blanket comprised a driver region with 2 w/o $^{233}UO_2$-ThO_2 rods and a reflector region of ThO_2 rods.

Eigenvalues obtained with RCP01 and ENDF/B-IV data are shown in Table XII. The particular detailed cell configuration which was calculated had a critical seed position of ~2.0 inches below the blanket.

It is judged that analysis of the measured parameters is not likely to be fruitful for cross section testing purposes mainly because of the complexity of these cores, and no attempt has been made to calculate them.

Table XII - Eigenvalues of LWBR Criticals Calculated with RCP01 and ENDF/B-IV Data

Core	$K_{eff} \pm \sigma$
Detailed Cell	.9940±.0012
BMU-1B	.9963±.0014

G. Resonance Integrals for Thorium Capture. Measurements of the dilute resonance capture integral have usually been made by the cadmium ratio method relative to the dilute resonance integral of gold. In this method, resonance and thermal activation ratios are compared by irradiating dilute gold and thorium detector foils, bare and cadmium-covered, in a pseudo 1/E flux spectrum. Normalization depends on the thorium and gold thermal capture cross sections and the gold dilute resonance integral:

$$I_{Th232} = \frac{(A_{res}/A_{ther})_{Th232}}{(A_{res}/A_{ther})_{Au}} \times \frac{\sigma_{Th232}}{\sigma_{Au}} I_{Au} \qquad (1)$$

The measured resonance and thermal specific activation (A_{res} and A_{ther}) of Equation (1) must be suitably corrected for cadmium cutoff energy, detector foil shielding and neutron flux spectrum.

Grenèche[21] has recently reviewed the available integral experiments. On the basis of fourteen measurements he obtains a dilute resonance integral

$$I_{Th232} = 85.8 \pm 0.9\text{b (experimental)} \pm 1.6\text{b (normalization)}$$

This represents all capture above 0.5 eV and is normalized as follows:

$$\sigma_{Au} = 98.8 \pm 0.3\text{b}$$

$$\sigma_{Th232} = 7.40 \pm 0.08\text{b}$$

$$I_{Au} = 1560 \pm 22\text{b}$$

The BNL-325[22] value is 85±3b.

Complementing lattice experiments as a test of shielded resonance capture are measurements of effective resonance integrals for thorium metal and ThO_2 rods of various diameters. The methods, problems of interpretation and results have been summarized by Hellstrand[23].

For thorium, the experiments were done by activation techniques in which a cadmium-covered rod was irradiated in a pseudo-1/E flux spectrum. Thorium captures were sampled by counting the capture activity of a ground-up portion of the ThO_2 rod or (for a metal rod) of a thorium metal detector foil. Normalization was explicitly to the dilute resonance integral of thorium:

$$I'(S/M,T) = \left(\frac{A'_{res}(S/M,T)}{A_{res}} \right)_{Th232} \times I_{Th232} \qquad (2)$$

where I' and A'_{res} are the effective resonance integral and specific thorium resonance capture activation for a rod of surface/mass ratio S/M cm^2/gm at temperature T. In some experiments, normalization was directly to the gold resonance integral via Equation (1).

In comparison to lattice measurements, the thorium activation counting techniques are similar, but there is the additional complication of determining the actual flux spectrum impinging on the rod. In this sense an effective resonance integral measurement is more difficult to interpret than a lattice experiment, although in principle it is more specific (i.e., not subject to interference from competing reactions).

On the basis of two experiments[24,25] for metal and three for oxide rods[27,23,26], Hellstrand[23] recommends the following room-temperature effective resonance integrals:

Thorium metal	$I' = 5.05 + 15.5 \sqrt{S/M}$
ThO_2	$I' = 5.85 + 16.2 \sqrt{S/M}$

Here, S/M is the surface-to-mass ratio (cm^2/gm) of metal or of oxide. These expressions apply over the range $0.30 < \sqrt{S/M} < 0.90$, with an assigned uncertainty of $\pm 4.5\%$ and include all capture above 0.5 eV.

A connection with lattice measurements of thorium resonance capture can be established via the LWBR thorium capture data evaluation[12]. The LWBR data set produced calculated effective resonance integrals for ThO_2 rods which are well represented by the expression

$$I' = 5.74 + 15.54 \sqrt{S/M} \quad (300^\circ K)$$

The calculated effective resonance integral is approximately 3% below the Hellstrand recommendation, and the dilute integral is 85.2b. The ENDF/B-IV thorium (as will be shown subsequently) produces approximately 3% less resonance capture than the LWBR set. On this basis, it is inferred that the ENDF/B-IV thorium would produce effective resonance integrals approximately 6% below the Hellstrand recommendation.

H. Consistency of Capture Measurements. There are only a very limited number of integral Th232 capture measurements potentially useful for data testing purposes. For room temperature ThO_2 rods, these are:

(1) Effective resonance integrals of ThO_2 rods.
(2) ρ^{02} measurements in the Th-U233 BNL exponentials (H_2O and D_2O moderated).
(3) ρ^{02} measurements in the D_2O-moderated, hard-spectrum ETA-I (Th-U235) and ETA-II (Th-U233) lattices.

The consistency of these measurements can be seen from Figure 7, which shows experiment/ENDF/B-IV calculation ratios. The experiments range from 10% high to 3% low, with experimental uncertainties ranging from ±2% to ±5%. In addition, there are several questions of interpretation which should be mentioned:

(1) The measured ThO_2 rod resonance integrals are directly proportional to the dilute resonance integral I. Integral measurements of I are directly proportional to the thorium thermal capture cross section. (Normalization at present is to σ_a = 7.40b, consistent with ENDF/B-IV.)
(2) ρ^{02} measurements do not depend on any such normalization. However, calculated ρ^{02} depends inversely on the thorium thermal σ_a. Without a firm value of σ_a, it is difficult to draw conclusions about resonance capture.
(3) In the ETA cores, ρ^{02} calculations are somewhat sensitive to data other than Th232 capture itself (through leakage corrections and competing absorptions). For example, the ENDF/B-IV calculated δ^{25} is 7% above experiment. A 10b reduction of the U235 fission integral can remove about half of this difference. Such a change would lower calculated ρ^{02} by 1% and raise calculated CR* by about the same amount.

Altogether, these experiments, assuming that the ENDF/B-IV σ_a^{Th232} = 7.40b is fixed, favor an amount of thorium resonance capture slightly above - or at least, not much below - ENDF/B-IV.

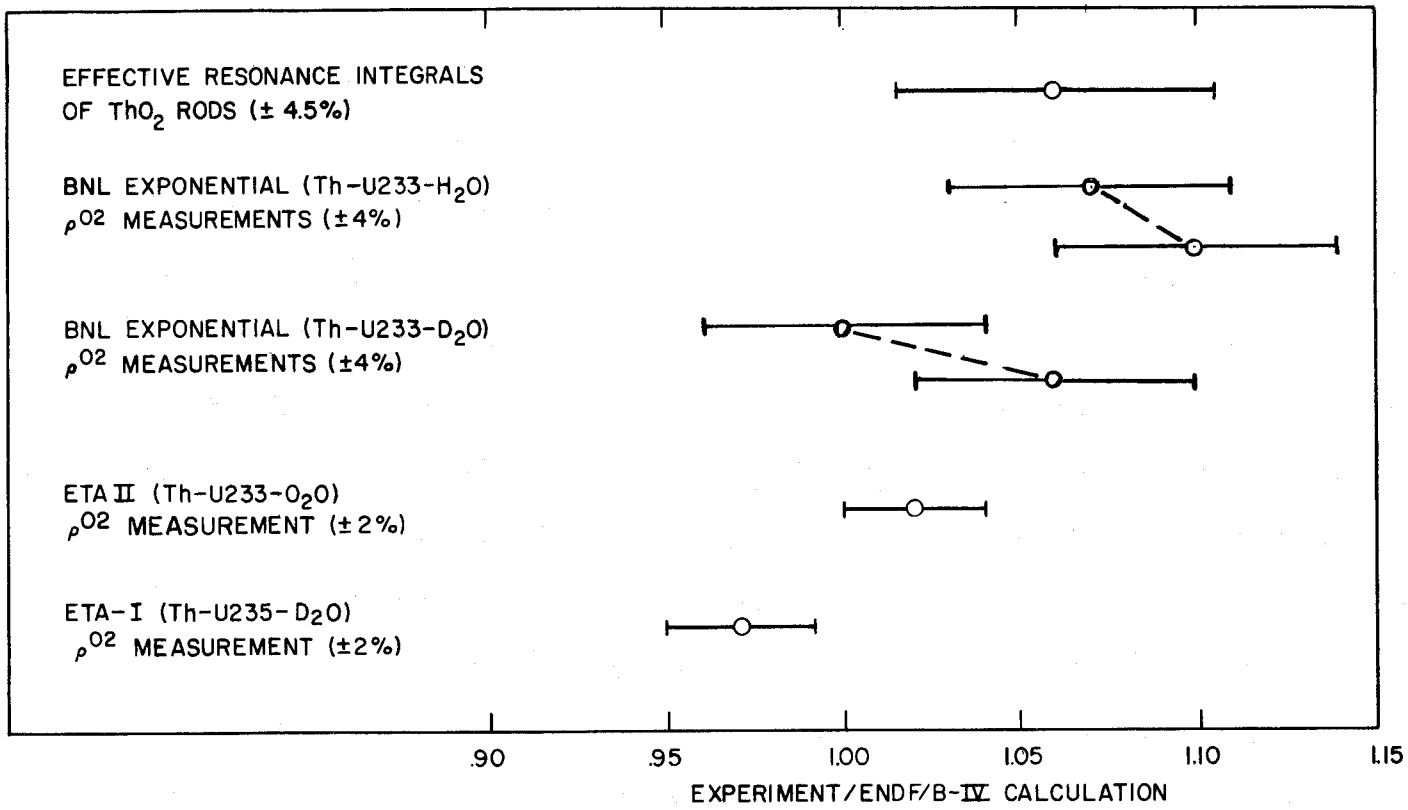

Figure 7 - Comparison of Thorium Capture Predictions Based on ENDF/B-IV

II. Testing of Alternative Data Sets for Thorium and Other Data Sensitivities

In Part I of this paper we established a data base to assess how well ENDF/B-IV cross sections do in predicting the neutron economies of thorium-uranium cores. Although, ENDF/B-IV does a reasonably good job, improvements are desirable in some areas. In what follows, we report on calculated sensitivities of selected experiments covered in Part I to several alternate thorium data sets. The experiments include the ETA-I and ETA-II cores, two TUPE lattices, the BNL exponential experiments, and the BMU-1B core. In addition, we mention a comparison of ENDF/B-IV and the Leonard thorium sets which was made for the High Temperature Lattice Test Reactor (HTLTR) U233-Th lattices[10]. Other data sensitivities, notably to the fission neutron spectrum representation, were determined for the homogeneous U233 criticals and selected lattice experiments.

A. Testing of Alternate Thorium Evaluations. In addition to ENDF/B-IV material 1296, three alternate thorium data sets were used to analyze selected lattice experiments. These evaluations were:

(1) The Leonard evaluation[10] up to 50 keV, ENDF/B-IV above. Mat. 600.
(2) The Derrien evaluation[11]. Mat. 445.
(3) The LWBR data set, based on the 1970 evaluation by N. M. Steen[12].

In each case, all data other than that for thorium were from ENDF/B-IV.

Table XIII shows dilute resonance capture integrals and 2200 m/s capture cross sections for the several thorium data sets. A more detailed comparison of the recent evaluations (Mat. 445 and Mat. 600) appears in Table XIV, which shows dilute resonance capture integrals in three ranges. Above 67.4 keV, the difference of smooth capture integral is small. The 3.2 barn difference below 454 eV is nearly all in the resonances and in fact mostly in the large resonances just above 20 eV.

In the middle range*, Derrien added additional capture (in file 3) above that contributed by the resolved and unresolved resonances. This was done to make up the $\sigma_c(E)$ adopted by Derrien, as shown in Figure 8 which is taken from [11]. This extra capture was significant down to 450 eV. Since resonance

---

* NOTE: It appeared after some initial work that Mat. 445 had the unresolved resonance capture cross section duplicated in file 3. This duplication was eliminated by reducing the smooth capture cross section in MUFT groups 27-30 (the total reduction was 1.2568b of resonance integral).

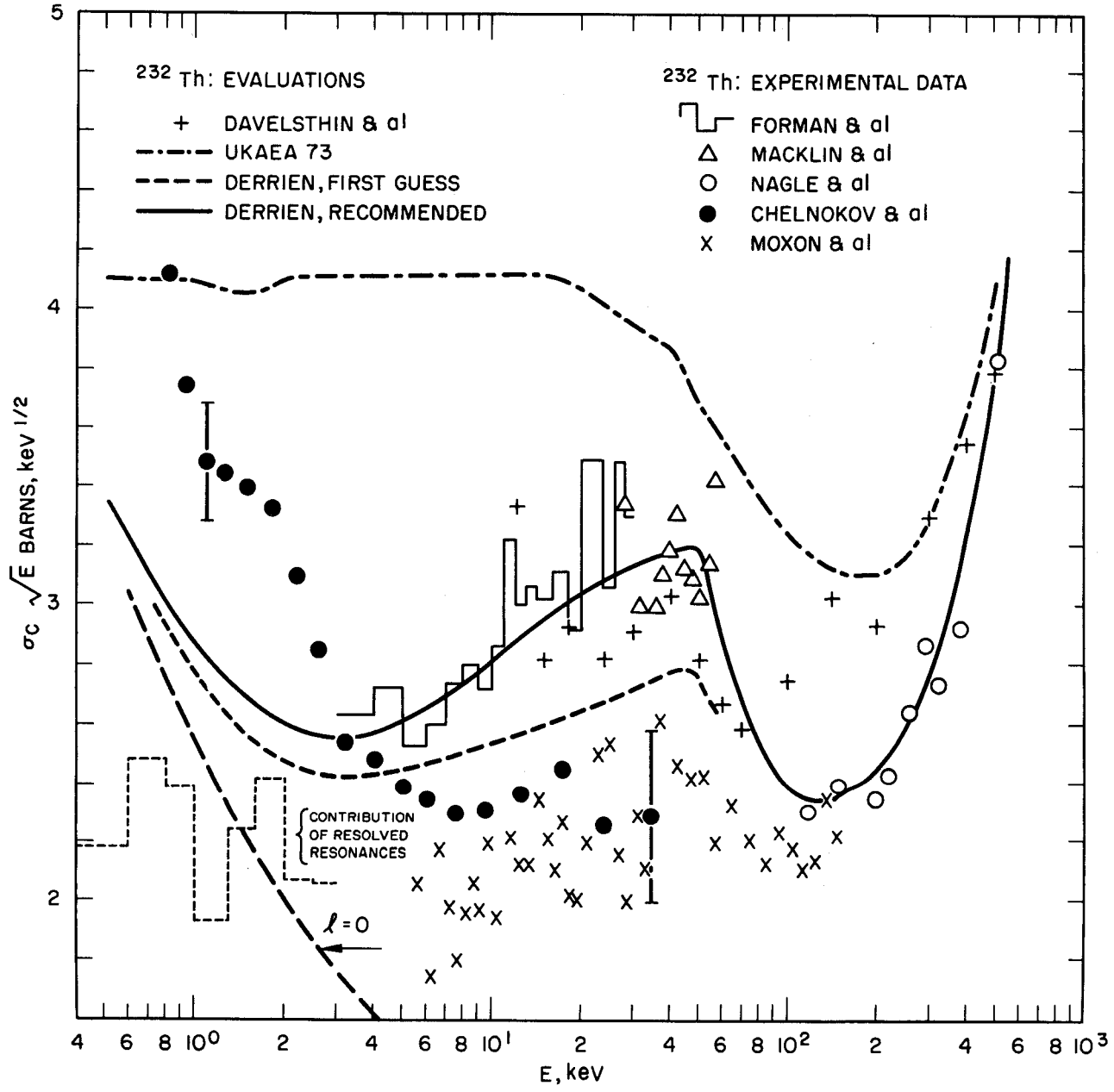

Figure 8 - Thorium Capture Cross Section Between 1 keV and 500 keV

shielding is quite strong in these lattices (the effective resonance integral is only approximately 12 barns), such added capture can be very important, particularly in file 3 where it is not shielded. For this same reason, the accuracy of the $\sigma_c(E)$, shown in Figure 8 becomes significant. As will appear below, 0.1b of unshielded resonance capture integral is worth 1% in ρ^{02} in the ETA-I lattice.

Table XIII - Comparison of Resonance Integrals and Thermal Capture Cross Sections for Several Thorium Data Sets

	I(>0.625 eV)	σ_c(.0253 eV)
ENDF/B-IV	85.2	7.40
Leonard	79.0	7.62
Derrien	83.5	7.40
LWBR	84.8	7.34

Table XIV - Comparison of Dilute Capture Integrals for Mat. 600 and Mat. 445

Energy Range	MUFT Groups	Resonance Integrals (barns) Mat. 600	Mat. 445	Mat. 445 - Mat. 600
21.1 meV - 67.4 keV	1-23	.674	.637	-.037
67.4 keV - 454 eV	24-33	6.312	7.630*	1.318
454 eV - 0.625 eV	34-57	72.022	75.254	3.232
		79.0	83.5	4.5

* Reduced by 1.257b in MUFT groups 27-30 to remove duplicated unresolved resonance capture from file 3.

NOTE:

		Resonance Ranges	
Mat. 445	resolved	0 eV - 3008 eV	MUFT groups 30-57
	unresolved	3008 eV - 10 keV	MUFT groups 27-30
Mat. 600	resolved	5 eV - 4000 eV	MUFT groups 29-50
	unresolved	4 keV - 50 keV	MUFT groups 24-29

Table XV compares the resonance and background (file 3) MUFT-group smooth capture cross sections for materials 445 and 600. The extra capture in deck 445 is apparent - the cumulative difference in this range is 1.318b of resonance integral.

Cell reaction rates in ETA-I were calculated with RCP01, with leakage corrections obtained with P7MG. Resulting integral parameters are shown in Table XVI. The Derrien set is also shown with a 1.0b reduction of smooth capture integral (in MUFT groups 27-33).

A similar calculation was done for the ETA-II experiment with Leonard's thorium. Results are shown in Table XVII.

The following points are noteworthy:

(1) The LWBR thorium produces 1.5% more resonance capture than ENDF/B-IV Mat. 1296.

(2) The Derrien data set produces high ρ^{02} and CR* relative to experiment. Removal of 1.0b of smooth (file 3) capture leads to much better agreement.

Table XV - Comparison of Dilute Capture Cross Sections Between 454 eV and 67.4 keV

MUFT Group	σ_c (barns) Mat. 445 (Derrien) File 3	Resonance	Mat. 600 (Leonard) File 3	Resonance	Mat. 445 - Mat. 600 σ_c(b)	I(b)*
24	.42120	0	.23604	.13628	.04888	.02444
25	.55843	0	0	.43024	.12818	.06409
26	.69254	0	0	.55563	.13692	.06846
27	.69321	.15016	0	.69241	.15096	.07548
28	.09306	.92594	0	.85301	.16598	.08299
29	.10753	1.1474	.00174	.89829	.35476	.17738
30	.26742	1.3581	.00588	1.1988	.42086	.21043
31	.42183	1.9689	.00755	1.9016	.48160	.24080
32	.51998	1.9417	.00970	1.8870	.56494	.28247
33	.22942	3.7643	.01245	3.7990	.18220	.09110
						1.31764

*
$\Delta u = 0.5$

Table XVI - Integral Parameters in ETA-I Calculated with ENDF/B-IV and Various Thorium Data Sets

		Calculation*				
	Experiment	Mat. 1296 Th232	LWBR Th232	Mat. 600 Th232	Mat. 445≠** Th232	Mat. 445#*** Th232
ρ^{02}	10.54±.15	10.9±.06	11.2	10.1	11.6	10.5
δ^{25}	1.74±.02	1.86±.01	1.86	1.86	1.84	1.85
δ^{02}	.0166±.0009	.0141±.0001	.0158	.0141	.0142	.0140
CR*	.867±.009	.857±.003	.871	.812	.915	.830

* Calculations used ENDF/B-IV data, and thorium data as indicated. Uncertainties in each case are the same as shown for Mat. 1296 Th232.

** Mat. 445≠ has unresolved resonance capture removed from file 3 in groups 27-30, totaling 1.2568b of resonance integral.

*** Mat. 445# has reduced smooth capture in groups 27-33 totaling 1.0b of resonance integral (relative to Mat. 445≠).

Table XVII - Integral Parameters in ETA-II Calculated with ENDF/B-IV and Leonard Thorium Data Sets

		Calculation	
	Experiment	Mat. 1296 Th232	Mat. 600 Th232
ρ^{02}	8.89±.15	8.71±.05	8.15
δ^{23}	2.96±.08	2.90±.02	2.93
δ^{02}	.0181±.0014	.0165±.0001	.0164
CR*	1.047±.02	1.034±.004	.981

(3) The Leonard thorium produces ρ^{02} and CR* significantly below experiment in both ETA-I and ETA-II. Lowering the thermal σ_a could improve ρ^{02} but has small effect on CR*.

(4) The Leonard set produces a dilute resonance integral (79.0b) significantly below the value 85.8±0.9 (exp), ±1.6 (norm) obtained by Grenêche[21] from integral experiments. Raising σ_a (.0253 eV) from 7.40b to 7.62b would raise the integral value by 3%, increasing the discrepancy.

TUPE lattices 15A and 15D were reanalyzed with the Leonard thorium data set (Mat. 600). Eigenvalues are shown in comparison with ENDF/B-IV (Mat. 1296) in Table XVIII. The effects of the reduced resonance capture and increased thermal capture of Mat. 600 nearly cancel in lattice 15D. The tighter 15A lattice shows more sensitivity to the reduced resonance capture.

Table XVIII - Comparison of K_{eff} Values Calculated for the TUPE Lattices with Mat. 1296 and Mat. 600 Thorium Data Sets

Lattice	Mod./Fuel Vol. Ratio	Calculated K_{eff} Mat. 1296 Th^{232}	Calculated K_{eff} Mat. 600 Th^{232}	ΔK_{eff} (Mat. 600-Mat. 1296)
15A	1.379	1.0002±.0014	1.0058±.0017	+.0056±.0022
15D	2.945	1.0056±.0014	1.0074±.0019	+.0018±.0024

The sensitivities of the 2D Monte Carlo (corrected for axial inleakage) results for the BNL light water lattices to the various thorium evaluations were calculated. Results are shown in Table XIX and are plotted vs. (M/F) volume ratio in Figure 9. For each lattice K_{eff} from use of the LWBR thorium is higher than that based on ENDF/B-IV thorium. A comparison of reaction rates for the tighter lattices reveals that the increase in LWBR thorium resonance capture more than compensates for the reduction in the thermal capture cross section. However, the higher scattering cross section of the LWBR thorium reduces the core neutron leakage fraction and contributes to raise K_{eff}. For the looser lattices, the reduced thermal capture nearly compensates for the increased resonance capture. Since these core leakage fractions are smaller, the increased LWBR thorium scattering cross section only acts to raise K_{eff} by a slight amount above that using the ENDF/B-IV thorium. The Leonard thorium set

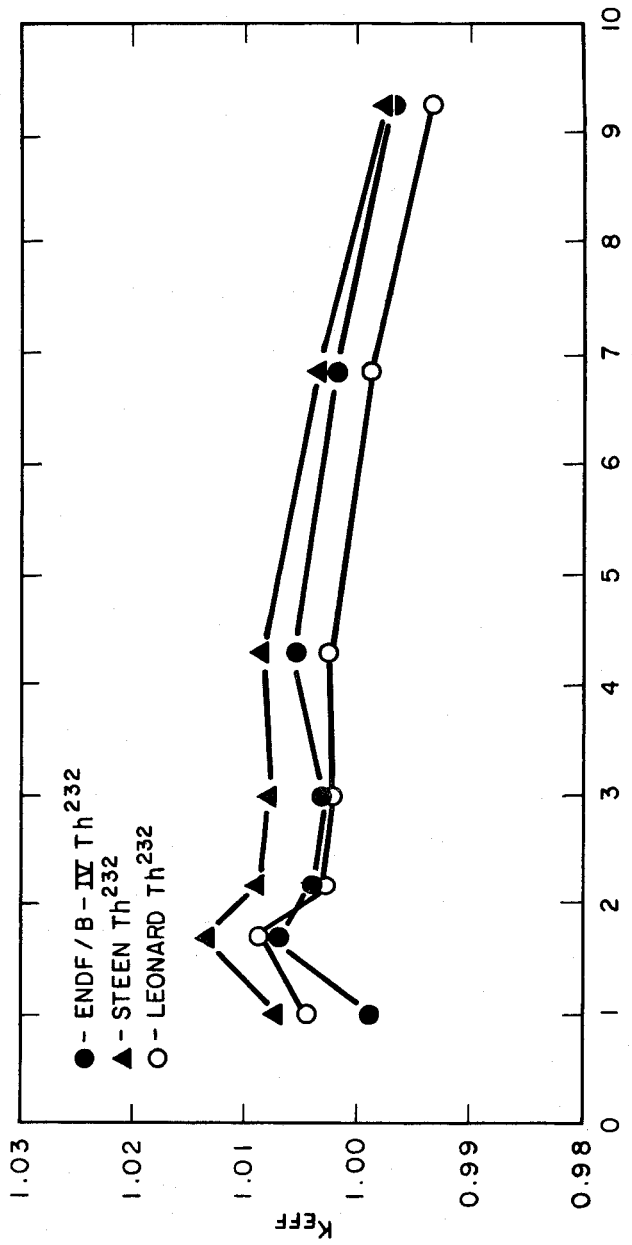

Figure 9 - BNL U233-ThO_2-H_2O Exponential Lattices, Sensitivity of K_{eff} to Thorium Evaluations

Table XIX - Comparison of K_{eff} Values Calculated for the BNL Exponential Light Water Lattices Using Different Thorium Evaluations

V(Moderator) / V(Fuel)	Calculation* Mat. 1296 Th232	LWBR Th232	Mat. 600 Th232	Mat. 445 Th232
0.997	0.9986±0.0020	1.0072	1.0046	0.9982
1.384	0.9907±0.0022	0.9948	0.9918	0.9885
1.713	1.0077±0.0028	1.0134	1.0084	1.0071
2.1943	1.0040±0.0019	1.0090	1.0036	1.0037
3.0043	1.0028±0.0024	1.0078	1.0019	1.0034
4.2722	1.0055±0.0025	1.0086	1.0028	1.0052
6.8449	1.0015±0.0025	1.0037	0.9986	1.0015
9.2747	0.9969±0.0023	0.9974	0.9934	0.9962

*Errors are Monte Carlo statistics at 1σ.

produces higher K_{eff} values for the tighter lattices due to reduced resonance capture. For values of (M/F) > 2.0, the higher Leonard thorium thermal capture cross section over-compensates the reduced resonance capture, resulting in lower values for K_{eff}. Core leakage fractions were similar from use of the Leonard and ENDF/B-IV thorium sets.

Use of the Derrien thorium set yielded values for K_{eff} (not plotted) which were relatively unchanged from those based on the ENDF/B-IV thorium.

The sensitivity of the calculated parameter ρ^{02} to several of the thorium data sets considered above was determined. Results are summarized in Table XX, and values of ρ^{02}(calc.)/ρ^{02}(meas.) are plotted for comparison in Figure 10. As yielded by RCP cell calculations discussed in Part I, the values of ρ^{02} based on the ENDF/B-IV thorium are ~8% below experiment. As expected with its reduced resonance capture and higher thermal capture cross section, the Leonard thorium yields values of ρ^{02} which are lower still, they being 14% below experiment. The LWBR thorium produces better agreement with experiment than ENDF/B-IV through increased resonance capture and reduced thermal capture.

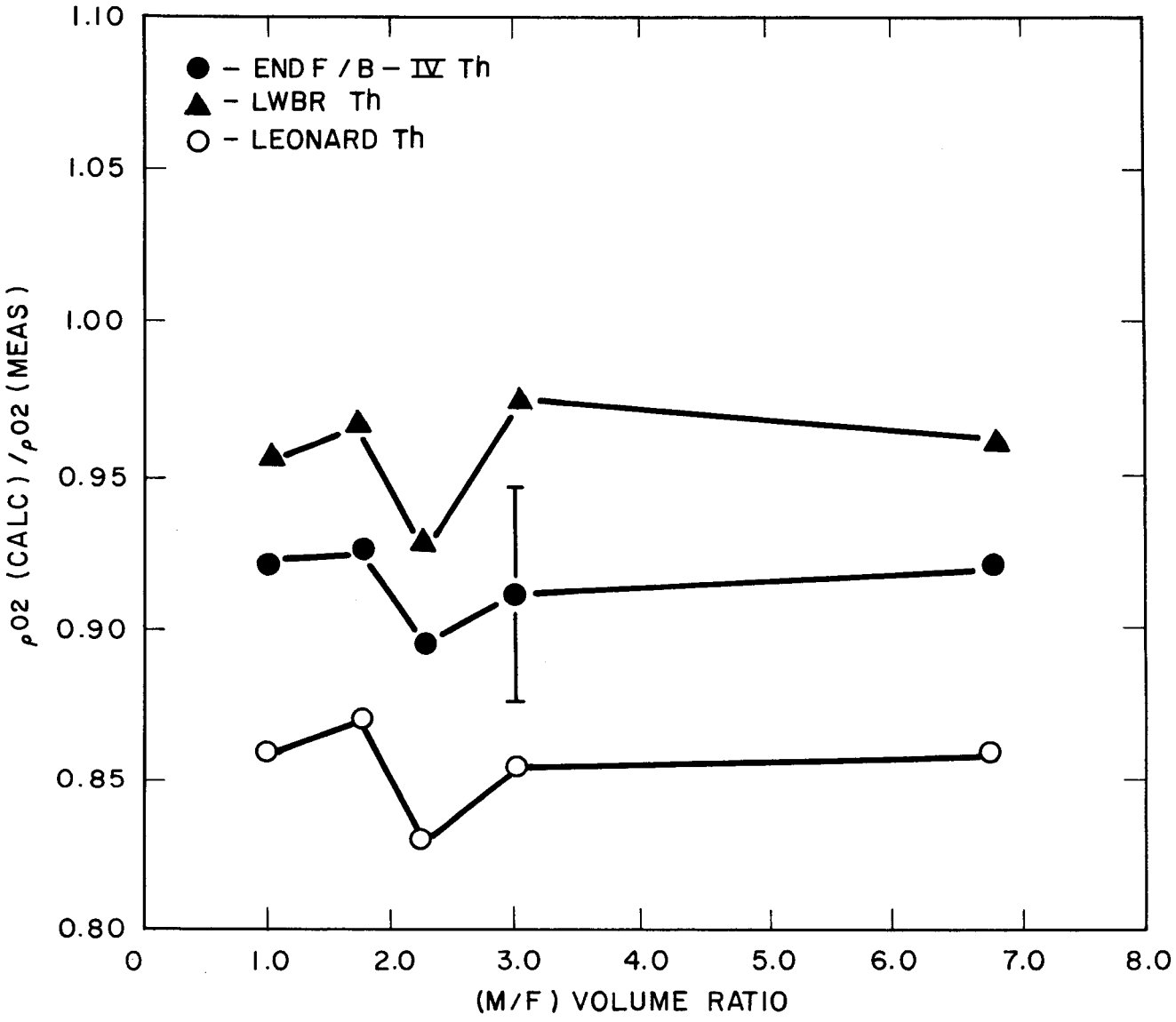

Figure 10 - BNL U233-ThO_2-H_2O Exponential Lattices, Sensitivity of ρ^{02} to Thorium Evaluations

Table XX - Comparison of ρ^{02} Values Calculated for the BNL Exponential Light Water Lattices Using Different Thorium Evaluations

V(Moderator)/V(Fuel)	Measured ρ^{02}	Calculated ρ^{02} Mat. 1296 Th232	LWBR Th232	Mat. 600 Th232
0.997	1.380±0.042	1.271	1.317	1.185
1.713	0.754±0.024	0.698	0.728	0.656
2.1943	0.607±0.026	0.543	0.563	0.504
3.0043	0.435±0.013	0.396	0.424	0.372
6.8449	0.218±0.008	0.201	0.209	0.187

Similarly, values of ρ^{02} for several of the BNL D_2O moderated lattices were calculated using the LWBR and Leonard thorium evaluations. They are compared with the measurements and values based on the ENDF/B-IV thorium in Table XXI. The ρ^{02} values for the LWBR thorium are about 4% higher than those yielded by the ENDF/B-IV thorium and ~3% above experiment. Leonard's thorium yields ρ^{02} values which are generally 9% below experiment and about 7% below ENDF/B-IV. These results are compared further with other integral measurements related to thorium capture in Section II.B.

Table XXI - Comparison of ρ^{02} Values Calculated for Several BNL Heavy Water Exponential Lattices Using Different Thorium Evaluations

V(Moderator)/V(Fuel)	Measured ρ^{02}	Calculated ρ^{02}* Mat. 1296 Th232	LWBR Th232	Mat. 600 Th232
11.716	0.794±0.028	0.759 (0.956±0.035)	0.793 (1.000)	0.724 (0.912)
29.113	0.297±0.011	0.297 (1.000±0.037)	0.308 (1.035)	0.275 (0.927)
55.226	0.166±0.006	0.164 (0.987±0.036)	0.171 (1.031)	0.150 (0.903)

*Numbers in parentheses are ρ^{02}(calc.)/ρ^{02}(meas.).

The BMU-1B core was also analyzed with two alternate thorium data sets: the Leonard evaluation and the LWBR data set based on the Steen evaluation. All other data were from ENDF/B-IV. Major full-core reaction rates and eigenvalues are shown in Table XXII. Mat. 600 produces 2.9% less thorium resonance capture than Mat. 1296 (ENDF/B-IV). The LWBR deck produces 2.8% more. These differences are counteracted thermally by the increased thorium capture of Mat. 600 and the decreased capture of the LWBR set. The fact that the epithermal U233 fission rate is higher with LWBR thorium than with ENDF/B-IV (despite the higher epithermal capture of LWBR thorium) appears to be due to reduced leakage.

Another recent test of ENDF/B-IV and the Leonard thorium sets was part of a detailed study[10] of the three High Temperature Lattice Test Reactor (HTLTR) U233 lattices (Table XXIII). This work was intended to assess the ability of methods and nuclear data to predict the temperature coefficient of reactivity for HTGR's. The basic assumption of this work was that the possible systematic uncertainties in the measured values of $k_\infty(T)$ were relatively temperature independent, and therefore the existing data base of k_∞ versus T is adequate for verification of neutronic predictions of $\frac{1}{k_\infty(T)}\frac{dk_\infty(T)}{dT}$. The calculations were based primarily on ENDF/B-IV cross section data, and sensitivities to alternate cross section data for U233 were also determined.

Correlations between calculated and measured temperature coefficients of the HTLTR lattices provided an interesting comparison of thorium data sets. The particular correlation employed had the form

$$k_\infty^{meas.}(T) = k_\infty^{calc.}(T)\,[A+B(T-293)] \tag{3}$$

$$\left[\frac{1}{k_\infty(T)}\frac{dk_\infty(T)}{dt}\right]_{meas.} = \left[\frac{1}{k_\infty(T)}\frac{dk_\infty(T)}{dt}\right]_{calc.}$$

$$+\left(\frac{B}{A+B(T-293)}\right) \simeq \left[\frac{1}{k_\infty(T)}\frac{dk_\infty(T)}{dT}\right]_{calc.} + B \tag{4}$$

since A ~1.0, B ~10^{-5}, and T ~10^3. The parameter A plays the role of a normalizing coefficient, and the parameter B expresses the bias in the calculated temperature coefficients. The dependence of the bias parameter B on different sources of cross section data were studied (Table XXIV). There were negligible effects on B from the use of the alternate U233 data, which was

Table XXII - Comparison of Major Reaction Rates and Eigenvalues for BMU-1B Obtained with ENDF/B-IV and Various Thorium Data Sets

		Mat. 1296 Th232	Mat. 600 Th232	LWBR Th232
Fast	Th fiss.	.0081±.00002	.0081	.0088
	Cap.	.1991±.0004	.1913	.2047
	U233 fiss.	.1692±.0003	.1705	.1706
	Q(0.625 eV)	.5725±.0010	.5786	.5652
Thermal	Th Cap.	.2220±.0006	.2260	.2168
	U233 fiss.	.2213±.0005	.2233	.2239
	K_{eff}	.9963±.0014	1.0045 ±.0016	1.0079 ±.0021

Note: Mat. 1296 is ENDF/B-IV Th232.

Mat. 600 is Leonard's evaluation.

Uncertainties in each case are the same as shown for Mat. 1296. These are one standard deviation from Monte Carlo statistics.

Table XXIII - Characteristics of the HTLTR U233 ThO_2 Lattices

	Lattice #2	Lattice #3	Lattice #5
C/U-233*	10470	13990	9460
C/Th-232**	193	282	146
Fuel Rod Radius (cm)	0.5969	0.5969	0.9982
Square Lattice Pitch (cm)	1.905	1.905	4.763

* Ratio of carbon to U233 atoms.

** Ratio of carbon to Th232 atoms.

effectively a decrease in the thermal eta from 2.2972 to 2.284. The values of B obtained using the alternate Leonard thorium were uniformly 0.4 X $10^{-5}{}^{o}K^{-1}$ lower than those based on ENDF/B-IV and generally improved the agreement between the calculated and measured temperature coefficients of reactivity for the three $^{233}UO_2$-ThO_2 fueled HTLTR lattices. Due to the reduced effective resonance integral, the Leonard thorium produces a smaller negative contribution to the temperature coefficient from the thorium Doppler effect. On this basis it was concluded[10] that the Leonard thorium evaluation is preferred over ENDF/B-IV for predicting temperature coefficients of thorium fueled lattices.

Unfortunately, due to systematic uncertainties direct comparisons of calculated $k_\infty(T)$ with experiment are not fruitful from a data testing point of view.

Table XXIV - Calculated Values* of the Temperature Coefficient Bias Parameter B for the HTLTR Lattices

	Lattice #2	Lattice #3	Lattice #5
ENDF/B-IV Data	$+0.21\pm0.07X10^{-5}$	$+1.55\pm0.19X10^{-5}$	$+0.41\pm0.09X10^{-5}$
Leonard Thorium (Mat. 600)	$-0.18\pm0.07X10^{-5}$	$+1.08\pm0.19X10^{-5}$	$+0.03\pm0.09X10^{-5}$
Leonard Thorium and Alternate U233	--	$+1.11\pm0.19X10^{-5}$	--

*All values are in units of $^{o}K^{-1}$.

B. Overall Comparison of Thorium Evaluations and Capture Measurements. In Figure 11, experiment/calculation ratios are displayed for the limited number of integral Th232 capture measurements for three of the thorium evaluations considered in this work. Errors which are shown are experimental. The ENDF/B-IV results are the same as in Figure 7 and were discussed in Section I.H. The results based on the LWBR thorium evaluation are in slightly better overall agreement with experiment. This is due to greater thorium resonance capture and a 1% smaller thermal capture cross section. The effects of a 3% higher thermal capture cross section and reduced resonance capture are readily apparent in the results produced by Leonard's thorium evaluation. Particular note is made of the bias of +13% vs. +6% for ENDF/B-IV for the ThO_2 rod resonance integrals. Almost half of this increase is due to the higher σ_a^{Th232}, which is used for normalization of the experimental rod resonance integrals, adopted

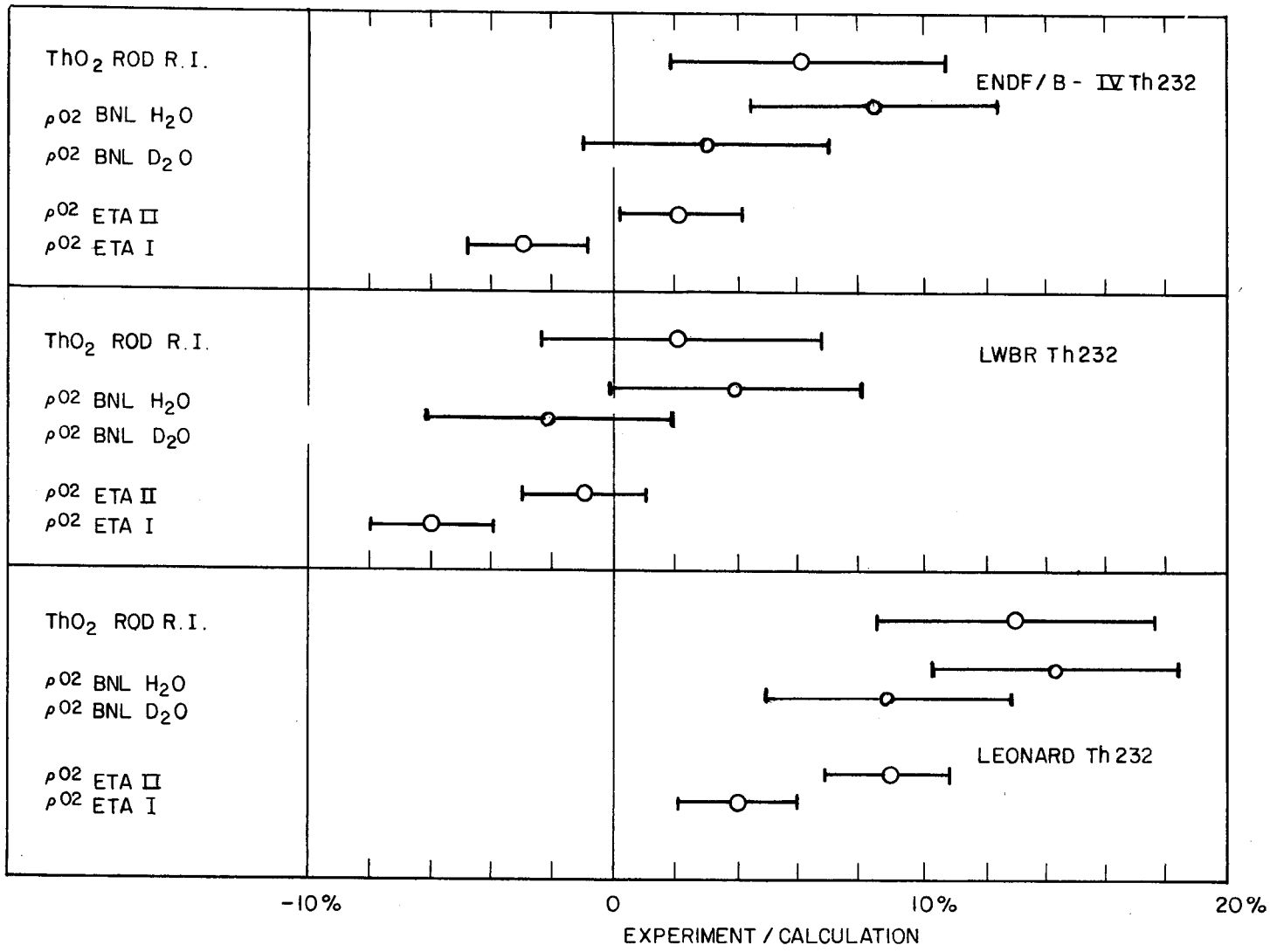

Figure 11 - Comparison of Thorium Capture Predictions for Several Thorium Evaluations

by Leonard. This again points out the need to firm up the value of σ_a^{Th232} before substantive conclusions can be drawn about resonance capture. Collectively, these comparisons suggest that thorium resonance capture should be slightly above - or at least not much below - ENDF/B-IV and that σ_a^{Th232} should not be increased - or at least not much - over 7.4b.

C. Sensitivities of Calculated Eigenvalues to Other Nuclear Data. Sensitivities of calculated eigenvalues to several nuclear data changes were determined for selected U233 homogeneous criticals. These changes included the hydrogen thermal absorption cross section, the uranium capture and fission resonance integrals, the uranium inelastic cross sections, the ENDF/B version of oxygen, and representations of the fission neutron spectra.

A reference eigenvalue was computed for each assembly with P7MG and ENDF/B-IV data. Then for each change in data δK_{eff} was determined relative to this reference value. The sensitivities of K_{eff} to the various parameters are summarized in Table XXV. The following points are noteworthy:

(1) The uranium capture and fission resonance integrals were varied as shown in Table XXV. In each case this was achieved by a uniform percentage change of the smooth multigroup cross sections. Although there were significant sensitivities for the U235 systems[1], this is not so for U233.

(2) Reducing the hydrogen 2200 m/sec absorption cross section from 0.332b to 0.330b increases the reactivity of the thermal assemblies by 0.3% with negligible effect on the high-leakage assemblies.

(3) A 20% reduction of the inelastic cross sections produced negligible changes of reactivity.

(4) Sensitivities to the ENDF/B version of oxygen are worth as much as 0.6% in K_{eff} for the high-leakage assemblies and are negligible for the large assemblies. The successive versions of oxygen (ENDF/B-I to ENDF/B-IV) show an increase in backscattering.

(5) The fission neutron spectrum significantly affects fast neutron leakage. Eigenvalue sensitivities to mean energy (for a Maxwellian shape) and to the difference between Watt and Maxwellian shapes (for the same mean energy) are shown in Table XXV.

Eigenvalue sensitivity to selected cross section variations was calculated for TUPE cores 15A, 15D, and 25$\sqrt{2}$B, THUD456, and three BNL exponentials, with results shown in Table XXVI. The smooth epithermal multigroup cross sections were increased by a uniform percentage to obtain the changed resonance integrals integrated. Thermal $\sigma_f(E)$ and $\sigma_c(E)$ were increased 1%. As expected, these lattices are most sensitive to the effective thorium resonance integral. The next greatest sensitivity is generally to revisions of the fission neutron spectra.

Table XXV - Sensitivities of U233 Critical Assemblies to Changes in Nuclear Data

Data Component	Change in Data Component	Change in Eigenvalue (δK_{eff}) H/U233=154(L2)*	381(L3)	1535(L5)	1986(L11)
Hydrogen Cross Sections	Reduced thermal absorption cross section from 0.332b to 0.330b.	+0.0004	+0.0009	+0.0026	+0.0030
Uranium-233 Scattering Cross Sections	Reduced the inelastic cross section by 20%.	-0.0004	-0.0001	0.0000	0.0000
	Inelastic cross sections reduced by 20% and the elastic cross section increased by an equivalent amount to maintain the same total cross section.	-0.0003	-0.0001	0.0000	0.0000
Oxygen Cross Sections	ENDF/B-IV → ENDF/B-III	-0.0041	-0.0031	-0.0008	-0.0001
	ENDF/B-IV → ENDF/B-I	-0.0062	-0.0044	-0.0012	-0.0002
Fission Spectrum**	Maxwellian spectrum $\bar{E}$=2.0 meV	+0.0036	+0.0029	+0.0009	+0.0003
	Maxwellian spectrum $\bar{E}$=2.1 meV	-0.0134	-0.0109	-0.0049	-0.0024
	Watt spectrum ($\bar{E}$=2.0 meV)	-0.0001	+0.0001	+0.0005	+0.0004
Smooth Capture Integral Increased by 6.0b (I_C=132±6b ENDF/B-IV)***		-0.0017	-0.0007	-0.0002	----
Smooth Fission Integral Increased by 13.0b (I_F=733±13b ENDF/B-IV)***		+0.0016	+0.0009	+0.0005	----

*Experiment ID's correspond to those in Table I.
**All δK_{eff} are relative to the ENDF/B-IV fission neutron spectrum for U233.
***Resonance integrals above 0.625 eV.

Table XXVI - Sensitivity of Eigenvalues to Selected Data Changes

		$(K_{eff}/K_{eff}^{base}-1)$						
		TUPE Lattices			THUD Lattice	BNL Exponential Lattices		
Data Type	Change	Core 15A	Core 15D	Core 25$\sqrt{2}$B	456	(M/F)-0.997:1.0	3.0043:1.0	6.845:1.0
Th232 I_c	+1.0b	-0.0093	-0.0048	-0.0030	-0.0065	-0.0150	-0.0060	-0.0029
Th232 thermal $\sigma_c(E)$	+1.0%	-0.0011	-0.0011	-0.0016		-0.0013	-0.0021	-0.0019
U235 I_F	+5.0b	+0.0020	+0.0011	+0.0005	+0.0012	--	--	--
U235 I_c	+6.0b	-0.0029	-0.0015	-0.0006	-0.0015	--	--	--
U235 thermal $\sigma_F(E)$	+1.0%	+0.0024	+0.0031	+0.0044	+0.0034	--	--	--
U235 thermal $\sigma_c(E)$	+1.0%	-0.0010	-0.0010	-0.0009	-0.0010	--	--	--
U233 I_F	+13.0b	--	--	--	--	+0.0044	+0.0020	+0.0074
U233 I_c	+6.0b	--	--	--	--	-0.0024	-0.0009	-0.0060
U233 thermal $\sigma_f(E)$	+1.0%	--	--	--	--	+0.0027	+0.0038	+0.0014
U233 thermal $\sigma_c(E)$	+1.0%	--	--	--	--	-0.0001	-0.0004	-0.0002
U235 fission spectrum	ENDF/B-IV → Adams	-0.0041	-0.0044	-0.0021	-0.0009	--	--	--
U233 fission spectrum	ENDF/B-IV → Steen	--	--	--	--	-0.0034	-0.0041	-0.0013

From our study of U235 and U233 homogeneous criticals[1] (parts of which are reproduced in this review) using ENDF/B-IV data, it was concluded that leakage was being underpredicted. For U235 systems, a suitable hardening of the fission spectrum and adoption of the Watt shape seemed to account for half the discrepancy. The other half seemed to be due to a $\bar{\nu}^{235}$ which was 10.0b too high. The sensitivities of the TUPE and THUD456 lattices to the more recent Adams U235 fission neutron spectrum[28] are shown in Table XXVI and Figure 12 (TUPE only). This spectrum has a Watt shape and a mean energy of 2.016 meV vs. 1.985 meV for ENDF/B-IV. Better agreement with experiment also was achieved for the U235 homogeneous criticals with Adams' spectrum[29].

Steen[30] has reevaluated the fission spectra for both U235 and U233. It was found that the Watt and his standard models represented the U235 data, which was the same as used by Adams, with about equal reliability. In the case of the standard model, it was possible to obtain a prompt fission neutron mean energy as high as 2.07 meV. For U233, the same standard model represented best the existing data and yielded a mean prompt neutron energy of ~2.08 meV. The effects of this spectrum on K_{eff} for the BNL exponential lattices have been calculated and are depicted in Figure 12. A substantial improvement is obtained.

The overall effect of Steen's new U233 fission neutron spectrum on K_{eff} for the homogeneous U233 criticals, the BNL H_2O moderated exponential experiments, and the two LWBR criticals considered in this work is depicted in Figures 13 and 14. Figure 13 shows K_{eff} vs. total neutron leakage fraction based on ENDF/B-IV. The BNL exponentials and the LWBR cores fit nicely into the pattern that was established for the homogeneous criticals. These same K_{eff} results are shown in Figure 14a when Steen's harder U233 fission neutron spectrum is employed. Much of the rising trend in K_{eff} vs. leakage is eliminated with the result that most of these experiments, which are H_2O moderated, form a reasonably consistent set. However, the BNL D_2O moderated exponentials are not consistent with this picture since K_{eff} is already underpredicted by 1.5% using ENDF/B-IV. It is expected that a harder U233 fission neutron spectrum would worsen this underprediction.

In addition to the fission spectrum change, the effects of replacing the ENDF/B-IV thorium by the LWBR and Leonard evaluations, respectively, are depicted in Figure 14b and c. The consistency of the results is lessened for the LWBR thorium, but this is due mostly to the effects of the higher thorium scattering cross section which was adopted in that evaluation and which acts to reduce leakage and raise K_{eff}. As seen previously in Figure 9, Leonard's thorium tends to increase K_{eff} for the tighter BNL lattices and lower K_{eff} for the looser lattices. This reintroduces a slight rising trend in K_{eff} vs. leakage for those thorium bearing lattices in Figure 14c, but the overall consistency is not much disturbed.

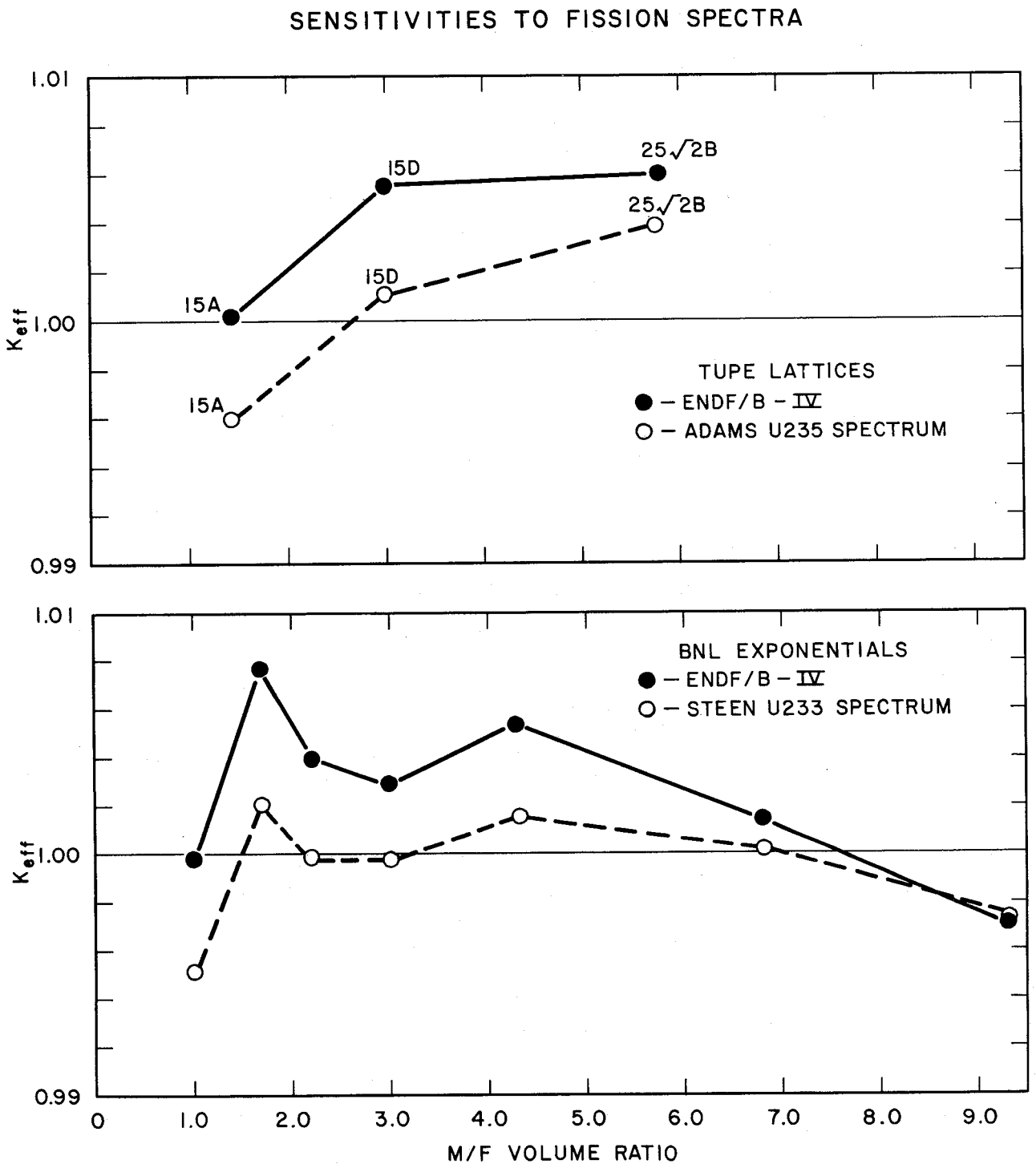

Figure 12 - Sensitivities of K_{eff} to Alternate Fission Neutron Spectra

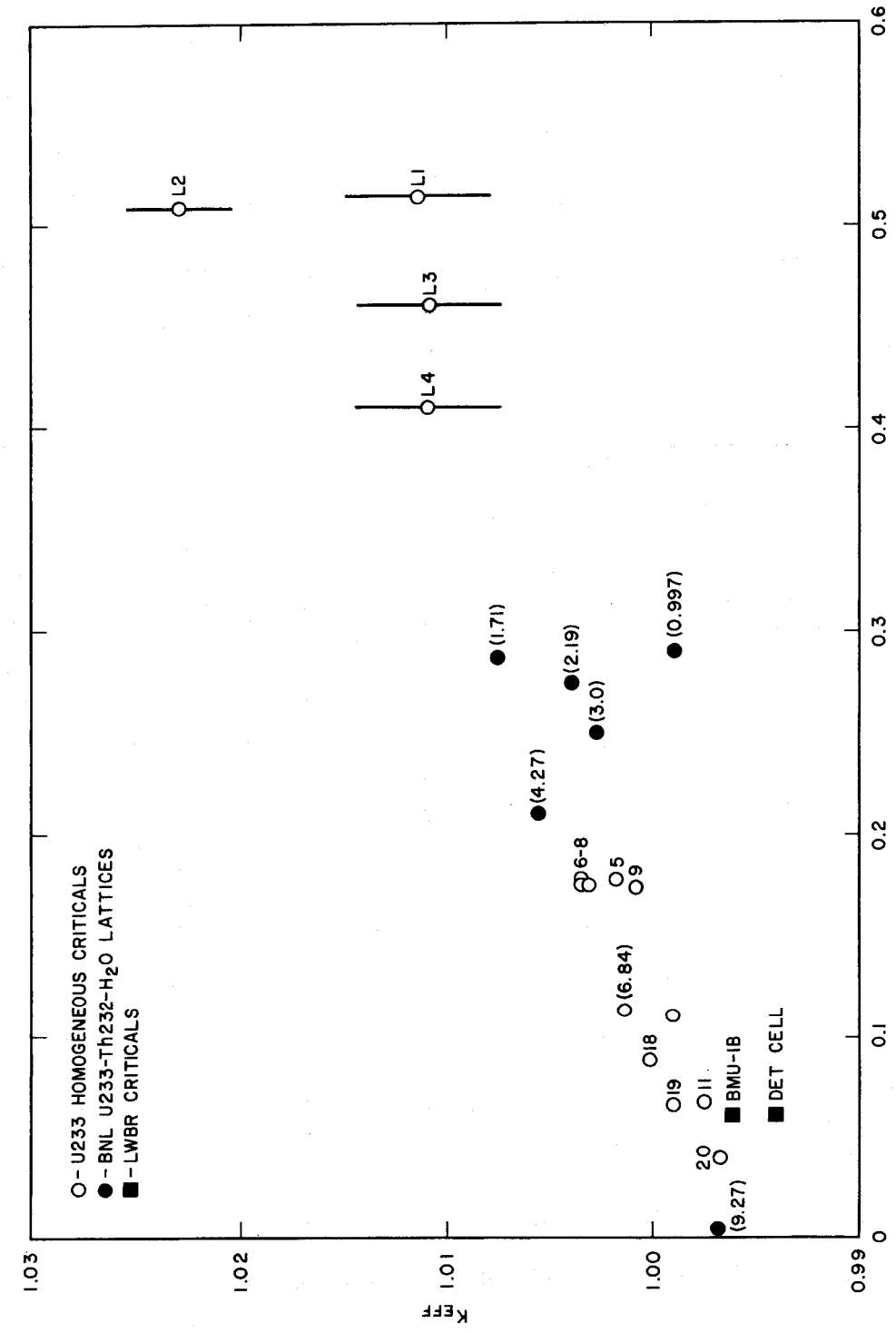

Figure 13 - K_{eff} vs. Neutron Leakage Fraction for U233 Systems

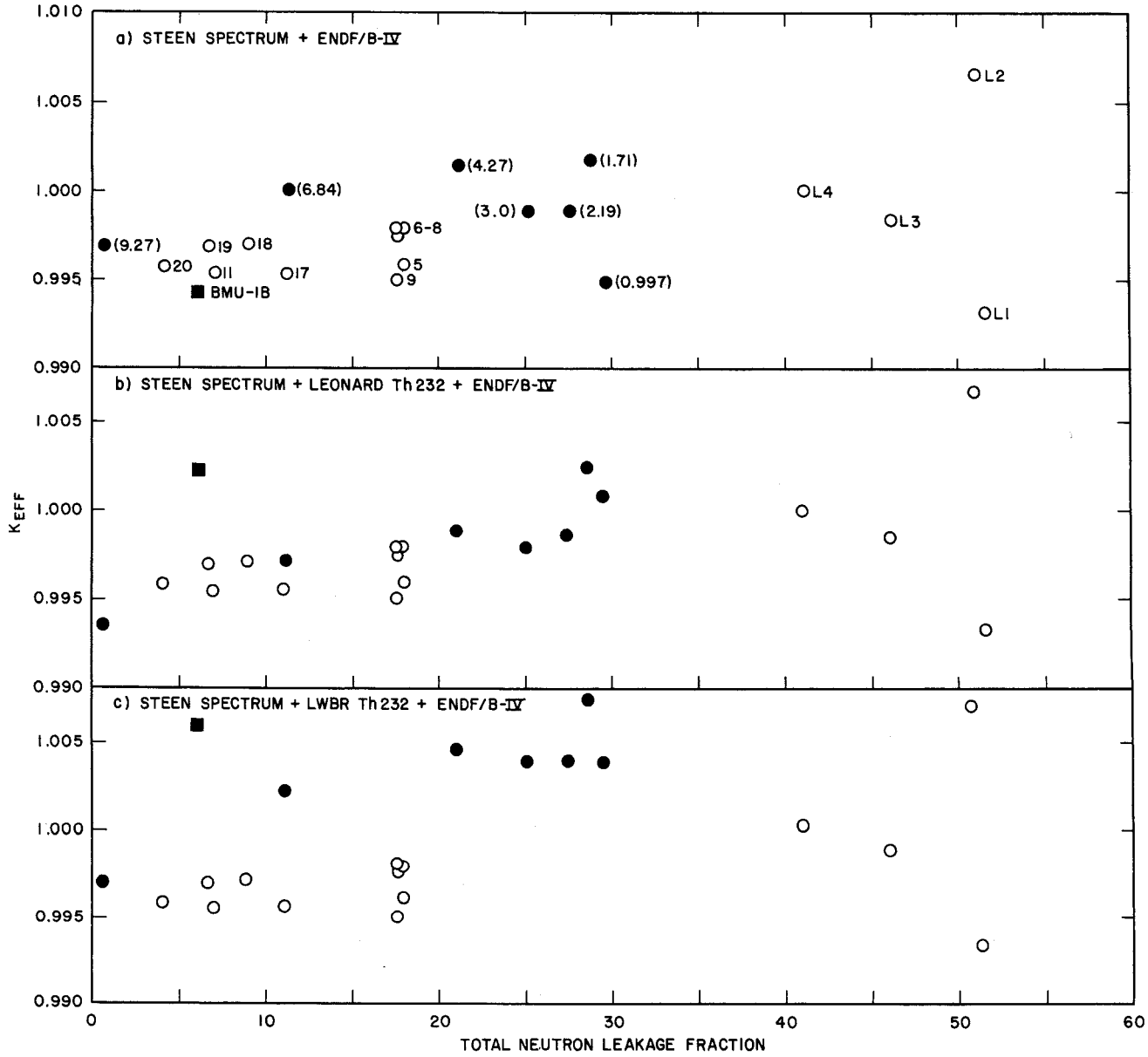

Figure 14 - K_{eff} vs. Neutron Leakage Fraction: a) ENDF/B-IV and the Harder Steen U233 Fission Neutron Spectrum, b) Case a plus the Leonard Th232, and c) Case a plus the LWBR Th232

The LWBR thorium raises K_{eff} for the BMU-1B core by 1.2%. This is thought to be attributed to reduced leakage with the LWBR set since the overall thorium capture rate was virtually unchanged compared to that for ENDF/B-IV. The Leonard thorium evaluation also raised the BMU-1B K_{eff} significantly by 0.8%. In this case though, the effect was due mainly to the reduced resonance capture which was not compensated by the increased thermal capture. The implication here is that if Leonard's thorium resonance evaluation is firm, then an even higher σ_a^{Th232} is required to bring the BMU-1B core back into line with the other experiments. This is considered to be unlikely and suggests, as do the integral thorium capture measurements, that resonance absorption is underpredicted by the Leonard set.

III. Summary

This study was intended to provide a systematic review of selected U233 and thorium-uranium experiments using ENDF/B-IV data. A second aim was to test the performance of thorium data sets, which have recently been proposed, to predict measured integral parameters and to examine sensitivities to various nuclear data changes.

K_{eff} for critical homogeneous U233 systems, calculated with ENDF/B-IV data, show an upward trend of approximately 2% with decreasing H/U, and there is a similar trend for homogeneous U235 systems. These trends appear to be due mostly to an underprediction of fast leakage.

Based on full energy range, explicit geometry Monte Carlo calculations, K_{eff} for many of the H_2O moderated thorium-uranium lattices (TUPE's, THUD's, BNL exponentials) also tends to be overpredicted with ENDF/B-IV data. Since many of these cores have leakage fractions between 20-30%, this trend is not inconsistent with that for leaky homogeneous criticals and therefore partly may be associated with an underprediction of leakage. On the other hand, K_{eff} for the BNL D_2O moderated exponentials appears to be underpredicted by 1.5%.

In the area of measured integral parameters, it was judged that interpretation of ρ^{02} measurements for the TUPE and THUD lattices would require detailed study and are unpromising. For the BNL H_2O moderated exponential lattices, the ENDF/B-IV predicted values for ρ^{02} were generally ~8% below experiment, as were the predictions for the D_2O lattices by 3%. ρ^{02} for ETA-I was overpredicted by 3%, and ρ^{02} for ETA-II was 2% low. Overall, the consistency among predictions of integral thorium capture measurements based on ENDF/B-IV is reasonable (Figure 7).

Three alternate thorium evaluations due to Derrien, Steen (LWBR), and Leonard were tested besides ENDF/B-IV. The most unambiguous test of these cross section sets were the measured

ρ^{02} values for the BNL exponential and ETA lattices. Calculated K_{eff} values were also sensitive to the thorium set used, but here the fission neutron spectrum was an additional factor. How well these evaluations predict thorium capture measurements is depicted in Figure 11.

The additional unshielded capture in the resonance and unresolved resonance ranges assumed in the Derrien evaluation is a questionable alternative. As a result, testing of this evaluation has not been pursued as far as that for the other evaluations and those results that were obtained have not been plotted in Figure 11.

The consistency among various experiment/calculation comparisons using the LWBR thorium set is similar to that for ENDF/B-IV. However, agreement with experiment is slightly better for the LWBR set.

The high thorium thermal capture cross section of 7.61b adopted by Leonard has a nontrivial implication as far as the measured dilute resonance capture integral is concerned. Based on the review by Grenêche, which assumed $\sigma_a^{Th232} = 7.4 \pm 0.08$b, the dilute integral would be raised to 88.5b. This would also serve to raise the measured shielded resonance integrals. It is noted in connection with the Leonard evaluation that measured integral parameters such as ρ^{02} and I'^{Th232} are furthest discrepant from the differential data, which underpredicts them (Figure 11).

There is a good deal of evidence from these analyses to support hardening of the fission neutron spectra of both U235 and U233. Calculations of K_{eff} for several TUPE lattices are improved somewhat (Figure 12) by using the harder Adams spectrum for U235. Predictions of the parameter δ^{02} for the ETA-I lattice are 15% (Table XVI) below experiment and also could be improved with a harder fission spectrum. An even harder U235 fission neutron spectrum has resulted from an evaluation due to Steen. In a similar manner, Steen has reevaluated the U233 fission spectrum. This spectrum is also significantly harder than the ENDF/B-IV U233 spectrum. Use of Steen's U233 fission spectrum virtually eliminates the bias trend in the predictions of K_{eff} vs. neutron leakage for the U233 homogeneous criticals and the BNL H_2O moderated exponential lattices (Figure 14) and should also improve the low predicted δ^{02} value for the ETA-II lattice.

REFERENCES

1. J. J. Ullo and J. Hardy, Jr., "Analysis of Homogeneous U233 and U235 Critical Assemblies with ENDF/B-IV Data," WAPD-TM-1299, October 1977.
2. N. L. Snidow, et al., "Thorium Uranium Physics Experiments," BAW-1191, Babcock and Wilcox, May 1960.

3. W. C. Redman, et al., "Critical Experiments with Thoria-Urania Fuel in Heavy Water," ANL-6378, December 1961.
4. G. A. Price, et al., "Organic-Cooled, Heavy Water-Moderated U233 Fueled Lattice Experiments," BNL-50012 (T-434) (1966).
5. H. H. Windsor, et al., Nucl. Sci. Eng., 42, 150 (1970).
6. J. Hardy, Jr., J. J. Volpe, and D. Klein, "Measurement and Analysis of Parameters in Tight Th232-U235 and Th232-U233 Lattices Moderated with D_2O," WAPD-TM-1089, January 1974. Also Nucl. Sci. Eng., 55, 401 (1974).
7. B. L. Palowitch and J. Hardy, Jr., "Study of the ThO_2 Doppler Effect in a Tight $U^{235}O_2$-ThO_2 Lattice Moderated with D_2O," WAPD-TM-1090, January 1974.
8. S. Milani, et al., "BMU Series of ^{233}U Fueled Critical Experiments," WAPD-TM-1117, January 1975.
9. S. Milani, et al., "^{233}U Oxide-Thorium Oxide Detailed Cell Critical Experiments," WAPD-TM-1101, October 1974.
10. D. F. Newman, et al., "Evaluation of Temperature Coefficients of Reactivity for U233-Thorium Fueled Lattices," EPRI-NP-222, May 1977.
11. H. Derrien, "Evaluation of Th232 Resonance Parameters," Specialists Meeting on "Resonance Parameters of Fertile Nuclei and Pu239," Saclay, P. Ribon, Ed., NEANDC(E) 163U, May 1974.
12. N. M. Steen, "An Evaluation of the Radiative Neutron Capture Cross Sections of Thorium-232 for the Range 0.0 eV to 15 meV," WAPD-TM-971, December 1970.
13. S. R. McNeany and J. D. Jenkins, "Comparison of Hanson-Roach and ENDF/B-IV Cross Sections for U233 Criticality Calculations," ORNL-TM-5113, 1976.
14. N. R. Candelore, R. C. Gast, and L. A. Ondis II, "RCP01 - A Monte Carlo Program for Solving Neutron and Photon Transport Problems in Three-Dimensional Geometry with Detailed Energy Description," WAPD-TM-1267, 1978.
15. H. Bohl Jr., et al., "P3MG-1, A One-Dimensional P-3 Program for the Philco-2000 Computer," WAPD-TM-272, 1963.
16. H. Bohl Jr. and A. P. Hemphill, "MUFT-5 - A Fast Neutron Spectrum Program for the Philco 2000," WAPD-TM-218, February 1961.
17. S. C. Bhatt, et al., Trans. Am. Nucl. Soc., 27, 920 (1977).
18. N. L. Shapiro, et al., "Assessment of Thorium Fuel Cycles in Pressurized Water Reactors," EPRI NP-359, February 1977.
19. B. R. Sehgal, et al., Trans. Am. Nucl. Soc., 23, 559 (1976).
20. J. J. Weiss and B. K. Malaviya, Trans. Am. Nucl. Soc., 27, 890 (1977).
21. D. Grenêche, "Evaluation of the Th232 Capture Resonance Integral," Specialists Meeting on "Resonance Parameters of Fertile Nuclei and Pu239," Saclay, P. Ribon, Ed., NEANDC(E) 163 U, May 1974.

22. S. F. Maghabghab and D. I. Garber, "Neutron Cross Sections," BNL-325, Third Edition, June 1973.
23. E. Hellstrand, "Measurement of Resonance Integrals," in Reactor Physics in the Resonance and Thermal Regions, Vol. II, Proceedings of the National Topical Meeting, San Diego, February 7-9, 1966, A. J. Goodjohn and G. C. Pomraning, Eds., M.I.T. Press, Cambridge, Mass., 1966.
24. E. Hellstrand and G. Lundgren, Nucl. Sci. Eng., 12, 435 (1962).
25. W. Pettus, M. Baldwin, and C. Samuel, BAW-1286, 1963.
26. J. Weitman, Nucl. Sci. Eng., 18, 246 (1964).
27. B. Palowitch and J. Hardy, Jr., Nucl. Sci. Eng., 29, 111 (1967).
28. J. M. Adams, "Prompt Fission Neutron Spectra of U235," AERE-R-8636, NEANDC(UK) 170L, NEACRP 476.
29. J. Hardy, Jr., "The Performance of ENDF/B-IV Data in Thermal Reactor Benchmark Testing - Some Results with Version IV and Prospects for Version V," to appear in Trans. Am. Nucl. Soc., June 1978.
30. N. M. Steen, "Status of Nuclear Data for Th232 and U233," to be presented at the June 1978 Meeting of the American Nuclear Society.

Section 10

INTEGRAL DECAY-HEAT MEASUREMENTS AND COMPARISONS TO ENDF/B-IV AND V

INTEGRAL DECAY-HEAT MEASUREMENTS AND COMPARISONS TO ENDF/B-IV AND V

T. R. England
Los Alamos Scientific Laboratory, University of California
Theoretical Division
Los Alamos, New Mexico 87545

and

R. E. Schenter and F. Schmittroth
Hanford Engineering Development Laboratory
Richland, Washington 99352

ABSTRACT

Results from recent integral decay-power experiments are presented and compared with summation calculations. The experiments include the decay power following thermal fission of ^{233}U, ^{235}U, and ^{239}Pu. The summation calculations use ENDF/B-IV decay data and yields from Versions IV and V. Limited comparisons of experimental β and γ spectra with summation calculations using ENDF/B-IV are included. Generalized least-squares methods are applied to the recent ^{235}U and ^{239}Pu decay-power experiments and summation calculations to arrive at evaluated values and uncertainties. Results for ^{235}U imply uncertainties less than 2% (1 σ) for the "infinite" exposure case for all cooling times greater than 10 seconds. The uncertainties for ^{239}Pu are larger. Accurate analytical representations of the decay power are presented for $^{235,238}U$, and ^{239}Pu for use in light water reactors and as the nominal values in the new ANS 5.1 Draft Standard (1978). Comparisons of the nominal values with ENDF/B-IV and the 1973 ANS Draft Standard in current use are included. Gas content, important to decay-heat experiments, and absorption effects on decay power are reviewed.

*Work supported by Reactor Research and Technology Division of the U. S. Department of Energy and by the U.S. Nuclear Regulatory Commission.

Integral Decay-Heat Measurements And Comparisons To ENDF/B-IV And V*

T. R. England
Los Alamos Scientific Laboratory, University of California
Theoretical Division
Los Alamos, New Mexico 87545

and

R. E. Schenter and F. Schmittroth
Hanford Engineering Development Laboratory
Richland, Washington 99352

INTRODUCTION

Coordinated research by the authors at the Los Alamos Scientific Laboratory (LASL) and the Hanford Engineering Development Laboratory (HEDL) on the development, evaluation, testing, and application of fission-product nuclear data has been in progress since 1973. The range of our activity is indicated by the source term summary of Ref. 1. A comprehensive review of the decay-heat (decay-power) source term through mid-Summer of 1977, including contributions from other researchers, is given in Ref. 2. These two reports contain extensive references to recent publications; the respective conference reports in which these are published also contain review papers by other researchers that provide some basic source material on decay-heat and related fission-product data.

Decay heat from the thermal fission of ^{235}U was emphasized in the earlier publications. The present report also contains decay-heat comparisons with very recent experiments following the thermal fission of ^{233}U and ^{239}Pu and calculated ^{238}U Decay-heat. These new comparisons and the ^{235}U comparisons directly associated with a revised American Nuclear Society Decay Heat Standard (ANS 5.1) are emphasized in this report. The final standard has not been formally adopted but its data base and methodology, as summarized in this report, has the approval of the ANS 5.1 Working Group and preliminary ANS 5 and ANSI approval.†

*Work supported by Reactor Research and Technology Division of the U.S. Department of Energy and by the U.S. Nuclear Regulatory Commission.

†The fitted functions and uncertainties were formally accepted by the ANS 5.1 Working Group on June 21, 1978 as the basis of the new standard. (Note added in proof.)

Since 1973 there has been extensive progress in developing the data base used in summation codes and in benchmark experiments of decay heat. Fission-product data libraries have been developed in the United States, England, France, Japan, and Sweden. In addition, several groups have studied and published uncertainty analyses of the summation calculations, and least-squares methods have been used to combine the experimental data and calculational results and to produce functional representations of the standard. An extensive, global review of decay-heat research would be largely redundant with the review in Ref. 2 and is not included in this report. Rather, the background, source data and methodology for the proposed revision of the ANS Decay-Heat Standard is used as a focal point for the included ENDF/B comparisons.

ENDF/B Data Base[3]

Table 1 lists the general content of ENDF/B-IV and approximate content of ENDF/B-V. Version V decay data is not yet (5/78) complete but we have included comparisons of decay heat using preliminary, but near final, Version V yields. The plexus of 824 coupled nuclides in Version IV are used in the comparisons in this report. A listing of all nuclide parameters used (decay energies, decay constants, branching fractions, cross sections, etc.) is given in

Table 1

ENDF/B Fission Product Files; General Content

Type Data, Comment	Number In ENDF/B-IV	Approximate Number In ENDF/B-V
Total Nuclides	824	~ 838
Stable	113	~ 114
Unstable	711	~ 724
Ground State	701	~ 702
1st Excited State	117	~ 127
2nd Excited State	6	~ 7
Delayed Neutron Precursors	57	102
Nuclides with α Decay Data	6	~ 6
Nuclides with β^+ Decay Data	17	~ 17
Nuclides with Line Data	180	250-270
Nuclides with Evaluated Cross Sections	181	~ 182
Yield Sets	10	20

Ref. 4, and the yields are listed in Ref. 5. References 6 and 7 also provide information on the file content, and Ref. 8 contains the results of earlier and varied integral data tests. Uncertainty analyses for decay heat using ENDF/B-IV data have been published in Refs. 9-11. Otherwise, there are a plethora of publications using the ENDF/B-IV fission-product data base, as indicated in Refs. 1 and 2.

Integral Measurements

Approximately one year after the task force effort to compile the ENDF/B-IV evaluated data began, four benchmark quality experiments were initiated. Two were funded by the Electric Power Research Institute (EPRI), respectively, at the University of California, Berkeley (UCB) and Intelcom Rad Tech (IRT). The other two experiments were funded by the U.S. Nuclear Regulatory Commission (NRC), respectively, at the Los Alamos Scientific Laboratory (LASL) and the Oak Ridge National Laboratory (ORNL). These and the earlier measurements at Fontenay-aux-Roses (F-a-R), France, are included in the proposed standard.

Table 2 lists the experiments used in the decay-heat standard and other integral comparisons of ENDF/B-IV with recent experiments (1970 - 1977).

Revised Decay-Heat Standard

The current American Nuclear Society (ANS) Draft Decay-Heat Standard[25] and its uncertainty limits of + 20% and - 40% (for times $< 10^3$ s) reflects the state of knowledge when it was prepared (1971 and slightly revised in 1973). The mean value is based on ^{235}U thermal fission for an "infinite" period prior to shutdown and no neutron absorption by fission products. For the important cooling time ($\leq 10^3$ s) of interest in the hypothetical loss-of-coolant accident (LOCA), reactor designs in the U.S.A. and other countries are required to use this mean value plus 20% (ANS 5.1 + 20). This value, if conservative, is an extremely expensive design criterion. However, neither a smaller mean value nor a smaller uncertainty would have been justifiable based on data available through 1973.

The initial motivation for the ENDF/B-IV fission-product data was for use in improving our knowledge of decay heat using summation calculations. Based on encouraging results from preliminary calculations, a new ANS Working Group (ANS 5.1) was formed in 1974 chaired by V. E. Schrock for the purpose of defining a new standard. The subsequent funding of benchmark experiments was unexpected, but these were very much needed in the process of establishing a new standard of high quality. The new ANS 5.1 Working Group was expanded to include those involved with the new experiments as well as experts from NRC, industry and the national laboratories. This report benefits from the close cooperation of all members of the ANS 5.1 Working Group. Some of the ENDF/B-IV comparisons, for example, include experimental results that are still being prepared

Table 2

Integral Comparisons With ENDF/B-IV[a]

Fissionable Nuclide	Quantity	Exposures	Approx. Cooling Range	Laboratory	Ref.
^{235}U	TOT	2×10^4 s	$10 - 10^5$ s	LASL (Yarnell and Bendt)	12
	β, γ, TOT	1, 10, 100 s	$2 - 1.4 \times 10^4$ s	ORNL (Dickens, et al.)	13
	β, γ, TOT	24 h	$1 - 10^5$ s	IRT (Friesenhahn and Lurie)	14
	TOT HEAT	100, 1000, 5000 s	$70 - 7 \times 10^4$ s	F-a-R (Lott, et al.)	15
	TOT HEAT	1, 4, 22.4 h	$10 - 10^4$ s	UC Berkeley (Schrock, et al.)	16
	TOT HEAT	Long, Variable	$5 \times 10^4 - 10^7$ h	BAPL (Gumst, et al.)	17
	β	10, 100 s	0.2 - 26 s	SURRC (Alan and Scobie)	18
	γ	2.5×10^4 s	$29 - 1.5 \times 10^5$ s	LASL (Jurney)	19, 24
	γ	4, 10, 100 s	$10 - 1.5 \times 10^3$ s	Studsvik (Johansson and Nilsson)	20, 2
^{233}U	TOT HEAT	2×10^4 s	$20 - 10^5$ s	LASL (Yarnell and Bendt)	19
	TOT HEAT	50 to 2.5×10^4 s	$60 - 10^5$ s	F-a-R (Fiche, et al.)	21
	γ	2.5×10^4 s	$29 - 1.5 \times 10^5$ s	LASL (Jurney)	19, 24
^{239}Pu	TOT HEAT	2×10^4 s	$20 - 10^5$ s	LASL (Yarnell and Bendt)	19
	TOT HEAT	50 to 2.5×10^4 s	$60 - 10^5$ s	F-a-R (Fiche, et al.)	21
	β, γ, TOT	1, 5, 100 s	$2 - 1.4 \times 10^4$ s	ORNL (Dickens, et al.)	22
	γ	2.5×10^4 s	$29 - 1.5 \times 10^5$ s	LASL (Jurney)	19, 24
		- - - - SPECTRA - - - -			
~ 130 β and γ spectra compared with: a) All ^{235}U values from ORNL and LASL Measurements b) LASL γ Measurements for ^{233}U and ^{239}Pu c) β spectra measured at UI (^{235}U irradiation for 15 ms and 8 hours - see Refs. 23 and 24).					

[a]Only completed comparisons are listed. All experiments were made since 1970, and except for BAPL, UI, and SURRC, since 1976.

for publication.

As already noted, a new standard has been proposed by ANS 5.1 and received preliminary acceptance. Unlike the existing standard, the proposed standard

a) incorporates ^{239}Pu and ^{238}U in addition to ^{235}U,
b) incorporates neutron absorption effects,
c) includes a continuous functional representation for each fuel (to 10^9 s); these permit heating following any finite irradiation including a fission pulse.

For ^{235}U and ^{239}Pu, the proposed standard combines experiments with summation calculations in the cooling interval $1\text{-}10^5$ s. For all longer times, and for all times in the case of ^{238}U, the proposed standard is based entirely on summation calculations using ENDF/B-IV.

*The reader is cautioned that the final approved standard may differ in its uncertainties and from the functional representations in this report. The draft standard includes functional and tabular data and precise prescriptions for applications. The combined experimental and calculational results to date are referred to here as nominal values. The intent in this report is to present the basic data comparisons and accepted methodology in combining experimental and calculated data as of May 1978.**

DIRECT ENDF/B-IV COMPARISONS WITH EXPERIMENTS

In the case of finite irradiation, the comparisons in this section are mostly with the quantity F(t,T), the "integral decay-heat function" which is given in the units

$$\text{MeV/Fission} \equiv \frac{\text{MeV/s}}{\text{Fissions/s}} \quad .$$

This is possible because all experiments have essentially a constant fission rate prior to shutdown. The measurement intervals of energy release after shutdown are sufficiently short, that an average over the counting or measurement intervals can be applied to the mid-point of the interval.

In some cases the results follow a very short irradiation period. In all cases we ultimately generate a pulse-equivalent for the nominal value or "differential decay-heat function", f(t), given in the units.

$$\text{MeV/Fission-s} \equiv \frac{\text{MeV/s}}{\text{Fissions}} \quad .$$

*See the footnote on page 1.

These two quantities are precisely defined and functionally related in a subsequent section (Eqs. 1-4). The reader should note that the numerator of these expressions refers to times after fission and the denominator to the fission interval.

The irradiation times and flux levels in the experiments are not sufficient to cause significant effects due to neutron absorption coupling. However, a nuclide having a large cross section such as ^{135}Xe could have a lower concentration; therefore, all comparison calculations did include cross sections and flux levels typical of the experiments.

Comparisons with the derived nominal decay-heating, including the ENDF/B-IV pulse and finite irradiation values, and the 1973 ANS Draft Standard, are made in following sections. This section compares only ENDF/B-IV summation calculations, not the nominal values, with measurements.

Calculational Uncertainties and Data Tests

Several studies of calculational uncertainties have been made[2,9-11] and all are in basic agreement. Table 3 shows typical results at selected cooling times for a fission pulse and for extended irradiation. In addition, the current uncertainty estimates for the nominal decay-heat values discussed in a following section are given in parentheses for comparison; these are somewhat more conservative[1,2,31] than initial values obtained on combining experiments and calculations (for ^{235}U and ^{239}Pu), but are the current accepted values. For clarity only the experimental uncertainties, not the calculational values, are shown on the comparison plots in this section.

Table 3

Total Decay-Heat Uncertainties (%) in Summation Calculations and in Proposed 5/78 Nominal[a]

Cooling Times(s)	^{235}U Thermal		^{239}Pu Fast		^{238}U Fast	
	Pulse	10^7 s	Pulse	10^7 s	Pulse	10^7 s
1.0	19. (40.)	6.9 (3.3)[a]	27.2 (54.)	8.4 (5.6)	22. (23.)	10. (12.)
2.0	17. (8.3)	6.4 (2.4)	22.5 (12.)	7.9 (4.5)	21. (21.)	9.5 (12.)
5.0	16. (3.8)	5.6 (2.2)	18.8 (5.4)	7.0 (4.4)	19. (20.)	8.1 (11.)
10.0	15. (3.2)	4.8 (2.0)	17.1 (4.9)	6.3 (4.2)	17.7 (18.)	6.9 (9.5)
20.0	14. (2.4)	3.8 (1.9)	16. (4.4)	5.4 (4.2)	16. (17.)	5.6 (8.4)
50.0	10. (2.0)	2.8 (1.8)	13. (4.0)	4.4 (4.2)	13. (15.)	3.9 (7.8)
1×10^2	6.8 (1.8)	2.5 (1.8)	9.8 (3.9)	3.9 (4.2)	9.6 (10.)	3.0 (5.9)
1×10^3	4.6 (1.8)	2.4 (1.8)	5.5 (3.8)	3.6 (4.4)	4.7 (5.6)	2.5 (4.9)
1×10^4	4.3 (1.8)	2.0 (1.8)	5.9 (4.6)	2.6 (4.8)	4.7 (5.6)	2.1 (4.4)
1×10^5	3.2 (1.7)	1.4 (2.0)	3.7 (5.0)	1.9 (5.0)	3.3 (4.5)	1.6 (3.9)
1×10^6	1.5 (2.0)	1.1 (2.0)	2.0 (5.0)	1.5 (5.0)	1.8 (3.5)	1.5 (3.9)
1×10^7	1.6 (2.0)	1.4 (2.0)	1.9 (5.0)	1.9 (5.0)	2.1 (3.7)	2.1 (4.4)
1×10^8	2.2 (2.0)	2.0 (2.0)	3.8 (5.0)	3.6 (5.0)	3.8 (5.0)	3.7 (5.0)

[a]Uncertainty in the nominal value is given in parentheses. The value under the 10^7 s column applies to the infinite ($\equiv 10^{13}$ s) irradiation, but the result is only slightly different for 10^7 s. The nominal uncertainty incorporates experimental data for ^{235}U and ^{239}Pu and contains a conservative component. The analysis for fast neutron fission energy of ^{239}Pu also applies to thermal fission.

Uncertainty studies of the basic summation results are basically sensitivity analyses that propagate uncertainties in the basic nuclear data such as fission yields and average decay energies. This approach is desirable; one can ascertain which basic data have the largest impact on the accuracy of the calculations so that future work on the nuclear data libraries can be properly directed. In addition, in comparisons with experimental measurements, an independent assessment of the summation uncertainties allows one to decide whether or not any observed discrepancies are normal or are indicative of undetected errors. Except for fission yields, all the decay data are the same for different fissionable nuclides. Thus, an understanding of the sensitivity of summation calculations to the basic data allows one to extrapolate experimental results for one nuclide, such as ^{235}U, to other less studied fissioning nuclides.

A particularly important aspect of these uncertainty calculations is to delineate the relationship between the uncertainties for a pulse irradiation and for a finite irradiation more typical of actual reactor operations. *Because the summation uncertainties turn out to be much smaller for the longer irradiations, a comparison of the discrepancies between calculated and experimental decay-heat values for a very short irradiation is not indicative of the accuracy of summation calculations for the longer irradiations, even for short cooling times.*

Uncertainties in summation calculations are from several sources. These include errors in fission-product yields, average decay energies, and half-lives. One must also consider metastable states and branching ratios. For short cooling times ($t < 10^4$ s), one can neglect uncertainties due to secondary corrections such as neutron capture. Despite different approaches to the various sources of error by different workers, a number of general conclusions can be drawn. As seen in Figs. 1-4 taken from Ref. 10, the total uncertainties for cooling times greater than 100 s are quite small for both ^{235}U and ^{239}Pu. Also as seen in Figs. 1-4 and emphasized in Fig. 5, there is a sharp reduction in the calculated uncertainties with increased irradiation times, especially for the shorter cooling times. Work by Spinrad[11] is in quantitative agreement with these conclusions for ^{235}U, although his approach to yield uncertainties is quite different.

For cooling times greater than 100 s, decay-heat uncertainties due to decay-energy uncertainties are on the order of 1-3% for a fission burst and ~ 1% for a long irradiation. For shorter cooling times, the use of model Q-values results in possible correlations in average decay energies that leads to increased decay-heat uncertainties. This effect is readily apparent in Figs. 1-4, especially in the decay-energy component.

In general, half-life uncertainties are relatively unimportant in decay-heat calculations. Nevertheless, one must recognize that gross errors in an individual nuclide can alter this conclusion. As an example, the ENDF/B-IV library contains a value of 2.3 m for the half-life of ^{96}Y while recent measurements indicate both a

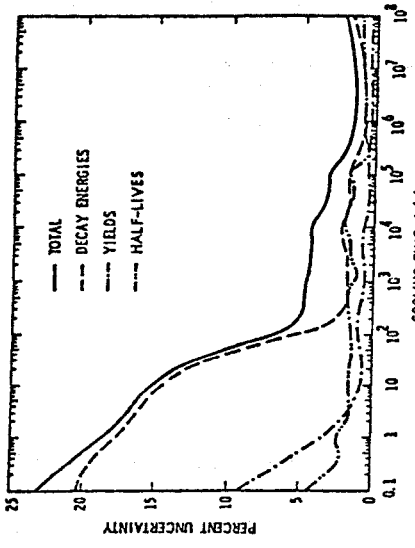

Fig. 1. ^{235}U (Thermal) T = 0 s.

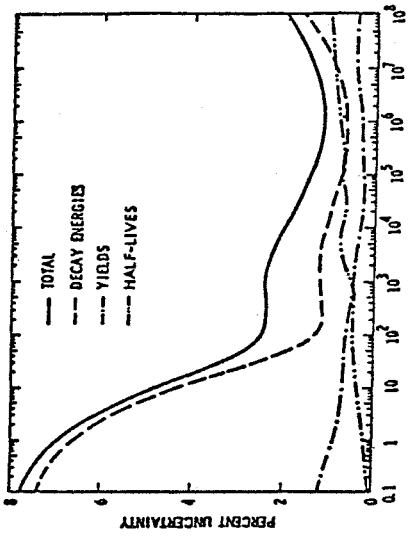

Fig. 2. ^{235}U (Thermal) T = 10^7 s.

Fig. 3. ^{239}Pu (Fast) T = 0 s.

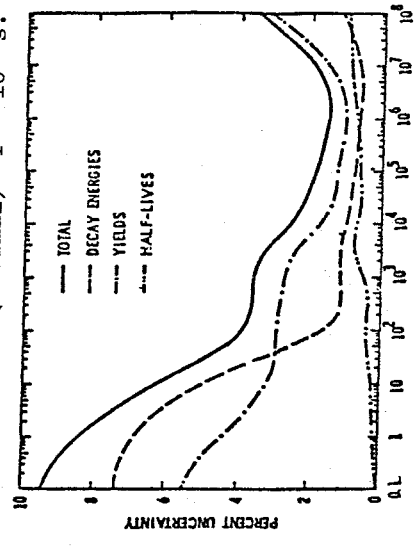

Fig. 4. ^{239}Pu (Fast) T = 10^7 s.

ground and metastable state with respective half-lives of 6.0 s and 10.0 s. This drastic change, which is far beyond the expected uncertainties, changes the decay-heat calculations for a pulse irradiation by as much as 8%. Fortunately, the effect is much smaller for longer irradiations (~ 2.5% for an infinite irradiation).

The problem of gross errors discussed for half-lives in the previous paragraph is also of concern for metastable states and their associated branching ratios. A branching ratio error can shift the decay of a parent nuclide between daughter states of widely different half-lives with an effect equivalent to a large half-life change. In one study,[9] the metastable states were excluded from the ENDF/B library in order to test their significance. As long as decay energies were consistently changed to reflect conservation of decay energy in the mass chains, the main consequence of eliminating the metastable states was to alter the time dependence of when the energy was released and the split between beta and gamma energy. For a longer irradiation ($T = 10^7$ s), which tends to average out time variations, the maximum change in decay-heat was ~ 6%. However, a major portion of this change can arise from

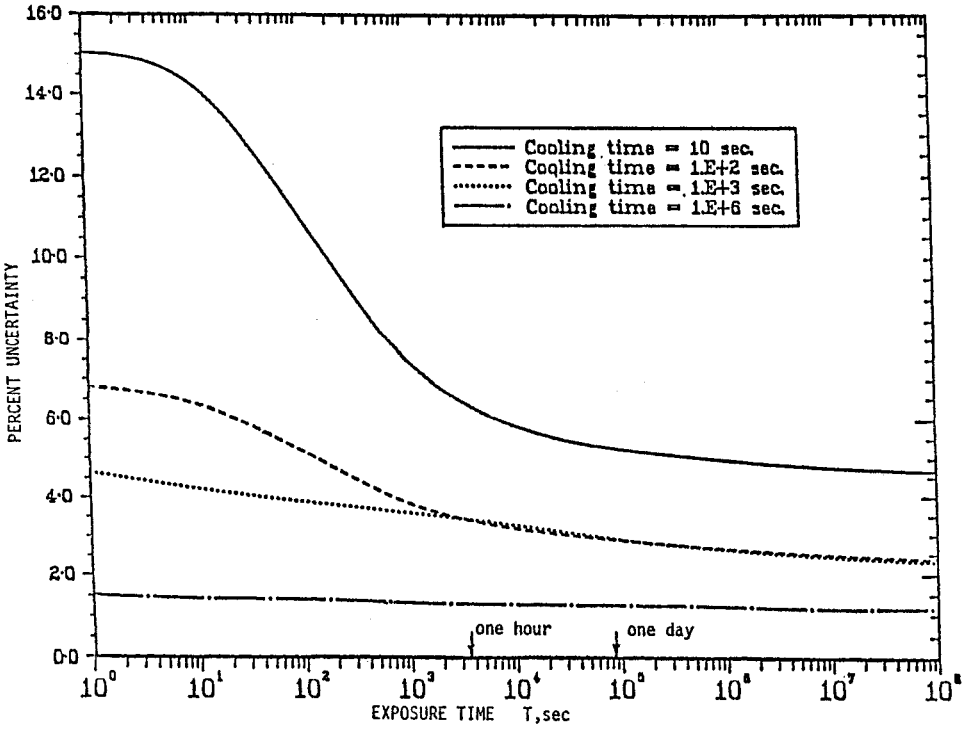

Fig. 5. Decay-heat uncertainty vs exposure time, T, and cooling time, t, for ^{235}U (Thermal).

a single nuclide near the mass yield peaks, as was found to be the case for ^{98}Zr. In the original ENDF/B-IV library, this nuclide is mistakenly listed as branching to the metastable state of ^{98}Nb.* Experience with these types of errors indicates that errors in a single nuclide can affect decay-heat values by a few per cent for a finite-irradiation exposure. Nevertheless, large errors are very unlikely. Constraints on decay energies, statistical cancellation of errors, the small contributions of individual nuclides, and the time-averaging that occurs in finite irradiations all combine to keep these problems at a minimum. In order to crudely account for additional errors of this sort, the total uncertainties in Figs. 1-4 include an extra term (not separately shown) that is as large as 4% for a burst exposure at short cooling times.[2,31]

In spite of the need for further testing and library improvements, summation methods are already useful for decay-heat calculations <u>including</u> the short cooling times less than 1000 s important for loss-of-coolant accidents. In the case of ^{238}U, only summation calculations are used to produce a nominal value.

Comparisons With LASL Measurements[12,19]

The best single agreement with ENDF/B-IV is given in Fig. 6 for ^{235}U thermal fission,[12] based on a 2×10^4 s irradiation. However, one expects the ultimate (1 σ) uncertainty in decay heat to be 2-5%, and Fig. 6 is not sufficient to show such small deviations.

For ^{233,235}U and ^{239}Pu thermal fission, Figs. 7-9 show the <u>ratio</u> of experiment to calculation of F(t,T) vs cooling time. ^{233}U is included for completeness, but is not currently used in the proposed ANS Standard. The uncertainty in the calculated ^{233}U value has not been evaluated, but we expect it to be 4 to 5% based on the analysis of ^{235}U, ^{239}Pu, and ^{238}U (Table 3). The ^{233}U results are essentially in agreement within 1 σ uncertainties. For ^{235}U, the comparison is remarkably good.

For ^{239}Pu the comparison is outside the range of evaluated uncertainties. This has received considerable attention and is discussed further in this report, but the reason for the discrepancy is not yet resolved.

Table 4 provides some comparisons of the LASL experimental data and Fig. 10 compares the ratio of all three results to calculation on a common axis. The shape deviations around 500 s and 5000 s are believed to be due to potential errors in ENDF/B-IV. Considerable effort has been made to locate this problem. The effort will be renewed if it persists in Version V. Currently, the systematic deviation of ^{239}Pu is of more concern. *It is emphasized that these data apply to a 2×10^4 s (5.56 h) irradiation.*

The LASL experiments also include measurements of gamma spectra.

---

*Some figures in this report are denoted as ENDF (Zr 98) indicating this correction, but <u>all</u> comparisons contain this important correction.

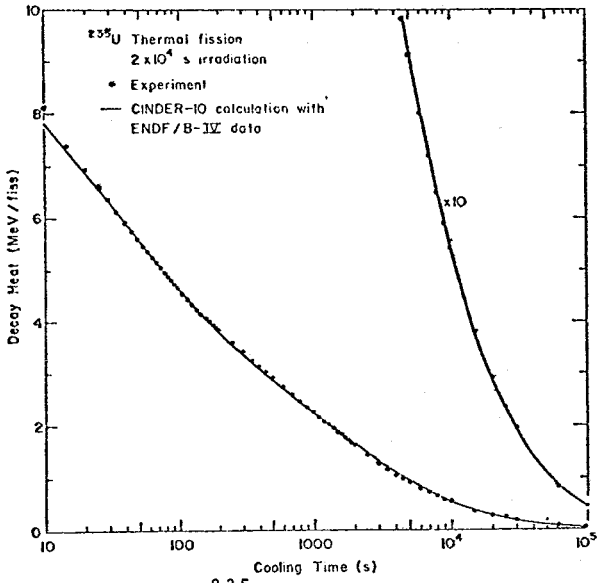

Fig. 6. LASL ^{235}U experimental decay heat and calculation for a 2 x 10^4 s irradiation at constant flux (Ref. 12).

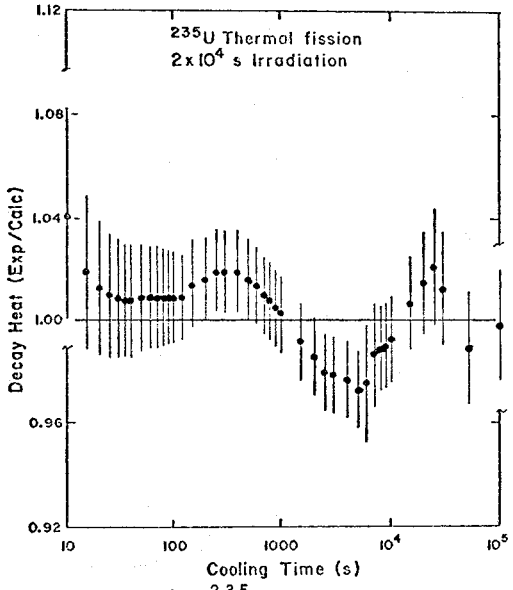

Fig. 7. LASL ^{235}U experimental decay-heat ratio to calculation. (Calculation uses ENDF/B-IV.)

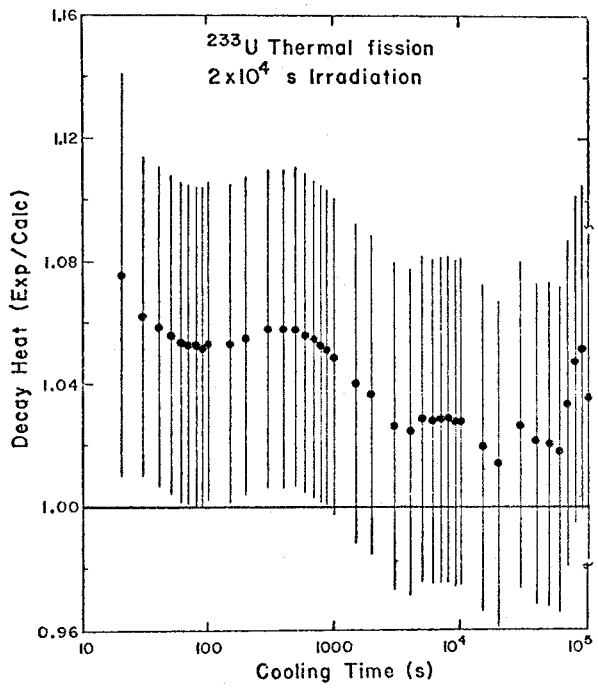

Fig. 8. LASL ^{233}U experimental decay-heat ratio to calculation. (Calculation uses ENDF/B-IV.)

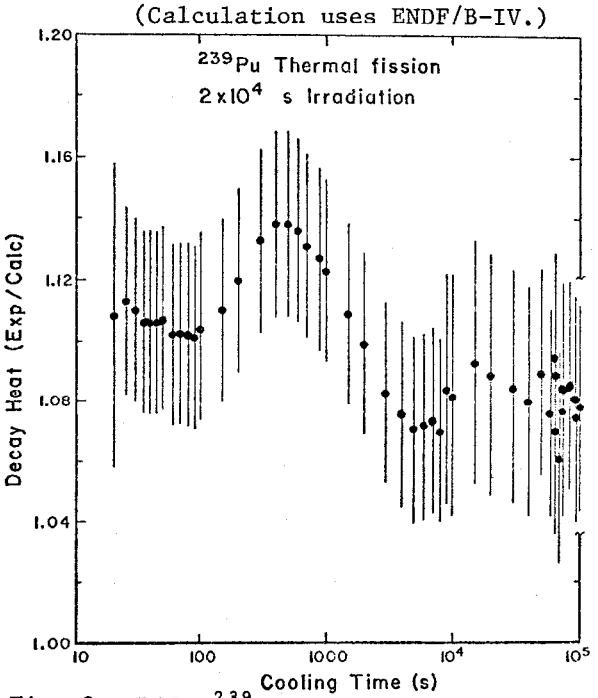

Fig. 9. LASL ^{239}Pu experimental decay-heat ratio to calculation. (Calculation uses ENDF/B-IV.)

Table 4

Some Comparisons of ^{233}U, ^{235}U, and ^{239}Pu Decay Heating From LASL Measurements[a]

(20000 s Irradiation)

Cooling Time(s)	F(t,T) in MeV/Fission ^{235}U	^{233}U	^{239}Pu
10	8.10	-	-
20	6.93	6.43	6.48
50	5.61	5.34	5.37
10^2	4.67	4.54	4.49
5×10^2	2.92	2.95	2.89
10^3	2.26	2.31	2.21
5×10^3	0.911	0.980	0.797
10^4	0.540	0.591	0.457
10^5	0.0454	0.0466	0.0467

[a] ^{235}U data are taken from Ref. 12. The ^{233}U and ^{239}Pu values are preliminary results, supplied by J. Yarnell prior to publication.

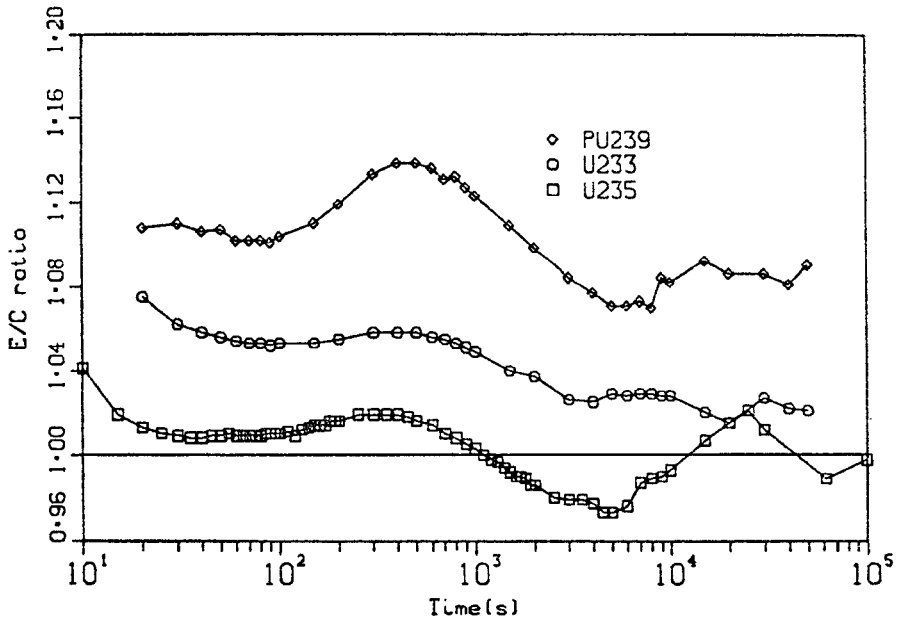

Fig. 10. Ratio of LASL decay heat measurements to ENDF/B-IV calculations (20 000 s irradiation).

Comparisons With ORNL Measurements[13,22]

The ORNL measurements are for β and γ spectra following short (1-100 s) irradiations. Figures 11 and 12 show comparisons of the energy-integrated results for ^{235}U[13] and Figs. 13 and 14 the comparisons for ^{239}Pu.[22] These comparisons are based on equivalent pulse results in order to combine, in each case, three irradiation times (1, 10, 100 s for ^{235}U and 1, 5 and 100 s for ^{239}Pu). The t f(t) ordinate is the product of the differential decay-heat function, f(t), and the cooling time in units of MeV/Fission.

For the total heating it is necessary to sum the β and γ heating. This is done and compared with the nominal and with LASL (for ^{239}Pu) in another section of this report. It will be seen that the total heating for ^{235}U is less than the calculated result by a few per cent except at times $\lesssim$ 10 s and near 10^2 s. For ^{239}Pu, the agreement is very good, being well within overlaping 1 σ uncertainties at all times.

ORNL is completing similar measurements for ^{241}Pu thermal fission, but these will not be available in time for a detailed comparison in this report. Preliminary comparison indicates good agreement with summation calculations and decay-heat values close to that of ^{235}U.

Comparison With IRT Measurements[14]

These include total β and total γ heating for several irradiation times for ^{235}U thermal fission. Only the 24 h irradiation result has been published and used in producing the nominal. The comparison with ENDF/B-IV is given in Fig. 15 for the total β + γ result. The agreement is very good, but this will be more evident in comparisons with the nominal values, shown in a later section, because of the condensed scale. There are also IRT measurements of ^{239}Pu which are not yet available for comparison.

Comparisons With The F-a-R[15,21] And UCB Measurements[16]

These calorimetric measurements have larger uncertainties than the LASL, ORNL and IRT data but are included in producing the nominal values. Results for ^{235}U are shown in Figs. 16 and 17. ^{239}Pu results by the French[21] are shown in a following section as a comparison with the nominal values.

The UCB data (^{235}U only) exceeds the calculation below a few hundred seconds (even allowing for its 1 σ uncertainty).

The ^{235}U French measurements[15] apply after ~ 100 s and within their (1 σ) uncertainty agree with calculations after ~ 200 s. Their ^{239}Pu measurement[21] has been quoted only as a derived pulse value. After ~ 300 s it deviates from the calculation about as much as the LASL result; however, the French uncertainties are much larger.

All of these comparisons will be shown in the discussion of the nominal decay heat as deviations from the nominal values.

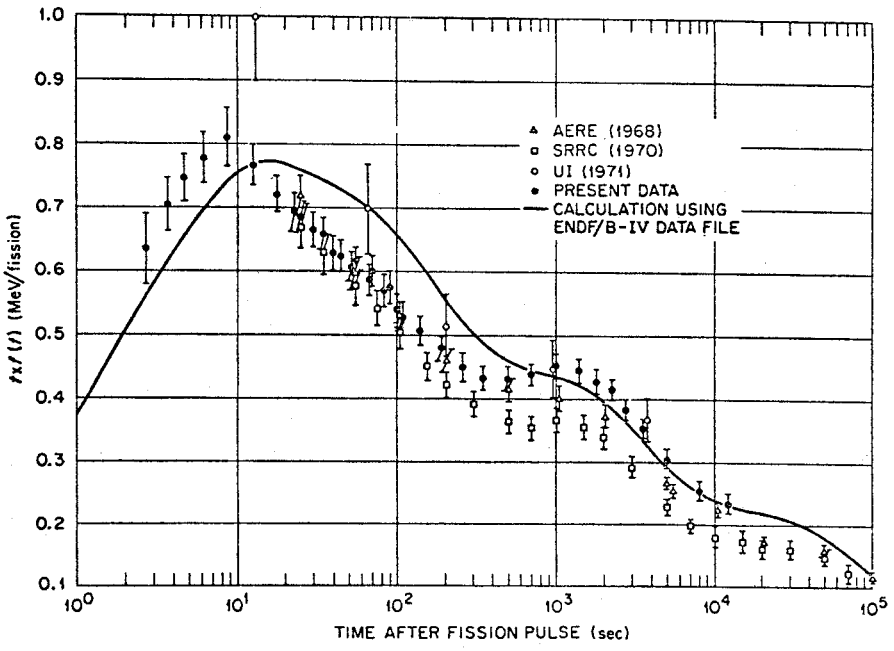

Fig. 11 ORNL ^{235}U beta experimental decay heat compared to calculation (Ref. 13). (Three irradiation times combined on a pulse basis.)

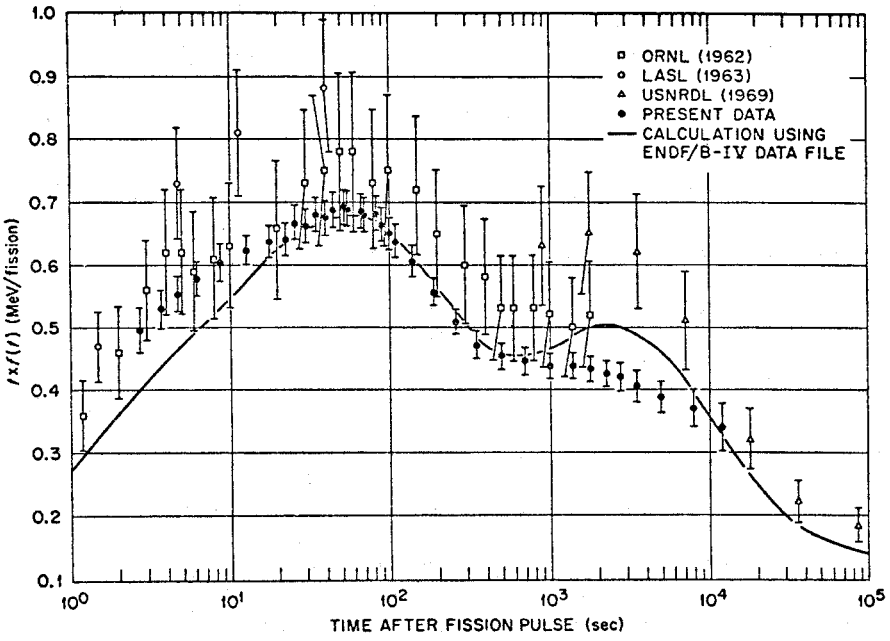

Fig. 12 ORNL ^{235}U gamma experimental decay heat compared to calculation (Ref. 13). (Three irradiation times combined on a pulse basis.)

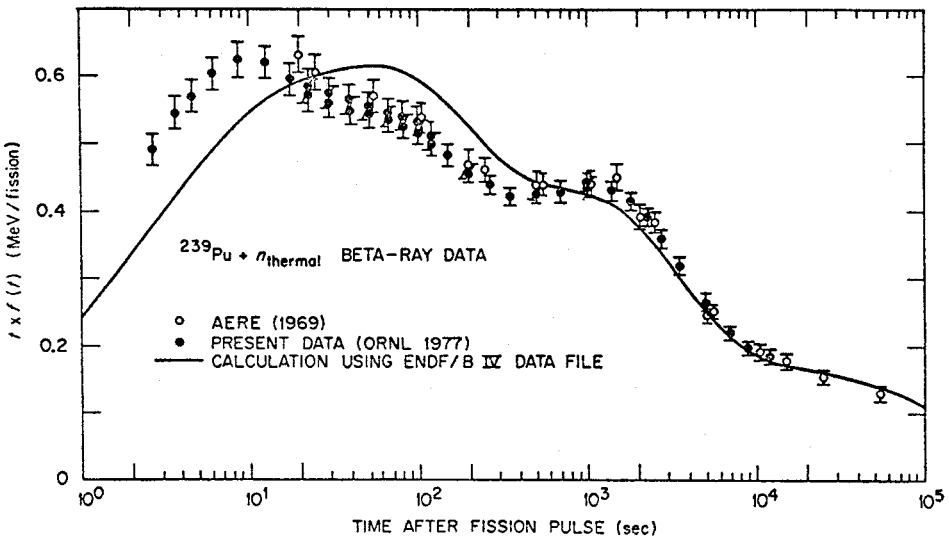

Fig. 13. ORNL ^{239}Pu beta experimental decay heat compared to calculation (Ref. 22). (Three irradiation times combined on a pulse basis.)

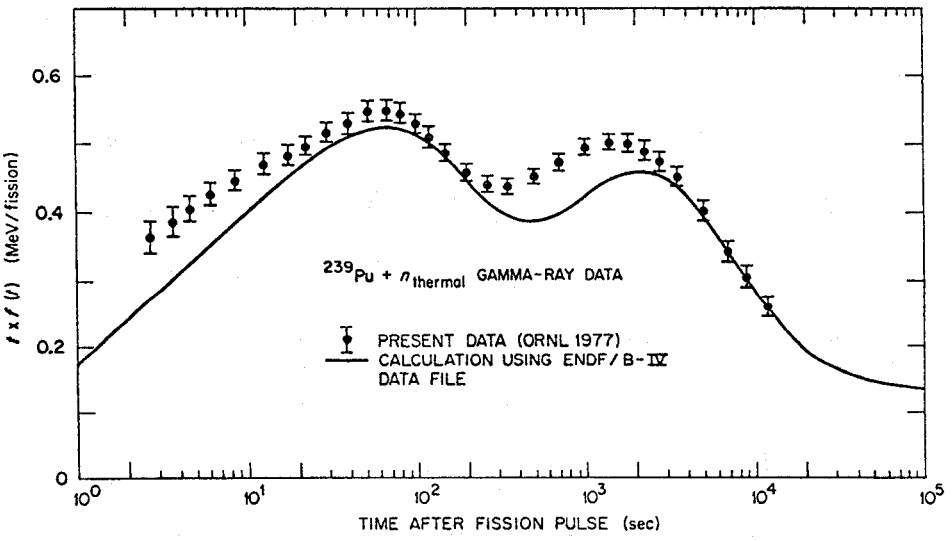

Fig. 14 ORNL ^{239}Pu gamma experimental decay heat compared to calculation (Ref. 22). (Three irradiation times combined on a pulse basis.)

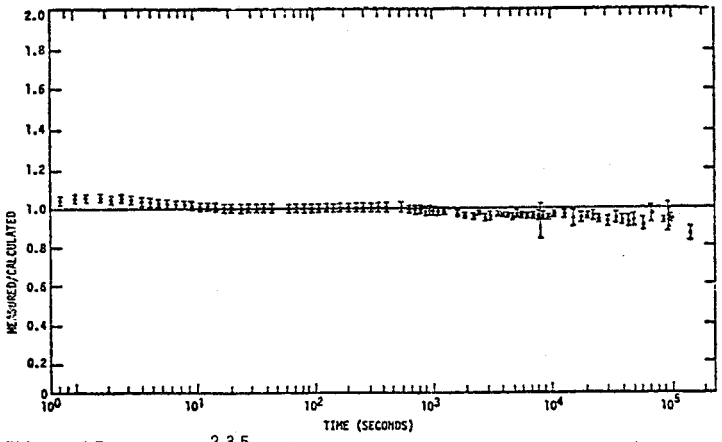

Fig. 15. IRT ^{235}U decay-heat ratio to ENDF/B-IV calculation.

Other Comparisons

A number of comparisons have also been made with older experiments, and where available, with the β and γ components. The component heating was not used in producing a nominal value and is not included in this report (see Ref. 2).

Spectral Comparisons. As noted in Table 2, approximately 130 comparisons have been made with ORNL, UI, and LASL measurements. All ^{235}U comparisons are shown in Ref. 24. Eight of the 102 ^{235}U comparisons in Ref. 24 are shown in Figs. 18-25. Figures 18-21 use 150 γ-energy groups and Figs. 22-25 use 75 β-energy groups.

Spectral comparisons constitute a stringent test of the data base. These could be expected to reveal errors in the data but to date no specific nuclide error has been identified. The comparisons are much better than originally anticipated.

We have made comparisons with the recent, unpublished ^{233}U and ^{239}Pu gamma spectra measured at LASL (E. T. Jurney and P. J. Bendt). These are equally good.

For use in reactor design codes an extensive effort has been made to reduce the calculated pulse data to 11-groups and to provide a simple functional fit to each group. The pulse functions can then be folded into any power history. Accurate, but preliminary results, including neutron absorption effects, will be presented at the semiannual ANS Meeting (June 78) in San Diego.[26]

GAS CONTENT IN FISSION PRODUCTS

Extensive calculations of the gas content (noble gases and halogens) in several irradiated fuels have been made using ENDF/B-IV data and partially reported in Ref. 27. The results are of importance to decay-heat experiments because the energy release is

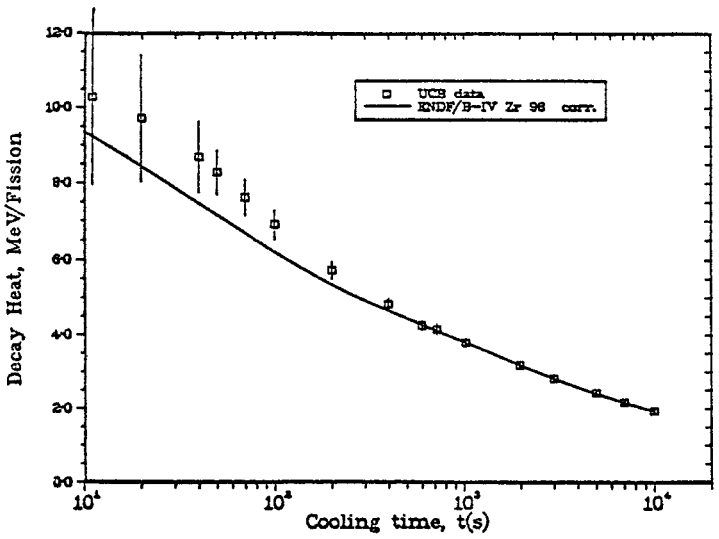

Fig. 16. UCB ^{235}U experimental decay heat compared to calculation. *(Note that values use calculation to extrapolate data to infinite irradiation.)*

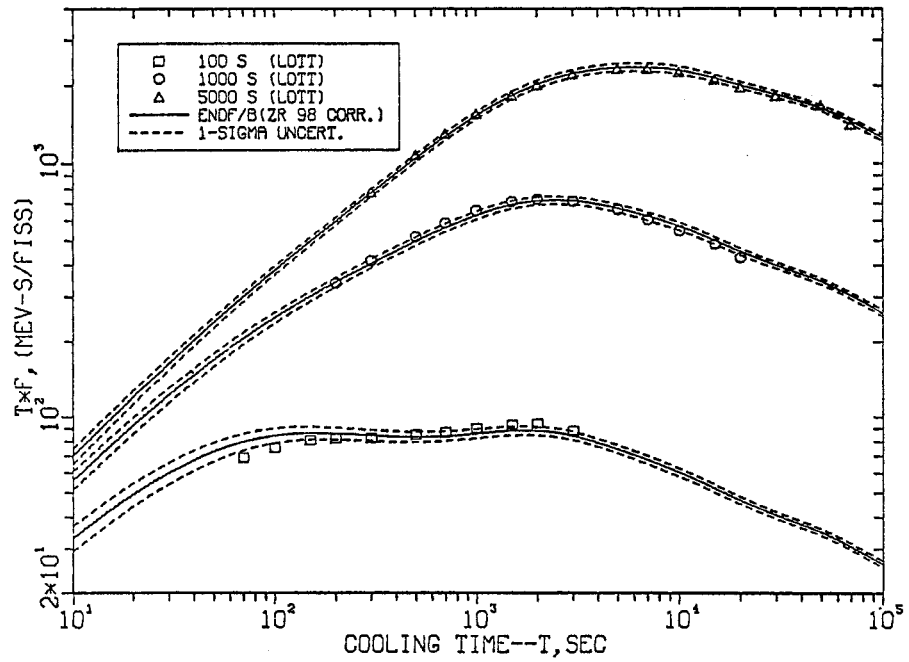

Fig. 17. F-a-R ^{235}U experimental decay-heat data compared to calculation.

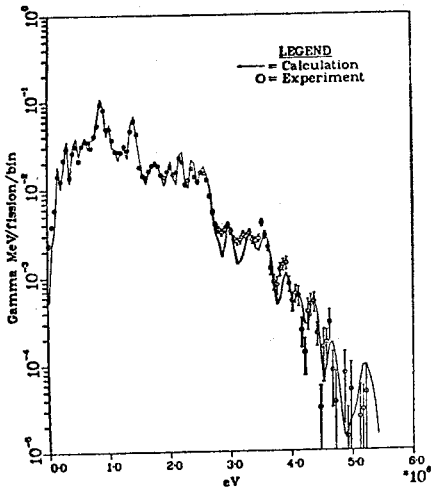

Fig. 18. LASL 5.56 h IRRAD, 660 s decay.

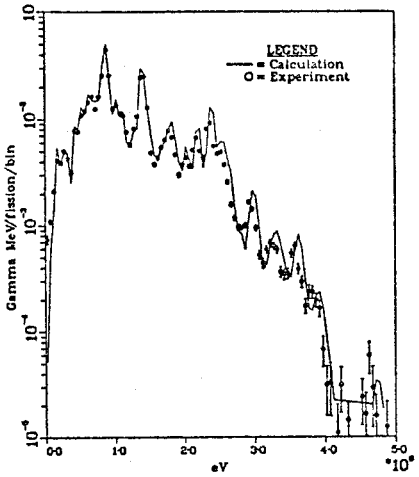

Fig. 19. LASL 5.56 h IRRAD, 5000 s decay.

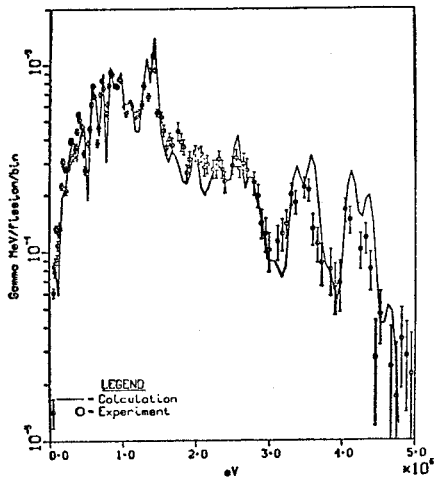

Fig. 20. ORNL 10 s IRRAD, 184.7 s decay.

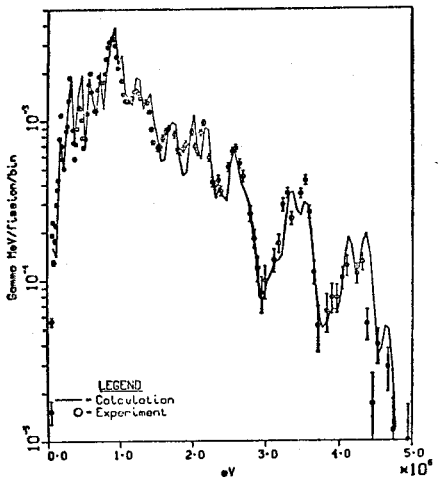

Fig. 21. ORNL 100 s IRRAD, 650.0 s decay.

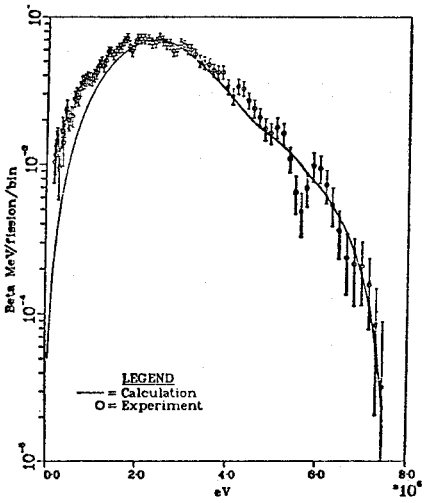

Fig. 22. ORNL 1 s IRRAD, 2.2 s decay.

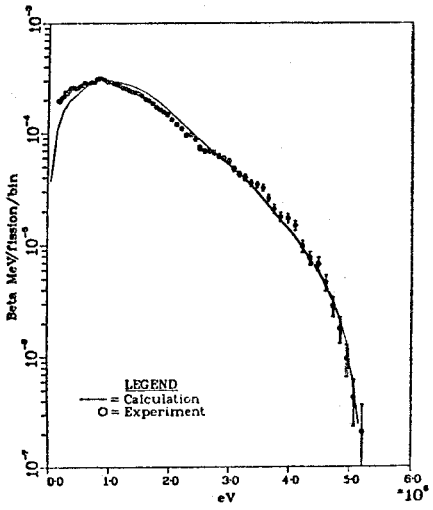

Fig. 23. ORNL 100 s IRRAD, 4950 s decay.

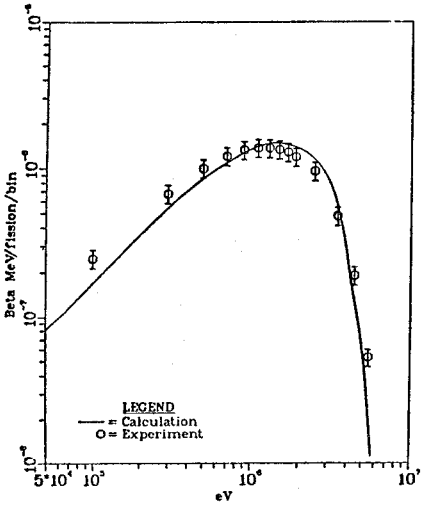

Fig. 24. UI 15 ms IRRAD, 204 s decay.

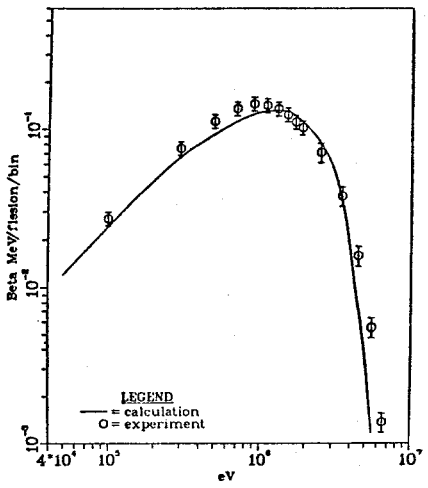

Fig. 25. UI 8 h IRRAD, 21 s decay.

considerable by comparison with the fraction of fission products that are gases. That is, a relatively small gas loss could constitute a significant loss in decay energy. Realization of the importance and potential magnitude of a gas loss in decay-heat experiments has been based on these calculations. The recent experiments have included a detection method for gas loss through the cladding of irradiated samples during and following irradiation. The ORNL measurements also include a correction for diffusion of gas through the polyethylene window.

Figures 26 and 27 show the time-dependent results following a ^{235}U and ^{239}Pu fission pulse, and Fig. 28 shows the values following an extended ^{235}U fission interval (20 000 h). Results in these plots are expressed as fractions of the corresponding quantity in the total fission-product ensemble. The fractional density curves include all gases having half-lives less than 10^{10} y but not the stable gases.

The potential seriousness of a gas loss is illustrated by the contrast at ~ 10^4 s cooling. For the ^{235}U thermal fission pulse, ~11% of the fission products are noble gases plus halogens and these constitute greater than 45% of the total gamma energy release rate. The contrast is even larger for the extended fission interval (Fig. 28) where the fractional density is only 0.5% and this fraction constitutes 34% of the total gamma energy at 10^4 s.

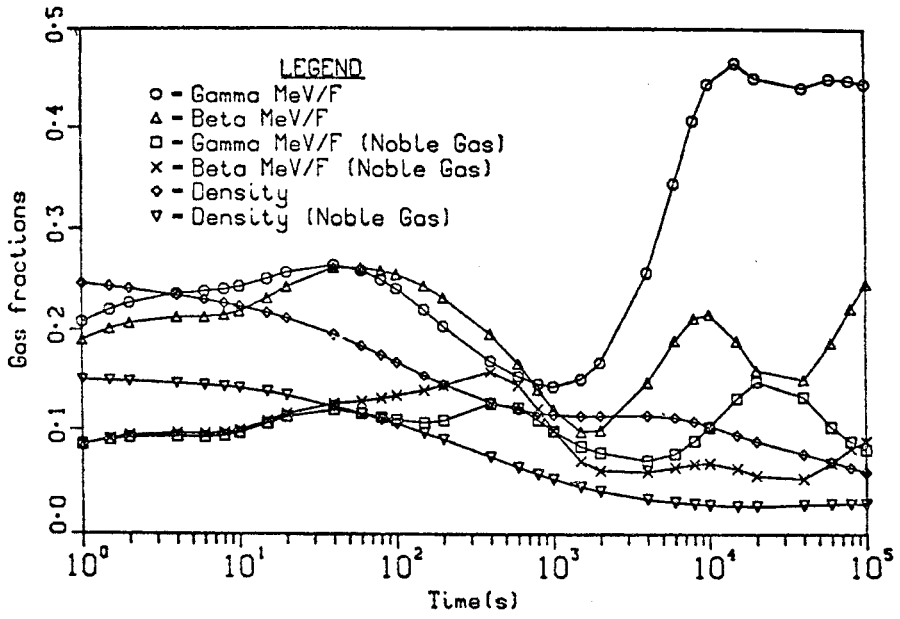

Fig. 26. Fractional gas content following a ^{235}U fission pulse (fraction of total products).

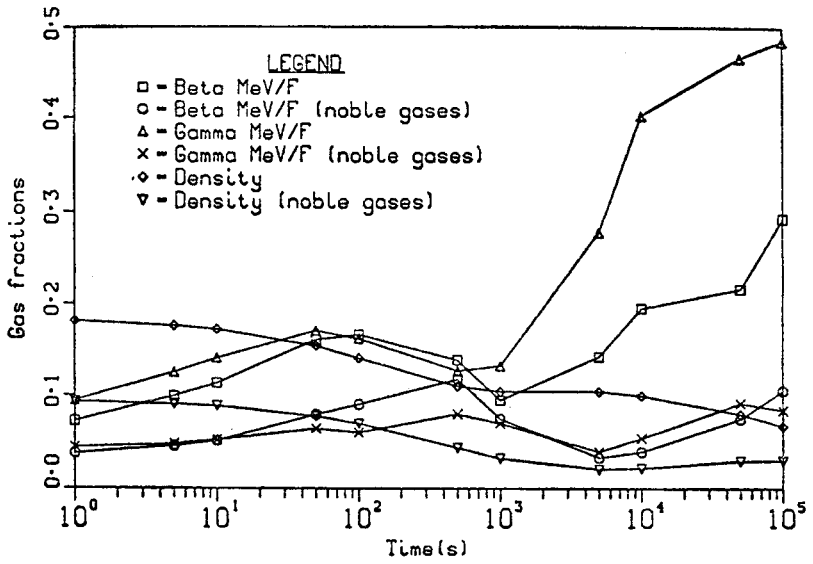

Fig. 27. Fractional gas content following a ^{239}Pu fission pulse (fraction of total products).

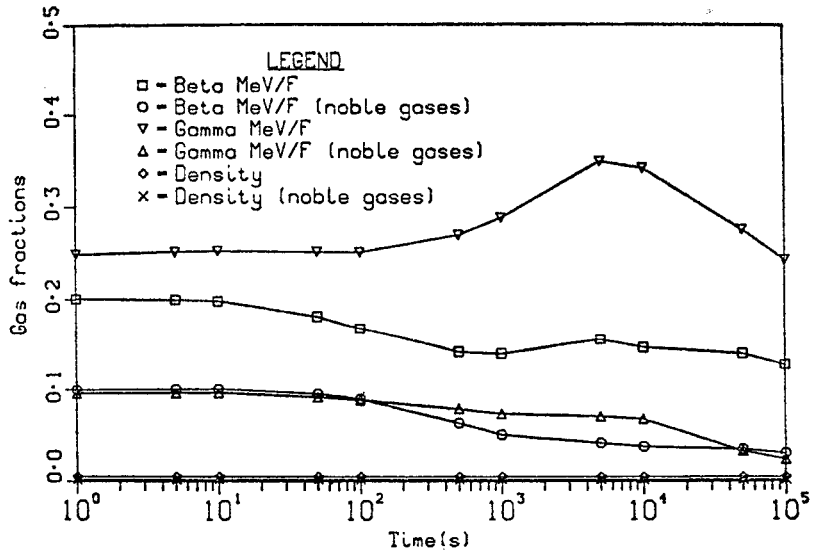

Fig. 28. Fractional gas content following a ^{235}U thermal irradiation of 20 000 h, no depletion (fraction of total products).

NEUTRON ABSORPTION EFFECT ON DECAY HEAT

For short fission intervals characteristic of the recent benchmark experiments, neutron absorption in the fission products is not important, and it is not included in the nominal values presented in the following section. It is important in realistic reactor histories, particularly at long cooling times. Nuclide coupling in the stable and long-lived nuclides tends to buildup the concentration of more unstable nuclides. The effect has been evaluated for typical reactor lifetimes and a range of flux levels. The net effect for cooling times less than 10^3 s and a thermal flux of 10^{13} n/cm^2-s is less than 1% for a 20 000 h irradiation. The effect increases with the flux level and irradiation time. For example, the effect on total heating at a thermal flux of 10^{14} n/cm^2-s reaches 2.4% for ^{235}U at a 10^3 s cooling compared to 0.1% at 10^{13} n/cm^2-s; the increase for ^{239}Pu is approximately three times these values for cooling times less than 10^3 s.

At long cooling times, (~ 8 x 10^7 s) the effect is very large, (~ 60% for a flux of 10^{14} n/cm^2-s following a 4-year irradiation, and the gamma energy increases several hundred per cent). This is due primarily to absorption in the stable nuclide ^{133}Cs which produces the shielded nuclide ^{134}Cs. The effect is dependent on the flux spectrum and particularly on the ratio of the resonance to the thermal flux.

Figures 29 and 30 show the deviation in heating for one case based on a rather large flux of 10^{14} n/cm^2-s.[1] The large gamma increase at 8 x 10^7 s due to absorption in ^{133}Cs so dominates the plot of Fig. 29 that the plot to 10^6 seconds in Fig. 30 is needed to show the result at short cooling times.

The positive effect of neutron capture on total (β plus γ) heating results primarily from the shielded nuclides ^{134}Cs, ^{136}Cs, ^{148m}Pm, ^{148}Pm, and ^{154}Eu. The contribution of ^{135}Xe to ^{136}Cs is an important exception; absorption in ^{135}Xe decreases the heating rate and this persists for greater than 10^6 s. The effect on β heating is much smaller than the γ component for times > 100 s; here, the contribution from the nuclides ^{90}Y, ^{140}La is significantly increased by absorption. All nuclides and their precursors found to be important to the absorption effect on heating are listed in Table 5.

NOMINAL DECAY HEAT

The nominal decay-heat values are produced in two steps:

a) For ^{235}U and ^{239}Pu the calculated values are combined with measurements over the cooling range of 1-10^5 s. A linear, but generalized least-squares procedure is used to produce nominal values and uncertainties following a fission pulse out to 10^5 s. The results of calculation and experiments are shown in this section

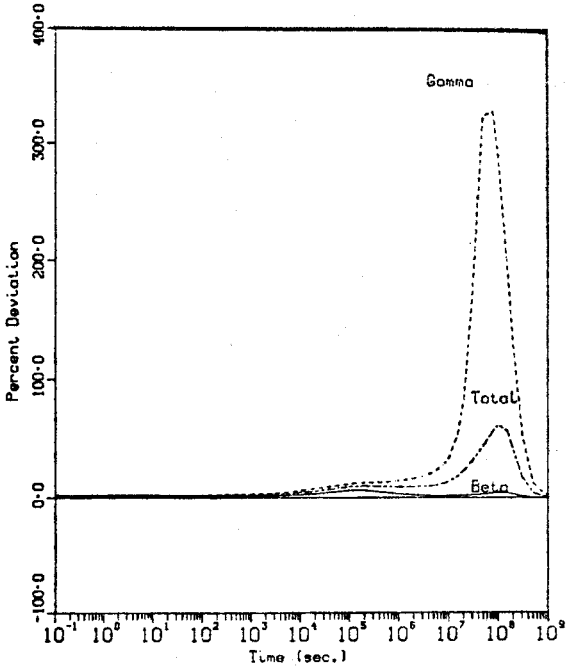

Fig. 29. Per cent deviation of decay-heating due to neutron absorption (^{235}U irrad. for 20 000 h, no dep.), $\Phi=10^{14}$.

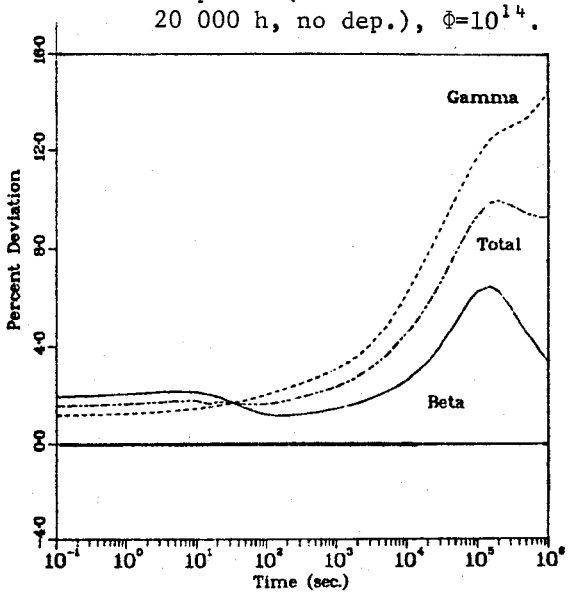

Fig. 30. Per cent deviation of decay-heating due to neutron absorption (^{235}U irrad. for 20 000 h, do dep.), $\Phi=10^{14}$.

Table 5

FISSION PRODUCTS IMPORTANT IN DETERMINATION OF NEUTRON ABSORPTION EFFECTS ON DECAY POWER

NUCLIDE	PRECURSOR(S)	NUCLIDE	PRECURSOR(S)
^{90}Y	^{89}Y, ^{90}Sr	^{148}Pm	^{147}Nd, ^{147}Pm
^{100}Tc	^{99}Tc	^{148}Pm	^{147}Nd, ^{147}Pm
^{104}Rh	^{103}Ru	^{149}Pm	^{147}Nd, ^{147}Pm
^{105}Rh	^{105}Ru		^{148}Pm, ^{148m}Pm
^{116}In	^{115}In	^{150}Pm	^{147}Nd, ^{147}Pm
^{130}I	^{129}I, ^{130m}I		^{148}Pm, ^{148m}Pm
^{134}Cs	^{133}Cs		^{149}Pm
^{135}Xe	^{135}I	^{151}Sm	^{150}Sm
^{136}Cs	^{135}Xe, ^{135}Cs	^{153}Sm	^{152}Sm
^{140}La	^{140}Ba, ^{139}La	^{154}Eu	^{153}Eu
^{142}Pr	^{141}Pr	^{156}Eu	^{155}Eu
^{144}Pr	^{144}Ce, ^{143}Pr		
^{147}Nd	^{146}Nd		

in graphical comparisons to the nominal values over the $1\text{-}10^5$ s time range.

b) The pulse values are augmented by calculated values out to 10^{13} s for ^{235}U and ^{239}Pu. For ^{238}U, only the calculated values are used. Each result is then fitted to a simple function using a non-linear least-squares code. The resulting pulse function parameters constitute the total range of the nominal heating; these functions are then used for any irradiation and cooling time.

Recommended uncertainties in the nominal values were presented in Table 4 and will not be repeated in this section.

Least-Squares Evaluation of Decay-Heat

As already noted, least-squares methods[28,29] were used to evaluate the results of recent decay-heat experiments along with summation calculations based on ENDF/B-IV. There are several reasons to use the least-squares approach. First of all, since the different experiments represent various irradiation times, one must use some means to place these data on a common irradiation basis in order to compare the various results. One technique is to use calculated values to extrapolate measured data to some common irradiation time. This method provides a useful comparison of the different experimental results but suffers from the deficiency

that one cannot easily weight the various results to obtain an average or evaluated decay-heat curve. Furthermore, the uncertainties one assigns to such an average are necessarily somewhat subjective. The least-squares method in use automatically accounts for different irradiation histories and objectively propagates quoted experimental uncertainties to obtain uncertainties for the evaluated results. Another advantage of the generalized least-squares approach is that important correlations that affect the weight of each experiment can be incorporated. Specifically, decay-heat experiments typically exhibit normalization uncertainties that affect the entire decay-heat curve in a strongly correlated fashion. And finally, simple statistical tests are available to check for experimental biases and inconsistencies.

While the least-squares method is a useful evaluation tool, one must recognize its limitations. No level of sophistication in data analysis can substitute for a physical understanding of the potential for undetected systematic errors. Also, the confidence one has in the final uncertainties as generated by the least-squares approach much in turn depend on the confidence one has in the quoted experimental uncertainties.

The least-squares method requires a linear model. For this application, the pulse decay-heat function was represented by a linear sum of decaying exponentials, a form that is easily integrated to obtain an analytic representation for the decay heat for any finite exposure. A large number of terms was used (about 5 exponentials per decay of cooling time) to ensure that the least-squares results reflected the input values rather than the underlying exponential model.

The least-squares method was applied to the measurements of LASL, ORNL, IRT, UCB, and F-a-R for ^{235}U and to the LASL, ORNL, and F-a-R data for ^{239}Pu along with values obtained by summation calculations using ENDF/B-IV. The experimental uncertainties initially used were those quoted by the experimentalists, although some additional judgement was needed to completely specify the required correlations. No attempt was made to reanalyze the experiments to obtain independently assessed uncertainties.

^{235}U Evaluation. The initial evaluation disclosed that the ORNL values were inconsistent in normalization and that the IRT data showed fluctuations that were large compared to their quoted statistical errors. Consequently, a second evaluation was performed with the ORNL normalization uncertainty increased by about a factor of 2 and with the IRT statistical uncertainties increased by a factor of 2.

Uncertainties in the resulting pulse values do not reflect experimental biases or inconsistencies that are not accounted for in the input uncertainties.

Detailed comparisons are shown in Figs. 31 and 32 which display the fractional deviations of the different inputs from the evaluated or nominal values (the pulse values from the ENDF/B results are shown [Fig. 32] only for comparison; the 20 000 s ENDF/B

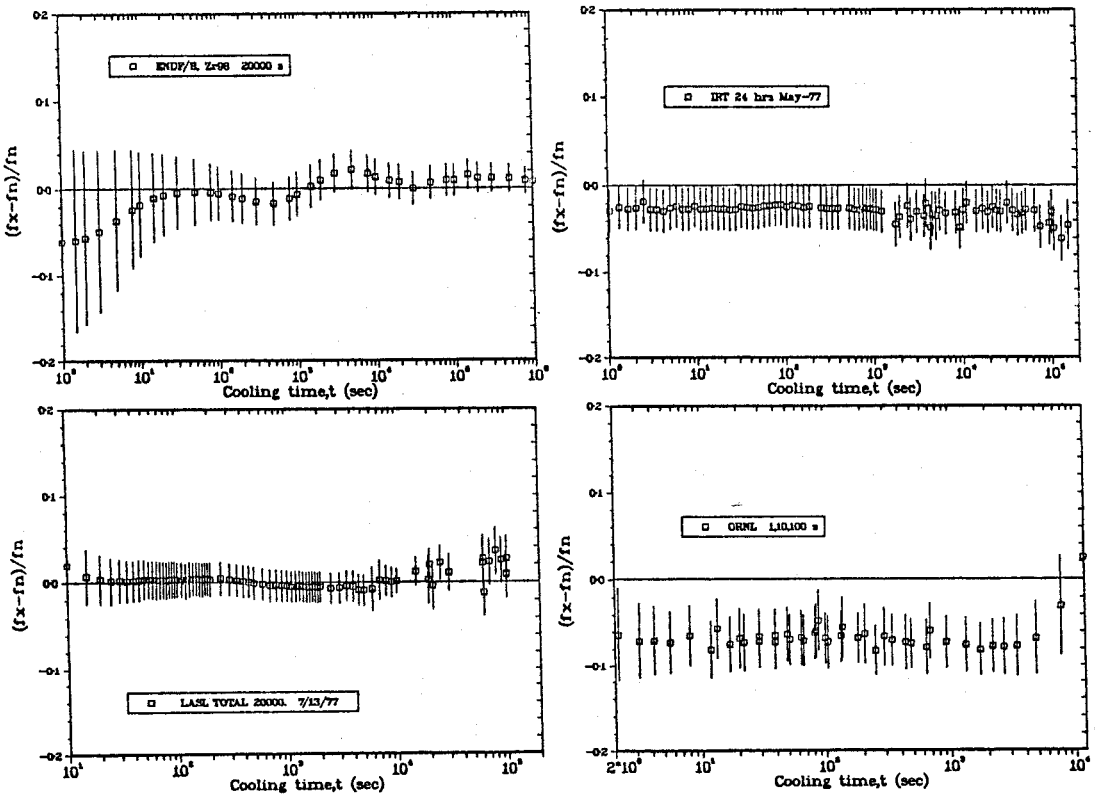

Fig. 31. Fractional deviation of decay-heat measurements and calculations from nominal values as determined by least-squares method for ^{235}U. (Uncertainties are 1 σ.)

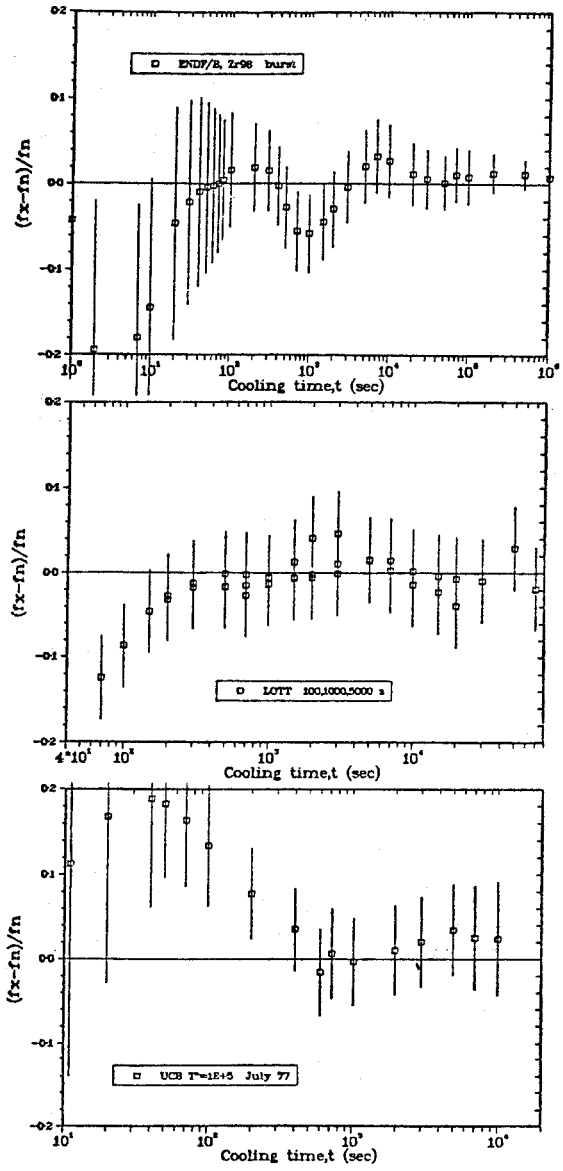

Fig. 32. Fractional deviation of decay-heat measurements and calculations from nominal values as determined by least-squares method for ^{235}U (cont.). (Uncertainties are 1 σ.)

values were used as input in the evaluation to take some advantage of the previously discussed time averaging of any errors in the ENDF/B-IV data base).

The inconsistency of the ORNL normalization with the evaluated values is readily apparent in the figure. *It is important to emphasize that this inconsistency is a direct consequence of the constraining influence of the LASL and ENDF results.* In order to conclude that the ORNL values are actually low as shown in the figure, one must have confidence that the LASL and ENDF uncertainties used in the evaluation fairly reflect the true uncertainties in the corresponding values. If the quoted ORNL uncertainties represent a truer estimate of the actual uncertainties, the picture would obviously change. The power of the least-squares method lies in its ability to compare the various results and obtain an objective evaluation. It cannot guarantee the validity of quoted uncertainties in the input data sets.

^{239}Pu Evaluation. ^{239}Pu data are more limited and inconsistent. For example, the LASL and ORNL ratios to calculations are compared in Fig. 33. In this case we have "extrapolated" the ORNL data to a 20 000 s irradiation using summation calculations. The deviation at ~ 500 s was discussed in a previous section; here it is interesting that both the LASL and ORNL measurements show the same shape deviation from calculation. Figure 34 shows the ratio of the LASL to the ORNL measurements, again using an extrapolation of the ORNL data to a 20 000 s irradiation. Clearly, the measured data are inconsistent.

We initially believed that there was a normalization error in the LASL ^{239}Pu measurement, but subsequent, unpublished measurements by J. Yarnell have essentially eliminated this possibility. Also he has repeated the ^{235}U measurements since the ^{239}Pu measurements and obtained essentially the same result as shown in an earlier section of this report. In addition, the LASL, ORNL, and F-a-R measurements all have a smaller decay-heat ratio of ^{235}U to ^{239}Pu than is calculated. Thus the measured ratios are more consistent than the absolute heating values. However, it is also true that calculated ratios using independent data compilations (UK and French) are more consistent with the ENDF/B-IV calculations than with ratios of the measurements. If the LASL data are correct, then the ENDF/B-IV data (and the ORNL measurements) are deficient for ^{239}Pu. In the event of ENDF/B-IV being in error, one first suspects the yield data. However, we have examined the ENDF/B-IV mass chain yields and model parameters for the independent yields, and have also compared in the following section, calculations using Version V yields. It appears to be very unlikely that the calculations are in error due to ^{239}Pu yield errors. The ^{239}Pu yields do emphasize different mass chains; those chains having large ^{239}Pu - ^{235}U yield differences have been examined for errors in decay parameters; none were found. This work is still in progress.

The nominal value is necessarily based on the existing data and uncertainties even though more consistent data are desirable.

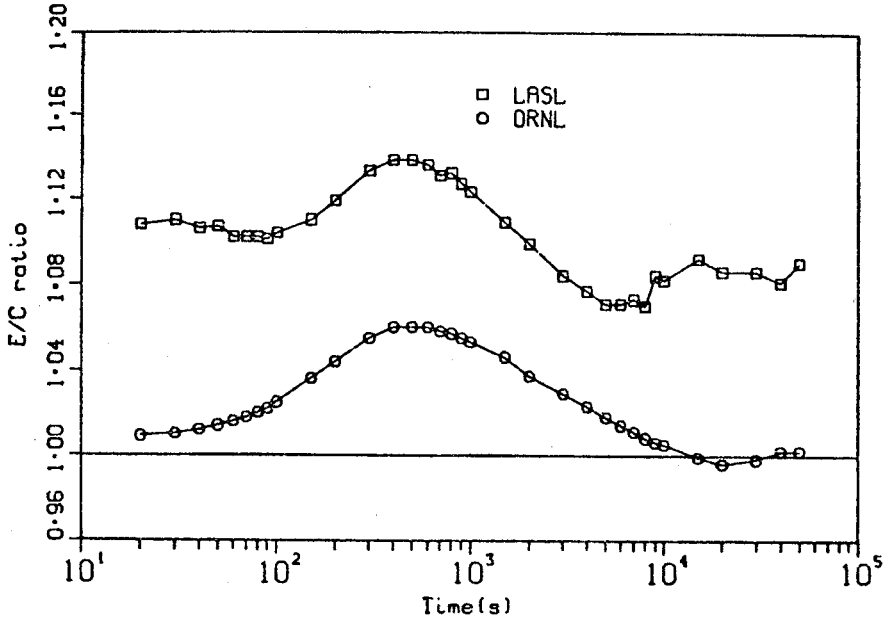

Fig. 33. ^{239}Pu decay-heat ratio of experiment to calculation following a 20 000 s irradiation (calculation uses ENDF/B-IV).

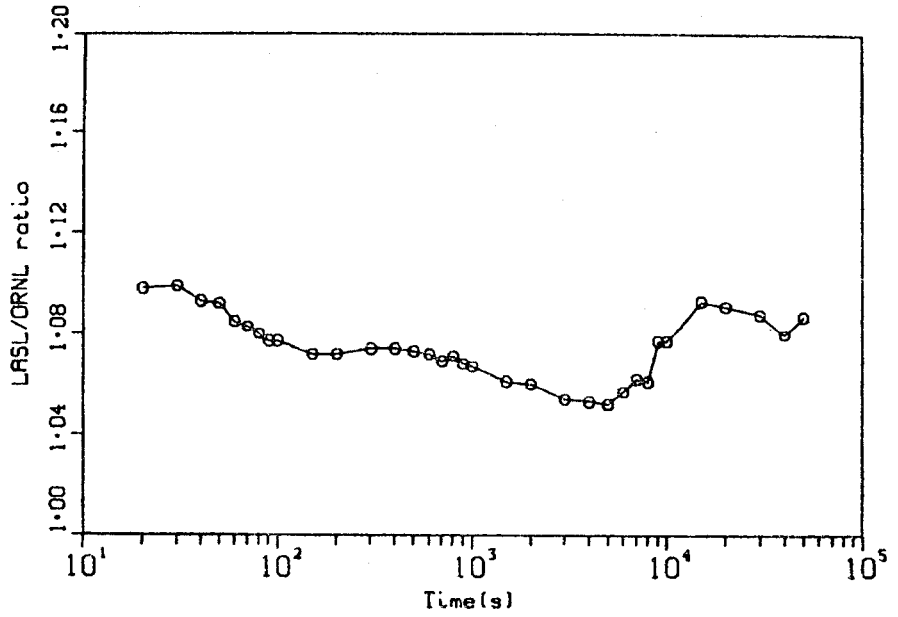

Fig. 34. ^{239}Pu decay-heat ratio of LASL to ORNL following a 20 000 s irradiation.

There is no reason to expect an overall normalization error in summation calculations, but one was permitted in this case (2%) because of the unresolved discrepancy with the LASL data. The effect was an upward shift of the nominal by about 0.8%.

The final comparisons with the nominal values are shown in Fig. 35 for ^{239}Pu.

Functional Fits To The Nominal Values

As noted, the ^{235}U and ^{239}Pu nominal pulse was augmented by calculation between 10^5 and 10^{13} s (~ 300 000 years) cooling. This is necessary because the experiments do not account for heating at long cooling times and for long irradiation times. For ^{238}U, only the calculated pulse is used for all cooling times.

Let

$f(t)$ = the "differential decay-heat function" for the fission pulse at a cooling time t in units of MeV/fission-s.

$F(t,T)$ = the "integral decay-heat function" at a cooling time t following an extended, constant fission rate for an interval T in units of MeV/Fission (t and T in seconds).

In the absense of neutron capture

$$F(t,T) = \int_{t}^{t+T} f(t')dt' \quad . \tag{1}$$

The f(t) pulse function, once obtained, is very convenient for applications, but if the above integral is carried out to infinity (conceptually possible only in the absence of neutron absorption effects), then the resulting $F(t,\infty)$ function has the same informational content. Thus

$$F(t,T) = F(t,\infty)-F(t+T,\infty) \quad . \tag{2}$$

As in the generalized least-squares analysis, we chose a sum of decaying exponentials to represent f(t):

$$f(t) \simeq \sum_{i=1}^{m} \alpha_i \, e^{-\lambda_i t} \tag{3}$$

In this case, we found that it was necessary to use a non-linear least-squares fit[1,26] in order to reduce the number of exponentials while maintaining an accurate fit. In addition, we found it was necessary to use ~ 6 points per time decay of cooling (~ 80 points)

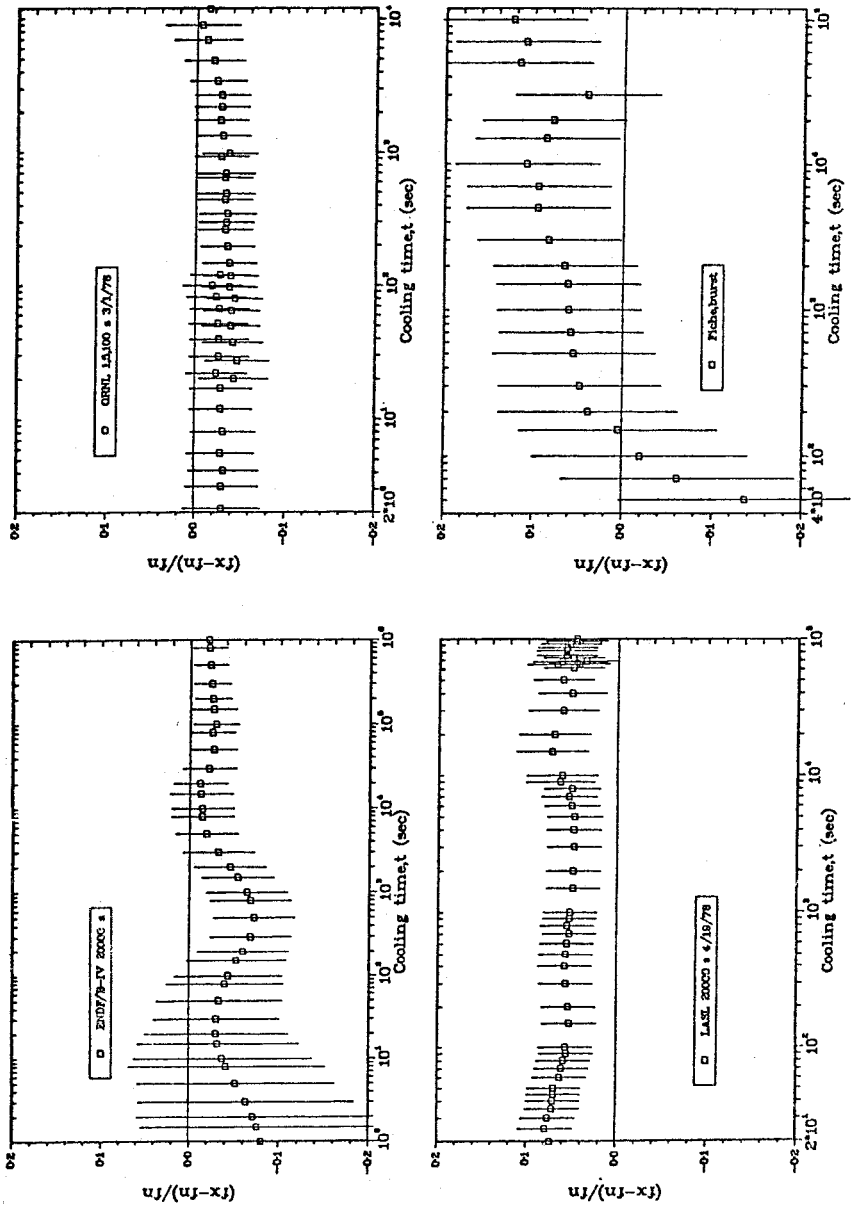

Fig. 35. Fractional deviation of decay-heat measurements and calculations from nominal values as determined by least-squares methed for ^{239}Pu. (Uncertaintie are 1 σ.)

to maintain an accurate calculation of the F(t,T) value. In this application the reader should recall that the uncertainty in the nominal is, for ^{235}U, < 2% for most decay times, so that a highly accurate fit is essential.

At the worst fitted point, accuracy within a few tenths per cent for the pulse and within a few hundreths per cent for the finite irradiation (within ~ $\sigma/10$) was achieved using 23 exponentials. The resulting α, λ coefficients are listed in Table 6.

Values in Table 6 can be used with Eq. (3) for the pulse. For finite irradiation times at a constant fission rate for T seconds the heating is

$$F(t,T) = \sum_{i=1}^{m} \frac{\alpha_i}{\lambda_i} e^{-\lambda_i t} (1-e^{-\lambda_i T}) \quad . \tag{4}$$

The methodology in the new ANS 5.1 proposed standard uses the functional fits to generate all tabular data. However, it should be noted that for practical reasons 10^{13} s is used for infinity, i.e.,

$$F(t,\infty) \equiv F(t,10^{13}) \quad . \tag{5}$$

The reader is reminded that these nominal functions do not account for neutron absorption effects discussed in a previous section.

COMPARISONS USING ENDF/B-V YIELDS

It was originally expected that preliminary ENDF/B-V decay data, in addition to yields, would be available for some decay-heat comparisons in this report, as is indicated by the title. The expected decay file content, summarized in Table 1, for ENDF/B-V are not yet complete. We have evaluated the effects of some new or improved decay data, particularly in seeking the cause of the anomalous deviations at 500 s and 5 000 s evident in Figs. 10 and 33; this effort is discussed in Ref. 2.

More importantly, the problem with ^{239}Pu decay heating has focused attention on the yield data, as already noted. There is a preliminary, near final set of ENDF/B-V yields. These have been incorporated with ENDF/B-IV decay data and the results of pulse calculations compared for ^{235}U and ^{239}Pu thermal fission. The results are given in Table 7.

Clearly, the new yield evaluation does not explain the large deviation of the LASL experiment from calculation even though many individual yields have changed significantly and particularly so for ^{239}Pu.

Preliminary comparison calculations by Tobias[30] using the ENDF/B-IV and the UK independent yield evaluation by Crouch also indicate that the yield data will not explain discrepancies between

^{239}Pu calculations and the LASL experiments. (The decay file used by Tobias could be considered intermediate to ENDF/B-IV and -V; he has corrected errors previously identified[4] and others, and attempted to merge the best data from the UK and ENDF/B-IV files.[30])

Table 7

EFFECT OF ENDF/B-IV YIELDS
% DIFFERENCE OF VERSION V FROM VERSION IV
- PULSE VALUES ONLY -

Cooling Time(s)	^{235}U β	^{235}U γ	^{235}U Total	^{239}Pu β	^{239}Pu γ	^{239}Pu Total
10^0	- 2.4	- 0.3	- 2.4	+ 1.3	- 0.3	+ 0.6
5×10^0	- 2.2	- 2.0	- 2.1	+ 1.0	- 1.0	+ 0.2
10^1	- 1.1	- 1.2	- 1.0	+ 1.0	- 0.8	+ 0.3
5×10^1	- 0.3	- 0.1	- 0.2	+ 0.5	0.0	+ 0.2
10^2	- 0.4	0.0	- 0.2	- 0.3	- 0.2	- 0.2
5×10^2	- 0.1	+ 1.0	+ 0.4	+ 0.4	+ 1.2	+ 0.7
10^3	+ 0.1	+ 0.9	+ 0.5	- 0.1	0.0	+ 0.1
5×10^3	+ 0.3	+ 0.7	+ 0.5	+ 0.3	+ 1.5	+ 1.0
10^4	- 0.1	+ 0.4	+ 0.2	+ 1.1	+ 2.8	+ 2.2
5×10^4	- 0.3	- 0.1	- 0.2	+ 0.2	+ 0.6	+ 0.4
10^5	- 0.3	0.0	- 0.2	+ 0.4	+ 1.2	+ 0.9

Parenthetically, there are other a priori reasons to expect that the yields are <u>not</u> the cause of the decay-heat discrepancy with the LASL measurements, and as already shown in Fig. 34, the ORNL measurement differs from LASL by almost as much as the calculation.

COMPARISON OF NOMINAL VALUES WITH THE 1973 ANS DRAFT STANDARD AND ENDF/B-IV

Table 8 includes some tabular comparisons of the ^{235}U and ^{239}Pu nominal values with ENDF/B-IV and associated 1 σ uncertainties. Graphical comparisons were included in a previous section (Figs. 31, 32 and 35), for the pulse and 20 000 s cases.

Figure 36 compares the proposed ^{235}U "infinite" irradiation (no absorption) nominal values with the 1973 ANS 5.1 Draft Standard

Table 6

Parameters
For
Pulse and finite irradiation decay-heat
Functions f(t) and F(t , T)
(5/78)

U-235 Thermal		U-238 Fast		Pu-239 Thermal	
α	λ	α	λ	α	λ
6.5057E-01	2.2138E+01	1.2311E+00	3.2881E+00	2.0830E-01	1.0020E+01
5.1264E-01	5.1587E-01	1.1486E+00	9.3805E-01	3.8530E-01	6.4330E-01
2.4384E-01	1.9594E-01	7.0701E-01	3.7073E-01	2.2130E-01	2.1860E-01
1.3850E-01	1.0314E-01	2.5209E-01	1.1118E-01	9.4600E-02	1.0040E-01
5.5440E-02	3.3656E-02	7.1870E-02	3.6143E-02	3.5310E-02	3.7280E-02
2.2225E-02	1.1681E-02	2.8291E-02	1.3272E-02	2.2920E-02	1.4350E-02
3.3088E-03	3.5870E-03	6.8382E-03	5.0133E-03	3.9460E-03	4.5490E-03
9.3015E-04	1.3930E-03	1.2322E-03	1.3655E-03	1.3170E-03	1.3280E-03
8.0943E-04	6.2630E-04	6.8409E-04	5.5158E-04	7.0520E-04	5.3560E-04
1.9567E-04	1.8906E-04	1.6975E-04	1.7873E-04	1.4320E-04	1.7300E-04
3.2535E-05	5.4988E-05	2.4182E-05	4.9032E-05	1.7650E-05	4.8810E-05
7.5595E-06	2.0958E-05	6.6356E-06	1.7058E-05	7.3470E-06	2.0060E-05
2.5232E-06	1.0010E-05	1.0075E-06	7.0465E-06	1.7470E-06	8.3190E-06
4.9948E-07	2.5438E-06	4.9894E-07	2.3190E-06	5.4810E-07	2.3580E-06
1.8531E-07	6.6361E-07	1.6352E-07	6.4480E-07	1.6710E-07	6.4500E-07
2.6608E-08	1.2290E-07	2.3355E-08	1.2649E-07	2.1120E-08	1.2780E-07
2.2398E-09	2.7213E-08	2.8094E-09	2.5548E-08	2.9960E-09	2.4660E-08
8.1641E-12	4.3714E-09	3.6236E-11	8.4782E-09	5.1070E-11	9.3780E-09
8.7797E-11	7.5780E-10	6.4577E-11	7.5130E-10	5.7300E-11	7.4500E-10
2.5131E-14	2.4786E-10	4.4983E-14	2.4188E-10	4.1380E-14	2.4260E-10
3.2176E-16	2.2384E-13	3.6654E-16	2.2739E-13	1.0880E-15	2.2100E-13
4.5038E-17	2.4800E-14	5.6293E-17	9.0536E-14	2.4540E-17	2.6400E-14
7.4791E-17	1.5699E-14	7.1602E-17	5.6098E-15	7.5570E-17	1.3800E-14

and with this value plus 20% and - 40% to 10^3 s; for times > 10^3 s the envelope is plus 10% and - 20%. For the hypothetical LOCA, LWR designs now use the ANS 5.1 + 20% heating for infinite irradiation for all fuels. The 1973 draft standard specified the above ranges as uncertainties and, in a footnote, noted that the upper limit "refers to the interval above the standard within which the true value may reside". Thus the meaning of the uncertainty was not adequately defined. As noted earlier, the draft standard was based on measurements that were incomplete (e.g., gamma measurements only in some time ranges), and decidely inadequate to support an uncertainty of less than 15 to 20%. Therefore the ANS 5.1 + 20% value was not, at the time, at all unreasonable.

In our comparison we have assumed that the + 20% is an ill-defined confidence limit, whatever was originally intended by the 20% uncertainty, and used 2 σ uncertainty bars on the nominal points.

The 20% ^{235}U "uncertainty" can now be reduced to a well supported 2 σ of ~ 4% (see 1 σ values in Table 3). Representatives of the reactor venders have noted that such a large reduction in uncertainty is worth many millions of dollars to the reactor industry.

Figure 37 compares the ^{239}Pu and ^{238}U heating values with ^{235}U for the infinite irradiation case.

These figures have been plotted only to 10^5 s because of the interest in LOCA analysis, but the nominal value is intended to apply to 10^9 s (finite irradiation). As noted earlier, absorption effects can be very important at long cooling times; this is incorporated into the new, but preliminary ANS 5.1 standard.

SUMMARY

This report is itself essentially a summary document of the very significant progress represented by ENDF/B-IV as a nuclide data base. We have used the recent, high quality decay-heat experiments and the generation of a new nominal decay-heat function, having very significant economical import, as a focal point to present comparisons. However, many more comparisons have been made than presented in this report, particularly in the area of spectra.

While the improvement in decay heat in the range of interest to the LOCA would justify all effort to date, there are other uses for the data base, and some data are definitely in need of improvement:

- Short-lived nuclides far from stability require greatly improved decay energy data.
- We did not show the comparisons with the beta and gamma components of the total energy. This split in the total energy is not as well determined as is the total.

TABLE 8

PER CENT DEVIATION OF ENDF/B-IV FROM NOMINAL VALUES
- 5/15/78 -

COOLING TIME(S)	^{235}U PULSE	^{235}U INFINITE	^{239}Pu PULSE	^{239}Pu INFINITE
10^0	- 8.5 (19., 40.)[A]	- 5.6 (6.9, 3.3)	-22.3 (27., 54.)	- 7.1 (8.4, 5.6)
10^1	-14.2 (15., 3.2)	- 1.8 (4.8, 2.0)	-14.7 (17., 4.9)	- 3.3 (6.3, 4.2)
10^2	+ 0.9 (6.8, 1.8)	- 0.5 (2.5, 1.8)	+ 3.0 (9.8, 3.9)	- 3.5 (3.9, 4.2)
10^3	- 6.0 (4.6, 1.8)	- 0.3 (2.4, 1.8)	-10.6 (5.5, 3.8)	- 4.1 (3.6, 4.4)
10^4	+ 2.2 (4.3, 1.8)	+ 0.4 (2.0, 1.7)	- 1.5 (5.9, 4.6)	- 1.0 (2.6, 4.8)
10^5	+ 0.8 (3.2, 1.7)	+ 0.02 (1.4, 2.0)	- 2.0 (3.7, 4.0)	- 0.1 (1.9, 5.0)

[A] VALUES IN PARENTHESES ARE EVALUATED UNCERTAINTIES (1 σ) IN SUMMATION CALCULATIONS FOLLOWED BY PROPOSED 1 σ UNCERTAINTIES IN NOMINAL VALUES.
FOR LONGER TIMES AND FOR ALL ^{238}U VALUES, THE NOMINAL VALUES ARE BASED ENTIRELY ON ENDF/B-IV DATA USED IN SUMMATION CALCULATIONS.

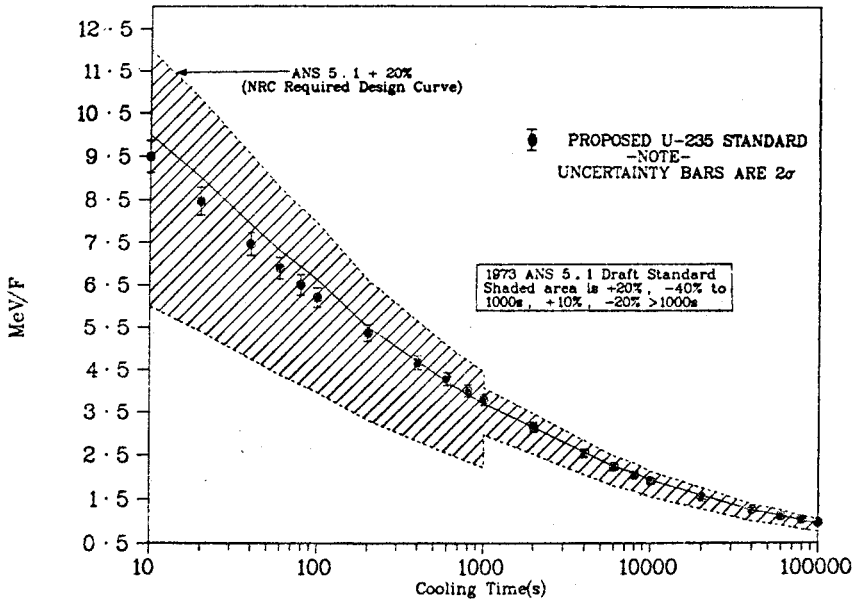

Fig. 36. Comparison of Proposed Nominal (2 σ Uncertainty Bars) With ANS 5.1 (Infinite Irradiation, No Depletion or Absorption Effects).

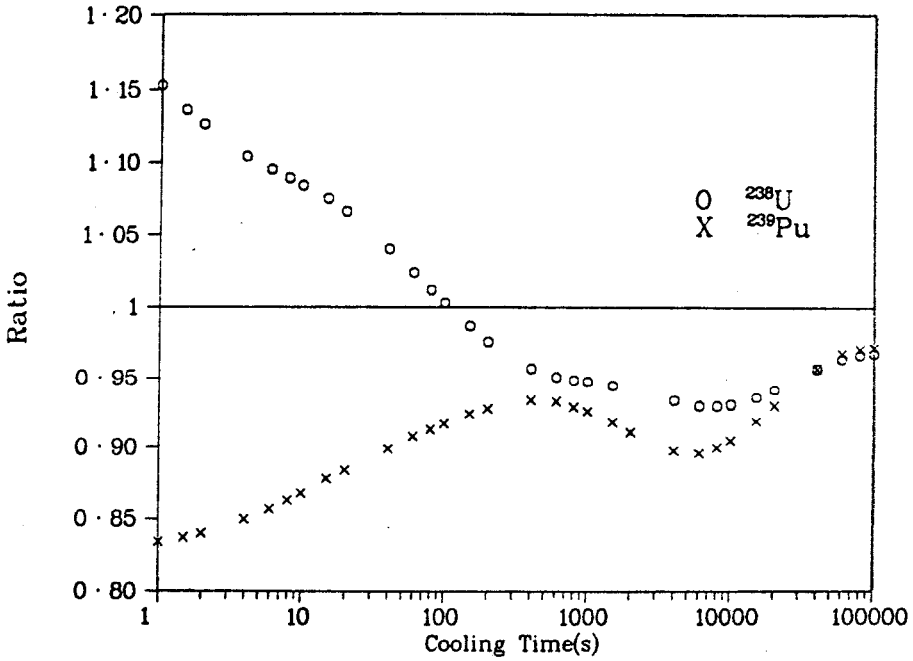

Fig. 37. Ratio of ^{239}Pu and ^{238}U Nominal Decay Heating to ^{235}U Nominal
-------- Infinite Irradiation --------.

- There are clearly gaps in our knowledge of, or errors in, some of the longer-lived nuclides.
- Spectral data are very inadequate for use at short cooling times.
- Long-lived nuclides important to fuel cycles, transportation and waste management have not been adequately examined.
- For some applications it is important to know independent fission yields; this is an area of considerable theoretical attention but sparse experimental data. For example, we are on the threshold of being able to accurately calculate delayed neutron yields and spectra, and such quantities as prompt neutron emission, and the total energy release in fission. All of these areas have been examined using the ENDF/B data, succeeding remarkably well in some cases and failing in others.
- Experimental and calculational discrepancies for ^{239}Pu heating are unresolved as of 5/78.
- The subject of absorption buildup has been recently reviewed.[32] Based on the most extensive measurements available, the review noted that the calculated resonance absorption may be significantly low.

Nevertheless, we believe that the comparisons in this and other reports[1,2,32] have demonstrated the value of summation calculations and the need for continued support in improving and expanding the data base.

ACKNOWLEDGMENT

We have been fortunate in having the close cooperation of those people involved in recent measurements, particularly J. L. Yarnell and E. T. Jurney (LASL), J. K. Dickens and R. W. Peelle (ORNL), N. R. Lurie (IRT) and V. E. Schrock (UCB).

We would also like to thank N. L. Whittemore and H. M. Holleman for their assistance in the preparation of this report.

REFERENCES

1. T. R. England, M. G. Stamatelatos, R. E. Schenter, and F. Schmittroth, Fission-Product Source Terms for Reactor Applications, Conference 770708, Proceedings of Topical Meeting on Thermal Reactor Safety, Sun Valley Idaho (July 31 - Aug. 4, 1977). Also LA-NUREG-6917-MS (August 1977).
2. R. E. Schenter, F. Schmittroth, and T. R. England, Integral Determination of Fission Product Inventory and Decay Power, Review Paper No. 15 Presented at the Second IAEA Advisory Group Meeting on Fission Product Nuclear Data, Petten, Netherlands (Sept. 5-9, 1977).

3. Fission Product Decay Library of the Evaluated Nuclear Data File, Version IV (ENDF/B-IV). [Available from, and maintained by, the National Nuclear Data Center (NNDC) at the Brookhaven National Laboratory, these data were compiled by a task force chaired by R. E. Schenter.]
4. T. R. England and R. E. Schenter, ENDF/B-IV Fission-Product Files: Summary of Major Nuclide Data, LA-6116-MS [ENDF-223], (October 1975).
5. M. E. Meek and B. F. Rider, Compilation of Fission-Product Yields, NEDO-12154-1 (January 1974).
6. C. W. Reich, R. G. Helmer, and M. H. Putnam, Radioactive-Nuclide Decay Data for ENDF/B, ANCR-1157 (ENDF-120) (August 1974).
7. P. F. Rose and T. W. Burrows, ENDF/B Fission-Product Decay Data, BNL-NCS-50545 [ENDF-243], Vols. 1 and 2 (August 1976, issued May 1977).
8. R. E. Schenter, Ed., Benchmark Test of ENDF/B-IV, BNL-NCS-21118 [ENDF-230], Vol. 1 (1976).
9. F. Schmittroth, Nucl. Sci. Eng. 59, 117 (1976).
10. F. Schmittroth and R. E. Schenter, Nucl. Sci. Eng. 63, 276 (1977).
11. B. I. Spinrad, Nucl. Sci. Eng. 62, 35 (1977).
12. J. L. Yarnell and P. J. Bendt, Decay Heat From Products of ^{235}U Thermal Fission by Fast-Response Boil-Off Calorimetry, LA-NUREG-6713 (Sept. 1977). [Additional data points for use in the ANS 5.1 Standard were supplied in a personal communication, Yarnell to England].
13. J. K. Dickens, J. F. Emery, T. A. Love, J. W. McConnell, K. J. Northcutt, R. W. Peelle, and H. Weaver, Fission-Product Energy Release for Times Following Thermal-Neutron Fission of ^{235}U Between 2 and 14000 Seconds, ORNL/NUREG-14 (October 1977).
14. S. J. Friesenhahn, N. A. Lurie, V. C. Rogers, and N. Vagelatos, U-235 Fission Product Decay Heat from 1 to 10^5 Seconds, EPRI NP-180, Prepared for EPRI by IRT Corporation (February 1976). [Updated data published in Conference 770708, Sun Valley Idaho -- see Ref. 1].
15. M. Lott, G. Lhiaubet, and F. DuFreche, J. Nucl. Energy 27, 597 (1973) [See also translation AEC-TR-7472 and Report No. 73-83, Centre d'Etudes Nuclaires de Cadarache, 1974].
16. V. E. Schrock, L. M. Grossman, S. G. Prussin, K. C. Sockalingam, F. Nuh, C-K Fan, N. Z. Cho, and S. J. Oh, A Colorimetric Measurement of Decay Heat From ^{235}U Fission Products From 10 to 10^5 Seconds, NP-616, Vol. 1, prepared for EPRI by the University of California, Berkeley (February 1978).
17. S. B. Gunst, D. E. Conway, and J. C. Connor, Nucl. Sci. Eng. 56, 241 (1975).
18. B. Alam and J. Scobie, Ann of Nucl. Sci. and Eng. 1, 537 (1974).

19a. The report on total heating from ^{233}U and ^{239}Pu is in preparation by J. L. Yarnell and P. J. Bendt. Preliminary Comparisons are included in this report.

b. Beta and Gamma Spectra are largely unpublished. For ^{235}U the LASL, ORNL and UI comparisons with ENDF/B-IV calculations are published in Ref. 24.

20. P.-I. Johansson and G. Nilsson, Nukleara Resteffektdata Fordrojd Gammastalning fran ^{235}U, AE-FN-38, in Swedish (January 14, 1977).

21. C. Fiche, F. DuFreche, and A. M. Monnier, Calorimetric Measurements of the Total After Power Released by the Thermal Fission Products of ^{233}U and ^{239}Pu, SEN-022, in French (June 1976).

22. J. K. Dickens, A. F. Emery, T. A. Love, J. W. McConnell, K. J. Northcutt, R. W. Peelle, and H. Weaver, Fission-Product Energy Release for Times Following Thermal-Neutron Fission of ^{239}Pu Between 2 and 14000 Seconds, ORNL/NUREG-34 (April 1978).

23. N. Tsoulfanidis, B. W. Wehring, and M. E. Wyman, Nucl. Sci. Eng. 43, 42 (1971).

24. T. R. England and M. G. Stamatelatos, Comparisons of Calculated and Experimental Delayed Fission-Product Beta and Gamma Spectra from ^{235}U Thermal Fission, LA-NUREG-6896-MS, (July 1977).

25. American Nuclear Society, Draft Standard ANS 5.1, approved by Subcommittee ANS-5 of the ANS Standards Committee, October 1971 (revised 1973).

26. R. J. LaBauve and T. R. England, Trans. Am. Nucl. Soc. 28, 749 (June, 1978).

27. T. R. England, R. E. Schenter, and N. L. Whittemore, Gamma and Beta Decay Power Following 235U and 239Pu Fission Bursts, LA-6021-MS (July, 1975).

28. F. Schmittroth and R. E. Schenter, Nucl. Sci. Eng. (accepted for publication).

29. F. Schmittroth, Generalized Least-Squares for Data Analysis, HEDL-TME-77-51 (March 1978).

30. A. Tobias, Decay Heat Testing of the UK-ENDF/B-IV Format Fission Product Decay Data File, RD/B/N4179 (Dec. 1977).

31. "Core Engineering Technical Progress Report July-September 1977," HEDL-77-48 (Dec. 1977).

32. W. B. Wilson and T. R. England, Status of Fission-Product Data for Absorption Calculations, LA-UR-78-1452, Contribution to the Seminar on "Nuclear Data Problems for Thermal Reactor Applications, at the Brookhaven National Laboratory May 22-24, 1978 (to be published).

Section 11

STATUS OF FISSION-PRODUCT DATA FOR ABSORPTION CALCULATIONS

Status of Fission-Product Data For Absorption Calculations

W. B. Wilson and T. R. England
Los Alamos Scientific Laboratory, University of California
Theoretical Division
Los Alamos, New Mexico 87545

ABSTRACT

Progress in fission-product nuclear data for absorption buildup calculations in thermal power reactors is reviewed. Important nuclides and chain parameters are identified based on ENDF/B-IV data. The results of extensive sensitivity studies are provided and comparisons are made with integral experiments.

*Work supported by the Electric Power Research Institute and Department of Energy.

Status of Fission-Product Data For Absorption Calculations

W. B. Wilson and T. R. England
Los Alamos Scientific Laboratory, University of California
Theoretical Division
Los Alamos, New Mexico 87545

INTRODUCTION

The well known book by Weinberg and Wigner (1958)[1] stated that "Fission-product poisoning in natural uranium thermal reactors is one of the most important questions in reactor technology, since it is intimately tied to the problem of how long a chain reactor can run without reprocessing ..." The text then summarized the meager knowledge of cross sections (noting, for example, that Walker had found only 24 fission products had measured cross sections), and the formidable task of calculating the poison (i.e., absorption) buildup if data were available. Prior to early 1960 or late 1959, the Weinberg and Wigner text is an adequate summary of the knowledge of absorption buildup, and the importance they note still continues.

Following a brief summary of the subsequent development of fission-product absorption since ~ 1960, this report contains:

a) a summary of the ENDF/B-IV and anticipated ENDF/B-V content,
b) a list of the major thermal and epithermal absorbers in light water reactors (LWRs), and their contribution to the aggregate absorption rates,
c) sensitivity studies of the parameters important in the production of the major absorbers, and
d) comparisons of ENDF/B-IV with integral experiments, including a brief review of the experiments.

We anticipate that two other papers at this conference will review the specific status and uncertainties of microscopic data and the subject of decay heat.

PROGRESS SINCE 1960

Since the review in Ref. 1, the major effort has been in greatly improved summation codes, cross sections, and yields. (However, in the extensive list of nuclides contributing > 0.1% to absorption, only 22 contribute > 1/2% to the thermal absorption; of these only one, ^{134}Cs, is not included in the 1962 list by England,[2] but specific nuclide contributions have changed.)

*Work supported by the Electric Power Research Institute and Department of Energy.

Beginning in early 1960 there was significant progress. Walker,[3] and Greenhow and Hansen[4] used approximations and simplified chain structures (e.g., 2 to 3 coupled nuclides assumed to be stable) to estimate absorption buildup. The Greenhow and Hansen calculation was probably the most extensive effort at the time it was published. A more general method permitting decay loss and decay or (n,γ) fractional coupling was summarized by England and Eckert in 1961,[5] along with preliminary results using 5 nuclides per chain. By 1962 the CINDER code[6] was published further generalizing the method (any number of nuclides coupled by any combination of decays and (n,γ) branching, and no numerical integration) based on Markovian chains. Data from a variety of sources were compiled and evaluated by personnel in the Naval Reactor Program. The sources included theoretical cross-section estimates by Garrison and Roos,[7] and data from Nephew,[8] Katcoff,[9] Schuman and Berreth,[10] Walker,[3,11] Stehn,[13] BNL 325,[12] extensive private contributions by Norm Holden, Don Harris, David Goldman, Eric Hansen and other sources.[14-18] These were organized into chains for the CINDER code. The resulting absorption buildup for a variety of fuels and irradiation histories was published by England in 1962,[2] including a comparison with an integral measurement. This study used 163 products, in 67 chains including decay branching and nuclides having half-lives $\gtrsim$ 4 hours, and chains having up to 15 nuclides. Of these nuclides, 139 had thermal and epithermal cross sections. Some cross sections were theoretically based, especially in the epithermal range.

It was found in the 1962 study that decay branching and multiple coupling are important to the aggregate absorption. The buildup of ^{149}Sm was found to double over the value normally incorporated in depletion codes. Subsequently some widely used depletion codes, such as PDQ-HARMONY,[19] incorporated CINDER for actinides and the more important fission-product chains. Vondy,[20] working independently, developed a code based on a generalization of the Bateman Equations[21] similar to CINDER but did not attempt similar calculations of so many fission products at that time or incorporate the fractional (n,γ) branching which proved to be important to ^{149}Sm.

Since 1962 a number of other codes have been developed in this country, differing in capability and data bases, the best known being RIBD-II[22] and ORIGEN.[23] FISSPROD, published by Lane[24] in 1969 and recently extended by Walker, is familiar to some CSEWG members. There are several non-U.S.A. codes now in existence and data compilations similar to ENDF/B-IV. Several codes use a generic form of CINDER, but RIBD-II uses a "grid processor" method and ORIGEN uses an exponential matrix method first discussed by Joanou, et al.[25]

There has been a steady improvement in yields, cross sections, branching ratios, etc., and numerous publications, but no great surprises in aggregate absorption buildup since 1962. The need for more accurate evaluated data has continued. Prior to ENDF/B-IV there was no central source of such data; earlier

versions of ENDF/B were inadequate and largely ignored in thermal reactor design except for the energy dependent cross sections of a few nuclides.

The first comparison of calculations with preliminary integral experiments of extensively irradiated fuel (^{235}U) was also made in 1962.[2,26] Surprisingly, the comparison in Ref. (2) appears to be in as good agreement as is the final experimental data with ENDF/B-IV reported here. This can only be fortuitous. Values at only two U-235 depletions were reported in contrast to the current extensive temporal comparisons using data in a more appropriate group structure.

Lumped Absorbers

The idea of using lumped absorbers according to the ill-defined (i.e., reactor dependent) concepts of non-saturating, slowly saturating, and rapidly saturating absorbers appears to us to have only predagogical value or, at best, to be of value in crude survey calculations. The lumping concept has been used in, e.g., Garrison and Roos,[7] but even there the reader is warned that it is only used as an approximate check on absorption buildup. It is possible to accurately represent the absorption behavior, including transients and major spectrum dependencies using only 5 to 12 real nuclide chains plus one pseudo-nuclide.[27] The pseudo-nuclide or pseudo-chain we suggest is a lumped result, but it includes primarily those nuclides which will buildup only linearly with depletion.

Spatial Depletion

Prior to 1962, spatial depletion codes used coding for specific actinide and fission product chains. The fission product absorption was estimated by incorporation of ^{135}Xe and ^{149}Sm from the mass 135 and 149 yields and a rough aggregate estimate of all other products (e.g., the assumption of 50 barns/fission). At the time, this was adequate because ^{135}Xe and the partial contribution of ^{149}Sm considered were the major fraction of the absorption buildup for the reactor lifetimes then considered, and because the resulting uncertainty was comparable to that of other parasitic absorption. All requirements are now more stringent.

Summary

In summary, there were major developments in calculational methods of absorption buildup and in data bases by 1962. The need for improved data for added confidence was evident then. Subsequently, the amount and quality of data has increased, but there have been no startling developments.

The most significant development since 1962 is, we believe, the ENDF/B-IV[28-32] evaluated fission-product data; this has greatly improved our knowledge of microscopic data, and concomitantly, the

detailed effort required in calculations.

GENERAL CONTENT OF ENDF/B-IV

Table 1 summarizes the content of ENDF/B-IV[28-32] and approximate content expected in ENDF/B-V. Table 2 shows the content of actinide yield sets in both of these versions of ENDF/B. For fission products, the primary difference between Version IV and V is an expansion of decay data, delayed neutron precursors, and yield sets; the latter two quantities have doubled, and it is likely that the decay data will have a similar expansion, at least as to the number of energies tabulated. (A major expansion is in the heavy nuclides generally referred to as actinides; approximately 49 "actinides"extending to einsteinium will have cross-section and decay data.)

Calculation of fission-product behavior requires (n,γ) branching. This was not included in ENDF/B-IV (see Ref. 29) but is to be included in ENDF/B-V.

Of the 181 nuclides having (n,γ) cross-section evaluations in ENDF/B-IV, essentially all had some experimental data (in contrast to the 24 noted in 1958).[1]

Thermal reactor life-time predictions in the U.S.A. have used, with minor revisions, the fission product data from 1962[2] with considerable success. The use of the more detailed fission-product data in ENDF/B-IV is expected to offer the first significant improvement. However, this is more difficult to document than is the remarkable agreement with decay properties.[33-35] The latter had the benefit of several high quality experiments of decay heat, β, and γ spectra. Reference (34) (Schenter, et al.)

TABLE 1

FISSION PRODUCT FILES; GENERAL CONTENT

Type Data, Comment	Number In ENDF/B-IV	Approximate Number In ENDF/B-V
Total Nuclides	824	~ 838
Stable	113	~ 114
Unstable	711	~ 724
Ground State	701	~ 702
1st Excited State	117	~ 127
2nd Excited State	6	~ 7
Delayed Neutron Precursors	57	102
Nuclides with α Decay Data	6	~ 6
Nuclides with β^+ Decay Data	17	~ 17
Nuclides with Line Data	180	250-270
Nuclides with Evaluated Cross Sections	181	~ 182
Yield Sets	10	20

TABLE 2

FISSION YIELD SETS[a]

Fissionable Nuclide	ENDF/B-IV Thermal	ENDF/B-IV Fast	ENDF/B-IV 14 MeV	ENDF/B-IV Spon.	ENDF/B-V Thermal	ENDF/B-V Fast	ENDF/B-V 14 MeV
^{232}Th		X				X	X
^{237}Np						X	
^{233}U	X				X	X	X
^{235}U	X	X	X		X	X	X
^{236}U						X	
^{238}U		X	X			X	X
^{239}Pu	X	X			X	X	X
^{240}Pu						X	
^{241}Pu	X				X	X	
^{242}Pu						X	
^{252}Cf				X			

[a] Yield sets for fissionable nuclide and neutron fission energies are noted. There are other differences. ENDF/B-IV data included only independent yields. ENDF/B-V includes independent yields (before $\bar{\nu}_d$ emission), cumulative yields along each mass chain (after $\bar{\nu}_d$ emission) and uncertainties.

contains an extensive summary and reference list of publications based on ENDF/B-IV and other libraries, primarily of decay properties. This report, limited to absorption, essentially completes the testing of ENDF/B-IV.

OVERVIEW OF PROCESSED DATA FOR ABSORPTION

A modification of the original CINDER code and an extensive processed ENDF/B-IV library was produced for the Electric Power Research Institute (EPRI).[36] As in the original work in 1962, the primary objective of this code version and existing library is the computation of absorption buildup in thermal reactors.

(Other recent versions are used for, e.g., short term decay heat and spectra.) The library describes 186 nuclides formed into 84 chains. The (n,γ) reactions are described by 4-group cross sections based on a 154-group set in a structure proposed by LaBauve and Wilson,[37] and processed from ENDF/B-IV using NJOY.[38] The weighting function we used for the multigroup processing and collapsing is based on a typical Light Water Reactor (LWR) spectrum at mid-life.[39]

The 154-group cross sections are sufficiently detailed that they are suitable for collapsing using very different spectra than used in the initial processing. These data and a general collapsing code TOAFEW prepared by Wilson[39] are available from RSIC, as is the EPRI-CINDER code and library used in this report.

The actual chain data in EPRI-CINDER includes all significant nuclides for neutron absorption and all radioactive nuclides having half-lives $\gtrsim$ 4 hours. The code and library is therefore sufficient for many decay studies on long ($\gtrsim$ 10 h) shutdown with the addition of a decay energy library using, e.g., the data summarized in Ref. (29).

All studies in this report use EPRI-CINDER and the data of Ref. (36). However, the sensitivity calculations and some other studies were facilitated by (unpublished) code options added for use in this report.

The EPRI-CINDER library also contains a recommended 12-chain library, with a 4-element pseudo-chain, for use in spatial design codes. Parameters are provided for all nuclides including those of the pseudo-chain.

IMPORTANT PARAMETERS

In the sensitivity studies of important absorbers we have selected, for each case, the more important parameters. Surprises are possible, and we suggest a thorough study is in order, but examination of chain systematics is a sufficient bases in most cases to pick the important nuclide parameters. Many readers are probably familiar with the following type of comments, but misconceptions still exist. The comments are offered without detailed explanation.

- The magnitude of a nuclide's cross section is <u>not</u> an adequate indication of its importance (even apart from the consideration of its yield). For example:
  a) the increase of a cross section (such as ^{147}Nd) can decrease the aggregate buildup, have little or no effect (such as ^{149}Pm, ^{149}Sm) or increase the aggregate (such as ^{105}Pd),
  b) in some cases a small cross section in a precursor is more important than large values in daughter products (for Example ^{150}Sm → ^{151}Sm → etc.) because it controls the buildup of several subsequent products.

- In the absence of consideration of the known uncertainties in parameters, the mass chain fission yields are as important as cross sections on the aggregate absorption at steady-state power. For example, during the early part of reactor life, the ^{149}Sm absorption results from the mass 149 yield; it is only necessary to know that ^{149}Sm has a large cross section (> 40,000 b) to know its contribution to the aggregate absorption - that is, once that ^{149}Sm is saturated, its contribution may be calculated from the yield without knowledge of its cross section. (Later in life, ^{149}Sm is also determined by other mass chains in multiple couplings through ^{147}Nd). In most cases, the absorption cross section is sufficiently small such that, to first order, the contribution is a product of the effective yield and cross section. The effective yield, however, may be increased by (n,γ) absorption in other mass chains.

- Half-lives are important as coupling mechanisms and in determining the transient behavior during power changes. Only a few nuclides that are important absorbers are significantly affected by their own half-lives (e.g., ^{135}Xe). However, there are cases where the buildup of important nuclides is affected significantly by decay even when it already dominates the (n,γ) branching (^{147}Nd is an example).

- Independent yields are not very important to absorption calculations during steady state power operation. (Independent yields are very important to decay heat and spectral calculations.)

- Flux level and spectrum are important where the cross section is important and where (n,γ) branching at radioactive nuclides is important.

All of these general statements result from the fact that fission products have both a source and depletion mechanism. The parameter(s) of importance can only be determined by an examination of chain systematics or by a very general sensitivity study of parameters affecting all products. In this report we examine the most important contributors to absorption buildup.

LIGHT WATER REACTOR (LWR) FISSION-PRODUCT ABSORPTION CALCULATIONS

A number of calculations have been performed with the EPRI-CINDER code and data library to identify the major fission-product absorbers generated in reactor fuel and the various nuclide parameters important to such calculations. The data library used in the calculations and the pertinent reactor parameter assumptions are examined in this section.

EPRI-CINDER Data Library

The EPRI-CINDER library describes all fission-product nuclides with half-lives exceeding 4 hours and important to the temporal description of the neutron absorption of fission-product nuclides. Cross sections for the library were processed from ENDF/B-IV with the NJOY code.[38] This procedure requires the formation of a Doppler-broadened point-energy cross-section representation (PENDF)[40] from which neutron flux-weighted average group values are calculated. Of the 181 nuclides described with evaluated cross sections in the ENDF/B-IV fission-product files, 20 are also included in the ENDF/B-IV general purpose files; multigroup cross sections for these 20 nuclides were calculated from 900 K PENDF files retained from previous general purpose file processing. Multigroup cross sections for the remaining 161 nuclides were processed from 1000 K PENDF files generated from the fission-product file. Each of the 181 nuclides have evaluated (n,γ) reaction cross sections. Also, 36 of these have additional evaluated cross sections for other neutron-absorption reactions, such as (n,p), (n,α), etc. All reaction cross sections were processed, although cross sections for neutron absorption reactions other than radiative capture were found to be negligable and were not included in the library.

Multigroup cross-section processing and collapsing were performed with the Power Reactor Studies (PRS) Neutron Flux Weighting Function, typical of LWRs.[39] The 4-group energy structure of the library cross sections, along with the typical LWR group (integral) flux ratios derived from the weighting function and employed in these and semilar calculations, are given in Table 3.

Table 3

4-Group Energy Structure and Flux Ratios

Group i	Energy Boundary E_i (eV)	Lethargy Width μ_i	LWR FLUX Ratio ϕ_i/ϕ_4
	1.0000×10^{7}		
1		2.5	1.4759
	8.2085×10^{5}		
2		5.0	2.3401
	5.5308×10^{3}		
3		9.088	1.7833
	6.2506×10^{-1}		
4		8.412	1.0
	1.0000×10^{-5}		

An indication of the degree of hardness of a flux spectrum is the thermal (group 4) flux-weighted average value of a cross section equal to unity at 2200 m/s and varying inversely with velocity. This value for the PRS flux description is

$$\langle \sigma_{1/v} \rangle = 0.554018 \quad . \tag{1}$$

Not all of the 181 ENDF/B-IV fission-product nuclides having evaluated cross sections are included in the EPRI-CINDER fission-product data library. Examination of chain systematics indicated that 23 of the 181 were insignificant absorbers and/or negligable precursors. Some 28 of the 186 nuclides included in the library thus have no evaluated cross sections in ENDF/B-IV. Only 1 of these, ^{79}Se, appears in absorption coupling. The 4-group cross-section values used for ^{79}Se were taken from previous CINDER libraries. The remaining 27 nuclides have short half-lives, affect only transient absorption properties or simply satisfy the $\gtrsim$ 4-hour half-life criterion; these nuclides were assigned cross-section values of zero. Radioactive decay constants and branching fractions for competing radioactive decay and absorption reactions were taken from the data of Ref. 29. Yield fractions were taken from ENDF/B-IV evaluated yields. In some instances, effective fission yield fractions and branching fractions were formulated to accomodate the branching through short-lived nuclides or metastable states not explicitly included in the chain structure.

Basic Depletion Conditions

The neutron absorption calculations performed to identify major absorbers and nuclide parameters have assumed the following:

1. LWR flux spectrum of the PRS flux description, with the group flux ratios of Table 3.
2. 3.3% enriched uranium fuel.
3. Continuous fuel irradiation for 3 years (26,400 hours) to a burnup of 33 Gwd/MT at a constant power of 30 Mw/MT.
4. Power and fission-product production from ^{235}U, ^{238}U and ^{239}Pu only. Actinide cross sections not changed with temporal fuel composition for resonance self-shielding.

Absorption Buildup Calculations

EPRI-CINDER calculations were performed to trace the buildup of fission-product absorption through thirty-three 800-hour (1 Gwd/MT) time increments. The macroscopic fission-product absorption cross-section Σ, shown in Fig. 1, indicates the continuous increase in fission-product absorption throughout the 3-year fuel lifetime. It is customary in depletion calculations to represent the fission-product absorption cross section in terms of a barns-per-fission absorption cross section, $\hat{\sigma}$, equal to the

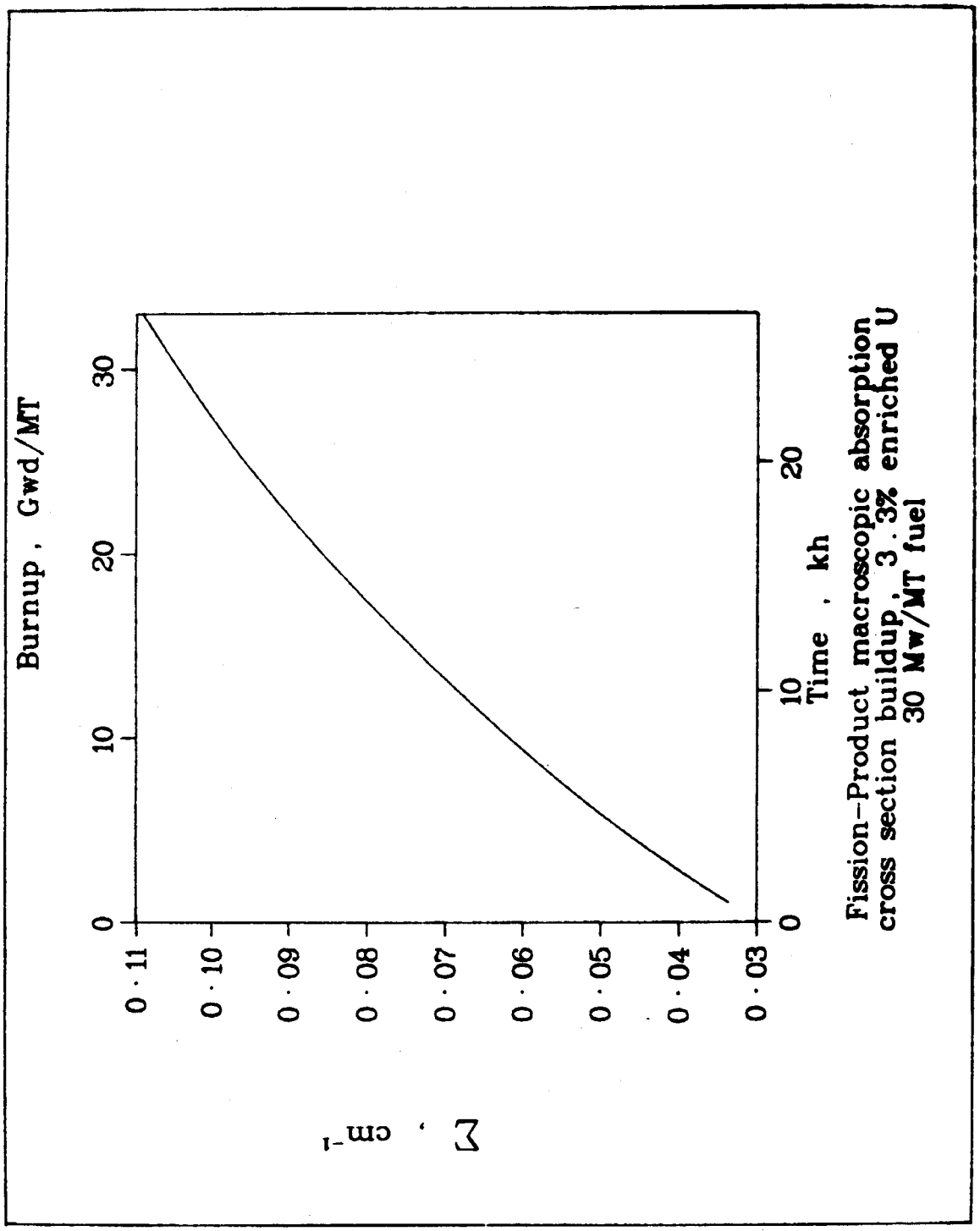

FIGURE 1. Fission-Product macroscopic absorption cross section buildup, 3.3% enriched U 30 Mw/MT fuel.

macroscopic absorption cross section, Σ, divided by the total number of fissions per cm^3 that have occured. This quantity, generated by the EPRI-CINDER code at each time increment, is shown in Fig. 2.

The quantities Σ and $\hat{\sigma}$ described above have been generated from 4-group values. The distribution of the fission-product absorption rate among the four energy groups is shown in Fig. 3. The fission-product absorption rate is dominated by thermal (group 4) absorption throughout the fuel lifetime, although the percentage of absorption in the thermal group decreases from 96% at 800 hours to 56% at the end of life. The balance of absorption almost entirely occurs in the epithermal group 3. The combined fast absorption in groups 1 and 2 accounts for less than 1% of the total fission-product absorption rate throughout the fuel lifetime.

Identification of Major Absorbers

The total fission-product absorption rate, R_T, is computed at any time increment as the sum of the group values, or

$$R_T = \sum_{i=1}^{4} \phi_i \Sigma_i \quad , \tag{2}$$

where

ϕ_i = the group i flux integral, and

Σ_i = the group i macroscopic fission-product absorption cross section.

Similarily, the thermal (R_4), epithermal (R_3) and resonance (R_R) absorption rates are given by

$$R_4 = \phi_4 \Sigma_4 \quad , \tag{3}$$

$$R_3 = \phi_3 \Sigma_3 \quad , \tag{4}$$

and

$$R_R = \sum_{i=1}^{3} \phi_i \Sigma_i \quad . \tag{5}$$

Because of the magnitude of fission-product absorption in groups 1 and 2, the epithermal absorption rate is very nearly equal to the resonance absorption rate.

The group macroscopic absorption cross sections Σ_i are computed as the sum of the individual values of the 186 nuclides of the data library. Special edits to the EPRI-CINDER code have been

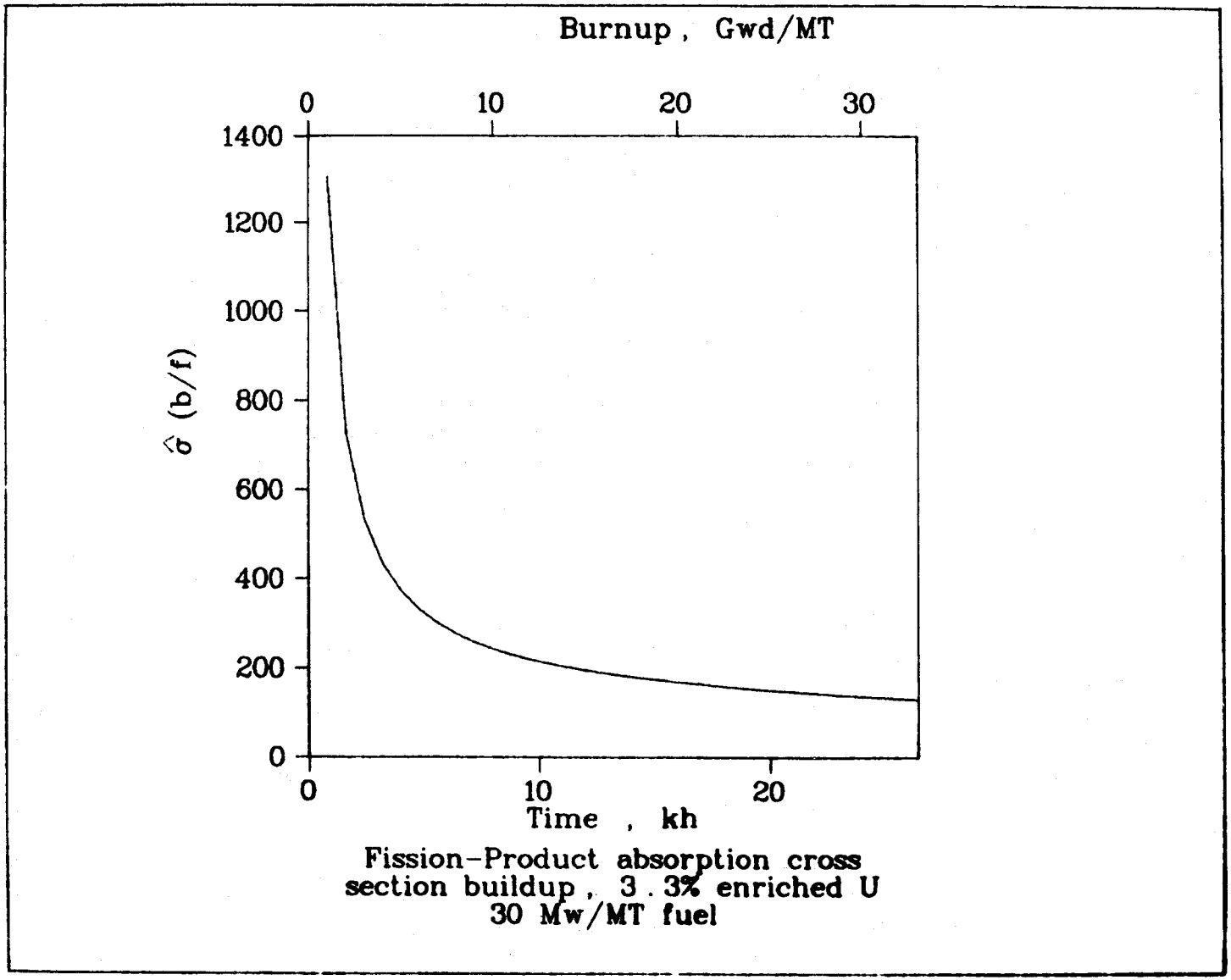

FIGURE 2. Fission-Product absorption cross section buildup, 3.3% enriched U 30 Mw/MT Fuel.

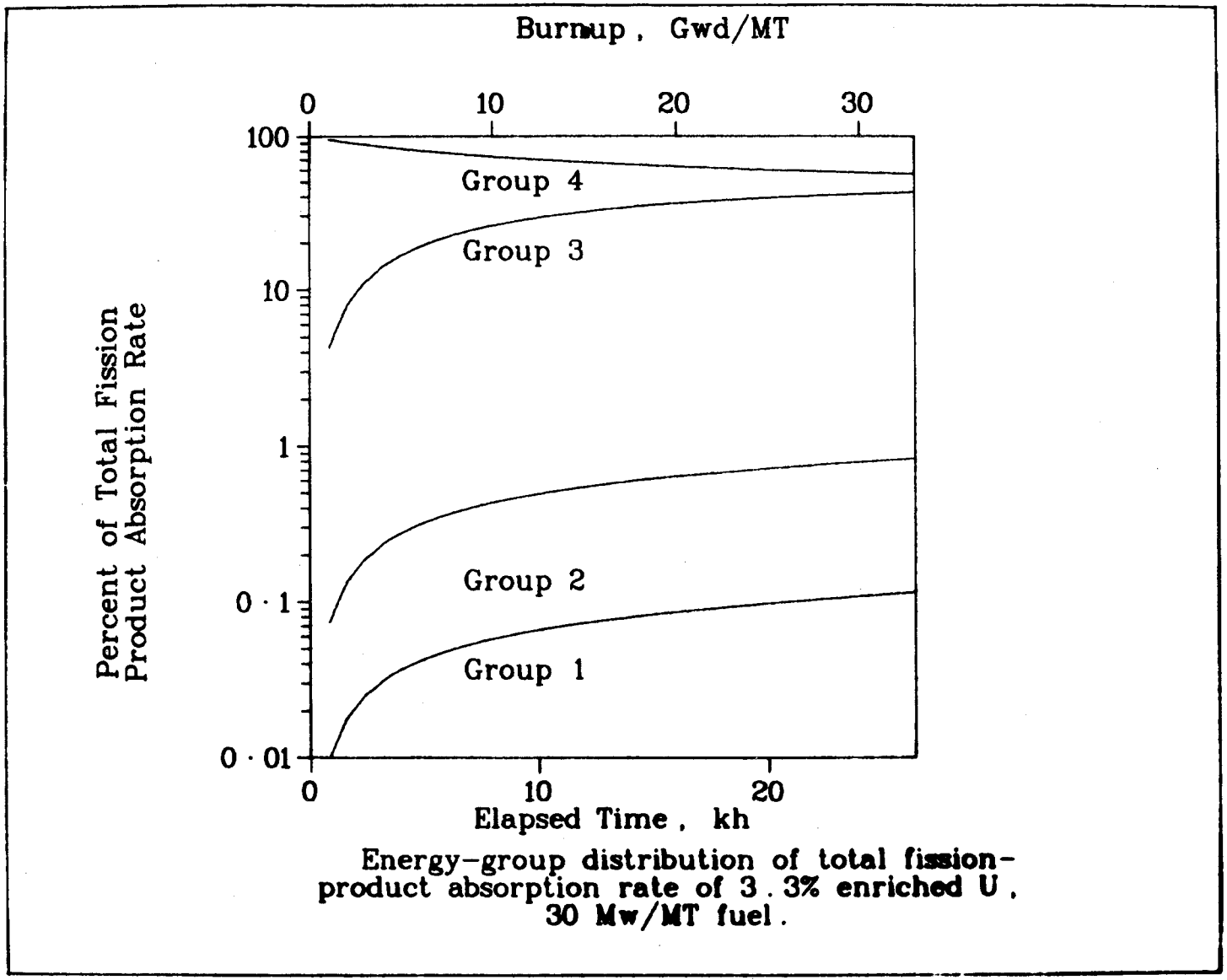

FIGURE 3. Energy-group distribution of total fission-product absorption rate of 3.3% enriched U, 30 Mw/MT fuel.

added to identify and order, at each time increment, the major contributors to R_T, R_4, R_3 and R_R.

All nuclides contributing, at 4000 hours, greater than 0.1% of R_T, R_4 and R_3 are tabulated in Tables 4-6. Similar tabulations are given at 16000 hours in Tables 7-9 and at the end of life in Tables 10-12. R_T is dominated by ^{135}Xe and ^{149}Sm early in fuel lifetime, as shown in Fig. 4; ten nuclides, listed in Table 13, dominate throughout the fuel history. However, the percentage of the total absorption rate not accounted for by these ten nuclides steadily increases throughout the fuel history.

Parameter Sensitivity Studies

Examination of Tables 4-12 shows that 64 individual nuclides each, at some time, account for greater than 0.1% of one or more of the group absorption rates tabulated. These nuclides are listed in Table 14. As previously described, the absorption by each of these nuclides is determined by a combination of parameters associated with the absorber, its precursors, and the fuel.

The chain systematics associated with each of these 64 nuclides have been examined to identify a total of 291 parameters that effect, to some extent, the total fission-product absorption rate R_T.

Edits to the EPRI-CINDER code have been added to perturb an individual nuclide parameter of the data library, calculate the total perturbed absorption rate, R_T', and evaluate the sensitivity of the total absorption rate to the parameter perturbed. The sensitivity, S, of R_T to a parameter is calculated as

$$S = \frac{(R_T' - R_T) \; / \; R_T}{\Delta p / p} \quad , \tag{6}$$

where Δp is the perturbation to parameter p.

Throughout these studies parameters were individually increased by 10%. Parameters studied include decay constants, thermal (group 4) absorption cross sections, epithermal (group 3) absorption cross sections, effective yield fractions from each of the three fissionable nuclides, and radioactive decay and absorption branching fractions. In the case of branching fractions, complementary branching fractions were decreased to preserve unity. However, no attempt was made to adjust yield fractions to nuclides other than that directly perturbed.

The sensitivity of R_T at each time increment to each of these parameters was evaluated, requiring 291 seperate EPRI-CINDER calculations. These parameters and R_T sensitivity values at three times during fuel lifetime are listed in Tables 15-20. Calculated sensitivity values less than 1.0×10^{-5} are recorded as zero. The 40 parameters to which R_T is most sensitive are ordered, for each of the three times, in Tables 21-23.

Table 4

SUMMARY OF MAJOR FISSION-PRODUCT TOTAL ABSORBERS AT 4000 HOURS

NUCLIDE	PERCENT OF TOTAL ABSORPTION (GROUPS 1-4)	PERCENT OF THERMAL ABSORPTION (GROUP 4)	PERCENT OF EPITHERMAL ABSORPTION (GROUP 3)	PERCENT OF RESONANCE ABSORPTION (GROUPS 1-3)
XE135	51.66877	62.25804	.11979	.11758
SM149	13.64641	16.28261	.82427	.81274
SM151	4.87625	5.28924	2.89994	2.86568
ND143	4.72617	5.06554	3.05532	3.07406
PM147	3.84727	1.03728	17.74753	17.52700
RH103	2.88576	1.29927	10.71796	10.60918
XE131	2.64281	.77094	11.94299	11.75554
CS133	2.38660	.61488	11.04344	11.01176
TC 99	1.91200	.37562	9.41367	9.39149
SM152	1.58060	.36688	7.61827	7.48928
PM148M	1.26102	1.47567	.21755	.21607
ND145	1.19667	.52806	4.47278	4.45166
RH105	.65107	.62619	.78595	.77220
EU153	.53709	.29189	1.73731	1.73080
RU101	.49444	.05294	2.52978	2.64382
SM150	.41197	.35620	.66846	.68346
EU155	.38497	.41294	.24903	.24883
KR 83	.34854	.32251	.46944	.47526
MO 95	.31201	.09792	1.34417	1.35424
PR143	.27672	.19653	.66838	.66711
XE133	.25333	.19356	.55340	.54433
PM148	.24959	.11543	.91820	.90268
CD113	.24338	.29297	.00195	.00195
ZR 93	.23937	.04997	1.15644	1.16140
LA139	.22821	.18864	.41419	.42088
PR141	.21542	.15979	.46206	.48621
AG109	.19883	.04410	.96633	.95210
GD157	.18819	.22641	.00215	.00213
PD105	.18198	.06566	.68771	.74826
CE141	.15961	.15063	.19272	.20334
ND147	.14174	.03452	.67001	.66372
MO 97	.13916	.04204	.52592	.61199
CS135	.11925	.05473	.43583	.43334
PM149	.10907	.11192	.09292	.09522
RU103	.10723	.03021	.46006	.48218
ALL OTHERS	1.17850	.51830	3.93406	4.39249

Table 5

SUMMARY OF MAJOR FISSION-PRODUCT THERMAL ABSORBERS AT 4000 HOURS

NUCLIDE	PERCENT OF TOTAL ABSORPTION (GROUPS 1-4)	PERCENT OF THERMAL ABSORPTION (GROUP 4)	PERCENT OF EPITHERMAL ABSORPTION (GROUP 3)	PERCENT OF RESONANCE ABSORPTION (GROUPS 1-3)
XE135	51.66877	62.25804	.11979	.11758
SM149	13.64641	16.28261	.82427	.81274
SM151	4.87625	5.28924	2.89994	2.86568
ND143	4.72617	5.06554	3.05532	3.07406
PM148M	1.26102	1.47567	.21755	.21607
RH103	2.88576	1.29927	10.71796	10.60918
PM147	3.84727	1.03728	17.74753	17.52700
XE131	2.64281	.77094	11.94299	11.75554
RH105	.65107	.62619	.78595	.77220
CS133	2.38660	.61488	11.04344	11.01176
ND145	1.19667	.52806	4.47278	4.45166
EU155	.38497	.41294	.24903	.24883
TC 99	1.91200	.37562	9.41367	9.39149
SM152	1.58060	.36688	7.61827	7.48928
SM150	.41197	.35620	.66846	.68346
KR 83	.34854	.32251	.46944	.47526
CD113	.24338	.29297	.00195	.00195
EU153	.53709	.29189	1.73731	1.73080
GD157	.18819	.22641	.00215	.00213
PR143	.27672	.19653	.66838	.66711
XE133	.25333	.19356	.55340	.54433
LA139	.22821	.18864	.41419	.42088
PR141	.21542	.15979	.46206	.48621
CE141	.15961	.15063	.19272	.20334
PM148	.24959	.11543	.91820	.90268
PM149	.10907	.11192	.09292	.09522
ALL OTHERS	3.11251	.99038	12.71032	13.44354

Table 6

SUMMARY OF MAJOR FISSION-PRODUCT EPITHERMAL ABSORBERS AT 4000 HOURS

NUCLIDE	PERCENT OF TOTAL ABSORPTION (GROUPS 1-4)	PERCENT OF THERMAL ABSORPTION (GROUP 4)	PERCENT OF EPITHERMAL ABSORPTION (GROUP 3)	PERCENT OF RESONANCE ABSORPTION (GROUPS 1-3)
PM147	3.84727	1.03728	17.74753	17.52700
XE131	2.64281	.77094	11.94299	11.75554
CS133	2.38660	.61488	11.04344	11.01176
RH103	2.88576	1.29927	10.71796	10.60918
TC 99	1.91200	.37562	9.41367	9.39149
SM152	1.58060	.36688	7.61827	7.48928
ND145	1.19667	.52806	4.47278	4.45166
ND143	4.72617	5.06554	3.05532	3.07406
SM151	4.87625	5.28924	2.89994	2.86568
RU101	.49444	.05294	2.52978	2.64382
EU153	.53709	.29189	1.73731	1.73080
MO 95	.31201	.09792	1.34417	1.35424
ZR 93	.23937	.04997	1.15644	1.16140
AG109	.19883	.04410	.96633	.95210
PM148	.24959	.11543	.91820	.90268
SM149	13.64641	16.28261	.82427	.81274
RH105	.65107	.62619	.78595	.77220
PD105	.18198	.06566	.68771	.74826
ND147	.14174	.03452	.67001	.66372
SM150	.41197	.35620	.66846	.68346
PR143	.27672	.19653	.66838	.66711
XE133	.25333	.19356	.55340	.54433
MO 97	.13916	.04204	.52592	.61199
KR 83	.34854	.32251	.46944	.47526
PR141	.21542	.15979	.46206	.48621
RU103	.10723	.03021	.46006	.48218
CS135	.11925	.05473	.43583	.43334
LA139	.22821	.18864	.41419	.42088
SM147	.08353	.02046	.39366	.39054
PD108	.06101	.01060	.30946	.30641
EU155	.38497	.41294	.24903	.24883
MO 98	.04644	.00242	.23108	.26074
EU154	.08505	.05670	.22474	.22308
PM148M	1.26102	1.47567	.21755	.21607
ND148	.05051	.01421	.20524	.22718
ZR 96	.03681	.00032	.20246	.21445
CE141	.15961	.15063	.19272	.20334
NB 95	.03772	.00635	.16779	.19044
IN115	.03522	.00857	.16775	.16499
PD107	.04295	.01478	.16714	.18008
MO100	.03230	.00415	.14619	.16931
I129	.07536	.06112	.13279	.14466
XE135	51.66877	62.25804	.11979	.11758
ZR 91	.02960	.01068	.10987	.12175
I127	.02112	.00277	.10854	.11043
ALL OTHERS	1.08152	.93646	1.46437	1.78773

Table 7

SUMMARY OF MAJOR FISSION-PRODUCT TOTAL ABSORBERS AT 16000 HOURS

NUCLIDE	PERCENT OF TOTAL ABSORPTION (GROUPS 1-4)	PERCENT OF THERMAL ABSORPTION (GROUP 4)	PERCENT OF EPITHERMAL ABSORPTION (GROUP 3)	PERCENT OF RESONANCE ABSORPTION (GROUPS 1-3)
XE135	24.19192	38.27335	.02599	.02548
ND143	9.48034	13.34132	2.84028	2.85416
RH103	8.33864	4.92939	14.35283	14.18957
SM149	8.07239	12.64639	.22597	.22253
PM147	5.60915	1.98563	11.99147	11.82780
XE131	5.48054	2.09911	11.47786	11.28372
CS133	5.16617	1.74758	11.07859	11.03313
TC 99	4.07030	1.04990	9.28723	9.25388
SM151	3.71043	5.28434	1.02263	1.00930
SM152	3.62459	1.10464	8.09624	7.94931
ND145	2.42531	1.40518	4.20107	4.17606
EU153	2.11214	1.50712	3.16624	3.15046
PM148M	2.10630	3.23627	.16840	.16705
MO 95	1.55383	.64029	3.10227	3.12163
SM150	1.10130	1.25025	.82814	.84568
RU101	1.09953	.15456	2.60712	2.72127
EU155	1.06962	1.50641	.32066	.32000
EU154	.99966	.87496	1.22422	1.21366
AG109	.93008	.27085	2.09483	2.06144
KR 83	.63206	.76791	.39453	.39892
PR141	.59201	.57658	.58850	.61849
RH105	.58417	.73769	.32681	.32070
PD105	.57280	.27135	1.00318	1.09015
SM147	.55966	.18000	1.22240	1.21123
ZR 93	.49228	.13494	1.10219	1.10556
LA139	.48896	.53066	.41126	.41738
PM148	.46927	.28496	.80008	.78558
CS134	.42340	.45151	.37436	.37515
MO 97	.30357	.12040	.53168	.61793
PD108	.29528	.06736	.69413	.68644
CS135	.25103	.15126	.42519	.42224
I129	.20143	.21451	.16449	.17898
GD157	.18972	.29968	.00100	.00100
PD107	.18872	.08528	.34034	.36623
CD113	.18164	.28708	.00067	.00067
PR143	.14209	.13250	.15905	.15855
XE133	.13972	.14016	.14145	.13896
ND144	.12646	.12279	.11168	.13275
ND148	.11084	.04096	.20875	.23078
MO 98	.10256	.00703	.23649	.26652
ALL OTHERS	1.81011	1.08783	2.64973	3.04968

Table 8

SUMMARY OF MAJOR FISSION-PRODUCT THERMAL ABSORBERS AT 16000 HOURS

NUCLIDE	PERCENT OF TOTAL ABSORPTION (GROUPS 1-4)	PERCENT OF THERMAL ABSORPTION (GROUP 4)	PERCENT OF EPITHERMAL ABSORPTION (GROUP 3)	PERCENT OF RESONANCE ABSORPTION (GROUPS 1-3)
XE135	24.19192	38.27335	.02599	.02548
ND143	9.48034	13.34132	2.84028	2.85416
SM149	8.07239	12.64639	.22597	.22253
SM151	3.71043	5.28434	1.02263	1.00930
RH103	8.33864	4.92939	14.35283	14.18957
PM148M	2.10630	3.23627	.16840	.16705
XE131	5.48054	2.09911	11.47786	11.28372
PM147	5.60915	1.98563	11.99147	11.82780
CS133	5.16617	1.74758	11.07859	11.03313
EU153	2.11214	1.50712	3.16624	3.15046
EU155	1.06962	1.50641	.32066	.32000
ND145	2.42531	1.40518	4.20107	4.17606
SM150	1.10130	1.25025	.82814	.84568
SM152	3.62459	1.10464	8.09624	7.94931
TC 99	4.07030	1.04990	9.28723	9.25388
EU154	.99966	.87496	1.22422	1.21366
KR 83	.63206	.76791	.39453	.39892
RH105	.58417	.73769	.32681	.32070
MO 95	1.55383	.64029	3.10227	3.12163
PR141	.59201	.57658	.58850	.61849
LA139	.48896	.53066	.41126	.41738
CS134	.42340	.45151	.37436	.37515
GD157	.18972	.29968	.00100	.00100
CD113	.18164	.28708	.00067	.00067
PM148	.46927	.28496	.80008	.78558
PD105	.57280	.27135	1.00318	1.09015
AG109	.93008	.27085	2.09483	2.06144
I129	.20143	.21451	.16449	.17898
SM147	.55966	.18000	1.22240	1.21123
RU101	1.09953	.15456	2.60712	2.72127
CS135	.25103	.15126	.42519	.42224
XE133	.13972	.14016	.14145	.13896
ZR 93	.49228	.13494	1.10219	1.10556
PR143	.14209	.13250	.15905	.15855
ND144	.12646	.12279	.11168	.13275
MO 97	.30357	.12040	.53168	.61793
PM149	.08271	.11143	.03265	.03342
CE141	.08783	.10883	.04915	.05179
ALL OTHERS	2.33698	1.06821	4.04764	4.51443

Table 9

SUMMARY OF MAJOR FISSION-PRODUCT EPITHERMAL ABSORBERS AT 16000 HOURS

NUCLIDE	PERCENT OF TOTAL ABSORPTION (GROUPS 1-4)	PERCENT OF THERMAL ABSORPTION (GROUP 4)	PERCENT OF EPITHERMAL ABSORPTION (GROUP 3)	PERCENT OF RESONANCE ABSORPTION (GROUPS 1-3)
RH103	8.33864	4.92939	14.35283	14.18957
PM147	5.60915	1.98563	11.99147	11.82780
XE131	5.48054	2.09911	11.47786	11.28372
CS133	5.16617	1.74758	11.07859	11.03313
TC 99	4.07030	1.04990	9.28723	9.25388
SM152	3.62459	1.10464	8.09624	7.94931
ND145	2.42531	1.40518	4.20107	4.17606
EU153	2.11214	1.50712	3.16624	3.15046
MO 95	1.55383	.64029	3.10227	3.12163
ND143	9.48034	13.34132	2.84028	2.85416
RU101	1.09953	.15456	2.60712	2.72127
AG109	.93008	.27085	2.09483	2.06144
EU154	.99966	.87496	1.22422	1.21366
SM147	.55966	.18000	1.22240	1.21123
ZR 93	.49228	.13494	1.10219	1.10556
SM151	3.71043	5.28434	1.02263	1.00930
PD105	.57280	.27135	1.00318	1.09015
SM150	1.10130	1.25025	.82814	.84568
PM148	.46927	.28496	.80008	.78558
PD108	.29528	.06736	.69413	.68644
PR141	.59201	.57658	.58850	.61849
MO 97	.30357	.12040	.53168	.61793
CS135	.25103	.15126	.42519	.42224
LA139	.48896	.53066	.41126	.41738
KR 83	.63206	.76791	.39453	.39892
CS134	.42340	.45151	.37436	.37515
PD107	.18872	.08528	.34034	.36623
RH105	.58417	.73769	.32681	.32070
EU155	1.06962	1.50641	.32066	.32000
MO 98	.10256	.00703	.23649	.26652
SM149	8.07239	12.64639	.22597	.22253
ND148	.11084	.04096	.20875	.23078
ZR 96	.07851	.00089	.20014	.21173
PM148M	2.10630	3.23627	.16840	.16705
ND147	.07644	.02444	.16746	.16569
I129	.20143	.21451	.16449	.17898
PR143	.14209	.13250	.15905	.15855
I127	.06673	.01150	.15893	.16150
ZR 91	.09201	.04356	.15825	.17515
RU103	.07953	.02942	.15812	.16552
IN115	.07093	.02266	.15655	.15379
MO100	.07206	.01216	.15116	.17485
XE133	.13972	.14016	.14145	.13896
RU104	.05726	.01215	.11184	.13468
ND144	.12646	.12279	.11168	.13275
ALL OTHERS	25.77991	39.79116	1.41494	1.73393

Table 10

SUMMARY OF MAJOR FISSION-PRODUCT TOTAL ABSORBERS AT 26400 HOURS

NUCLIDE	PERCENT OF TOTAL ABSORPTION (GROUPS 1-4)	PERCENT OF THERMAL ABSORPTION (GROUP 4)	PERCENT OF EPITHERMAL ABSORPTION (GROUP 3)	PERCENT OF RESONANCE ABSORPTION (GROUPS 1-3)
XE135	15.09836	26.77836	.01371	.01342
ND143	9.90337	15.62377	2.50825	2.51536
RH103	9.81659	6.50558	14.28416	14.09282
CS133	6.21505	2.35690	11.26709	11.19792
XE131	6.03893	2.59298	10.69177	10.48944
SM149	5.69759	10.00653	.13483	.13251
TC 99	4.93791	1.42788	9.52478	9.47118
PM147	4.59155	1.82217	8.29825	8.16826
SM152	3.89481	1.33069	7.35464	7.20642
SM151	3.23823	5.17014	.75449	.74313
EU153	3.21177	2.56920	4.07021	4.04165
ND145	2.88226	1.87209	4.22063	4.18692
EU154	2.23714	2.19512	2.31606	2.29140
EU155	2.18896	3.45605	.55475	.55249
MO 95	2.09987	.97005	3.54423	3.55906
PM148M	1.83657	3.16345	.12413	.12288
SM150	1.54143	1.96175	.97988	.99859
AG109	1.44728	.47249	2.75572	2.70625
RU101	1.42170	.22404	2.84980	2.96850
CS134	.91132	1.08947	.68118	.68123
PD105	.87408	.46420	1.29412	1.40344
SM147	.79702	.28738	1.47167	1.45524
PR141	.77187	.84276	.64865	.68031
KR 83	.66512	.90590	.35097	.35416
LA139	.61911	.75325	.44022	.44586
ZR 93	.60368	.18550	1.14261	1.14376
RH105	.58694	.83091	.27759	.27184
PD108	.51431	.13153	1.02206	1.00867
PM148	.49921	.33984	.71952	.70504
MO 97	.38887	.17290	.57576	.66779
PD107	.32190	.16308	.49077	.52702
CS135	.30709	.20745	.43972	.43578
I129	.28230	.33702	.19489	.21162
ND144	.22832	.24854	.17046	.20221
GD157	.21670	.38375	.00097	.00096
ND148	.14303	.05925	.22772	.25123
CD113	.13790	.24433	.00043	.00043
MO 98	.13324	.01024	.25971	.29209
RU102	.12987	.09197	.10409	.17882
ZR 91	.11696	.06208	.17006	.18784
XE133	.11005	.12376	.09418	.09234
PR143	.10586	.11066	.10017	.09965
EU156	.10472	.11108	.09860	.09651
ALL OTHERS	2.13118	1.34390	2.77646	3.14797

Table 11

SUMMARY OF MAJOR FISSION-PRODUCT THERMAL ABSORBERS AT 26400 HOURS

NUCLIDE	PERCENT OF TOTAL ABSORPTION (GROUPS 1-4)	PERCENT OF THERMAL ABSORPTION (GROUP 4)	PERCENT OF EPITHERMAL ABSORPTION (GROUP 3)	PERCENT OF RESONANCE ABSORPTION (GROUPS 1-3)
XE135	15.09836	26.77836	.01371	.01342
ND143	9.90337	15.62377	2.50825	2.51536
SM149	5.69759	10.00653	.13483	.13251
RH103	9.81659	6.50558	14.28416	14.09282
SM151	3.23823	5.17014	.75449	.74313
EU155	2.18896	3.45605	.55475	.55249
PM148M	1.83657	3.16345	.12413	.12288
XE131	6.03893	2.59298	10.69177	10.48944
EU153	3.21177	2.56920	4.07021	4.04165
CS133	6.21505	2.35690	11.26709	11.19792
EU154	2.23714	2.19512	2.31606	2.29140
SM150	1.54143	1.96175	.97988	.99859
ND145	2.88226	1.87209	4.22063	4.18692
PM147	4.59155	1.82217	8.29825	8.16826
TC 99	4.93791	1.42788	9.52478	9.47118
SM152	3.89481	1.33069	7.35464	7.20642
CS134	.91132	1.08947	.68118	.68123
MO 95	2.09987	.97005	3.54423	3.55906
KR 83	.66512	.90590	.35097	.35416
PR141	.77187	.84276	.64865	.68031
RH105	.58694	.83091	.27759	.27184
LA139	.61911	.75325	.44022	.44586
AG109	1.44728	.47249	2.75572	2.70625
PD105	.87408	.46420	1.29412	1.40344
GD157	.21670	.38375	.00097	.00096
PM148	.49921	.33984	.71952	.70504
I129	.28230	.33702	.19489	.21162
SM147	.79702	.28738	1.47167	1.45524
ND144	.22832	.24854	.17046	.20221
CD113	.13790	.24433	.00043	.00043
RU101	1.42170	.22404	2.84980	2.96850
CS135	.30709	.20745	.43972	.43578
ZR 93	.60368	.18550	1.14261	1.14376
MO 97	.38887	.17290	.57576	.66779
PD107	.32190	.16308	.49077	.52702
GD155	.08491	.14881	.00240	.00238
PD108	.51431	.13153	1.02206	1.00867
XE133	.11005	.12376	.09418	.09234
PM149	.07952	.12009	.02654	.02711
EU156	.10472	.11108	.09860	.09651
PR143	.10586	.11066	.10017	.09965
ALL OTHERS	2.48985	1.29853	3.50912	4.02846

Table 12

SUMMARY OF MAJOR FISSION-PRODUCT EPITHERMAL ABSORBERS AT 26400 HOURS

NUCLIDE	PERCENT OF TOTAL ABSORPTION (GROUPS 1-4)	PERCENT OF THERMAL ABSORPTION (GROUP 4)	PERCENT OF EPITHERMAL ABSORPTION (GROUP 3)	PERCENT OF RESONANCE ABSORPTION (GROUPS 1-3)
RH103	9.81659	6.50558	14.28416	14.09282
CS133	6.21505	2.35690	11.26709	11.19792
XE131	6.03893	2.59298	10.69177	10.48944
TC 99	4.93791	1.42788	9.52478	9.47118
PM147	4.59155	1.82217	8.29825	8.16826
SM152	3.89481	1.33069	7.35464	7.20642
ND145	2.88226	1.87209	4.22063	4.18692
EU153	3.21177	2.56920	4.07021	4.04165
MO 95	2.09987	.97005	3.54423	3.55906
RU101	1.42170	.22404	2.84980	2.96850
AG109	1.44728	.47249	2.75572	2.70625
ND143	9.90337	15.62377	2.50825	2.51536
EU154	2.23714	2.19512	2.31606	2.29140
SM147	.79702	.28738	1.47167	1.45524
PD105	.87408	.46420	1.29412	1.40344
ZR 93	.60368	.18550	1.14261	1.14376
PD108	.51431	.13153	1.02206	1.00867
SM150	1.54143	1.96175	.97988	.99859
SM151	3.23823	5.17014	.75449	.74313
PM148	.49921	.33984	.71952	.70504
CS134	.91132	1.08947	.68118	.68123
PR141	.77187	.84276	.64865	.68031
MO 97	.38887	.17290	.57576	.66779
EU155	2.18896	3.45605	.55475	.55249
PD107	.32190	.16308	.49077	.52702
LA139	.61911	.75325	.44022	.44586
CS135	.30709	.20745	.43972	.43578
KR 83	.66512	.90590	.35097	.35416
RH105	.58694	.83091	.27759	.27184
MO 98	.13324	.01024	.25971	.29209
ND148	.14303	.05925	.22772	.25123
ZR 96	.09936	.00127	.21411	.22604
GD156	.09286	.00538	.20306	.20585
I127	.09969	.01927	.20073	.20356
I129	.28230	.33702	.19489	.21162
PD104	.09593	.00829	.18172	.20910
ND144	.22832	.24854	.17046	.20221
ZR 91	.11696	.06208	.17006	.18784
MO100	.09404	.01779	.16676	.19250
RU104	.08479	.02016	.14001	.16825
SM149	5.69759	10.00653	.13483	.13251
IN115	.07048	.02524	.13150	.12891
PM148M	1.83657	3.16345	.12413	.12288
RU103	.07255	.03009	.12194	.12739
SM148	.06968	.02331	.11397	.12957
ND147	.05958	.02136	.11035	.10895
RU102	.12987	.09197	.10409	.17882
PR143	.10586	.11066	.10017	.09965
ALL OTHERS	16.95996	28.81303	1.40022	1.65149

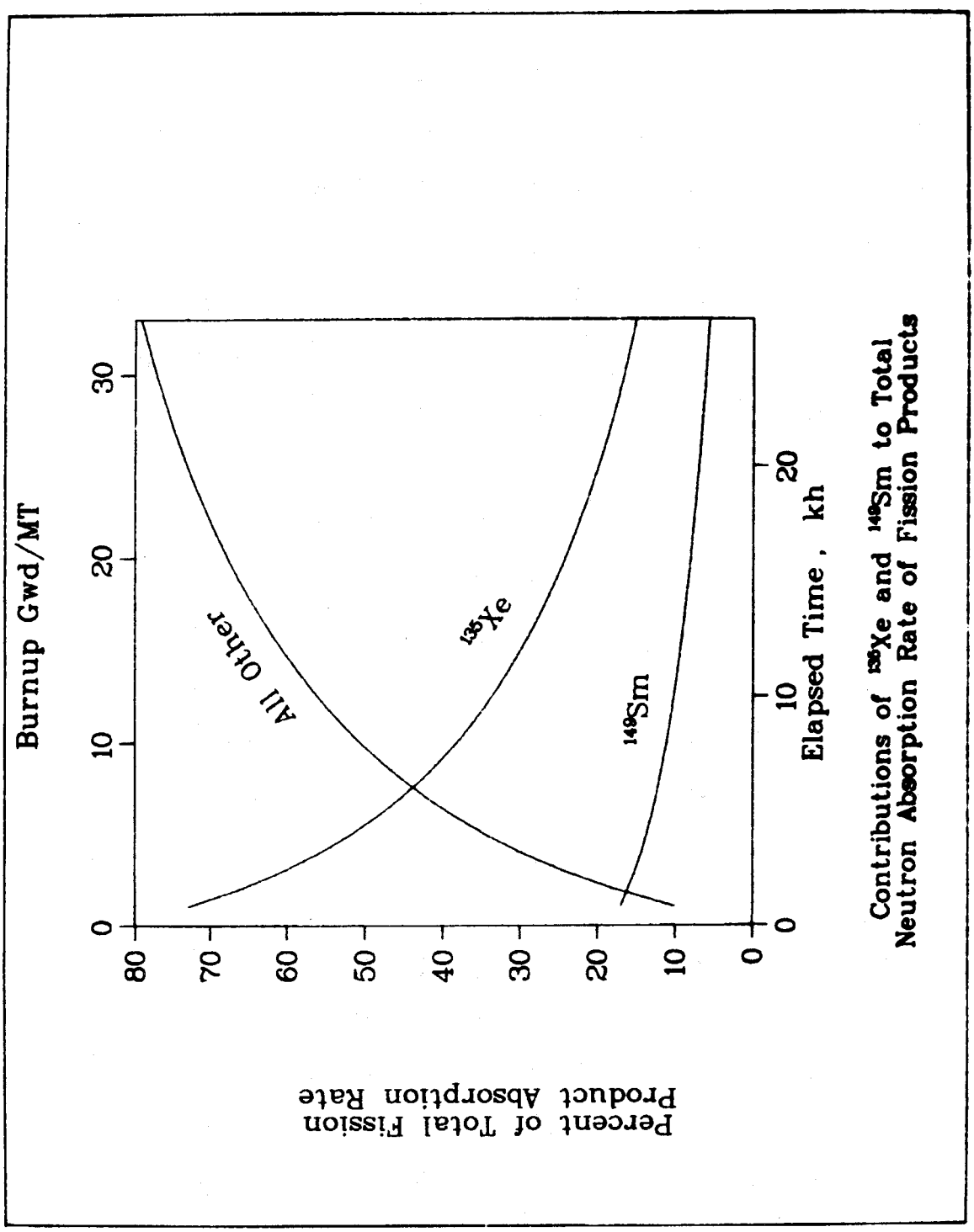

FIGURE 4. Contributions of ^{135}Xe and ^{149}Sm to Total Neutron Absorption Rate of Fission Products.

Table 13

CONTRIBUTIONS OF TEN MAJOR NUCLIDES TO THE TOTAL NEUTRON ABSORPTION RATE OF FISSION PRODUCTS

Elapsed Time, hours	Burnup GWd/MT	Percent of Total Fission-Product Absorption Rate										
		^{99}Tc	^{103}Rh	^{131}Xe	^{135}Xe	^{133}Cs	^{143}Nd	^{147}Pm	^{149}Sm	^{151}Sm	^{152}Sm	All Others
800	1	0.49	0.29	0.55	72.97	0.52	0.76	0.79	16.98	2.46	0.30	3.89
1600	2	0.94	0.88	1.21	65.87	1.12	1.97	1.82	16.05	3.79	0.64	5.71
2400	3	1.32	1.56	1.77	60.25	1.61	3.05	2.66	15.11	4.46	0.98	7.23
3200	4	1.64	2.24	2.24	55.60	2.03	3.96	3.32	14.33	4.77	1.29	8.58
4000	5	1.91	2.89	2.64	51.67	2.39	4.73	3.85	13.65	4.88	1.58	9.81
4800	6	2.16	3.49	3.00	48.28	2.70	5.39	4.27	13.04	4.88	1.84	10.95
5600	7	2.37	4.04	3.31	45.32	2.99	5.96	4.61	12.50	4.83	2.08	11.99
6400	8	2.57	4.55	3.59	42.69	3.24	6.46	4.88	12.01	4.75	2.29	12.97
7200	9	2.75	5.02	3.84	40.34	3.48	6.90	5.10	11.56	4.65	2.48	13.88
8000	10	2.91	5.45	4.07	38.21	3.69	7.29	5.27	11.14	4.55	2.65	14.77
8800	11	3.07	5.84	4.27	36.27	3.89	7.63	5.41	10.74	4.44	2.80	15.64
9600	12	3.21	6.21	4.46	34.50	4.07	7.94	5.51	10.38	4.34	2.94	16.44
10400	13	3.34	6.55	4.63	32.87	4.24	8.22	5.59	10.03	4.25	3.06	17.22
11200	14	3.46	6.87	4.79	31.36	4.39	8.47	5.64	9.71	4.16	3.17	17.98
12000	15	3.58	7.16	4.93	29.96	4.54	8.69	5.67	9.40	4.07	3.27	18.73
12800	16	3.69	7.43	5.06	28.65	4.68	8.89	5.69	9.11	3.99	3.36	19.47
13600	17	3.79	7.68	5.18	27.43	4.81	9.06	5.69	8.83	3.91	3.44	20.18
14400	18	3.89	7.92	5.29	26.28	4.94	9.22	5.67	8.57	3.84	3.51	20.87
15200	19	3.98	8.14	5.39	25.20	5.05	9.36	5.65	8.31	3.77	3.57	21.58
16000	20	4.07	8.34	5.48	24.19	5.17	9.48	5.61	8.07	3.71	3.62	22.26
16800	21	4.16	8.53	5.56	23.24	5.27	9.59	5.56	7.84	3.65	3.67	22.93
17600	22	4.24	8.70	5.64	22.34	5.37	9.68	5.51	7.62	3.60	3.71	23.59
18400	23	4.31	8.86	5.71	21.48	5.47	9.76	5.45	7.41	3.55	3.75	24.25
19200	24	4.39	9.00	5.77	20.68	5.56	9.82	5.38	7.21	3.50	3.78	24.91
20000	25	4.46	9.14	5.82	19.91	5.65	9.87	5.30	7.01	3.46	3.81	25.57
20800	26	4.53	9.26	5.87	19.19	5.73	9.91	5.23	6.82	3.42	3.83	26.21
21600	27	4.59	9.37	5.91	18.51	5.81	9.94	5.14	6.64	3.39	3.85	26.85
22400	28	4.66	9.47	5.94	17.86	5.89	9.96	5.06	6.47	3.35	3.86	27.48
23200	29	4.72	9.56	5.97	17.25	5.96	9.97	4.97	6.30	3.32	3.87	28.11
24000	30	4.78	9.64	6.00	16.66	6.03	9.96	4.88	6.14	3.30	3.88	28.73
24800	31	4.83	9.71	6.02	16.11	6.09	9.95	4.78	5.99	3.28	3.89	29.35
25600	32	4.89	9.77	6.03	15.59	6.16	9.93	4.69	5.84	3.26	3.89	29.95
26400	33	4.94	9.82	6.04	15.10	6.22	9.90	4.59	5.70	3.24	3.89	30.56

Table 14

NUCLIDES CONTRIBUTING GREATER THAN 0.1% OF THERMAL, EPITHERMAL OR TOTAL FISSION-PRODUCT ABSORPTION RATE AT SOME TIME DURING FUEL HISTORY (to 33 000 MWd/MT)

Z SYM	Thermal	Epithermal	Total
36 Kr	^{83}Kr	^{83}Kr	^{83}Kr
40 Zr	^{93}Zr	$^{91,93,95,96}Zr$	$^{91,93}Zr$
41 Nb		^{95}Nb	
42 Mo	$^{95,97}Mo$	$^{95,97,98,99,100}Mo$	$^{95,97,98}Mo$
43 Tc	^{99}Tc	^{99}Tc	^{99}Tc
44 Ru	^{101}Ru	$^{101,102,103,104}Ru$	$^{101,102,103}Ru$
45 Rh	$^{103,105}Rh$	$^{103,105}Rh$	$^{103,105}Rh$
46 Pd	$^{105,107,108}Pd$	$^{104,105,107,108}Pd$	$^{105,107,108}Pd$
47 Ag	^{109}Ag	^{109}Ag	^{109}Ag
48 Cd	^{113}Cd		^{113}Cd
49 In		^{115}In	
53 I	^{129}I	$^{127,129}I$	^{129}I
54 Xe	$^{131,133,135}Xe$	$^{131,133,135}Xe$	$^{131,133,135}Xe$
55 Cs	$^{133,134,135}Cs$	$^{133,134,135}Cs$	$^{133,134,135}Cs$
56 Ba		^{140}Ba	
57 La	^{139}La	$^{139,140}La$	^{139}La
58 Ce	^{141}Ce	$^{141,143}Ce$	^{141}Ce
59 Pr	$^{141,143}Pr$	$^{141,143}Pr$	$^{141,143}Pr$
60 Nd	$^{143,144,145}Nd$	$^{143,144,145,147,148}Nd$	$^{143,144,145,147,148}Nd$
61 Pm	$^{147,148,148m,149}Pm$	$^{147,148,148m,149,151}Pm$	$^{147,148,148m,149}Pm$
62 Sm	$^{147,149,150,151,152}Sm$	$^{147,148,149,150}Sm$ $^{151,152,153}Sm$	$^{147,149,150,151,152}Sm$
63 Eu	$^{153,154,155,156}Eu$	$^{153,154,155}Eu$	$^{153,154,155,156}Eu$
64 Gd	$^{155,157}Gd$	^{156}Gd	^{157}Gd

Table 15

SENSITIVITY OF TOTAL FISSION-PRODUCT ABSORPTION
RATE TO MASS 81--100 NUCLIDE PARAMETERS

NUCLIDE	PARAMETER	SENSITIVITY OF TOTAL FISSION-PRODUCT ABSORPTION TO PARAMETER		
		4.0 KHRS 5 GWD/MT	16.0 KHRS 20 GWD/MT	26.4 KHRS 33 GWD/MT
35-BR- 81	THERMAL N,G X-SEC	.00001	.00003	.00004
35-BR- 81	EF.YLD.FRAC. U235TH	.00011	.00021	.00025
35-BR- 82	DECAY CONSTANT VALUE	.0	.0	.0
35-BR- 82	EF.YLD.FRAC. U235TH	.0	.0	.0
36-KR- 82	THERMAL N,G X-SEC	.0	.0	.00002
36-KR- 82	EPITHERMAL N,G X-SEC	.0	.00001	.00003
36-KR- 82	EF.YLD.FRAC. U235TH	.0	.0	.0
36-KR- 83	THERMAL N,G X-SEC	.00258	.00408	.00352
36-KR- 83	EPITHERMAL N,G X-SEC	.00076	.00121	.00105
36-KR- 83	EF.YLD.FRAC. U235TH	.00321	.00513	.00477
38-SR- 90	THERMAL N,G X-SEC	.00013	.00026	.00031
38-SR- 90	EF.YLD.FRAC. U235TH	.00015	.00027	.00030
38-SR- 91	DECAY CONSTANT VALUE	.0	.0	.0
38-SR- 91	EF.YLD.FRAC. U235TH	.00040	.00085	.00096
39- Y- 91	DECAY CONSTANT VALUE	.00006	.00004	.00003
39- Y- 91	EF.YLD.FRAC. U235TH	.0	.0	.0
40-ZR- 91	THERMAL N,G X-SEC	.00009	.00027	.00035
40-ZR- 91	EPITHERMAL N,G X-SEC	.00018	.00057	.00072
40-ZR- 92	THERMAL N,G X-SEC	.00004	.00008	.00010
40-ZR- 92	EF.YLD.FRAC. U235TH	.00010	.00018	.00020
39- Y- 93	DECAY CONSTANT VALUE	.00001	.0	.0
39- Y- 93	EF.YLD.FRAC. U235TH	.00219	.00396	.00434
40-ZR- 93	THERMAL N,G X-SEC	.00041	.00084	.00103
40-ZR- 93	EPITHERMAL N,G X-SEC	.00193	.00394	.00479
40-ZR- 93	EF.YLD.FRAC. U235TH	.0	.0	.0
40-ZR- 94	EF.YLD.FRAC. U235TH	.00004	.00007	.00008
40-ZR- 95	DECAY CONSTANT VALUE	.00188	.00231	.00165
40-ZR- 95	EF.YLD.FRAC. U235TH	.00343	.01278	.01509
41-NB- 95	DECAY CONSTANT VALUE	.00106	.00105	.00075
42-MO- 95	THERMAL N,G X-SEC	.00081	.00395	.00519
42-MO- 95	EPITHERMAL N,G X-SEC	.00224	.01092	.01431
40-ZR- 96	EF.YLD.FRAC. U235TH	.00033	.00060	.00067
42-MO- 96	THERMAL N,G X-SEC	.0	.00001	.00002
40-ZR- 97	DECAY CONSTANT VALUE	.00001	.0	.0
40-ZR- 97	EF.YLD.FRAC. U235TH	.00123	.00223	.00246
42-MO- 97	THERMAL N,G X-SEC	.00035	.00076	.00097
42-MO- 97	EPITHERMAL N,G X-SEC	.00088	.00191	.00244
42-MO- 97	EF.YLD.FRAC. U235TH	.0	.0	.00001
42-MO- 98	THERMAL N,G X-SEC	.00002	.00005	.00007
42-MO- 98	EPITHERMAL N,G X-SEC	.00039	.00091	.00125
42-MO- 98	EF.YLD.FRAC. U235TH	.00041	.00079	.00093
42-MO- 99	EF.YLD.FRAC. U235TH	.01684	.02949	.03035
42-MO- 99	EF.YLD.FRAC. U238FST	.00087	.00205	.00291
42-MO- 99	EF.YLD.FRAC.PU239TH	.00147	.00936	.01659
43-TC- 99	THERMAL N,G X-SEC	.00307	.00622	.00705
43-TC- 99	EPITHERMAL N,G X-SEC	.01552	.03127	.03526
42-MO-100	THERMAL N,G X-SEC	.00003	.00008	.00011
42-MO-100	EPITHERMAL N,G X-SEC	.00025	.00055	.00074
42-MO-100	EF.YLD.FRAC. U235TH	.00028	.00052	.00059
44-RU-100	THERMAL N,G X-SEC	.00001	.00014	.00036

Table 16

SENSITIVITY OF TOTAL FISSION-PRODUCT ABSORPTION RATE TO MASS 101--115 NUCLIDE PARAMETERS

NUCLIDE	PARAMETER	SENSITIVITY OF TOTAL FISSION-PRODUCT ABSORPTION TO PARAMETER		
		4.0 KHRS 5 GWD/MT	16.0 KHRS 20 GWD/MT	26.4 KHRS 33 GWD/MT
44-RU-101	THERMAL N,G X-SEC	.00044	.00096	.00122
44-RU-101	EPITHERMAL N,G X-SEC	.00421	.00922	.01169
44-RU-101	EF.YLD.FRAC. U235TH	.00423	.00755	.00818
44-RU-102	THERMAL N,G X-SEC	.00016	.00045	.00070
44-RU-102	EPITHERMAL N,G X-SEC	.00014	.00038	.00060
44-RU-102	EF.YLD.FRAC. U235TH	.00034	.00072	.00092
44-RU-103	DECAY CONSTANT VALUE	.01005	.00638	.00413
44-RU-103	THERMAL N,G X-SEC	.00024	.00013	.00009
44-RU-103	EPITHERMAL N,G X-SEC	.00073	.00039	.00026
44-RU-103	EF.YLD.FRAC. U235TH	.02364	.04591	.03950
44-RU-103	EF.YLD.FRAC. U238FST	.00238	.00629	.00788
44-RU-103	EF.YLD.FRAC.PU239TH	.00392	.03217	.05206
45-RH-103	THERMAL N,G X-SEC	.01029	.02421	.02122
45-RH-103	EPITHERMAL N,G X-SEC	.01709	.04003	.03486
44-RU-104	THERMAL N,G X-SEC	.00003	.00008	.00013
44-RU-104	EPITHERMAL N,G X-SEC	.00015	.00043	.00066
44-RU-104	EF.YLD.FRAC. U235TH	.00015	.00027	.00032
44-RU-105	DECAY CONSTANT VALUE	.0	.0	.0
44-RU-105	EF.YLD.FRAC. U235TH	.00422	.00311	.00267
45-RH-105	DECAY CONSTANT VALUE	-.00566	-.00489	-.00469
45-RH-105	THERMAL N,G X-SEC	.00496	.00428	.00409
45-RH-105	EPITHERMAL N,G X-SEC	.00126	.00108	.00104
46-PD-105	THERMAL N,G X-SEC	.00054	.00167	.00250
46-PD-105	EPITHERMAL N,G X-SEC	.00114	.00353	.00527
44-RU-106	EF.YLD.FRAC. U235TH	.00001	.00004	.00005
46-PD-106	THERMAL N,G X-SEC	.0	.00001	.00002
46-PD-106	EPITHERMAL N,G X-SEC	.00001	.00009	.00022
46-PD-107	THERMAL N,G X-SEC	.00012	.00055	.00098
46-PD-107	EPITHERMAL N,G X-SEC	.00028	.00126	.00222
46-PD-107	EF.YLD.FRAC. U235TH	.00014	.00026	.00030
46-PD-108	THERMAL N,G X-SEC	.00009	.00049	.00094
46-PD-108	EPITHERMAL N,G X-SEC	.00054	.00289	.00548
46-PD-108	EF.YLD.FRAC. U235TH	.00015	.00031	.00039
46-PD-109	DECAY CONSTANT VALUE	.00001	.00001	.00002
46-PD-109	EF.YLD.FRAC. U235TH	.00034	.00049	.00040
47-AG-109	THERMAL N,G X-SEC	.00035	.00136	.00167
47-AG-109	EPITHERMAL N,G X-SEC	.00153	.00592	.00718
46-PD-110	EF.YLD.FRAC. U235TH	.0	.0	.00001
47-AG-111	EF.YLD.FRAC. U235TH	.00002	.00003	.00004
46-PD-112	EF.YLD.FRAC. U235TH	.0	.00001	.00001
48-CD-112	THERMAL N,G X-SEC	.0	.00001	.00002
48-CD-112	EPITHERMAL N,G X-SEC	.0	.00001	.00003
48-CD-112	EF.YLD.FRAC. U235TH	.0	.0	.0
48-CD-113	THERMAL N,G X-SEC	.00004	.0	.0
48-CD-113	EPITHERMAL N,G X-SEC	.0	.0	.0
48-CD-113	EF.YLD.FRAC. U235TH	.00111	.00032	.00013
48-CD-114	EF.YLD.FRAC. U235TH	.0	.0	.00001
48-CD-115	DECAY CONSTANT VALUE	.00001	.0	.0
48-CD-115M	DECAY CONSTANT VALUE	.00001	.00001	.00001

Table 17

SENSITIVITY OF TOTAL FISSION-PRODUCT ABSORPTION RATE TO MASS 128--135 NUCLIDE PARAMETERS

NUCLIDE	PARAMETER	SENSITIVITY OF TOTAL FISSION-PRODUCT ABSORPTION TO PARAMETER		
		4.0 KHRS 5 GWD/MT	16.0 KHRS 20 GWD/MT	26.4 KHRS 33 GWD/MT
51-SB-128	DECAY CONSTANT VALUE	.0	.0	.0
51-SB-128	EF.YLD.FRAC. U235TH	.0	.0	.0
52-TE-128	THERMAL N,G X-SEC	.0	.0	.00001
52-TE-128	EPITHERMAL N,G X-SEC	.00001	.00002	.00003
52-TE-128	EF.YLD.FRAC. U235TH	.00001	.00002	.00003
52-TE-128	BF, N,G TO ISO STATE	.0	.0	.0
52-TE-129M	EF.YLD.FRAC. U235TH	.00012	.00026	.00030
53- I-129	THERMAL N,G X-SEC	.00050	.00133	.00183
53- I-129	EPITHERMAL N,G X-SEC	.00022	.00058	.00081
53- I-129	EF.YLD.FRAC. U235TH	.00047	.00085	.00092
53- I-130	EF.YLD.FRAC. U235TH	.0	.0	.0
54-XE-130	THERMAL N,G X-SEC	.0	.00001	.00003
52-TE-131M	DECAY CONSTANT VALUE	.00004	.00002	.00001
52-TE-131M	EF.YLD.FRAC. U235TH	.00287	.00464	.00406
52-TE-131M	EF.YLD.FRAC. U238FST	.00009	.00020	.00026
52-TE-131M	EF.YLD.FRAC.PU239TH	.00043	.00272	.00436
53- I-131	DECAY CONSTANT VALUE	.00174	.00076	.00045
53- I-131	EF.YLD.FRAC. U235TH	.01976	.03164	.02765
53- I-131	EF.YLD.FRAC. U238FST	.00120	.00264	.00335
53- I-131	EF.YLD.FRAC.PU239TH	.00210	.01302	.02083
54-XE-131	THERMAL N,G X-SEC	.00612	.01061	.00906
54-XE-131	EPITHERMAL N,G X-SEC	.01906	.03278	.02765
52-TE-132	EF.YLD.FRAC. U235TH	.00013	.00025	.00031
54-XE-132	THERMAL N,G X-SEC	.00005	.00014	.00022
54-XE-132	EPITHERMAL N,G X-SEC	.00006	.00016	.00025
53- I-133	EF.YLD.FRAC. U235TH	.02355	.04131	.04438
53- I-133	EF.YLD.FRAC. U238FST	.00112	.00264	.00387
53- I-133	EF.YLD.FRAC.PU239TH	.00219	.01330	.02422
54-XE-133	THERMAL N,G X-SEC	.00155	.00075	.00050
54-XE-133	EF.YLD.FRAC. U235TH	.0	.0	.00001
55-CS-133	THERMAL N,G X-SEC	.00512	.01103	.01298
55-CS-133	EPITHERMAL N,G X-SEC	.01851	.03978	.04657
54-XE-134	THERMAL N,G X-SEC	.00009	.00020	.00028
54-XE-134	EPITHERMAL N,G X-SEC	.00005	.00010	.00014
54-XE-134	EF.YLD.FRAC. U235TH	.00017	.00033	.00037
55-CS-134	THERMAL N,G X-SEC	.00032	.00267	.00542
55-CS-134	EPITHERMAL N,G X-SEC	.00015	.00126	.00258
53- I-135	THERMAL N,G X-SEC	.0	.0	.0
53- I-135	EF.YLD.FRAC. U235TH	.40290	.12636	.05091
53- I-135	EF.YLD.FRAC. U238FST	.02271	.01336	.01114
53- I-135	EF.YLD.FRAC.PU239TH	.06426	.08408	.07575
54-XE-135	DECAY CONSTANT VALUE	-.14269	-.05411	-.02513
54-XE-135	THERMAL N,G X-SEC	.13693	.05143	.02363
54-XE-135	EPITHERMAL N,G X-SEC	.00006	.00002	.00001
54-XE-135	EF.YLD.FRAC. U235TH	.01615	.00506	.00204
54-XE-135	EF.YLD.FRAC. U238FST	.00005	.00003	.00003
54-XE-135	EF.YLD.FRAC.PU239TH	.01174	.01536	.01384
55-CS-135	THERMAL N,G X-SEC	.00045	.00094	.00114
55-CS-135	EPITHERMAL N,G X-SEC	.00073	.00151	.00182
55-CS-135	EF.YLD.FRAC. U235TH	.0	.0	.0

Table 18

SENSITIVITY OF TOTAL FISSION-PRODUCT ABSORPTION RATE TO MASS 136--146 NUCLIDE PARAMETERS

NUCLIDE	PARAMETER	SENSITIVITY OF TOTAL FISSION-PRODUCT ABSORPTION TO PARAMETER		
		4.0 KHRS 5 GWD/MT	16.0 KHRS 20 GWD/MT	26.4 KHRS 33 GWD/MT
54-XE-136	EF.YLD.FRAC. U235TH	.00003	.00005	.00006
55-CS-137	EF.YLD.FRAC. U235TH	.00005	.00013	.00018
56-BA-138	EF.YLD.FRAC. U235TH	.00007	.00013	.00015
57-LA-139	THERMAL N,G X-SEC	.00156	.00333	.00418
57-LA-139	EPITHERMAL N,G X-SEC	.00069	.00147	.00185
57-LA-139	EF.YLD.FRAC. U235TH	.00203	.00366	.00401
56-BA-140	EF.YLD.FRAC. U235TH	.00027	.00027	.00027
57-LA-140	EF.YLD.FRAC. U235TH	.0	.0	.0
58-CE-140	THERMAL N,G X-SEC	.00009	.00021	.00027
58-CE-140	EPITHERMAL N,G X-SEC	.00001	.00003	.00005
58-CE-141	DECAY CONSTANT VALUE	-.00065	-.00038	-.00027
58-CE-141	THERMAL N,G X-SEC	.00124	.00067	.00051
58-CE-141	EPITHERMAL N,G X-SEC	.00032	.00017	.00013
58-CE-141	EF.YLD.FRAC. U235TH	.00331	.00505	.00547
59-PR-141	THERMAL N,G X-SEC	.00133	.00365	.00478
59-PR-141	EPITHERMAL N,G X-SEC	.00077	.00213	.00279
58-CE-142	THERMAL N,G X-SEC	.00016	.00038	.00054
58-CE-142	EF.YLD.FRAC. U235TH	.00019	.00040	.00051
58-CE-142	EF.YLD.FRAC. U238FST	.00001	.00002	.00004
58-CE-142	EF.YLD.FRAC.PU239TH	.00001	.00010	.00021
59-PR-142	DECAY CONSTANT VALUE	.0	.0	.0
59-PR-142	THERMAL N,G X-SEC	.0	.0	.0
60-ND-142	THERMAL N,G X-SEC	.0	.00007	.00020
58-CE-143	DECAY CONSTANT VALUE	.00052	.00019	.00010
58-CE-143	THERMAL N,G X-SEC	.00001	.0	.0
58-CE-143	EPITHERMAL N,G X-SEC	.00003	.00001	.00001
58-CE-143	EF.YLD.FRAC. U235TH	.04532	.07393	.06563
58-CE-143	EF.YLD.FRAC. U238FST	.00185	.00413	.00529
58-CE-143	EF.YLD.FRAC.PU239TH	.00292	.01846	.02985
59-PR-143	DECAY CONSTANT VALUE	.00319	.00119	.00060
59-PR-143	THERMAL N,G X-SEC	.00152	.00057	.00029
59-PR-143	EPITHERMAL N,G X-SEC	.00104	.00039	.00020
60-ND-143	THERMAL N,G X-SEC	.04025	.06709	.05337
60-ND-143	EPITHERMAL N,G X-SEC	.00491	.00829	.00672
60-ND-143	EF.YLD.FRAC. U235TH	.0	.0	.0
58-CE-144	DECAY CONSTANT VALUE	.00009	.00036	.00045
58-CE-144	THERMAL N,G X-SEC	.00012	.00016	.00015
58-CE-144	EF.YLD.FRAC. U235TH	.00034	.00101	.00139
60-ND-144	THERMAL N,G X-SEC	.00012	.00081	.00153
60-ND-144	EPITHERMAL N,G X-SEC	.00006	.00042	.00080
60-ND-144	EF.YLD.FRAC. U235TH	.0	.0	.0
59-PR-145	EF.YLD.FRAC. U235TH	.01067	.01837	.01886
60-ND-145	THERMAL N,G X-SEC	.00432	.00829	.00917
60-ND-145	EPITHERMAL N,G X-SEC	.00737	.01413	.01560
60-ND-146	THERMAL N,G X-SEC	.00013	.00042	.00072
60-ND-146	EPITHERMAL N,G X-SEC	.00009	.00028	.00049
60-ND-146	EF.YLD.FRAC. U235TH	.00024	.00062	.00090

Table 19

SENSITIVITY OF TOTAL FISSION-PRODUCT ABSORPTION RATE TO MASS 147--150 NUCLIDE PARAMETERS

NUCLIDE	PARAMETER	SENSITIVITY OF TOTAL FISSION-PRODUCT ABSORPTION TO PARAMETER		
		4.0 KHRS 5 GWD/MT	16.0 KHRS 20 GWD/MT	26.4 KHRS 33 GWD/MT
60-ND-147	DECAY CONSTANT VALUE	.00531	.00155	.00097
60-ND-147	THERMAL N,G X-SEC	.00021	.0	-.00006
60-ND-147	EPITHERMAL N,G X-SEC	.00084	.00001	-.00022
60-ND-147	EF.YLD.FRAC. U235TH	.06181	.08410	.06440
60-ND-147	EF.YLD.FRAC. U238FST	.00371	.00720	.00855
60-ND-147	EF.YLD.FRAC.PU239TH	.00467	.02753	.04101
61-PM-147	DECAY CONSTANT VALUE	-.00259	-.01530	-.01790
61-PM-147	THERMAL N,G X-SEC	.01391	.01594	.00927
61-PM-147	EPITHERMAL N,G X-SEC	.04775	.05378	.03069
61-PM-147	EF.YLD.FRAC. U235TH	.0	.0	.0
61-PM-147	BF, N,G TO GND STATE	-.02297	-.04150	-.03967
61-PM-147	BF, N,G TO ISO STATE	.02037	.03680	.03518
62-SM-147	THERMAL N,G X-SEC	.00017	.00100	.00123
62-SM-147	EPITHERMAL N,G X-SEC	.00064	.00387	.00467
60-ND-148	THERMAL N,G X-SEC	.00023	.00055	.00078
60-ND-148	EPITHERMAL N,G X-SEC	.00067	.00160	.00227
60-ND-148	EF.YLD.FRAC. U235TH	.00085	.00169	.00209
60-ND-148	EF.YLD.FRAC. U238FST	.00006	.00015	.00025
60-ND-148	EF.YLD.FRAC.PU239TH	.00007	.00051	.00102
61-PM-148	DECAY CONSTANT VALUE	-.00374	-.00776	-.00887
61-PM-148	THERMAL N,G X-SEC	.00163	.00323	.00366
61-PM-148	EPITHERMAL N,G X-SEC	.00261	.00517	.00585
61-PM-148	EF.YLD.FRAC. U235TH	.0	.0	.0
61-PM-148M	DECAY CONSTANT VALUE	-.00512	-.00861	-.00698
61-PM-148M	THERMAL N,G X-SEC	.00697	.00834	.00649
61-PM-148M	EPITHERMAL N,G X-SEC	.00022	.00026	.00021
61-PM-148M	BF,BETA TO GND STATE	-.00086	-.00158	-.00142
61-PM-148M	BF,ISOMERIC TRANSITN	.00005	.00010	.00009
62-SM-148	THERMAL N,G X-SEC	.00001	.00013	.00029
62-SM-148	EPITHERMAL N,G X-SEC	.00005	.00049	.00107
62-SM-148	EF.YLD.FRAC. U235TH	.0	.0	.0
61-PM-149	DECAY CONSTANT VALUE	.00040	.00012	.00013
61-PM-149	THERMAL N,G X-SEC	.00005	.00009	.00005
61-PM-149	EPITHERMAL N,G X-SEC	.00001	.00001	.00001
61-PM-149	EF.YLD.FRAC. U235TH	.10208	.04288	.03081
61-PM-149	EF.YLD.FRAC. U238FST	.00900	.00625	.00643
61-PM-149	EF.YLD.FRAC.PU239TH	.01840	.02673	.02922
62-SM-149	THERMAL N,G X-SEC	.00105	.00040	.00028
62-SM-149	EPITHERMAL N,G X-SEC	.00001	.0	.0
60-ND-150	THERMAL N,G X-SEC	.00004	.00013	.00023
60-ND-150	EPITHERMAL N,G X-SEC	.00019	.00065	.00112
60-ND-150	EF.YLD.FRAC. U235TH	.00021	.00056	.00082
62-SM-150	THERMAL N,G X-SEC	.00478	.01752	.02939
62-SM-150	EPITHERMAL N,G X-SEC	.00181	.00665	.01118
62-SM-150	EF.YLD.FRAC. U235TH	.0	.00001	.00001

Table 20

SENSITIVITY OF TOTAL FISSION-PRODUCT ABSORPTION RATE TO MASS 151-- 157 NUCLIDE PARAMETERS

NUCLIDE	PARAMETER	SENSITIVITY OF TOTAL FISSION-PRODUCT ABSORPTION TO PARAMETER		
		4.0 KHRS 5 GWD/MT	16.0 KHRS 20 GWD/MT	26.4 KHRS 33 GWD/MT
61-PM-151	DECAY CONSTANT VALUE	.00023	.00013	.00018
61-PM-151	THERMAL N,G X-SEC	.00002	-.00002	-.00006
61-PM-151	EPITHERMAL N,G X-SEC	.00001	-.00002	-.00005
61-PM-151	EF.YLD.FRAC. U235TH	.04173	.03012	.02564
61-PM-151	EF.YLD.FRAC. U238FST	.00439	.00473	.00564
61-PM-151	EF.YLD.FRAC.PU239TH	.00854	.02302	.03135
62-SM-151	DECAY CONSTANT VALUE	-.00001	-.00005	-.00007
62-SM-151	THERMAL N,G X-SEC	.01462	.00414	.00330
62-SM-151	EPITHERMAL N,G X-SEC	.00174	.00049	.00039
62-SM-151	EF.YLD.FRAC. U235TH	.0	.0	.0
62-SM-152	THERMAL N,G X-SEC	.00299	.00697	.00735
62-SM-152	EPITHERMAL N,G X-SEC	.01242	.02842	.02945
62-SM-152	EF.YLD.FRAC. U235TH	.00695	.01300	.01407
62-SM-152	EF.YLD.FRAC. U238FST	.00072	.00180	.00268
62-SM-152	EF.YLD.FRAC.PU239TH	.00136	.00879	.01647
62-SM-153	DECAY CONSTANT VALUE	.00001	.00019	.00042
62-SM-153	THERMAL N,G X-SEC	.00004	.00002	-.00003
62-SM-153	EPITHERMAL N,G X-SEC	.00010	.00006	-.00008
62-SM-153	EF.YLD.FRAC. U235TH	.00377	.00814	.00761
63-EU-153	THERMAL N,G X-SEC	.00266	.01220	.01721
63-EU-153	EPITHERMAL N,G X-SEC	.00318	.01460	.02055
63-EU-153	EF.YLD.FRAC. U235TH	.0	.0	.0
62-SM-154	THERMAL N,G X-SEC	.00002	.00007	.00012
62-SM-154	EPITHERMAL N,G X-SEC	.00005	.00017	.00028
62-SM-154	EF.YLD.FRAC. U235TH	.00005	.00011	.00014
63-EU-154	DECAY CONSTANT VALUE	-.00001	-.00041	-.00117
63-EU-154	THERMAL N,G X-SEC	.00054	.00581	.00922
63-EU-154	EPITHERMAL N,G X-SEC	.00043	.00466	.00742
63-EU-154	EF.YLD.FRAC. U235TH	.0	.0	.0
64-GD-154	THERMAL N,G X-SEC	.0	.00004	.00015
64-GD-154	EPITHERMAL N,G X-SEC	.0	.00004	.00014
63-EU-155	DECAY CONSTANT VALUE	.00010	.00005	-.00002
63-EU-155	THERMAL N,G X-SEC	.00193	.00234	.00290
63-EU-155	EPITHERMAL N,G X-SEC	.00024	.00030	.00038
63-EU-155	EF.YLD.FRAC. U235TH	.00223	.00110	.00050
64-GD-155	THERMAL N,G X-SEC	.00002	.00001	.00001
64-GD-155	EPITHERMAL N,G X-SEC	.0	.0	.0
63-EU-156	DECAY CONSTANT VALUE	-.00012	-.00030	-.00072
63-EU-156	THERMAL N,G X-SEC	.0	.0	.0
63-EU-156	EPITHERMAL N,G X-SEC	.0	.0	.0
63-EU-156	EF.YLD.FRAC. U235TH	.00006	.00006	.00006
64-GD-156	THERMAL N,G X-SEC	.0	.00002	.00006
64-GD-156	EPITHERMAL N,G X-SEC	.00008	.00057	.00168
63-EU-157	DECAY CONSTANT VALUE	.0	.0	.0
63-EU-157	THERMAL N,G X-SEC	.0	.0	.0
63-EU-157	EPITHERMAL N,G X-SEC	.0	.0	.0
63-EU-157	EF.YLD.FRAC. U235TH	.00058	.00017	.00007
64-GD-157	THERMAL N,G X-SEC	.0	.0	.00001
64-GD-157	EPITHERMAL N,G X-SEC	.0	.0	.0
64-GD-157	EF.YLD.FRAC. U235TH	.0	.0	.0

Table 21

NUCLIDE PARAMETERS TO WHICH CALCULATED TOTAL FISSION-PRODUCT ABSORPTION RATE AT 4000 HOURS (5 GWD/MT) IS MOST SENSITIVE

ORDER	NUCLIDE	PARAMETER	SENSITIVITY
1	53- I-135	EF.YLD.FRAC. U235TH	.40290
2	54-XE-135	DECAY CONSTANT VALUE	-.14269
3	54-XE-135	THERMAL N,G X-SEC	.13693
4	61-PM-149	EF.YLD.FRAC. U235TH	.10208
5	53- I-135	EF.YLD.FRAC.PU239TH	.06426
6	60-ND-147	EF.YLD.FRAC. U235TH	.06181
7	61-PM-147	EPITHERMAL N,G X-SEC	.04775
8	58-CE-143	EF.YLD.FRAC. U235TH	.04532
9	61-PM-151	EF.YLD.FRAC. U235TH	.04173
10	60-ND-143	THERMAL N,G X-SEC	.04025
11	44-RU-103	EF.YLD.FRAC. U235TH	.02364
12	53- I-133	EF.YLD.FRAC. U235TH	.02355
13	61-PM-147	BF, N,G TO GND STATE	-.02297
14	53- I-135	EF.YLD.FRAC. U238FST	.02271
15	61-PM-147	BF, N,G TO ISO STATE	.02037
16	53- I-131	EF.YLD.FRAC. U235TH	.01976
17	54-XE-131	EPITHERMAL N,G X-SEC	.01906
18	55-CS-133	EPITHERMAL N,G X-SEC	.01851
19	61-PM-149	EF.YLD.FRAC.PU239TH	.01840
20	45-RH-103	EPITHERMAL N,G X-SEC	.01709
21	42-MO- 99	EF.YLD.FRAC. U235TH	.01684
22	54-XE-135	EF.YLD.FRAC. U235TH	.01615
23	43-TC- 99	EPITHERMAL N,G X-SEC	.01552
24	62-SM-151	THERMAL N,G X-SEC	.01462
25	61-PM-147	THERMAL N,G X-SEC	.01391
26	62-SM-152	EPITHERMAL N,G X-SEC	.01242
27	54-XE-135	EF.YLD.FRAC.PU239TH	.01174
28	59-PR-145	EF.YLD.FRAC. U235TH	.01067
29	45-RH-103	THERMAL N,G X-SEC	.01029
30	44-RU-103	DECAY CONSTANT VALUE	.01005
31	61-PM-149	EF.YLD.FRAC. U238FST	.00900
32	61-PM-151	EF.YLD.FRAC.PU239TH	.00854
33	60-ND-145	EPITHERMAL N,G X-SEC	.00737
34	61-PM-148M	THERMAL N,G X-SEC	.00697
35	62-SM-152	EF.YLD.FRAC. U235TH	.00695
36	54-XE-131	THERMAL N,G X-SEC	.00612
37	45-RH-105	DECAY CONSTANT VALUE	-.00566
38	60-ND-147	DECAY CONSTANT VALUE	.00531
39	55-CS-133	THERMAL N,G X-SEC	.00512
40	61-PM-148M	DECAY CONSTANT VALUE	-.00512

Table 22

NUCLIDE PARAMETERS TO WHICH CALCULATED TOTAL FISSION-PRODUCT ABSORPTION RATE AT 16000 HOURS (20 GWD/MT) IS MOST SENSITIVE

ORDER	NUCLIDE	PARAMETER	SENSITIVITY
1	53- I-135	EF.YLD.FRAC. U235TH	.12636
2	60-ND-147	EF.YLD.FRAC. U235TH	.08410
3	53- I-135	EF.YLD.FRAC.PU239TH	.08408
4	58-CE-143	EF.YLD.FRAC. U235TH	.07393
5	60-ND-143	THERMAL N,G X-SEC	.06709
6	54-XE-135	DECAY CONSTANT VALUE	-.05411
7	61-PM-147	EPITHERMAL N,G X-SEC	.05378
8	54-XE-135	THERMAL N,G X-SEC	.05143
9	44-RU-103	EF.YLD.FRAC. U235TH	.04591
10	61-PM-149	EF.YLD.FRAC. U235TH	.04288
11	61-PM-147	BF, N,G TO GND STATE	-.04150
12	53- I-133	EF.YLD.FRAC. U235TH	.04131
13	45-RH-103	EPITHERMAL N,G X-SEC	.04003
14	55-CS-133	EPITHERMAL N,G X-SEC	.03978
15	61-PM-147	BF, N,G TO ISO STATE	.03680
16	54-XE-131	EPITHERMAL N,G X-SEC	.03278
17	44-RU-103	EF.YLD.FRAC.PU239TH	.03217
18	53- I-131	EF.YLD.FRAC. U235TH	.03164
19	43-TC- 99	EPITHERMAL N,G X-SEC	.03127
20	61-PM-151	EF.YLD.FRAC. U235TH	.03012
21	42-MO- 99	EF.YLD.FRAC. U235TH	.02949
22	62-SM-152	EPITHERMAL N,G X-SEC	.02842
23	60-ND-147	EF.YLD.FRAC.PU239TH	.02753
24	61-PM-149	EF.YLD.FRAC.PU239TH	.02673
25	45-RH-103	THERMAL N,G X-SEC	.02421
26	61-PM-151	EF.YLD.FRAC.PU239TH	.02302
27	58-CE-143	EF.YLD.FRAC.PU239TH	.01846
28	59-PR-145	EF.YLD.FRAC. U235TH	.01837
29	62-SM-150	THERMAL N,G X-SEC	.01752
30	61-PM-147	THERMAL N,G X-SEC	.01594
31	54-XE-135	EF.YLD.FRAC.PU239TH	.01536
32	61-PM-147	DECAY CONSTANT VALUE	-.01530
33	63-EU-153	EPITHERMAL N,G X-SEC	.01460
34	60-ND-145	EPITHERMAL N,G X-SEC	.01413
35	53- I-135	EF.YLD.FRAC. U238FST	.01336
36	53- I-133	EF.YLD.FRAC.PU239TH	.01330
37	53- I-131	EF.YLD.FRAC.PU239TH	.01302
38	62-SM-152	EF.YLD.FRAC. U235TH	.01300
39	40-ZR- 95	EF.YLD.FRAC. U235TH	.01278
40	63-EU-153	THERMAL N,G X-SEC	.01220

Table 23

NUCLIDE PARAMETERS TO WHICH CALCULATED TOTAL FISSION-PRODUCT ABSORPTION RATE AT 26400 HOURS (33 GWD/MT) IS MOST SENSITIVE

ORDER	NUCLIDE	PARAMETER	SENSITIVITY
1	53- I-135	EF.YLD.FRAC.PU239TH	.07575
2	58-CE-143	EF.YLD.FRAC. U235TH	.06563
3	60-ND-147	EF.YLD.FRAC. U235TH	.06440
4	60-ND-143	THERMAL N,G X-SEC	.05337
5	44-RU-103	EF.YLD.FRAC.PU239TH	.05206
6	53- I-135	EF.YLD.FRAC. U235TH	.05091
7	55-CS-133	EPITHERMAL N,G X-SEC	.04657
8	53- I-133	EF.YLD.FRAC. U235TH	.04438
9	60-ND-147	EF.YLD.FRAC.PU239TH	.04101
10	61-PM-147	BF, N,G TO GND STATE	-.03967
11	44-RU-103	EF.YLD.FRAC. U235TH	.03950
12	43-TC- 99	EPITHERMAL N,G X-SEC	.03526
13	61-PM-147	BF, N,G TO ISO STATE	.03518
14	45-RH-103	EPITHERMAL N,G X-SEC	.03486
15	61-PM-151	EF.YLD.FRAC.PU239TH	.03135
16	61-PM-149	EF.YLD.FRAC. U235TH	.03081
17	61-PM-147	EPITHERMAL N,G X-SEC	.03069
18	42-MO- 99	EF.YLD.FRAC. U235TH	.03035
19	58-CE-143	EF.YLD.FRAC.PU239TH	.02985
20	62-SM-152	EPITHERMAL N,G X-SEC	.02945
21	62-SM-150	THERMAL N,G X-SEC	.02939
22	61-PM-149	EF.YLD.FRAC.PU239TH	.02922
23	53- I-131	EF.YLD.FRAC. U235TH	.02765
24	54-XE-131	EPITHERMAL N,G X-SEC	.02765
25	61-PM-151	EF.YLD.FRAC. U235TH	.02564
26	54-XE-135	DECAY CONSTANT VALUE	-.02513
27	53- I-133	EF.YLD.FRAC.PU239TH	.02422
28	54-XE-135	THERMAL N,G X-SEC	.02363
29	45-RH-103	THERMAL N,G X-SEC	.02122
30	53- I-131	EF.YLD.FRAC.PU239TH	.02083
31	63-EU-153	EPITHERMAL N,G X-SEC	.02055
32	59-PR-145	EF.YLD.FRAC. U235TH	.01886
33	61-PM-147	DECAY CONSTANT VALUE	-.01790
34	63-EU-153	THERMAL N,G X-SEC	.01721
35	42-MO- 99	EF.YLD.FRAC.PU239TH	.01659
36	62-SM-152	EF.YLD.FRAC.PU239TH	.01647
37	60-ND-145	EPITHERMAL N,G X-SEC	.01560
38	40-ZR- 95	EF.YLD.FRAC. U235TH	.01509
39	42-MO- 95	EPITHERMAL N,G X-SEC	.01431
40	62-SM-152	EF.YLD.FRAC. U235TH	.01407

We expect the results of these sensitivity studies will be very useful in defining the parameters in most need of Version V review and of more lasting use in defining the parameters requiring improved evaluations in future ENDF/B modules or versions.

EXAMINATION OF THE EXPERIMENTS OF GUNST, CONNOR, AND CONWAY AS A POTENTIAL BENCHMARK FOR FISSION-PRODUCT ABSORPTION IN THERMAL REACTORS

Description of Experiment

The experiments of Gunst, Connor, and Conway constitute the most extensive measurements of fission-product absorption in thermal reactors available.[41,42] In these experiments, samples of ^{233}U and natural thorium were irradiated to high depletion in consecutive three-week cycles in the Materials Testing Reactor (MTR) and Advanced Test Reactor (ATR). Three-group flux histories during irradiation cycles were obtained from flux monitors. Reactivity measurements following most of the irradiation cycles were made on each sample in the Advanced Reactivity Measurement Facility (ARMF-I). The TARMF analytical model[42] was used to extract fission-product absorption parameters from the measured sample reactivities using calculated actinide reactivity contributions and fission history. These absorption parameters were transformed to associated parameters appropriate to the MTR for comparison with calculated parameters specific to the irradiation facility.

The neutron-energy group structure of the irradiation flux history was determined by the flux spectrum description adopted for the MTR. This description incorporated a thermal Maxwellian distribution at 343.2 K extending from 0 to infinite energy, a 1/E epithermal distribution above 0.105 eV, plus some augmentation for fission spectrum neutrons. Samples irradiated in the MTR facility were actually irradiated in either aluminum or beryllium reflector assemblies, with the neutron spectrum of the latter hardened with the use of boron sample shrouds. Three-group microscopic absorption and fission cross sections for actinide nuclides in the MTR group structure, (0, 0.105 eV, 5.53 keV, 10 MeV) are given in Ref. 42, along with coefficients of a density-dependent exponential self-shielding treatment. Similar data are given for microscopic absorption cross sections of moderator, structural, and fission-product nuclei (based on pre-ENDF/BIV data).

Reactivity measurements were conducted in the ARMF-I with samples positioned at various locations in a central water hole and in fuel elements surrounding the water hole. The neutron flux spectrum of the water hole, in general, was described by a Maxwellian distribution at 299.6 K with a 1/E distribution added above 0.120 eV. The slightly harder neutron spectrum characteristic of fuel element locations was described by a Maxwellian distribution at 315.6 K with a 1/E distribution added above 0.098 eV. Associated with each region of the ARMF-I is a microscopic cross-section tabulation, similar to that for the MTR, reflecting the different

spectra and group structure (the upper limit of the thermal group being, in each case, the lower limit of the 1/E distribution).

Reactivity measurements and TARMF model calculations combined to produce values of the thermal fission-product absorption cross section $\hat{\sigma}_3$ and epithermal fission-product absorption cross section $\hat{\sigma}_2$ for the measurement location. The epithermal value $\hat{\sigma}_2$ tacitly includes all fast absorption. All values of $\hat{\sigma}_3$ and $\hat{\sigma}_2$ resulting from individual measurements were transformed to associated values appropriate to a reference water hole location, and a number of measurements were conducted at a variety of ARMF-I measurement positions to form a single set of fitted values of $\hat{\sigma}_3$ and $\hat{\sigma}_2$ for the reference water hole position for the irradiation/cooling time history.

The resulting values of $\hat{\sigma}_3$ were each transformed to an effective 2200 m/s thermal cross section, $\hat{\sigma}_{2200}$, by dividing $\hat{\sigma}_3$ by the $\langle\sigma_{1/v}\rangle$ quantity evaluated for the ARMF-I water hole spectrum. By assuming that $\hat{\sigma}_{2200}$ evaluated for the ARMF-I water hole spectrum is equivalent to the 2200 m/s value appropriate to the MTR spectrum (exact for truly 1/v cross sections), the values of $\hat{\sigma}_{2200}$ and $\hat{\sigma}_2$ were then used to construct cross-section values appropriate to the MTR spectrum. These values are the reasonance integral above 0.105 eV, $\hat{I}$, and an effective one-group cross section, $\hat{\sigma}_{eff}$, that, when multiplied by the effective 2200 m/s flux, ϕ_{2200}, accurately reproduces the total fission-product absorption. The values of $\hat{\sigma}_{2200}$, $\hat{I}$ and $\hat{\sigma}_{eff}$ are the quantities reported.

The limitations on the resulting values of $\hat{\sigma}_{2200}$, $\hat{I}$ and $\hat{\sigma}_{eff}$ are as follows:

1. Data used in the TARMF model calculations and transformations to the reference water hole location did not originate from the data library used in benchmark calculations.
2. Simplifying assumptions are required in the ARMF transformations and transformation to the MTR.[41,42]
3. The tacit inclusion of fast absorption in $\hat{\sigma}_2$ complicates the one-to-one correspondence of "measured" and calculated parameters.

LASL Comparison Calculations

The irradiation histories and measured values of $\hat{\sigma}_{2200}$, $\hat{I}$ and $\hat{\sigma}_{eff}$ for five samples each of ^{233}U and natural thorium are reported in Ref. (42). Two of the ^{233}U samples, irradiated to $\gtrsim$ 90% depletion, have been calculated with differing orders of detail. The three-group actinide cross sections reported in Ref. (42) have been used throughout. Three fission-product data libraries have been employed in the EPRI-CINDER comparison calculations:

1. Calculations with the 4-group EPRI-CINDER data library produce 4-group barns/fission cross sections appropriate to the MTR spectrum. The transformation of 3-group actinide cross sections to 4-group values for problem input and the transformation of 4-group results to the

reported quantities require the assumptions that actinide and fission-product cross sections vary as 1/v in the energy region 0.105 eV - 0.625 eV. It must also be assumed that the flux varies as 1/E in this region.

2. A 3-group MTR fission-product cross-section library was produced by collapsing the 154-group library[39] to the 3-group structure appropriate to the MTR, using the MTR flux description. This library, with energy boundaries of 10^{-5} eV, 0.105 eV, 5.53 keV and 10 MeV, permitted the direct computation and comparison of the reported values of $\hat{\sigma}_{2200}$, $\hat{I}$, and $\hat{\sigma}_{eff}$.
3. A three-group ARMF-I fission-product cross-section library was created by collapsing the 154-group library to the three-group structures appropriate to the ARMF-I water hole, using the appropriate flux description. This library, with energy boundaries of 10^{-5} eV, 0.120 eV, 5.53 keV and 10 MeV permitted direct comparison with the ARMF-I water hole values of $\hat{\sigma}_2$ and $\hat{\sigma}_3$ (from which the reported MTR values of $\hat{\sigma}_{2200}$, $\hat{I}$, and $\hat{\sigma}_{eff}$ were constructed) and with the reported values constructed in the exact fassion as reported.

Calculations with the 3-group ARMF-I library are performed parasitically with 3-group MTR library calculations. The MTR libary is used in the EPRI-CINDER depletion and fission-product absorption buildup calculation, yielding the fission-product nuclide densities at each time increment. These number densities are combined, at each time increment, with the ARMF-I library to produce $\hat{\sigma}_1$, $\hat{\sigma}_2$, and $\hat{\sigma}_3$ values appropriate to the ARMF-I water hole. The flow of these combined calculations is thus identical to that of the irradiation and measurement sequence of the experiment.

Irradiation histories of each sample, measured with sample flux monitors, are reported in Ref.(42) in great detail. The combined irradiation - cooling - measurement cycle history of each sample extends to approximately 3 years, represented in approximately 1300 time increments with three-group flux values. Initial fuel number densities of each sample are also reported.

Sample 46

^{233}U sample 46 was irradiated in the MTR beryllium reflector in a hard spectrum. Comparison calculations for this sample were performed with a simplified 72-timestep representation of the detailed and extensive irradiation history using each of the three data libraries. Measured and calculated values of the MTR quantities $\hat{\sigma}_{2200}$, $\hat{I}$, and $\hat{\sigma}_{eff}$ are given in Tables 24-26. The measured ARMF-I values $\hat{\sigma}_2$ and $\hat{\sigma}_3$, extracted from the reported MTR values $\hat{\sigma}_{2200}$, $\hat{I}$, and $\hat{\sigma}_{eff}$ using the inverse of algorythms reported in Ref. (42), are compared in Table 27 to the $\hat{\sigma}_1$, $\hat{\sigma}_2$, and $\hat{\sigma}_3$ values calculated with the 3-group ARMF-I library.

Table 24

MEASURED AND CALCULATED VALUES OF $\hat{\sigma}_{2200}$, Sample 46

Irradiation Cycle	Elapsed Time (h)	BAPL Values (Barns/Fission)		LASL Calculated Values (Barns/Fission)		
		Measured	Calculated	4-Gp (LWR)	3-Gp (MTR)	3-Gp (ARMF)
2	1641.12	128.0 ± 6.4	124.7	127.11	127.92	119.66
3	2719.87	105.2 ± 5.3	101.8	103.44	105.31	98.74
4	3490.08	183.4 ± 9.2	192.1	171.26	187.86	176.07
4	3706.08	81.0 ± 4.0	90.6	89.95	92.42	86.85
7	5619.46	67.2 ± 3.4	71.1	69.77	72.63	68.54
8	6388.68	90.6 ± 4.5	95.5	88.40	95.70	90.28
8	6775.68	61.5 ± 3.1	67.6	66.43	69.21	65.40
10	8045.58	54.6 ± 2.7	59.7	59.66	62.27	58.98
12	9369.95	62.3 ± 3.1	69.2	64.02	68.77	65.19
12	9716.95	49.0 ± 2.5	56.6	54.71	57.15	54.22
14	11057.24	46.9 ± 2.4	52.2	50.28	52.46	49.87
17	12807.80	47.6 ± 2.4	52.3	48.59	51.83	49.38
17	13200.80	39.8 ± 2.0	46.2	44.19	46.21	44.06
21	15913.79	42.1 ± 2.1	46.9	43.35	45.90	43.81
21	16244.79	37.2 ± 1.9	42.3	40.37	41.84	39.96
22	17708.61	35.2 ± 1.8	40.6	38.95	40.32	38.52
23	18683.63	35.6 ± 1.8	38.1	37.26	38.64	36.96
24	19378.63	37.1 ± 1.9	43.1	39.70	42.10	40.23
24	19839.63	36.7 ± 1.8	38.0	36.15	37.55	35.93
25	22368.50	37.1 ± 1.9	41.5	38.25	40.46	38.68
25	22777.50	33.1 ± 1.7	36.7	35.05	36.26	34.72
25	25399.50	32.9 ± 1.7	36.2	34.84	36.50	34.95

Table 25

MEASURED AND CALCULATED VALUES OF $\hat{I}$, Sample 46

Irradiation Cycle	Elapsed Time (h)	(Barns/Fission) BAPL Values		LASL Calculated Values		
		Measured	Calculated	4-Gp (LWR)	3-Gp (MTR)	3-Gp (ARMF)
2	1641.12	248.1 ± 17.4	196.4	212.50	224.51	218.34
3	2719.87	162.9 ± 11.4	196.8	200.56	218.37	213.66
4	3490.08	246.2 ± 17.2	220.8	237.83	232.23	228.51
4	3706.08	262.0 ± 18.3	195.6	192.62	213.08	209.25
7	5619.46	201.0 ± 14.1	185.3	175.44	196.54	194.01
8	6388.68	207.2 ± 14.5	193.3	185.58	199.93	198.06
8	6775.68	221.8 ± 15.5	184.1	173.20	193.46	191.23
10	8045.58	210.1 ± 14.7	177.8	165.51	185.40	183.60
12	9369.95	194.1 ± 13.6	176.4	164.17	179.93	178.78
12	9716.95	209.8 ± 14.7	170.9	158.52	176.33	174.88
14	11057.24	180.9 ± 12.7	164.6	151.95	168.80	167.62
17	12807.80	177.2 ± 12.4	158.8	145.65	159.75	159.15
17	13200.80	182.8 ± 12.8	155.2	142.64	157.30	156.53
21	15913.79	168.2 ± 11.8	148.0	136.04	148.01	147.59
21	16244.79	175.0 ± 12.3	144.9	133.72	146.01	145.43
22	17708.61	175.2 ± 12.3	141.6	130.73	142.41	141.88
23	18683.63	148.3 ± 10.4	138.7	127.90	139.21	138.78
24	19378.63	170.6 ± 11.9	138.9	128.09	138.20	137.93
24	19839.63	133.4 ± 9.3	136.0	125.44	136.06	135.68
25	22368.50	159.6 ± 11.2	135.8	125.29	134.81	134.58
25	22777.50	147.7 ± 10.3	133.1	122.88	132.90	132.57
25	25399.50	149.4 ± 10.5	132.4	122.40	131.61	131.37

Table 26

MEASURED AND CALCULATED VALUES OF $\hat{\sigma}_{eff}$, Sample 46

Irradiation Cycle	Elapsed Time (h)	(Barns/Fission) BAPL Values		LASL Calculated Values		
		Measured	Calculated	4-Gp (LWR)	3-Gp (MTR)	3-Gp (ARMF)
2	1641.12	185.6 ± 5.6	170.3	155.77	180.37	170.67
3	2719.87	143.2 ± 4.3	147.7	132.56	156.51	148.84
4	3490.08	241.0 ± 7.2	243.8	200.10	242.58	229.93
4	3706.08	142.4 ± 4.3	136.4	119.19	142.68	136.21
7	5619.46	114.1 ± 3.4	114.3	97.97	118.81	114.14
8	6388.68	138.8 ± 4.2	140.5	116.25	142.65	136.80
8	6775.68	113.1 ± 3.4	110.5	94.36	114.65	110.32
10	8045.58	103.1 ± 3.1	100.7	86.59	105.43	101.73
12	9369.95	106.7 ± 3.2	109.5	89.94	110.27	106.42
12	9716.95	96.9 ± 2.9	95.6	80.58	97.82	94.56
14	11057.24	88.0 ± 2.6	89.7	75.24	91.24	88.38
17	12807.80	87.6 ± 2.6	88.2	72.33	88.29	85.70
17	13200.80	81.1 ± 2.4	81.2	67.84	82.11	79.80
21	15913.79	80.0 ± 2.4	80.3	65.74	79.66	77.47
21	16244.79	76.6 ± 2.3	75.0	62.64	75.15	73.13
22	17708.61	74.6 ± 2.2	72.5	60.74	72.72	70.80
23	18683.63	69.0 ± 2.1	69.3	58.69	70.33	68.55
24	19378.63	75.5 ± 2.3	74.4	60.90	73.59	71.65
24	19839.63	66.7 ± 2.0	68.6	57.23	68.56	66.86
25	22368.50	73.1 ± 2.2	72.1	59.06	71.19	69.35
25	22777.50	66.4 ± 2.0	66.7	55.74	66.56	64.94
25	25399.50	66.5 ± 2.0	66.0	55.46	66.50	64.90

Table 27

MEASURED AND CALCULATED ARMF-I VALUES OF $\hat{\sigma}_1$, $\hat{\sigma}_2$ AND $\hat{\sigma}_3$, Sample 46

Irradiation Cycle	Elapsed Time (h)	$\hat{\sigma}_3$ (Barns/Fission)		$\hat{\sigma}_2$ (Barns/Fission)		$\hat{\sigma}_1$ (Barns/Fission)
		BAPL Measured	LASL 3-Gp (ARMF) Calculated	BAPL Measured	LASL 3-Gp (ARMF) Calculated	LASL 3-Gp (ARMF) Calculated
2	1641.12	112.18	104.976	22.52	19.489	.19530
3	2719.87	92.20	86.628	14.69	19.176	.19709
4	3490.08	160.74	154.469	22.09	20.104	.19560
4	3706.08	70.99	76.199	24.03	18.835	.19763
7	5619.46	58.90	60.135	18.41	17.525	.19611
8	6388.68	79.40	79.207	18.88	17.775	.19558
8	6775.68	53.90	57.372	20.37	17.284	.19670
10	8045.58	47.85	51.740	19.31	16.613	.19516
12	9369.95	54.60	57.190	17.79	16.129	.19331
12	9716.95	42.94	47.570	19.31	15.830	.19389
14	11057.24	41.10	43.749	16.63	15.181	.19217
17	12807.80	41.72	43.321	16.28	14.397	.18965
17	13200.80	34.88	38.657	16.84	14.184	.18995
21	15913.79	36.90	38.435	15.47	13.355	.18687
21	16244.79	32.60	35.056	16.13	13.177	.18700
22	17708.61	30.85	33.794	16.15	12.855	.18598
23	18683.63	31.20	32.427	13.65	12.576	.18510
24	19378.63	32.52	35.291	15.72	12.478	.18424
24	19839.63	32.16	31.525	12.25	12.294	.18435
25	22368.50	32.52	33.935	14.69	12.176	.18340
25	22777.50	29.01	30.459	13.60	12.012	.18348
25	25399.50	28.83	30.662	13.76	11.899	.18343

Table 28

MEASURED AND CALCULATED VALUES OF $\hat{\sigma}_{eff}$, $\hat{\sigma}_{2200}$, and $\hat{I}$, SAMPLE 44

Elapsed Hours	Irad Cycle	$\hat{\sigma}_{eff}$ (b/f) BAPL Meas	$\hat{\sigma}_{eff}$ (b/f) BAPL Calc	$\hat{\sigma}_{eff}$ (b/f) EPRI-CINDER Calc 72-TS	$\hat{\sigma}_{eff}$ (b/f) EPRI-CINDER Calc 1692-TS	$\hat{\sigma}_{2200}$ (b/f) BAPL Meas	$\hat{\sigma}_{2200}$ (b/f) BAPL Calc	$\hat{\sigma}_{2200}$ (b/f) EPRI-CINDER Calc 72-TS	$\hat{\sigma}_{2200}$ (b/f) EPRI-CINDER Calc 1692-TS	$\hat{I}$ (b/f) BAPL Meas	$\hat{I}$ (b/f) BAPL Calc	$\hat{I}$ (b/f) EPRI-CINDER Calc 72-TS	$\hat{I}$ (b/f) EPRI-CINDER Calc 1692-TS
1640.12	2	159.3	139.7	131.04	130.32	146.0	126.2	116.13	115.43	194.7	198.1	217.66	217.37
2720.17	3	126.5	113.8	108.43	107.26	120.6	100.0	93.54	92.40	85.2	200.2	214.75	214.36
3453.99	4	210.3	218.0	193.98	196.51	193.3	202.5	178.07	180.56	248.3	226.4	231.16	231.72
3668.99	4	102.1	101.2	95.33	95.90	80.4	87.5	80.77	81.33	317.1	200.0	211.48	211.64
5667.99	7	82.3	80.3	77.07	77.35	66.0	67.0	63.11	63.38	237.7	194.5	202.36	202.42
6449.04	8	107.1	111.8	104.88	104.11	88.9	97.8	90.46	89.71	264.9	204.1	208.35	208.15
6836.04	8	78.3	77.2	74.46	74.28	61.6	63.7	60.51	60.33	241.6	195.2	201.62	201.54
8176.66	10	72.9	70.0	68.64	67.56	56.8	56.9	55.10	54.05	234.2	191.2	196.61	196.18
9517.83	12	80.2	83.3	78.59	78.38	63.9	70.2	65.23	65.03	240.3	192.8	195.56	195.55
9862.83	12	65.9	67.2	64.97	64.99	49.7	54.4	51.88	51.89	237.3	187.6	191.79	191.81
11220.66	14	61.1	62.9	60.99	60.93	45.7	50.5	48.26	48.21	226.6	183.6	187.02	187.01
13047.66	17	65.7	68.3	64.60	65.15	50.3	56.1	52.22	52.75	228.3	181.9	182.89	183.12
13441.66	17	55.3	57.9	55.90	56.17	40.0	46.0	43.72	43.99	226.4	177.9	179.79	179.90
16240.66	21	60.5	63.3	60.16	60.04	46.5	51.9	48.64	48.51	213.1	174.2	174.57	174.57
16585.66	21	53.0	54.3	52.39	52.45	38.8	43.2	41.07	41.13	216.3	170.1	171.46	171.48
18088.66	22	50.3	52.3	50.54	50.57	34.9	41.4	39.43	39.47	235.6	167.7	168.59	168.61
19067.66	23	49.0	50.0	48.92	48.40	36.3	39.3	38.02	37.51	195.0	165.2	165.95	165.73
19762.66	24	55.6	58.5	55.77	55.73	41.8	47.7	44.85	44.81	212.2	166.8	166.55	166.58
20223.66	24	48.7	49.9	48.13	48.20	35.1	39.3	37.42	37.49	209.5	162.9	163.35	163.38
22770.16	25	54.2	56.4	53.24	53.43	41.5	45.8	42.56	42.74	196.5	164.1	163.22	163.32
23179.16	25	47.0	48.6	46.67	46.82	34.6	38.2	36.18	36.32	190.6	160.4	160.39	160.45
25814.16	25	46.3	48.0	46.56	46.70	33.0	37.7	36.17	36.31	204.5	159.6	158.82	158.87

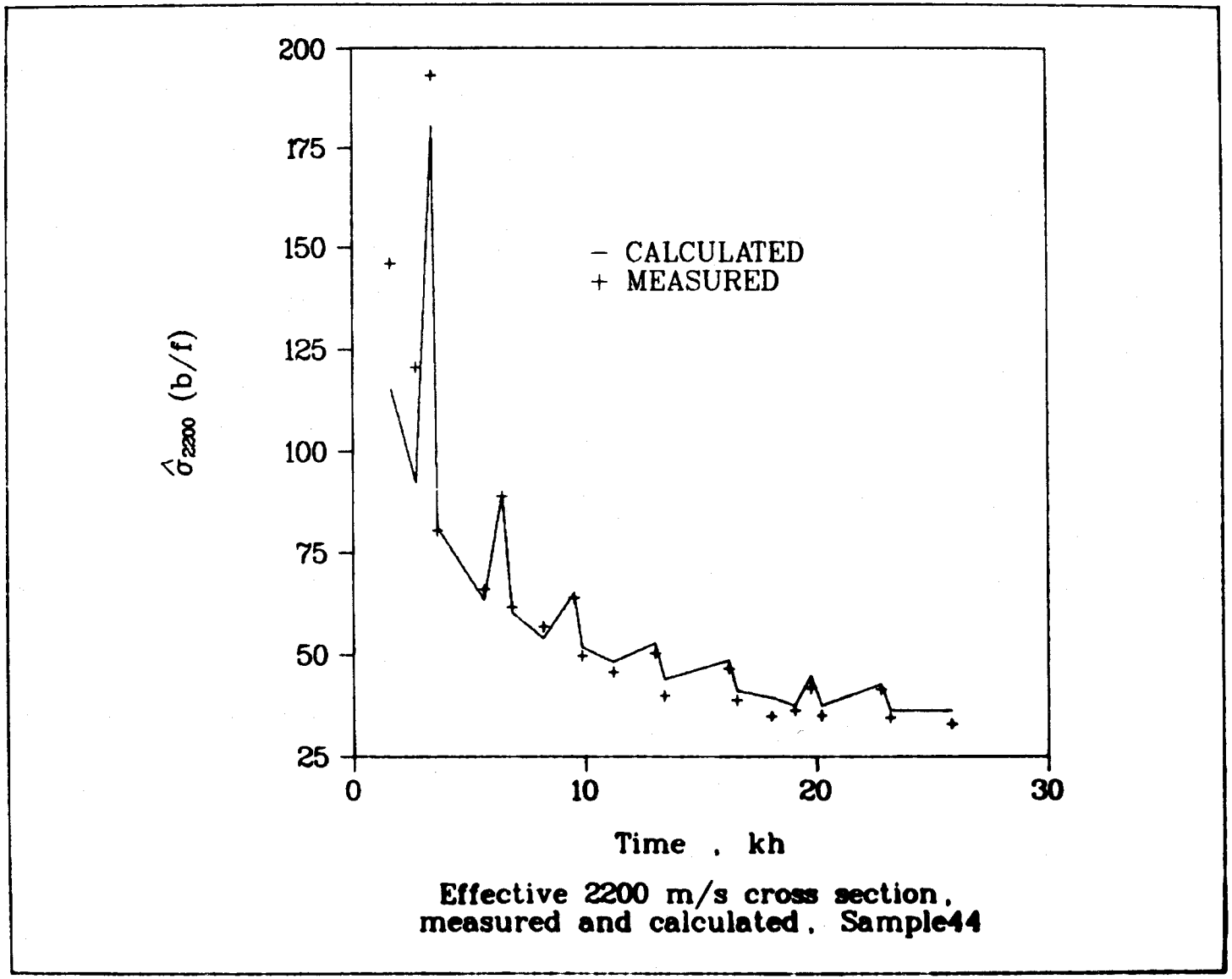

FIGURE 5. Effective 2200 m/s cross section, measured and calculated, Sample 44.

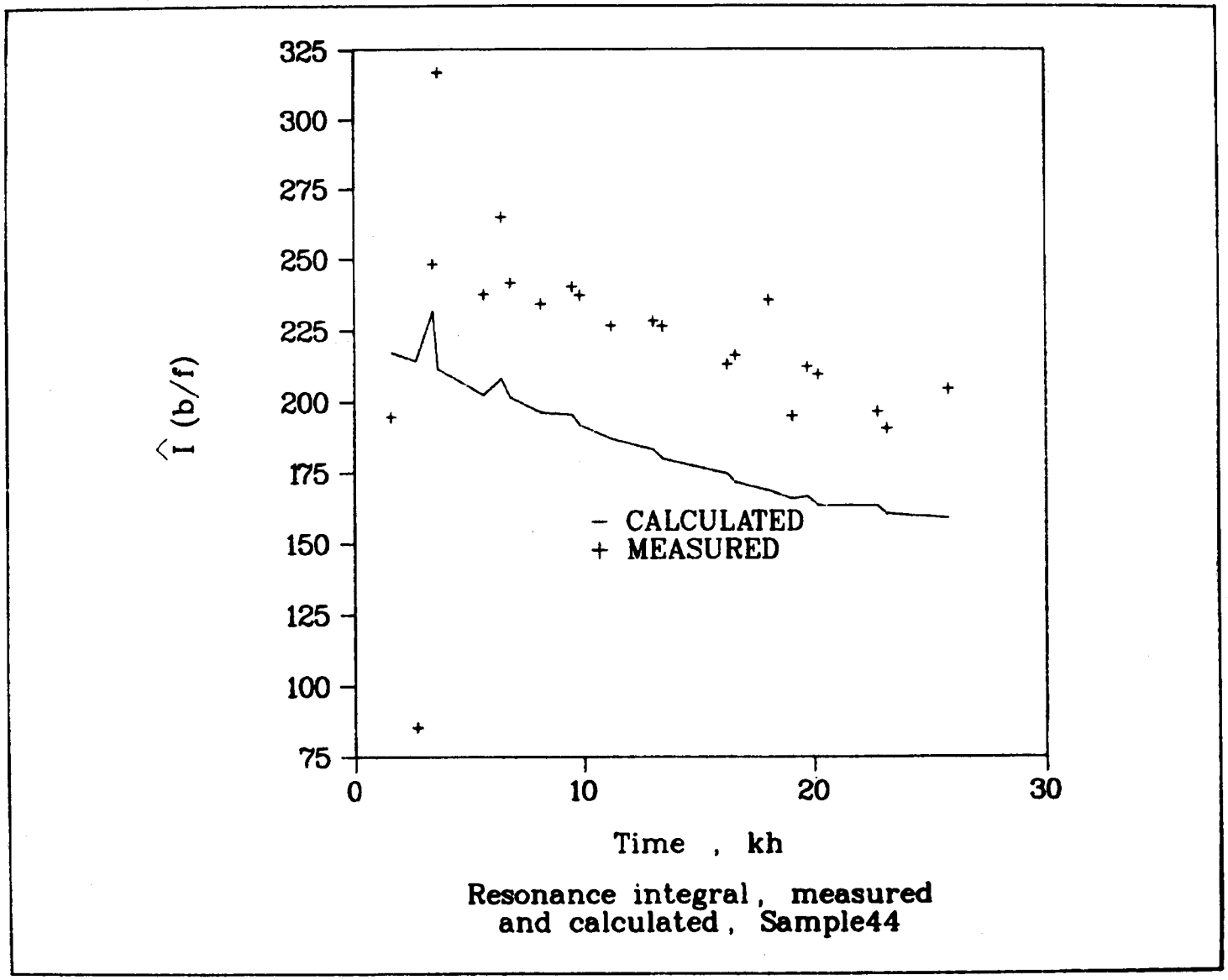

FIGURE 6. Resonance integral, measured and calculated, Sample 44.

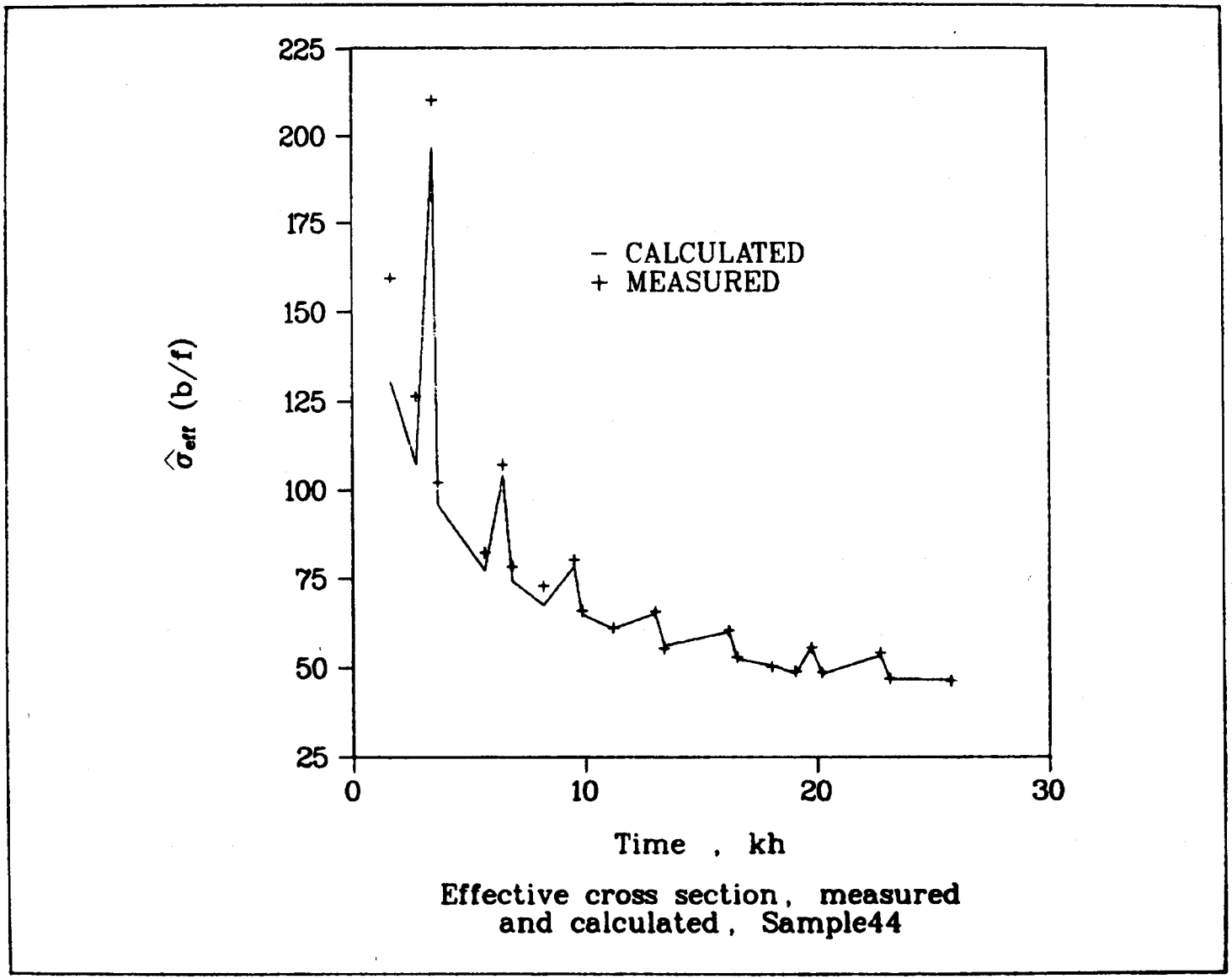

FIGURE 7. Effective cross section, measured and calculated, Sample 44.

Table 29

Measured and Calculated Values of $\hat{\sigma}_1$, $\hat{\sigma}_2$, and $\hat{\sigma}_3$, Sample 44

Elapsed Hours	Irad Cycle	$\hat{\sigma}_3$ (Barns/Fission) BAPL Meas	$\hat{\sigma}_3$ BAPL Calc	$\hat{\sigma}_3$ EPRI-CINDER Calc 72-TS	$\hat{\sigma}_3$ EPRI-CINDER Calc 1692-TS	$\hat{\sigma}_2$ (Barns/Fission) BAPL Meas	$\hat{\sigma}_2$ BAPL Calc	$\hat{\sigma}_2$ EPRI-CINDER Calc 72-TS	$\hat{\sigma}_2$ EPRI-CINDER Calc 1692-TS	$\hat{\sigma}_1$ (Barns/Fission) EPRI-CINDER Calc 72-TS	$\hat{\sigma}_1$ EPRI-CINDER Calc 1692-TS
1640.12	2	128.0	110.6	101.81	101.19	17.5	17.9	19.45	19.42	.19565	.19561
2720.17	3	105.7	87.7	82.00	81.00	7.4	18.2	19.31	19.28	.19777	.19776
3453.99	4	169.5	177.5	156.10	158.29	22.2	20.2	20.34	20.38	.19614	.19605
3668.99	4	70.5	76.7	70.81	71.30	29.2	18.2	19.08	19.09	.19842	.19838
5667.99	7	57.9	58.7	55.32	55.56	21.8	17.8	18.33	18.34	.19808	.19804
6449.04	8	77.9	85.7	79.30	78.64	24.3	18.6	18.73	18.72	.19770	.19769
6836.04	8	54.0	55.8	53.04	52.89	22.2	17.9	18.28	18.27	.19903	.19901
8176.66	10	49.8	49.9	48.30	47.38	21.6	17.5	17.85	17.81	.19807	.19806
9517.83	12	56.0	61.5	57.19	57.00	22.1	17.6	17.69	17.69	.19694	.19693
9862.83	12	43.6	47.7	45.48	45.49	21.9	17.2	17.42	17.42	.19767	.19766
11220.66	14	40.1	44.3	42.31	42.26	20.9	16.9	16.99	16.99	.19663	.19662
13047.66	17	44.1	49.2	45.77	46.24	21.0	16.7	16.59	16.61	.19522	.19520
13441.66	17	35.1	40.3	38.33	38.56	20.9	20.9	16.35	16.36	.19560	.19559
16240.66	21	40.8	45.5	42.64	42.53	19.6	16.0	15.83	15.84	.19336	.19335
16585.66	21	34.0	37.9	36.01	36.06	20.0	15.6	15.59	15.59	.19359	.19358
18058.66	22	30.6	36.3	34.57	34.60	21.8	15.4	15.33	15.33	.19300	.19299
19067.66	23	31.8	34.5	33.33	32.88	18.0	15.2	15.10	15.08	.19237	.19236
19762.66	24	36.6	41.8	39.32	39.28	19.6	15.3	15.11	15.11	.19170	.19168
20223.66	24	30.8	34.5	32.80	32.86	19.4	15.0	14.86	14.86	.19186	.19185
22770.16	25	36.4	40.1	37.31	37.47	18.1	15.1	14.82	14.82	.19119	.19118
23179.16	25	30.3	33.5	31.71	31.84	17.6	14.8	14.59	14.59	.19130	.19129
25814.16	25	28.9	33.0	31.71	31.83	18.9	14.7	14.44	14.45	.19131	.19130

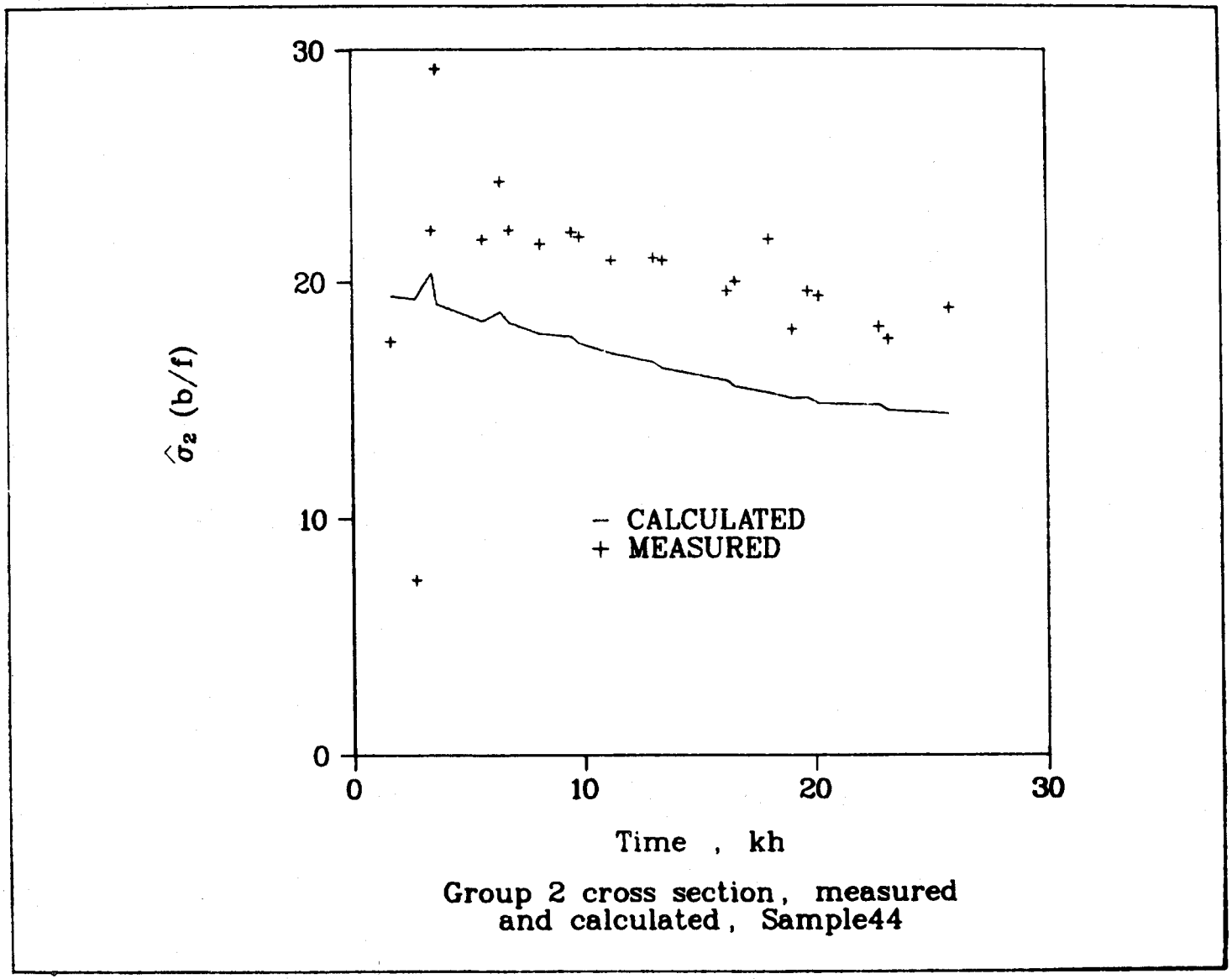

FIGURE 8. Group 2 cross section, measured and calculated, Sample 44.

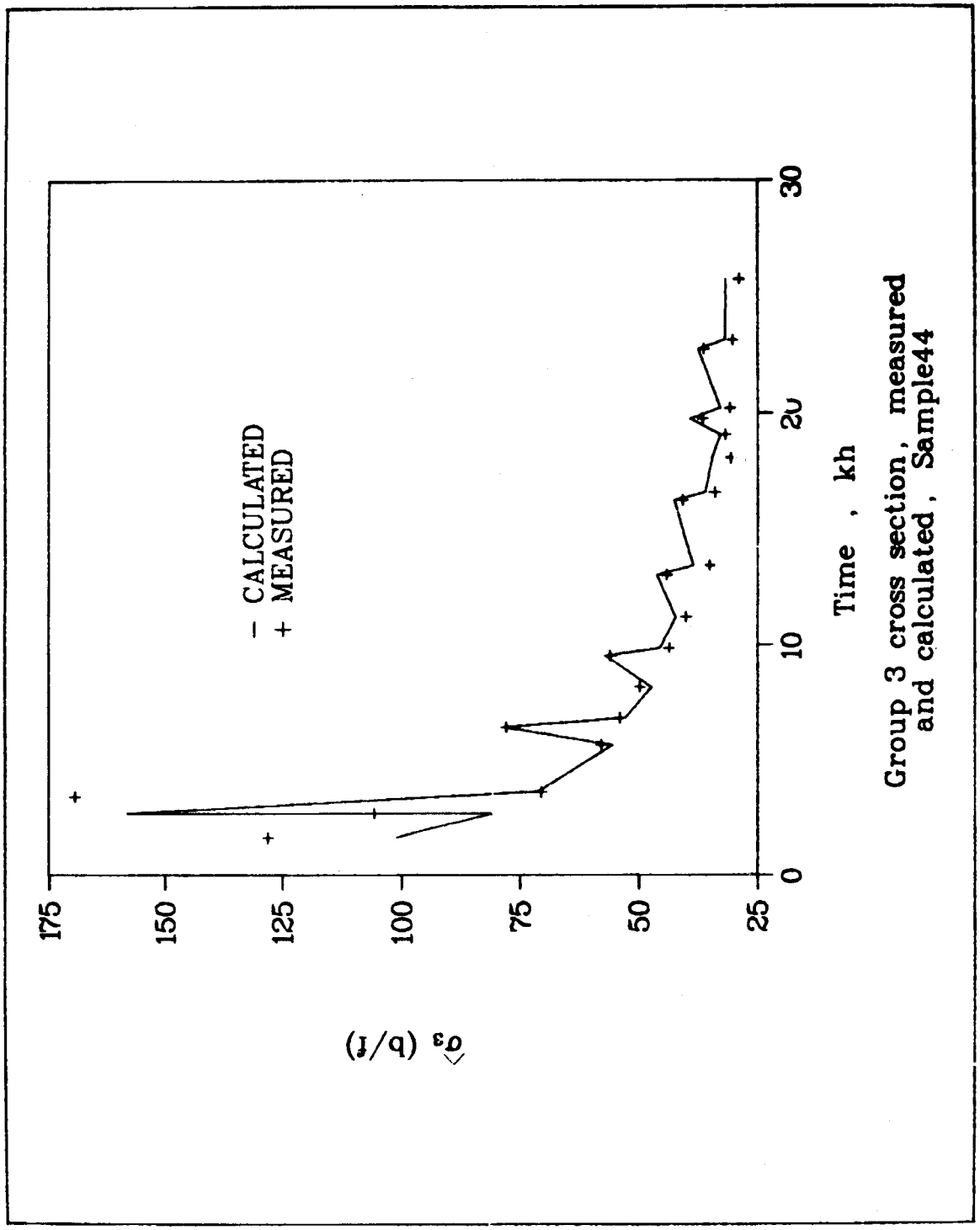

FIGURE 9. Group 3 cross section, measured and calculated, Sample 44.

Sample 44

^{233}U sample 44 was irradiated in the soft spectrum of the aluminum reflector of the MTR. Comparison calculations were performed with a simplified 72-timestep representation of the irradiation history and with a 1692-timestep history. This detailed history is an augmentation of the reported history, using small time increments to represent the reported longer cooling-measurement periods to display rapid quantity variations at measurement times shortly following irradiations.

Measured and calculated values of $\hat{\sigma}_{eff}$, $\hat{\sigma}_{2200}$, and $\hat{I}$ are reported in Table 28 and shown in Figs. 5-7. All calculated values, for the two timestep histories, were produced from the 3-group ARMF-I library values of $\hat{\sigma}_2$ and $\hat{\sigma}_3$. The calculated values of $\hat{\sigma}_2$ and $\hat{\sigma}_3$ are compared in Table 29 and Figs. 8-9 with measured values extracted from the reported values of $\hat{\sigma}_{2200}$, $\hat{I}$, and $\hat{\sigma}_{eff}$.

Summary

The detailed and simplified history calculations of sample 44 have shown that the simplified history is very adequate for calculating the fission-product absorption buildup. Calculations with the three-group libraries show improvement over calculations with the 4-group EPRI-CINDER library. In all calculations the values calculated for the thermal quantities $\hat{\sigma}_{2200}$ and $\hat{\sigma}_3$ are in reasonably good agreement. *Values calculated for the epithermal quantities $\hat{I}$ and $\hat{\sigma}_2$ are consistently lower than measured values; these discrepancies greatly exceed any consideration of the tacit inclusion of fast absorption in measured values of $\hat{\sigma}_2$. Calculated and measured values of $\hat{\sigma}_{eff}$ are in reasonably good agreement because of the dominence of thermal absorption.*

Because of the complex nature of the Gunst, et al., experiments, particularly the reactivity model used to extract only fission product absorption, their experiments do not have the desired simplicity for benchmark data. However, we know of no other data comparable in scope.

An alternate, unexplored approach would be to use the measured number densities available from, e.g., W. Maeck's cumulative yield measurements. The densities depend on cross sections and it would be possible to use the measured densities with ENDF/B-IV, V cross sections and compare with summation calculations. This could possibly be a benchmark comparison for a large subgroup of the important absorbers.

ACKNOWLEDGMENTS

We particularly appreciate the intensive efforts of H. Holleman in typing and compiling this report and N. L. Whittemore in preparing tables and plots.

REFERENCES

1. A. M. Weinberg and E. P. Wigner, Univ. of Chicago Press, Chicago (1958).
2. T. R. England, Time-Dependent Fission-Product Thermal and Resonance Absorption Cross Sections, WAPD-TM-333, November 1962. (Rev. Addendum 1965).
3. W. H. Walker, Yields and Effective Cross Sections of Fission Products and Pseudo-Fission-Products, CRRP-913 (AECL 1054), (March 1960).
4. C. R. Greenhow and E. C. Hansen, Thermal and Resonance Fission-Product Poisoning for U-235 Systems, KAPL-2172, October 1961; (also see KAPL-2057, Dec. 1, 1959).
5. T. R. England and R. J. Eckert, Trans. Am. Nucl. Soc. 4, (1) 321 (November 1961).
6. T. R. England, CINDER - A One-Point Depletion and Fission Product Program, WAPD-TM-334, August 1962. (Rev. 1964).
7. J. D. Garrison and B. W. Roos, Nucl. Sci. Eng. 12, 115-134 (1962).
8. E. A. Nephew, Thermal and Resonance Absorption Cross Sections of the U^{233}, U^{235}, and Pu^{239} Fission Products, ORNL-2869, (March 1, 1960).
9. S. Katcoff, Nucleonics 18 (11) 201-208 (1960).
10. R. P. Schuman and J. R. Berreth, Nucl. Sci. Eng. 12, 519-522 (1962).
11. W. H. Walker, Fission Product Poisoning from the Fast Fission of U-238, CRRP-1090, (AECL-1537) (June 1962).
12. D. J. Hughes and R. B. Schwartz, Neutron Cross Sections, BNL-325 (2nd. Ed.), U.S. Government Printing Office, Washington, D.C., (1958) (also 2nd Ed. and Suppl. 1, 1960 by D. J. Hughes, B. A. Magurno, and M. K. Brussel).
13. J. F. Stehn, Nucleonics 18 (11), 186-195 (1960).
14. R. L. Ferguson and G. D. O'Kelley, A Survey and Evaluation of U-233 Fission Yield Data, ORNL-3305 (July 1962).
15. H. Farrar and R. H. Tomlinson, Nucl. Phys. 34 (1962).
16. H. Farrar, H. R. Fickel, and R. H. Tomlinson, Can. J. Phys. 40, (1962).
17. D. T. Goldman and J. F. Stehn, Chart of the Nuclides, 7^{th} Ed., Knolls Atomic Power Laboratory.
18. A. E. McArthy, P. J. Persiani, B. I. Spinrad, and L. J. Templin, Neutron Resonance Integral and Age Data, Reactor Physics Constants Center Newsletter No. 1, Argonne National Laboratory (June 30, 1961).
19. W. R. Cadwell, C. J. Pfeifer, and P. F. Burger, PDQ-5 and PDQ-6 Programs for the Solution of the Two-Dimensional Neutron Diffusion-Depletion Program, WAPD-TM-477 (1964), and R. J. Breen, O. J. Marlowe, and C. J. Pfeifer, HARMONY: System for Nuclear Reactor Depletion Computation, WAPD-TM-478 (1964).

20. D. R. Vondy, Development of a General Method of Explicit Solution to the Nuclide Chain Equations for Digital Machine Calculations, ORNL-TM-361, (October 1962), (Addendum August 1963).
21. H. Bateman, Proc. Camb. Philos. Soc. 16, 423 (1910).
22. D. R. Marr, A User's Manual for Computer Code RIBD-II, A Fission Product Inventory Code, HEDL-TME 75-26 (January 1975).
23. M. J. Bell, ORIGEN - The ORNL Isotope Generation and Depletion Code, ORNL-4628 (1973).
24. F. E. Lane, FISSPROD, A G-20 Computer Program, AECL-3038, (November 1969); and W. H. Walker, et al., FISSPROD-2; An Improved Fission Product Accumulation Program, AECL-5106 (August 1975).
25. G. D. Joanou, et al., Nucl. Sci. Eng. 18, 363-69 (1964).
26. S. B. Gunst, J. C. Connor, E. D. McGarry, D. E. Conway, and S. Stein, Trans. Am. Nucl. Soc. 5 (1) 50-51 (1962).
27. Addendum to WAPD-TM-333 Substitled Data Revision and Calculational Extensions, (January 1965).
28. Fission Product Decay Library of the Evaluated Nuclear Data File, Version IV (ENDF/B-IV). [Available from, and maintained by, the National Nuclear Data Center (NNDC) at the Brookhaven National Laboratory, these data were compiled by a task force chaired by R. E. Schenter.]
29. T. R. England and R. E. Schenter, ENDF/B-IV Fission-Product Files: Summary of Major Nuclide Data, LA-6116-MS [ENDF-223], (October 1975).
30. C. W. Reich, R. G. Helmer, and M. H. Putnam, Radioactive-Nuclide Decay Data for ENDF/B, ANCR-1157 (ENDF-120) (August 1974).
31. P. F. Rose and T. W. Burrows, ENDF/B Fission-Product Decay Data, BNL-NCS-50545 [ENDF-243], Vols. 1 and 2 (August 1976, issued May 1977).
32. M. E. Meek and B. F. Rider, Compilation of Fission Product Yields, NEDO-12154-1 (January 1974).
33. R. E. Schenter, Ed., Benchmark Test of ENDF/B-IV, BNL-NCS-21118 [ENDF-230], Vol. 1 (1976).
34. R. E. Schenter, F. Schmittroth, and T. R. England, Integral Determination of Fission Product Inventory and Decay Power, (August 1977) (HEDL-SA-11346, To be published as Rev. Paper 15 of the IAEA Second Advisory Group Meeting on Fission Product Nuclear Data, Petten, Netherlands, Sept. 1977).
35. T. R. England and M. G. Stamatelatos, Comparisons of Calculated and Experimental Delayed Fission-Product Beta and Gamma Spectra from ^{235}U Thermal Fission, LA-NUREG-6896-MS (July 1977).
36. T. R. England, W. B. Wilson, and M. G. Stamatelatos, Fission Product Data for Thermal Reactors, Part 1: A Data Set for EPRI-CINDER Using ENDF/B-IV, LA-6745-MS (Dec. 76); Fission Product Data for Thermal Reactors, Part 2: Users Manual for EPRI-CINDER, LA-6746-MS (Dec. 76), also issued as EPRI-ND-367 (Dec. 1976).

37. R. J. LaBauve and W. B. Wilson, Proposal to Extend CSEWG Neutron and Photoneutron Multigroup Structure for Wider Applications, LA-6240-P (Feb. 1976).

38. R. E. MacFarland and R. M. Boicourt, Trans. Am. Nucl. Soc. 22, 720 (November 1975).

39. W. B. Wilson, T. R. England, and R. J. LaBauve, Multigroup and Few-Group Cross Sections for ENDF/B-IV Fission Products; The TOAFEW Collapsing Cide and Data File of 154-Group Fission-Product Cross Section, LA-7174-MS (March 1978).

40. R. J. LaBauve, C. R. Weisbin, R. E. Seamon, M. E. Battat, D. R. Harris, P. G. Young, and M. M. Klein, PENDF: A Library of Nuclear Data for Monte Carlo Calculations Derived from Data in the ENDF/B Format, LA-5687 (Oct. 1974).

41. S. B. Gunst, J. C. Connor, and D. E. Conway, Nucl. Sci. Eng. 58, 387 (1975).

42. S. B. Gunst, J. C. Connor, and D. E. Conway, Measurements and Calculations of Heavy Isotopes in Irradiated Fuels and of ^{233}U Fission-Product Poisoning, WAPD-TM-1182 (1974).

Section 12

NUCLEAR DATA FOR ACTINIDE PRODUCTION AND DEPLETION CALCULATIONS

Nuclear Data for Actinide Production and Depletion Calculations*

Richard W. Benjamin
Savannah River Laboratory, E. I. du Pont de Nemours & Co.,
Aiken, South Carolina 29801

ABSTRACT

The status of nuclear cross section data required for actinide depletion calculations in thermal reactors is summarized and recommendations made for future work. The primary fertile and fissile nuclides (^{232}Th, ^{233}U, ^{235}U, ^{238}U, and ^{239}Pu) are not reviewed. Nuclear data for the transactinium mass region are, with few exceptions, reasonably complete and adequate for current thermal reactor depletion calculations. There is a real need, however, for well-documented reactor production studies to use as benchmarks for data testing.

INTRODUCTION

The ability to calculate accurately fuel element contents as a function of thermal reactor history is of considerable value for a variety of applications. Such calculations depend fundamentally upon the calculational models of the reactor codes and the quality of the nuclear data that go into the codes. This paper reviews the current (April 1978) status of neutron cross section data for thermal reactor production and depletion calculations: it essentially updates a more extensive paper[1] completed three years ago. The primary fertile and fissile nuclides (^{232}Th, ^{233}U, ^{235}U, ^{238}U, and ^{239}Pu) have not been included in either review, for they are examined regularly and extensively.

The actinide nuclides involved in the thermal reactor production path are shown in three segments in Figures 1 through 3. The following conventions are used in these figures:

- neutron capture, an arrow to the right
- appreciable neutron-induced fission, a bold vertical arrow
- significant γ,n or n,2n reactions, an arrow to the left
- important radioactive decay (α, β, EC), an arrow in the appropriate direction accompanied by the half-life

* The information contained in this article was developed during the course of work under Contract No. AT(07-2)-1 with the U. S. Department of Energy.

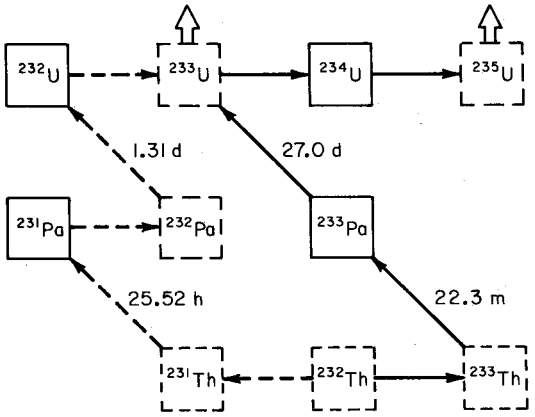

FIGURE 1. Thorium Target Path

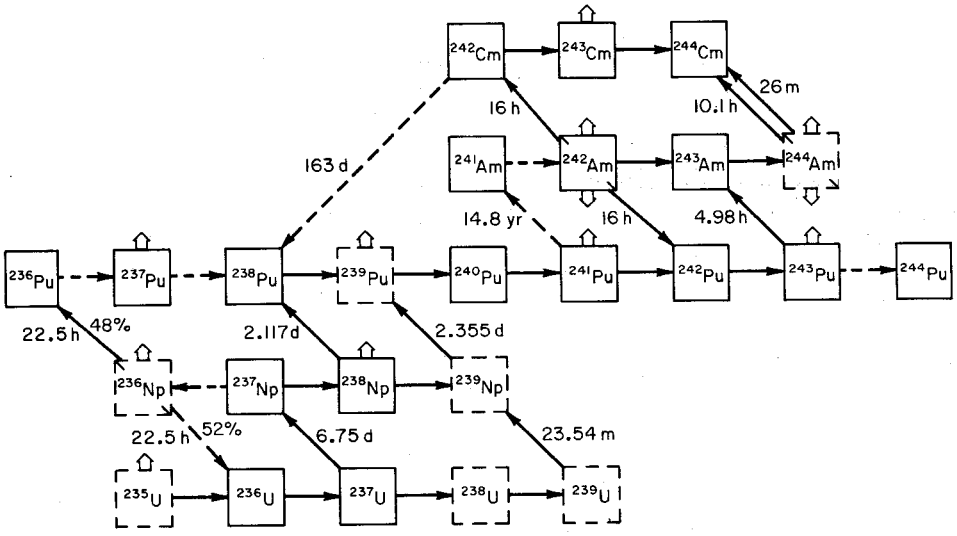

FIGURE 2. Uranium Target Path

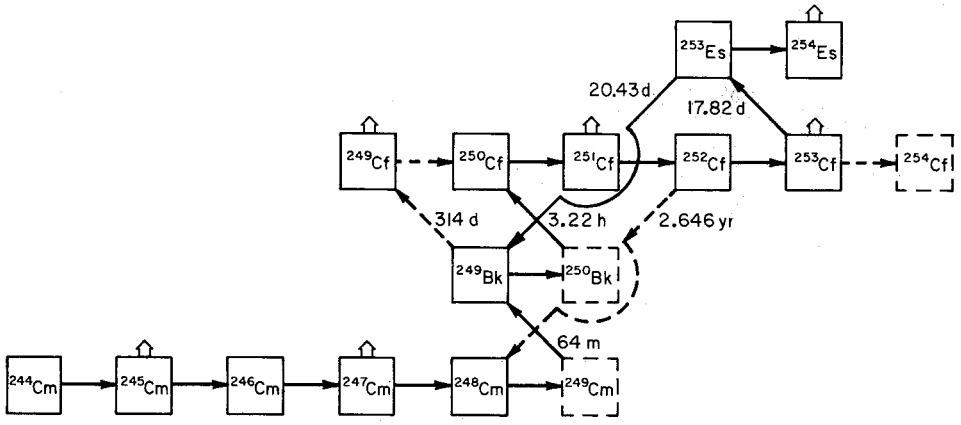

FIGURE 3. Curium Target Path

- nuclides surveyed are enclosed in solid boxes
- primary production links are shown as solid lines

These actinide data have been surveyed with the dual requirements of adequate experimental cross section data to satisfy current and projected needs, and an adequate evaluated library of these data.

RECOMMENDATIONS

The following recommendations appear valuable in terms of foreseeable user needs. The measurements should be within the capabilities of current technology. Projects which are in progress and have a good chance of meeting the needs are not listed here, but in the next section.

Experimental Measurements

- ^{233}Pa — Capture from 0 to 2 eV with ∿5% accuracy (note that current accuracy is about 12%). Differential data would be best, but integral measurements might be acceptable.
- ^{237}Np — Better description of the n,2n and γ,n reactions. Either differential or integral data would be acceptable.
- ^{240}Pu* — Differential descriptions of the first resonance. Self-indication measurements would be very worthwhile.
- ^{241}Am — Capture branching ratios as a function of neutron energy (hard).
- ^{242m}Am — Thermal capture cross section and capture resonance integral <10%.
- ^{242}Cm — Thermal capture cross section and capture resonance integral <20%.
- ^{246}Cm — Differential total or capture data <20 eV with a highly enriched sample. A good integral thermal capture cross section would help.
- ^{247}Cm — Differential fission below 30 eV.
- ^{250}Cf — Thermal measurements of any kind.
- ^{251}Cf — Differential fission measurements above 0.01 eV.

---

* Probably the most valuable data listed.

EVALUATIONS

A complete series of new and revised actinide evaluations has just been completed and reviewed. These evaluations will be issued with ENDF/B-V General-Purpose and Special-Actinide Files. Data inadequacies which can be improved by further evaluation will only be revealed after significant data testing. A few isotopes are currently being re-evaluated because of their location in the production chain or the availability of significant new experimental data: these include ^{241}Am, ^{242m}Am, ^{245}Cm, and ^{249}Bk. Only one other isotope could be re-evaluated profitably at present, ^{242}Cm.

REACTOR PRODUCTION BENCHMARKS

To determine the adequacy of data for reactor production-depletion calculations, well-documented benchmark-quality depletion measurements need to be made, or identified if they exist. Such measurements are important for all production chain regions shown in Figures 1 through 3. Beginning and ending assays, flux history, and flux spectra as a function of time need to be well-characterized. At the same time, depletion codes must be examined to ensure their adequacy for the calculations. Good quality depletion measurements are essential to improving both the depletion codes and the nuclear data.

WORK IN PROGRESS

Measurements and evaluations of the actinides are in progress or planned for the immediate future at several laboratories in the United States. A summary of these programs is given in Table 1.

STATUS AND DATA SUMMARIES

The status of experimental actinide cross section data is summarized in Tables 2 through 5. Data were reviewed through April 30, 1978. Requests indicated in Tables 3 through 5 were drawn primarily from the April 1977 "Compilation of Requests for Nuclear Data":[2] a few pertinent requests were drawn from the World Request List (WRENDA).[3] All requests used were for thermal reactor applications.

Table 2 gives a general summary of the current experimental status for each nuclide, as well as measurement recommendations. The condition of the low-energy differential data can be inferred from the location of the first resonance and the thermal cross section shape. A "very poor" listing under the status column should not be construed to encourage a crash measurement program, for most isotopes so listed have little influence in current reactor operations. The most useful of the recommendations would be a careful measurement of the first resonance in ^{240}Pu. This

Table 1

Measurement and Evaluation Programs

Nuclide	Reaction	Work	Energy Range	Laboratory	Status
^{228}Th	All	Eval	0 to 20 MeV	HEDL	In progress
^{230}Th	All	Eval	0 to 20 MeV	HEDL	In progress
^{231}Th	All	Eval	0 to 20 MeV	HEDL	In progress
^{233}Th	All	Eval	0 to 20 MeV	HEDL	In progress
^{232}U	All	Eval	0 to 20 MeV	HEDL	In progress
^{237}Np	n,γ	Meas	Thermal to MeV	ORNL	Beginning
^{241}Am	All	Eval	Thermal	SRL	Beginning
^{241}Am	n,f	Meas	Subthreshold	ORNL	Planned
^{242m}Am	n,f	Meas	Thermal to 20 MeV	LLL	Nearly complete
^{242m}Am	All	Eval	<10 keV	SRL	Planned
^{243}Cm	n,f	Meas	Thermal to MeV	ORNL	Analysis
^{245}Cm	All	Eval	<10 keV	SRL	Beginning
^{245}Cm	n,f	Meas	Thermal to MeV	ORNL	Analysis
^{245}Cm	n,f	Meas	Thermal to MeV	RPI	Nearly complete
^{249}Bk	n,T	Meas	0.03 to 100 eV	SRL-ORNL	Nearly complete
^{249}Bk	All	Eval	<10 keV	SRL	Beginning
^{249}Cf	n,T	Meas	0.03 to 100 eV	SRL-ORNL	Analysis
^{249}Cf	n,f	Meas	Thermal to MeV	LLL	Planned

Table 2

Summary of Actinide Neutron Cross Sections in the Thermal and Resonance Regions

Element(Z)	Isotope	Status	Thermal Shape	First Resonance, eV	Recommendation
Pa(91)	231	Good	∿1/v < 0.1 eV	0.396	-
	233	Acceptable	∿1/v	0.795	Better thermal capture data
U(92)	232	Good	∿1/v	5.98	-
	234	Good	∿1/v	5.17	-
	236	Good	∿1/v	5.45	-
	237	Very poor	Unknown	Unknown	-
Np(93)	237	Good	1/v < 0.15 eV	0.489	More γ,n and n,2n data
	238	Very poor	Unknown	Unknown	-
Pu(94)	236	Very poor	Unknown	Unknown	-
	237	Very poor	Unknown	Unknown	-
	238	Good	Non 1/v	2.90	-
	240	Good	∿1/v < 0.5 eV	1.056	Better parameters for first resonance
	241	Very good	Non 1/v	0.257	-
	242	Very good	1/v	2.67	-
	243	Poor	Unknown	Unknown	-
	244	Poor	Unknown	Unknown	-
Am(95)	241	Good	1/v < 0.06 eV	0.308	Capture branching ratio as a function of energy
	242	Very poor	Unknown	Unknown	-
	242m	Acceptable	Non 1/v	0.173	Capture
	243	Very good	1/v < 0.3 eV	0.420	-
Cm(96)	242	Acceptable	Unknown	13.6	Capture
	243	Poor	Unknown	∿1.49	Analysis of extant fission data
	244	Good	1/v	7.67	-
	245	Good	Non 1/v	0.85	-
	246	Acceptable	1/v	4.32	Differential total or capture < 20 eV
	247	Poor	Unknown	Unknown	Differential fission < 30 eV
	248	Good	1/v	7.25	-
Bk(97)	249	Acceptable	Non 1/v	0.197	-
Cf(98)	249	Acceptable	Non 1/v	0.70	-
	250	Poor	Unknown	Unknown	Thermal capture (difficult)
	251	Poor	Unknown	Unknown	Differential fission < 30 eV
	252	Acceptable	Unknown	Unknown	Any lower-energy measurements (difficult)
	253	Very poor	Unknown	Unknown	-
Es(99)	253	Poor	Unknown	Unknown	-
	254	Very poor	Unknown	Unknown	-
	254m	Very poor	Unknown	Unknown	-

Table 3

Thermal Neutron Cross Sections

Element(Z)	Isotope	$\sigma_{n\gamma}^{2200}$ Recommended Experimental Value, barns	$\sigma_{n\gamma}^{2200}$ Accuracy, % Experiment	$\sigma_{n\gamma}^{2200}$ Accuracy, % Requested	σ_{nf}^{2200} Recommended Experimental Value, barns	σ_{nf}^{2200} Accuracy, % Experiment	σ_{nf}^{2200} Accuracy, % Requested
Pa(91)	231	210	10	5-10	0.01	50	-
	233	41	12	5	≤1	-	-
U(92)	232	73.1	2	2-5	75.2	7	-
	234	100.2	1.5	3	<0.65	-	-
	236	5.2	6	10	-	-	-
	237	378	33	-	≤0.35	-	-
Np(93)	237	169	2	3	0.019	16	-
	238	-	-	-	2070	2	-
Pu(94)	236	-	-	-	162	20	-
	237	-	-	-	2200	20	-
	238	532	4	-	17.3	3	-
	240	289.5	0.5	3	0.03	150	-
	241	362	3	3	1015	<1	1
	242	18.5	4-5	3	0	-	-
	243	87.4	15	-	180	15	-
	244	1.7	6	-	-	-	-
Am(95)	241	831.8	8	10-15	3.15	3	-
to 242		748	3	10	-	-	-
to 242m		83.8	8	10	-	-	-
	242	-	-	10	2100	10	10-20
	242m	-	-	10	6900	5	10-20
	243	77	5	10	0.2	50	-
Cm(96)	242	20	50	20	≤5	-	-
	243	130.7	7	15[a]	609.6	5	10[a]
	244	10.6	20	10	1.1	10	-
	245	383	10	10	2020	5	10
	246	1.4	10	10	0.14	35	-
	247	58	10	5-10	81	6	5-10
	248	2.44	10	-	0.37	15	-
Bk(97)	249	1150	15	10	-	-	-
Cf(98)	249	497	6	-	1660	3	-
	250	1700	15	10	-	-	10
	251	2850	10	10	4800	10	10
	252	20.4	8	10	32.0	10	10
	253	12	20	-	1100	20	-
Es(99)	253	158	13	-	-	-	-
to 254		<3	-	-	-	-	-
to 254m		155	13	-	-	-	-
	254	-	-	-	2900	5	-
	254m	-	-	-	1840	5	-

a. IAEA Requests from WRENDA 76/77.[3]

Table 4

Infinite Dilution Resonance Integrals

Element (Z)	Isotope	$I_{n\gamma}$ Recommended Experimental Value, barns	$I_{n\gamma}$ Accuracy, % Experiment	$I_{n\gamma}$ Accuracy, % Requested	I_{nf} Recommended Experimental Value, barns	I_{nf} Accuracy, % Experiment	I_{nf} Accuracy, % Requested
Pa(91)	231	1500	7	5-10	0.05	26	-
	233	895	4	5-10	-	-	-
U(92)	232	280	6	5	320	15	-
	234	630	12	6	<10	-	-
	236	365	6	10	-	-	-
	237	1200	18	-	-	-	-
Np(93)	237[a]	660	8	10	-	-	-
	238	-	-	-	880	8	-
Pu(94)	236	-	-	-	-	-	-
	237	-	-	-	-	-	-
	238	164	10	-	25	20	-
	240	8013	12	3	-	-	-
	241	162	0.4	3	570	~3	10
	242	1275	4	3	4.7	-	-
	243	264	25	-	542	25	-
	244	42.5	10	-	-	-	-
Am(95)	241	1538	13	-	23	9	-
to 242		1330	9	10	-	-	-
to 242m		208	9	10	-	-	-
	242	-	-	-	<300	-	-
	242m	-	-	10	1570	7	10-20
	243	1927	3	5-10	17.3	8	-
Cm(96)	242	150	30	-	-	-	-
	243	214.4	10	15[b]	1575	9	10[b]
	244	585	10	50	18	10	-
	245	104	7	10	772	6	10
	246	115	7	10	10	4	10
	247	500	15	5-10	762	6	5-10
	248	246	10	-	13.2	6	-
Bk(97)	249	1200	15	10	-	-	-
Cf(98)	249[a]	625	10	-	1610	10	-
	250	11500	7	10	-	-	10
	251	1590	4	10	5380	15	10
	252	43.4	8	10	110	20	10
	253	12.1	25	-	2000	25	-
Es(99)	253	7308	8	-	-	-	-
to 254		4299	5	-	-	-	-
to 254m		3009	6	-	-	-	-
	254	-	-	-	2200	5	-
	254m	-	-	-	-	-	-

a. I is not very meaningful for ^{249}Cf or ^{237}Np because of large resonances in the 0.5-eV region.

b. IAEA Requests from WRENDA 76/77.[3]

Table 5

Resonance Parameters

Element(Z)	Isotope	Resolved Resonance Range, eV	Γ_n Accuracy, %		Γ_f Accuracy, %		Comments on Measurements
			Experiment	Requested	Experiment	Requested	
Pa(91)	231	0-100	5	10	50	-	Fission 0.4-1.3 eV
	233	0-17	10	10	-	-	
U(92)	232	0-75	10	10	12	-	
	234	0-1500	5	6	10	-	Fission 5-1500 eV
	236	0-4100	5	10	30	-	Fission 5-380 eV
	237	45-225	-	-	20-50	-	$\frac{1}{2}\pi\sigma_o\Gamma_f$ only
Np(93)	237	0-235	<5	5	30-100	-	Fission 0.1-155
	238	-	-	-	-	-	
Pu(94)	236	-	-	-	-	-	
	237	-	-	-	-	-	
	238	0-496	∿10	-	∿40	-	No fission <18.6 eV
	240	1-5700	∿4	10	∿20	10	Fission 700 eV-3.5 keV
	241	0-160	∿5	5	∿10	5	
	242	0-4000	5-10	10	10	-	No fission <50 eV
	243	-	-	-	-	-	
	244	-	-	-	-	-	Fission threshold meas
Am(95)	241	0-150	2-5	10	-	-	Limited fission data avail
	242	-	-	-	-	-	
	242m	0-∿20	∿10	10	-	10	
	243	0-250	<5	10	-	-	
Cm(96)	242	0-265	∿10	20	-	20	
	243	1-30	15	-	20	-	
	244	0-520	10	-	10	-	Fission 20-972 eV
	245	0-60	10-15	10	14	10	
	246	0-160	5	10	20	-	Fission 20-382 eV
	247	20-60	-	5-10	-	5-10	Fission only
	248	0-2400	7	-	20	-	Fission 20-100 eV
Bk(97)	249	0-100	∿5	20	-	20	
Cf(98)	249	0-70	∿10	-	∿10	-	
	250	-	-	10	-	10	
	251	-	-	10	-	10	
	252	-	-	-	-	-	
	253	-	-	-	-	-	
Es(99)	253	-	-	-	-	-	
	254	-	-	-	-	-	
	254m	-	-	-	-	-	

resonance is very large and self-shields significantly at low ^{240}Pu concentrations. Thus, the precise shape of the wings of the resonance are very important. Self-indication techniques at one of the electron LINAC laboratories could be usefully employed.

Tables 3 and 4 summarize thermal cross sections; infinite dilution resonance integrals, and comparisons of experimental accuracies with user-requested accuracies. The listed thermal cross sections are nominal 2200 m/sec 1/v cross sections: those values determined from differential measurements have been converted to the 2200 m/sec cross section that would be appropriate to a 1/v cross section measured in a room temperature Maxwellian neutron spectrum. The lower energy cutoff for the resonance integrals is nominally 0.5 eV, but variations may exist because of differing experimental conditions. The values given represent evaluations by the author, and do not necessarily conform to the new ENDF/B-V actinide file. It is interesting to note that in these tables most of the requests have already been met.

The resolved resonance parameter data for the actinide production chain nuclides are summarized in Table 5. The energy range is listed with comparisons of the experimental and requested accuracies for the neutron and fission widths. The accuracies for the widths are approximate because they vary from resonance to resonance: the values listed are representative of the larger low-energy resonances important in thermal reactor calculations.

Version V of the Evaluated Nuclear Data Files (ENDF/B-V) contains new evaluations for all the actinides. These evaluations are listed in Table 6. A full evaluation indicates that both decay and cross section data are included. Decay denotes evaluations having only decay data. File GP denotes the General Purpose File: only evaluations having complete cross section and secondary neutron data can be included in the General Purpose File. Other isotopes are put into the Special Purpose Actinide File (A), which has less stringent conditions. Many isotopes for which no differential data are shown in Table 5 have been included in the evaluations. For these nuclides, differential data were fabricated using a technique developed by McCrosson.[4] This technique combined the available integral data with nuclear systematics to produce a picket fence description of the resolved resonance region. Most of the actinide cross section evaluations below 10 keV for ENDF/B-V are described in References 5 and 6.

Almost all of the actinide evaluations for ENDF/B-V have been completed and reviewed (the exceptions are some of the thorium cycle isotopes). The evaluations will be released in the very near future. They represent the best data currently available in evaluated form. There are a few nuclides in these evaluations for which significant new data have become available since the evaluations were completed, e.g.

Table 6

Actinide Evaluations for ENDF/B-V

Isotope	Evaluation	File[a]	Isotope	Evaluation	File[a]
^{228}Th[b]	Full	A	^{240}Am	Decay	A
^{230}Th[b]	Full	A	^{241}Am	Full	GP
^{231}Th[b]	Full	A	^{242}Am	Full	A
^{232}Th	Full	GP	^{242m}Am	Full	GP
^{233}Th[b]	Full	A	^{243}Am	Full	GP
			^{244}Am	Decay	A
^{231}Pa[b]	Full	A	^{244m}Am	Decay	A
^{233}Pa	Full	GP			
			^{241}Cm	Full	A
^{232}U[b]	Full	A	^{242}Cm	Full	A
^{233}U	Full	GP	^{243}Cm	Full	GP
^{234}U	Full	GP	^{244}Cm	Full	GP
^{235}U	Full	GP	^{245}Cm	Full	GP
^{236}U	Full	GP	^{246}Cm	Full	GP
^{237}U	Full	A	^{247}Cm	Full	A
^{238}U	Full	GP	^{248}Cm	Full	A
^{239}U	Decay	A	^{249}Cm	Decay	A
^{236}Np	Decay	A	^{249}Bk	Full	A
^{236m}Np	Decay	A	^{250}Bk	Decay	A
^{237}Np	Full	GP			
^{238}Np	Full	A	^{249}Cf	Full	A
^{239}Np	Decay	A	^{250}Cf	Full	A
			^{251}Cf	Full	A
^{236}Pu	Full	A	^{252}Cf	Full	A
^{237}Pu	Full	A	^{253}Cf	Full	A
^{238}Pu	Full	GP			
^{239}Pu	Full	GP	^{253}Es	Full	A
^{240}Pu	Full	GP			
^{241}Pu	Full	GP			
^{242}Pu	Full	GP			
^{243}Pu	Full	A			
^{244}Pu	Full	A			

a. A — Special Purpose Actinide File.
GP — General Purpose File.

b. Evaluations in progress at HEDL.

- ^{242m}Am(n,f) from thermal to 20 MeV[7]
- ^{242}Cm(n,T) resonance parameters from 1 to 265 eV[8]
- ^{243}Cm(n,γ) integral cadmium difference measurements[9]
- ^{245}Cm(n,f) resonance parameters from thermal to 30 eV[10] and the fission cross section from 1 eV to 100 keV[11]
- ^{249}Bk(n,T) resonance parameters from thermal to 100 eV[12]

Three of these isotopes, ^{242m}Am, ^{245}Cm, and ^{249}Bk, will be re-evaluated by SRL within the next six months because of the new data. Re-evaluation of ^{242}Cm with the inclusion of the low-lying resonance parameters instead of the "picket-fence" model which is in ENDF/B-V would also be of value.

The major deficiency in establishing the quality of nuclear data and/or codes for actinide depletion and production calculations is a complete lack of established reactor irradiation benchmarks with which to test the data. This is a problem as yet not addressed by the Data Testing Subcommittee of the Cross Section Evaluation Working Group (CSWG) which is responsible for ENDF/B. A very worthwhile contribution would be the measurement and/or identification of well-documented depletion benchmarks for a range of starting points in the production chain (see Figures 1 through 3) and a variety of neutron energy spectra. At the same time the adequacy of the models and assumptions of the depletion codes used in the calculations must be examined.

Nuclear data and evaluations for the actinides are reasonably complete and of sufficient accuracy for current production-depletion calculations with thermal reactors. The present need is for practical methods of testing the ENDF/B-V data.

DATA ADDITIONS SINCE 1975 BY NUCLIDE

The following experimental data have become available since the completion of the 1975 Karlsruhe paper.[1]

^{231}Pa - I_{nf} (>0.55 eV) = 0.049 ±0.013 b.[13]

^{234}U - The James et al.[14] work quoted in Reference 1 was published.

^{237}Np - Reference 1, p. 29 should read $I_{\gamma n}$ = 12.2 mb. This value is from a more recent manuscript[15] rather than the source quoted.

- A new fission measurement from 3 eV to 2 MeV[16] yields $2g\Gamma_n^o$, Γ_f, and some Γ_γ from 3.86 eV to 155 eV. The Γ_f values are an improvement over earlier measurements.

^{240}Pu - The Weston and Todd[17] work quoted in Reference 1 was analyzed and published. It forms the basis for the ENDF/B-V evaluation (by Weston).

- Subthreshold fission was measured and fission widths for 82 resonances between 500 eV and 10 keV were obtained.[18]

^{241}Pu - Differential fission, capture, and total cross section measurements have been completed and published. These works refine the resonance parameter information from 1 to 104 eV[19] and add substantial smooth capture[20] and fission[21] data to the rather extensive data already available.

^{241}Am - Two integral measurements have been reported. The Gavrilov et al.[22] work described in Reference 1 has been published and an integral fission measurement[23] has been done. The results of these measurements were consistent with earlier work, but the capture branching ratios add confidence to the established values.

- Two analyses of already reported total cross section measurements have been published.[24,25] Weston's results[25] were normalized to ENDF/B-IV at thermal and form the basis of the ENDF/B-V evaluation.

^{242m}Am - An additional integral measurement of the fission cross section was published by Zuravlev et al.[23] Both the thermal cross section and the resonance integral are inconsistent with earlier results.

- Preliminary results are coming from Browne's (LLL)[7] differential fission measurements. The 2200 m/sec fission cross section is 7040 ±350 b. Combining this value with the measured shape yields an equivalent 1/v thermal cross section of ∿7700 b.

^{243}Am - A substantial amount of Russian work[22,23,24,26] has been published recently on ^{243}Am.

^{242}Cm - A very significant paper has been published on ^{242}Cm. Artamonov et al.[8] have derived the resonance parameters for resolved resonances below 265 eV from a total cross section measurement.

^{243}Cm - An excellent and unique integral capture measurement has been reported by Bemis et al.[9] using the cadmium difference technique and ^{59}Co monitors.

- The bomb shot results from LASL have been published in an ERDA report.[27] The fission cross section is tabulated from 15 eV to 3.25 MeV.

^{244}Cm - There has been some Russian work on ^{244}Cm which gives added confidence to the earlier work.[23,28]

^{245}Cm - Several significant differential total[28-30] and fission[10] measurements have been reported as well as two integral measurements.[22,23] The low-energy fission measurements of Browne et al.[10] provide sufficient new shape and resonance information for a complete new evaluation. There are also two Russian integral fission measurements.[22,23] A differential fission measurement from 1 eV well into the MeV range from the RPI lead slowing-down spectrometer will be available within about a month.[11]

^{246}Cm - The new Russian differential and integral data[23,28,30] give added confidence to the earlier work.

^{247}Cm - Three resonances in the ^{245}Cm measurements of Belanova et al.[29,30] were attributed to ^{247}Cm.

^{248}Cm - Same comment as for ^{246}Cm.

^{249}Bk - The integral capture measurements of Gavrilov et al.[22] and the total cross section measurements of Benjamin et al.[12] provide sufficient data for a complete new evaluation. In addition, the bomb-shot fission measurements have recently been published.[31]

^{249}Cf - Differential total cross section[12] and integral fission measurements[22,23] have been reported. The total cross section data analysis is not yet complete.

REFERENCES

1. R. W. Benjamin. "Status of Measured Neutron Cross Sections of Transactinium Isotopes for Thermal Reactors." Transactinium Isotope Nuclear Data (TND), Vol. II, p 1, IAEA-186, IAEA, Vienna (1976).

2. Compilation of Requests for Nuclear Data, ERDA Report BNL-NCS-50632, Brookhaven National Laboratory, Upton, NY (April 1977).

3. R. W. Lessler, Ed. WRENDA 76/77, World Request List for Nuclear Data. IAEA Report INDC(SEC)-55/URSF, IAEA, Vienna (August 1976).

4. F. J. McCrosson. "A Practical Method for Generating Resonance Energy Cross Sections for Heavy Nuclides." Proc. Third Conference on Neutron Cross Sections and Technology, Knoxville, TN (1971) 714.

5. R. W. Benjamin, F. J. McCrosson, and P. L. Roggenkamp. "Conversion of ^{238}Pu and ^{252}Cf Production Chain Cross Section to ENDF/B Format." Report EPRI NP-161, Electric Power Research Institute, Palo Alto, CA (December 1975).

6. R. W. Benjamin, F. J. McCrosson, and W. E. Gettys. "Evaluation of Neutron Cross Sections for ^{244}Cm, ^{246}Cm, and ^{248}Cm." ERDA Report DP-1447, E. I. du Pont de Nemours and Company, Savannah River Laboratory, Aiken, SC (January 1977).

7. J. C. Browne, Lawrence Livermore Laboratory (to be published).

8. V. S. Artamanov, R. N. Ivanov, S. M. Kalebin, G. V. Rukolaine, V. A. Anifriev, S. I. Babich, T. S. Belanova, N. G. Kocherygin, A. G. Kolesov, S. N. Nikolskii, V. N. Nefedov, V. A. Poruchikov, V. A. Safonov, and V. V. Tihomirov. "Neutron Resonances in ^{242}Cm." Proc. 4th All Union Conf. on Neutron Physics, Kiev, 18-22 April (1977) in Russian.

9. C. E. Bemis, Jr., J. Oliver, R. Eby, and J. Halperin. "Thermal-Neutron Capture and Fission Cross Sections and Resonance Integrals for Cm-243." Nucl. Sci. Eng. 63, 413 (1977).

10. J. C. Browne, R. W. Benjamin, and D. G. Karraker. "Fission Cross Section for ^{245}Cm from 0.01 to 35 eV." Nucl. Sci. Eng. 65, 164 (1978).

11. R. C. Block, Rensselaer Polytechnic Institute (to be published).

12. R. W. Benjamin, J. A. Harvey, and N. W. Hill. "Neutron Total Cross Section Measurements for ^{249}Bk and ^{249}Cf." Trans. Am. Nucl. Soc. 27, 872 (1977).

13. Gryntakis (1976) as quoted in CINDA 76/77 Supplement 3, International Atomic Energy Agency, Vienna, p 330 (1977).

14. G. D. James, J. W. T. Dabbs, J. A. Harvey, N. W. Hill, and R. H. Schindler. "Intermediate Structure Studies of ^{234}U Cross Sections." Phys. Rev. C 15, 2083 (1977).

15. C. E. Ahlfeld and N. P. Baumann. "The Measurement of α,n Cross Sections for ^{232}Th, ^{233}U, and ^{237}Np with Aluminum Capture Gamma Rays." (Private Communication.)

16. S. Platlard, J. Blons, and D. Paya. "Fission Cross Section of Neptunium-237 from 3 eV to 2 MeV." Nucl. Sci. Eng. 61, 477 (1976).

17. L. W. Weston and J. H. Todd. "Neutron Capture Cross Section of Plutonium-240." Nucl. Sci. Eng. 63, 143 (1977).

18. G. F. Auchampaugh and L. W. Weston. "Parameters of the Subthreshold Fission Structure in ^{240}Pu." Phys. Rev. C 12, 1850 (1975).

19. J. Blons and H. Derrien. "Analyse Multiniveaux des Sections Efficoce Totale et de Fission de ^{241}Pu de 1 a 104 eV." Journal de Physique 37, 659 (1976).

20. L. W. Weston and J. H. Todd. "Neutron Capture and Fission Cross Sections of Plutonium-241." Nucl. Sci. Eng. 65, 454 (1968).

21. G. W. Carlson, J. W. Behrens, and J. B. Czirr. "A Measurement of the Fission Cross Section of Plutonium-241 from 8 eV to 70 keV." Nucl. Sci. Eng. 63, 149 (1977).

22. V. D. Gavrilov, V. A. Goncharov, V. V. Ivanenko, V. N. Kustov, and V. P. Smirnov. "Thermal Cross Sections and Resonance Integrals of Fission and Capture of ^{241}Am, ^{243}Am, ^{245}Cm, ^{249}Bk, and ^{249}Cf." Sov. Nucl. En. 41, 808 (1976).

23. K. D. Zuravlev, N. I. Kroshkin, A. P. Chetverikov. "Cross Sections and Resonance Integrals for the Fission of ^{239}Pu, Am, Cm, and ^{249}Cf." Sov. Nucl. En. 39, 907 (1975).

24. S. M. Kalebin, V. S. Artamanov, R. N. Ivanov, G. V. Pukolaine, T. S. Belanova, A. G. Kolesov, and V. A. Safonov. "Total Neutron Cross Section and Neutron Resonance Parameters of ^{241}Am in the Energy Range 0.004-30 eV." Sov. Nucl. En. 40, 373 (1976).

25. L. W. Weston and J. H. Todd. "Neutron Absorption Cross Section of Americium-241." Nucl. Sci. Eng. 61, 356 (1976).

26. T. S. Belanova, A. G. Kolesov, V. A. Poruchikov, G. A. Timofeev, S. M. Kalebin, V. S. Artamanov, and R. N. Ivanov. "Total Neutron Cross Sections and Neutron Resonance Parameters of ^{243}Am in the Energy Range 0.4-35 eV." Sov. Nucl. En. 40, 368 (1976).

27. M. G. Silbert. "Cross Section of ^{243}Cm from the Underground Nuclear Explosion, PHYSICS-8, Table of Values." ERDA Report LA-6239-MS (UC-34c), Los Alamos Scientific Laboratory, NM (1976).

28. S. M. Kalebin. "Total Neutron Cross Section Measurements on the Transactinium Isotopes ^{241,243}Am, ^{244,245,246,248}Cm." Transactinium Isotope Nuclear Data TND, International Atomic Energy Agency IAEA-186, Vol. II, p 121 (1976).

29. T. S. Belanova, Ur. S. Zamyatnin, A. G. Kolesov, V. M. Lebedev, and V. A. Poruchikov. "Neutron Resonance Parameters for ^{245}Cm in the Energy Range from 1-30 MeV." Atomnaya Energiya 42, 52 (1977) in Russian.

30. T. S. Belanova, Ur. S. Zamyatnin, A. G. Kolesov, V. A. Poruchikov, S. E. Babich, N. G. Kocherygin, V. N. Nefodov, S. A. Safonov, S. N. Nikopskin, V. A. Anufriev, V. N. Nikopaev, V. A. Lebedev, Ur. Tolorov, A. V. Klinov, S. M. Kalebin, V. S. Artamonov, and R. N. Ivanov. "Neutron Resonance Parameters of Some Curium Isotopes." Proc. 4th All Union Conf. on Neutron Physics Kiev, 18-22 April (1977) in Russian.

31. M. G. Silbert. "Fission Cross Section of Berkelium-249 between 0.7 and 3 MeV." Nucl. Sci. Eng. 63, 198 (1977).

Section 13

DATA PROCESSING FOR POWER REACTOR FUEL CYCLE CODES

DATA PROCESSING FOR POWER REACTOR FUEL CYCLE CODES*

Robert E. MacFarlane
Los Alamos Scientific Laboratory, University of California
Theoretical Division
Los Alamos, New Mexico 87545

ABSTRACT

A power reactor fuel cycle code must compute the isotopic composition of the fuel as a function of both time and position. The most difficult part of such a calculation is computing the self-shielded cross sections and fluxes for the wide range of compositions seen over the power history of the fuel. The EPRI-CELL and EPRI-CPM codes use the background cross section method for self-shielding. This paper reviews the background cross section method with special emphasis on the interaction between the approximations used in CELL and CPM and the methods used for processing multigroup constants. Specific examples using data processed with NJOY are used to illustrate the effects of non-1/E flux, intermediate resonance parameters, elastic scattering self-shielding, transport corrections, and heterogeniety methods.

INTRODUCTION

An accurate knowledge of the isotopic compostion of power reactor fuel as a function of time is important for operating considerations such as control and fuel shuffle procedures, for economic effects such as core life and fissile isotope production, and for long-term problems such as storage criticality and final disposal. Such a calculation is difficult and expensive. In addition to a fairly complete knowledge of fission-product yields and decay paths and actinide-transmutation paths, a good representation of space and energy self-shielding is required over a wide range of compostions.

In order to make such a calculation tractable, approximations must be made. For example, reduced transmutation chains can be chosen that are still capable of representing fuel depletion/production and fission product absorption accurately,[1] and self-shielding can be represented using the background cross section methods.[2] This approach is used in the codes EPRI-CELL and EPRI-CPM.[3] This paper will discuss the nuclear data requirements of these codes from the processing point of view, with special emphasis on the problem of self-shielding. Specific examples using data produced by NJOY[4] will be used to illustrate the interaction between the approximations used in CELL and CPM and the methods used for producing multigroup constants.

*Work supported by Electric Power Research Institute and US Department of Energy.

BURNUP CODE METHODOLOGY

The basic structure of the burnup codes EPRI-CELL and EPRI-CPM is shown in Fig. 1. Starting with a specified initial composition, the code computes self-shielded cross sections for the fuel pins. These cross sections are then used to compute the flux at criticality for a specified power level. This flux, together with the self-shielded cross sections, is then used to compute the production and burnup of isotopes for this time step. The new composition is then used to repeat the entire procedure for the next time step. The process is continued for the entire power history of the fuel.

Consider the production and burnup calculation. CELL uses the CINDER[5] code with (currently) 69 linearized chains for fission products and 16 chains for the actinides. CPM also uses the method of linearized chains, but with 14 fission-product chains and 5 actinide chains. Both representations are reasonably adequate for following fuel economy and fission product absorption. CELL provides additional detail for the production of the higher actinides and a good enough representation of the fission products for storage and reprocessing calculations. For difficult problems like shutdown after-heat, the flux history and shielded cross sections from CELL or CPM can be used with CINDER-10,[6] which has very extensive chains.

The flux calculation in CELL is divided into thermal and fast parts. The thermal calculation uses the method of THERMOS[7] -- a detailed integral transport calculation for a cylindrical cell using 35 group P_0 transport-corrected cross sections. The fast flux calculation uses the 68 group structure and B_1 method from GAM-I[8] with self-shielded cross sections. The two flux solutions are connected, adjusted to give the desired power, and used to collapse the cross sections to a few-group structure for the burnup calculation and later multidimensional flux calculations. CPM first carries out a 69-group cylindrical collision probability solution for the flux in each type of fuel pin, then collapses to a coarser structure and uses the same method to compute the flux in the homogenized multipin cell. If needed, a two-dimensional collision probability calculation is made in a still coarser group structure. In any case, leakage is accounted for by a B_1 calculation, the flux is normalized to the desired power, and the cross sections are condensed to the few-group structure.

The self-shielded cross sections required for these calculations are obtained by using the background cross-section method (also called the shielding-factor method and the Bondarenko method). This is in contrast to previous practice in the thermal reactor community where shielding is normalized to experimental resonance integral correlations as in LASER[9] or computed from resonance parameters using the Nordheim method as in GAM-I and its successors. The background cross section methods in CELL and CPM

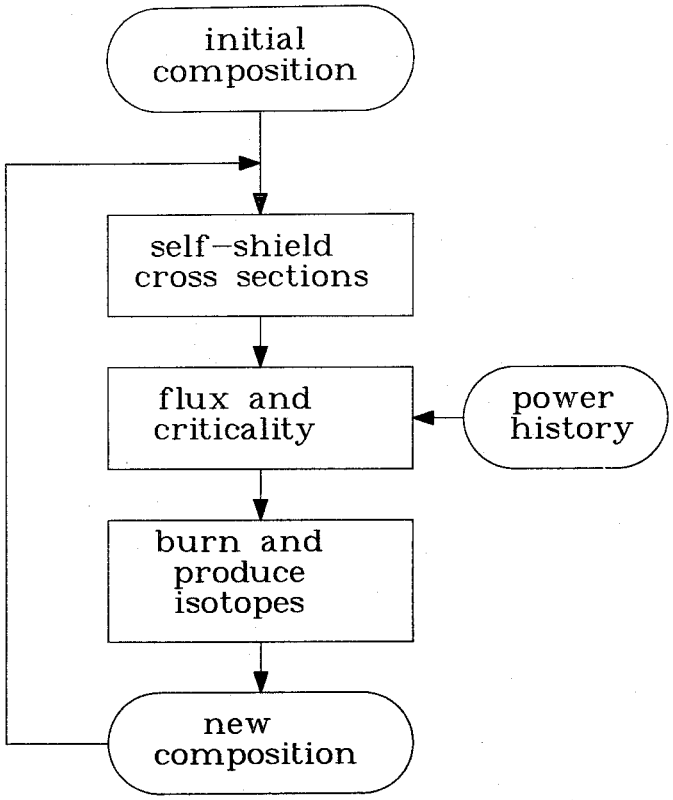

Fig. 1. Basic structure of a fuel cycle burnup code.

are based on those in the British code WIMS.[10] Similar methods are widely used in fast-reactor analysis.

THE BACKGROUND CROSS SECTION METHOD

The average cross section for group g, material i, and reaction x is

$$\sigma^i_{xg} = \frac{\int_g \sigma^i_x(E)\phi(E)dE}{\int_g \phi(E)dE} \quad . \tag{1}$$

Since the flux ϕ is not known, some model flux must be assumed. For example, in a large homogeneous system where the narrow resonance approximation is valid,

$$\phi(E) = \frac{S(E)}{\Sigma_t(E)} \quad , \tag{2}$$

where S(E) is a smooth function of energy representing the scattering and fission sources into E, and Σ_t is the total macroscopic cross section.

In evaluating the numerator of Eq. (1), it is assumed that the important effect is the interaction between a resonance in σ_x and the dip in ϕ caused by that same resonance (hence, "self-" shielding). The cross section becomes

$$\sigma^i_{xg} = \frac{\int_g \frac{\sigma^i_x(E)}{\sigma^i_0 + \sigma^i_t(E)} S(E)dE}{\int_g \frac{S(E)}{\sigma^i_0 + \sigma^i_t(E)}} \quad , \tag{3}$$

where

$$\sigma^i_0 = \frac{1}{N_i} \sum_{j \neq i} N_j \sigma^j_t \quad , \tag{4}$$

and where N_i is the number density for material i in the mixture. It is now further assumed that the background cross section σ^i_0 is constant in each group. This allows a nearly problem-independent library to be constructed; the processing code simply evaluates

Eq. (3) for a range of values of σ_0. The self-shielding code determines σ_0 and interpolates for the corresponding cross section.

It is the use of this single σ_0 parameter that characterizes the background cross-section method. The accuracy of the method depends on (1) obtaining accurate cross sections $\sigma_x(\sigma_0)$ and (2) making good choices for σ_0.

INTERMEDIATE RESONANCE SELF-SHIELDING

As an example of these two influences, consider the problems of obtaining accurate self-shielded cross sections and choosing σ_0 in the range below 200-300 eV where the resonances are not well represented by the narrow resonance approximation. In the method originally developed for WIMS, Eq. (2) is solved in detail for an infinite homogeneous mixture of the heavy fuel isotope (σ_f) with varying amounts of hydrogen (σ_m) using a point-energy or super-fine-group integral transport code such as RABBLE.[11] This detailed flux can then be used to compute effective multigroup cross sections versus $\sigma_0 = N_m\sigma_m/N_f$.

The NJOY code uses a simpler variation of this approach. For an infinite homogeneous system of two isotopes with isotropic scattering in the center-of-mass frame, Eq. (2) becomes

$$[\sigma_f(E)+\sigma_0]\phi(E) = \int_E^{E/\alpha_m} \frac{\sigma_0}{(1-\alpha_m)E'}\,\phi(E')dE' + \int_E^{E/\alpha_f} \frac{\sigma_{sf}(E')}{(1-\alpha_f)E'}\,\phi(E')dE' \quad , \qquad (5)$$

where α is the maximum fractional energy change in scattering, and σ_{sf} is the fuel scattering cross section. If ϕ were 1/E, the first source integral would become σ_0/E independent of moderator mass. The flux that results has the property desired for the background cross-section method — it depends only on the single parameter σ_0 -- and, moreover, it has exactly the same form as Eq. (2), with S(E) being the solution of the integral equation

$$S(E) = \frac{\sigma_0}{E} + \int_E^{E/\alpha} \frac{\sigma_{sf}(E)}{(1-\alpha)E'}\,\frac{S(E')}{\sigma_f(E') + \sigma_0}\,dE' \quad . \qquad (6)$$

Since this equation only requires data over a limited energy range above E, it is practical to solve it by iteration using detailed pointwise cross sections. The NJOY solution proceeds from low energy to high and switches over to the narrow resonance result above some specified cutoff energy. Table 1 compares cross sections computed with the computed weighting flux and cross sections computed using the narrow resonance approximation flux.

Table 1

Comparison of Cross Sections Using Computed Flux to Narrow Resonance (NR) Cross Sections for U-238 at 100 b Background

Energy Range	Computed Absorption	NR Absorption
4-9.88 eV	11.75 b	11.78 b
9.88-15.97	0.4518	0.4509
15.97-27.7	8.614	7.729
27.7-48.1	6.012	4.713
48.1-75.5	2.796	2.285
75.5-149	3.178	2.737
149-367	1.955	1.760

This derivation depends on the flux having a 1/E shape. In a real thermal power reactor, the flux increases somewhat less rapidly with decreasing energy due to absorption. Assuming that $\phi = E^{-p}$ throughout the range E to E/α_m ($p \sim 0.94$ for a PWR), the moderator source becomes

$$S_m = \left[\frac{1 - \alpha_m^p}{p(1-\alpha_m)}\right] \frac{\sigma_0}{E^p} \quad . \tag{7}$$

The bracketed factor can be absorbed into the arbitrary normalization of the flux. Equation (6) is recovered with the first term on the right changed to σ_0/E^p. NJOY allows the user to input an arbitrary function for this term.

The second assumption made in deriving Eq. (6) is that any resonance dips in the flux are narrow enough so that they do not contribute appreciably to the moderator integral (i.e., resonances are narrow with respect to moderator scattering but not with respect to fuel scattering. This problem can be attacked using a variation of the intermediate resonance approximation.[12] The source term is assumed to be intermediate between the narrow and wide resonance limits

$$S_m(E) = \lambda\sigma_0 C + (1-\lambda)\sigma_0\phi(E) \quad , \tag{8}$$

where λ and C are both slowly varying functions of energy. Equation (5) becomes

$$[\sigma_f+\lambda\sigma_0]\phi(E) = \lambda\sigma_0 C + \int_E^{E/\alpha_f} \frac{\sigma_{sf(E')}}{(1-\alpha_f)E'}\ \phi(E')dE' \quad . \tag{9}$$

Therefore, the self-shielded cross sections already computed can be used, even when the narrow resonance approximation fails for moderator scattering, by simply interpolating for the cross section appropriate for $\lambda\sigma_0$.

For its intended use in the background cross section method, an effective λ value must be chosen for each group. It can be obtained by comparing the source into the group obtained using a full treatment of the moderator term in Eq. (5) for various moderators with the corresponding source using the simplified form. Values used by WIMS, CELL, and CPM are given in Tables 2 and 3. A detailed re-evaluation of these parameters and investigation of the range of validity of Eq. (8) is underway.

Table 2

Intermediate Resonance λ From EPRI-CELL and WIMS

Isotope	CELL	WIMS
SS	0.5	
Zirc	0.5	
Inconel	0.5	
H-1	1.	1.
H-2		1.
B-10	0.9	
C-12		1.
O-16	0.94	0.94
Al		0.9
Fe		0.5
U and Pu	0.2	0.2

Table 3

Intermediate Resonance λ From EPRI-CPM Library

Group	H-1	H-2	O-16	Fe	U & Pu
15					0.99
16					0.98
17					0.97
18					0.96
19				0.99	0.95
20			0.99	0.98	0.90
21	0.99		0.98	0.85	0.60
22	0.987	0.99	0.92	0.80	0.32
23	0.987	0.98	0.914	0.75	0.32
24	0.963	0.94	0.784	0.45	0.073
25	0.955	0.93	0.74	0.37	0.05
26	1.	1.	0.984	0.95	0.80
27	0.894	0.845	0.49	0.121	0.01

(omitted numbers are 1.0)

HETEROGENEITY

In an infinite system of two regions (fuel and moderator), the neutron balance equations are

$$V_f \Sigma_f \phi_f = (1-P_f) V_f S_f + P_m V_m S_m \quad , \tag{10}$$

$$V_m \Sigma_m \phi_m = P_f V_f S_f + (1-P_m) V_m S_m \quad , \tag{11}$$

where V_f and V_m are the volumes of the regions, Σ_f and Σ_m are the total macroscopic cross sections, S_f and S_m are the source per unit volume in each region, P_f is the probability that a neutron born in the fuel will suffer its next collision in the moderator, and P_m is the probability that a neutron born in the moderator will suffer its next collision in the fuel. The reciprocity theorem[13] requires that $V_f \Sigma_f P_f = V_m \Sigma_m P_m$. It is further assumed that the fuel escape probability can be represented using the Wigner rational approximation[13]

$$P_f = \frac{\Sigma_e}{\Sigma_e + \Sigma_f} \quad , \tag{12}$$

where the fuel escape cross section Σ_e is assumed to be a slowly varying function of energy. The flux in the fuel region then satisfies

$$(\Sigma_f + \Sigma_e)\,\phi_f = \frac{\Sigma_e S_m}{\Sigma_m} + S_f \quad . \tag{13}$$

If the moderator term on the right-hand-side is a slowly varying function of energy, Eq. (12) is clearly equivalent to Eq. (5) with Σ_e/N_f being the equivalent background self-shielded cross section. Therefore, the homogeneous self-shielded cross sections computed as described above are also suitable for heterogeneous systems that meet the following qualifications: (1) the moderator scattering and absorption are slowly varying, and (2) all resonances are narrow with respect to moderator scattering.

The equivalence is less evident when there are significant resonance dips in the moderator flux. Using the intermediate resonance approximation as in the preceeding section,

$$S_m = \lambda\Sigma_m C + (1-\lambda)\Sigma_m\phi_m \quad . \tag{14}$$

Substituting this into Eq. (13) and using the sum of Eqs. (10) and (11) to eliminate ϕ_m gives the result

$$(\lambda'\Sigma_e+\Sigma_f)\phi_f = \lambda'\Sigma_e C + S_f \quad , \tag{15}$$

where the effective λ value is

$$\lambda' = \frac{\lambda}{\lambda + \dfrac{V_f\Sigma_e}{V_m\Sigma_m}(1-\lambda)} \quad . \tag{16}$$

For an external moderator that is a mixture of several isotopes (e.g., H_2O), λ in Eq. (16) is to be replaced by the average $\bar{\lambda}$ given by

$$\bar{\lambda} = \frac{\sum_{i\varepsilon m}\lambda_i\Sigma_i}{\Sigma_m} \quad . \tag{17}$$

Once again, the heterogeneous system will have multigroup cross sections equivalent to the homogeneous ones, but with a background cross section equal to $\lambda'\Sigma_e/N_f$. The physical meaning of Eq. (16) is clear. The parameter $(V_f\Sigma_e/V_m\Sigma_m)$ describes how much of each resonance dip in the fuel flux appears in the moderator flux; if it is zero, the effective λ is 1.0 because there are no resonance

dips in the moderator flux; if the parameter is 1.0 (close-packed lattices), the flux in the moderator is equal to the fuel flux and the effective λ is equal to the homogeneous value. This effect is only partially included in CELL and CPM.

To evaluate the practical importance of intermediate resonance corrections, a simple pin cell with a 0.5 cm radius oxide pin, zirconium clad, and 0.9 cm water moderator was run with CPM. Table 4 compares some results obtained using the standard library to results with two modified libraries: one with $\lambda = 1$ for all groups of hydrogen and one with $\lambda = 1$ for all groups of hydrogen and oxygen (in both fuel and moderator). These differences are large enough to justify careful attention to the calculation of λ by the processing code and to the use of λ in the fuel cycle code. In particular, CELL should be extended to use energy-dependent λs, and both CELL and CPM should allow for region-dependence in λ.

Table 4

Effect of Moderator Intermediate Resonance Parameter for CPM Pin Cell Problem

Computed Quantity	Standard Library	$\lambda = 1$ for H-1	$\lambda = 1$ for H-1 & O-16
U-238 σ_a for 4-10 eV group	7.904 b	+2.14%	+7.55%
k_∞	1.08109	-0.21%	-0.69%
U-238 absorptions at critical	0.2977	+0.69%	+2.24%

ELASTIC SELF-SHIELDING

The elastic scattering cross section and the elastic group-to-group transfer matrix are self-shielded just like fission and capture; however, neither CELL nor CPM carries the corresponding shielding factors. The libraries for both codes contain totally shielded elastic data for U-238; all other isotopes have only infinitely dilute elastic data. The first processing code capable of consistently shielding all the elements of the elastic matrix is NJOY. In the process of generating an ENDF/B-IV library for EPRI-CPM, data sets were prepared for U-238 with and without elastic self-shielding. A comparison for several quantities is shown in Table 5. As might be expected, the effect on the transport cross section is large. Since the U-238 background cross section

Table 5

Effects of Shielding Elastic Scattering for CPM Pin Cell Test with LASL U-238

Quantity Calculated	Standard Library	Elastic* @ σ_0 = 10b	Elastic* @ σ_0 = ∞
k_∞	1.08109	1.02431	+0.029%
Transport for 0.625 eV to 5.5 keV	0.3566	0.3469	+32.7%
Buckling	0.000968	0.000282	+9.7%
U-238 Absorptions at Critical	0.2977	0.3487	-0.35%

*All isotopes same as in Standard Library except for U-238 from ENDF/B-IV and NJOY.

will change with burnup, a more sophisticated treatment of shielding for U-238 elastic scattering might be necessary.

THERMAL LIBRARY PROCESSING

The cross section data required by EPRI-CELL and EPRI-CPM can be produced using the NJOY nuclear-data processing system. The basic structure of NJOY in this application is shown in Fig. 2.

First, ENDF/B-IV or V data are converted into pointwise form using the RECONR module. RECONR is similar to RESEND[14] and outputs an accurate linearly interpolable representation of resonances and non-linear cross sections at 0 K. The results are broadened to any desired temperature using the highly accurate SIGMA1[15] method in the BROADR module. Thermal coherent and incoherent scattering is produced in THERMR for free and bound scatterers. The results of these modules are saved in point-ENDF (PENDF) format.

The GROUPR module produces self-shielded cross sections and group-to-group matrices including intermediate resonance effects and elastic matrix self-shielding as discussed above. The results are saved in group-ENDF (GENDF) format.

The multigroup output can then be reformated into a variety of specific library formats, including (1) EPRI-CELL fast, (2) EPRI-CELL thermal, (3) EPRI-CPM, and (4) DTF/ANISN format for discrete ordinates transport calculations.

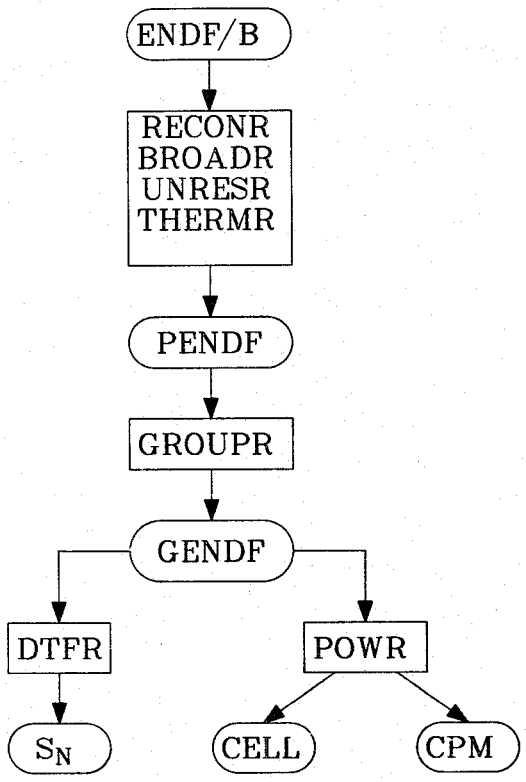

Fig. 2. Processing sequence used for generating NJOY thermal libraries.

A CELL library produced using NJOY with ENDF/B-IV has been tested by comparison with the original CELL library (based on ENDF/B-I or II) for a fuel element that was irradiated for two cycles in the Carolina Power and Light Company's H. B. Robinson Pressurized Water Reactor. Because of the well-known problem with U-238 absorption in ENDF/B-IV, a modified library with U-238 absorption reduced by 15% in every resonance group was also used. The results in Tables 6 and 7 show reasonably good agreement when the corrected U-238 cross sections are used. Table 5 shows this same effect when using Version IV U-238 in CPM.

Table 6

NJOY vs CELL Library for CP+L Problem Criticality

Integral Parameter	Original Library	NJOY Library	Modified Library*
k_{eff}	1.00224	-0.41%	-0.04%
Total absorption	0.8985	+3.3	+0.12
Total fission	0.4068	-0.10	+0.32
U-238 abs.	0.2955	+10.9	+0.07
Buckling	0.00201	-31.0	-1.5

*U-238 absorption reduced by 15% in every resonance group.

Table 7

NJOY vs CELL Library for CP+L Problem Isotopics

Ratio	Experiment*	CELL	NJOY (Mod)
U235/U	0.604±0.052	0.602	+4.3%
Pu239/Pu	54.11±1.15	53.72	+6.0
Pu240/Pu	25.14±0.32	25.14	-3.5
Pu241/Pu	13.07±0.30	15.21	+5.0
Pu242/Pu	6.02±5.0	6.12	-3.1

*For 30.92 MWD/kg burnup.

CONCLUSIONS

The application of the background cross section method to power reactor fuel cycle codes shows promise of providing calculations of practical accuracy at relatively low cost. New cross section libraries, improved fission-product and actinide chains, and extended methods (e.g., intermediate resonance equivalence principles and elastic self-shielding) will further increase the utility of codes like EPRI-CELL and EPRI-CPM.

REFERENCES

1. T. R. England, W. B. Wilson, and M. G. Stamatelatos, Fission Product Data for Thermal Reactors, Electric Power Research Institute report NP-356, December 1976.
2. I. I. Bondarenko, Ed., Group Constants for Nuclear Reactor Calculations, Consultants Bureau, New York, 1964.
3. EPRI-CELL and EPRI-CPM are part of the proprietary Advanced Recycle Methodology Program developed by Nuclear Associates International and AB Atomenergie, Studsvik, for the Electric Power Research Institute (EPRI). Additional information can be obtained from EPRI.
4. R. E. MacFarlane and R. M. Boicourt, Trans. Am. Nucl. Soc. 22, 702 (1975).
5. T. R. England, CINDER - A One-Point Depletion and Fission-Product Program, Westinghouse Corporation report WAPD-TM-334 (Rev.), June 1964.
6. T. R. England, et al, CINDER-7: An Interim Report for Users, Los Alamos Scientific Laboratory report LA-5885-MS, April 1975. (CINDER-10 is described in Applied Nuclear Data Research and Development, p. 13, Los Alamos Scientific Laboratory report LA-6472-PR, 1976.
7. H. C. Honeck, THERMOS, A Thermalization Transport Theory Code for Reactor Lattice Calculations, Brookhaven National Laboratory report BNL-5826, 1961.
8. G. D. Joanou and J. S. Dudek, GAM-I: A Consistent P_1 Multigroup Code for the Calculation of Fast Neutron Spectra and Multigroup Constants, General Atomic report GA-1850, 1961.
9. C. G. Poncelet, LASER - A Depletion Program for Lattice Calculations Based on MUFT and THERMOS, Westinghouse Electric Corporation report WCAP-6073, 1966.
10. J. R. Askew, F. J. Fayers, and P. B. Kemshell, J. Brit. Nucl. Energy Soc. 5, 564 (1966).
11. P. H. Kier and A. A. Robba, RABBLE, A Program for Computation of Resonance Absorption in Multiregion Reactor Cells, Argonne National Laboratory report ANL-7326, 1967.
12. R. Goldstein and E. R. Cohen, Nucl. Sci. Eng. 13, 132 (1962).
13. L. Dresner, Resonance Absorption in Nuclear Reactors, Pergamon Press, 1960.

14. O. Ozer, RESEND: A Program to Preprocess ENDF/B Materials with Resonance Parameters into A Pointwise Form, Brookhaven National Laboratory report BNL-17134, 1972.
15. D. E. Cullen and C. R. Weisbin, Nucl. Sci. Eng. 60, 199, 1976.

Section 14

THE RELATIONSHIP BETWEEN BASIC NUCLEAR DATA AND LWR FUEL CYCLE PARAMETERS

The Relationship Between Basic Nuclear Data and LWR Fuel Cycle Parameters

M. Becker, D.R. Harris, B. Quan, and J.M. Ryskamp
Rensselaer Polytechnic Institute, Troy, N. Y.

ABSTRACT

An interactive system has been developed at RPI to analyze the sensitivity of water reactor fuel cycle parameters and costs to uncertainties in nuclear data. A sequence of batch depletion, core analysis, and fuel cost codes (referred to as Path B) determines the changes in fuel cycle parameters and costs for changes in few-group microscopic cross sections, in fission yields, and in decay data. For cases that are found to be significant from Part B analysis, the sensitivities of few-group data to basic nuclear data are determined by detailed calculations (referred to as Path A). Analyses of pressurized and boiling water reactors with recycle and throwaway options show substantial sensitivities of fuel cycle parameters and costs, particularly to thermal and resonance nuclear data for fissile nuclides. The results bring out the importance for power reactor sensitivity analysis of dealing with the full fuel cycle including depletion of initially-loaded fuel and the building-in of actinides and fission products.

INTRODUCTION

An interactive system has been developed at RPI to analyze the sensitivity of water reactor fuel parameters and cycle costs to uncertainties in nuclear data. Uncertainties in nuclear data impose penalties in reactor economy through margins that are necssary to ensure that reactor performance meets requirements. Sensitivity analyses of these effects are important both in establishing worthwhile directions for improvement in the data and in verifying proper margins.

Improvements in nuclear data can be costly, involving continuing support for measurement facilities and for evaluating, processing and testing data. Power reactor costs are on a much larger scale, however, and design margins are correspondingly important. Our sensitivity analyses indentify certain data as being important to LWR fuel cycle operation and economy, while other data are found to be relatively unimportant. In some cases, these patterns of importance are found to differ from those suggested by tabulations of requests for improved data.[1]

Improvements in nuclear data can benefit reactor operation and economy other than through fuel cycle parameters. For example, greater confidence in nuclear data can lead to a reduction in number of control rods, thus decreasing initial capital costs.[2] Factors other than nuclear data uncertainties affect design margins

also, and design margins are applied for safety, licensing and other objectives as well.[3] Fuel cycle parameter and cost sensitivities, however, are significant[4,5,6] and are subjected to systematic analysis. Many of the sensitivities determined here, such as for core reactivities and batch inventories through time, are important also for objectives other than reducing fuel cycle costs.

Improvements in nuclear data can permit a reduction in the margin of enrichment that is provided in the unexposed reactor fuel to ensure that the core achieves the required cycle length at the required power. The reduced fuel enrichment results in decreased fuel cycle cost. Sensitivity analyses of this effect must include changes in core reactivity and important changes in nuclide inventories resulting directly from the original change in nuclear data and indirectly from changes in neutron flux distributions in energy and space. These changes are determined through a linked series of data processing, reactor cell, core, and cost codes either by perturbation theory methods[7] or by the direct method. In the direct method the code sequence is run for a base case. Then each nuclear datum is changed, and the code sequence is run through to determine changes in cost and in physics parameters. The direct method, which would be prohibitively expensive if industry codes were used for the survey, becomes feasible when inexpensive special-purpose codes are used. Such special-purpose codes have been developed and are applied through the RPI interactive investigator-computer-graphics system.[8]

The sensitivity analysis system is outlined first including recent improvements. Then sensitivity analyses are described for a PWR and for a BWR for various fuel and recycle options.

REACTOR SENSITIVITY ANALYSIS SYSTEM

The structure of the reactor sensitivity analysis system is influenced both by the complexity of the nuclear design process and by the large number of potentially important nuclear data. The system relates nuclear data to fuel cycle costs by two sequences of operations broken at the few-group level. In Path A, basic cross sections are processed to multigroup cross sections and collapsed to few-group cross sections. In Path B, few-group microscopic cross sections, radioactive decay data, and fission yields are used in depletion of a fuel batch at power levels determined by core analysis, reactor parameters and inventories are computed, and fuel cycle costs are determined.[9]

The cost implications of nuclear data uncertainties at the few-group level are determined first by Path B analysis; then for cases thus shown to be important, Path A analyses are carried out. At the few-group dividing level, the uncertainties arising from data processing are indistinguishable from uncertainties in the basic nuclear data, and data processing effects are included in Path A analyses. The data processing uncertainties investigated

here are not numerical in nature (these we judge should be under control) but physical, particularly in the detailed distributions of neutron flux in energy and space that are used to average cross sections.

Path B

Fuel cycle costs are determined for fuel batch inventories before and after exposure by the code module COSTR. Fuel cycle costs are grouped into conventional cost components for which present worth values are determined referred to the mid-point of the fuel in-core residence time. Front end cost components include the costs of mining and milling ore, of conversion, of separation and of fuel fabrication. Tails enrichment has either an assigned value or the optimum value in terms of feed and enrichment costs. Plutonium or ^{233}U values in fresh fuel are determined consistent with uranium cost, enrichment cost, and fuel handling penalties. Back end costs include storage, transportation, and disposal for the throwaway case as well as the reprocessing cost and the values of materials in spent fuel for recycle cases. Payments for materials and services, including progress payments, are on an assigned schedule relative to the fuel in-core residence time. The discount rate used for present value calculations is either assigned or is determined from more basic information such as debt and equity fractions. Unit costs at required points in time are determined by projecting as shown in Table 1. Costs for a given year are in terms of current dollars.

The pre- and post-exposure fuel batch inventories and other batch parameters are determined by Path B by the few-group batch exposure code module FASTCELL. Exposure-dependent few-group microscopic cross sections are determined by a base run of an industry cell code, e.g., LEOPARD[10] or LASER,[11] and stored at major time-steps during exposure. Modifications in these few-group microscopic cross sections are relagated to Path A detailed analysis. FASTCELL accurately follows nuclear concentrations by forward differencing (or more accurately, in the case of a few fission products) for minor time steps between the major time steps. The fission product chains used are largely those of EPRI-CPM[12] and of the EPRI-CINDER reduced chain structure,[13] and data are obtained from ENDF/B-IV[14] as well. Few-group fluxes scaled by demand power are recomputed at each minor time step so power demand, few-group microscopic data, few group fluxes and nuclear concentrations are always consistent. The accuracy and cost of the calculation are controlled through the frequency of minor time steps between the major time steps. FASTCELL, which costs less than one dollar on the PDP-15[8] to expose a fuel batch over several years, is orders of magnitude cheaper than industry cell codes.

The power demand imposed on a fuel batch is determined by the power demand on the core, by the distribution of power density in the core, and by cycle loading patterns for the fuel elements

Table 1

Fuel Cycle Cost Projections (UO_2 Cycle)

	1980	1985	1990	1995	2000	2005	2010
Ore ($/lb$U_3O_8$)	38.3	48.9	62.4	79.6	101.6	138.5	230.3
Conversion ($/lb)	4.5	5.7	7.2	9.1	11.8	12.2	15.6
Enrichment ($/kg/SWU)	78.6	103.0	139.0	188.0	254.0	324.0	414.0
Fabrication UO_2 ($/kg)	122.3	152.0	190.0	238.0	299.0	377.0	477.0
Fabrication Mixed Oxide($/kg)	262.5	326.8	406.5	509.6	641.2	809.1	1025.2
Shipment ($/kg)	17.9	22.8	29.1	37.1	47.4	60.5	77.2
Reprocessing ($/kg)	221.0	230.0	241.0	256.0	275.0	299.0	329.0
Disposal ($/kg)	64.0	81.0	104.0	133.0	169.0	216.0	276.0
Plutonium ($/kg)	28.4	37.3	49.0	64.1	839.0	121.0	185.0

making up the batch. For small cross section changes the fuel loading patterns do not change. The distribution of power density in the core is determined by operator control and by thermal-hydraulic factors as well as by depletion. The Haling strategy, whereby design and control contribute to maintaining a nearly constant power shape, is often followed for BWR's and we find that PWR operation approximates this strategy. The power demand on the core, the cycle loading patterns, and the constant core power shape determined from analysis of industry experience are combined in a code module FASTCORE to yield the required batch power demand.

The Path B code system exposes a fuel batch for the base case and fuel batch costs C are determined for the base case. Then a few-group microscopic cross section or fission yield or decay parameter (x) is changed (by δx), the fuel batch is reexposed, and the end-of-cycle core reactivity and other parameters are found to differ from those of the base case. Core parameter sensitivities are determined at this point. Because the cycle length must be unchanged to achieve the required energy production, the enrichment of fresh fuel is changed until the end-of-cycle core reactivity returns to that of the base case. For mixed oxide recycle the proportion of oxides in fresh fuel may be altered as well as enrichment. Fuel batch parameters and costs are redetermined for this doubly-perturbed exposure, and the change δC from the base case and the sensitivity coefficient

$$S_x = \frac{x}{C}\frac{\delta C}{\delta x} \quad , \tag{1}$$

is determined.

Path A

The LWR sensitivity analyses to be described shortly bring out the importance of thermal and resonance group cross sections. Thus most Path A analysis has been directed to these phenomena, although a fast slowing-down code combining features of GAM[15] and MUFT[16] with adjoint capability has been prepared. The resonance code module FASTR solves the slowing down equations numerically across a resonance using region-to-region collision probabilities and using resonance cross sections from the RPI multilevel code module MLEVL. Resonance group sensitivities are determined from FASTR by the direct method.[17] Resonance group sensitivities are found to result primarily from uncertainties in the resonance parameters and in Dancoff factors with lesser contributions from multilevel effects and Doppler broadening treatments.

In contrast, thermal group sensitivities are determined using the perturbation method.[18] The thermal group code module FASTT combines features of the LEOPARD-SUFFOCATE and LASER-THERMOS methods and adds an adjoint capability. A striking feature of our Path A thermal analyses has been the (usually) overwhelming importance of the Maxwellian energy region.

SENSITIVITY ANALYSES FOR CURRENT LIGHT WATER REACTORS

Sensitivity analyses have been carried out for large pressurized and boiling water reactors using slightly enriched UO_2 fuel prepared from ore.[19] The back end of the fuel cycle is considered as two alternatives, one with spent fuel reprocessing including fissile uranium and plutonium credits, and the other the throwaway case with storage and disposal costs. The fuel batch for the representative large PWR[20] has an initial enrichment of 2.8 w/o ^{235}U and is exposed for three equilibrium cycles over three years. For the first cycle the batch is exposed on the core periphery and for the second and third cycles is checkerboard loaded in the core interior. Reference characteristics for the BWR are based on data for the Montague plants.[21] The BWR fuel batch is exposed for four equilibrium cycles over four years using a scatter loading pattern.

Path B sensitivity coefficients for 1985 are shown in Table 2 for both pressurized and boiling water reactors and for both back end alternatives.[22] Sensitivity coefficients for the BWR are generally less in absolute value than for the PWR. Detailed examination indicates that the lower BWR sensitivities occur because of lower initial enrichment and lower discharge exposure. Table 2 also shows lower sensitivities for the closed cycle than for the throwaway case. This occurs largely because changes in fissile credits after exposure tend to defray in part the changes in initial enrichment required to compensate for nuclear data changes.

The sensitivities shown in Table 2 demonstrate the importance of considering fuel exposure in contrast to examining sensitivites at a point in time or in a mockup. For example, sensitivity to ^{240}Pu data turns out to be small, because of the high worth of the ^{241}Pu produced from neutron capture in ^{240}Pu. Similarly, sensitivities to ^{238}U capture data are less than might have been expected because of the buildup of fissile plutonium in the throwaway case and, additionally, its credit in the recycle case. We have shown earlier[9] that these fuel cycle sensitivities can be aggravated by applying a bias like k-reset which is determined from critical experiments.

The sensitivities shown in Table 2 are abstracted from complete surveys for all relevant nuclear data. Neutron yields ν per fission (Table 3) and energy yields κ per fission are found to be very important, including some of the largest sensitivities found from the study. Nuclear data for certain fission products (Table 4) are somewhat important. The results shown in Tables 3 and 4 are for the BWR. Fast neutron fission in ^{238}U and a few other fast neutron reactions are also important. The results shown in these tables emphasize, however, the major importance of thermal and resonance data for fissile isotopes and to a lesser extent for ^{238}U, fission products and hydrogen. When it is considered that a single fuel batch for a single reactor has a cost of some tens of millions of dollars, it can be seen that these sensitivity

Table 2

Fuel Cycle Cost Sensitivity to Few-Group Data

	BWR		PWR	
	Closed End	Throwaway	Closed End	Throwaway
^{235}U (Epithermal, Capture)	0.092	0.094	0.131	0.128
^{235}U (Epithermal, Fission)	-0.070	-0.089	-0.114	-0.134
^{235}U (Thermal, Capture)	0.221	0.231	0.229	0.232
^{235}U (Thermal, Fission)	-0.429	-0.521	-0.489	-0.544
^{236}U (Epithermal, Capture)	0.017	0.019	0.027	0.029
^{238}U (Fast, Fission)	-0.118	-0.128	-0.137	-0.142
^{238}U (Epithermal, Capture)	0.057	0.203	0.160	0.332
^{238}U (Thermal, Capture)	0.054	0.139	0.078	0.139
^{239}Pu (Thermal, Capture)	0.480	0.537	0.575	0.610
^{239}Pu (Thermal, Fission)	-0.567	-0.678	-0.659	-0.744
^{240}Pu (Epithermal, Capture)	-0.005	0.005	-0.002	0.008
^{241}Pu (Thermal, Fission)	-0.104	-0.122	-0.117	-0.130
Fis. Prod.(Epithermal,Capture)	0.115	0.131	0.158	0.169
Fis. Prod. (Thermal, Capture)	0.129	0.152	0.137	0.152
Hydrogen (Thermal Capture)	0.138	0.164	0.120	0.134
Zirconium (Epithermal, Capture)	0.028	0.032	0.024	0.026

Table 3

Fuel Cycle Cost Sensitivity to Fission Neutron Yield ($\bar{\nu}$)

	Recycle	Throwaway
$\bar{\nu}(^{235}U)$	-1.41	-1.76
$\bar{\nu}(^{238}U)$	- .14	- .18
$\bar{\nu}(^{239}Pu)$	-1.35	-1.70
$\bar{\nu}(^{241}Pu)$	- .27	- .34
All $\bar{\nu}$	-3.17	-3.95

Table 4

Fuel Cycle Cost Sensitivity to Important Fission Product Data

	Recycle	Throwaway
^{135}Xe Thermal Capture σ	.017	.023
Decay Constant	-.017	-.023
U Fission Yield	.028	.038
Pu Fission Yield	.031	.042
^{149}Sm U Fission Yield	.008	.011
Pu Fission Yield	.012	.016
^{103}Rh Thermal Capture σ	.008	.011
Pu Fission Yield	.014	.018
^{131}Xe Pu Fission Yield	.006	.008
^{133}CS Pu Fission Yield	.005	.007
^{143}Nd Thermal Capture σ	.018	.025
Pu Fission Yield	.008	.011
^{147}Pm Decay Constant	-.005	-.007
Pu Fission Yield	.007	.009
^{151}Sm Pu Fission Yield	.009	.012

coefficients indicate large potential benefits from data improvement.

It was noted earlier that Path A analyses for these reactors bring out the importance of individual resonance parameters and Dancoff factors in the resonance range and of the Maxwellian range for thermal group cross sections. The latter point is illustrated in Figure 1 by the case of the important ^{239}Pu fission cross section which is more than five times as large at its 0.3 ev resonance than at the Maxwellian peak; yet its detailed sensitivity is about 50% larger at the Maxwellian peak than at the resonance. This result is for a PWR at middle of exposure. At beginning of exposure the detailed resonance-to-Maxwellian sensitivity ratio is somewhat larger, and at end of exposure it is somewhat smaller. Figure 2 shows the detailed sensitivity profile for the ^{135}Xe cross section. Again the hardened Maxwellian region is dominant.

THORIUM CYCLE SENSITIVITIES

Thorium utilization is being considered for light water reactors for two possible objectives. One of these is to capitalize on thorium resources. The other is to utilize fuel cycles which might prove more resistant to proliferation of capability to obtain strategic nuclear materials. Fuel cycle cost sensitivities to data uncertainties have been evaluated[23] for a basic thorium cycle[24] and for a denatured cycle related to the basic cycle.

As may be expected, thorium fuel cycle costs are less sensitive to ^{235}U data than are conventional fuel cycle costs, since ^{235}U constitutes only a portion of the fuel loaded in the thorium cycle. Also, as may be expected, sensitivities to fertile material data (thorium) are small because conversion to fissile material compensates for reactivity effects from the fertile material itself.

One interesting result in the denatured cycle is the influence of plutonium. The epithermal capture cross-section of ^{238}U in the denatured cycle is substantially higher than in a conventional cycle because of lower self-shielding. Thus, with one-eighth the amount of ^{238}U, the denatured cycle leads to one-third the amount of plutonium of a conventional cycle. Thus, the economics of the denatured cycle is sensitive to data for plutonium. The denatured cycle leads to higher conversion of fertile material, because the ^{238}U leads to more fissile material than the ^{232}Th it replaces.

PLUTONIUM RECYCLE SENSITIVITIES

Sensitivities have been evaluated for plutonium recycle, i.e., cycles in which plutonium is loaded into the reactor as mixed oxide fuel. By comparison with conventional cycles, sensitivity

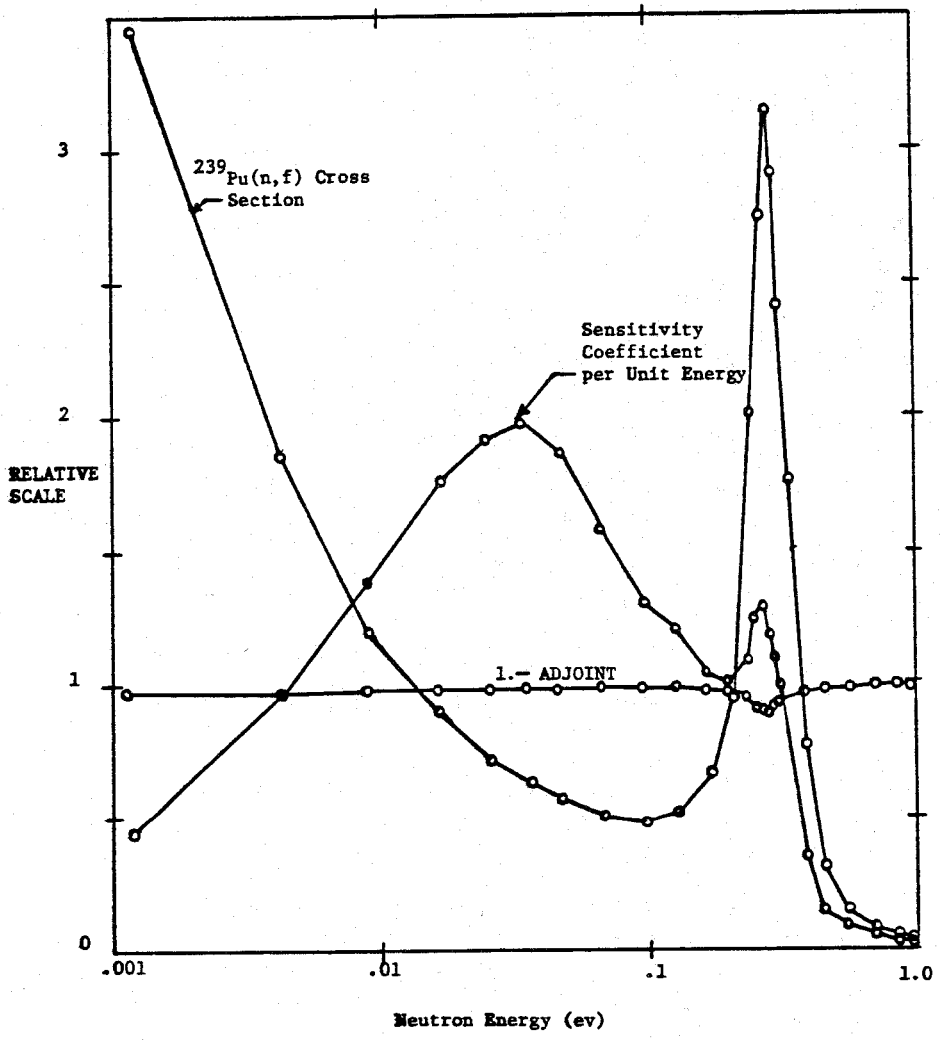

Figure 1 Detailed Pu-239 Thermal Fission Cross Section, Sensitivity Coefficient, and Adjoint for the Maine Yankee II PWR at Middle of Batch Exposure.

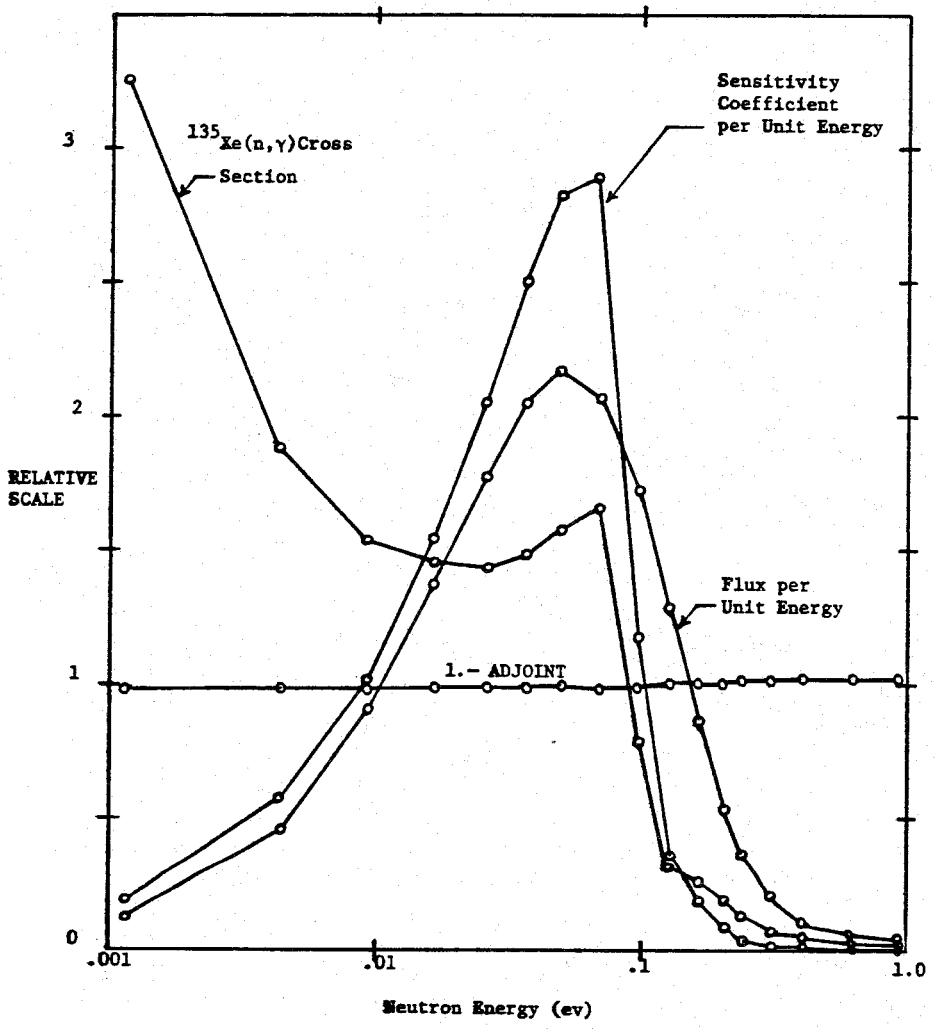

Figure 2 Detailed Xe-135 Thermal Capture Cross Section, Sensitivity Coefficient, Adjoint, and Flux for the Montague BWR at Middle of Batch Exposure.

to ^{235}U is reduced (again, it no longer is the only fuel), and sensitivity to plutonium data is enhanced, particularly for ^{241}Pu. Sensitivities for fertile materials still are small, including both ^{238}U and ^{240}Pu. Sensitivities can differ considerably depending on whether criticality is determined by enrichment of the uranium oxide fuel (the reference assumption) or by plutonium content in the mixed oxide fuel.

SUMMARY

Procedures have been developed and implemented which permit relating uncertainties in nuclear data to implications for nuclear fuel cycle parameters and cost. These procedures have been applied to a number of fuel cycle options. The importance of considering the full fuel cycle, as opposed to integral parameters at startup or in a critical assembly, has been shown. Particularly notable are the major sensitivities of thermal and resonance data for fissile isotopes and to a lesser extent for ^{238}U, ^{232}Th, fission products, and hydrogen. Also of note is the enhanced importance of certain data (e.g. for plutonium) because of influence on the end-of-cycle conditions that determine initial fuel loadings. These methods and results should prove useful in setting priorities for experimental and analytical efforts aimed at the reduction of uncertainties in basic nuclear data.

REFERENCES

1. WRENDA 74, "World Request List for Nuclear Data Measurements: Fission Reactor Programmes," International Atomic Energy report INDC (SEC)-38/U (1974).
2. S. Ramchandran, "Impact of the New LASL Delayed Neutron Data on FTR Design," Proc. Nat. Topical Meeting on New Developments in Reactor Physics and Shielding, Kiamesha Lake, New York, CONF-720901, p. 660.
3. C. G. Poncelet, O. Ozer and D. R. Harris, "Proprietary, Standard, and Government-Supported Nuclear Data Bases," Los Alamos Scientific Laboratory Report LA-6023-MS (1975).
4. V.O. Uotinen, J. D. Robertson, and J. S. Tulenko, "The Light Water Reactor Industry - Nuclear Data Needs," in Nuclear Cross Sections and Technology, Vol. I, R. A. Schrack and C. D. Bowman, Eds., NBS-SP-495, U. S. Government Printing Office, Washington, D. C., 1975, p. 7.
5. P. Greebler, B. A. Hutchins, and R. B. Linford, "Sensitivity of Fast-Reactor Economics to Uncertainties in Nuclear Data," Nucl. Applic., 4, 297 (1968).
6. P. Greeber, B. A. Hutchins, and C. L. Cowan, "Implications Nuclear Data Uncertainties to Reactor Design," International Atomic Energy Agency report IAEA-CN-26/102, (1970).

7. D. R. Harris and M. Becker, "Nonlinear Perturbation Technique for the Nuclear Fuel Cycle," Trans. Am. Nucl. Soc. 23, 534 (1976).
8. M. Danchak, W. R. Moyer and M. Becker, "The Rensselaer Interactive Graphics Analysis System," Trans.Am.Nucl.Soc. 18, 159 (1974).
9. M. Becker, D. R. Harris, J. Parillo, A. Parvez, and J. M. Ryskamp, "Fuel Cycle Sensitivity Analysis System for Light-Water Reactors," Trans.Am.Nucl.Soc. 24, 216 (1976).
10. R. F. Barry, "LEOPARD-A Spectrum Dependent Non-Spatial Depletion Code for the IBM-7094," Westinghouse Electric Corporation Report, WCAP-3269 (Sept. 1963).
11. C. F. Poncelet, "LASER, A Depletion Program for Lattice Calculations Based on MUFT and THERMOS," VWCAP-6073 (1966).
12. A. Ahlin and M. Edenius, "The Collision Probability Module EPRI-CPM," Studsvik AB Atomenergi Sweden report (1975).
13. T. R. England, W. B. Wilson and M. G. Stamatelatos, "Fission Product Data for Thermal Reactors, Part I, A Data Set for EPRI-CINDER Using ENDF/B-IV," EPRI NP-356 (1976).
14. P. F. Rose and T. W. Burrows, "ENDF/B Fission Product Decay Data," BNL-NCS-50545 (1976).
15. G. G. Joanou and J. S. Dudek, "GAM-II-a B_3 Code for the Calculation of Fast Neutron Spectra and Associated Multigroup Constants," Gulf General Atomics Report GA-4265 (1963).
16. W. R. Cadwell, "PDQ-7 Reference Manual," Westinghouse Electric Corporation Report WAPD-TM-678 (1967).
17. A. Parvez, D. R. Harris and M. Becker, "Interactive Graphics Investigation of Relationships of Detailed Epithermal Data to Nuclear Fuel Cycle Cost," Trans.Am.Nucl.Soc. 27, 897 (1977).
18. J. M. Ryskamp, D. R. Harris and M. Becker, "Sensitivity of Light-Water Reactor Parameters to Uncertainties in Thermal Nuclear Data," Trans.Am.Nucl.Soc. 26, 581 (1977).
19. A. Parvez, M. Becker, D. Boguslawski, D. R. Harris and J. M. Ryskamp, "Fuel Cycle Cost Sensitivity Analysis for Boiling and Pressurized Water Reactors," Trans.Am.Nucl.Soc. 27, 468 (1977).
20. "Interim Design Report 17x17 Subassemblies," Westinghouse Electric Corporation, 1973.
21. "Preliminary Safety Analysis Report, Montague Nuclear Power Station Units 1 and 2," 1974.
22. M. Becker, D. R. Harris, A. Parvez, B. Quan, and J. M. Ryskamp, "Sensitivity of LWR Fuel Cycle Costs to Uncertainties in Nuclear Data," Proc. Topical Meeting on Advances in Reactor Physics, Gatlinburg, Tenn., April 10-12, 1978.
23. A. Parvez, M. Becker, D. R. Harris, B. Quan, "Fuel Cycle Cost Sensitivity Analysis for LWR's Utilizing Thorium," Trans.Am. Nucl. Soc., Vol. 28, in press.
24. R. A. Matzie, J. R. Rec, "Practical Considerations in the Use of a Thorium Cycle in PWRs," Trans.Am.Nucl.Soc. 24, 220 (1976).

ACKNOWLEDGMENT

This work was sponsored by the Electric Power Research Institute under Contract RP-975-4. The guidance of Dr. Odelli Ozer, EPRI Project Manager, is appreciated.

Section 15

TEMPERATURE EFFECTS IN THERMAL REACTOR ANALYSIS

Temperature Effects in Thermal Reactor Analysis

M Edenius *)
Oskarshamnsverkets Kraftgrupp AB (OKG), Stockholm, Sweden

INTRODUCTION

One important quantity in determining the operating characteristics and safety of nuclear reactors is the temperature coefficient of reactivity. The isothermal temperature coefficient in Light Water Reactors varies considerably with the design, the moderator temperature and the boron concentration in the moderator etc. Typical values for a fresh BWR core is -5 pcm/°C (1 pcm = 10^{-5}) at 200C and -25 pcm/°C at 280°C. Typical values for a PWR are in the range 0 to -50 pcm/°C.

Much effort has been devoted to the development of proper methods for the calculation of temperature coefficients. Despite this, the methods in current use to calculate the temperature dependence of reactivity in light water reactors are not altogether successful. The calculated temperature coefficient is usually 2-4 pcm/°C too negative compared to the measured value. The literature lacks information about clean (simple, well-defined) and precise high temperature experiments. The extensive series of experiments that have been performed in the high temperature critical facility KRITZ at Studsvik have, however, provided measured data to compare with calculated ones.[1]

Detailed analyses of the KRITZ experiments and comparisons between theoretical results and experimental information have been carried out. The influence of approximations in the theoretical methods and uncertainties in nuclear data on the temperature coefficient have been investigated. The present paper summarizes the work, part of which has been described in more detail in a separate report.[2]

COMPARISON WITH KRITZ EXPERIMENTS

The KRITZ facility has been used for studying BWR and PWR lattices as well as uniform pin cell lattices over a temperature range from 20°C to 245°C (68°F - 473°F). Both UO_2 and mixed PuO_2-UO_2 (MO_2) fuel have been used and the enrichment ranged from 1.2% to above 3%. The PuO_2 content in MO_2 fuel varied between 1.5% and 6%.

---

*) The work presented here was carried out by the author while employed by AB Atomenergi, Studsvik, Sweden.

The experiments have been used for benchmarking of EPRI-CPM and CASMO. [3] This benchmarking as well as experience from power reactor calculations show that there is a difference in the predicted reactivity level for cold and hot lattices. The discrepancy exists for all types of lattices which have been investigated. We have therefore chosen to study the simplest geometries, i.e. the uniform pin cell lattices, in more detail. These experiments are the most appropriate ones for the purpose of revealing fundamental discrepancies between theory and experiment in determining the temperature effect.

The cell calculations referred to in this paper were carried out with the Studsvik code CASMO using a 69 group library based on the UK Nuclear Data Library (UKNDL), when not otherwise stated. Comparisons have been made with ENDF/B-III data. The core calculations necessary to obtain the reactivity values were performed with the two-dimensional (x, y) diffusion theory code DIXY. In most cases CASMO generated cross sections in five energy groups were used for the core calculations. The axial leakage was accounted for by using the measured axial buckling.

Calculated k_{eff}-values versus temperature are plotted in fig.1 for some pin cell lattices with UO_2 fuel enriched to 1.35% and 1.9% and for mixed oxide fuel containing 1.5% PuO_2 in depleted UO_2. It is seen that the calculated reactivity always is lower at high temperature than at room temperature. The difference is 0.1-0.7% corresponding to 0.4 - 3.7 pcm/°C ($0.2 \cdot 10^{-5}$ - $2.1 \cdot 10^{-5}$/°F). The deviation between measured and calculated reactivity coefficients is the same at low and high temperatures.

Similar analyses of BWR and PWR lattices studied in KRITZ give theoretical temperature coefficients which are 2-4 pcm/°C ($1.1 \cdot 10^{-5}$ - $2.2 \cdot 10^{-5}$ /°F) more negative than the experimental values.

In the experiments criticality is established with high accuracy (within a few pcm). However, in the theoretical analysis the uncertainty in the measured axial buckling, in the boron concentration etc must be considered. These uncertainties could typically correspond to 50 to 100 pcm in k. This means that discrepancies between calculated and measured temperature coefficients of less than 0.5 pcm/°C are generally not significant.

THE COMPONENTS OF THE TEMPERATURE COEFFICIENT

Many phenomena in a reactor system contribute to the temperature coefficient of reactivity. Lack of agreement between theoretical and experimental values of the isothermal temperature coefficient, dk/dT, may therefore be due to errors in the calculation of one or several of the different components. Furthermore, agreement obtained in a limited study does not necessarily mean that the calculations are correct in all respects. Compensating errors may appear and care must be exercised in drawing conclusions.

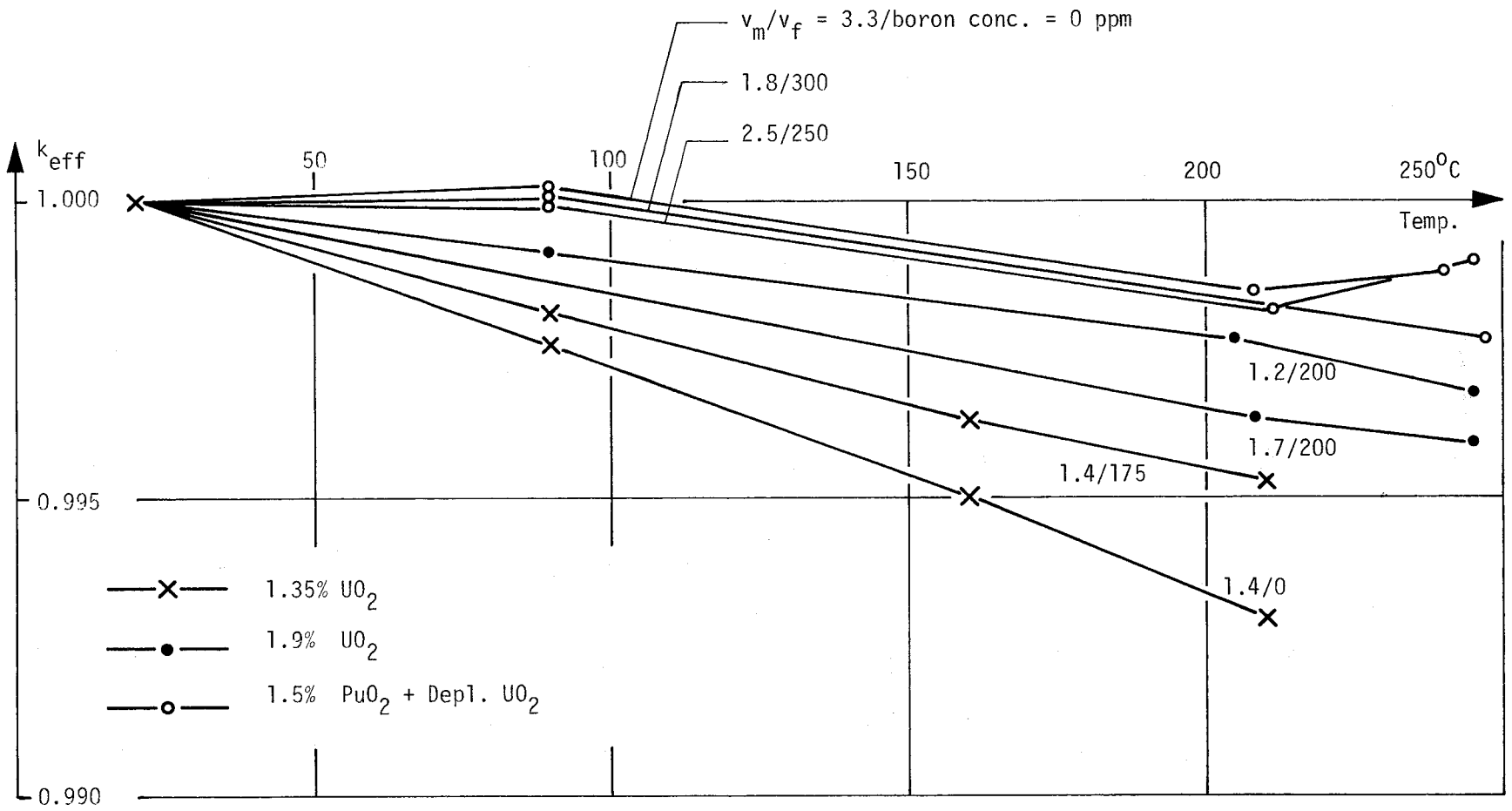

Fig. 1 Calculated k_{eff} versus temperature (normalized to unity at 20°C).

dk/dT may be written

$$\frac{dk(T_f, T_c, T_m, \theta)}{dT} = \frac{\partial k}{\partial T_f} + \frac{\partial k}{\partial T_c} + \frac{\partial k}{\partial T_m} + \frac{\partial k}{\partial \theta}\frac{d\theta}{dT} \qquad (1)$$

T_f, T_c and T_m = fuel, canning and moderator temperature, resp.
θ = moderator density

Table 1 shows calculated partial temperature coefficients for some lattices. Results are given for the reactivity temperature coefficient of the critical lattice at 55°C and 185°C. At these temperatures experimental values of the total temperature coefficients are available from the KRITZ measurements. The term $\partial k/\partial T_c$ can be neglected compared to the other terms.

The fuel temperature coefficient is in all lattices less negative at 185°C than at 55°C. This should be expected due to the approximate $T^{-1/2}$ dependence of the Doppler coefficient. The contribution to $\partial k/\partial T_f$ from thermal scattering in UO_2 is about one tenth of the Doppler coefficient.

$\partial k/\partial T_m$ is negative in the UO_2 lattices and positive in the MO_2 lattices. The different signs of $\partial k/\partial T_m$ for the two types of fuel are due to the 0.3 eV resonance in Pu-239 and the non-$1/v$ dependence of the thermal U-235 cross section. Thus, an analysis of both UO_2 and MO_2 systems constitutes a severe test of the ability to predict the thermal neutron spectrum. An error in the calculated temperature dependence of the spectrum can be expected to give different errors in the predicted temperature coefficient for UO_2 and MO_2 lattices. Our analysis of the KRITZ experiments has, however, given approximately the same discrepancy between calculated and measured temperature coefficients in both UO_2 and MO_2 systems. This indicates that the change of the thermal neutron spectrum with temperature has been correctly calculated.

$\frac{\partial k}{\partial \theta}\frac{d\theta}{dT}$ is more negative at high temperatures than at low ones due to the variation of $d\theta/dT$ with temperature. The discrepancy between calculated and measured temperature coefficients is, however, about the same at low and high temperatures. This indicates that the calculated "density coefficient", $\frac{\partial k}{\partial \theta}$, is correct.

APPROXIMATIONS IN THE CALCULATIONAL METHODS

In reactor physics calculations a number of approximations are done. We have tried to verify the adequacy of all approximations, which could be suspected to influence the calculated temperature coefficients.

Table 1. Calculated partial temperature coefficients at 55°C and 185°C for some KRITZ lattices

Fuel	V_m/V_f	Boron conc. (ppm)	$\partial k/\partial T_f$		$\partial k/\partial T_m$		$\partial k/\partial \theta \cdot d\theta/dT$		dk/dT	
			55°C	185°C	55°C	185°C	55°C	185°C	55°C	185°C
UO_2,1.35%	1.4	0	-4.1	-3.6	-5.1	-4.7	-10.6	-29.0	-19.8	-37.3
	1.4	175	-4.1	-3.7	-4.3	-4.0	- 6.9	-20.2	-15.3	-27.9
UO_2,1.9%	1.2	200	-4.8	-4.2	-3.7	-3.5	-13.2	-34.3	-21.7	-42.0
	1.7	200	-3.8	-3.4	-4.1	-4.1	-10.9	-30.3	-18.9	-37.8
MO_2	1.8	300	-4.1	-3.7	+2.5	+3.8	-13.7	-39.5	-15.3	-39.4
	2.5	250	-3.3	-3.0	+5.1	+6.7	-11.4	-36.5	- 9.6	-32.8
	3.3	0	-2.7	-2.5	+4.1	+6.2	-14.4	-44.3	-13.0	-40.5

For example, calculations using various number of energy groups and spatial regions verified that the choice used in our analyses is fine enough to produce accurate results. Comparisons between calculations using isotropic (transport corrected) and anisotropic (P1-) scattering showed that calculated k -values and dk / dT did agree very well for the two types of calculations. The cylindricalization of the square pin cells in our cell calculations was also found to give negligibly small errors. Inadequacies in the core calculations could have given rise to an error in the absolute value of k, but the effect in the temperature dependence would have been small in the clean KRITZ lattices.

Summing up we have not found any single known approximation in the calculational methods which is likely to cause an error in the predicted temperature coefficients of the magnitude quoted for the KRITZ analysis.

INFLUENCE OF NUCLEAR DATA ON THE CALCULATED TEMPERATURE COEFFICIENT

Comparison of temperature coefficients calculated by use of ENDF/B and UKNDL data

The CASMO calculations referred to above were made with the cross section library traditionally used in Sweden. This cross section set was originally based on a version of UKNDL that is now partly out of date. To check the dependence of the results on the data library, several lattices studied in KRITZ were re-calculated using a data library generated from ENDF/B-III. The levels of the calculated k_∞ and M^2 differ, but partial and total temperature coefficients calculated with the two different libraries are equal.

The two libraries are in principle entirely independent as most of the basic nuclear data and the processing codes used for generating group cross sections differ. Scattering matrices for water are based on the Nelkin model in the UKNDL-library and on the Haywood model in the ENDF/B-library.

The Doppler coefficient

Calculated resonance integrals and their temperature dependence were compared with experimental integrals and Doppler coefficients. [4] The calculated Doppler coefficients were found to be within the experimental uncertainty which is about 10%. The Doppler coefficient is 3-4 pcm/^{o}C at temperatures below 250^{o}C, so the uncertainty in the fuel temperature coefficient is expected to be less than 0.4 pcm/^{o}C.

Thermal scattering data

Moderator temperature coefficients calculated using the Nelkin, the Effective width and the Haywood model are compared in table 2. Considering that three entirely different models have been used, the agreement in calculated coefficients is very good.

Table 2 also shows calculated reaction rate ratios in the fuel. The reaction rates obtained with the Nelkin and the Effective width model are equal, whereas the Haywood model gives a harder spectrum at both low and high temperature.

Calculations using the UO_2 scattering model in ENDF/B-III have been compared with calculations using the free gas model for both uranium and oxygen in UO_2. Although the scattering cross sections differ considerably in the two cases, the influence on calculated reactivities and coefficients is negligible. This is due to the small importance of the thermal scattering in the fuel in light water reactors.

Thermal data for U-235 and U-238

The temperature coefficient is sensitive to the energy dependence of the fuel cross sections in the thermal energy region. Checks were therefore made to investigare the effect of a given change in the energy dependence for certain U-235 and U-238 cross sections on the calculated temperature coefficients.

First a change in $\alpha(E)$ (capture-to-fission ratio) for U-235 within the experimental error band was made at thermal energies. It was found that the uncertainty in $\alpha(E)$ corresponded to an uncertainty of about 1 pcm/^{o}C in the predicted temperature coefficient.

Secondly the effect of a variation in the U-238 capture cross section was studied. This cross section is generally assumed to obey the 1/v-law at thermal energies. When deriving the thermal capture cross section it is necessary to take into account the contribution from one or several bound levels. For most choices of negative energy resonances the contribution to the capture cross section will be proportional to $E^{-1/2}$. It is, however, possible to choose a resonance level around zero energy. If such a resonance exists, its contribution to the thermal capture cross section will be such that the gradient of σ_c versus energy will be more negative than for a 1/v-cross section.

In order to investigare how a non-1/v cross section affects the predicted temperature coefficient a change of the capture cross section below 0.3 eV was tested. The modification was made so that the reaction rate in a 20^{o}C Maxwellian spectrum was preserved. Modified and unmodified cross sections are shown in fig. 2 and results from the calculations for some KRITZ lattices with the modified data are collected in table 3. The modification is quite modest but the effect on the calculated temperature coefficient is significant. It is obvious that for all these lattices a close agreement between theory and experiments can be obtained by

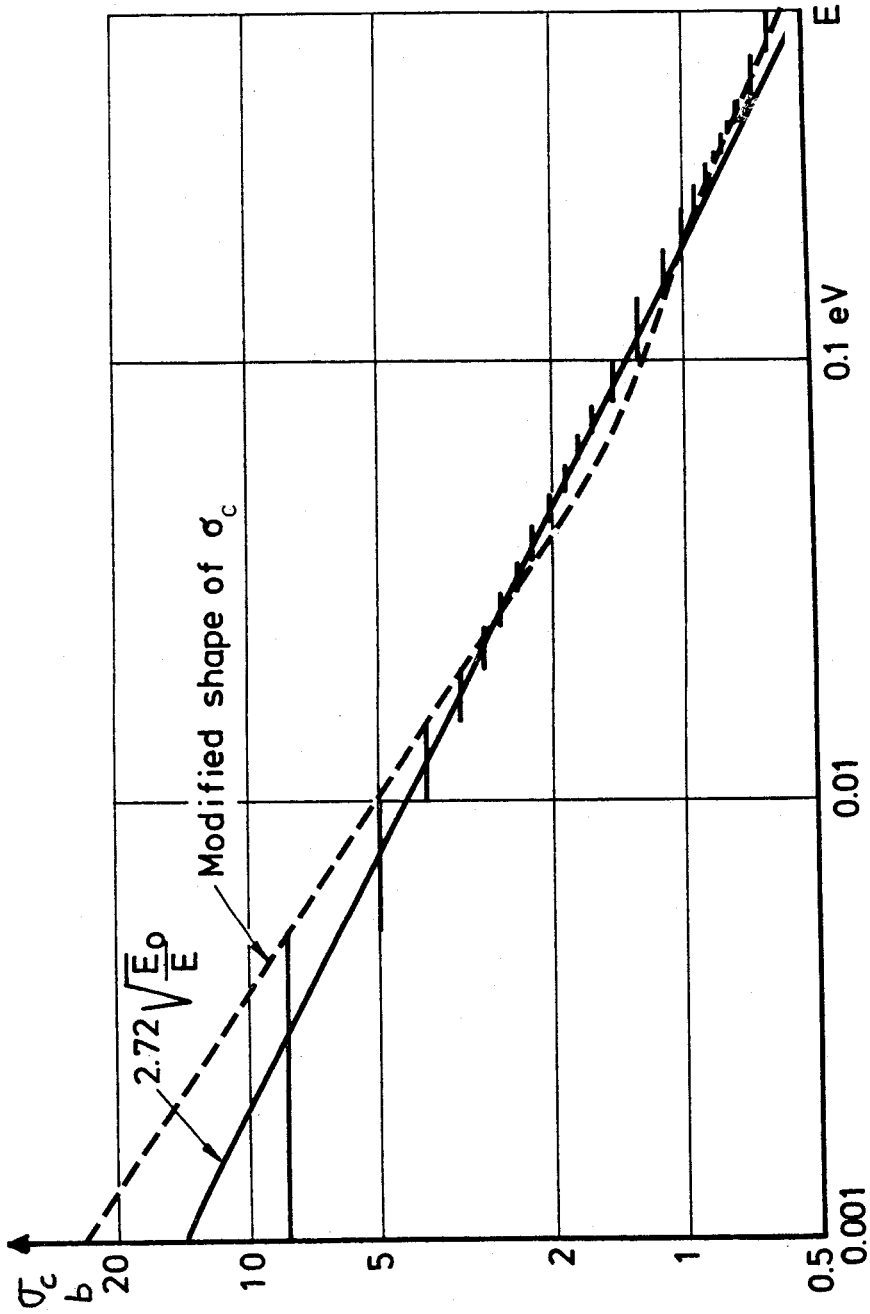

Fig. 2 σ_c for U-238

Table 2. Calculated moderator temperature coefficients and reaction rate ratios (fission) using different scattering models for water

Fuel	V_m/V_f	Boron conc. (ppm)	Scattering model	$\partial k/\partial T_m$ (pcm/°C)		(U-235/1/v)		(Pu-239/1/v)	
				55°C	185°C	20°C	210°C	20°C	210°C
UO_2,1.35%	1.4	175	Nelkin	-4.2	-3.9	.993	.968	1.288	1.498
			Eff.width	-4.5	-4.1	.994	.968	1.286	1.500
			Haywood	-4.1	-3.8	.990	.966	1.307	1.514
UO_2,1.9%	1.7	200	Nelkin	-4.0	-3.9	.993	.969	1.305	1.515
			Eff.width	-4.6	-4.3	.994	.969	1.304	1.517
			Haywood	-3.9	-3.9	.990	.967	1.326	1.531
MO_2	2.5	250	Nelkin	+5.0	+6.3	.997	.973	1.185	1.357
			Eff.width	+5.5	+6.4	.997	.974	1.184	1.357
			Haywood	+4.7	+6.2	.994	.971	1.197	1.365

Table 3. Change in dk/dT due to modified thermal σ_c for U-238

Fuel	V_m/V_f	Boron conc. (ppm)	dk/dT (pcm/°C)		
			Original discrepancy theory-exp.	Change due to modified thermal σ_c for U-238	Discrepancy after modification of σ_c for U-238
UO_2, 1.35%	1.4	0	-4.4	+3.1	-1.3
	1.4	175	-3.3	+3.1	-0.2
UO_2, 1.9%	1.2	200	-1.4	+2.1	+0.7
	1.7	200	-1.8	+2.3	+0.5
MO_2	1.8	300	-0.4	+1.3	+0.9
	2.5	250	-1.0	+1.4	+0.4
	3.3	0	-0.6	+1.5	+0.9

modifying the shape of the thermal U-238 capture cross section.

TEMPERATURE COEFFICIENTS IN POWER REACTORS

Among the different partial temperature coefficients it is only the Doppler coefficient which has any significant influence on the operating characteristics of a BWR. The moderator temperature coefficient is important mainly for determining the reactivity gap between the hot and cold reactor. The bias in the predicted temperature coefficient is therefore easily handled in the core analysis by accepting different k_{eff}-levels for cold and hot cores. Results from the Swedish BWRs show that the calculated k_{eff} for a critical reactor is about 1% higher at room temperature than at operating conditions.

In a PWR the moderator temperature coefficient is of great importance also for the operating characteristics. Furthermore, the Doppler coefficient is more important for a PWR than for a BWR. Although the KRITZ experiments have revealed a bias in the calculated temperature coefficient, both the Doppler and the moderator temperature coefficient are predicted accurately enough not to create any problem in static PWR analysis. So once again it is a matter of normalization of k_{eff}-levels.

Transient calculations are more sensitive to the predicted coefficients. It is therefore usually necessary to correct for the known bias, which is 3-4 pcm/°C for both BWR and PWR analyses.

Based on the KRITZ analyses we may assume that the different calculated k_{eff}-levels for cold and hot cores are mainly due to the few-group cross sections used in the core calculations. There are, however, several other uncertainties which influence predicted temperature coefficients in power reactors. At operating conditions the thermal hydraulics part of the calculations is of great importance.

For example, the calculated fuel temperature versus power is sensitive to which assumptions are made for the swelling of the fuel and cracking within the pellets. This uncertainty is of the same size or larger than the uncertainty in the predicted Doppler coefficient. In BWR calculations with three-dimensional nodal codes the representation of control rods and the choice of albedo values at the core boundary introduce additional uncertainties. Both the control rod reactivity worth and the albedo values are temperature dependent.

There is a possibility that an error in the temperature coefficient generated by a cell code is not detected if only measured data from power reactors are available for benchmarking.

SUMMARY

An extensive program of high temperature measurements in KRITZ have been analysed. Results for uniform pin cell lattices as well as BWR and PWR assemblies show that the theoretical methods are able to predict the reactivity with reasonable accuracy for a wide

range of different lattices with different fuel. It was, however, observed that the predicted k_{eff} always is lower at high temperature than at room temperature. The deviation between room temperature and 245°C is typically 0.4 - 1% in k_{eff}, corresponding to 2-4 pcm/°C ($1.1 \cdot 10^{-5}$ - $2.2 \cdot 10^{-5}$/°F).

The adequacy of approximations in the theoretical methods was verified. We did not find any approximation which is likely to cause the observed bias in predicted temperature coefficients.

A theoretical study of the partial temperature coefficients in combination with experimental information indicates that the temperature dependence of the thermal spectrum was correctly predicted. It also indicates that the inconsistency between theory and experiment is not due to effects caused by the variation of water density with temperature.

Calculations using UKNDL and ENDF/B-III data gave the same temperature coefficients. Further, temperature coefficients using the Nelkin, Effective width and Haywood scattering models for water were the same. Calculated Doppler coefficients were found to be within 10% from experimental values.

The influence of uncertainties in the thermal U-235 and U-238 cross sections on the calculated temperature coefficients was investigated. Uncertainties in U-235 data may cause an error of about 1 pcm/°C. It was found that good agreement between measured and calculated temperature coefficients can be obtained if the thermal U-238 capture cross section is modified to a non-1/v-shape, which could be explained by a resonance at a level very close to zero energy. The modification of the thermal U-238 cross section is an interesting hypothesis since it is the simplest way to eliminate the observed discrepancies. However, it cannot be excluded that the observed discrepancy is a result of several small contributions from inadequate theoretical models and data.

The observed bias in predicted temperature coefficients does not cause any problems in reactor physics calculations for BWRs and PWRs. In certain applications it should, however, be corrected for.

ACKNOWLEDGEMENT

Extensive contributions to the analyses of the KRITZ experiments have been obtained from E Hellstrand, R Persson and other colleagues at AB Atomenergi.

REFERENCES

1. R Persson, E Blomsjö and M Edenius, High Temperature Critical Experiments with H_2O-moderated Fuel Assemblies in KRITZ, Technical meeting No. 2/11, NUCLEX 72.
2. M Edenius, Studies of the Reactivity Temperature Coefficient in Light Water Reactors, AE-RF-76-3160, AB Atomenergi, 1976.

3. Å Ahlin and M Edenius, Trans. Am. Nucl. Soc. 26, 604 (1977).

4. M Edenius, in Seminar on U-238 Resonance Capture, S Pearlstein, Editor, p 87, BNL-NCS-50451, 1975.

Section 16

FEEDBACK OF BWR BENCHMARKS TO CROSS SECTION DATA

Section 16

FEEDBACK OF BWR BENCHMARKS TO CROSS SECTION DATA

S. C. Bhatt, R. L. Crowther, C. M. Kang, R. A. Wolters, and J. E. Wood
(General Electric Company, San Jose, California 95125)

This paper was not submitted for publication.

Section 17

REQUIREMENTS FOR THE PHYSICS ANALYSIS OF PWR FUEL ASSEMBLIES

Requirements for the Physics Analysis of PWR Fuel Assemblies

A. Jonsson, J. R. Rec, U. N. Singh
Combustion Engineering, Inc.

I. INTRODUCTION

The verification of physics design procedures for PWR fuel comprises verification of basic cross section data, data processing codes, multigroup libraries and calculational methods all contributing to the final product: the prediction of reactivity levels, reactivity differences and reaction rate distributions. Each of these elements contribute to the overall uncertainty level of the final solution and to some extent, one can separate these contributions by the analysis of experimental information. Three sources of such information are commonly used in the verification process viz., integral measurements of cross-section data, critical experiments for uniform and non-uniform lattices and information from operating power plants.

This paper discusses briefly the uncertainties in basic cross-sections taken from ENDF/B-IV as derived from analyses of selected uniform lattices measured in critical experiments. Against this background, the contribution to the overall uncertainty from calculational methods is discussed for the specific application to PWR fuel designs. Methods uncertainties are quantified in terms of error levels for reactivity and cross-sections using a detailed physics model for the calculation of PWR fuel. The accuracy of this model is verified in comparisons with critical experiments involving non-uniform lattices.

II. SOME METHODS RELATED UNCERTAINTIES FOR THE ANALYSIS OF PWR FUEL GEOMETRIES

In the analysis of thermal benchmarks approximating the PWR fuel assembly geometry (as well as in design analyses), several physics approximations are usually made. The effects of these approximations may equal, and in some instances overshadow, uncertainties in basic cross-sections so that conclusions concerning the quality of the latter may not be legitimate unless the physics model recognizes all relevant circumstances.

Methods related uncertainties for PWR fuel include uncertainties which are present also in uniform lattices, for example:
-The choice of resonance cross-section model.
-The choice of energy group structure.
-Details of method accounting for the influence of leakage.
-Anisotropic scattering.

-Choice of Transport Calculation, for example, S_n, integral transport theory, etc.
-Representation of geometry: cylindricized cell.
-Choice of spatial mesh.
These and other methods approximations are fairly well understood. They are possible to quantify individually. The literature contains numerous studies that do this. Additional work is desirable, however, to systematically compare the uncertainties with corresponding uncertainties for basic cross-section data so that meaningful conclusions can be drawn from simple thermal benchmark lattices.

Less well known are the additional uncertainties introduced by the non-uniform nature of the PWR fuel geometry. These uncertainties are important, however, since there is a lack of high quality uniform lattice thermal benchmarks and one does therefore rely to a great extent also on thermal benchmark measurements for non-uniform lattices in the process of verifying both basic cross-section data and methods. This section lists some of the physics approximations that are commonly made. They are quantified in terms of their effect on reactivity and in terms of their effect on calculated few-group cross-sections. The latter effects may be interpreted as uncertainties and compared to uncertainties in basic cross-section data. This is a possible path for comparing methods and cross-section uncertainties on a systematic basis. In addition,a discussion follows on the requirements posed by the use of diffusion theory in design and in benchmark analyses.

II.1 Spectrum Interactions in the Thermal Energy Region

Three structural components can interact in a PWR fuel assembly viz., fuel, absorbers and vacant positions (waterholes). Usually these interactions are accounted for by repeated 1-D calculations where the component in question is surrounded by a homogenized cylindrical environment. For example, a burnable absorber may be modelled explicitly with its associated water and then surrounded by a volume weighted mixture of fuel, clad and water. (Flux-volume weighting would be preferred here but is more difficult to do since the weighting is energy dependent.) As a result, the thermal spectrum is normally calculated to be too hard compared to a direct calculation for the correct geometry. An approximation of this kind results, typically, in an underestimate of the average thermal cross-section (0.0-0.625eV) for the absorbing material by 3-4%. In a critical experiment or in a design situation with about 5000 - 8000 pcm reactivity (1 pcm = $1 \cdot 10^{-5}$), tied in absorbers, the overall effect on reactivity would be seen as an uncertainty of 0.15-0.30%k which is outside the range of accuracy generally sought.

Similar effects are observed for waterholes (locations for control rods and instruments) which generally have a softer thermal spectrum than predicted by simple models. Since the water

may be borated to a high concentration, the reactivity effect of a typical 3% error in the B^{10} cross-section will be noticeable. For example, 0.11%k in a fully borated critical experiment modelling fuel with large waterholes (occupying 2x2 fuel locations each) or 0.09%k for a lattice having about 20 single waterholes per assembly.

The presence of absorbers and waterholes has an effect also on the neutron energy spectrum in the fuel which is often determined from infinite lattice calculations kept critical by a combination of soluble boron concentration and leakage. Some codes model fuel located near lattice perturbations by one-dimensional calculations where the environment to the fuel is suitably weighted to account for the various structural elements. Simplifications of this character are only partially successful in predicting the details of the softening of the thermal spectrum in the vicinity of waterholes. The opposite effect occurs around absorbers which are particularly difficult to incorporate as constituents of the fuel environment in 1-D models. In general, the net consequences on reactivity from these modelling uncertainties are ameliorated, Fig. 1, because the spectrum variations act similarly on both production and absorption cross-sections so that the two reactivity errors tend to cancel. The spectrum variations are quite significant, i.e., -4 to -5% in terms of their effect on a 1/v-type group averaged cross-section in the vicinity of an absorber and +3 to +4% around waterholes at operating temperatures. The effects are larger at room temperature so that some temperature dependence of this type of uncertainty may be noted. These thermal spectrum interactions die out fairly quickly so that they are less significant for locations other than nearest neighbors in the lattice. For a fuel design with 20 single waterholes, 60-70% of all fuel pins are neighbors of a waterhole, all with an average of say 3% effect on the thermal group averaged absorption cross-section. Because of counteracting movements of the flux level, this does result in less error for the total absorption rate, usually around 1/2 of that amount. This does still correspond to a quite considerable reactivity: 0.6-0.7%k. Cancelling errors of this magnitude are not desirable in analyses used for design or benchmarking of thermal data. Cancellation of errors is not always complete. Examples of this are mixed oxide fuel (where net reactivity effects as large as 0.7% cold and 0.3% hot have been observed) and depleted fuel. It should also be remembered that, although net reactivity is insensitive to thermal spectrum shifts, local reaction rate distributions are more directly affected. This is discussed in more detail below.

II.2 Interactions in the Resonance Region

In this region of the neutron energy spectrum, interactions between various components of the lattice may be classified as Dancoff correction interactions and other spectrum interactions.

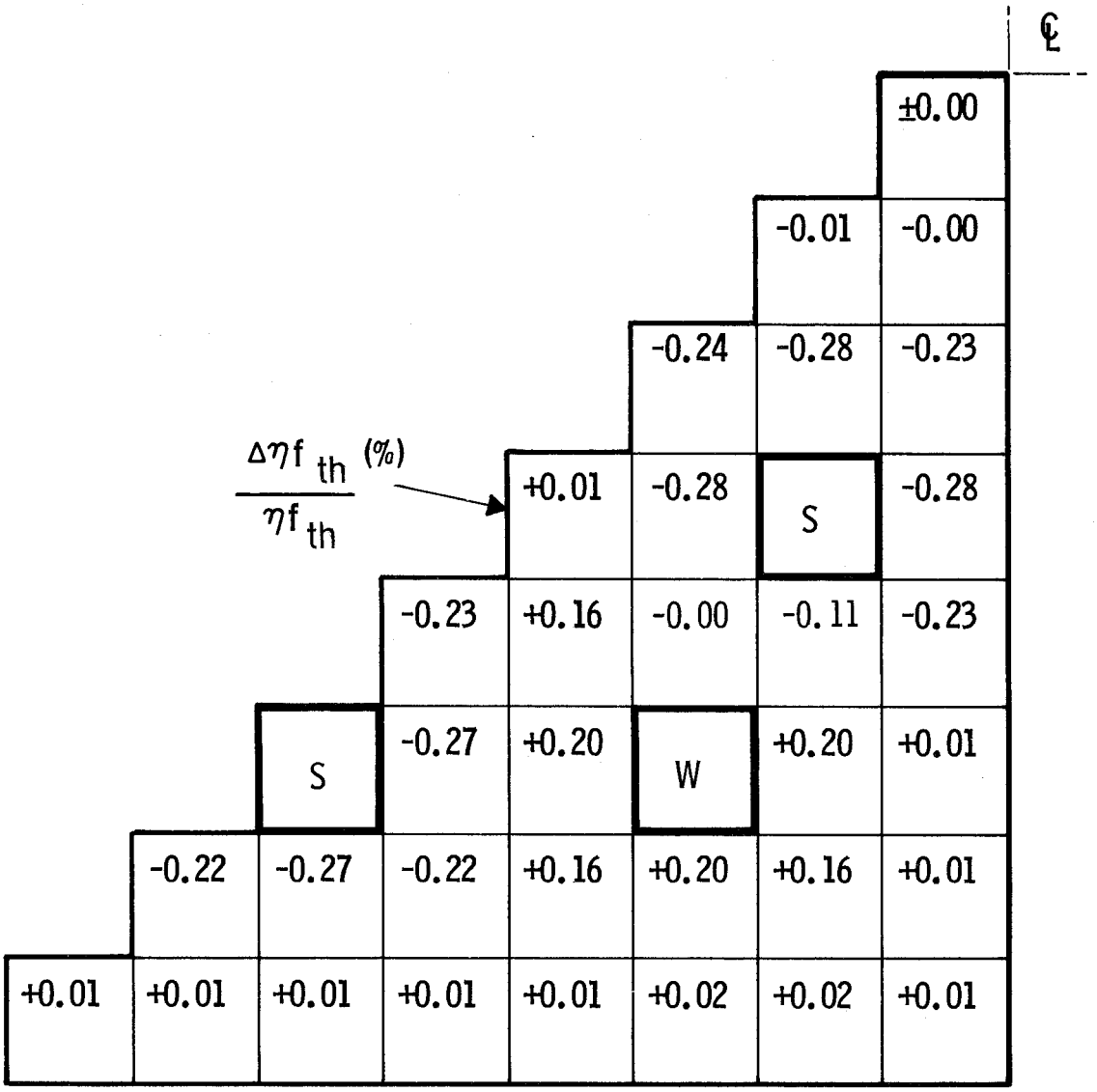

Figure 1

VARIATION OF THERMAL ηf WITHIN 1/8 OF A 16 x 16 PWR FUEL ASSEMBLY WITH SINGLE WATERHOLES AND BURNABLE ABSORBERS, (S)

TABLE 1. NON-UNIFORM LATTICES. EFFECTS OF THERMAL SPECTRUM INTERACTIONS ON REACTIVITY

Fuel Type	Temperature	Physical Effect	Effect on Reactivity
UO_2	Operating	Hardening of spectrum for fuel close to absorbers.	-0.10 to -0.15%k
UO_2	Operating	Softening of spectrum for fuel close to waterholes.	
		a) Effect due to change in σ_a	-0.65%k
		b) Effect due to change in $\nu\sigma_f$	+0.70%k
		c) Net effect	+0.05%k
UO_2	Cold condition	As above, net effect	+0.20 - 0.25%k
Mixed oxide	Operating	As above, net effect	+0.70%k
Mixed oxide	Cold condition	As above, net effect	+0.25%k
UO_2	Operating	Softening of spectrum in burnable absorber relative to simple 1-D method.	-0.15 to -0.30%k

TABLE 2. NON-UNIFORM LATTICES. EFFECTS OF EPITHERMAL SPECTRUM INTERACTIONS ON REACTIVITY

Fuel Type	Physical Effect	Effect on Reactivity[1)]
UO_2	Softening of Resonance region spectrum for fuel near waterholes.	
Without burnable absorbers.	Effect on slowing down.	+0.55%k
With burnable absorbers	Effect on slowing down.	+0.10%k
Without burnable absorbers.	Effect on resonance absorption	-0.30%k
With burnable absorbers	Effect on resonance absorption.	-0.15 to -0.20%k

1) Relative to conditions for infinite lattice.

TABLE 3. NON-UNIFORM LATTICES. EFFECT OF SPECTRUM INTERACTIONS ON FUEL CELL CROSS-SECTIONS AT INDICATED LOCATIONS

		"Asymptotic"[1] Location	Average[1] Assembly	Facing Waterhole	Facing Absorber
U-235	σ_{a4}	Ref.	---	+3.09%	-4.03%
	$\nu\sigma_{f4}$	Ref.	---	+3.12	-4.07
Pu-239	σ_{a4}	Ref.	---	-3.06	+0.07
	$\nu\sigma_{f4}$	Ref.	---	-2.49	+0.00
Pu-240	σ_{a3}	Ref.	---	-1.03	+1.70
U-238	σ_{a1}	---	Ref.	+0.17	-1.29
	σ_{r1}	---	Ref.	-0.41	-0.84
	σ_{a3}	---	Ref.	+1.85	+0.52
	σ_{a3}	Ref.	---	+2.95	+1.66
H	σ_{r1}	---	Ref.	-1.26	+0.56
	σ_{r3}	---	Ref.	+2.89	-0.63
	σ_{r3}	Ref.	---	+3.83	+0.31
	σ_{a4}	Ref.	---	+2.89	-3.74
Sol.Boron	σ_{a4}	Ref.	---	+2.89	-3.24
Oxygen	σ_{a1}	---	Ref.	+2.10	-1.50
	σ_{r1}	---	Ref.	+1.63	+1.15

1) Percentage values are relative to these reference locations.

The local variation of group averaged slowing down cross-sections would be an example of the latter while the increased value of resonance integrals around vacancies in the lattice are of the former kind. Figure 2 is a visualization of the combined effects of these two interactions.

In general, one finds an increase of group removal cross-sections for fuel cells adjacent to waterholes. These effects are typically of the order of 3.5 to 4% and are due to a shift to lower energies of the spectrum in the range 2eV to 5keV. The net reactivity effect in a PWR assembly with about 20 waterholes is around 0.5 to 0.6%k. It is always counteracted by an increase of the local value of the Dancoff factor worth typically some -0.3%k. The effects on slowing down cross-section stretch further in the lattice than do resonance self-shielding phenomena. The consequence may be larger net effects on resonance escape probability for corner pins than for pins directly facing a waterhole although the details of such variations may be sensitive to the particular models chosen for doing the spectrum calculation and for the computation of location dependent Dancoff factors. Close to absorbers, one may find that Dancoff effects dominate so that a local loss in reactivity is the net result. See Fig. 2. For fuel pins located between both a waterhole and an absorber, the combined effects of increases in Dancoff factor attributable to the two cells may be particularly large so that a large reduction is seen for the resonance escape probability. The intricacies of local variations of this type are not reproducible with simple models relying on the usage of an average spectrum and an average value for the Dancoff correction. In particular, it is difficult to accurately represent the presence of burnable absorbers. However, most models do achieve acceptable accuracy on net reactivity averaged over entire fuel assemblies.

II.3 Net Reactivity Effects of Spectrum Interactions

Interactive effects in the high energy portion (above 10kev) are generally small and do not affect reactivity or group averaged cross-sections to a great extent. (Spatial flux weighting is important, however, and is discussed below.)

Thus, the combined effects of thermal and resonance region interactions do determine the net effect on local reactivity, Fig. 3. In general, local reactivity is high near waterholes and low near absorbers.

Average (i.e., for an entire assembly or for an entire core) reactivity level uncertainties are listed in Tables 1 and 2 and uncertainties on individual cross-sections in Table 3. Although in the epithermal region, many models do achieve correct reactivity levels by successfully calculating group averaged cross-sections in the spatially averaged spectrum, we have listed typical spatial variations in Table 3. The reason is that some of these variations, in particular those in slowing down cross-

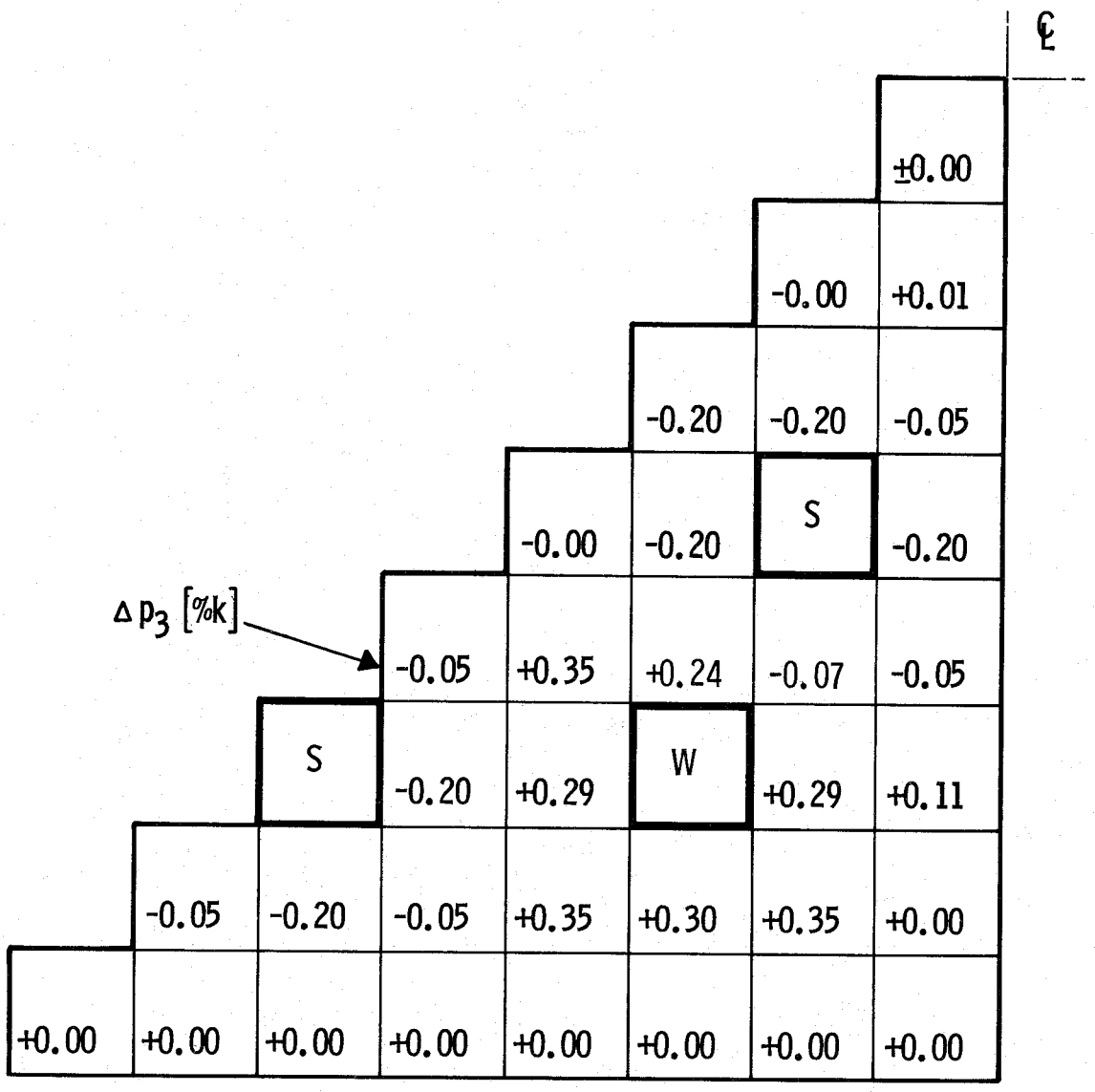

Figure 2

VARIATION OF RESONANCE ESCAPE PROBABILITY WITHIN 1/8 OF A 16 x 16 PWR FUEL ASSEMBLY WITH SINGLE WATERHOLES AND BURNABLE ABSORBERS

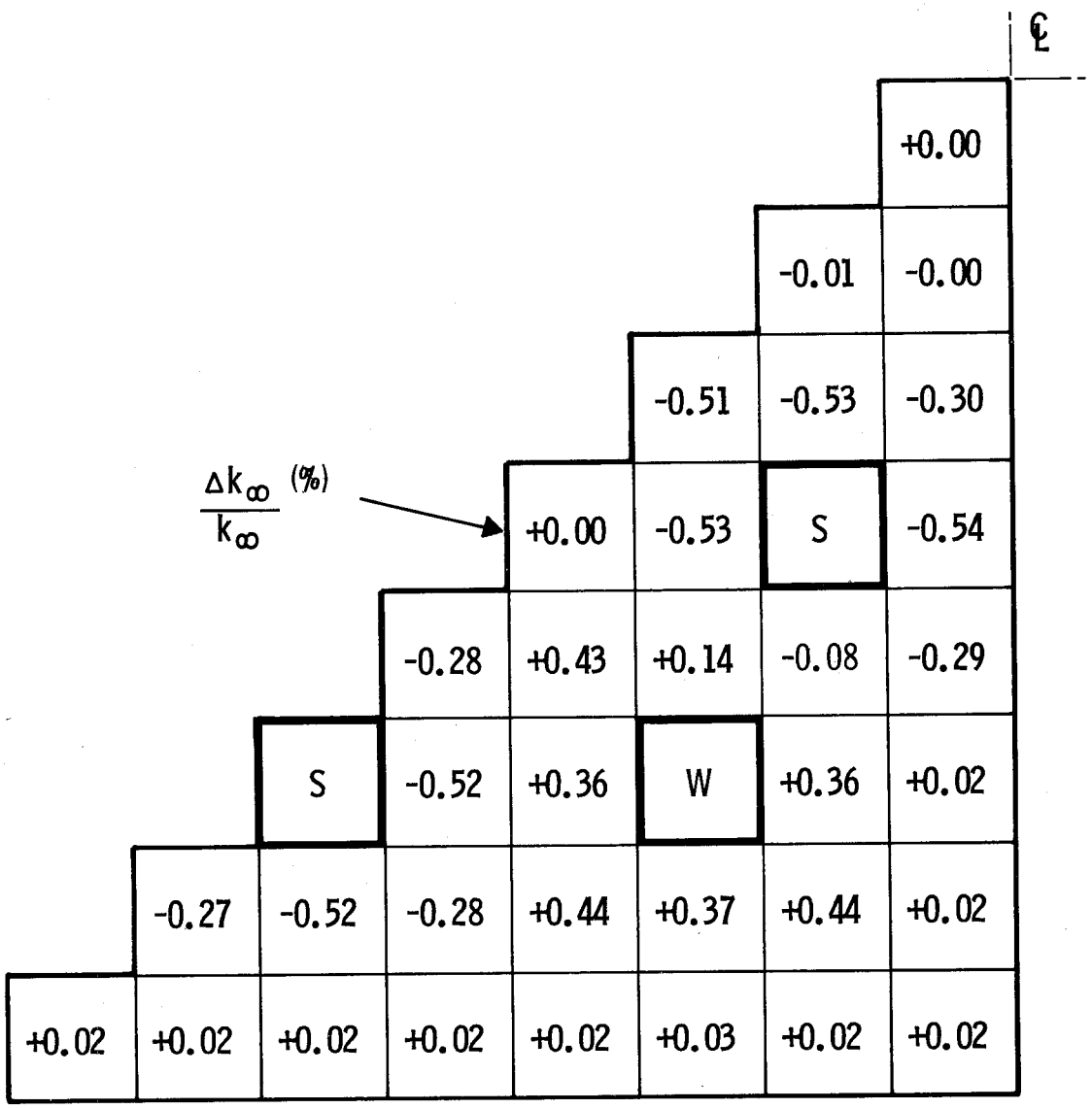

Figure 3

VARIATION OF LOCAL k_∞ WITHIN 1/8 OF A 16 x 16 PWR FUEL ASSEMBLY WITH SINGLE WATERHOLES AND BURNABLE ABSORBERS

sections do have an effect on local reaction rate distributions both epithermally and thermally. The prediction of such distributions is an important objective in design and in the simulation of benchmark experiments used for verification of design methods. Thus, the local variations of 1-4% observed in Table 3 for group 3 (5.5keV to 0.625eV) slowing down cross-sections are indicative of significant model uncertainties. The values in the table are typical for operating temperatures in a PWR. For cold, critical experiments, these variations may be stronger. For example, the group averaged slowing down cross-section inside waterholes may be as much as 15% higher than in the average spectrum. Such uncertainties do significantly exceed current uncertainties in basic data, i.e., chiefly in the ENDF/B-IV value of 20.45 barns for the hydrogen elastic cross-section in this energy region.

II.4 Cross Section Requirements Dictated by the Use of Diffusion Theory

Thermal reactor benchmark analyses are often, and design analyses for power reactor cores are always done using diffusion theory as the primary means of predicting reactivity and core-side reaction rate distributions. These analyses are performed with the few-group spectrum averaged cross-section data for which some methods related uncertainties were quantified above. The two elements of the analysis viz., the diffusion theory and the process for generating few-group data are not independent however. Each supplies a component to the overall uncertainty. One should therefore be aware of the possibility that the contribution of the former may be significant and possibly be mistaken for uncertainties in basic cross-section data. So that the diffusion approximation may yield accurate results, the few-group data must be defined and calculated to fit the particular form of diffusion theory used, i.e., to the finite difference formulation employed and the mesh density chosen. This is achieved by comparing the diffusion theory results with results from higher order approximations for some particular situation approximating the end use. Few group cross sections for non-diffusion regions of the lattice such as absorbers are thus forced to duplicate higher order results for that particular situation.

This element of the cross-section generating process is particularly important since design analyses do always involve diffusion theory methods and hence these are an integral part of the analysis system to be benchmarked. A few examples of uncertainties in the end results (reactivity and reaction rates) will be discussed in the next paragraphs.

Reaction rates for heavy absorbers such as burnable absorbers and control rods are not accurately predicted by unmodified diffusion theory constants. Absorption and slowing down cross-sections are, therefore, routinely adjusted, as discussed above,

to compensate for the overpredicted flux level in this type of region. In regions of the geometry where flux peaking occurs, adjustments in the opposite direction are required. Although this method is effective in dealing with the reactivity contribution of the non-diffusion region, there are certain side effects which are of interest, particularly when conclusions are to be drawn from benchmark measurements of reactivity and reaction rate distributions. Thus, for example, one finds that by compensating in the absorption cross-section for an absorber, the flux level predicted by diffusion theory in that absorber does move further away from reality and, since the transient difference between transport theory and diffusion theory is not confined to the absorber itself but encompasses also the neighboring fuel, both reactivity and reaction rates in this fuel are affected by the adjustments made. This type of effect is of the order of 1-2% equivalent cross-section uncertainty in the thermal energy range. To eliminate such errors, it is desirable to employ methods that modify the diffusion coefficients rather than the reaction rate cross sections so that, ideally, the correct flux levels are predicted by diffusion theory for all different components of the fuel assembly design. Such an approach does also ensure that changes in flux levels, which are important contributions to reactivity coefficients and reactivity differences hot to cold, may be correctly predicted.

A source of methods-related uncertainty which is particularly noticeable in the diffusion theory analysis of small critical, experimental cores is connected with leakage effects in the heterogeneous lattice. Leakage is dominated by fast events (i.e., above about 100 keV). In this energy region, local flux perturbations are caused chiefly by the presence of waterholes into which the flux distribution dips noticeably. Diffusion theory does always predict a flux level too high in this situation and the same type of correction as discussed above for the thermal region is required but often omitted since a separate transport theory computation is necessary to find the correct amount of flux dipping. In a critical experiment, the leakage may amount to some 35%k of which say 3.5%k takes place in waterholes. An error of 10% in the flux level does contribute to an error in overall reactivity of about 0.35%k which is outside the accuracy required and may cloud conclusions drawn about basic cross-section data from the analyses. An example of this is given in Section V below. Direct effects on k-infinity are small. However, if no measures are taken to correct the fast flux level in waterholes, errors corresponding to some 3% in assembly average slowing-down cross-sections may be observed for a design with waterholes. This amounts to about 0.10 + 0.15%k and may exhibit symptoms similar to uncertainties in the hydrogen and U-238 inelastic cross-sections for slowing down.

III. CALCULATIONAL MODEL

Elimination of methods related uncertainties in the range 0.1-0.5%k as discussed above, require explicit account of geometry-induced spectrum and spatial interactions. The DIT calculational model is visualized in Fig. 4. Although some important differences are present, it is similar in structure to codes such as WIMS[1] and EPRI-CPM[2]. Three major components make up computational models of this kind, viz., (1) A spectrum calculation in approximated assembly geometry, (2) a spatial calculation in the assembly geometry and (3) a depletion routine followed by editing routines.

DIT includes the following additional features:

A. Spatial interaction uncertainties are minimized by avoiding homogenizations. Thus, the transport calculation is done in explicit-pin geometry for the assembly using integral transport methods[3,4]. Individual cells are coupled by interface currents. The name DIT refers to the method of integrating the transport equation within each individual cell as originally developed by Carlvik[5]. The spatial mesh within cells may be both radial and azimuthal. Most frequently, one uses a radial mesh combined with an expansion in harmonics azimuthally, subsequently referred to as the k=n option where n is the number of harmonics retained in the expansion.

B. Spectral interactions are accounted for in an 85-group structure by performing explicit-geometry transport calculations for spectrum geometries which are portions of the assembly and using boundary currents generated in the assembly calculation. Typical spectrum geometries consist of 1 to 3 cells with diagonal symmetry. See Fig. 4.

C. Upon completion of the assembly calculation, excess reactivity (i.e., reactivity not accounted for by chemical shim) is removed by leakage in an 85-group B1 calculation with a buckling search. Thus, criticality is always maintained and the few-group averaged cross-sections produced are always obtained in a critical spectrum.

D. The depletion takes place for each individual pin in the assembly and, when required, also for subdivisions of fuel or absorber pins. Editing routines supply cross-sections for both fine mesh PDQ and coarse mesh nodal codes.

E. Cross-sections are processed from ENDF/B via ETOG[6],FLANGE-II[7], GGC-3[8] and RABBLE[9]. The cosine current approximation has been removed from RABBLE and replaced with an integral transport routine. The fine-group averaged resonance cross-sections are converted to a two-dimensional table parametric in temperature and a background cross-section via an equivalence theorem linking lattices of differing geometry.

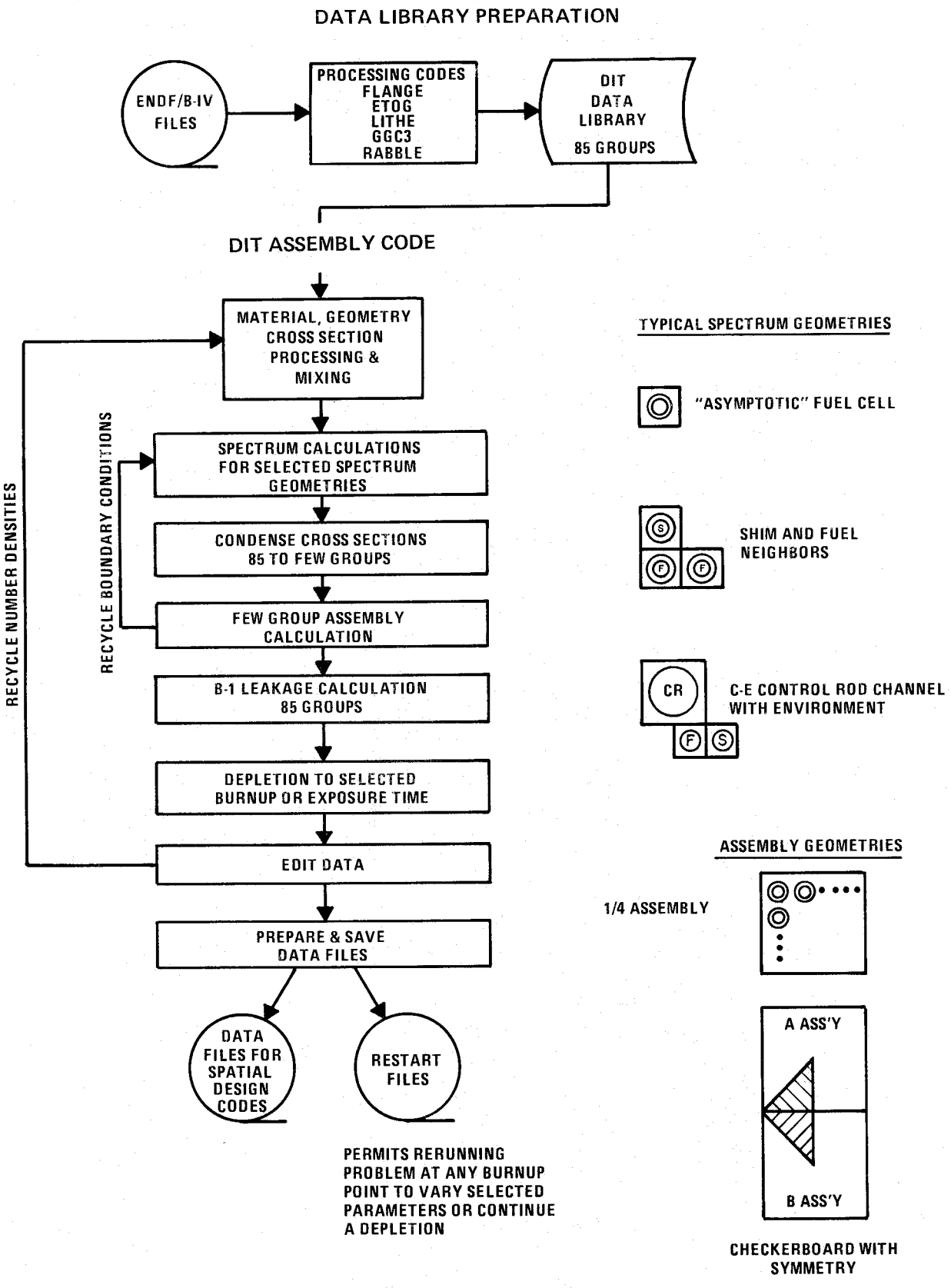
DATA LIBRARY PREPARATION
ENDF/B-IV FILES
PROCESSING CODES FLANGE ETOG LITHE GGC3 RABBLE
DIT DATA LIBRARY 85 GROUPS
DIT ASSEMBLY CODE
MATERIAL, GEOMETRY CROSS SECTION PROCESSING & MIXING
SPECTRUM CALCULATIONS FOR SELECTED SPECTRUM GEOMETRIES
CONDENSE CROSS SECTIONS 85 TO FEW GROUPS
FEW GROUP ASSEMBLY CALCULATION
B-1 LEAKAGE CALCULATION 85 GROUPS
DEPLETION TO SELECTED BURNUP OR EXPOSURE TIME
EDIT DATA
PREPARE & SAVE DATA FILES
RECYCLE NUMBER DENSITIES
RECYCLE BOUNDARY CONDITIONS
DATA FILES FOR SPATIAL DESIGN CODES
RESTART FILES
PERMITS RERUNNING PROBLEM AT ANY BURNUP POINT TO VARY SELECTED PARAMETERS OR CONTINUE A DEPLETION
TYPICAL SPECTRUM GEOMETRIES
"ASYMPTOTIC" FUEL CELL
S
F
F
SHIM AND FUEL NEIGHBORS
CR
F
S
C-E CONTROL ROD CHANNEL WITH ENVIRONMENT
ASSEMBLY GEOMETRIES
1/4 ASSEMBLY
A ASS'Y
B ASS'Y
CHECKERBOARD WITH SYMMETRY

Figure 4

Interaction effects between different resonance absorbers are accounted for in the equivalence. In the process of reading its library, DIT uses the same equivalence theorem to interpolate in the table. This method does not, therefore, rely on an equivalence theorem to perform the more difficult function of relating heterogeneous resonance integrals to homogeneous data. Its sole function is to serve as a convenient means of tabulating and retrieving the data which itself is generated with an accurate space dependent slowing-down calculation (RABBLE in this case). A similar procedure based on homogeneous slowing down calculations with the SDR code[10], was originally developed for WIMS[1] with suitable equivalence theorems provided by Leslie et.al[11].

IV. UNIFORM LATTICES ANALYZED WITH ENDF/B-IV DATA

The calculational method described above has been applied to the analysis of a limited range of uniform critical lattices selected for their quality. ENDF/B-IV data was processed through ETOG, FLANGE, RABBLE, and GGC-3 as described in Section III. The analysis of uniform lattices complements the main body of verification analyses composed of non-uniform lattices in critical experiments and in operating power reactor cores. Uniform lattices are used to indicate the quality of basic cross-section data for undepleted fuel. A brief discussion of the results obtained with ENDF/B-IV will be given followed by results from a repeat of the analyses using a modified ENDF/B-IV library. The latter was adopted for application to non-uniform lattice results which are described in Section V below.

Four sets of experiments have been analyzed:

1) UKAEA, Winfrith R/100H series of 3% enriched UO_2[12].
2) TRX -1,2, 1.3% enriched metal in light water[13].
3) EPRI-BNWL lattices, 2.35% enriched UO_2[14].
4) KRITZ, Studsvik series of 1.35% enriched UO_2 at a range of temperatures[15].

The analyses were done using the experimental buckling as an input to DIT, i.e., the influence of leakage on spectrum and on reactivity was accounted for by a fundamental mode solution in the B1 approximation using 85 groups. Except in the case of the EPRI-BNWL lattices, this approximation does not lead to large errors in the predicted criticality. For the EPRI-BNWL lattices, corrections were made on the basis of 2-D, ANISN core calculations reported by Ozer and Fiarman[16].

Table 4 and Figure 5 show results using an ENDF/B-IV library. Several conclusions were drawn:

1) Calculated Relative Conversion Ratios and rho-28's were too high by 2-4%. A reduction of U-238 resonance capture data

TABLE 4 Uniform Lattices Analyzed with ENDF/B-IV Data

Lattice	Vm/Vf	k_{eff}	ρ^{28}		RCR		δ^{28}		δ^{25}	
			Meas.	Calc.	Meas.	Calc.	Meas.	Calc.	Meas.	Calc.
Winfrith: 3% U-235(UO_2)										
R1/100H(20°C)	1.0	1.00359	---	---	4.158	4.293	0.0858	0.0825	---	---
R1/100H(80°C)	1.0	0.99993	---	---	4.293	4.416	0.0895	0.0844	---	---
R2/100H(20°C)	3.16	1.00437	---	---	---	---	---	---	---	---
R3/100H(20°C)	0.78	1.00140	---	---	4.789	4.980	0.1066	0.0978	---	---
TRX: 1.3% U-235 U-Metal										
TRX-1	2.35	0.99630	1.320	1.364	---	---	0.0946	0.0940	0.0987	0.1044
TRX-2	4.02	0.99546	0.837	0.851	---	---	0.0693	0.0674	0.0614	0.0640
EPRI-BNWL:2.35% U-235(UO_2)										
U-L66	2.41	1.00974[1]	---	---	---	---	---	---	---	---
U-L162	3.69	1.00401[1]	---	---	---	---	---	---	---	---
U-L73	2.41	1.00573[1]	---	---	---	---	---	---	---	---
U-L143	3.69	1.00211[1]	---	---	---	---	---	---	---	---
KRITZ: 1.35% U-235(UO_2)										
20°C	1.44	0.99795	---	---	---	---	---	---	---	---
90°C	1.44	0.99479	---	---	---	---	---	---	---	---
160°C	1.44	0.99122	---	---	---	---	---	---	---	---
210°C	1.44	0.98954	---	---	---	---	---	---	---	---

1) Including ANISN corrections of OZER and Fiarman[16].

Figure 5
UNIFORM LATTICES - ENDF/B-IV

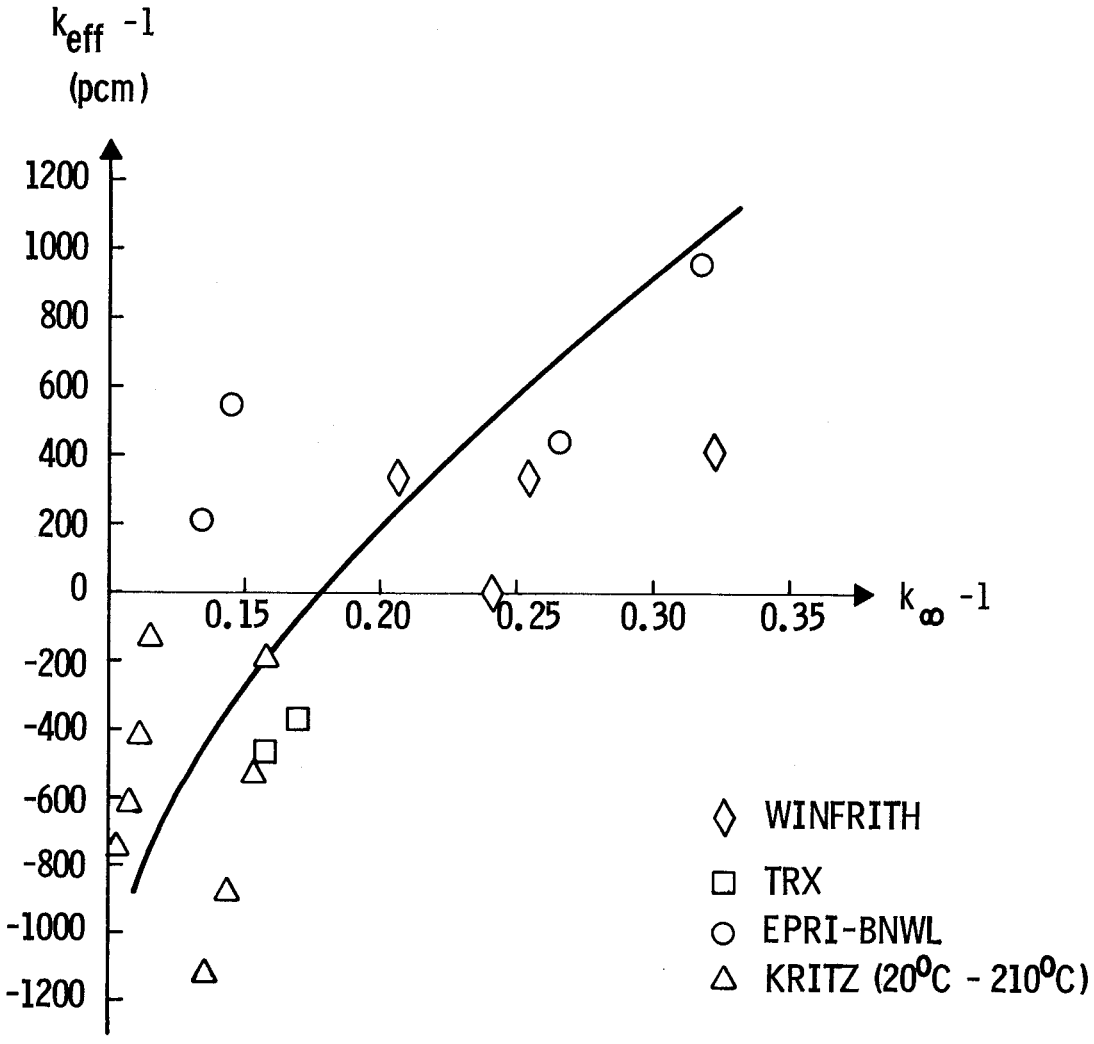

was indicated.

2) The calculated fast fission ratio was low by an average of some 4.5%. Going to ENDF/B-V fission spectra would improve this situation.

3) The thermal fine structure, i.e., the coolant-to-fuel flux ratio, was underpredicted by up to 2% for the Winfrith lattices. See Table 5. This was expected because use of the Haywood scattering kernel for hydrogen leads to a spectrum which is too hard. It is also expected on the grounds of the method used for evaluating collision probabilities which in these lattices used a cylindricized outer boundary for each cell. This is an instance where the relative magnitudes of uncertainties in data and methods both need to be quantified.

TABLE 5

Thermal Fine Structure, U-235 Fission Rates

Lattice	Vm/Vf	Measured[12]	Calculated	Difference %
R1/100H(20°C)	1.00	1.260 ± .015	1.237	-1.9
R1/100H(80°C)	1.00	1.233 ± .007	1.221	-1.0
R3/100H(20°C)	0.78	1.223 ± .016	1.207	-2.1

4) Delta-25 for the TRX lattices is calculated high by as much as 5%. An improvement is required but no modification of the library has been studied.

5) The reactivity error was both negative and positive within 1%k. It varied approximately linearly with the amount of leakage, Figure 5. We concluded that there could be an underprediction of M^2 by as much as 4% and noted that the harder fission spectra anticipated in ENDF/B-V would increase M^2.

6) There is a definite trend in the reactivity error with temperature for the KRITZ lattices. A similar behavior was reported by Wikdahl, et.al.[17] for a range of lattices and the existence of a discrepancy of this type was recognized as possibly originating from basic cross-section data.

The overprediction of U-238 capture was, of course, expected. The 1975 "Seminar on ^{238}U Resonance Capture" held at the National Neutron Cross Section Center[18] indicated that such overpredictions were well known. A direct comparison between the ENDF/B-IV library and measured[19] resonance integrals did also lead to this conclusion. Table 6 shows such a comparison indicating a 2-3% reduction of the ENDF/B-IV data would be justified. Thus, the integral measurements are consistent with conversion ratio measurements as claimed by Hellens, et.al[20].

TABLE 6

Comparison of U-238 Resonance Integrals with Best Estimate Measured Values [19]

	$\frac{S}{M}$ = .418	$\frac{S}{M}$ = .370	$\frac{S}{M}$ = .310
		barns	
300°K			
DIT(ENDF/B-IV)	23.12	22.19	20.92
Measured	22.61	21.59	20.25
Diff.	0.51	0.60	0.67
570°F			
DIT(ENDF/B-IV)	24.17	23.16	21.80
Measured	23.72	22.62	21.17
Diff.	0.45	0.54	0.63
1100°F			
DIT(ENDF/B-IV)	25.79	24.66	23.14
Measured	25.30	24.07	22.48
Diff.	0.49	0.59	0.66

The following modifications were made to the library:

1) Fission spectra were generated from ENDF/B-V recommendations, i.e., Maxwell spectra were replaced by Watt spectra.
2) U-238 resonance cross-sections were reduced from their ENDF/B-IV level by a flat 0.07 barns (i.e., about 2.5-3.0% of a resonance integral) on the cross-section in the range 3eV to 9keV. This reduction does not necessarily simulate ENDF/B-V but has been used over the past years as a simple expedient to force agreement of calculated reaction rates with measured single rods and uniform lattices.

Table 7 and Figure 6 give the results for the modified library. Conclusions are:

1) Calculated relative conversion ratios and rho-28's are now in good agreement with all measurements. Slight overestimates are still observed by up to 1% for the Winfrith lattices but for the TRX lattices there is an underestimate by 1-2%. These numbers are comparable to the measurement uncertainties. It is likely also that the adoption of the ENDF/B-V data will show differences in detail from the effect observed here which is based on the flat reduction of the cross section. Thus, Hardy[21] has shown that going to recently measured resonance parameters as well as going to revised scattering data for U-238 and to a Reich-Moore multilevel formalism will reduce rho-28 for the TRX-1 lattice by 3%, i.e., very close to the amount needed to bring the Table 4 ENDF/B-IV value into agreement with the measured value.

TABLE 7 Uniform Lattices Analyzed with Modified ENDF/B-IV Data

Lattice	Vm/Vf	k_{eff}	ρ^{28}		RCR		δ^{28}		δ^{25}	
			Meas.	Calc.	Meas.	Calc.	Meas.	Calc.	Meas.	Calc.
Winfrith: 3% U-235 in UO_2										
R1/100H(20°C)	1.00	1.00915	---	---	4.158	4.185	0.0858	0.0851	---	---
R1/100H(80°C)	1.00	1.00570	---	---	4.293	4.306	0.0895	0.0871	---	---
R2/100H(20°C)	3.16	1.00302	---	---	----	----	----	----	---	---
R3/100H(20°C)	0.78	1.00925	---	---	4.789	4.840	0.1066	0.1006	---	---
TRX:1.3% U-235 U-metal										
TRX-1	2.35	1.00262	1.320	1.314	---	---	0.0946	0.0968	0.0987	0.1044
TRX-2	4.02	0.99872	0.837	0.823	---	---	0.0693	0.0696	0.0614	0.0640
EPRI-BNWL:2.35% U-235 in UO_2										
U-L66	2.41	1.00920[1]			---	---	---	---	---	---
U-L162	3.69	1.00333[1]			---	---	---	---	---	---
U-L73	2.41	1.00765[1]			---	---	---	---	---	---
U-L143	3.69	1.00284[1]			---	---	---	---	---	---
KRI : 1.35% U-235 in UO_2										
20°C	1.44	1.00260	---	---	---	---	---	---	---	---
90°C	1.44	0.99960	---	---	---	---	---	---	---	---
160°C	1.44	0.99643	---	---	---	---	---	---	---	---
210°C	1.44	0.99516	---	---	---	---	---	---	---	---

1) Including ANISN corrections of OZER and Fiarman[16]

Figure 6

UNIFORM LATTICES - MODIFIED ENDF/B-IV

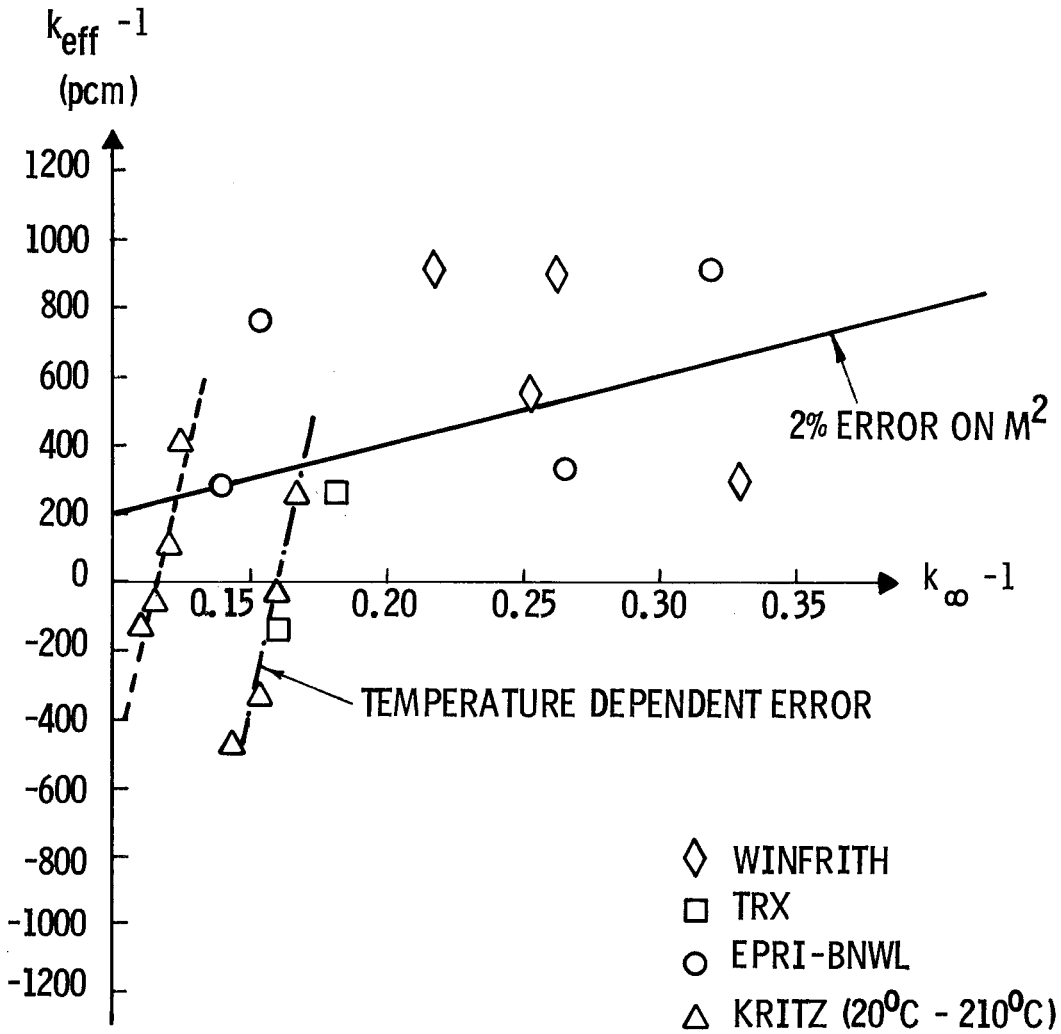

2) Calculated fast fission ratios are now an average of 1.4% low, a considerable improvement achieved through the hardening of the fission spectrum. The increased fast fission which are a result of this hardening does also have the effect to increase k-infinity by typically 0.15%k. The net effect on k-effective is usually negative, however, since the leakage does also increase and prevails in these high leakage criticals. The Winfrith and the TRX lattices do, however, lead to opposite conclusions for the fast fission ratio. The underestimate for the Winfrith lattices is still significant in one case and the overestimate for TRX-1 may also be significant. We conclude that there might still be some improvement necessary in either the fast cross-section data or in our ability to calculate the fast spectrum in the very high energy region or in the apparently inconsistent lattice measurements.

3) Agreement on Delta-25 is virtually unchanged by the modifications of the library as expected. The calculated values are a significant 5% high and it is worth noting that our values are higher than those reported by most evaluators for the TRX lattices. A reduction of the U-235 fission resonance integral from its ENDF/B-IV value to a level of about 275 barns indicated by integral measurements would reduce the discrepancy to about 2%, i.e., just outside the uncertainty of the measurement. Methods uncertainties are a possibility in this area and one should examine the methods used to account for interaction effects between various resonance absorbers.

4) The temperature dependent trend observed for the calculated reactivity of the KRITZ latties was only marginally reduced by the changes made.

5) The previously strong trend of calculated k-effective with leakage was considerably reduced through the higher energies for fission neutrons resulting from the use of the Watt spectrum. This corresponded to an increase of typically 1.5% in M^2. The trend is still visible though and the effect of a remaining error of 2% in M^2 is indicated in Figure 6. The elimination of such an error would both reduce the level of predicted k-effective and remove the trend. Forthcoming changes to the U-238 inelastic scattering data in ENDF/B may influence the conclusions reached here. The discrepancies are small, however, (the average k-effective is 1.00323) and the source of the discrepancy may well lie elsewhere. An additional source of uncertainty may be found in the theoretical treatment of the leakage rather than in the data. Differences of the order of 2% of total leakage between various methods (viz., GGC-3, MUFT and DIT) have been observed during the course of this evaluation. These differences arise in the resonance region contribution to the leakage when using the B1 approximation.

V. PWR FUEL BENCHMARKS ANALYZED WITH MODIFIED ENDF/B-IV DATA

C-E has sponsored a number of critical experiments, e.g., at the Westinghouse CRX reactor, the KRITZ facility at Studsvik, Sweden and the BNWL, PRCF facility, to provide a data base applicable to the C-E assembly design. Measurements included core reactivity, relative fission rate distributions, soluble boron concentrations, bucklings and, in selected cases, spectral indices, temperature effects and rod worths. In this section, the effects discussed in Section II are explored further to evaluate their impact on assembly design parameters. The results of analyses of selected critical experiments using various calculational models are included to illustrate various effects as well as to indicate the level of agreement between calculation and experiment.

V.1. Calculational Comparisons for PWR Assembly Designs

Before discussing the results of comparisons between calculations and measurements, several of the effects discussed in Section II are illustrated by comparing the results from various calculational methods. As part of the benchmarking effort on DIT, comprehensive comparisons were made among DIT, MORSE[22] and DOT[23]. A comparison of the thermal flux levels in the fuel cells as predicted by each method, with MORSE as a base, for a 14x14 assembly with large waterholes and power flattening absorber rods is summarized in Figure 7. The agreement is good between DIT and MORSE with DIT tending to slightly underpredict the flux levels in fuel pins near the absorber rods. Near the large waterholes, DIT tends to overestimate the flux levels. Overall, the agreement is within the statistical uncertainty of the MORSE results. In general, a difference of 1-2% in peaking is observed between heterogeneous DIT and homogeneous DOT or homogeneous DIT. Thus, homogeneous transport calculations in x-y geometry are not sufficient for highly accurate power peaking predictions.

In the following discussion, the results of calculations employing DIT with the k=1 option (azimuthal flux variation) are used as the basis of comparisons. The azimuthal variation of the thermal flux as predicted with DIT (k=1) for a fuel cell adjacent to a waterhole is shown in Fig. 8. In Fig. 9, in which fission rate distribution and reactivity differences are presented, neglect of the azimuthal variation of the flux in a cell (the k=0 option) significantly impacts the predicted fission rate distribution and reactivity level. The thermal flux gradients near the large waterholes are underpredicted in this case. The difference in reactivity of about 0.23%$\Delta\rho$ is due essentially to the underprediction of the thermal flux peak in the waterholes. Using the diffusion constants generated by DIT directly in the diffusion code, PDQ, and employing a mesh point assignment typically used in reactor design, illustrates further the

Figure 7

14 x 14 ASSEMBLY (2 x 2 WATER HOLES) WITH ABSORBER RODS

COMPARISON OF THERMAL FLUX DISTRIBUTION

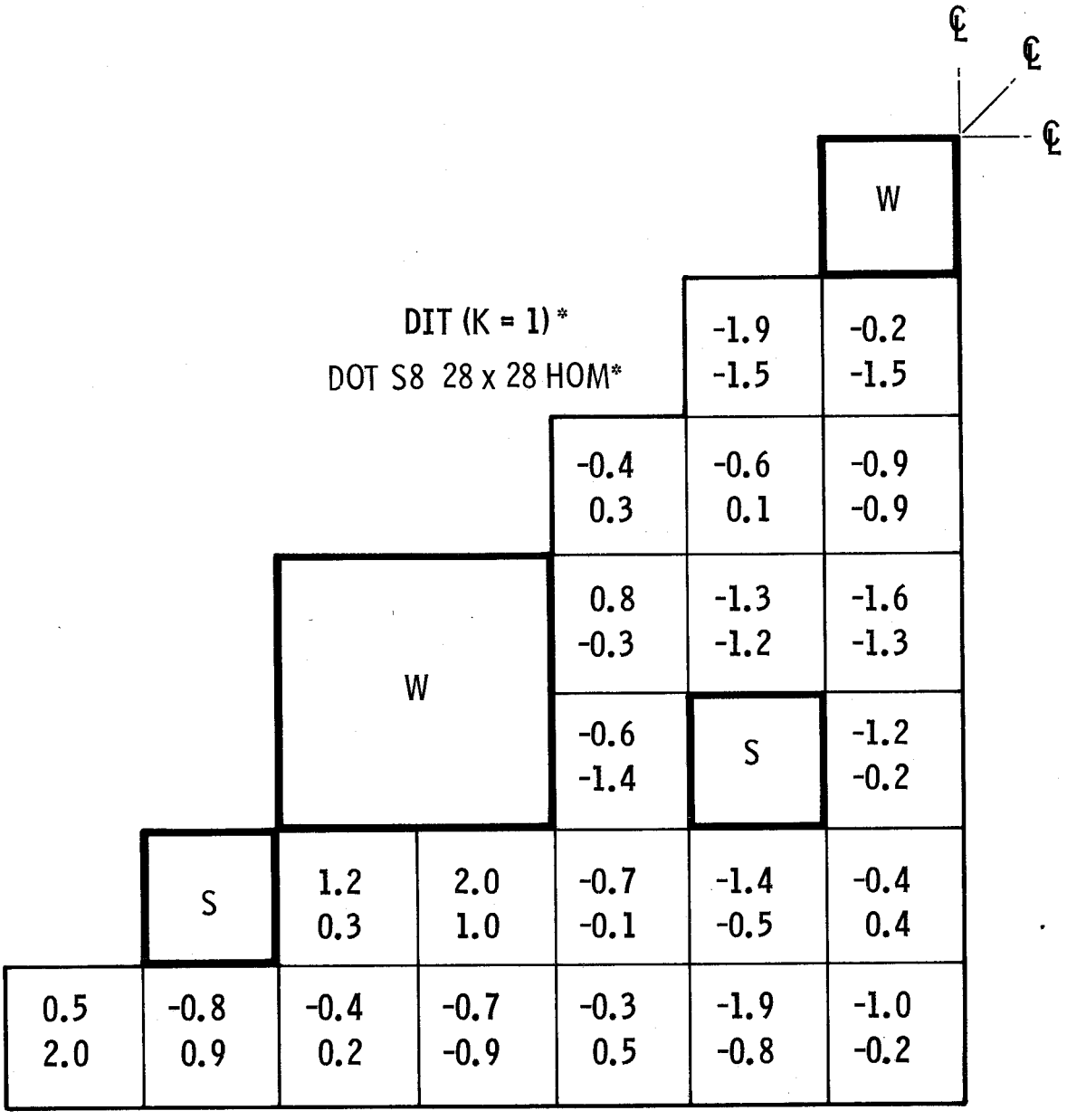

*PERCENTAGE DIFFERENCES IN CALCULATED THERMAL FLUX LEVELS RELATIVE TO MORSE (MORSE STATISTICAL UNCERTAINTY ± 1.0%)

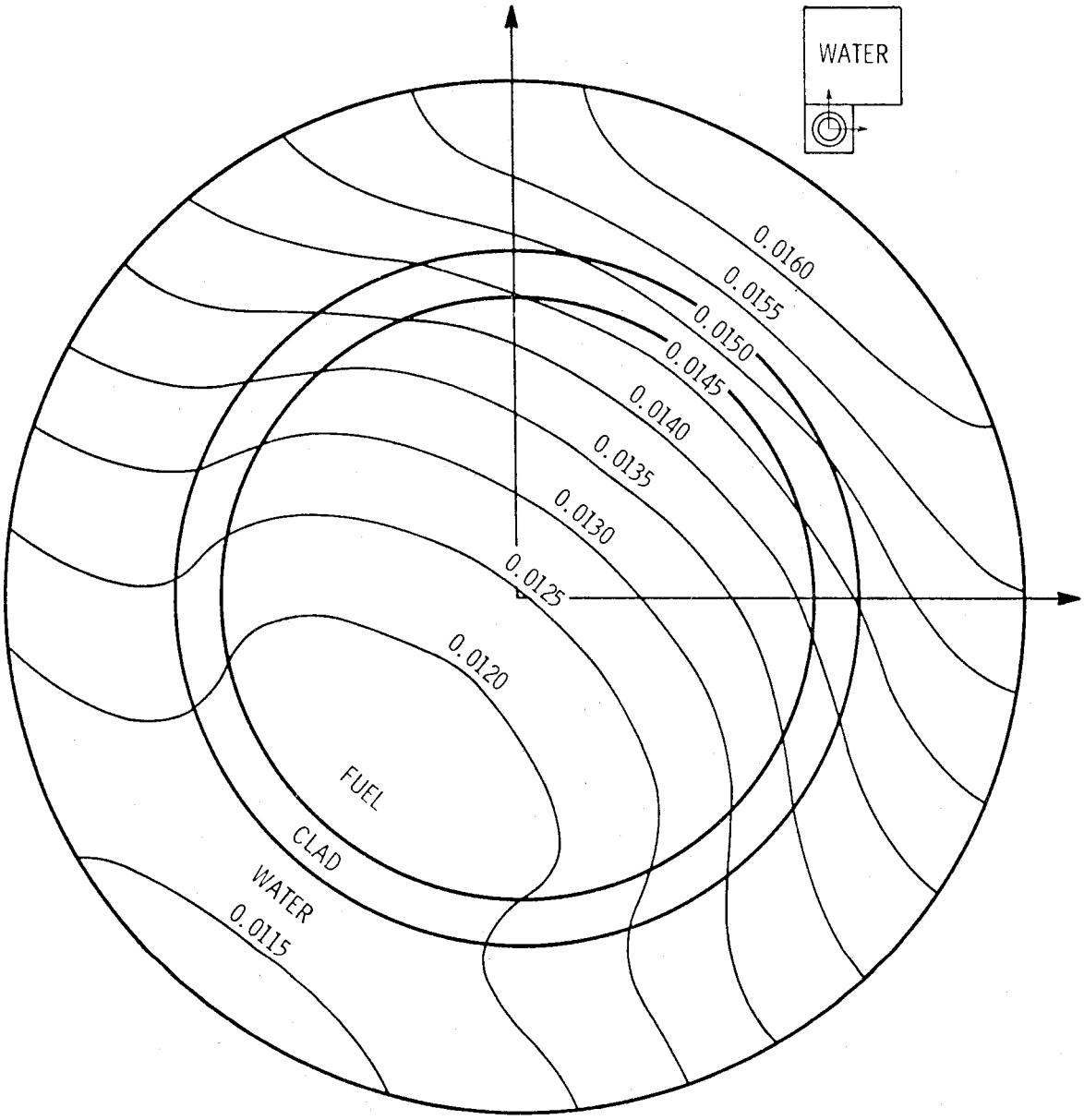

Figure 8
THERMAL FLUX CONTOURS IN A UO_2 PIN
NEAR A WATERHOLE

17-25

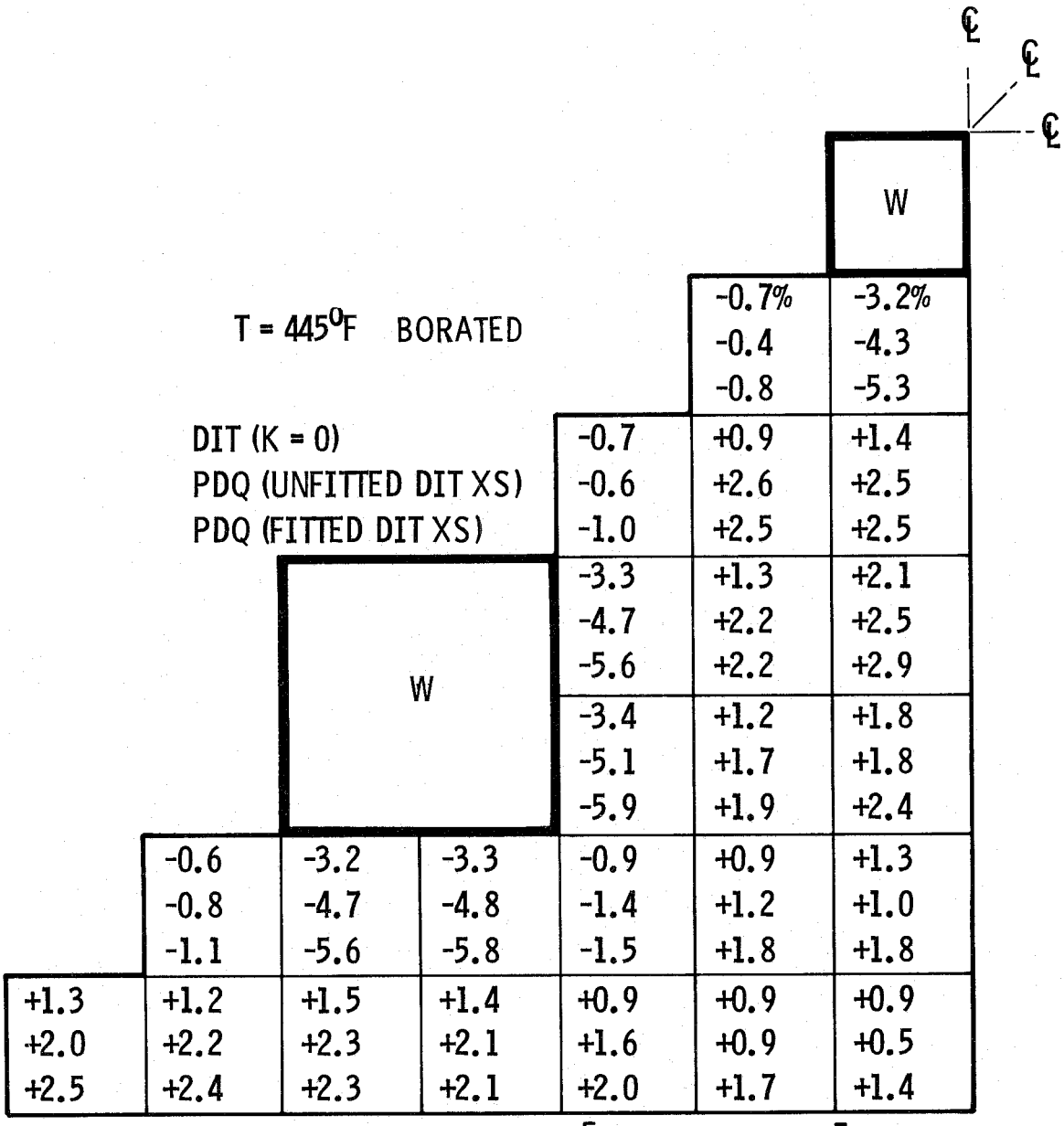

DIFFERENCES RELATIVE TO DIT (K = 1): [CALC - DIT(K = 1)] x 100

	% Δρ	Δ WATER HOLE ABS FRACTION
DIT (K = 0)	+0.232	0.00218
PDQ (UNFITTED WATER HOLE XS)	+0.866	0.00874
PDQ (FITTED WATER HOLE XS)	+0.007	0.0

Figure 9

14 x 14 ASSEMBLY WITH LARGE WATER HOLES
COMPARISON OF RELATIVE FISSION RATE DISTRIBUTION
AND REACTIVITY

magnitude of the differences introduced by simplifying the physical modelling in the calculations. As shown in Fig. 9, the fission rate distribution predicted by the diffusion code using averaged fuel cell constants is substantially flatter than the DIT (k=1) distributions. These differences are due basically to (1) the limitation of diffusion theory in regions where strong flux gradients exist and (2) the neglect of spectrum interaction effects near heterogenieties when averaged cross sections are used. The two effects contribute about equally to the underprediction of fission rate at the waterholes, while the former essentially accounts for the rather large reactivity overprediction of about 0.87%$\Delta\rho$ by the diffusion code. The underprediction of the thermal flux peak in the large waterhole leads to the observed underestimate of its reactivity worth. This limitation of diffusion theory can be alleviated to a degree by dividing the regions with a finer mesh. For example, a 4x4 mesh structure per fuel cell reduces the differences in fission rate in fuel cells adjacent to the waterholes by about 0.7% and decreases the reactivity difference to about 0.69%$\Delta\rho$. However, this small degree of improvement does not warrant the large increase in computer storage and time needed to implement this approach.

A more powerful approach is to fit cross sections in heterogeneous regions, i.e., waterholes and absorber rods, to match the transport predicted reaction rates in these regions. This is illustrated in Fig. 9 where the waterhole cross sections for the diffusion calculation were fitted to give the DIT (k=1) reaction rates. The difference in reactivity level is essentially eliminated, but the fission rate distribution is further flattened across the assembly. This is due to the fact that the flux levels in the waterholes are adversely perturbed by the fitting process. A further consequence of perturbing the flux levels in the waterholes is to increase the global leakage from the assembly. The increased leakage is worth about 0.15%$\Delta\rho$ and further adjustments must be made to the diffusion constants to eliminate this artificiality. Fig. 9 illustrates that although this method succeeds reasonably well to match integrated reaction rates and reactivity, it still fails to provide the correct distribution of reaction rates. A method that achieves both has been developed. As discussed in Section II, this is accomplished via a definition of diffusion coefficients geared to the particular finite difference formulation used. It has been found that this is most easily accomplished in a mesh centered formulation and Fig. 10 shows that the transport theory fission rate distribution and reactivity are both essentially duplicated by such a diffusion calculation.

Each of the effects discussed serves to illustrate the importance of fully considering the physical modelling approximations in the methods used to evaluate the impact of data uncertainties on various parameters. This is especially true in the

Figure 10

COMPARISON OF FISSION RATES

DIT (K=1) vs MESH CENTERED DIFFUSION THEORY

	k_∞
DIT (K = 1)	1.3499
MC DIFF THEORY	1.3502

%DIFF= (DIT - FC) x 100

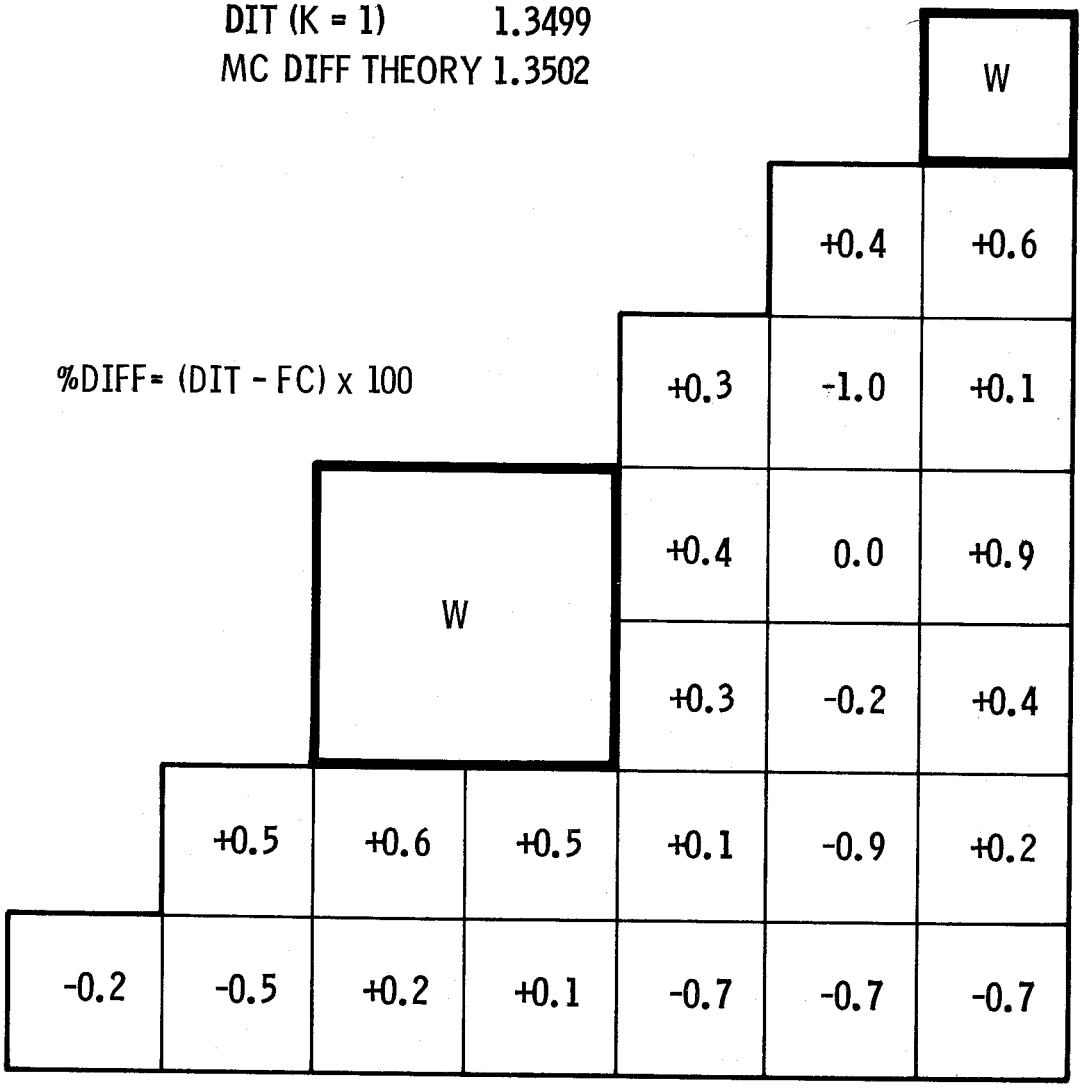

analysis of critical experiments which are used to validate reactor design methods. The possibility of compensating errors masking the results is quite high with their neglect leading to fortuitous agreement. In the next section, the results of the analysis of selected heterogeneous critical experiments are examined to demonstrate the levels of uncertainty observed and to establish their relationship to basic data uncertainties.

V.2. Comparisons Between Calculation and Experiments for PWR Benchmarks

The analysis of non-uniform experimental cores provides a means for verifying the methods and the data to be used for reactor design. Unlike uniform cores which can be treated as asymptotic regions, the heterogenieties in the non-uniform cores require that detailed spatial calculations be performed. Since the entire core geometries typically cannot be modelled explicitly in detailed transport codes, such as DIT, the comparisons between experiment and calculation must be indirect. This can be done in several ways among them including the use of an intermediary, spatial code or the correction of measurements to eliminate global effects occurring in the core. The former is required to compare reactivity levels while the latter is more appropriate for comparisons of fission rate distributions.

For this analysis, several critical experiments, the central regions of which model the C-E 14x14 assembly design, were selected to illustrate the effects discussed above. The experiments labeled as C-E criticals were performed for C-E by Westinghouse at the CRX facility. The cores were configured in a square array of about 900 fuel rods with certain rods removed to simulate large waterholes. About half the cores had waterholes only in the central 14x14 region while the rest had waterholes distributed throughout the core. The experiments were conducted at room temperature and were fully reflected at the sides. The measured axial bucklings were obtained for critical conditions and relative fission rate distributions were measured. Soluble boron poison was employed in two of the selected cores. An additional experiment from a C-E sponsored program at the KRITZ facility in Studsvik, Sweden is also included to provide data at a temperature more representative of operating reactors. Basically, the same measurements were made for this core as were made for the C-E criticals although the techniques were somewhat different. The calculated reactivity levels together with pertinent parameters are given in Table 8. The values were obtained from 2-D spatial diffusion calculations using cross sections generated by DIT. A 1x1 mesh assignment per fuel rod location and explicit radial reflector representation were employed. Axial leakage was accounted for through a DB^2 term employing the measured axial buckling. Fitted diffusion constants were employed in the waterholes to reproduce the transport predicted reaction rates.

TABLE 8. Non-Uniform Lattices. Comparison of Reactivity Levels
Calculation vs. Experiment

MODIFIED ENDF/B-IV

Core	Vol.Mod / Vol.Fuel	No. of Large Waterholes	Soluble Boron Conc. PPM	k_{eff}	k_{eff} With Reflector Corrections
C-E Criticals 2.7 % U-235, 68°F					
#12	1.49	5	0	0.9956	1.0002
#32	1.49	17	0	0.9930	0.9991
#43	1.49	5	323	0.9973	1.0017
#53	1.26	17	0	0.9945	1.0006
#56	1.26	17	302	0.9935	0.9991
KRITZ 3.1% U-235, 445°F	1.79	21	959	0.9983	1.0023

The column labeled k_{eff} in Table 8 gives the calculated multiplication constants obtained from diffusion theory. All the lattices are predicted to be subcritical for the reported conditions. Analysis of core-reflector interactions based on transport calculations indicate that the fast leakage in the radial direction is too large. Matching the core-reflector albedos predicted by transport theory in the diffusion calculations adds about $0.4\%\Delta\rho$ to the k_{eff} of each lattice. The far right column of Table 8 gives the calculated multiplication constants with reflector corrections. Overall agreement with experiment is significantly improved. These results suggest that substantial reactivity swings can occur as physical modelling improves and compensating effects are eliminated. The latter can be quite substantial in reactor design calculational models and can mask, to a large extent, the need for improvements in basic cross section data.

A comparison between the calculated and the measured fission rate distribution for the central 14x14 region of the KRITZ experimental core is given in Fig. 11. The measured values were corrected for the global flux shape in the core, such that the corrected values would be those expected to be measured in an infinite array of assemblies. This procedure allows the results of the DIT (k=1) assembly calculation to be compared most directly with measurements. The measurement uncertainty is of the order of $\pm$1%, so that overall agreement is quite good. This and similar comparisons for the C-E criticals indicate that DIT(k=1) slightly overpredicts the thermal flux peak in the waterholes resulting in too large a gradient from the waterholes to the "asymptotic" regions of the assembly. This results in a small overprediction of the fission rate in fuel pins directly surrounding the waterholes and an underprediction in fuel pins away from the waterholes. An additional consequence is that the waterhole worth is overpredicted by about 3% which if corrected would raise calculated reactivity in the critical cores by up to about $0.07\%\Delta k$ depending on the number of waterholes.

VI. CONCLUSIONS

Modifications to ENDF/B-IV data anticipating, in part, Version V have brought calculations into better agreement with thermal benchmark experiments for both uniform and non-uniform lattices. Remaining discrepancies may be attributed to either or all of experimental, calculational and basic cross-section uncertainties. In particular, we conclude that cross-section and methods uncertainties are now of comparable size and often competing, for example, in the following areas:

Thermal Flux Fine Structure and Spectrum

ENDF/B-IV choice of thermal scattering model for H_2O. - Cylindricized cells in one-dimensional calculations.

Figure 11
DIT (K=1) vs MEASUREMENT FISSION RATE DISTRIBUTION

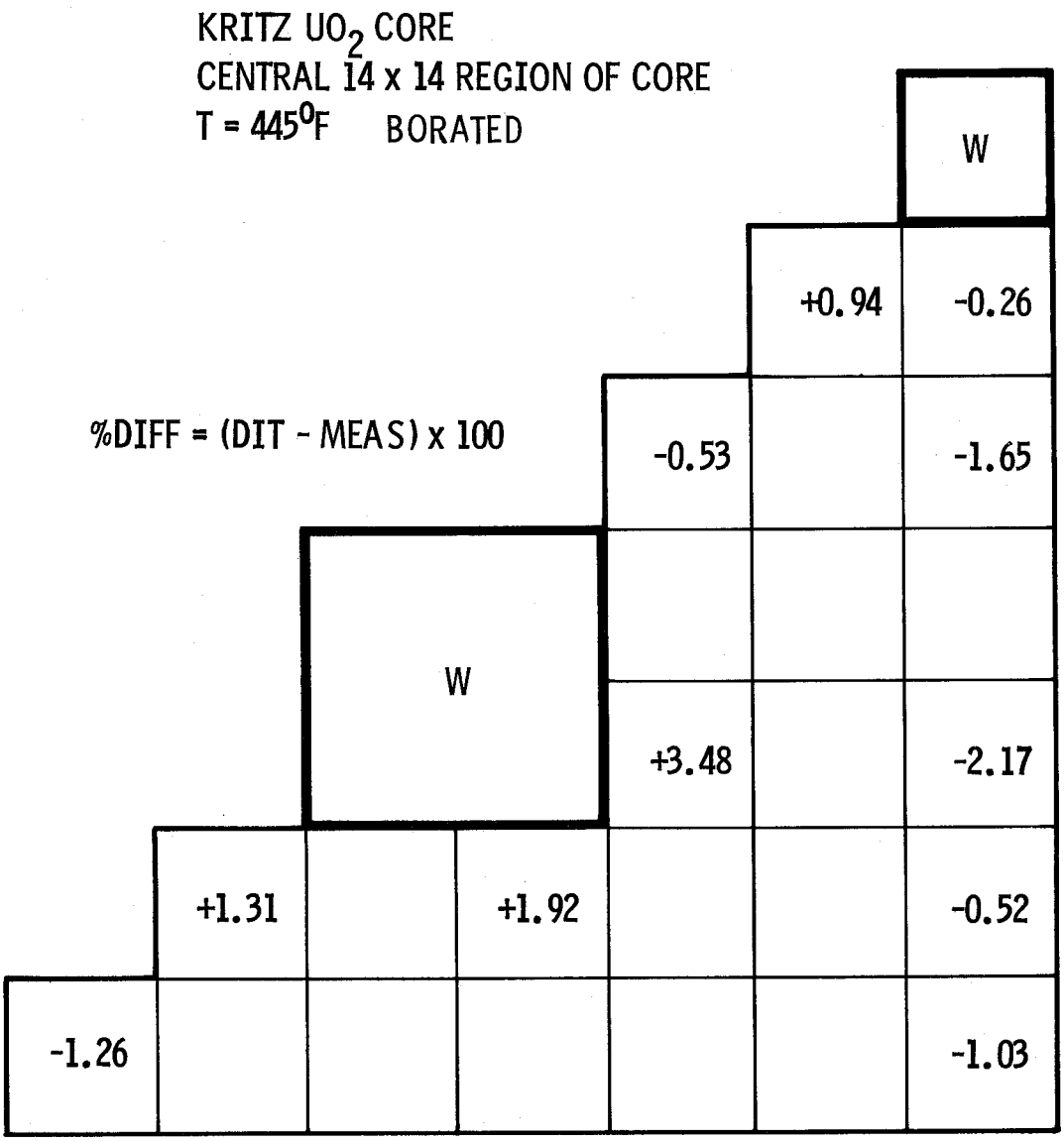

U-235 Resonance Fission

Both calculated reactivity levels and δ^{25} may indicate high values for U-235 resonance fission using ENDF/B-IV. On the other hand, theoretical models for interference between resonance absorbers may not be accurate enough to draw this conclusion.

Leakage Representation and Fast Spectrum

Representation of leakage via B1, fundamental mode or full core Monte Carlo calculations represent the spectrum of approaches open to the analyst. - Basic data uncertainties, for example, in U-238 inelastic cross-sections and fission spectra may be important when drawing conclusions about the accuracy of calculated fast leakages.

Resonance Absorption

Basic ENDF/B-V U-238 resonance data is expected to have uncertainty levels comparable to the following calculational and processing uncertainties:
-Transport calculation (in RABBLE for example).
-Slowing down calculation.
-Multilevel formalism vs. single level.
-Resonance region spectrum interactions in broad groups.
-Usage of equivalence theorem.

Two-dimensional transport codes executed in realistic fuel geometry are necessary to minimize calculational uncertainties in PWR fuel geometry. In applications to both uniform and non-uniform lattices, PWR design codes generally need attention to the details of processing and using resonance data.

VII. REFERENCES

1. J. R. Askew, et.al., "A General Description of the Lattice Code WIMS," Journal Brit. Nucl. Energy Soc., 5,4,(1966).
2. B. A. Zolotar and W. J. Eich, "Advanced Recycle Methodology Program: Preliminary Specifications for a New Nuclear Computational Capability," EPRI SR-2 (July 1974); W.J.Eich, "Advanced Recycle Methodology Program: Project Status Report," EPRI 118-1 (December 1975); R.D.Mosteller, et.al. "UO_2 and MO_2 Assembly Analysis: Collision Probability and Few-Group Diffusion Comparisons," Trans. Am. Nucl. Soc. 24, 443 (1976).
3. A. Jonsson, et.al., "Discrete Integral Transport Theory Extended to the Case with Surface Sources," Atomkernenergie, 24, 79-84,(1974).
4. A. Jonsson, et.al., "Integral Transport Theory with Cell Couplings Involving Arbitrarily Distributed Currents," Trans. Am. Nucl. Soc., 21, 231, (1975).

5. I. Carlvik, "Integral Transport Theory in One-dimensional Geometries," Nukleonik, 10, 104, (1967).

6. D. E. Kusner, et.al, "ETOG-1, A Fortran IV Program to Process Data from the ENDF/B File to the MUFT, GAM and ANISN Formats," WCAP-3845-1, (ENDF-114), (1969).

7. H. C. Honeck, D. R. Finch, "FLANGE-II, A Code to Process Thermal Neutron Data from an ENDF/B Tape," DP-1278, ENDF-152, (1971).

8. J. Adir, K. D. Lathrop, "Theory of Methods Used in the GGC-3 Multigroup Cross Section Code," GA-7156, (1967).

9. P. Kier, A. Robba, "RABBLE, A Program for Computation of Resonance Absorption in Multiregion Reactor Cells," ANL-7326, (1967).

10. R. J. Brissenden, C. Durston, "The Calculation of Neutron Spectra in the Doppler Region," Converence on the Application of Computing Methods to Reactor Proglems, ANL-7050. P. 51, (1965).

11. D. C. Leslie, et.al., "Improvements to the Theory of Resonance Escape in Heterogeneous Fuel,"
    I. Regular Arrays of Fuel Rods.
    Nucl. Sci. Eng. 22, 78, (1965)
    II. Dancoff Factor and Equivalence Theorem in Chapter-type Fuel.
    Nucl. Sci. Eng. 23, 82, (1965).

12. P. B. Kemshell, "Some Integral Properties of Nuclear Data Deduced from WIMS Analyses of Well Thermalized Uranium Lattices," AEEW-R786, (1972).

13. J. Hardy, Jr., et.al., "A Study of Physics Parameters in Several Water-moderated Lattices of Slightly Enriched and Natural Uranium," WAPD-TM-931, (1970).

14. R. Smith, G. Konzeh, "Clean Critical Experiment Benchmarks for Plutonium Recycle in LWR's," EPRI-NP-196, Vol. 1, (1976).

15. R. Persson, et.al., "High Temperature Critical Experiment with H_2O-moderated UO_2 Rod Lattices in KRITZ," Reactor Meeting of Deutsches Atomforum, Sektion 1, Paper 128, 1972.

16. O. Ozer, S. Fiarman, "ENDF/B-IV Eigenvalue Calculations for UO_2 and Mixed-Oxide Critical Lattice Experiments," Trans. Am. Nucl. Soc., 26, 596, (1977).

17. C. E. Wikdahl, et.al., "Studies of Single-Rod Lattices of UO_2, PuO_2 and ThO2 in Heavy Water," The Physics Problems in Thermal Reactor Design. Conference of the British Nuclear Energy Society, Proceedings, P 103, (1967).

18. S. Pearlstein, Editor, "Seminar on ^{238}U Resonance Capture," ENDF-217, (1975).

19. E. Hellstrand, "Measurement of Resonance Integrals," Am. Nucl. Soc. Topical Meeting Reactor Physics in the Resonance and Thermal Regions, Vol. II, P 151, (1966).

20. R. L. Hellens, et.al., "A comparative Analysis of Some Graphite and Water Moderator Reactor Lattices," The Physics Problems in Thermal Reactor Design. Conference of the British Nuclear Energy Society, Proceedings, P 27, (1967).

21. J. Hardy, Jr., "Monte Carlo Analyses of TRX Slightly Enriched Uranium - H_2O Critical Experiments with ENDF/B-IV and Related Data Sets," WAPD-TM-1307, (1977).

22. RSIC Computer Code Collection, "MORSE-CG", CCC-203, ORNL.

23. R. G. Soltesz, et.al., "Users Manual for the DOT-IIW Discrete Ordinates Transport Computer Code," WANL-TME-1982, (1968).

Section 18

LWR ASSEMBLY REACTION RATE REPRESENTATION

LWR Assembly Reaction Rate Representation

W. J. Eich
Electric Power Research Institute
Palo Alto, California

INTRODUCTION

As a consequence of both the realities of current reactor designs and also the resources available for their analyses, complex treatments have been developed for accuracy in reactor core simulation. In contrast, analysis of most critical experiments has generally required only the application of a subset of this general capability. The context of this review paper is the structure of codes and associated engineering procedures documented as the Advanced Recycle Methodology Program.[1,2,3,4] These codes and procedures have been adopted by a large (and an increasing) number of domestic utilities in order to simulate Light Water Reactor (LWR) cores.

The basic ARMP project was completed by Nuclear Associates International under the sponsorship of the Electric Power Research Institute (EPRI). The ARMP system is open-ended in the sense that development, as well as support, modification and benchmarking of codes and associated engineering continues, especially in the area of three-dimensional simulators. The engineering techniques in those physics codes which are the precursors to the core simulators, however, have achieved that degree of stability signifying the completion of basic development. These codes process the cross sections generated from the Evaluated Nuclear Data Files together with other information into various types and kinds of reaction rates crucial to LWR assembly analysis. The purpose of this paper is to explain some of the engineering techniques or models that have been evolved for the representation of these assembly reaction rates. In the course of this explication, it is hoped that some notion will be gained of the constraints on both the developers and also the utility users of ARMP who must optimize, to a certain stringent degree, various considerations of accuracy, time of preparation, computer power, etc.

The organization of this paper is as follows: the total ARMP code structure required for detailed analysis will be discussed; the particular codes pertinent to assembly reaction rates will be described in more detail; finally, the details of specific ARMP assembly reaction rate models will be presented.

GENERAL ARMP STRUCTURE

Introduction

A primary goal of the ARMP is to present U.S. Electric Utility Companies with the capability of generating a three-dimensional (nodal) simulation of a Light Water Reactor (LWR) core in the various configurations planned or encountered throughout mutlicycle operation. This capability encompases cores that contain not only UO_2 assembly designs but also the more complex Mixed Oxide (MO_2) designs.

The Primary Calculational Sequence

The interrelationship of the primary codes and the general flow of data through the system is discussed in this subsection. The four main sequence physics codes are briefly discussed below:

1. With due recognition of simplification in the explanation, EPRI-CELL may be said to treat a fuel rod or burnable poison in explicit cylindrical geometry; it approximates less exactly the surrounding environment. Various engineering modifications have been developed in the course of ARMP to improve this environmental approximation. Depletion of the fuel rod or burnable poison can be conducted and various depletion-dependent quantities can then be edited.
2. PDQ-7/HARMONY: PDQ-7, as generally used in ARMP, geometrically approximates a fuel assembly in X-Y geometry with the lattice components each homgenized in their respective cells. In terms of energy, the neutronics distribution and reaction rates are derived from a representation in 2 to 4 groups with the homogenized group constants derived from EPRI-CELL and various consistent parameterizations. The HARMONY code refers to the particular, highly flexible tabular general framework concomitant to PDQ whereby one represents the depletion dependence of the few group cross sections and the associated isotopic number densities.
3 and 4. EPRI-NODE-P and -B: These programs utilize the nodal approximations; i.e., at each of 12 axial positions, each assembly is approximated by a node or point. Associated with each node are a set of precalculated equations which account, in a fashion integrated with the global solution, for the local variations in assembly characteristics due to temperature effects, moderator density, depletion, etc. Given the input parameters for these equations, one has a powerful and cost-effective tool available for X-Y-Z LWR core simulation.

The interrelationship among the main sequence codes and the data processing modules is illustrated in Figure 1. This figure and the functions of the various processing modules will now be discussed. The letters A, B, C, D and E designate specific data transferred between the various modules. The three EPRI-CELL libraries are "fixed" input files for EPRI-CELL. EPRI-CELL produces few group cross-sections defined as data type A. These

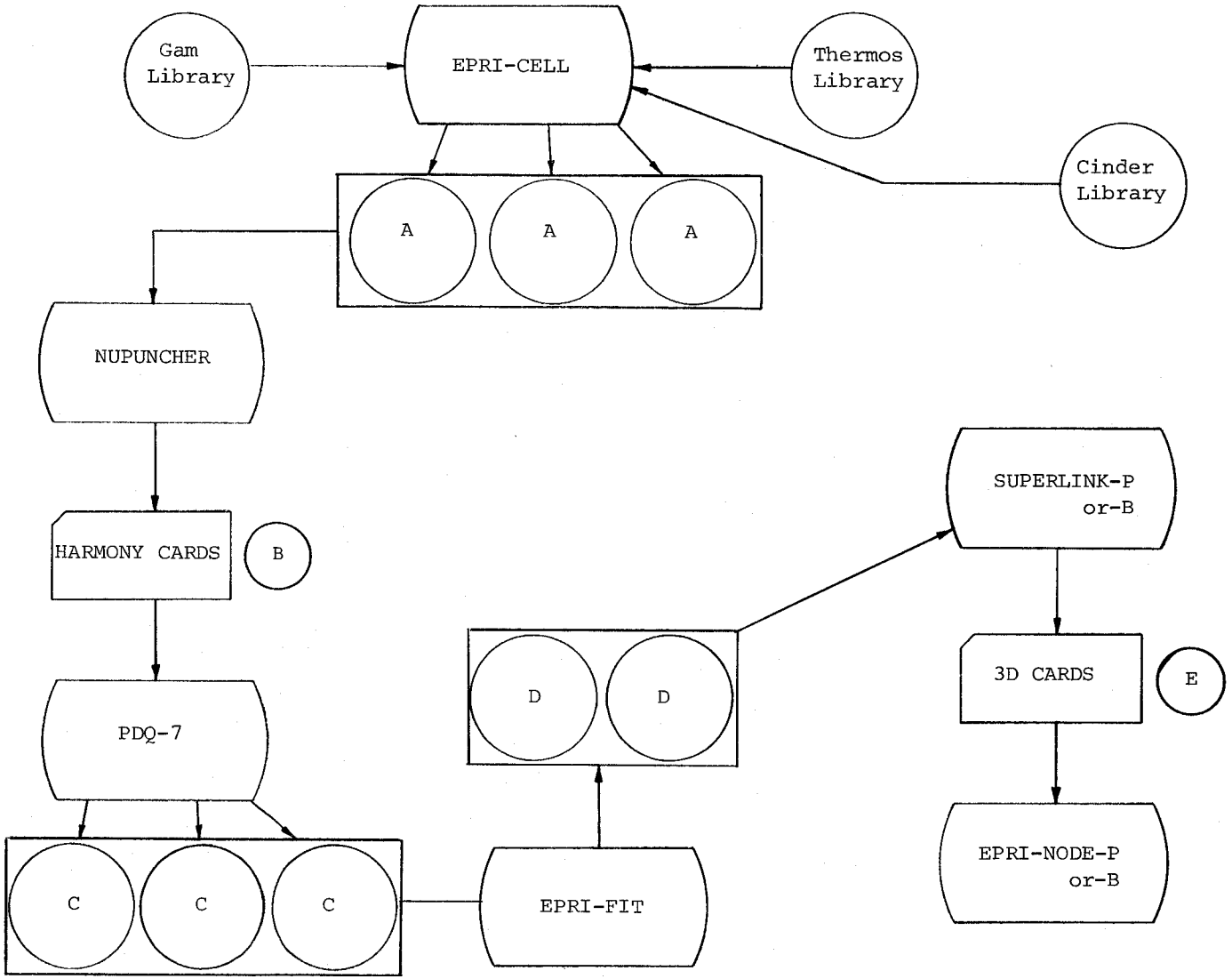

Figure 1 ARMP Main Sequence Codes

data are used by NUPUNCHER which processes the type A files and produces HARMONY cards, data type B, for input into PDQ-7. PDQ-7 creates the regular PDQ-7 integral files referred to here as data type C. The module EPRI-FIT processes the PDQ-7 integral files and produces the specific color files, data type D. Color is defined for PWR's as a particular combination of enrichment/ burnable poison type and complement characterizing an assembly; for BWR's, the term signifies an assembly type. SUPERLINK reads the color files, data type D, and produced fitted files (type E) for the three-dimensional core simulators, EPRI-NODE-P and -B.

Primary Auxiliary Codes

These six codes, originally developed as ancillary to the main sequence, are briefly described below:

1. EPRI-CPM, developed by AB Atomenergi (AE) acting as a subcontractor to NAI, is a multigroup transport code that constitutes a highly accurate calculational tool suitable for analyzing an LWR assembly with almost any kind of complexity. Because of its unique internal computational sequence, it essentially calculates a multigroup spectrum at each lattice location at each depletion step. Its analytic strength is such that, having been benchmarked against certain specific experimental configurations, one may with confidence regard its analysis of other similar configurations as constituting a benchmark or standard. One may then proceed, as has been done in this Program, in parameterizing simpler and less expensive methods so that the latter match the essential results of CPM.
2. MICBURN, also developed by AE, is a sequence auxiliary to CPM which solves the problem of depletion of a gadolinium-loaded fuel pin with an elegant time-dependent spatial solution.
3. EPRI-SHUFFLE is a program auxiliary to PDQ-7 which allows the rearrangement and/or replacement of individual fuel assemblies within a given array. Such a program is essential if PDQ-7 is used to simulate a PWR beyond the first cycle.
4 and 5. EPRI-THERM-P and -B are thermal-hydraulic codes capable of a macroscopic analysis of an entire core; THERM-P also can perform a detailed subchannel analysis. Part of the output of each code is required as input to the corresponding nodal code.
6. EPRI-LIBRARY refers to a set of environmental subroutines required by the ARMP programs. For IBM application, these routines must be assembled or compiled and then loaded into a library data set for linking with many ARMP codes.

PWR Calculational Flow

The primary purpose of the ARMP PWR sequence is to provide accurate parameterized data to the nodal code EPRI-NODE-P so that it may simulate the three-dimensional behavior of the actual core. These parameters include data characteristic of the full core and data unique to each fuel assembly type, or "color". A color is

defined as a unique combination of fuel enrichment and the number of burnable poison rods (BPR's) present for an assembly. The data for each color is extracted from two-dimensional PDQ-7/HARMONY "color set" calculations, a color set being the adjacent quadrants of four different assemblies. A color set, therefore, may contain up to four distinct colors, and a sufficient number of color set runs must be made to include each color which is present in the core. The input data for the color set calculations, in turn, is taken from separate EPRI-CELL calculations for each fuel pin enrichment and for each type of water hole included in the lattice. RCC element and BPR data for the color sets normally will be taken from the parameterizations described in Section 4 of this paper.

Figure 2 presents a flow chart for the ARMP calculational sequence. This chart shows the data processing codes (NUPUNCHER, EPRI-FIT, SUPERLINK-P) which prepare input for one code from the output of the previous code and also indicates where user interaction may be required.

BWR Calculational Flow

The primary purpose of the ARMP BWR sequence is to provide accurate parameterized data to the nodal code EPRI-NODE-B so that it may simulate the three-dimensional behavior of the actual core. These parameters include data characteristics of the full core and data unique to each fuel assembly type. The data for each assembly are extracted from two-dimensional PDQ-7/HARMONY assembly calculations. The input data for the assembly calculations, in turn, are taken from separate EPRI-CELL depletion calculations for each fuel pin enrichment type. These depletion sets are suitably modified by a very few data items taken from BOL EPRI-CELL calculations, e.g., for each enrichment/dancoff combination. The representation of gadolinia-loaded pins requires some extra cards to modify the normal HARMONY input for fuel pins of the same enrichment. These extra cards are generated from an auxiliary EPRI-CELL sequence described in Section 4 of this paper.

Figure 3 presents a flow chart for the ARMP calculational sequence. This chart shows the data processing codes (NUPUNCHER, EPRI-FIT, SUPERLINK-B) which prepare input for one code from the output of the previous code and also indicates where user interaction may be required.

Reprise

Figure 4 schematically indicates the basic relationships among the primary codes as originally predicated in ARMP. CPM stood outside the main automated sequence: an assembly analysis code to be used as a synthetic experiment. Its role was either to verify EPRI-CELL/PDQ/HARMONY procedures or to act as a source for parameterizing selected aspects of such procedures. It should be noted that user convenience has altered this picture so that today

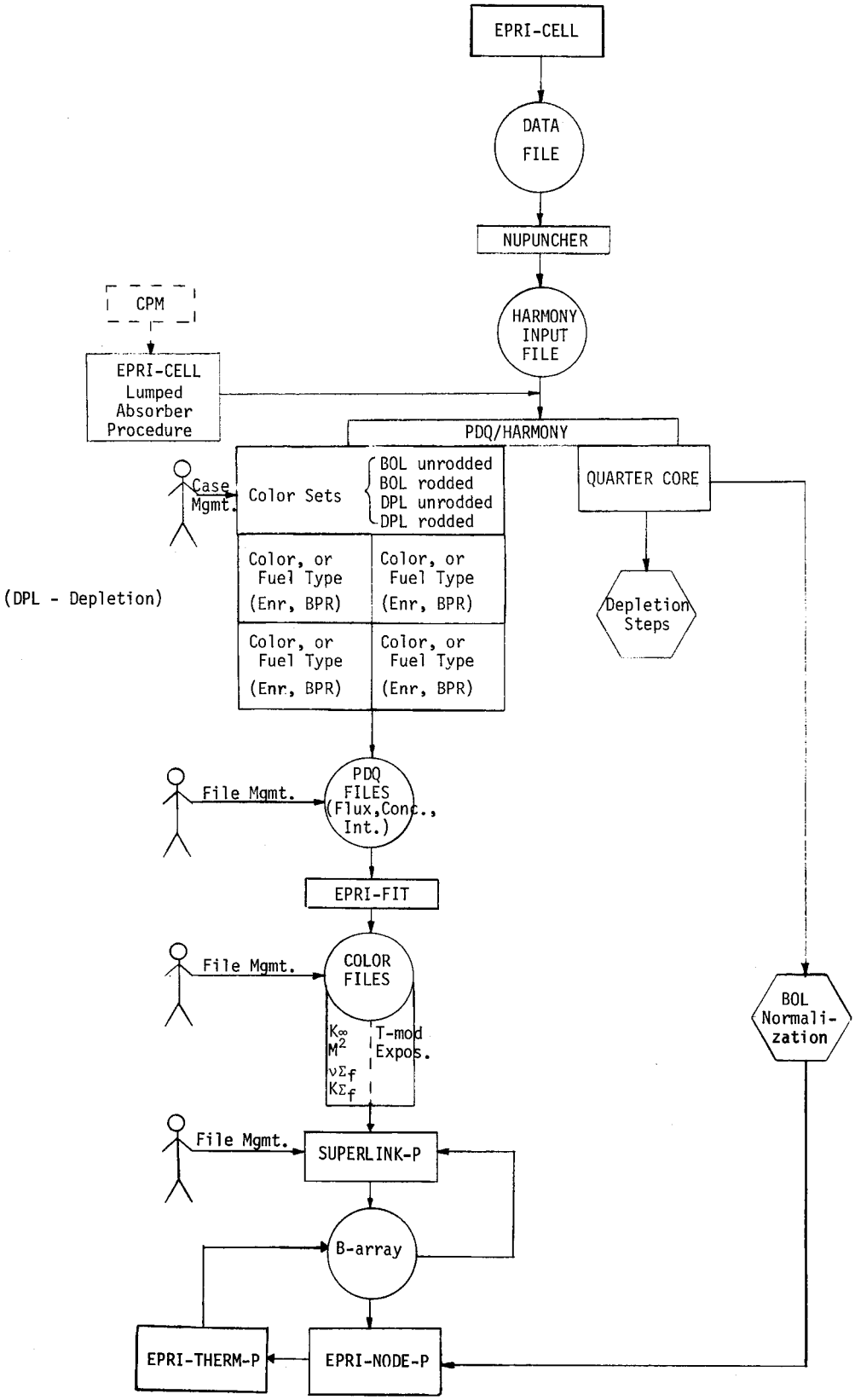

Figure 2 PWR Calculational Flow

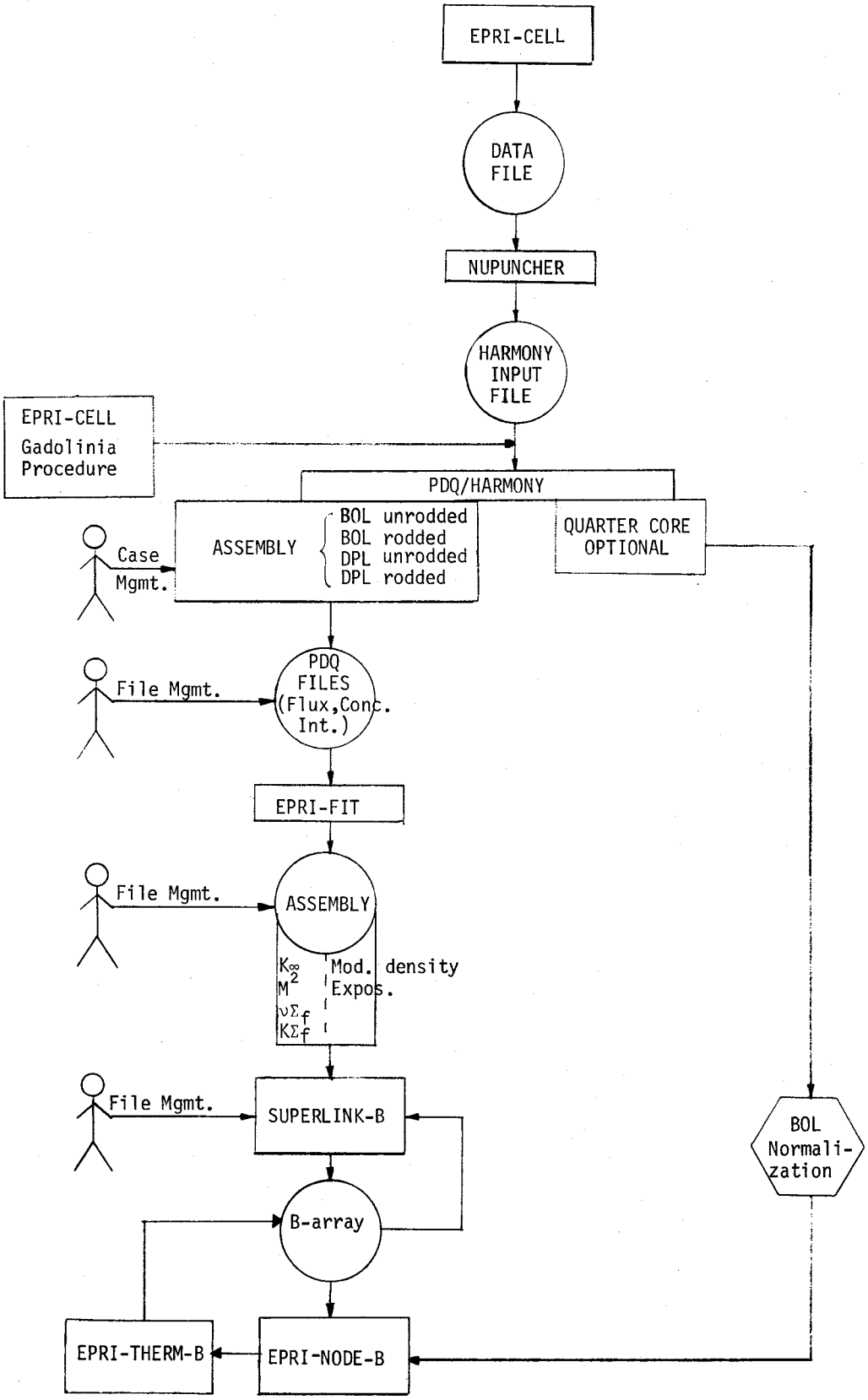

Figure 3 BWR Calculational Flow

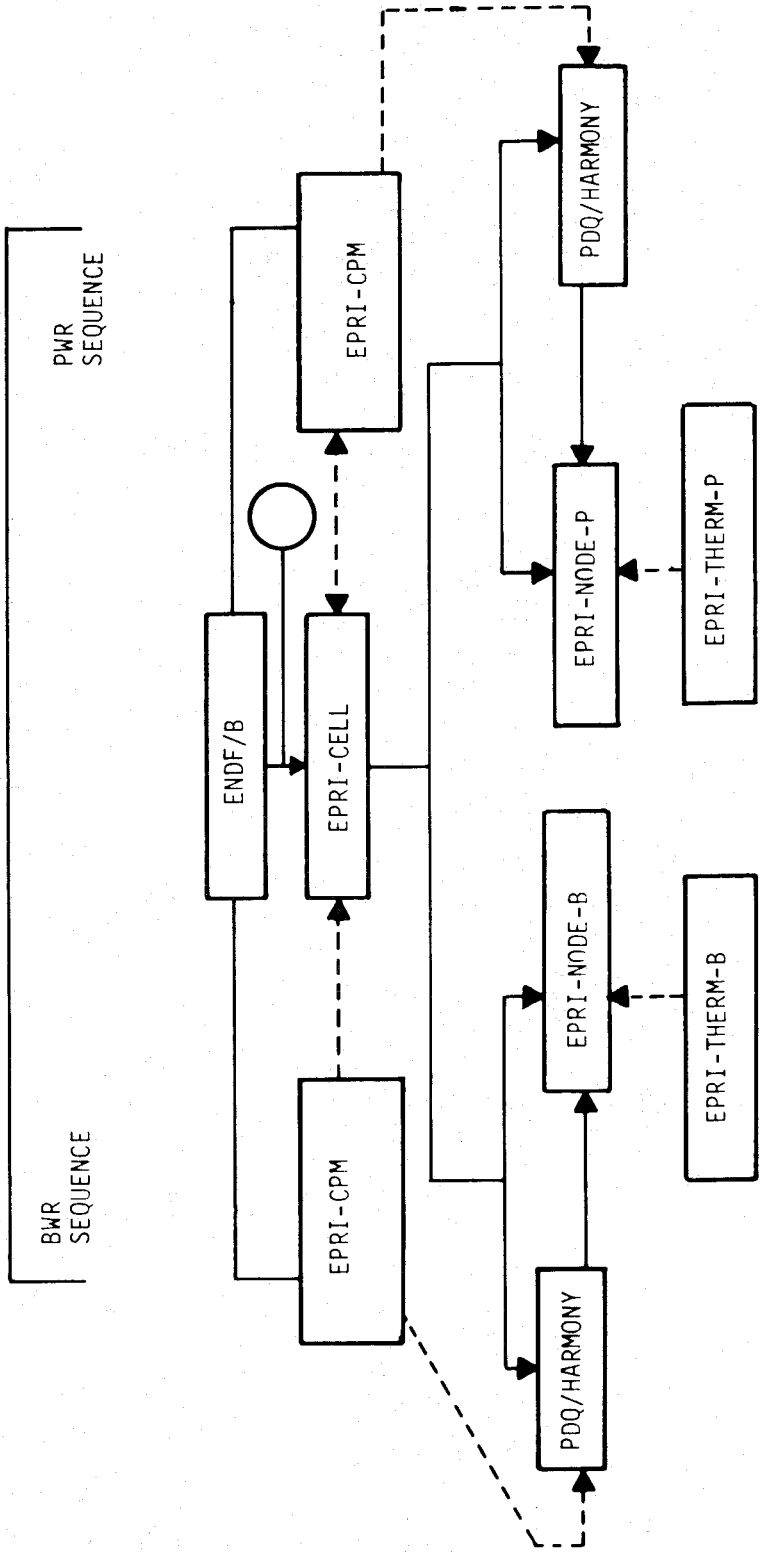

Figure 4 Main Calculational Sequence

the various BWR utility analysts are using CPM directly to provide input to EPRI-NODE-B. The EPRI-CELL/PDQ procedure is available, however, and can be used for certain applications outside the specialized capability of CPM. It is the relationships discovered and developed between CELL, CPM and PDQ that constitute Section 4 of this paper. Section 3, following, describes the three codes in somewhat greater detail.

CODES FOR ASSEMBLY ANALYSIS

EPRI-CELL

The three primary physics modules in EPRI-CELL consist of modified versions of the GAM, THERMOS and CINDER codes. Figure 5 schematically illustrates the calculational flow within EPRI-CELL.

The original GAM resonance treatment has been replaced in toto by an efficient parameterization of group-wise resonance integral shielding factors tabulated as functions both of effective potential scattering per absorber atom (σ_p^*) and also temperature. Heterogeneous fast effects are accounted for in EPRI-CELL by applying "advantage" factors to the GAM cross sections above 0.821 MeV. This prescription is based on intracell escape probabilities with a specially-derived effective chord length for the fuel region. GAM, essentially a point calculation, is superior to the well-known MUFT code in that it utilizes a general slowing down treatment.

The THERMOS portion of the code, however, consists of a specific spatial (cylindrical) treatment with up to 30 space points combined with a 35-group energy structure. Unlike the restrictive LASER version, the EPRI-CELL THERMOS is quite flexible in terms of space point designation and material placement within a maximum of 10 material zones and 30 space points. An analytic isotropic boundary condition has been installed which is a default in the engineering input version. A grain shielding treatment has been installed for the analysis of the particulate fuel.

One can represent a cylindrical lumped absorber surrounded by an annulus containing homogenized fuel. Typical configurations would be gadolinium-loaded fuel, B_4C in Al_2O_3, boron-loaded glass annuli, etc. Depletion of such absorbers can be conducted. This geometry consisting of a lumped cylindrical absorber and surrounding fuel environment is required in order to factor spectral and mesh effects into the ultimate PDQ assembly description.

Depletion within EPRI-CELL is conducted at each THERMOS space point so designated. A CINDER calculation is performed for each such point. The CINDER module contains 90 linear chains: 21 of these chains involving 116 nuclides account for the fuel, transuranic isotopes and burnable poisons which may be present in the calculation; the remaining chains determine the formation of 367 fission product nuclides.

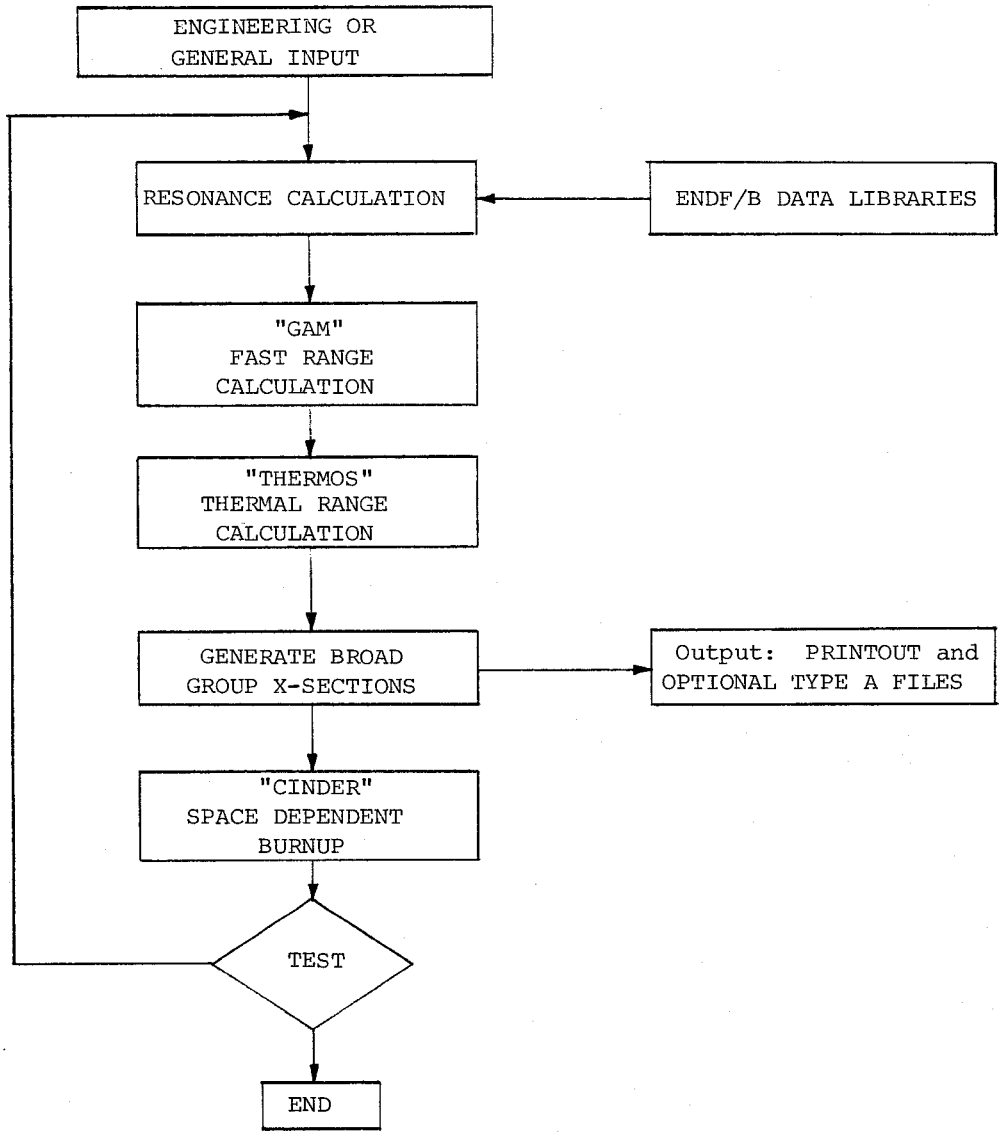

Figure 5 EPRI-CELL Flow Diagram

PDQ-7/HARMONY

The PDQ-7 program solves neutron diffusion problems in one, two, or three dimensions in rectangular, cylindrical or spherical geometries. Up to five energy groups are permitted and thermal groups can be represented as a pair of overlapping groups. The associated HARMONY program provides a flexible representation of time-dependent cross sections and a general format for specification of nuclide chains.

In PDQ-7, for an initial description of the reactor (geometry and material description), the neutron flux distribution for neutrons in several energy groups is obtained at discrete spatial mesh points in the reactor and surrounding reflector regions. In the solution of the spatial problem, either an eigenvalue, which is a measure of the closeness of the described reactor to criticality, is found or some parameter (poison, buckling, control rod position) is varied to yield neutron balance. The spatial flux is combined with the material inventory and nuclear cross sections to obtain the power distribution.

Once the spatial flux and power distributions have been obtained, the second step in diffusion-depletion programs is to simulate reactor operation during a specified time interval. Using the power normalized flux from the spatial calculation, the differential equations describing the time behavior of the nuclide concentrations are solved for that time interval. The solution yields a new distribution of nuclide concentrations in the reactor which are used in the generation of few-group macroscopic cross sections for the next spatial calculation.

In this Program, the preparation of the input to HARMONY has been greatly expedited by the creation of the default depletion chains and default cross section tables. Furthermore, for the purposes to which PDQ/HARMONY has been directed in this Program, one-dimensional tables are completely adequate, thus greatly minimizing associated computer costs. Finally, deviations from these default tables are easily specified should such be desired by a user.

The individual using PDQ-7 in the ARMP mode need only run X-Y problems in two to four groups. These X-Y problems will generally be individual BWR assemblies or (simultaneous) four quadrant representations of adjacent PWR assemblies. Implicit in the overall procedure is normalization to or verification by the more exact CPM code.

CPM

EPRI-CPM, developed by AB Atomenergi, is a multigroup two-dimensional collision probability code which can analyze, with all their heterogeneities, the complex geometry of PWR and BWR assemblies. Its power is such that it has been used in this program as a synthetic experiment against which PDQ assembly analyses have been compared and verified. This process of PDQ verification has

required the prior parameterization of some specific assembly reaction rates to those determined by CPM.

CPM encompasses lattice and non-fuel specifications of very general flexibility, some of which utilize engineering subroutines which are generally incorporated within the sequence. For example, one may specify cylindrical fuel rods of varying composition in a square pitch array, an assembly can, fuel rods loaded with burnable poison, poison rods within the lattice, BWR water slots and cruciform absorber blades in the regions separating fuel assemblies, in-core instrument channels, boron steel curtains, etc.

The flow sequence within CPM including the relationship of MICBURN is schematically illustrated in Figure 6. Figure 7 schematically illustrates the two basic types of microgroup calculations performed at the front end of CPM. Figure 8 provides, for a specific example, the geometric relationship between the optional second stage depicted in Figure 6, the macro group calculation, and the actual X-Y BWR recycle assembly configuration. Figure 9 shows the geometric detail permissible in the final rectilinear calculation.

In each step in the overall automated procedure, energy groups are collapsed sequentially as spatial detail is increased and made to correspond more closely to reality. The two annular macro calculations, distinguished principally by water gap widths, are edited and logically combined to account for the actual proximity of each pin to each type of gap. Further, if a control rod is inserted, it is represented in the wide gap run. Accordingly, the two sets of 25 group spectra corresponding to a particular rod type (a given annular or central region) are weighted differently for each rod location within a given X-Y array. These various spectra are then edited down to the 4 to 12 group parameters required in the final explicit X-Y calculation.

For the 2D-treatment in CPM, a multigroup integral transport routine based on the method of collision probabilities is used. The collision probabilities are evaluated in two-dimensional Cartesian geometry (x-y geometry). Sets of equidistant parallel lines are superimposed on the grid comprising the physical description of the assembly at a number of equally spaced angles - see Figure 10. The lines are reflected at the boundary a number of times, sufficient to allow the neutrons to be tracked a specified optical length. The accuracy of the collision probabilities is determined by the number of integration lines, the number of integration directions and the optical distance the neutrons are followed after reflection.

The resonance treatment is generally similar to that of EPRI-CELL, both programs having modeled this aspect of core physics against the WIMS (British) technology. Also, the final rectilinear calculation includes energy breakpoints consistent with the few-group EPRI-CELL/PDQ runs. Thus, the few-group PDQ input, which is to be corrected, will be completely consistent with the few-group reaction rate edits from CPM. Since EPRI-CELL and CPM

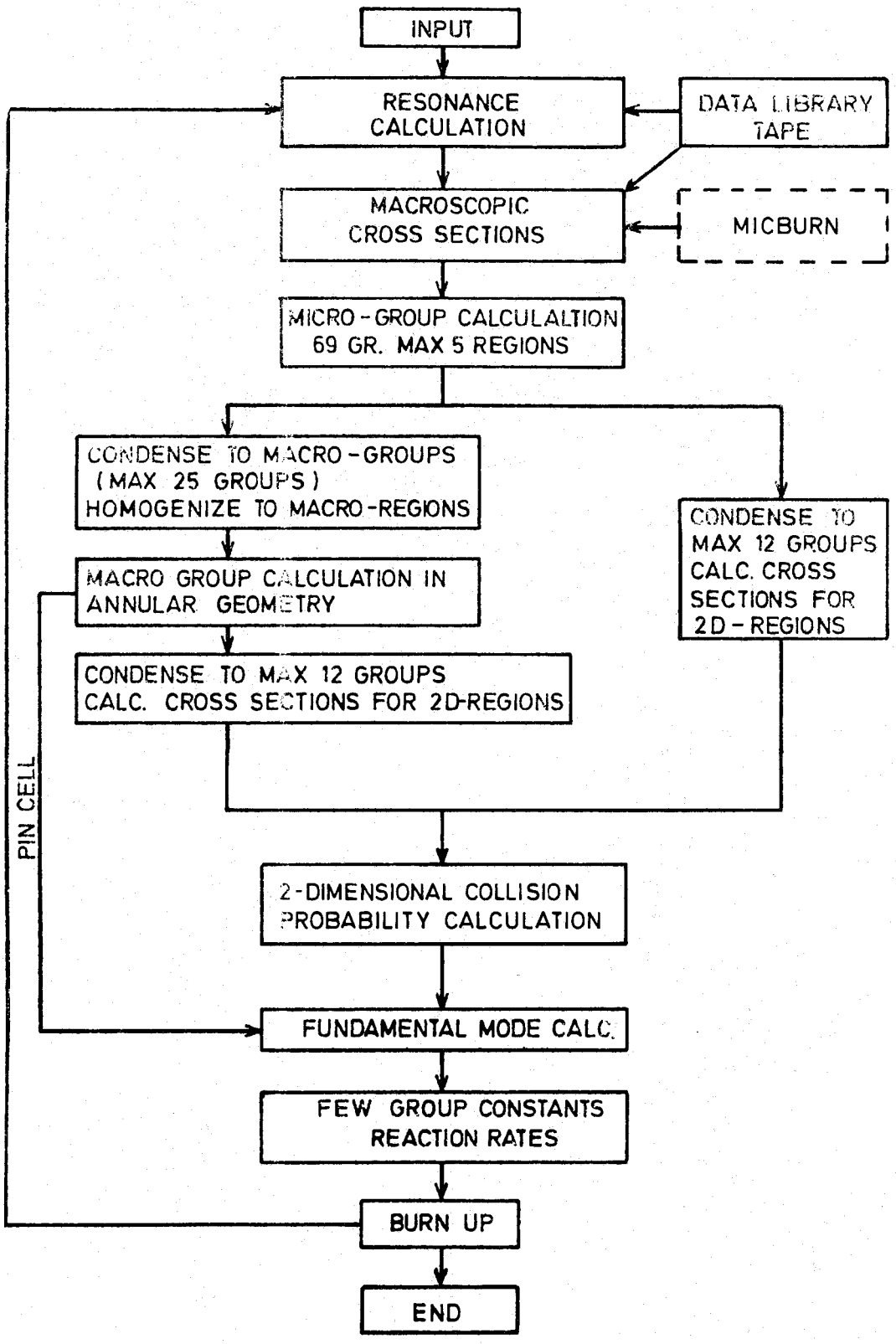

Figure 6 Flow Diagram of CPM

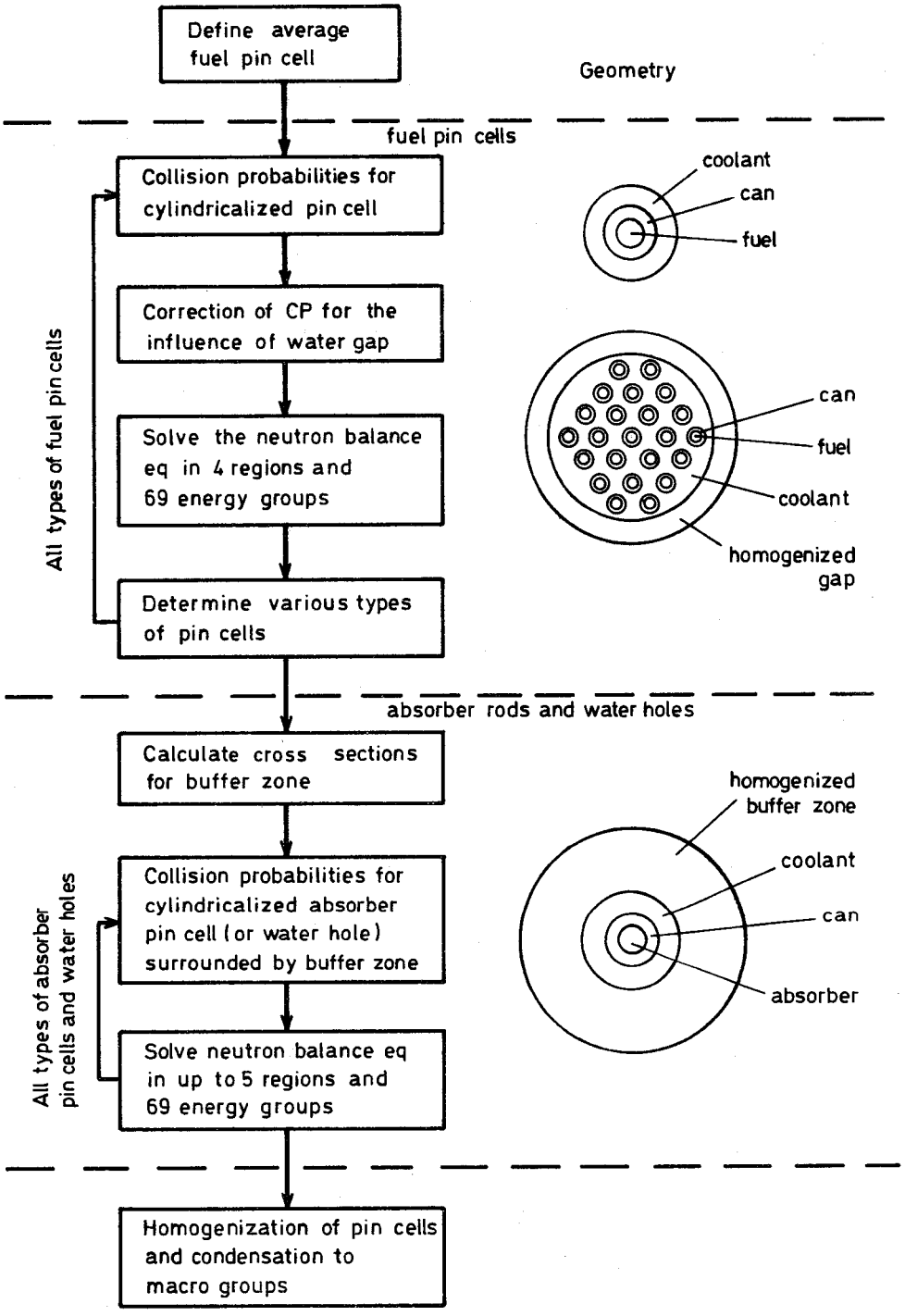

Figure 7 Flow Chart of Micro Group Calculation

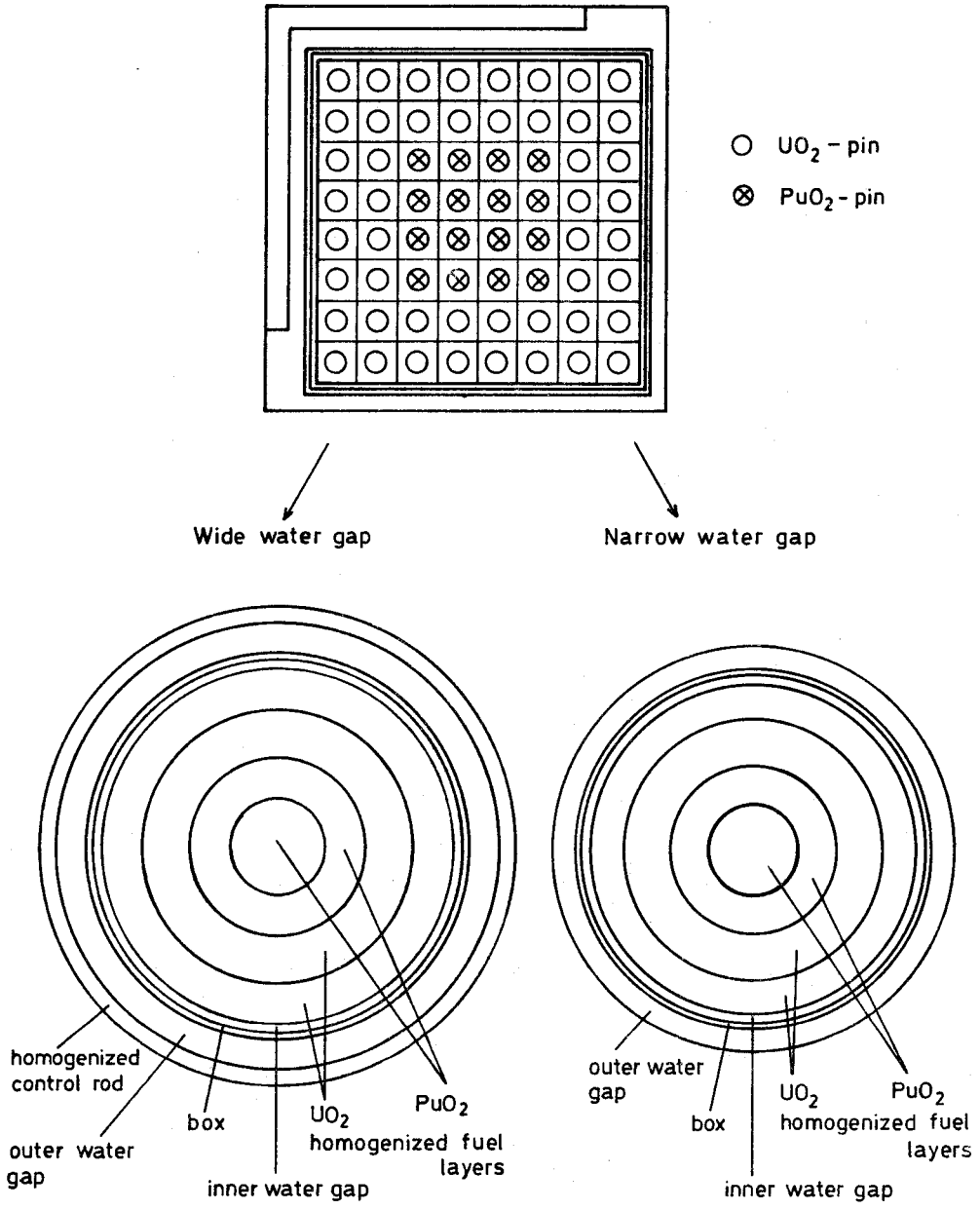

Figure 8 Example of Geometry in Macro Group Calculation

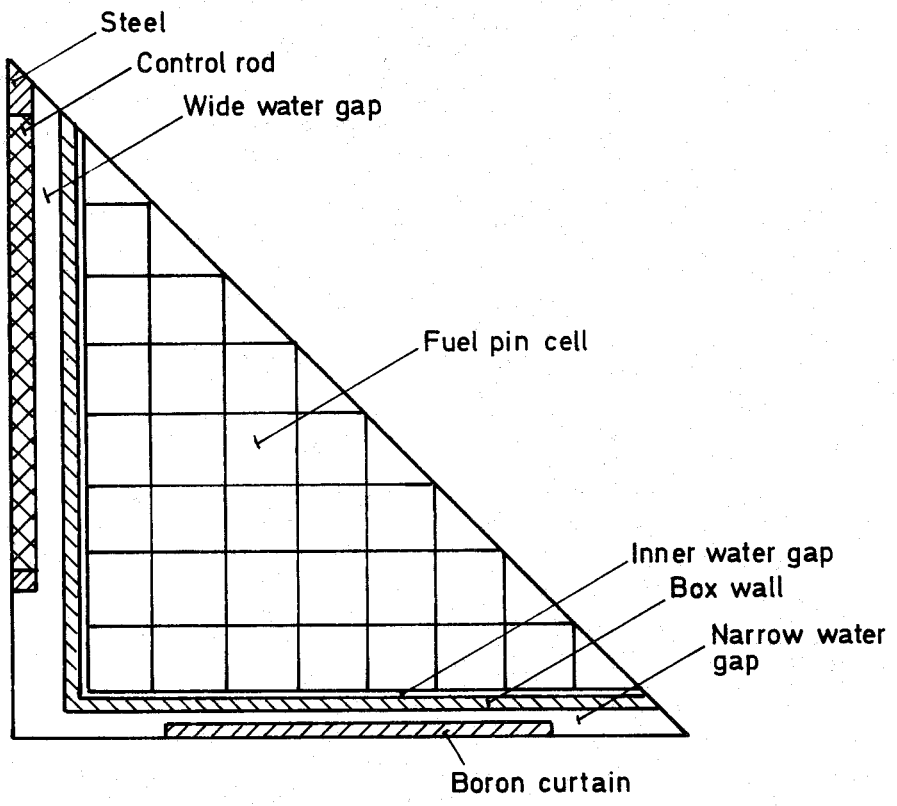

Figure 9 Example of BWR Cell Geometry in the 2D Calculation

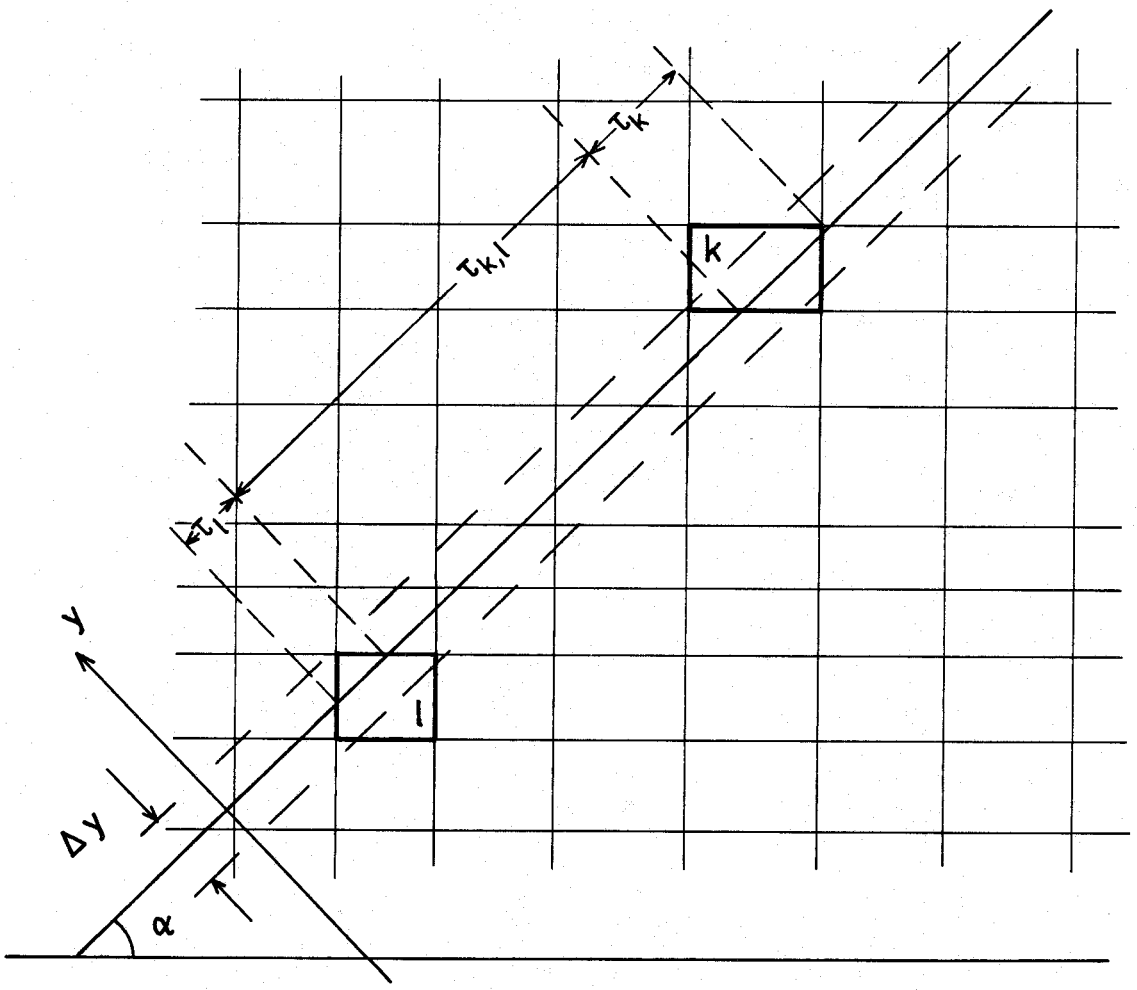

Figure 10 Calculation of Collision Probabilities

derive their basic data from the ENDF/B file, and because the two codes agree in the limit of application to an infinite lattice (by virtue of a prior EPRI-CELL/CPM unit-cell-equivalent normalization), the differing multigroup structure between CPM (69) and EPRI-CELL (97) presents no practical problems.

ASSEMBLY REACTION RATE MODELS

PWR Assemblies

Assemblies with Water Holes. A default path in the NUPUNCHER code produces HARMONY input from EPRI-CELL in an efficient mode. This procedure generates depletion-dependent microscopic and macroscopic constants. In combination with a cost-effective approach emplying two neutron groups and one mesh space per lattice cell location, the Ginna reactor has been modeled and the results have been tested against corresponding results from CPM. The model also utilizes a simple, infinite medium calculation for the water hole spectrum calculation. Mixed Number Density thermal cross sections are used; the main advantage in this application is the reduction of numerous depletion-dependent cross sections to values that are constant or almost constant with depletion.

Figures 11 and 12 provide radial plane power profiles in an assembly quadrant at two extremes of moderator boron concentration. It is of interest to observe that slight quantitative corrections to the PDQ eigenvalues at these extremes are quantitatively identical to corrections one might calculate using diffusion theory: four group, fine mesh equivalent PDQ runs.

Figure 13 shows the good agreement in reactivity between CPM and PDQ with depletion of this assembly. The PDQ incorporates a $0.25\%\Delta\rho$ increase in xenon worth relative to that obtained with unmodified EPRI-CELL input. This has been traced to differences in the nonuniform spatial xenon distribution between CPM and PDQ: identical flat xenon distributions input to both codes produce the same worth. Utility users have observed that this xenon correction decreases with increasing homogeneity of the lattice, e.g., 17 by 17 arrays.

Good agreement in isotopics between CPM and PDQ depletion runs has also been observed. One refinement developed in the course of achieving this agreement is worth noting. Comparisons between CPM and EPRI-CELL runs have shown that the supercell approximation, as employed in EPRI-CELL and other codes, is an excellent overall approximation to a PWR assembly. By comparisons with CPM, however, it has become clear that the extra region of the supercell produces fluxes that disproportionately weight the reaction rate of the 1 ev Pu-240 resonance. This overestimation, slight in PWRs, has been corrected in the CINDER portion of EPRI-CELL and in HARMONY through the incorporation of a multiplication factor, slightly less than unity, operating on the epithermal Pu-240 reaction rate.

.960 .948						
.971 .963	.994 .995					
.987 .984	1.031 1.033	WATER HOLE				
1.010 1.016	1.051 1.060	1.057 1.072	1.039 1.056			
1.031 1.032	WATER HOLE	1.041 1.047	1.035 1.042	WATER HOLE		
.997 .999	1.017 1.016	.998 1.002	.996 1.000	1.009 1.008	.978 .980	
.971 .963	.972 .966	.971 .963	.976 .962	.966 .961	.958 .951	.950 .940

	CPM	EPRI-CELL/PDQ
k_{eff}	1.07809	1.07666
k_{∞}	1.10013	1.09924
M^2	49.66	51.49

CPM

EPRI-CELL/PDQ

Figure 11 Relative Power Distribution in Quarter Assembly HZP, 1610 PPM

.955 .940						
.969 .958	.994 .996					
.988 .985	1.035 1.040	WATER HOLE				
1.013 1.022	1.059 1.072	1.066 1.085	1.046 1.068			
1.035 1.039	WATER HOLE	1.046 1.056	1.039 1.049	WATER HOLE		
.997 .999	1.019 1.018	.998 1.003	.996 .999	1.008 1.006	.974 .973	
.967 .957	.969 .961	.967 .957	.964 .954	.961 .952	.951 .938	.941 .926

	CPM	EPRI-CELL/PDQ
k_{eff}	1.28864	1.28491
k_{∞}	1.31476	1.31279
M^2	52.37	53.27

CPM

EPRI-CELL/PDQ

Figure 12 Relative Power Distribution in Quarter Assembly HZP, No Soluble Boron

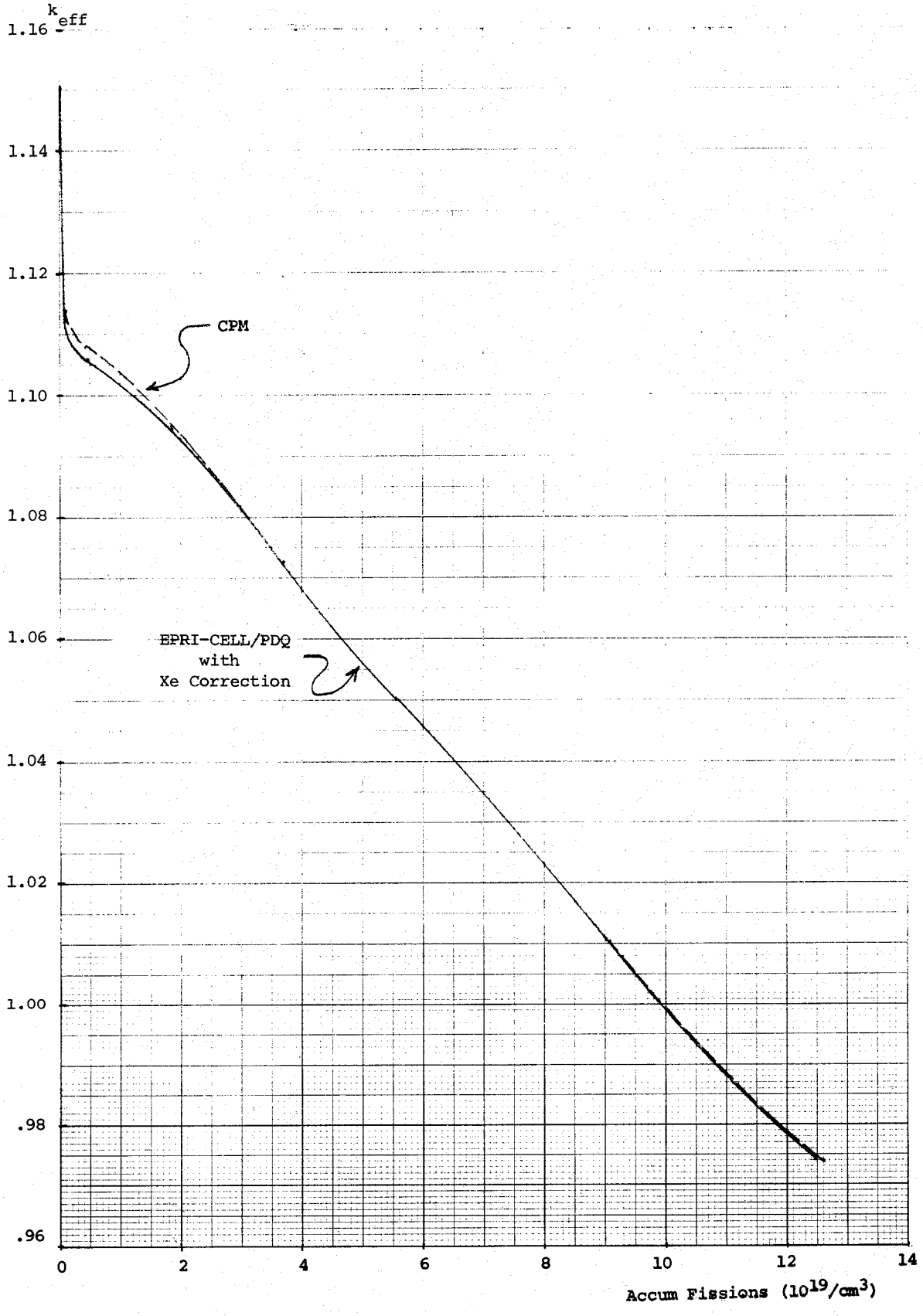

Figure 13 Assembly Multiplication Factor, 16 Water Holes

Of considerably greater importance in considerations involving the cell edit of the supercell is that particular technique dubbed the Improved Removal Treatment (IRT). Consider two applications that specify the proper functional form for a macroscopic removal cross section:

1. Given a homogeneous (point) epithermal calculation corresponding to a given geometric description, as in the GAM portion of EPRI-CELL, how does one determine the removal cross section for a subregion, i.e., for a number density mix corresponding to a geometric subdivision of the overall geometry on which this spectrum calculation is based?
2. Given a set of isotopic cross sections input to HARMONY based on a depletion sequence of EPRI-CELL output, by what mechanism are accurate macroscopic removal cross sections determined in the spatial PDQ for number density mixes not specifically calculated in the prior EPRI-CELL run, i.e., how does one obtain within the PDQ framework the equivalent of the results of EPRI-CELL depletion calculations reflecting the local lattice cell fast-to-thermal flux ratio instead of the (supercell) average?

In earlier cells codes using continuous slowing down theory, a so-called differential removal cross section was determined by repeating the spectrum calculation with one isotopic number density increased, usually by 10%. The change in macroscopic removal divided by the change in the number density defined a microscopic removal for the changed isotope. This procedure was repeated for each isotope in the mix and was thus time-consuming. It resulted in negative removal cross sections for isotopes having significant resonance absorption, thus providing unrealistic results in the limit of highly voided cells. The linear functional relationship was also improper. Finally, the validity of the calculated values of removal was severely restricted to number density mixes quite close to the original set.

By employing the GAM-1 integral slowing down theory in EPRI-CELL, microscopic removal cross sections may be obtained by straightforward weighting of the group-to-group scattering matrices. Thus, question one above poses no practical problem. Question two, however, is not resolved by the use of GAM-1 microscopic removals since they cannot represent the decrease in macroscopic removal which necessarily results, with depletion, from an increase in resonance group absorption without recomputation of the microgroup spectrum. For this reason, a method developed for use with continuous slowing down codes has been implemented.

The improved removal treatment (IRT) can be elucidated by citing results of Greuling and Goertzel. Although their method for treating resonance capture has been termed obsolete, the functional basis for the IRT is shown below by abstracting from the Greuling and Goertzel approach. Since IRT is applied to edited few group quantities in which the resonance capture has been smoothed and averaged, the functional relationship among moderating ratio, absorption and removal is quite valid and appropriate even though the original application to resonance escape

for slowly varying capture has passed into obsolescence. Note that the averaging of the capture corresponding to a single resonance in EPRI-CELL is performed over as many microgroups as necessary; this is in contradistinction to the coarser MUFT treatment in which resonance capture is a nonescape probability associated with a single microgroup.

With the usual terminology,

$$p\ (E) = \exp\left(- \int_{E}^{E_0} \frac{\Sigma_a}{\xi\Sigma_s + \gamma\Sigma_a} \frac{dE'}{E'} \right) \tag{1}$$

or

$$p(u_1,u_0) = \exp\left(- \int_{u_0}^{u_1} \frac{\Sigma_a\ (u)}{\xi\Sigma_s\ (u) + \gamma\Sigma_a} \, du \right) \tag{2}$$

The denominator in (2) is well approximated by a group-averaged $\xi\Sigma_s$, the numerator is replaced by the group-averaged cross section times the lethargy width, u, and p is replaced by its equivalent in few group macroscopic cross sections, $\frac{\Sigma_R}{\Sigma_R + \Sigma_a}$.

Accordingly

$$\Sigma_R = \frac{\Sigma_a}{\exp \frac{\Sigma_a \times \Delta u}{\xi\Sigma_s} - 1} \tag{3}$$

Microscopic absorption cross sections, σ_{ai}, are determined for each isotope i in the usual GAM calculation. Microscopic values of the slowing down power, $\xi\sigma_{si}$, are also averaged for each isotope i using the same GAM spectrum. The value of $\xi\sigma_s$ for hydrogen is modified slightly (to the order of 1 or 2%) so that equation (3) is exact in terms of the overall supercell edited values of Σ_a and Σ_R. This set of $\xi\sigma_{si}/\Delta u$, including the modified hydrogen value, is then used in conjunction with the microscopic σ_{ai} and equation (3) in the generation of Σ_a, Σ_R for subregions (number density subsets). The most important application of IRT directly in EPRI-CELL is the specification of the cell removal edits from a supercell (pin-cell plus extra region) calculation. By factoring eq. (3) into HARMONY and entering $\xi\sigma_{si}/\Delta u$ instead of σ_{ri}, removal cross sections are calculated for use in PDQ-7 which show the proper functional variation with local absorption.

The IRT approach shows promise in an important third application. Core simulators utilizing assembly-averaged two-group input cross sections instead of ΔK or $\Delta\rho$ input are receiving more attention. Such simulators are promising candidates for adoption, especially for BWR analysis. It has been noted in this connection that the removal cross section presents special problems in its representation. The reconstruction of removal using the IRT approach might have substantial potential in simplifying the input as a function of void level, depletion, doppler, etc.

Assemblies with Control Elements. A simple procedure for developing the representation of silver-indium-cadmium cluster control elements has been incorporated in the ARMP documentation. This method is a modification and extension to cylindrical elements of Bettis procedures summarized by Henry. It had, however, been tested against experimental PWR data in which moderator boron had been substituted as rod cluster groups (up to a worth of approximately 4.5% $\Delta\rho$) were fully inserted under hot, zero power conditions.

Confidence in this particular procedure as well as the other engineering techniques in which the cluster representation was imbedded led to the realization of the presence of a 7 to 11% worth overestimate for various cylindrical absorbers in CPM. The problem was traced to the spatial condensation procedure for lumped absorbers. EPRI extended the development of CPM to include a version that retained the cylindrical geometry in the final two-dimensional calculations of both fuel and absorbers occupying lattice positions and also authorized the development of an improved lumped absorber treatment for the homogeneous version of CPM. The net result of all the foregoing has been a substantial reinforcement of confidence in the results achieved using the standard (homogeneous) CPM with the cylindrical absorber treatment modified as discussed below.

Geometry A in Figure 14 depicts the original treatment by cylindrical lumped absorbers at the microgroup level of the CPM calculation. The buffer zone is 2.5 m.f.p. thick at the highest energy group below 0.625 ev; it contains flux and volume averaged cross sections corresponding to the average fuel cell. In the original procedure, the absorber cell cross sections were simply flux and volume weighted after the 69 group calculation; these cross sections were then collapsed to the group structure of the next stage of the calculation. The revised procedure involves an explicit microgroup recalculation, before group collapsing, in the Geometry B of Figure 14. Volume weighted fluxes corresponding to both geometries, collapsed to the (final) group structure of the 2-D calculation, are stored as ratios. The 2-D calculation is performed using the flux-volume homogenized cross sections stemming ultimately from the Geometry A calculations. Before determining reactivity, burnup, etc., however, the reaction rates calculated for the absorber cells in the 2-D calculation are scaled by those group-wise correction factors stored as the above-

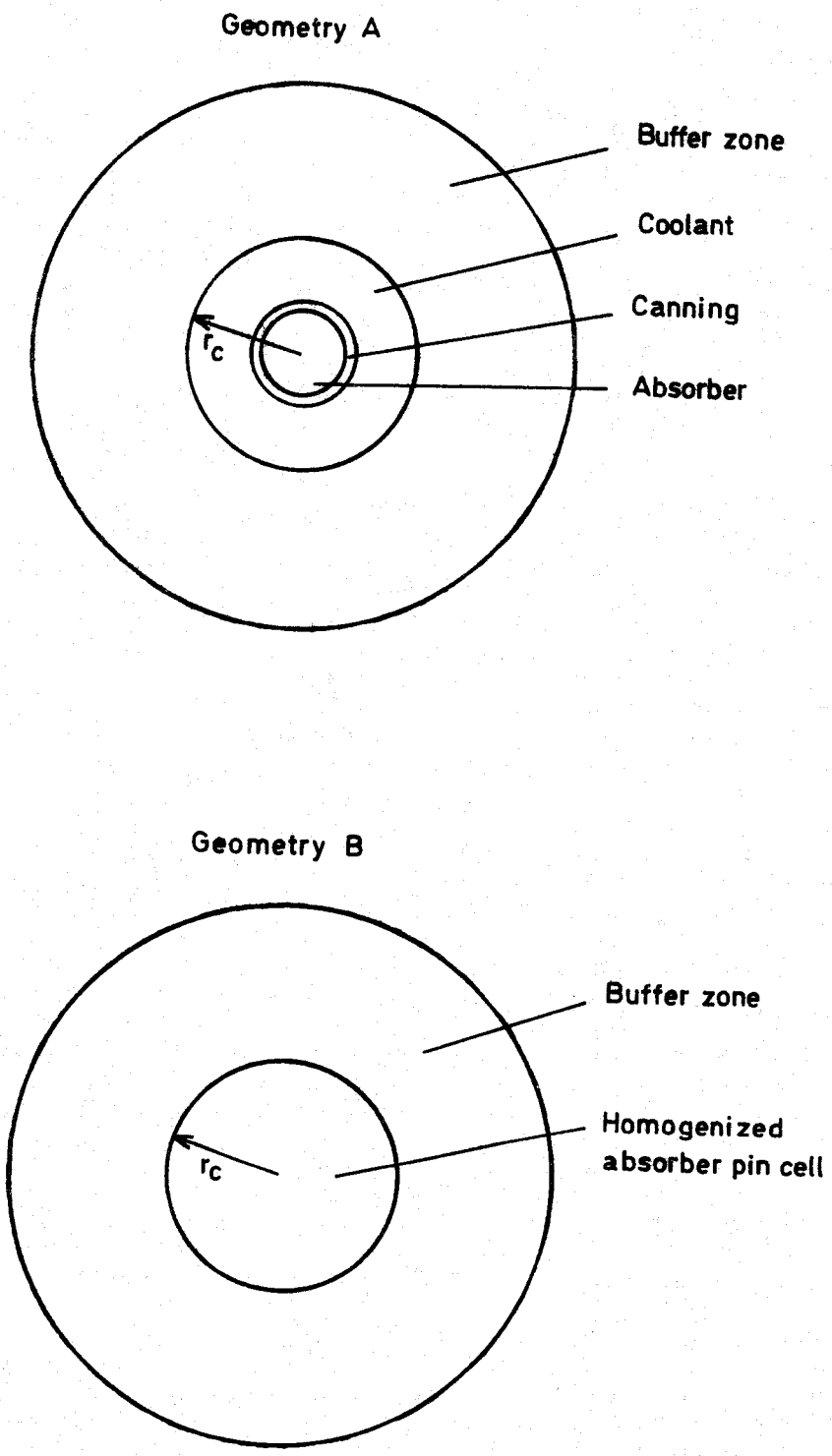

Figure 14 Geometries in the Absorber Pin Cell Calculation

mentioned ratios.

Assemblies with Burnable Poison Rods. The burnable poison rods (BPRs) utilized in the first core of the Ginna reactor were represented in PDQ/HARMONY by a parameterization of CPM quadrant assembly results. In the course of this parameterization, PDQ/HARMONY quadrant assembly depletion was performed in parallel fashion to this CPM. The fuel lattice constants and the so-called residual (i.e., boron free) representation of the homogenized BPR cell were taken from appropriate EPRI-CELL output.

Initially, macroscopic absorption cross sections for the BPR cell were found which matched the HZP BPR worth and fast-to-thermal absorption ratio from CPM. This was an iterative procedure, of course, but satisfactory cross sections were found after only a few PDQ runs. Thereafter, the cross sections were decomposed, on a straightforward basis, into three parts: B-10 in the BPR, soluble B-10 in the moderator of the BPR cell, and the balance of the cell contents or the residual component. The B-10 cross sections for the BPR at full depletion were taken to be the unshielded values; the cross sections at intermediate values of burnup were determined through iterative PDQ/HARMONY calculations at steps of increasing depletion. This procedure resulted in the curve of Figure 15 showing the shielded cross section variation versus fraction of B-10 remaining in the BPR. Figure 16 shows the relative worth between PDQ and CPM runs in which every thimble location was occupied by a BPR. Clearly, errors in the value of multiplication attributable to the PDQ representation of BPRs, computed for a full core with a realistic BPR complement, would be lower by a factor of three. Figures 17 and 18 provide further comparisons between the CPM and PDQ quadrant assembly runs. It is clear that the parameterization is most accurate in terms of the most important parameter, the BPR worth.

It was desirable to generalize this work so that it could be applied to BPRs without replicating the iterative PDQ/HARMONY/CPM calculations. In fact, a simple procedure involving only a BOL EPRI-CELL and an elementary one-group, fixed-source PDQ has been developed which utilizes selected results from the initial parameterization described above. This approach will now be outlined.

The requisite EPRI-CELL is run in a configuration similar to the Geometry A of Figure 14. EPRI-CELL, unlike the microgroup calculation of CPM, does allow preservation of true annular absorber geometry, if appropriate, in the thermal part of the calculation. An edit providing the ratio of absorber cell to supercell thermal absorption reaction rates has been added. A one-group, fixed-source rectilinear PDQ with two region geometry corresponding to the absorber cell and the buffer region is required. The mesh of the PDQ is identical to that which is to be used in quadrant assembly calculations; the buffer thermal constants are edited in to the appropriate region; several cases are run in a stack varying the absorption of the central region. That value which reproduces the cell/supercell reaction rate

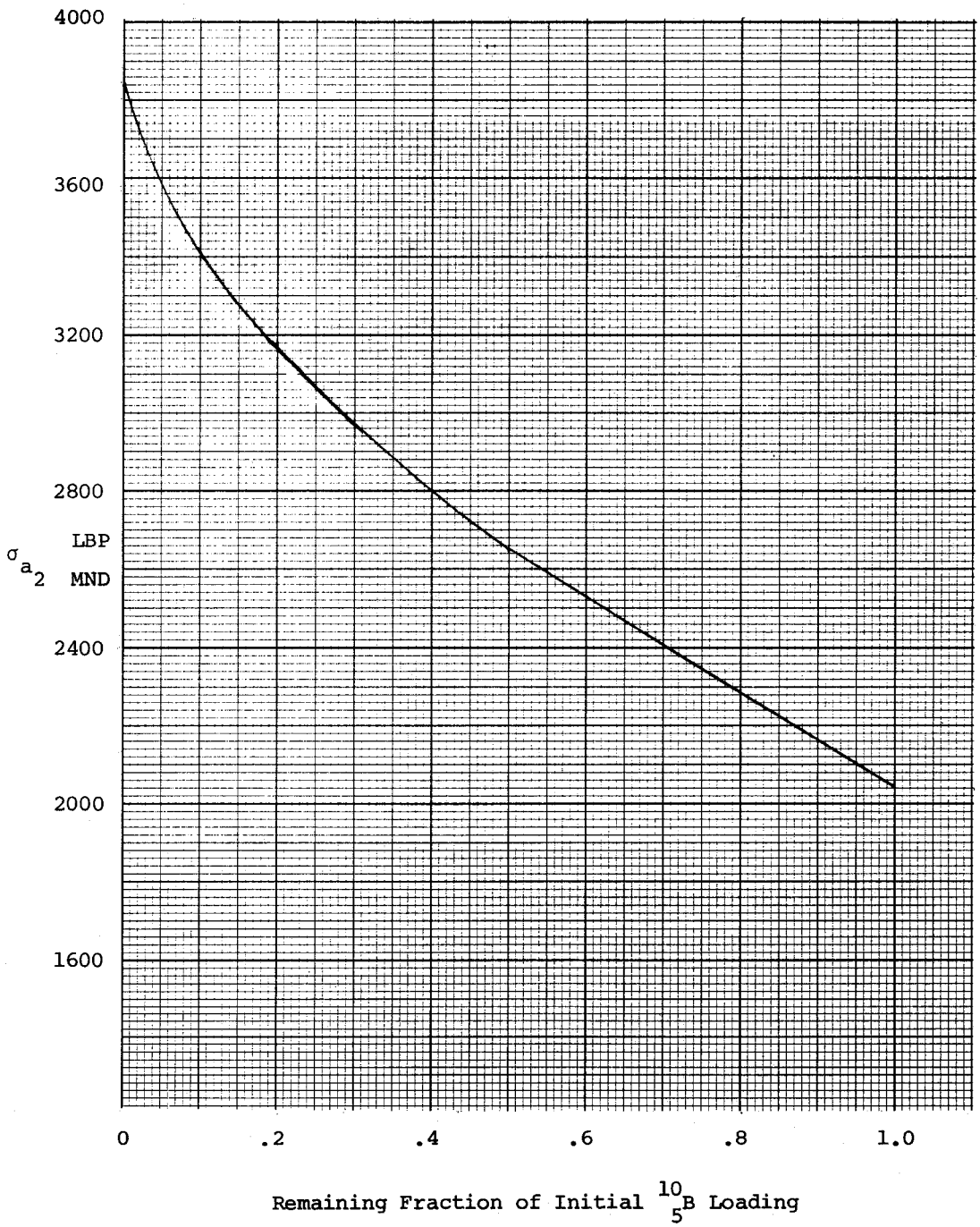

Figure 15 Microscopic MND Thermal Absorption (barns) for B-10 in LBP Cell

18-27

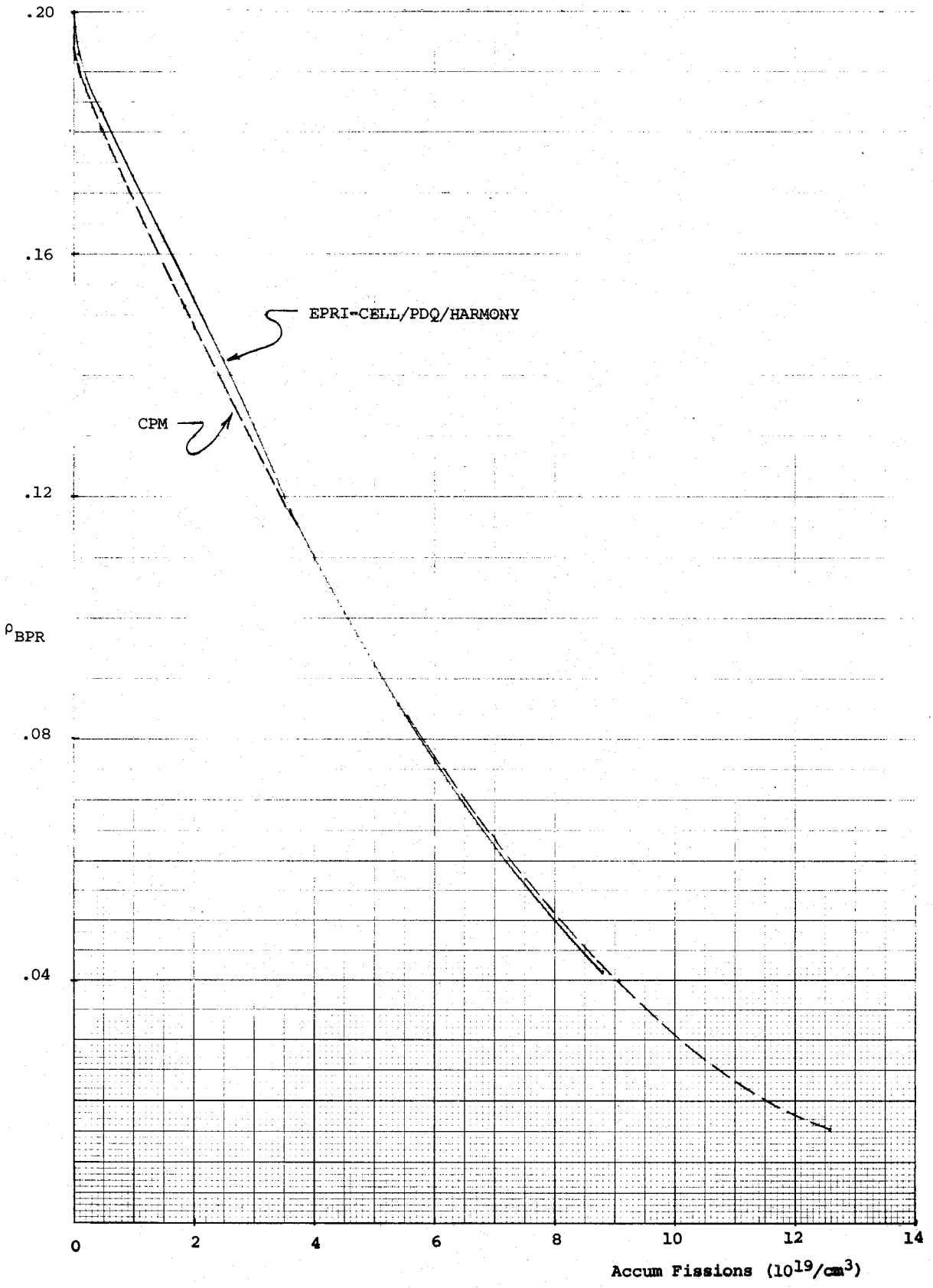

Figure 16 BPR Worth, 16 BPR's per Assembly

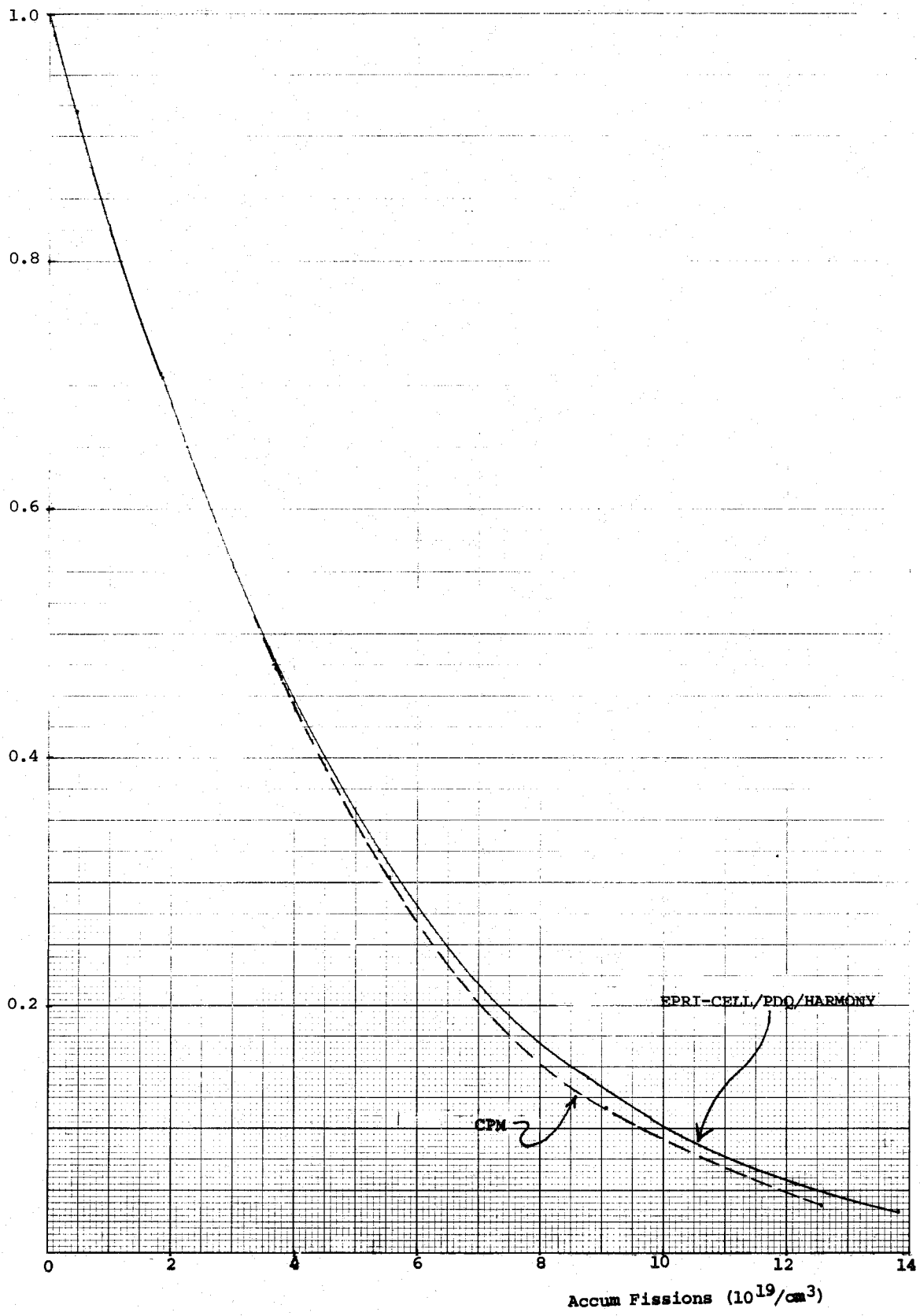

Figure 17 Remaining BPR Boron-10 Fraction

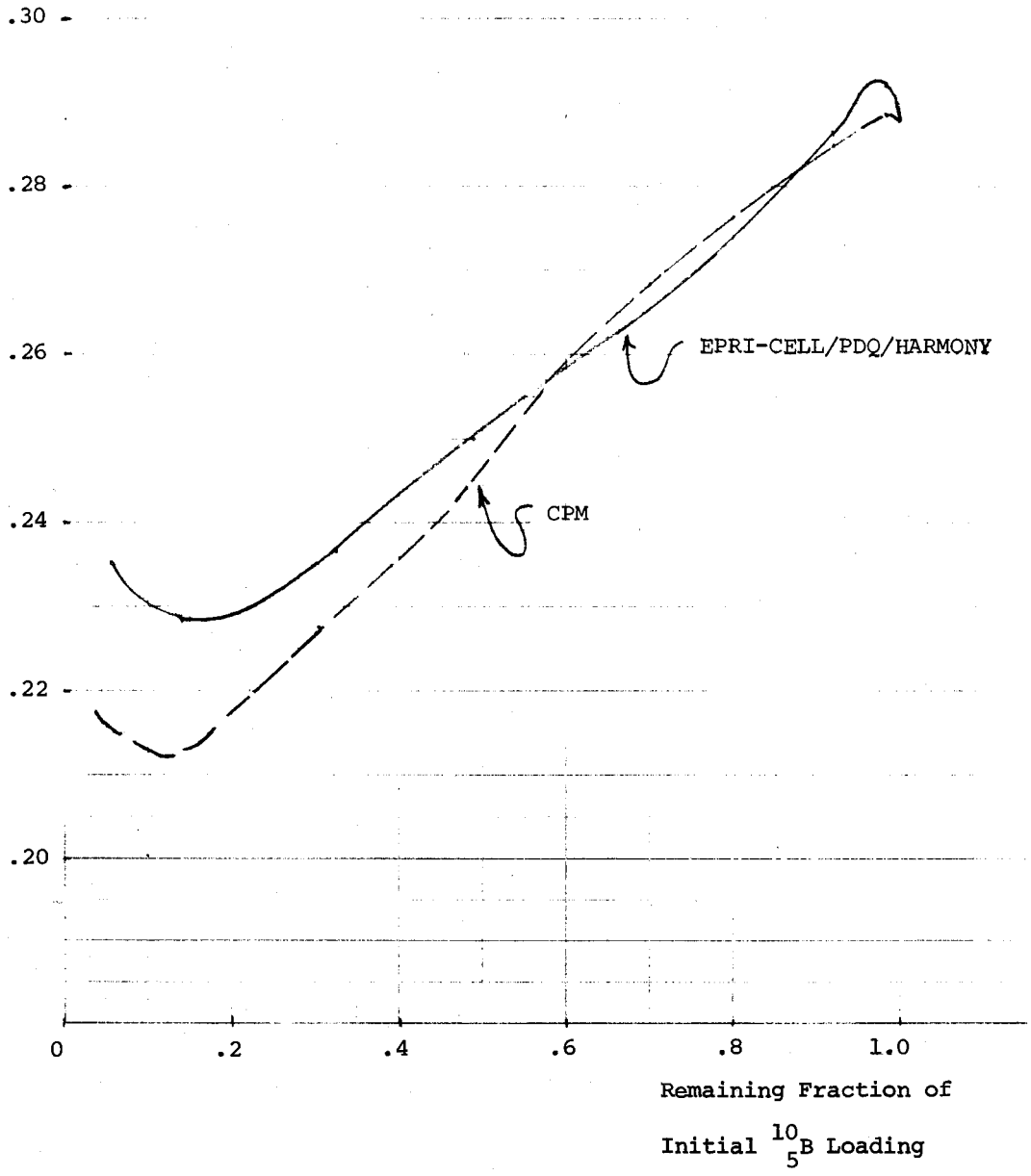

Figure 18 Fast-to-Thermal BPR Absorption Ratios

18-30

edited from the EPRI-CELL is the desired BOL thermal macroscopic absorption cross section for the BPR cell. Application of this EPRI-CELL procedure produced BPR worths very close to those determined from BOL CPM runs: worth differences, EPRI-CELL to CPM, of -3% to +5% were observed.

At this point, it is worth noting that, insofar as the heterogeneous CPM results differed slightly from those of the homogeneous CPM, they differ for PWR/BPR designs and the worth results from the heterogeneous runs generally coincided with those from EPRI-CELL. A possible explanation is that the revised BPR treatment in the homogeneous CPM, not utilized of course in the heterogeneous version, does not exactly preserve reaction rates in going from the geometrically explicit microgroup calculation to the final cell homogenized lattice calculation; the EPRI-CELL procedure is designed around such reaction rate preservation.

At any rate, the simplified procedure gives a result that can be decomposed, as above, into three elements, one being the shielded B-10 thermal cross section. As before, we know the unshielded cross section at full depletion. We now assume that the curve linking the two end points is that shape originally calculated together with a modest linear extrapolation. This is the basis for Figure 19; the known and calculated end points determine the limits of an ad hoc linear scale of B-10 fraction remaining. By this means, all information required for intermediate burnup points is determined. (Throughout this discussion, consideration of the much less variable fast cross section, contained in the documentation, has been excluded.)

This procedure has been widely applied by utilities exercising the PWR methods of ARMP. Although it might be the beneficiary of fortuitously canceling errors, the method has been generally evaluated as adequate in terms of helping utility calculations produce good agreement with the boron letdown predictions corresponding to the three domestic PWR manufacturers' diverse designs.

BWR Assemblies

The Supercell Approximation. Intercomparisons between EPRI-CELL/PDQ and CPM applied to BWR assembly representations are discussed in this section. They have shed much light on the validity and limitations of the supercell (SC) approximation in general and, in particular, in BWR applications. For example, the Pu-240 reaction rate overestimate discussed for PWRs was first observed in BWR lattices wherein the error is quite large; this will be discussed in more detail in the next section. In the epithermal range, use of the SC approximation in EPRI-CELLs providing input to PDQ has resulted in accurate values of assembly migration area (M^2). The extra region of the SC in the context of this paper consists of the water slots outside the can, the can itself, and the narrow water slot between the can and the outer boundary of the repeating lattice array, all prorated equally to the

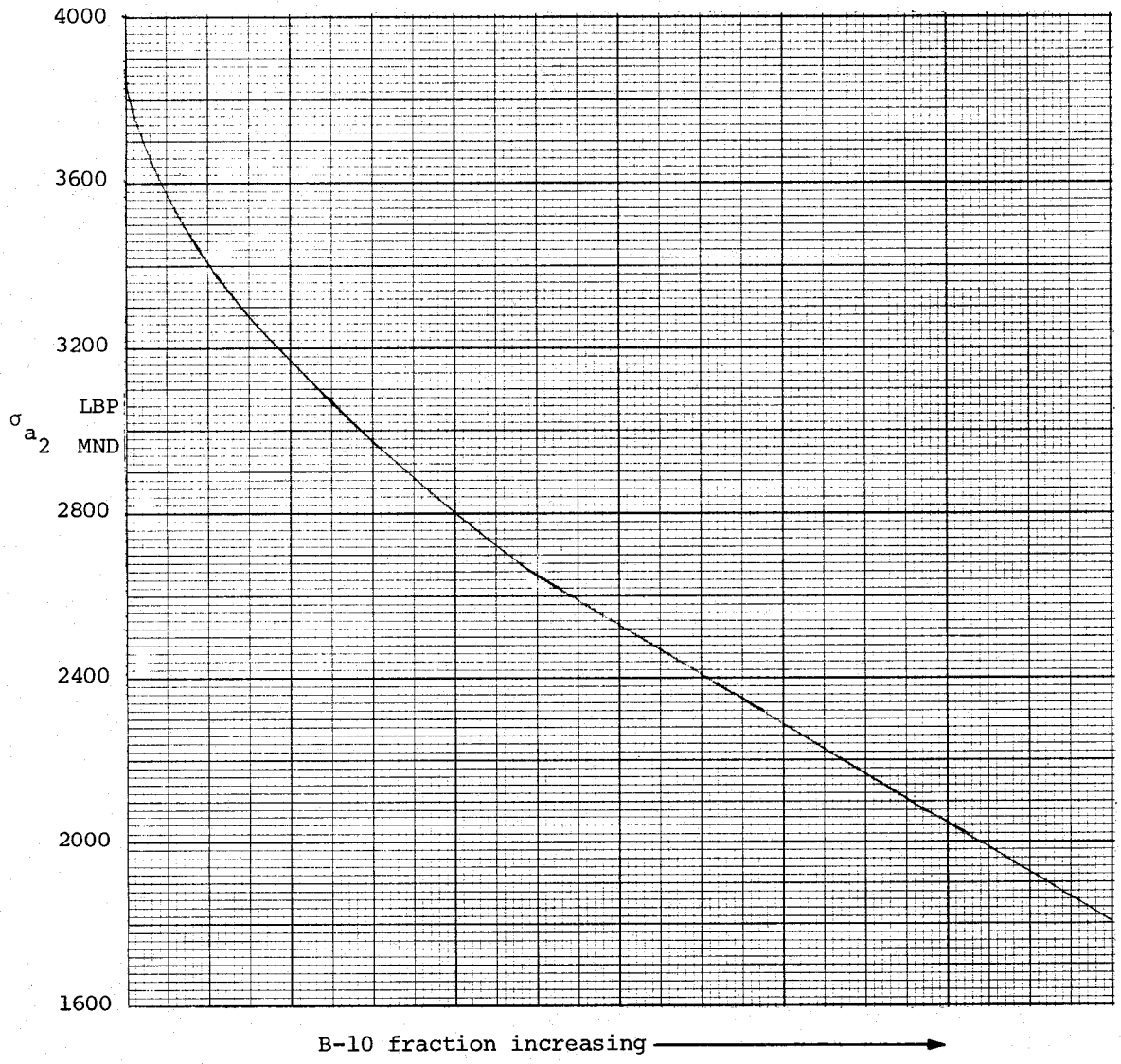

Figure 19 Microscopic MND Thermal Absorption (barns) for B-10 in LBP Cell

various pin cells in the assembly.

The validity of an older intuitive approach taken toward BWR assembly calculations has been disproven, namely, the notion of attaching, in the thermal description, both very large extra regions to cells corresponding to peripheral pins and also no extra regions to cells corresponding to internal lattice locations. In fact, within the context of PDQ representation, the composite lattice spectrum is more determined by the enrichments of the various pins than by proximity to the water slots. Figure 20 summarizes the results from two PDQs; in one, the lattice constants were generated from cell only EPRI-CELLS; in the other, they came from cell edits of SC runs. In all BWR assembly figures starting with 20, the wide slots are consistently placed adjacent to the top and left sides.

As one might infer from Figure 20, the problem in matching PDQ to CPM centered on reactivity, not power distribution. The basic problem to be countered is the fact that the supercell, consistently applied in various forms, is a very poor approximation in the thermal range to BWR assembly configurations. A measure of this statement is the 30 to 40% overestimate in the ratio of the group 3 to group 4 absorption reaction rate edited from an unmodified supercell run compared to the same ratio edited from PDQ or CPM for internal pins. A procedure described in the next section mitigates the magnitude of this error by a factor greater than two while, more importantly, solving the reactivity matching problem on a depletion basis utilizing BOL runs only.

Assemblies Without Gadolinium. The basic reactivity parameterization of PDQ/HARMONY to CPM, in the absence of gadolinium, is discussed in this section. The procedure for representing gadolinia-loaded pins, consistently superimposed on the basic parameterization, is briefly outlined in the next (and last) section.

The essence of the problem solved in the following discussion is the reactivity match of PDQ/HARMONY to CPM in as simple and, it is hoped, generic a manner as possible. Noting that the supercell approach is most approximate for a BWR in the thermal range, the Mixed Buckling Model (MBM) was devised. Negative values of thermal buckling, generic to void level, were input to EPRI-CELLS that ultimately produced PDQ agreement in reactivity with CPM at BOL by means of the following procedure. Supercell runs were made for each pin enrichment-average Dancoff combination in the assembly using a guess for the negative thermal buckling. Macroscopic cross sections, generated from the EPRI-CELLs as the cell edits of the supercells, were input to PDQ in conjunction with non-fuel cross sections edited from CPM; a reactivity comparison was then made with CPM. If the agreement was not satisfactory, the sequence was repeated with a new value of thermal buckling input to various EPRI-CELLS until an acceptable agreement in reactivity was reached between PDQ and CPM. This procedure was then applied at two other void levels (0 and 60% steam fraction

Monticello Cycle 1, BOL, 40% void

No curtains, No rod

Normalized Power

.942 .962							
.825 .836	1.066 1.077						
.745 .751	.936 .937	1.128 1.122					
1.061 1.073	1.204 1.204	1.041 1.028	.972 .955				
1.045 1.055	1.186 1.184	1,034 1.021	.975 .958	.982 .967			
1.094 1.108	1.258 1.263	1.110 1.102	1.052 1.041	1.062 1.053	1.145 1.142		
.789 .798	1.018 1.026	.912 .913	.871 .869	.879 .848	.939 .942	.692 .695	cell cell edit of supercell

	k_∞	M^2
cell	1.2127	86.68
cell of supercell	1.2152	89.84

Figure 20 PDQ Comparison: Cell Versus Cell Edit of Supercell Comparison

inside the fuel channel). Figures 21, 22, and 23 show the agreement at BOL in k, M^2 and power distribution between EPRI-CELL/PDQ and CPM calculations for the Monticello Cycle I assembly (unrodded and without curtains) at the three void conditions. Table 1 shows a BOL comparison of reaction rates ratios (groups 1 to 2, 2 to 3, and 3 to 4) between CPM and PDQ at 0, 40 and 60% void for the same assembly.

In connection with the use of this model, certain points are worth noting. The variation of PDQ assembly K with the particular value of negative buckling input to the various EPRI-CELLs is linear; thus, 2 trials should easily allow determination of the final value. Good initial guesses are available from a table in the ARMP documentation. In this process, we need run only one EPRI-CELL for each enrichment. That is, for the determination of BOL k_∞, the average dancoff is sufficient. Furthermore, since the procedure centers around the matching of k_∞ between CPM and PDQ at BOL with gadolinium suppressed, analysts have found 4 energy groups adequate for the 2-D portion of the CPM calculation.

One study showed that the total reactivity effect for buckling values input to EPRI-CELL from zero to the thermal value of $-.018\ cm^{-2}$ is $1.2\%\ \Delta\rho$. Thus, one may quanitify the MBM model as producing reactivity effects on the order of $1\%\ \Delta\rho$.

Although expected changes due to proximity to the water slot per se are not as great as anticipated, the EPRI-CELL procedure associated with the MBM takes no geometric account of this spectral effect. Furthermore, the EPRI-CELL removal cross sections do not match those of CPM. Yet, as will be seen later, the reactivity variation with depletion between EPRI-CELL/PDQ and CPM matches as well as at BOL. This model is clearly the beneficiary of fortuitously canceling errors that produce accurate absorption reaction rates at the various lattice positions.

By editing the Pu-240 group 3 of 4 absorption cross sections from CPM depletion runs and making assembly-averaged comparisons with corresponding EPRI-CELL/PDQ/HARMONY runs, it was discovered that $\sigma_{a3/4}$ for Pu-240 from EPRI-CELL was considerably overestimated. This was due, for the most part, to inflation within EPRI-CELL of the group 4/5 flux. This in turn has been traced to two mechanisms which are about equally effective in producing the overestimate: one is the very large extra region typical of the BWR supercell; the other is the large negative thermal buckling used in the MBM model. (Fortunately, no other important reaction rate besides that for Pu-240 occurs within the narrow group 4 of 5.) Table 2 illustrates these two effects. The correction to the Pu-240 $\sigma_{a3/4}$ was performed in HARMONY through the application of a depletion-independent "g" factor. A similar factor in EPRI-CELL corrects the Pu-240 CINDER $\sigma_{a3/4}$.

The special advantage of IRT to BWR assembly analysis is that it enables the generation of an accurate time-dependent representation of each pin cell enrichment-Dancoff combination with only a minimum of EPRI-CELL depletion runs (one for each enrichment) and corresponding generation through NUPUNCHER of HARMONY input. This

Monticello Cycle 1, BOL, 0 void

No curtains, No rod

Normalized Power

.931 .911							
.813 .799	1.049 1.036						
.735 .728	.915 .907	1.103 1.103					
1.060 1.065	1.183 1.187	1.017 1.017	.956 .958				
1.044 1.048	1.166 1.169	1.016 1.016	.967 .969	.984 .986			
1.101 1.102	1.253 1.255	1.106 1.109	1.060 1.066	1.080 1.084	1.178 1.183		
.793 .782	1.030 1.029	.926 .931	.893 .898	.908 .913	.978 .981	.718 .710	PDQ CPM

	k_∞	M^2
PDQ	1.2447	59.38
CPM	1.2463	61.01

Figure 21 PDQ/CPM Comparison

Monticello Cycle 1, BOL, 40% void

No curtains, No rod

Normalized Power

.957							
.960							
.834	1.077						
.831	1.068						
.750	.938	1.126					
.750	.927	1.117					
1.071	1.206	1.032	.959				
1.089	1.206	1.019	.946				
1.052	1.185	1.024	.962	.970			
1.069	1.182	1.011	.950	.959			
1.104	1.262	1.104	1.044	1.055	1.143		
1.122	1.263	1.098	1.040	1.051	1.144		
.794	1.023	.912	.868	.877	.940	.693	PDQ
.797	1.031	.917	.874	.883	.948	.690	CPM

	k_∞	M^2
PDQ	1.2274	90.29
CPM	1.2274	90.40

Figure 22 PDQ/CPM Comparison

Monticello Cycle 1, BOL, 60% void

No curtains, No rod

Normalized Power

.963 .981							
.841 .846	1.088 1.085						
.758 .759	.952 .940	1.143 1.131					
1.074 1.099	1.220 1.220	1.047 1.029	.969 .948				
1.054 1.077	1.196 1.192	1.035 1.015	.966 .945	.968 .948			
1.100 1.128	1.264 1.267	1.105 1.095	1.038 1.028	1.043 1.034	1.121 1.119		
.790 .801	1.016 1.028	.904 .908	.856 .859	.860 .863	.915 .924	.676 .673	PDQ CPM

	k_∞	M^2
PDQ	1.2102	118.19
CPM	1.2093	114.51

Figure 23 PDQ/CPM Comparison

Table 1

Reaction rate ratios: CPM versus PDQ Monticello Cycle 1, BOL, No curtain, no rod

Edit	steam void inside fuel channel	$\Sigma_{a1}\Phi_1/\Sigma_{a2}\Phi_2$		$\Sigma_{a2}\Phi_2/\Sigma_{a3}\Phi_3$		$\Sigma_{a3}\Phi_3/\Sigma_{a4}\Phi_4$	
		CPM	PDQ	CPM	PDQ	CPM	PDQ
Assembly	0	1.3694	1.2698	.1330	.1341	.2904	.2837
Fuel pin cells		1.3580	1.2553	.1346	.1357	.3043	.2969
2.95 w/o U-235		1.3284	1.2274	.1387	.1371	.3260	.3193
1.91 w/o U-235		1.4013	1.2752	.1387	.1369	.2524	.2498
1.13 w/o U-235		1.4082	1.3100	.1249	.1312	.2855	.2760
Assembly	40%	1.2179	1.1959	.1474	.1466	.3807	.3836
Fuel pin cells		1.2084	1.1833	.1493	.1485	.3992	.4011
2.95 w/o U-235		1.1822	1.1573	.1562	.1510	.4220	.4246
1.91 w/o U-235		1.2539	1.2038	.1548	.1497	.3198	.3291
1.13 w/o U-235		1.2547	1.2335	.1344	.1415	.3853	.3853
Assembly	60%	1.1219	1.1648	.1603	.1573	.4483	.4659
Fuel pin cells		1.1136	1.1532	.1624	.1595	.4701	.4867
2.95 w/o U-235		1.0897	1.1297	.1721	.1627	.4901	.5092
1.91 w/o U-235		1.1598	1.1731	.1692	.1608	.3671	.3929
1.13 w/o U-235		1.1567	1.1995	.1425	.1508	.4656	.4776

Table 2

Pu-240 BOL absorption cross sections edited from EPRI CELL

Monticello Cycle 1, BOL, 40% void, fuel pin of 2.95 w/o U-235

	$\phi_{3/5}/\phi_{4/5}$	$\sigma_{a_{3/5}}$	$\sigma_{a_{4/5}}$	$\sigma_{a_{5/5}}$	$\sigma_{a_{3/4}}$	$\sigma_{a_{4/4}}$
Pin cell 0 thermal buckling	9.57	16.24	7312.9	173.24	706.77	173.24
Super cell 0 thermal buckling	8.40	16.64	7381.8	174.31	799.87	174.31
Super cell $-.018\ cm^{-2}$ thermal buckling	7.06	16.64	7381.8	174.31	930.05	174.31

was achieved by the use of "g" factors applied to the group 3 U-238 absorption cross section. These factors were obtained from BOL EPRI-CELL calculations done for each pin enrichment-Dancoff combination.

Figure 24 shows a comparison between PDQ/HARMONY and CPM of k_∞ versus exposure for an unrodded cycle 1 assembly without curtains. Note that the excellent agreement in reactivity between PDQ and CPM, forced at BOL, is maintained throughout depletion without any further normalization or other intervention.

Assemblies With Absorbers. All calculations with absorbers of various types utilized a converged MBM fuel representation.

Four group macroscopic control rod cross sections were edited as an entity within the cruciform outline from CPM for use in PDQ. In going from a transport to a diffusion calculation, it was necessary to reduce somewhat the value of the thermal absorption cross section from CPM prior to its use in PDQ. A decrease of 5% produced good agreement in reactivity between CPM and PDQ rodded assembly calculations.

Boron loading was small enough so that there was virtually no self-shielding in the stainless steel curtains. An elementary treatment in PDQ/HARMONY was adequate for matching CPM.

An EPRI-CELL/PDQ procedure has been developed for the representation of gadolinia-loaded fuel pins. This procedure differs from those described previously in that it is virtually independent of CPM but provides depletion-dependent results that are in good agreement with those of CPM. The "virtually" preceding stems from a BOL normalization to CPM-calculated worth: unlike the case with PWR/BPRs, there is a slight dependence of worth on buffer size.

Again, as for PWRs, the EPRI-CELL is run in the Geometry A of Figure 14 and analogous one-group fixed-source PDQs are run. In this application, the transport-to-diffusion matching procedure is carried through depletion. Another significant departure is an especially useful application of the Mixed Buckling Model in the buffered EPRI-CELL: a rather large value of negative buckling is required to match the PDQ or CPM value of group 3 to group 4 absorption reaction rate ratio for the homogenized gadolinia-loaded pin cell.

The HARMONY description of the gadolinia-loaded pin cell is basically the same as that of a normal fuel cell of the same enrichment but with the following modifications:

1. A shielding factor is applied to the thermal cross sections to account for the spectral effects of gadolinium; these depletion-dependent cross sections are identically those automatically generated for fuel pins of the same enrichment (but gadolinium free) by the codes, EPRI-CELL and NUPUNCHER;
2. Microscopic cross sections for Gd-155 are present;

Monticello, Cycle 1, Assembly k_∞ versus exposure
No Curtain, No Rod, 40% void

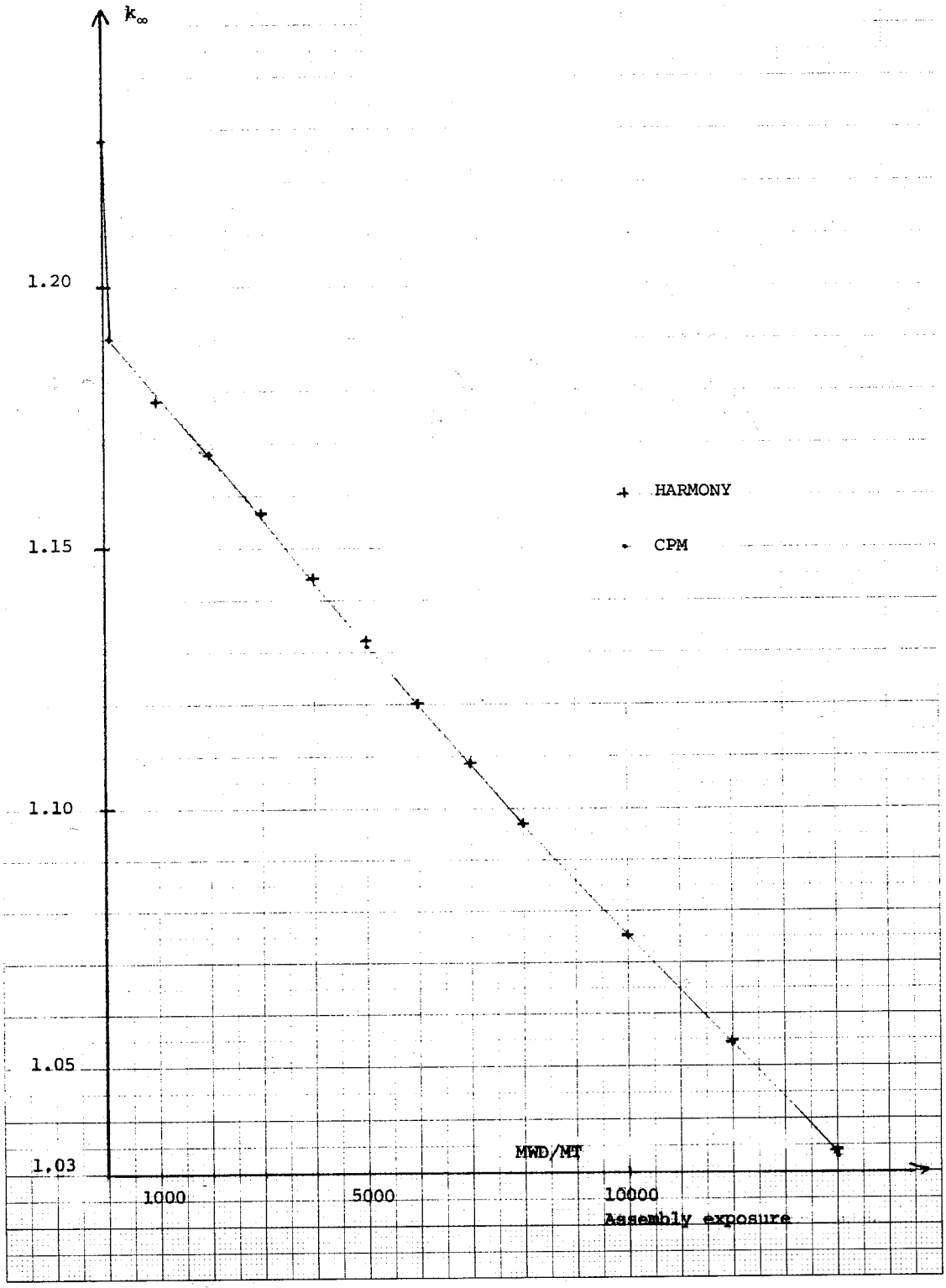

Figure 24 CPM/HARMONY Depletion Comparison

3. Effects of all gadolinium isotopes are lumped together into macroscopic cross sections.

Figure 25 shows a typical BOL comparison of pin-wise power between PDQ and CPM for a gadolinia-loaded assembly. The accuracy of the EPRI-CELL/PDQ-7/HARMONY parameterization of gadolinia-loaded fuel relative to CPM is shown in Figure 26 in terms of variation of K_∞ with depletion.

The gadolinia-loaded fuel parameterization within HARMONY is keyed to the depletion of a trace amount of Gd-155. The effective cross section of this isotope varies greatly with gadolinia depletion, e.g., over the 4 to 5 MWD/kg U step. The PDQ flux in the gadolinia pin location, however, varies by only 2% over this same step. Dr. Larry Matthews of Southern Company Services suggested that inclusion of the subinternal HARMONY depletion option might be advantageous in this application. Accordingly, 50-hour subinterval decomposition of the basic HARMONY depletion steps was applied to this trace isotope chain. Use of this option allowed depletion steps in PDQ/HARMONY twice as coarse (for asymptotic results) as those used in the efficient depletion procedure of CPM.

REFERENCES

1. W. J. Eich, "Advanced Recycle Methodology Program: Overview," to be published, Electric Power Research Institute, RP118-1, Final Report.

2. CCM-3, Research Project 118-1, "Advanced Recycle Methodology Program, System Documentation," Revision 0, September 1977, Electric Power Research Institute.

3. B. A. Zolotar and W. J. Eich, "Advanced Recycle Methodology Program: Preliminary Specification for a New Nuclear Computational Capability," EPRI SR-2, Special Report, July 1974.

4. W. J. Eich, "Advanced Recycle Methodology Program: Project Status Report." Research Project 118-1, December 1975, Electric Power Research Institute.

Monticello Cycle 2, BOL, 40% void

Gadolinia assembly

Normalized Power

1.132 1.143							
1.181 1.193	1.070 1.054						
1.058 1.071	1.128 1.112	.350 .336					
1.123 1.146	1.081 1.073	.872 .846	.819 .800				
1.125 1.148	1.102 1.098	.905 .887	.797 .769	.804 .785			
1.180 1.203	1.173 1.170	.952 .929	.334 .324	.863 .841	.976 .970		
1.160 1.181	1.066 1.073	1.124 1.139	1.010 1.014	1.037 1.053	1.135 1.158	1.037 1.057	PDQ* CPM

* With gadolinia pin cell Σ_{a_4}, $\nu\Sigma_{f_4}$ and $\kappa\Sigma_{f_4}$ edited from CPM reduced by 23% before input to PDQ.

	k_∞	M^2
PDQ	1.0963	85.99
CPM	1.0963	86.38

Figure 25 PDQ/CPM Comparison

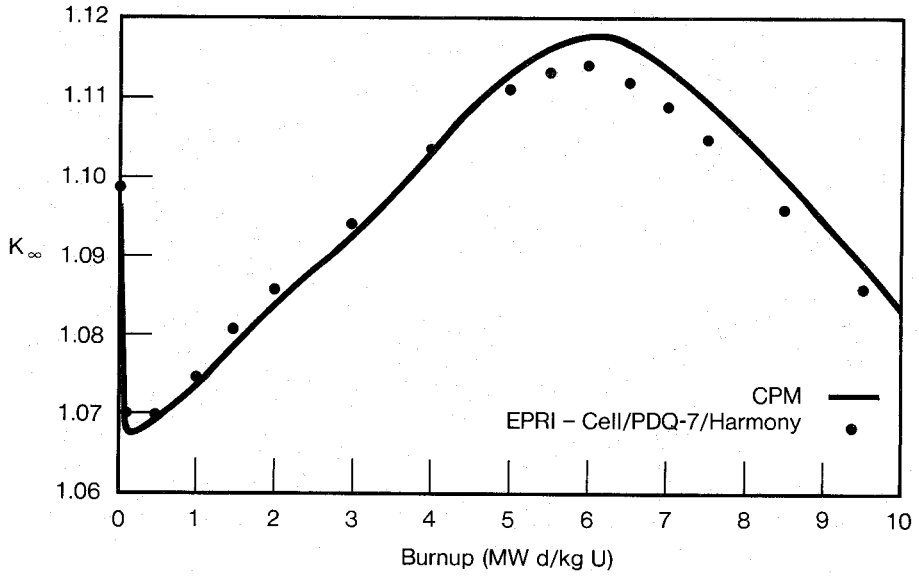

Figure 26 CPM/HARMONY Depletion Comparison

Section 19

TEMPERATURE DEPENDENT RESONANCE INTEGRALS USING RESONANCE PROFILES

Temperature Dependent Resonance Integrals using Resonance Profiles

E. Taviv and W. Rothenstein
Technion, Israel Institute of Technology, Haifa

INTRODUCTION

The change with temperature of effective resonance integrals of resonance nuclides in thermal reactor lattices depends to a considerable extent on the behaviour of the cross sections in the resonance wings, where resonance self shielding is relatively small. The increase of the cross sections with temperature at energies remote from the resonance peaks tends to zero in the far wings, where the natural line shape is reached. The accuracy of calculations of the temperature variation of the effective resonance integral is therefore greatly influenced by the precision with which the Doppler broadening and the shielding are evaluated at different temperatures over considerable energy ranges with respect to the resonance peaks.

As far as the resonance cross sections are concerned, these are represented for many resonance nuclides by the Breit Wigner Single Level formalism to which ψ,χ function Doppler broadening is applied. In numerical calculations of the effective resonance integrals, which are not based on narrow resonance, infinite mass, or intermediate resonance approximations, the numerical integrations may be restricted to a central portion near the resonance peaks and beyond this energy region wing corrections are applied. This is the case in particular in the Nordheim Integral Treatment[1]. The wing corrections are based on the natural line shape, so that errors in the temperature variation of the effective resonance integrals cannot be ruled out. In other treatments cross sections at each energy point in the numerical integrations may be evaluated from the contributions of a number of neighbouring resonances, and questions may arise what effects more distant resonances have on the effective resonance integrals and their temperature dependence. Finally, the ENDF/B files frequently contain smooth corrections to the cross sections calculated from the resonance formalism. These corrections are again not Doppler broadened, leading to a further possible source of error.

The resonance shielding calculation which leads to the difference between the effective and the infinitely dilute resonance integrals may also lead to inaccuracies. If individual resonance treatments are used, full flux recovery is assumed between the resonances of the same and of different nuclides in the fuel mixture. In addition, shielding of the wing corrections may be ignored. This is the case in the Nordheim Integral Treatment.

Most of the problems involved in the Nordheim procedure may be avoided by replacing it by a RABBLE-type integral transport treatment[2]. Instead of referring to a two region lattice unit cell, a multiregion subdivision is used so that the flux changes near the outer surface of the fuel rods can be determined with greater precision in the vicinity of the resonance peaks. There is no assumption relating to flux recovery between resonances, i.e. the flux above any resonance need not have its asymptotic energy dependence. Consequently, interference between the resolved resonances of all resonance nuclides is taken into account. Resonance reaction rates are determined directly, and from these effective resonance integrals can be determined according to:

$$R.I. = -\frac{\overline{\xi}\Sigma_s V_c}{N_o V_o} \ln(1-\alpha) \qquad (1)$$

where N_o is the atom density of the resonance absorber in the fuel volume V_o, $\overline{\xi}\Sigma_s V_c$ is the slowing down power in the lattice unit cell, and α the resonance absorption fraction in the energy range under consideration. However, the problems relating to the determination of the cross sections and their temperature changes remain.

On the other hand detailed profile tabulations in the resolved resonance region at the specified lattice temperature may be constructed in accordance with the ENDF/B specifications including smooth corrections from File 3, and with exact Doppler broadening. If they are utilised in a RABBLE-type treatment the effective resonance integrals of the resonance nuclides in the resolved resonance region in thermal reactor lattices may be determined at different temperatures.

A code utilising this approach was written for this purpose[3]. Calculations were made to determine the temperature variation of the effective resonance integral of natural and 3% enriched isolated UO_2 rods of different radii in a water moderator. Since the resonance profile tapes contain average cross sections in the unresolved resonance region, they cannot be used there to determine the resonance shielding. Consequently, the RABBLE-type evaluations in the resolved resonance region were combined with Nordheim TUZ calculations of the unresolved s-wave effective resonance integrals. The results were compared with calculations and measurements recently reported by M. Todosow and J.F. Carew[4]. The results also showed the interference effects between the effective resonance integrals of the two Uranium isotopes. They are specially noticeable in the temperature variation of the ^{235}U effective resonance integral which is reduced to a marked extent by the shielding caused by the large ^{238}U resonances.

PREPARATION OF TEMPERATURE DEPENDENT RESONANCE PROFILE TABULATIONS

The first step in the preparation of detailed resonance profile tabulations is carried out by the RESEND code[5] which prepares new ENDF/B File 3 cross sections consisting of the resolved resonance cross sections at $0^{o}K$, obtained from the formalism in File 2, together with any corrections contained in the original File 3. These tabulations are prepared so that they can be utilised with linear - linear interpolation to a chosen accuracy as specified in the problem input. In the unresolved energy region average cross sections are calculated at the energies at which the unresolved resonance parameters are given in the original ENDF/B tape. The remainder of the data are copied. The RESEND output tape contains a dummy File 2.

In order to Doppler broaden a RESEND tape it has to be linearised fully, i.e. also in the smooth cross section regions below and above the resonance region. For this the code LINEAR[6] is available. Again the complete transformation of the File 3 sections, referring to particular reactions, to linear - linear interpolation is carried out to an accuracy as specified in the input. The Doppler broadening itself is performed by the SIGMA1[7] code which has now been adapted to IBM computers by selective use of double precision, so that the smaller word length does not cause rounding errors. The final tabulations are thinned to the desired linear - linear interpolation accuracy criterion.

Detailed resonance profile tabulations have been prepared at different temperatures for ^{235}U and ^{238}U to an interpolation accuracy of 0.5 percent. In Table 1 the number of energy points in the different sections of File 3, which contain the resonance data, are shown. They clearly indicate that the cross sections become smoother with increasing temperature.

Table 1

Number of Energy Points of RESEND/SIGMA1 Output
(Convergence criterion 0.5 percent for linear-linear interpolation)

	U-238		U-235		
T°K	σ_s	σ_c	σ_s	σ_f	σ_c
0	14065	23940	1583	4408	5007
293	6018	11908	882	2786	3129
450	5375	10807	815	2502	2813
600	4757	10043	762	2315	2607
800	4563	9294	720	2128	2389
1200	4039	8360	625	1862	2103

The library for the resonance shielding code OZMA1[3] containing the RABBLE-type option was prepared from the temperature dependent tabulations by defining an equal grid in which each energy point is followed by the appropriate σ_s,σ_c for ^{238}U and by σ_s,σ_f, σ_c for ^{235}U. The grid chosen was that of the densest tabulation (in fact σ_c) and the other cross sections were added at the additional energy points by interpolation. A common grid is convenient for interpolating all the relevant data together in transport calculations of the resonance reaction rates. The grid was also inverted by the EQGRIV code[8] to read from high to low in energy as required for the evaluation of the slowing down integrals at the succesive lethargy points in the RABBLE treatment. The final library was set up in the MUFT group structure for convenience so that in the resonance treatment only parts of the long tabulations need to be in the memory at one time, and can be overwritten by the data in the next MUFT group subsequently. The resolved resonance region was defined to be that from the MUFT group containing the low energy limit of this region as given in the ENDF/B-IV tape (group 53 for both Uranium isotopes) through the group containing the high energy limit for ^{235}U (group 35), and the group below this energy limit for ^{238}U(group 27); group 26 was taken to belong to the unresolved resonance region for the purpose of calculation of resonance shielding by the TUZ code.

EFFECTIVE RESONANCE INTEGRALS AND THEIR TEMPERATURE VARIATION

The OZMA1 code (RABBLE-type option) was used to calculate the effective resonance integral of ^{238}U and ^{235}U for natural and 3% enriched isolated rods of UO_2 of different radii in light water. Sufficient water was placed between the rods in these calculations (volume ratio 25:1) to ensure very small Dancoff corrections. S/M values were corrected for the small lattice effect. The rods were subdivided into 3 subregions in the fuel with a smaller thickness near the fuel surface than in its interior. Three subregions were used outside the fuel, the thinnest again near its surface.

The capture integrals for ^{238}U in the resolved resonance region resulting from the OZMA1 run were combined with capture integrals outside it so that comparison could be made with results obtained by the Nordheim ZUT - TUZ treatment. In Table 2 a complete breakdown is given for the 0.5 cm radius UO_2 rod at room temperature. To the resonance integral obtained from the detailed profile tabulations in the resolved resonance region the resonance integral from TUZ for the s-wave unresolved resonances was added. p-wave unresolved resonances were converted to equivalent smooth σ_c values and their capture integral is shown separately; it is of course independent of temperature since it was calculated at infinite dilution. The unresolved resonance region covers MUFT groups 22 - 26. The capture integral obtained from the smooth ENDF/B-IV File 3 data in MUFT groups 1 - 26 and group 54 were also

added; they are again independent of temperature. The resonance integral in groups 27 - 53 includes that obtained from the ENDF/B-IV File 2 and File 3 data together with full Doppler broadening. For the Nordheim ZUT calculation a complete breakdown of the capture integral in the resolved resonance region is given.

Table 2

U-238 Capture Integral for 0.5 cm Radius Isolated Natural UO_2 rods at 293°K

$\sqrt{S/M}$ = 0.632 cm/gr$^{1/2}$

Energy Range 0.625 eV - 10 MeV

MUFT group	I_{eff} or $\int\sigma_c du$	code	barns	code	barns
27-53	I_{eff} (s-wave)	ZUT	19.07		
"	$\int\sigma_c du$ (p-wave)	ETOG	0.70		
"	$\int\sigma_c du$ (1/vtails)	ETOG	0.81		
"	$\int\sigma_c du$ (File 3)	ETOG	0.25		
	Total		20.83	OZMA1	20.10
22-26	I_{eff} (s-wave)	TUZ	0.68	TUZ	0.68
"	$\int\sigma_c du$ (p-wave)	ETOG	0.84	ETOG	0.84
1-26	$\int\sigma_c du$ (File 3)	ETOG	0.65	ETOG	0.65
54	$\int\sigma_c du$ (File 3)	ETOG	0.17	ETOG	0.17
	Total		23.17		22.44

It should be noted that the conversion of resolved p-wave resonances to equivalent smooth capture cross sections is overestimated in the original ETOG code. The value of 0.70 barns for the corresponding $\int\sigma_c du$ is based on this overestimate. A correction introduced into the current version of ETOG[8] reduces this contribution to the overall capture integral to 0.56 barns.

The results given by Todosow and Carew[4] for about the same rod diameter refer to a slightly lower S/M value (0.623 cm/gm$^{1/2}$). They quoted a value of 22.37 barns for the HAMMER/HELP capture integral, but it appears that the reduction of $\int\sigma_c du$ on account of the (n,2n) cross section was subtracted in the first two MUFT groups. This contribution amounts to 0.44 barns, so that their capture integral would be 22.81 barns. The difference between this value and the Nordheim ETOG value in Table 2 is largely due to the difference in S/M.

In Table 3 the total capture integrals of ^{238}U from 0.625 eV to 10 MeV for isolated natural UO_2 rods are given as a function of temperature and rod size. In Table 4 the corresponding results are given for 3 percent enriched rods.

Table 3

^{238}U Total Capture Integral for Natural UO_2 Rods
(0.625 eV - 10 MeV)

		R cm ($\sqrt{S/M}$ cm/gr$^{1/2}$)				
T°K	Code	0.125 (1.227)	0.250 (0.886)	0.500 (0.632)	1.00 (0.447)	2.00 (0.316)
293	OZMA1	39.44	29.63	22.44	17.26	13.49
	ZUT	39.45	30.09	23.17	18.23	14.84
450	OZMA1	41.10	30.60	23.03	17.65	13.76
	ZUT	41.01	31.01	23.75	18.62	15.13
600	OZMA1	42.51	31.41	23.52	17.96	13.97
	ZUT	42.40	31.83	24.25	18.95	15.37
800	OZMA1	44.21	32.39	24.09	18.32	14.22
	ZUT	44.09	32.83	24.84	19.33	15.65
1200	OZMA1	47.19	34.11	25.11	18.93	14.61
	ZUT	47.07	34.59	25.89	19.99	16.11

As expected there are only small differences between two results for the two enrichments.

The capture integrals I(T) including the shielding effect in the resonance region, as discussed in connection with Table 2, was expressed as a function $(\sqrt{T} - \sqrt{T_o})$. In general a linear fit is assumed, as expressed by

$$I(T) - \delta = [I(T_o) - \delta]\ [1 + \beta(\sqrt{T} - \sqrt{T_o})] \qquad (2)$$

where δ is the 1/v capture integral based on σ_c = 2.71 barns at 2200 m/sec above 0.55 eV. β is the Doppler coefficient. It was found that a quadratic fit including the $\gamma(\sqrt{T} - \sqrt{T_o})^2$ term in Eq. (2) is more satisfactory.

Table 4

^{238}U Total Capture Integral for 3 percent Enreched UO_2 Rods (0.625 eV - 10 MeV)

		R cm ($\sqrt{S/M}$ cm/gr$^{1/2}$)				
T°K	Code	0.125 (1.227)	0.250 (0.886)	0.500 (0.632)	1.00 (0.447)	2.00 (0.316)
293	OZMA1	39.73	29.73	22.34	16.94	12.93
	ZUT	39.87	30.39	23.40	18.43	15.04
450	OZMA1	41.42	30.71	22.94	17.34	13.20
	ZUT	41.46	31.33	23.98	18.83	15.34
600	OZMA1	42.85	31.54	23.44	17.65	13.41
	ZUT	42.88	32.17	24.49	19.17	15.59
800	OZMA1	44.59	32.54	24.02	18.01	13.65
	ZUT	44.61	33.18	25.10	19.57	15.87
1200	OZMA1	47.61	34.29	25.04	18.63	14.04
	ZUT	47.64	34.98	26.16	20.24	16.34

In Table 5 the values of β from the linear fit and β and γ for the quadratic fit are shown for the capture integrals resulting from the resonance profile tabulations in the resolved resonance region for the 3 percent enriched UO_2 rods.

Table 5

^{238}U Doppler Coefficients for 3 percent Enriched UO_2 Rods

	Linear Fit	Quadratic Fit	
R(cm)	$10^2\beta$	$10^2\beta$	$10^5\gamma$
0.125	1.17	1.06	6.5
0.250	0.91	0.82	5.1
0.500	0.73	0.68	2.6
1.00	0.61	0.60	0.5
2.00	0.54	0.56	-1.2

For the natural UO_2 rods the Doppler coefficients are not significantly different. There is also reasonable agreement with the Doppler coefficients which result from the Nordheim ZUT TUZ calculations, and the corresponding values given by Todosow and Carew[4].

For the ^{235}U effective absorption integral results are shown in Tables 6 and 7. They include the values obtained by the OZMA1 code in which there is no separation of the cross sections into smooth and resonance contributions and in which the effect of the flux depression due to the ^{238}U resonances on the ^{235}U absorption integral is taken into account. The ZUT values are also shown after addition of the absorption integral (43.55 barns) from the ENDF/B-IV File 3.

Table 6

^{235}U Absorption Integral for Natural UO_2 Rods
(0.834 - 101.3 eV)

		R(cm) ($\sqrt{S/M}$ cm/gr$^{1/2}$)				
		0.125 (1.227)	0.250 (0.886)	0.500 (0.632)	1.00 (0.447)	2.00 (0.316)
T°K	Code					
293	OZMA1	278.4	272.1	260.9	242.8	215.9
	ZUT	292.0	289.6	285.0	276.6	264.1
450	OZMA1	278.0	271.7	260.7	242.8	216.0
	ZUT	292.3	289.9	285.5	277.4	265.1
600	OZMA1	277.7	271.5	260.6	242.8	216.0
	ZUT	292.4	290.1	285.8	277.9	265.7
800	OZMA1	277.2	271.1	260.3	242.6	216.0
	ZUT	292.5	290.3	286.1	278.4	266.3
1200	OZMA1	276.3	270.2	259.6	242.2	215.7
	ZUT	292.5	290.5	286.5	279.0	267.1

Tables 6 and 7 clearly show the effect of the "mutual shielding". The ^{235}U effective resonance integral is considerably reduced when it is calculated in a flux which is shielded by the ^{238}U resonances. The effect becomes more pronounced for the larger rod diameters, i.e. greater heterogeneity.

The ^{235}U results obtained by the OZMA1 code also show considerably less temperature variation than in the case for the results obtained by the Nordheim method. This is again due to the interference between the resonances of the two Uranium isotopes.

Table 7

^{235}U Absorption Integral for 3 percent Enriched UO_2 Rods (0.834-101.3 eV)

		R(cm) ($\sqrt{S/M}$ cm/gr$^{1/2}$)				
T°K	Code	0.125 (1.227)	0.250 (0.886)	0.500 (0.632)	1.00 (0.447)	2.00 (0.316)
293	OZMA1	273.0	262.6	244.3	216.5	179.3
	ZUT	286.8	280.7	270.3	254.4	235.3
450	OZMA1	273.0	262.8	245.0	217.4	180.2
	ZUT	287.5	281.7	271.8	256.5	237.5
600	OZMA1	273.0	263.0	245.5	218.2	180.8
	ZUT	287.9	282.4	272.9	257.9	239.1
800	OZMA1	272.8	263.0	245.9	218.8	181.4
	ZUT	288.3	283.1	273.9	259.3	240.7
1200	OZMA1	272.2	262.7	246.0	219.4	182.2
	ZUT	288.8	284.0	275.4	261.4	243.1

For the thinnest rods the temperature change of the absorbtion integral obtained from the resonance profile tabulations is almost negligible. To estimate these small changes more reliably, a better accuracy criterion for producing the profile tabulations would be needed than the one used in the above calculations (0.5 percent). This would of course greatly increase computer storage requirements.

CONCLUSION

The use of accurately Doppler broadened resolved resonance profile cross section tabulations together with multiregion transport calculations overcomes many of the approximations frequently made in the evaluation of resonance reaction rates, or effective resonance integrals and their temperature variation.

Results are given for the ^{238}U resonance integral of UO_2 rods at different temperatures. The effect of these resonances on the ^{235}U resonance integral is shown. The additional flux depression not only reduces the absorption in ^{235}U, but has a marked effect on its temperature dependence.

A similar behaviour may be anticipated in the resonance absorption of fission products during their buildup throughout the fuel cycle. The methods used for the clean lattices could be

extended to Doppler effect studies in depleted systems.

REFERENCES

1. Kuncir, G.F.: "A Program for the Calculation of Resonance Integrals", GA-2525, General Atomic (1961).

2. Kier, P.H., Robba, A.A.: "RABBLE - A Program for Computation of Resonance Absorption in Multiregion Reactor Cells", ANL 7326, (1967).

3. Barhen, J., Rothenstein, W.: "Thermal Reactor Benchmark Lattice Calculations using Resonance Profiles", in Proceedings of the Seminar on "Nuclear Data Problems for Thermal Reactor Applications", May 22-24, 1978, N.N.D.C., Brookhaven National Laboratory.

4. Todosow, M.I., Carew, J.F.: "Evaluation of Temperature Dependent Resonance Integrals using the HAMMER Code", Trans. A.N.S., 27, 915, (1977).

5. Ozer, O.: "RESEND, A Program to Process ENDF/B Materials with Resonance Files into Point-Wise Form", BNL-17134, Brookhaven National Laboratory, (1973).

6. Cullen, D.E.; "Program LINEAR (Version 77-1): Linearize Data in the Evaluated Nuclear Data File / Version B (ENDF/B) Format", UCRL-50400, Vol. 17, Part A, Lawrence Livermore Laboratory, (1977).

7. Cullen, D.E.: "Program SIGMA-1 (Version 77-1): Doppler Broaden Evaluated Cross Sections in the ENDF/B Format", UCRL-50400, Vol. 17, Part B, Lawrence Livermore Laboratory, (1977).

8. Barhen, J., Rothenstein, W., Taviv, E.: "The HAMMER Code System, Technion Version", EPRI Report (Project RP709-1) to be published, (1978).

Section 20

THERMAL REACTOR BENCHMARK CALCULATIONS USING RESONANCE PROFILES

Thermal Reactor Benchmark Calculations using Resonance Profiles

J. Barhen and W. Rothenstein
Technion, Israel Institute of Technology, Haifa

INTRODUCTION

Thermal lattice benchmark calculations using ENDF/B-IV data were made by means of a modified version of the HAMMER code[1] which uses detailed resonance profile tabulations in the resolved resonance region. A number of different procedures were used to calculate the resonance reaction rates. These included the standard Nordheim Integral Treatment (NIT[2]), a similar treatment using resonance profiles (NITPRO[1]), as well as a RABBLE[3] multi-region treatment with profiles (RABPRO[1]) included directly in the HAMMER code. A more sophisticated procedure (OZMA-1) allowing for the computation of the anisotropic angular flux in the multi-region unit cell was developed separately. The resonance reaction rates produced by the OZMA-1 code were introduced into HAMMER for the subsequent lattice analysis.

The different methods are compared and results are given for the TRX-1 and TRX-2 lattices, as well as for the MIT benchmarks[4]. The new procedures give results which are quite close to previous Monte-Carlo calculations[5]. They are also in reasonable agreement with the latest experiments[6], within the limitations of the current ENDF/B specifications for the ^{238}U resonance cross sections. The recent multilevel formalisms developed by G. de Saussure[7] will probably suffice to close the remaining gap between calculations and experiment.

PREPARATION OF HAMMER ENDF/B-IV MULTIGROUP LIBRARY WITH RESONANCE PROFILE TABULATIONS

The HAMMER epithermal library in the MUFT group structure was prepared from the ENDF/B-IV data by means of the ETOG3[1] code. The fission spectrum was taken to be that of the neutrons produced by thermal fissions of ^{235}U. This spectrum was also used as the weighting function for cross section averaging above 67 keV and was joined to a 1/E weighting function below this energy. The (n,2n) cross section was replaced by inelastic scattering introducing the weight 2 for the extra neutron produced; $\sigma_{n,2n}$ was subtracted from σ_c to conserve σ_t. In the unresolved resonance region only the smooth corrections to σ_c of ^{238}U (from file 3 of the ENDF/B data) was entered into the smooth cross section library; the average resonance parameters of the s-wave and p-wave sequences in each of the relevant groups were included for shielding calculations. For ^{235}U the unresolved resonance parameters were converted to smooth cross sections at infinite dilution and combined with the file 3 corrections to produce σ_c

and σ_f. For the entire resonance region the smooth cross section library contained the potential scattering cross section (including file 3 corrections) of both Uranium isotopes.

In the resolved resonance region the smooth σ_c and σ_f for both ^{235}U and ^{238}U were set to zero. The library contained in the corresponding energy groups detailed resonance profile tabulations for σ_s, σ_f and σ_c. They were generated by means of the sequence of codes RESEND[8], SIGMA1[9], EQGRIV[1] and a modified version of HELP[1], maintaining throughout a 0.1 percent convergence criterion for linear-linear interpolation. The MUFT groups treated as groups with resolved resonance profile tabulations extended from the group containing the low energy limit of the resolved resonance region, to the group containing the high energy limit in the case of ^{235}U. For ^{238}U the group containing the energy boundary between the resolved and unresolved resonance region was taken to belong to the latter. The profile tabulation for σ_s was used for the slowing down treatment from which the resonance absorption rates were determined. It was also used to correct the smooth σ_s values on the standard MUFT library in these groups.

The thermal multigroup library for the THERMOS module of HAMMER was produced using FLANGEII[10] and LITHE[1], and the Haywood kernel for hydrogen in H_2O.

RESONANCE ABSORPTION TREATMENTS AVAILABLE IN THE MODIFIED HAMMER CODE

The Nordheim Integral Treatment using Resonance Parameters

The standard Nordheim Integral Treatment NIT[2] is one of the available options in the modified HAMMER code. It calculates the effective resonance integrals over the central portion of each resonance individually and adds wing corrections. No interference effects between different resonances are taken into account. A similar procedure is used in the unresolved resonance region. In the current version of HAMMER it is available both for the s-wave and the p-wave resonance sequences of fertile isotopes.

The Nordheim Integral Treatment using Resonance Profile Tabulations

The new Nordheim option (NITPRO) included in the HAMMER code preserves, as far as the material composition and geometrical subdivision of the lattice unit cell are concerned, the standard procedure outlined above, but it makes use of resonance profile tabulations instead of resonance parameters in the resolved resonance region. As a consequence the numerical integration of the slowing down equations is carried out over each MUFT group in its

entirety and not over the central portions only of the resonances contained in it. To this end a lethargy mesh is defined. The collision density is calculated at each mesh point by solving the integral equation using a Simpson partial integration technique based on stored backvalues to evaluate the slowing down integrals. Absorption rates are calculated subsequently by numerical integration over a finer lethargy grid, which sees the resonance profile shape and interpolates between the calculated collision densities. The procedure handles all the resolved resonances and smooth contributions (from ENDF/B-file 3) of the resonance nuclides in the fuel together, so that resonance interference effects are automatically included, both as far as the resonance sequences of a single nuclide are concerned, and for the resonances of different nuclides. However, only up to three nuclides with resonance profile tabulations can be treated together.

When the first MUFT group in the resolved resonance region for any of the fuel resonance nuclides is reached, the initial backvalues for the slowing down integration have to be specified for the asymptotic flux shape. This can be done also for each subsequent MUFT group. However, an alternative option is provided, which carries the numerical integration for the slowing down density across the group boundaries

When more than three resonance nuclides are included in the fuel region, it is possible to treat up to three of these nuclides with the resonance profile method NITPRO. The remainder can be handled by the standard Nordheim procedure NIT using resonance parameters, provided this does not conflict with the definition of "admixed nuclides" as defined in the HAMMER version of NIT.

The RABBLE Integral Treatment using Resonance Profiles

Contrary to the use of effective resonance integrals from which the corresponding reaction rates are determined, the RABBLE Code[3] calculates the resonance reaction rates directly. It avoids thereby any ambiguities in the definition and use of the effective resonance integrals, specially where mixtures of resonance nuclides are concerned.

The RABBLE treatment is a multiregion integral transport method in which the slowing down integrals are evaluated using recurrence formulas for very fine groups, and which assumes an isotropic flux in the laboratory system and isotropic scattering in the centre of mass system.

In the HAMMER Code an option based on the RABBLE procedure (RABPRO) has now been included which uses the resonance profile tabulations in the resolved resonance region. The slowing down treatment has been restructured. The slowing down integrals are computed over a discrete lethargy grid using Simpson partial integration techniques as in the Nordheim procedures. The Simpson partial integration algorithm has been generalized so that it can be used for an arbitrary number of nuclides in each of the

multiregion subdivisions of the lattice unit cell. The region to region collision probabilities are computed by the cosine currents-flat source approximation. An iteration procedure is used to calculate the collision density in all spatial subregions at each lethargy mesh point.

Whereas in the standard RABBLE code resonance parameters are used for the S.L.B.W. formalism with ψ-χ function Doppler broadening, the HAMMER version RABPRO uses the exactly Doppler broadened resonance profile tabulations. Thus there is no ambiguity how many resonances should be included to evaluate the cross sections at each energy point, and there is no longer any artificial separation of the resonance and smooth parts of the cross sections.

The resonance reactions rates calculated by the RABPRO option are used directly in HAMMER to evaluate integral lattice parameters including k_{eff}. It should be noted that the RABPRO option does not permit "mixed runs", in which some resonance nuclides are described by resonance profile tabulations, and others are represented by resonance parameters. As in NITPRO the calculation of resonance reaction rates is limited to mixtures of up to three materials with resonance profile tabulations in the fuel.

Introduction of Externally Calculated Resonance Reaction Rates into HAMMER

When dealing with benchmark calculations even more sophisticated treatments of resonance absorption may be required. Both Monte-Carlo programs such as the REPC[11] or RECAP[12] codes, or methods based on the integro-differential transport option included in the OZMA-1 code (which is described in the following section) may be used for this purpose. The resonance reaction rates calculated by these codes in the resolved resonance region can be entered optionally into the present version of HAMMER provided they are in the proper group structure. The code operates in such a way that these rates are preserved, at zero buckling, in the final slowing down MUFT calculations for the homogenised unit cell. The number of resonance nuclides in the fuel which can be represented by resonance profile tabulations then depends on the external codes used (such as REPC or OZMA-1) and is not limited to three as in the internally available resonance options in HAMMER.

THE OZMA-1 CODE

The OZMA-1 method was developed as a more accurate procedure to calculate resonance absorption in the resolved resonance region, which also overcomes most of the technical limitations in the HAMMER resonance treatments.

The code calculates resonance reaction rates and reaction fractions in a specified multigroup structure and in

one-dimensional geometries, for use in lattice analysis codes. In addition, effective resonance integrals are derived from the reaction rates and edited. The code also produces group averaged cross sections in the resonance region and cross sections in a collapsed group structure.

OZMA-1 is written in FORTRAN-IV*, for the IBM-370-series computers, with the aim of taking full advantage of the virtual storage operating system (OS/VS); the code has a modular structure, dynamical storage allocation capabilities, and uses variable dimensions and direct access block oriented programming techniques. The latter feature should permit easy conversion to CDC computers with E.C.S.

Except for available core storage or computer time limitations there are practically no restrictions on the complexity of the problem which can be handled. However, one should stress that all resonance nuclides are to be represented by profile tabulations. But resonance nuclides can have an arbitrary distribution within the cell, i.e. any mixture can, in principle, contain profile isotopes.

Two alternative approaches are available to calculate the flux.

- o As a first option the anisotropic angular flux in the multiregion unit cell is obtained by solving the integro-differential transport equation. A discrete-ordinates treatment was developed to solve the equation on a discrete lethargy grid, as required to handle resonance profile tabulations.
- o Alternatively one can compute the isotropic flux in the multiregion unit cell by solving the integral transport equation for the collision density using collision probability methods. The present option is analogous to the RABPRO procedure included in HAMMER, but without the technical limitations previously referred to.

In the integro-differential form of the neutron transport equation, the down-scattering source term

$$S(\bar{r},u,\bar{w}) = \sum_{j\,(\bar{r})} \int_{u-v_j}^{u} du' \int d\bar{w}'\ \Sigma_s^j\ (\bar{r},u'\to u,\bar{w}'\to\bar{w})\,\phi(\bar{r},u',\bar{w}') \qquad (1)$$

where $v_j = -\mathrm{Log}\alpha_j$ and $\alpha_j = [(A_j-1)/(A_j+1)]^2$

must be computed for each isotope j contained in the region in which $\bar{r}$ is located. If for example, a two term Legendre

---

* at the H-Extended compiler level, with the exception of a few system interface routines written in Assembler.

expansion of the scattering cross section is used, the source term takes the following form in region n and for direction m:

$$S^{j}_{n,m}(u) = SI^{j}_{n}(u) + SA^{j}_{n,m}(u) \tag{2}$$

where the isotropic source component is given by

$$SI^{j}_{n}(u) = \frac{1}{1-\alpha_j} \int_{u-v_j}^{u} du' \; \Sigma_s^{j,n}(u')\psi^{o}_{n}(u') \tag{3}$$

The anisotropic component may be written as

$$SA^{j}_{n,m}(u) = \frac{3}{2}\mu_m \frac{1}{1-\alpha_j} \left[S^{+}_{n,j}(u) - S^{-}_{n,j}(u)\right] \tag{4}$$

with

$$S^{+}_{n,j}(u) = (A_j+1)\cdot E^{1/2} \cdot \int_{u-v_j}^{u} du' \; \Sigma_s^{j,n}(u')\psi^{1}_{n}(u')/\sqrt{E'} \tag{5}$$

and

$$S^{-}_{n,j}(u) = (A_j-1)\cdot E^{-1/2} \cdot \int_{u-v_j}^{u} du' \; \Sigma_s^{j,n}(u')\psi^{1}_{n}(u')\sqrt{E'} \tag{6}$$

In the OZMA-1 method one does not use directly the flux or its moments; rather one defines

$$E\,\psi^{o}_{n}(u) = \phi^{o}_{n}(u) = \sum_{m} w_m \phi_{n,m}(u) \tag{7}$$

ψ^{o}_{n} is the flux per unit energy expressed as function of lethargy. In the same manner one defines $\psi^{1}_{n}(u)$.

The algorithms used to evaluate the source over a discrete lethargy grid are quite similar for all source components. Reference is made to the Simpson partial integration technique[1] which expresses the slowing down integrals in the form:

$$\int_{u_i - v}^{u_i} f(u')du' = M\varepsilon_g I(u_i) + \frac{1}{3} M\varepsilon_g f(u_i) \tag{8}$$

where isotope and region indices (j,n) have been omitted.

The interval between successive nodes is defined for a particular isotope by:

$$u_i - u_{i+1} = \frac{v}{N-1} = M\varepsilon_g \tag{9}$$

ε_g represents the lethargy spacing between successive points at which the collision density is calculated, while N denotes the number of backvalues for the isotope under consideration.

$I(u_i)$ is a partial Simpson integral, which does not include the contribution at node u_i. It is obtained from stored backvalues of f at previous grid notes u_ℓ (ℓ=i+1, ... i+N-1). The integer M controls the grid points at which the backvalues of the function f are stored for the isotope in question, and is determined so that the number of these storage points does not exceed a limit specified in the input. This ensures that the procedure can also be used for light nuclides.

If for an isotope M > 1 interpolation techniques may have to be used at some intermediate points. Defining $u_{i,k}$ as the k-th grid point on the "ε_g" mesh in $[u_i, u_{i-1}]$ width $1 \leq k \leq M$

$$\int_{u_{i,k}-v}^{u_{i,k}} f(u')du' = [I_1]_{u_i}^{u_{i,k}} + [I_2]_{u_{i+N-1}}^{u_i} - [I_3]_{u_{i+N-1}}^{u_{i,k}-v} \tag{10}$$

The main contribution to the source comes from I_2 which is evaluated by Simpson integration. The end corrections are obtained using composite trapezium integration. Since only backvalues at node points u_i are kept, intermediate values in the range $[u_{i+N-2}, u_{i+N-1}]$ have to be interpolated.

In OZMA-1 both the linear-linear and the linear-log options are available. If linear interpolation is used

$$f_{N,k} = f_N + \frac{k}{M_j} [f_{N-1} - f_N] \quad \text{for} \quad 1 < k \leq M$$

and

$$f_{N,1} = f_N \equiv f(u_{i+N-1}) \quad \text{for} \quad k = 1 \tag{11}$$

so that

$$[I_3]_{u_{i+N-1}}^{u_{i,k}-v} \simeq \frac{\varepsilon_g}{2}\,[f_{N,k} + f_{N,1}] + \varepsilon_g \sum_{h=2}^{h=k-1} f_{N,h} \qquad (12)$$

No interpolation is needed for $[I_1]$ since it is evaluated cumulatively at successive "ε_g" grid points from the most recently stored backvalue. For hydrogen a similar technique has been developed, using $M_H = 1$, notwithstanding the large range of integration. Instead of storing backvalues the two partial sums which make up I with different weights are kept, and modified when moving from one mesh point to the next.

RESULTS

The methods described above were applied to the study of thermal reactor lattice benchmarks[4]. Two H_2O moderated lattices of slightly enriched uranium rods, TRX-1 and TRX-2, and three D_2O moderated lattices of natural uranium rods, MIT-1-2-3, were analyzed. In every case the calculated quantities include the effective multiplication factor k_{eff} and the following integral parameters:

- o ρ_{28} = ratio of epithermal-to-thermal ^{238}U captures.
- o δ_{25} = ratio of epithermal-to-thermal ^{235}U fissions.
- o δ_{28} = ratio of ^{238}U fissions-to-^{235}U fissions.
- o CR = ratio of total ^{238}U captures-to-^{235}U fissions.

Sensitivity tests were made to determine the interval between the lethargy points at which the collision density is calculated when resonance profile tabulations are used. Changing the mesh interval successively by factors of two it was found that the results became fairly insensitive to the grid chosen when a density of about 4000 points per unit lethargy is reached. This value was subsequently adopted for all runs. The reaction rates were determined by a further subdivision of the grid in accordance with the average lethargy interval between resonance profile data in each MUFT group for the nuclide for which these data are the densest. Since the spacing of the data is closer than the average near the resonance peaks, an even finer subdivision was also tested, but produced practically identical results. The reaction rates were determined cumulatively throughout all the relevant MUFT groups so that interference effects between resonances in neighbouring groups were included.

In Table 1 results obtained by different resonance treatments for the TRX-1 benchmark are compared with experimental values as recently corrected by Sher and Fiarman[6]. The comparison between NIT and NITPRO shows the effect of replacing the resonance

parameter representation by resonance profiles; ρ_{28} is reduced from 1.408 to 1.384 but remains far outside the ^{28}experimental range; k_{eff} is improved by .3 of a percent; δ_{25} remains overpredicted. ^{eff}The three OZMA-1 options show clearly the improvements obtained when passing from a two region to a multiregion representation and subsequently from the integral transport-collision probabilities to the integro-differential transport formalisms. When the anisotropic flux option is used, ρ_{28} reaches almost the upper bound of the experimental range, while very good agreement is reached for δ_{25}, δ_{28} and CR. In the three OZMA-1 multiregion treatment options (RABPRO - integral transport and isotropic and linearly anisotropic integro-differential transport), the lattice unit cell was subdivided into 4 subregions in the fuel and 3 outside it. The subregion thicknesses were finer near the fuel surface. Tests with a greater number of subregions led to k_{eff} values differing from the ones quoted by no more than about .2 of a percent. The integro-differential treatment was based on an S_6 angular quadrature. A step function model was used in the flux computation scheme. The results agreed with those obtained with an S_4 quadrature to within .15 percent in k_{eff}. A comparable trend was observed when switching from the step function to the linear scheme. In the Table P_o and P_1 scattering in the laboratory system are compared.

The RECAP Monte-Carlo resonance reaction rates at zero buckling were introduced into the HAMMER analysis both at BNL[12] and at the Technion. The small difference in the results is due to the fact that the modified HAMMER treatment uses two iterations in the integral transport treatment in order to preserve neutron balance in the heterogeneity analysis and also treats the p-wave unresolved resonance shielding explicitely.

Tables 2 - 5 give similar comparisons for TRX-2 and MIT 1-3. The same trends are observed in comparing calculation and experiment as in the case of TRX-1.

CONCLUSION

The benchmark calculations presented here show that improved agreement with experiment can be obtained when resonance profile tabulations are used instead of resonance parameters in the resolved resonance region. A number of different calculational procedures were developed and tested. A multiregion transport calculation which allows for scattering anisotropy in the laboratory system appears to lead to closest agreement with experiment, but the differences with simpler treatments are not large. One of the major features of the use of profile tabulations lies in the fact that resonance interference effects are fully included, and in particular, those resulting from resonances of different nuclides. This led to improved values of δ_{25} which is affected by the proximity of the ^{238}U resonances.

Table 1

TRX - 1

	K_{eff}	ρ_{28}	δ_{25}	δ_{28}	CR
EPRI-Exp	1.0000	1.320 ±.021	.0987 ±.0010	.0946 ±.0041	.797 ±.008
NIT	.9832	1.408	.1052	.0950	.809
NITPRO	.9862	1.384	.1021	.0947	.803
OZMA-1:RABPRO	.9854	1.384	.0997	.0948	.805
OZMA-1: S_6P_0	.9896	1.350	.0984	.0943	.795
OZMA-1: S_6P_1	.9906	1.343	.0987	.0942	.792
BNL - REPC	.9880	1.367	.0994	.0944	.799
BNL - RECAP	.9882	1.368	.0999	.0944	.799
Tech- RECAP	.9895	1.353	.0995	.0943	.795

Table 2

TRX - 2

	K_{eff}	ρ_{28}	δ_{25}	δ_{28}	CR
EPRI-Exp	1.0000	.837 ±.016	.0614 ±.0008	.0693 ±.0035	.647 ±.006
NIT	.9885	.873	.0642	.0669	.648
NITPRO	.9905	.859	.0625	.0668	.644
OZMA-1	.9930	.837	.0601	.0666	.638
BNL - REPC	.9921	.846	.0612	.0666	.640
BNL - RECAP	.9934	.836	.0599	.0664	.637

Table 3
MIT-1

	K_{eff}	ρ_{28}	δ_{25}	δ_{28}	CR
EPRI-Exp	1.0000	.502 ±.010	.0469 ±.0019	.0588 ±.0030	1.017 ±.023
NIT	.9826	.530	.0490	.0573	.982
NITPRO	.9860	.513	.0462	.0570	.974
OZMA-1	.9924	.487	.0455	.0566	.958
BNL - REPC	.9905	.500	.0462	.0579	.965

Table 4
MIT-2

	K_{eff}	ρ_{28}	δ_{25}	δ_{28}	CR
EPRI-Exp	1.0000	.400 ±.004	.0335 ±.0030	.0587 ±.0030	.948 ±.020
NIT	.9833	.434	.0400	.0556	.926
NITPRO	.9860	.422	.0379	.0554	.920
OZMA-1	.9909	.402	.0374	.0551	.908
BNL - REPC	.9897	.411	.0376	.0562	.913

Table 5
MIT-3

	K_{eff}	ρ_{28}	δ_{25}	δ_{28}	CR
EPRI-Exp	1.0000	.313 ±.005	.0265 ±.0011	.0575 ±.0030	.859 ±.016
NIT	.9862	.338	.0309	.0540	.869
NITPRO	.9882	.328	.0295	.0538	.864
OZMA-1	.9918	.314	.0291	.0536	.855
BNL - REPC	.9921	.316	.0294	.0546	.856

The techniques have been formulated in such a way that they can be utilised also for more complicated systems.

REFERENCES

1. Barhen, J., Rothenstein, W., Taviv, E.,: "Improvement of Thermal Reactor Benchmark Procedures / The HAMMER Code System - Technion version", Research Contract EPRI-709-1, Final Report, Electric Power Research Institute, to be published (1978).

2. Kuncir, G.F.,: "A Program for the Calculation of Resonance Integrals", GA-2525, General Atomic (1961).

3. Kier, P.H., Robba, A.A.: "RABBLE - A Program for the Computation of Resonance Absorption in Multiregion Reactor Cells", ANL-7326 (1967).

4. N.N.C.S.C.: "Cross Section Evaluation Working Group Benchmark Specifications", BNL-19302, ENDF-202, Brookhaven National Laboratory (1974).

5. Rothenstein, W.: "Thermal Reactor Lattice Analysis Using ENDF/B-IV Data with Monte-Carlo Resonance Reaction Rates", Nucl. Sc. Eng., 59, 337 (1976).

6. Sher, R., Fiarman, S.: "Studies of Thermal Reactor Benchmark Data Interpretation: Experimental Corrections", EPRI-NP-209, Final Report, Electric Power Research Institute (1976).

7. de Saussure, G., Olsen, D.K., Periz, R.B.: "The ENDF/B-IV Representation of the Uranium-238 Total Neutron Cross Section in the Resolved Resonance Energy Region", Nucl. Sc. Eng., 61, 496, (1976).

8. Ozer, O.: "A Program to Process ENDF/B Materials with Resonance Files into Point-Wise Form", BNL-17134, Brookhaven National Laboratory (1973).

9. Cullen, D.E.: "Program SIGMA-1 (Version 77-1): Doppler Broaden Evaluated Cross Sections in the ENDF/B Format", UCRL-50400, Vol. 17, Part B, Lawrence Livermore Laboratory (1977).

10. Honeck, H.C., Finch, D.R.: "FLANGE-II (Version 71-1), A Code to Process Thermal Neutron Data from an ENDF/B Tape", DP-1278, ENDF-152, Savannah River Laboratory, (1971).

11. Rothenstein, W.: "Monte-Carlo Code REPC to Calculate Resonance Reaction Rates in Thermal Reactor Lattice Benchmarks", BNL-20400, Brookhaven National Laboratory (1975).

12. Levitt, L., Magurno, B., Rose, P.: "Improvement of Reference Nuclear Data for Commercial Power Reactor Analysis and Design", EPRI-NP-556, Project 708-1, Final Report, Electric Power Research Institute (1977).

APPENDIXES

Appendix A

SYMPOSIUM AGENDA
NUCLEAR DATA PROBLEMS FOR THERMAL REACTOR APPLICATIONS

May 22, 1978

9:10 a.m.	Welcoming Address, H. J. C. Kouts (BNL)
9:15 a.m.	Introductory Statement, O. Ozer (EPRI)
	SESSION I: Review of Microscopic Cross Sections of Importance to Reactor Design. Session Chairman: B. R. Leonard, Jr. (BNWL)
9:30 a.m.	1. L. W. Weston (ORNL): "Review of Cross Section Data Important to the Uranium Plutonium Fuel Cycle in Thermal Reactors"
10:00 a.m.	2. D. R. Mathews and W. R. Davison (GA): "The Adequacy of ^{232}Th and ^{233}U ENDF/B Data for HTGR Design Applications"
10:30 a.m.	Coffee Break
10:45 a.m.	3. W. H. Walker (AECL): "Cross Sections and Yields Important for Fission Product Absorption in Thermal Reactors"
11:15 a.m.	4. J. R. Smith (EG&G): "Status of ^{252}Cf $\bar{\nu}$ and Its Impact on Thermal Reactor Parameters"
	SESSION II: Review of Clean Critical Benchmarks and Analysis of Clean Critical Experiments. Session Chairman: J. Hardy, Jr. (BAPL)
1:00 p.m.	1. R. Sher and J. Adir (Stanford): "A Review of Plutonium Experiments"
1:30 p.m.	2. J. Hardy, Jr. (BAPL) and D. R. Finch (SRL): "Analysis of ^{235}U-^{238}U Thermal Reactor Benchmarks--Consistency and Interpretation"
2:00 p.m.	3. D. J. Pellarin, C. E. Ahlfeld, and N. P. Baumann (SRL): "Reactivity and Parameter Measurements in Coaxial Uranium Fuel-D_2O Moderated Critical Lattice"
2:30 p.m.	4. J. J. Ullo, J. Hardy, Jr., and N. M. Steen (BAPL): "Review of Thorium-^{233}U Cycle Thermal Reactor Benchmark Studies"
3:00 p.m.	Coffee Break
3:15 p.m.	SESSION III: Round Table Discussion of Sessions I and II. B. R. Leonard, Jr., and J. Hardy, Jr.
6:30 p.m.	Cocktails
7:30 p.m.	Banquet

May 23, 1978

SESSION IV: Dependence of Power Reactor Benchmarks on Nuclear Data.
Session Chairman: D. Diamond (BNL)

9:15 a.m. 1. T. R. England (LASL), R. E. Schenter, and F. Schmittroth (HEDL): "Integral Decay-Heat Measurements and Comparisons to ENDF/B-IV and -V"

9:45 a.m. 2. W. B. Wilson and T. R. England (LASL): "Status of Fission Product Data for Absorption Calculations"

10:15 a.m. Coffee Break

10:30 a.m. 3. R. W. Benjamin (SRL): "Nuclear Data for Actinide Production and Depletion Calculations"

10:50 a.m. 4. R. E. MacFarlane (LASL): "Data Processing for Power Reactor Fuel Cycle Codes"

11:15 a.m. 5. M. Becker, D. R. Harris, B. Quan, and J. M. Ryskamp (RPI): "The Relationship Between Basic Nuclear Data and LWR Fuel Cycle Parameters"

SESSION V: Interaction of Methods and Data in Industrial Experience.
Session Chairman: B. Zolotar (EPRI)

1:00 p.m. 1. M. Edenius (OKG, Sweden): "Temperature Effects in Thermal Reactor Analysis"

1:30 p.m. 2. S. C. Bhatt, R. L. Crowther, C. M. Kang, R. A. Wolters, and J. E. Wood (GE/San Jose): "Feedback of BWR Benchmarks to Cross Section Data"

2:00 p.m. 3. A. Jonsson, J. R. Rec, and U. N. Singh (CE): "Requirements for the Physics Analysis of PWR Fuel Assemblies"

2:30 p.m. 4. W. J. Eich (EPRI): "LWR Assembly Reaction Rate Representation"

3:00 p.m. Coffee Break

3:15 p.m. SESSION VI: Round Table Discussion of Sessions IV and V. D. Diamond and B. Zolotar

7:30 p.m. SESSION VII: Preparation of Summaries and Final Recommendations. S. Pearlstein and O. Ozer. All participants invited.

May 24, 1978

8:30 a.m. SESSION VIII: Preparation of Summaries and Final Recommendations. All participants invited.

10:30 a.m. SESSION IX: Presentation of Summaries and Final Recommendations (continued). All chairmen.

12:00 m. Adjournment

Appendix B

LIST OF PARTICIPANTS

Adir, J., Stanford University
Alapour, A., BNL
Anderl, R. A., EG&G Idaho
Aronson, A., BNL
Baker, V. C., ORNL
Barhen, J., Technion, Israel
Beer, M., MAGI
Benjamin, R. W., SRL
Bhat, M., BNL
Block, R. C., RPI
Bohn, T., EG&G Idaho
Buslik, A., BNL
Cacciapouti, R. J., Yankee Atomic
Cheng, H., BNL
Childs, R. L., ORNL
Cokinos, D., BNL
Craig, D. S., AECL
Crowther, R., GE/San Jose
Darnell, B. L., TVA
Darrouzet, M., CEA, France
Diamond, D. J., BNL
Divadeenam, M., BNL
Dudley, T., KAPL
Dunnenfeld, M., NRC
Durston, C., BNL
Edenius, M., OKG, Sweden
Eich, W., EPRI
England, T., LASL
Felvinci, J. P., Columbia University
Fieno, D., NRC
Finch, D..R., SRL
Fisher, J. R., NAI
Gibson, I. H., UKAEA
Goldstein, H., Columbia University
Gore, B., BNW
Griffiths, J., AECL
Grimesey, R., EG&G Idaho
Haggblom, H., Studsvik, Sweden
Hardy, J., BAPL
Harris, D. R., RPI
Havens, W. W., Columbia University
Heijboer, R. J., ECN, Netherlands
Henderson, W. B., WNES
Herczeg, J. W., BNL
Holden, N. E., BNL
Jenquin, U., BNW
Jonsson, A., CE
Kim, Y. S., NUS Corp.
Kujawski, E., GE/FBRD
Leonard, B., BNW
Levitt, L. B., BNL
Lichtenstein, H., MAGI
Liu, Y. W., Columbia University
Ludewig, H., BNL
MacFarlane, R., LASL
Magurno, B. A., BNL
Mahan, K., PSE&G, New Jersey
Mathews, D., GA
Melkonian, E., Columbia University
Moore, M. S., LASL
Mosteller, R., SAI
Nakahara, Y., BNL
Newman, D., BNW
Oden, D. R., BNW
Okazaki, A., AECL
Olsen, D. K., ORNL
Ozer, O., EPRI
Pearlstein, S., BNL
Peelle, R., ORNL
Pellarin, D. J., SRL
Pennington, E., ANL
Quan, B., RPI
Rec, J. R., CE
Reuss, P., CEA, France
Rose, P., BNL
Rothenstein, W., Technion, Israel
Rothleder, B., NAI
Ryskamp, J., RPI
Sher, R., Stanford University
Smith, J. R., EG&G Idaho
Stamatelatos, M., SAI
Stewart, L., LASL
Struble, G. L., LLL
Takahashi, H., BNL
Todosow, M., BNL
Ullo, J. J., BAPL
VerPlanck, D. M., Yankee Atomic
Walker, W. H., AECL
Wattecamps, E., Geel, Belgium
Weisbin, C. R., ORNL
Weston, L. W., ORNL
Williams, M. L., ORNL
Wilson, W. B., LASL
Wittkopf, W., B&W

Weston, L. W., ORNL
Williams, M. L., ORNL
Wilson, W. B., LASL
Wittkopf, W., B&W
Woodruff, W., ANL
Yamamoto, M., GE/San Jose
Zolotar, B., EPRI